



UNIVERSITAT DE
BARCELONA

Epigenomic and transcriptomic regulation of myeloid immunosuppression

Gerard Godoy Tena

ADVERTIMENT. La consulta d'aquesta tesi queda condicionada a l'acceptació de les següents condicions d'ús: La difusió d'aquesta tesi per mitjà del servei TDX (www.tdx.cat) i a través del Dipòsit Digital de la UB (diposit.ub.edu) ha estat autoritzada pels titulars dels drets de propietat intel·lectual únicament per a usos privats emmarcats en activitats d'investigació i docència. No s'autoritza la seva reproducció amb finalitats de lucre ni la seva difusió i posada a disposició des d'un lloc aliè al servei TDX ni al Dipòsit Digital de la UB. No s'autoritza la presentació del seu contingut en una finestra o marc aliè a TDX o al Dipòsit Digital de la UB (framing). Aquesta reserva de drets afecta tant al resum de presentació de la tesi com als seus continguts. En la utilització o cita de parts de la tesi és obligat indicar el nom de la persona autora.

ADVERTENCIA. La consulta de esta tesis queda condicionada a la aceptación de las siguientes condiciones de uso: La difusión de esta tesis por medio del servicio TDR (www.tdx.cat) y a través del Repositorio Digital de la UB (diposit.ub.edu) ha sido autorizada por los titulares de los derechos de propiedad intelectual únicamente para usos privados enmarcados en actividades de investigación y docencia. No se autoriza su reproducción con finalidades de lucro ni su difusión y puesta a disposición desde un sitio ajeno al servicio TDR o al Repositorio Digital de la UB. No se autoriza la presentación de su contenido en una ventana o marco ajeno a TDR o al Repositorio Digital de la UB (framing). Esta reserva de derechos afecta tanto al resumen de presentación de la tesis como a sus contenidos. En la utilización o cita de partes de la tesis es obligado indicar el nombre de la persona autora.

WARNING. On having consulted this thesis you're accepting the following use conditions: Spreading this thesis by the TDX (www.tdx.cat) service and by the UB Digital Repository (diposit.ub.edu) has been authorized by the titular of the intellectual property rights only for private uses placed in investigation and teaching activities. Reproduction with lucrative aims is not authorized nor its spreading and availability from a site foreign to the TDX service or to the UB Digital Repository. Introducing its content in a window or frame foreign to the TDX service or to the UB Digital Repository is not authorized (framing). Those rights affect to the presentation summary of the thesis as well as to its contents. In the using or citation of parts of the thesis it's obliged to indicate the name of the author.



UNIVERSITAT^{DE}
BARCELONA

EPIGENOMIC AND TRANSCRIPTOMIC REGULATION OF MYELOID IMMUNOSUPPRESSION

Memoria presentada per en **Gerard Godoy Tena** per optar al títol de
doctor per la Universitat de Barcelona

2024

UNIVERSITAT DE BARCELONA – FACULTAT DE FARMÀCIA
PROGRAMA DE DOCTORAT EN BIOMEDICINA

Tesis realitzada al grup d'Epigenètica i Malalties Immunitàries de
l'Institut Josep Carreras (IJC) sota la direcció del Dr. Esteban Ballestar

Dr. Esteban Ballestar
Director

Dra. Maria Del Carmen
Caelles Franch
Tutora

Gerard Godoy Tena
Doctorand

A l'avi i a la iaia

INDEX

- ACKNOWLEDGEMENTS1
- SUMMARY..... 7
- RESUMEN..... 9
- RESUM.....11
- ABBREVIATIONS..... 13
- 1. INTRODUCTION 21
 - 1.1. The Immune System 21
 - 1.1.1. Innate and Adaptive immunity..... 21
 - 1.1.2. Immune cell differentiation 24
 - 1.1.3. Monocytes..... 26
 - 1.1.4. Monocyte-derive cells and Dendritic Cells..... 28
 - 1.2. Mechanisms of immune suppression..... 33
 - 1.2.1. Immune suppression on epithelial barrier immunity, the role of Retinoic Acid..... 35
 - 1.2.2. Tumor immune-suppression 39
 - 1.2.3. COVID-19-associated Immune-supression 43
 - 1.3. DNA methylation as a major epigenetic mechanism in myeloid cells48
 - 1.3.1. Overview48
 - 1.3.2. Regulation of DNA methylation 50
 - 1.3.3. Transcription factors as mediators of DNA methylation changes 54
 - 1.3.4. DNA methylation alterations in immune mediated diseases.... 55
 - 1.3.5. Role of DNA methylation in monocyte differentiation and suppression 58
- 2. HYPOTHESIS..... 63
- 3. OBJECTIVES..... 65

3.	ARTICLES.....	69
	Director's report	69
3.1	ARTICLE 1. Retinoic Acid-Induced Epigenetic Modulation of VSIG4 via LXR α in Dendritic Cells Promotes Immunosuppression	73
3.2	ARTICLE 2. Epigenetic and transcriptomic reprogramming in monocytes of severe COVID-19 patients reflects alterations in myeloid differentiation and the influence of inflammatory cytokines	133
3.3	ARTICLE 3. Single-cell multi-omics analysis of COVID-19 patients with pre-existing autoimmune diseases shows aberrant immune responses to infection.....	197
5.	GLOBAL RESULTS.....	249
6.	GLOBAL DISCUSSION.....	257
	Overview	258
	DNA methylation and transcriptomic regulation	260
	Mechanisms of immune suppression	267
	Cell-cell communication	270
7.	CONCLUSIONS	273
8.	REFERENCES	279
9.	APPENDIX	307

ACKNOWLEDGEMENTS

Des del primer moment que vaig començar la tesis vaig estar pensant en aquest moment, en el moment d'agraïr a totes aquelles persones que d'alguna manera o altre m'ha ajudat en aquest camí, espero estar a l'altura.

Evidentment, res d'això no hagués estat possible si l'**Esteban** no hagués confiat cegament en mi per processar aquelles mostres de COVID-19 tan valuoses i tot seguit tornar a confiar en mi per formar part del seu equip i començar la tesis. Ja només per això t'estaré sempre agraït. Sempre hem tingut els nostres alts i baixos però sempre he sabut que és perquè compartim el mateix nervi per la ciència i per davant de tot se que sempre has posat que jo pugui fer una bona tesis.

Els inicis van ser estranys, vaig començar en un laboratori on no hi havia gent per culpa del confinament, tot i així no em vaig sentir sol, sempre tenia el suport dels meus companys de manera remota. La persona que més em va ajudar als meus inicis va ser en **Javi**. Gràcies Javi per ensenyar-me tant bé, sempre procurant que entengués cada detall. Donar-te les gràcies pel teu optimisme i passió per la ciència, però també pel teu bon humor i per saber escoltar quan ho he necessitat. Un altre persona amb la que em vaig sentir recolzada en els meus inicis va ser amb la **Laura**. Gràcies Laura per donar-me un cop de mà sempre que t'ho he demanat i per procurar per a que tothom del lab se senti còmode, sobretot jo. Sempre recordaré els nostre viatges al IRB amb cotxe.

Poc a poc van anar arribant els que serien els meus companys pels següents anys. Els primers en arribar van ser la Tian, en Carlos i l'Octavio. **Tian**, gràcies per ensenyar-me als meus inicis. També per ensenyar-me a ser ordenat, a procurar sempre tenir els meus protocols i sobretot a saber donar ajuda quan algú ho requereix. **Carlos**, sempre que he necessitat la teva ajuda ho has fet i amb molta dolçor, en procurar que el que m'estàs explicant ho entengui bé i t'estaré sempre agraït. També m'has sabut donar els millors consells pel meu doctorat, els qual he seguit al peu de la lletra. **Octavio**, gràcies per ensenyar-me a que amb autoaprenentatge es pot arribar molt alt. També per ensenyar-me a ser meticulós, a saber expressar els resultats de la millor manera i per la tranquil·litat que sempre m'has transmès. Amb vosaltres tres vaig fer uns dels viatges més bojos que he fet mai, vosaltres ja sabeu quin és (té alguna cosa a

veure amb una clínica a Jaca). Amb això m'agradaria també donar-vos les gràcies pel bon rollo que sempre m'heu transmès, no només dintre el laboratori sinó també fora.

Les últimes persones que vaig conèixer que ja formaven part del lab van ser l'Anna i en Ricardo. L'**Anna F.** ha sigut la millor compi de batalla que hauria pogut tenir pels meus 4 anys de tesis. Moles gràcies Anna per treballar colze a colze amb mi als inicis, se que els dos estàvem aprenent i tot i així tu em donaves la confiança que a mi sempre m'ha faltat. A nivell personal crec que no hi ha paraules per agrair-te el que ha significat tenir-te en el lab ja que sempre has sigut la persona que ha sabut notar quan no he estat bé i has procurat que no segueixi així i això significa molt per mi. **Ricardo**, tot i no estar sempre al lab, els mesos que estaves justament t'assentaves al meu costat i de tu vaig aprendre a centrar-me, a posar-me un objectiu i complir-lo. Per últim, i no per això menys important, donar les gràcies a les últimes incorporacions del lab, la **Cèlia**, en **Pep**, la **Cristina** i l'**Elkyn**. Gràcies per mirar sempre de portar bon rollo al lab i per ensenyar-me a que treballar pot ser professional i a la vegada divertit.

Van anar passant els mesos i cada cop teníem noves incorporacions al lab, ja siguin estudiants de màster, de grau, d'estància, etc. M'agradaria destacar als meus dos estudiants de màster preferits, en **Niko** i la **Lucía**. Gràcies, no només per l'ajuda en el meu projecte, sinó també pels bons moments que hem compartit.

M'agradaria també donar les gràcies a l'**Eva M.** per les reunions inicials que fèiem junt amb l'Esteban per discutir sobre els meus projectes i per donar-me el seu punt de vista des de la immunologia. També voldria donar-te les gràcies en ajudar-me a transmetre la meva ciència. Del grup de l'Eva m'emporto sobretot dues persones. El primer de tots és el *mio amore* **Fede**. Sento que des de que ens vam conèixer vam connectar súper bé i això ha fet que ens recolzem un en l'altre. Quan he tingut un dubte d'immunologia sempre has estat allà per ajudar-me i he de dir que he après moltíssim de tu. A nivell personal saps de sobres el que simbolitzes per mi. L'altre persona és la **Jana**, de la qual m'emporto el seu somriure incansable i tots els cafès que vam fer junts dia rere dia abans de començar la jornada i totes les nits de *board games*. Ja saps que junt amb en **Rob** sou els meus *unpaid therapists*.

Sento que sempre he sigut com un més als laboratoris veïns. Gràcies Josema, Andrés, **Anna G.** i **Maria** pels bons moments i per tots els viatges i coses que hem fet junts. Però sobretot volia agrair a en **Josema**, per ser un indispensable a la meua vida a Barcelona i per tot el que hem compartit junts. De l'Andrés parlaré més endavant. També vull destacar els meus *team desayuno*, en **Juan**, la **Cristina D.** i en **Pablo**, els quals sempre he necessitat per començar els dies amb energia i alegria. Destacar sobretot la **Cristina D.**, la qual ha suposat un gran recolzament emocional en els moments més durs. Com no, també donar les gràcies a l'**Oriol**, la **Mar**, l'**Ainara** i l'**Íngrid** per adoptar-me en els seus esmorzars i per les mil i una conversacions a cultius. Agrair també a l'**Alberto** la seva motivació constant que sempre m'ha meravellat i motivat a l'hora.

Aquest període no ha sigut només fer ciència sinó que m'agradaria destacar també la gran sort que he tingut de fer la tesis al IJC, amb molta gent meravellosa, amb la qual hem fet mil i una junts. Sobretot als inicis, quan tot estava tancat pel confinament, allà estaven la **Maria C.**, la **Gemma**, l'**Aleksey**, la **Carini**, l'**Eric** o en **James**, per passar una bona estona els divendres i per anar a jugar a vòlei a Badalona. També donar les gràcies a en **Noel**, en **Joan**, la **Clara**, en **Manu**, en **Louis**, l'**Eve**, la **Kathleen**, en **Hielke**, l'**Oliver**, la **Roser**, la **Lidia**, la **Noe**, l'**Adrià** i *el mas grande* **Jose**, amb els quals hem compartit grans moments. Gràcies a tots per fer possible aquesta foto:



També m'agradaria agrair totes aquelles persones que sento que m'han ajudat molt, tant per a arribar a fer la tesis com durant aquesta. Primer m'agradaria començar per les quatre persona més important en aquesta trajecte. Primer de tot al meu **Andrés**. Sento que no puc descriure en paraules tot el que has fet per mi. Vas ser la persona que em va ensenyar a tenir un propòsit a la vida, la persona que em va motivar a fer un doctorat, la persona amb la que he tingut les conversacions més profundes i enriquidores. Sento que el fet de coneixent va canviar totalment la meva menar de ser i de pensar. Ets a qui he acudit sempre que m'ha passat alguna cosa bona, però també quan m'ha passat alguna dolenta ja que sempre tens la millor resposta. Fer la tesis al teu costat ha sigut de les millors fortunes que he tingut mai. Després al meu **Marc**. Gràcies per convertir les eternes hores de classe de carrera en moments divertits i per ajudar-me amb els teus súper apunts aquelles nits al teu pis prèvies als exàmens. Però sobretot m'agradaria donar-te les gràcies per ser allà quan ho he necessitat, crec que això és el que defineix un bon amic i tu ets un dels grans. Al meu **Artur**, el meu indispensable. Gràcies per tots els bons moments que vam passar a la uni i durant el màster, i gràcies per fer-me un més del teu cercle a Teià. Ja saps que sense tu no hagués aconseguit tot el que he aconseguit. Per últim, la meva **Isa**, la millor no companya de màster. Gràcies per ensenyar-me a que si agafes les coses amb motivació pots aconseguir el que et proposis.

Destacar també aquells que durant la meva vida universitària van fer que millorés en molts aspectes. Primer de tot, com no començar pels meus *Caponasos*. L'**Uri C.**, la **Cris**, en **Domi**, la **Dome**, en **Guillem**, la **Bugui**, la **Marina**, l'**Arnau**, la **Marta** i en **Teti**. Gràcies per fer de l'etapa universitària de les millors que he viscut. Destacar també a l'**Ivan**, sense el qual no hagués après ni la meitat de coses que vaig aprendre. També donar les gràcies a les persones que vaig conèixer en el LEQUIA, destacant sobretot a en **Marc E.**, el qual sempre he tingut com a referent i model a seguir. Donar les gràcies a l'**Adri**, per ser el millor camp de màster. També a tots els membres del grup on vaig fer el TFM, destacant a en **Pablo F.**, l'**Alicia** i la **Cristina**, dels que vaig aprendre moltíssim i sempre m'he sentit recolzat.

Anant una mica més endarrere, voldria donar les gràcies a en **Miquel C.**, pel suport que va suposar tenir-lo durant el batxillerat i que em va permetre arribar on volia arribar. Donar les gràcies a tots els professors que, tot i les meves dificultats, es van esforçar per treure el millor de mi, sobretot al meu

gran metre, l'**Artur C.** També agrair a aquells que no van confiar en mi, ja que les meves ganes de demostrar que soc capaç de fer el que em proposi ha sigut el meu motor durant tot aquests temps.

Òbviament, donar les gràcies als *TUTs*, als meus amics de tota la vida, en **Pablo**, en **Boix**, l'**Oscar**, en **Soler**, l'**Uri**, en **Muni**, en **Nuñez**, en **Pich**, en **Ferrer**, la **Cinta**, en **Cuello**, en **Happy**, l'**Helena**, la **Clara** i en **Pere**, per sempre estar allà, per tots els moments que hem viscut fins ara i pels que ens queden. Se que he sigut molt pesat parlant de ciència, gràcies per la vostra paciència. També donar les gràcies a la **Júlia**, per ser el meu recolzament durant tants anys i per tots els bons moments viscuts.

Voldria donar les gràcies també a la meva família, en especial als **meus pares**, la **Judith**, en **David** i a tots els **Torracosins**, per donar-me l'oportunitat i recolzar-me en tot el que he volgut fet. Pel vostre sentiment d'orgull que sempre m'ha fet sentir bé amb el que faig. Sobretot voldria donar les gràcies a la **Laia**. Fa poc que formes part de la meva vida però has suposat una peça clau per a la recta final d'aquesta tesis. Per alegrar-me els dies, pel teu suport incondicional i per coneixem tant bé i sempre procurar treure la meva millor versió. Pel teu orgull cap a mi i tot el que hem aconseguit junts. No oblidar el teu suport en l'escriptura de la tesis i la súper portada que has dissenyat. Saps que el temps d'escriptura junts a Miami ha sigut de les millors coses que m'han passat mai.

No voldria acabar sense donar les gràcies a les dues persones més importants de la meva vida, que malauradament no han arribat al final d'aquest camí. Dues persones que malgrat les circumstancies sempre van lluitar pel bé de la seva família. Dues persones de les que he après moltíssim i m'han ensenyat a estimar el que faig. Dues persones amb les que sempre he tingut una connexió especial dels que sempre he estat orgullós. Dues persones que sempre m'han animat a seguir lluitant fins al final, i això he fet i seguiré fent. Vull dedicar aquesta tesis a ells, a l'**avi** i a la **iaia**.

SUMMARY

This doctoral thesis delves into the complex mechanisms of innate immune responses, focusing on the role of myeloid cells such as monocytes and monocyte-derived dendritic cells in immunosuppression. These cells dynamically shift between pro-inflammatory and immunosuppressive states influenced by their environment and interactions with specific molecules. This adaptability is crucial in various contexts, including epithelial barrier immunity or the tumor microenvironment, where retinoic acid (RA) can play a significant role, and in severe cases of COVID-19. However, the underlying regulatory mechanisms, especially the role of DNA methylation in these phenotypic changes, are not well understood. We have studied in these two different contexts, both *in vitro* and *ex vivo*, how DNA methylation is capable of regulating the suppressive phenotype in myeloid cells and, in turn, we have also examined how defects in suppression mechanisms associate with immune response to SARS-CoV-2 infection.

In the first study, we showed that RA influences the properties of monocyte-derived dendritic cells (moDCs), promoting a more macrophage-like phenotype and acquiring immunosuppressive capabilities. We determined that these changes were related to specific changes in DNA methylation, highlighting the role of epigenetics in acquiring this phenotype. We revealed that the nuclear receptor LXR α is crucial in the effects of RA, and its activation associates with DNA methylation reprogramming and expression of immunosuppressive elements such as VSIG4. The suppression of RXR α by RA was key to the function of LXR α . Lastly, we observed that macrophages in certain environments, such as in the colon or tumors, express both LXR α and VSIG4, suggesting a broader relevance of these mechanisms.

In the second study, we analyzed the methylome and transcriptome of monocytes from patients with severe COVID-19 and determined changes in DNA methylation at sites linked to interferon genes and antigen presentation, aligning with a suppressive gene expression profile. Some of these changes overlapped with those observed during bacterial sepsis, whereas others are alterations specific to viral infection. These changes in DNA methylation, reminiscent of those occurring during myeloid differentiation and inflammation, suggest the occurrence of an epigenetic and transcriptional reprogramming of monocytes. We also showed that this reprogramming could be related to the release of immature monocytes, the increase of systemic pro-inflammatory cytokines, and the disruption of interactions with other immune cells, contributing to the severity of the disease.

In the third study, we analyzed the transcriptome of peripheral immune cells from patients with rheumatoid arthritis, psoriasis, or multiple sclerosis infected with SARS-CoV-2. Although all three autoimmune groups showed a common increase in CD14⁺ HLA-DR_{low} monocytes, the specific characteristics of their immune response to the virus varied significantly. This included differences in type I interferon signaling and the inflammatory responses of T cells and monocytes. These variations highlight the complex and distinct immune responses in autoimmune patients when faced to SARS-CoV2 infections, underscoring the need for personalized approaches in their treatment and disease management.

RESUMEN

Esta tesis doctoral profundiza en los complejos mecanismos de la respuesta inmune innata, centrándose en el papel de las células mieloides como los monocitos y las células dendríticas derivadas de monocitos en la inmunosupresión. Estas células cambian dinámicamente entre estados proinflamatorios e inmunosupresores influenciados por su entorno y sus interacciones con moléculas específicas. Esta adaptabilidad es crucial en diversos contextos, incluida la inmunidad de barrera epitelial o los microambientes tumorales, dónde el ácido retinoico (RA) puede tener un papel importante, o en los casos graves de COVID-19. Sin embargo, los mecanismos reguladores subyacentes, especialmente el papel de la metilación del ADN en estos cambios fenotípicos, no se comprenden bien. Hemos estudiado en diferentes contextos, tanto *in vitro* como *ex vivo*, cómo la metilación es capaz de regular el fenotipo supresor en las células mieloides y a su vez, también hemos estudiado cómo los defectos en los mecanismos de supresión afectan la respuesta inmune frente a la infección por SARS-CoV-2.

En el primer estudio, mostramos cómo el RA influye en las células dendríticas derivadas de monocitos (moDC), promoviendo un fenotipo más parecido a macrófago y adquiriendo capacidades inmunosupresoras. Nuestro análisis reveló que estos cambios estaban relacionados con cambios específicos en la metilación del DNA, lo que destaca el papel de la epigenética en la adquisición de este fenotipo. Además, el análisis de los datos de transcriptómica reveló que el receptor nuclear LXR α es crucial en los efectos del RA, y su activación conduce a la remodelación en la metilación del DNA y expresión de elementos inmunosupresores como el VSIG4. La supresión de RXR α por parte del RA es clave para la función de LXR α . Por último, vimos que los macrófagos

en ciertos entornos, como en el colon o en tumores, expresan tanto LXR α como VSIG4, lo que sugiere una relevancia más amplia de estos mecanismos.

En el segundo estudio, se analizó el metiloma y transcriptoma de monocitos de pacientes con formas severas de COVID-19 y se pudo determinar cambios en la metilación del DNA en sitios vinculados a genes de interferón y presentación de antígenos, alineándose con un perfil de expresión genética supresora. Los cambios en el metiloma solapaban parcialmente con los que se producen en monocitos aislados de pacientes con sepsis, aunque, pero también se caracterizan por alteraciones únicas específicas de la infección viral. Estas alteraciones en la metilación del DNA, que son reminiscentes de los cambios que se producen durante la diferenciación mieloide y la inflamación. Estos cambios sugieren que reprogramación epigenética y transcripcional asociada con las formas severas de COVID-19 podría estar asociada a la liberación de monocitos inmaduros, el aumento de citocinas proinflamatorias sistémicas y la alteración de las interacciones con otras células inmunitarias, lo que contribuye a la gravedad de la enfermedad.

En el tercer estudio, analizamos el transcriptoma de las células inmunes periféricas de pacientes con artritis reumatoide, psoriasis o esclerosis múltiple infectados por SARS-CoV-2. A pesar de que los tres grupos autoinmunes mostraron un aumento común en los monocitos CD14⁺ HLA-DR^{low}, las características específicas de su respuesta inmune al virus variaron significativamente. Esto incluyó diferencias en la señalización del interferón tipo I y las respuestas inflamatorias de las células T y los monocitos. Estas variaciones destacan las respuestas inmunes complejas y distintas en pacientes autoinmunes cuando se enfrentan a COVID-19, lo que subraya la necesidad de enfoques personalizados en su tratamiento y manejo de la enfermedad.

RESUM

Aquesta tesi doctoral aprofundeix en els complexos mecanismes de la resposta immune innata, centrant-se en el paper de les cèl·lules mieloides com els monòcits i les cèl·lules dendrítiques derivades de monòcits en la immunosupressió. Aquestes cèl·lules canvien dinàmicament entre estats proinflamatoris i immunosupressors influenciats pel seu entorn i les seves interaccions amb molècules específiques. Aquesta adaptabilitat és crucial en diversos contextos, inclosa la immunitat de barrera epitelial o els microambients tumorals, on l'àcid retinoic (RA) pot tenir un paper important, o en els casos greus de COVID-19. Tot i això, els mecanismes reguladors subjacents, especialment el paper de la metilació de l'ADN en aquests canvis fenotípics, no es comprenen bé. Hem estudiat en diferents contextos, tant *in vitro* com *ex vivo*, com la metilació és capaç de regular el fenotip supressor a les cèl·lules mieloides i alhora també hem estudiat com els defectes en els mecanismes de supressió afecten la resposta immune davant la infecció per SARS-CoV-2.

Al primer estudi, mostrem com el RA influeix en les cèl·lules dendrítiques derivades de monòcits (moDC), promovent un fenotip més semblant a macròfag i adquirint capacitats immunosupressores. Vam veure com aquests canvis estaven relacionats amb canvis específics en la metilació del DNA, fet que destaca el paper de l'epigenètica en l'adquisició d'aquest fenotip. Vam veure que el receptor nuclear LXR α és crucial pels efectes del RA, i la seva activació condueix a la remodelació de la metilació i a l'expressió d'elements immunosupressors com el VSIG4. La supressió de RXR α per part del RA va ser clau per a la funció de LXR α . Finalment, vam veure que els macròfags en certs

entorns, com al còlon o en tumors, expressen tant LXR α com VSIG4, cosa que suggereix una rellevància més àmplia d'aquests mecanisme

En el segon estudi, vam analitzar el metiloma i el transcriptoma de monòcits de pacients greus de COVID-19 i vam veure canvis en la metilació del DNA en llocs vinculats a gens d'interferó i de presentació d'antígens, alineant-los amb un perfil d'expressió genètica supressora. Aquests canvis es van superposar amb els observats durant la sèpsia bacteriana, però també van incloure alteracions úniques específiques de la infecció viral. Aquestes modificacions de la metilació del DNA, que recorden les que es produeixen durant la diferenciació mieloide i la inflamació, suggereixen una reprogramació epigenètica i transcripcional dels monòcits. També vam veure que aquesta reprogramació podria estar relacionada amb l'alliberament de monòcits immadurs, l'augment de citocines proinflamatòries sistèmiques i l'alteració de les interaccions amb altres cèl·lules immunitàries, cosa que contribueix a la gravetat de la malaltia.

En el tercer estudi, vam analitzar el transcriptoma de les cèl·lules immunes de pacients amb artritis reumatoide, psoriasi o esclerosi múltiple infectats per SARS-CoV-2. Tot i que els tres grups autoimmunes van mostrar un augment comú en els monòcits CD14⁺ HLA-DR_{low}, les característiques específiques de la seva resposta immune al virus van variar significativament. Això va incloure diferències en la senyalització de l'interferó tipus I i les respostes inflamatòries de les cèl·lules T i els monòcits. Aquestes variacions ressalten les respostes immunes complexes i diferents en pacients autoimmunes quan s'enfronten a COVID-19, fet que subratlla la necessitat d'enfocaments personalitzats en el tractament i el maneig de la malaltia.

ABBREVIATIONS

5caC: 5-Carboxylcytosine

5fC: 5-Formylcytosine

5hmC: 5-Hydroxymethylcytosine

5mC: 5-Methylcytosine

9-cis-RA: 9-cis-Retinoic Acid

ACE: Angiotensin-converting enzyme

ALDHs: Aldehyde Dehydrogenases

AM-AR: Active Modification-Active Removal

AM-PD: Active Modification-Passive Dilution

AP-1: Activator Protein 1

APCs: Antigen-Presenting Cells

ATRA: all-trans retinoic acid

BCR: B cell receptor

BER: Base Excision Repair

BivFlnk: Flanking Bivalent Transcription Start Site/Enhancer

BS: Bisulfite

CCL: C-C Motif Chemokine Ligand

CCR: C-C Motif Chemokine Receptor

cDCs: Conventional Dendritic cells

CDPs: Common Dendritic Cell Precursors

CFSE: Carboxy Fluorescein Succinimidyl Ester

CGIs: CpG islands

CH₂₅H: Cholesterol 25-Hydroxylase

CLPs: Common Lymphoid Progenitors

CMs: Classical Monocytes

cMoPs: Common Monocyte Progenitors

CMPs: Common Myeloid Progenitors

CTLA-4: Cytotoxic T-Lymphocyte Associated protein 4

CTLs: Cytotoxic T Lymphocytes

DAMPs: Dangerous-recognition Molecular Patterns

DCs: Dendritic Cells

DEG: Differentially Expressed Gene

DMPs: Differentially Methylated Positions

DMRs: Differentially Methylated Region

DMSO: Dimethylsulfoxide

DNA: Deoxyribonucleic Acid

DNMT: DNA cytosine-5-methyltransferase

DoRothEA: Discriminant Regulon Expression Analysis

DSBH: Double-Stranded β -Helix

EGR2: Early Growth Response 2

ELISA: Enzyme-linked immunosorbent assay

Enh: Enhancers

EnhBiv: Bivalent Enhancer

EnhG: Genic Enhancers

FC: Fold change

FDR: False Discovery Rate

FXRs: Farnesoid X Receptors

GALT: Gut-Associated Lymphoid Tissue

GEO: Gene Expression Omnibus

GM-CSF: Granulocyte-Macrophage Colony-Stimulating Factor

GMPs: Granulocyte and Macrophage Progenitors

GO: Gene Ontology

GR: Glucocorticoid Receptors

GSEA: Gene Set Enrichment Analysis

HDs: Healthy Donors

Het: Heterochromatin

HIF-1 α : Hypoxia-Inducible Factor 1-Alpha

HLA: Human Leukocyte Antigen

HOMER: Hypergeometric Optimization of Motif EnRichment

HSC: Hematopoietic Stem Cell

IBD: Inflammatory Bowel Disease

ICU: Intensive Care Unit

iDCs: Immature Dendritic Cells

IFN: Interferon

IL: Interleukin

IM: Intermediate Monocytes

IRF: Interferon Regulatory Factor

KLF4: Krüppel-Like Factor 4

LPS: Lipopolysaccharides

LXR: Liver X Receptor

MAFB: MAF BZIP Transcription Factor B

MAIT: Mucosal-Associated Invariant T Cells

MAPK: Mitogen-Activated Protein Kinase

MCP-1: Monocyte Chemoattractant Protein-1

M-CSF: Macrophage Colony-Stimulating Factor

mDCs: Mature Dendritic Cells

MDP: Monocyte/Dendritic cell Progenitor

MDSCs: Myeloid-Derived Suppressor Cells

MEP: Megakaryocyte and Erythrocyte Progenitors

MHC: Major Histocompatibility Complex

MLN: Mesenteric Lymph Nodes

moDCs: Monocyte-derived DCs

MPP: Multipotent Progenitors

MS: Multiple Sclerosis

MyD88: Myeloid Differentiation Primary Response Gene 88

NCM: non-Classical Monocyte

NES: Normalized Enrichment Score

NF- κ B: Nuclear Factor Kappa-Light-Chain-Enhancer of Activated B Cells

NKs: Natural killer cells

NOS: Nitrogen Oxygen Species

PAMPs: Pathogen-Associated Molecular Patterns

PBMCs: Peripheral Blood Mononuclear Cells

PCA: Principal component analysis

PD-1: Programmed Cell Death Protein -1

pDCs: Plasmacytoid Dendritic Cells

PD-L1: Programmed Cell Death Ligand Protein -1

PEG-2: Prostaglandine-2

PI3K: Phosphoinositide 3-kinase

PPAR γ : Peroxisome Proliferator-Activated Receptor Gamma

Prolif. T: Proliferating T Cells

PRRs: Pattern-Recognition Receptor

Ps: Psoriasis

RA: Retinoic Acid

Ra: Rheumatoid Arthritis

RAR: Retinoic Acid Receptor

RARE: Retinoic Acid Response Elements

RB1: Retinoblastoma Tumor Suppressor Gene

RBC: Red Blood Cells

ReprPC: Repressed PolyComb

ReprPCWk: Weak Repressed PolyComb

RNA: Ribonucleic Acid

ROS: Reactive Oxygen Species

RPMI: Roswell Park Memorial Institute

RXR: Retinoid X Receptor

scRNA-seq: Single-cell RNA sequencing

SLE: Systemic Lupus Erythematosus

SOCS: Suppressor of Cytokine Signaling

SOFA: Sequential Organ Failure Assessment

STAT: Signal Transducer and Activator of Transcription

T₂DM: Type 2 Diabetes Mellitus

TAMs: Tumor-Associated Macrophages

TCR: T cell receptor

TD₁: Type 1 Diabetes mellitus

TET: Ten-Eleven Translocation

TGF- β : Transforming Growth Factor-Beta

Th: T helper

TLR: Toll-like receptor

TME: Tumor Microenvironment

TMPRSS₂: Transmembrane Protease Serine 2

TNF: Tumor Necrosis Factor

ToIDCs: Tolerogenic Dendritic Cells

Treg: Regulatory T cells

TSGs: Tumor Suppressor Genes

TssA: Active TSS

TssAFlnk: Flanking Active TSS

TssBiv: Bivalent/Poised TSS

Tx: Strong Transcription

TxFlnk: Transcr. at gene 5' and 3'

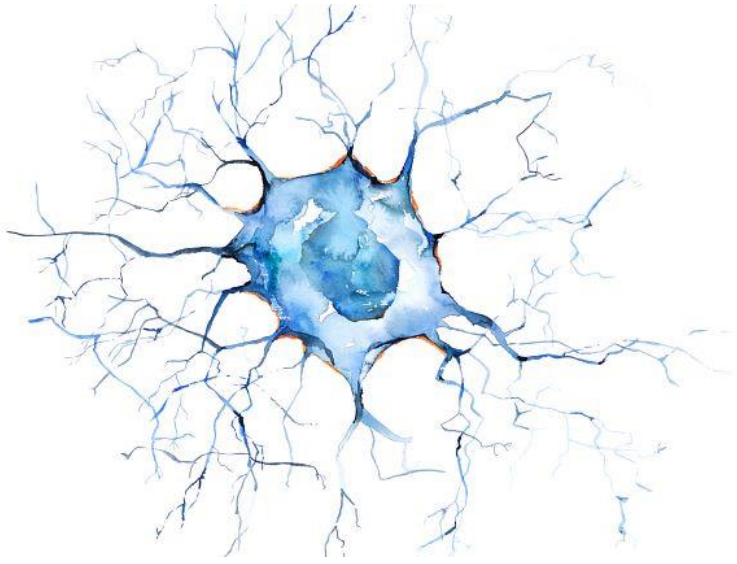
TxWk: Weak transcription

UHRF₁: Ubiquitin-Like Containing PHD and RING Finger Domains 1

UMAP: Uniform Manifold Approximation and Projection

VDR: Vitamin D Receptor

ZNF/Rpts: ZNF genes & repeats



INTRODUCTION

1. INTRODUCTION

1.1. The Immune System

1.1.1. Innate and Adaptive immunity

The immune system is composed by an intricate network of cells, tissues, and organs that collaboratively defend the body against pathogens, such as bacteria, viruses, and fungi, as well as abnormal cells, including cancerous ones. There are two fundamental branches governing its function: the innate immune response and the adaptive immune response (1).

The **innate immune** system serves as the first line of defense against invading pathogens. This response is characterized by nonspecific mechanisms that include physical barriers -such as the skin and mucosal surfaces-, cellular components -including myeloid cells like **monocytes**, macrophages, dendritic cells (**DCs**), neutrophils, and lymphocytes cells like natural killer cells (**NKs**)-, and soluble factors -such as cytokines and complement proteins- (2). Cells forming part of the innate immune system act rapidly, providing immediate protection upon encountering a threat. They are basically activated after the recognition of a pathogen-associated molecular patterns (**PAMPs**) or dangerous-recognition molecular patterns (**DAMPs**). These are recognized by the pattern-recognition receptors (**PRRs**), expressed in myeloid cells, B cells and NK lymphocytes (3). Toll-like receptors (TLRs) are the most well-known PRRs, with a variety of subtypes identified. For example, the lipopolysaccharide (LPS) from Gram-negative bacteria specifically triggers TLR₄, whereas Pam₃Cys-Ser-Lys₄ (P₃C), a synthetic mimic of the triacylated N-terminal portion of bacterial lipoproteins, engages TLR₂. Activation of TLR₂ or TLR₄ pathways stimulates inflammatory transcription factors (TFs), including nuclear factor kappa-light-chain-enhancer of activated B cells (NF- κ B),

Introduction

activator protein 1 (AP-1), and interferon regulatory factors (IRFs) (4, 5) leading to the generation of proinflammatory and antiviral cytokines and chemokines (6, 7).

In contrast, the **adaptive immune** response offers a tailored and precise defense against specific pathogens. This branch of immunity relies on the recognition of unique molecular markers, or antigens, present in pathogens or foreign substances. Through a process of antigen presentation, specialized cells known as **lymphocytes** -comprising **B cells and T cells**- generate highly specific responses targeted at neutralizing or eliminating the invading agent. Each B and T cell can recognize a specific antigen through its B cell receptor (BCR) or T cell receptor (TCR), respectively. B cells originate from precursor cells in the bone marrow and play several key roles including antibody production, serving as antigen-presenting cells, providing support to other mononuclear cells, and directly participating in inflammatory pathways. T lymphocytes also originate from precursor cells in the bone marrow and then undergo maturation and selection in the thymus before being released into the bloodstream. T cells exist in various subsets, including **naïve T** cells, which can react to new antigens; **memory T** cells -including CD4+ and CD8+ Tcells-, formed after previous encounters with antigens and regulatory T (**Treg**) cells, responsible for modulating immune responses. Importantly, the adaptive immune response exhibits immunological memory, enabling a swifter and more robust reaction upon re-exposure to the same pathogen.

The activation of the adaptive immune responses is dependent on the process of antigen presentation and processing by antigen-presenting cells (APCs), mostly myeloid cells. This process enables proteins from the major histocompatibility complex (MHC), referred to as human leukocyte antigen

(HLA) in humans, to be loaded with their appropriate ligands (8–10). Antigen presentation by DCs occurs through the TCR, which is expressed in naïve T cells and can recognize these antigens. T cells undergo activation upon receiving both a signal from the TCR and a costimulatory signal by CD28 binding, leading to the secretion of cytokines like IL-2. Once the TCR-MHC interaction has occurred, T cells initiate the process of activation and differentiation, known as T-cell priming. Activated T cells then carry out various immune responses, including killing infected cells, assisting B cells, and secreting cytokines.

The innate and adaptive immune responses collaborate extensively, forming a synergistic defense system. The innate response provides immediate protection while priming the adaptive response. Moreover, the adaptive immune system can modulate and enhance innate immune functions, ensuring a comprehensive and effective defense against pathogens.

However, the traditional classification of adaptive and innate responses has been challenged by the discovery of PRRs. Some evidence indicates that the innate immune system can adapt its functionality following a prior reaction (11). Reports of protection against re-infection by innate immune cells extend beyond plants and invertebrates lacking adaptive immunity demonstrate cross-protection between infections caused by different pathogens (12). These findings have led to the hypothesis that previous encounters with pathogens or their products can influence innate immunity giving rise to an epigenetic regulated process called "**trained immunity**" (13, 14).

1.1.2. Immune cell differentiation

The immune system's cellular composition originates from haematopoiesis, a meticulously orchestrated process where diverse cell types are generated from a singular progenitor cell known as the hematopoietic stem cell (**HSC**) (15, 16). This population located in the bone marrow has demonstrated its capability for self-renewal and gives rise to a heterogeneous array of multipotent progenitors (**MPPs**). These MPPs further specialize into two distinct lineages: common myeloid progenitors (**CMPs**) (17) and common lymphoid progenitors (**CLPs**) (18). CLPs contribute to the development of lymphoid cells including T, B, and NKs cells but lack potential for myeloid differentiation. Conversely, CMPs lose their lymphoid lineage capacity and instead differentiate into megakaryocyte and erythrocyte progenitors (**MEPs**) and granulocyte and macrophage progenitors (**GMPs**) (17). Subsequently, a monocyte/dendritic cell progenitor (**MDP**) population, likely derived from the GMP population, was identified. MDPs were also identified within the CMP compartment, possibly emerging directly from Flt3-expressing CMPs. Recent adoptive transfer experiments suggest that Ly6CHi monocytes can arise from both the GMP and MDP populations (19).

It is proposed that the MDP population undergoes a binary decision to differentiate into dedicated common dendritic cell precursors (**CDPs**) or unipotent common monocyte progenitors (**cMoPs**), although some MDP subpopulations may already be pre-committed to either lineage. In human bone marrow, cMoPs have also been identified within the GMP population (20). These monocytes, once released into the bloodstream and reach a tissue, can differentiate into other cell types like macrophages or DCs (**Figure 1**).

The advancements in single-cell RNA sequencing (scRNA-seq) have challenged the branching model of hematopoietic differentiation, suggesting that lineage commitment may already be predetermined in oligopotent progenitors (21). scRNA-seq sequencing combined with FACS sorting has revealed monocytic transcriptional programs within both **CMPs** and **GMPs** (22). The commitment to the **monocyte lineage** is governed by a distinct group of hematopoietic growth and transcription factors including SPI1 (encoding PU.1), IRF8, GATA2, and Krüppel-like factor 4 (KLF4) (23).

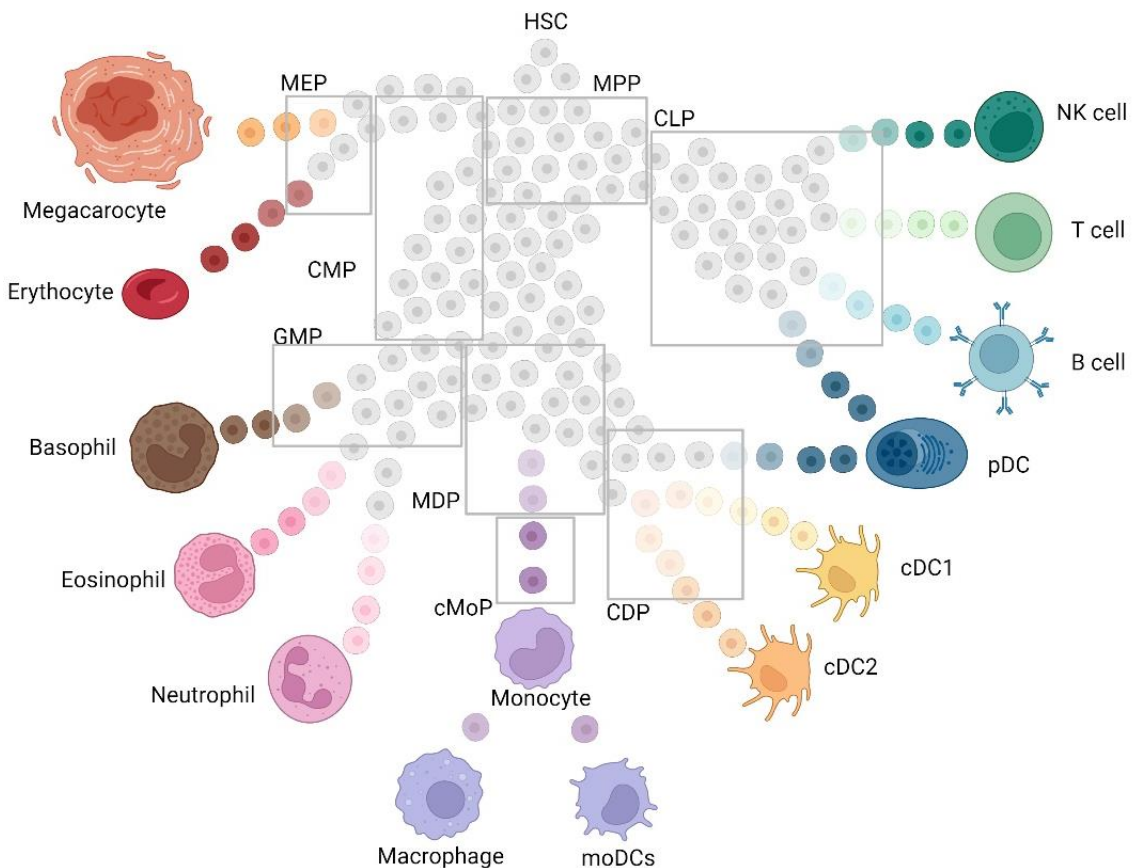


Figure 1. (See figure legend on the next page.)

Figure 1. Hematopoietic stem cells (HSC) or multipotent precursors (MPP) give rise, through intermediate precursor stages, to all types of circulating blood cells. Specific multipotent precursor populations, like granulocyte macrophage precursor (GMP), generate either the granulocytic lineage or further differentiate into monocyte-macrophage/dendritic cell precursor (MDP). Bipotent MDPs make binary decisions, branching into either common dendritic cell precursor (CDP) or common monocyte precursors (cMoP). cMoP ultimately differentiate into Ly6Chi cells, released into circulation, and capable of acquiring diverse cell fates as monocyte-derived cells in tissues including monocyte-derived DCs (moDCs) and Macrophages. Notably, the majority of plasmacytoid DC (pDC) originate from IL-7Ra-expressing common lymphocyte precursor (CLP), with a smaller fraction deriving from CDP (24).

1.1.3. Monocytes

Monocytes are part of the mononuclear phagocyte system originate from HSC in the bone marrow and migrate into the bloodstream post-birth. Monocytes constitute ~10% of the peripheral blood mononuclear cells (PBMCs) (24) and reside in the blood from 2 to 4 days (25). In the context of infection, the TLR response during infection promotes the expression of monocyte chemoattractant protein-1 (MCP-1), which binds to the C-C chemokine receptor type 2 (CCR2) on the surface of monocyte cells and triggers their release into the circulation (26).

Circulating monocytes are classified into three subsets based on the expression of the surface markers CD14 and CD16: “**classical**” CD14^{high}CD16⁻ monocytes (around 85% of monocytes), “**intermediate**” CD14⁺CD16⁺ monocytes (5–10%) and “**nonclassical**” CD14⁻CD16^{high} monocytes (5–10%) (27). This proportion of monocyte subsets can be modulated depending on the disease, for example several immune-related diseases present increased levels of intermediate and non-classical monocytes. However, the implication and role of this remains unclear (28). Furthermore, new studies using scRNA-seq on blood monocytes showed that CD14⁺CD16⁺ monocytes are a heterogeneous population with mixed transcriptional profiles (29, 30).

Monocytes are able to migrate inside tissues in response to damage signals. These play important roles in maintaining **tissue homeostasis** by initiating, propagating, and resolving immune responses against infection and injury. However, circulating monocytes subsets already possess functional roles before reaching the inflamed tissues. Typically, classical monocytes are pivotal in kickstarting innate immune reactions, engaging in phagocytosis, and migrating via the expression of chemokines, scavenger receptors, and pro-inflammatory cytokines (31). Intermediate subsets are linked to antigen processing and presentation, monocyte activation, inflammation, and differentiation (32). In healthy individuals, intermediate monocytes exhibit lower levels of CD163 compared to classical monocytes, while nonclassical monocytes have even lower levels (33). Given that CD163 is linked with anti-inflammatory or tissue-remodeling macrophages (34), this observation suggests that classical monocytes may possess anti-inflammatory properties under normal conditions. Additionally, CD86, associated with inflammatory macrophages (34), shows the highest expression on nonclassical monocytes, followed by intermediate monocytes, and lowest on classical monocytes. This pattern aligns with the inflammatory roles typically attributed to intermediate and nonclassical subsets (35).

Several studies have characterized the **cytokine production** capacities of monocytes following the activation of the TLR. CD16+ monocytes mainly produce tumor necrosis factor alpha (TNF- α) while intermediate subsets produce high levels of TNF- α , interleukin 1 beta (IL-1 β) and IL-6. In the case of classical monocytes, they have been reported to produce poor levels of several cytokines in response to LPS (36). Monocytes, mainly the classical subsets, are

also able to produce anti-inflammatory cytokines like IL-10 consistent with the more anti-inflammatory role of this subset (36, 37).

Finally, human monocytes can be identified by their antigen-presenting proteins (HLA-DR) expression, marking their possible **antigen presentation** capacities. The intermediate monocyte subset expresses high levels of MHC class II processing and presentation genes (38). Accordingly, these monocytes were shown to be the best inducers of *Staphylococcal* enterotoxin B-mediated T cell proliferation (32). Summarising, monocytes constitute a heterogeneous population with distinct subsets, each with specific roles in immune responses and tissue homeostasis, as well as varying cytokine production capacities, and antigen presentation abilities.

1.1.4. Monocyte-derive cells and Dendritic Cells

One of the most important roles of monocytes is their ability to be recruited in peripheral tissues and differentiate to several cell types, including DCs. DCs are professional APCs with the distinctive property of inducing priming and differentiation of naïve T cells like CD4⁺ and CD8⁺ T cells into helper and cytotoxic effector T cells, respectively. Phenotypic and functional criteria have been usually used to define three main DC subtypes, namely, conventional DCs (**cDCs**), plasmacytoid DCs (**pDCs**) and monocyte-derived DCs (**moDCs**), also known as inflammatory DCs (39).

On one hand, **cDCs**, are characterized by the expression of CD11c and are derived from CDPs in the bone marrow. cDCs can be further categorized into two main lineages: cDC1 and cDC2. cDC1s have an enhanced ability to cross-present exogenous antigens on MHC-I and to activate CD8⁺ T cells. In comparison, cDC2s, represent a heterogeneous population with enhanced

MHC-II antigen presentation capable of activating CD4⁺ T cells (40). However, a recent study has shown that cDC1s are also capable of activating CD4⁺ T cells (41). On the other hand, pDCs differentiate from both CDPs and CLPs (42, 43) (**Figure 1**) and similar to cDCs, pDCs express cytokine receptor Flt3 and are strictly dependent on its ligand Flt3L for their development (44). pDCs are recognized by their main function of producing high levels of interferon- alpha (IFN- α) in response to viruses and pathogens (45). In addition, pDCs promote both innate and adaptive immune responses through induction of NK cell migration, macrophage and DCs maturation, T cell response and antigen presentation (46).

Finally, monocytes are recruited during inflammation in a CCR2-dependent manner, and this gives rise to **mo-DCs** cells that are functionally distinct from resident macrophages (47). This subset has been described as activated effector monocytes (48), based on the pronounced proinflammatory signature. These cells have a similar phenotype to cDC2, however, can be distinguished by the absence of expression of CD26 (49). Recent reviews challenge the migratory ability of moDCs, suggesting a more localized function, where these cells may not migrate to the lymph nodes but can instead directly present antigens to effector T cells within the tissues (50). It has been established that moDCs are essential for CD8⁺ T cell activation and antitumor responses following local immunotherapy, however they can also present to CD4⁺ T cells (51, 52).

When immature dendritic cells (iDCs) encounter a PAMP or a DAMPs through their PRRs in tissues, they become activated. This activation process transforms them into mature dendritic cells (mDCs) (53). This transformation is marked by a heightened expression of MHC class II molecules, an increase in

Introduction

co-stimulatory molecules and cytokines, and the upregulation of the chemokine receptor CCR7 (54).

The moDC subset has been extensively studied using an *in vitro* model consisting of monocytes differentiating to moDCs in the presence of granulocyte-macrophage colony-stimulating factor (GM-CSF) and IL-4 (55). Through such experiments, it has been demonstrated that these cells exhibit remarkable adaptability, capable of differentiating, not only into typical moDCs, but also into various immunogenic or tolerogenic cell types in response to diverse growth factors, cytokines, or even compounds such as vitamins and drugs (56).

In vitro models for moDCs share features with other *in vitro* models for example monocyte-derived macrophages, classified as M1 or M2 macrophages, depending on if they were differentiating with GM-CSF or macrophage colony-stimulating factor (M-CSF) respectively, together with activation. M1 macrophages, known for their tissue-destructive and immune-stimulating roles, produce proinflammatory cytokines like IL-1, IL-6, IL-12 or TNF- α and exhibit anti-tumoral effects. Conversely, M2 macrophages facilitate tissue repair and exert immunosuppressive effects by releasing anti-inflammatory cytokines such as IL-10 and transforming growth factor-beta (TGF- β) (57). In addition, although both macrophages and moDCs can be found in similar tissues at steady-state and inflammatory conditions, they differ in function and cytokine expression. Both cells express TNF- α and IL-1 β in several tissues (58–60), however IL-12 production is specific to moDCs and only macrophages produce IL-10 (61, 62). Furthermore, moDCs but not macrophages can induce Th17 or Th1 polarization (63), and promote effector CD8+ T cell differentiation (61).

Other factors tested for their effects on *in vitro* moDCs include tumor-derived factors such as VEGF and prostaglandin-2 (PEG-2). These factors promote the acquisition of immunosuppressive properties and pro-tumoral functions, leading to phenotype similar to those of myeloid-derived suppressor cells (**MDSCs**) (64) or tumor-associated macrophages (**TAMs**) (56). Moreover, the addition of RANKL along with M-CSF can induce the differentiation of monocytes into osteoclasts (65), while the combination of TGF- β and GM-CSF can prompt the differentiation into Langerhans cells (66). RANKL alone promotes the downregulation of IL12, upregulation of IL10, and the conversion of immunogenic DCs into regulatory DCs (regDCs). Finally, IL-10, TGF- β , vitamin D or glucocorticoids can promote the differentiation into tolerogenic DCs (**ToIDCs**) that are a heterogenous pool of DCs with immuno-suppressive properties that present potential clinical applications (67-69) (**Figure 2**). In summary, depending on the cytokines, vitamins, or molecules they encounter, these cells have the capacity to differentiate into various cell types, each possessing distinct functions and capabilities.

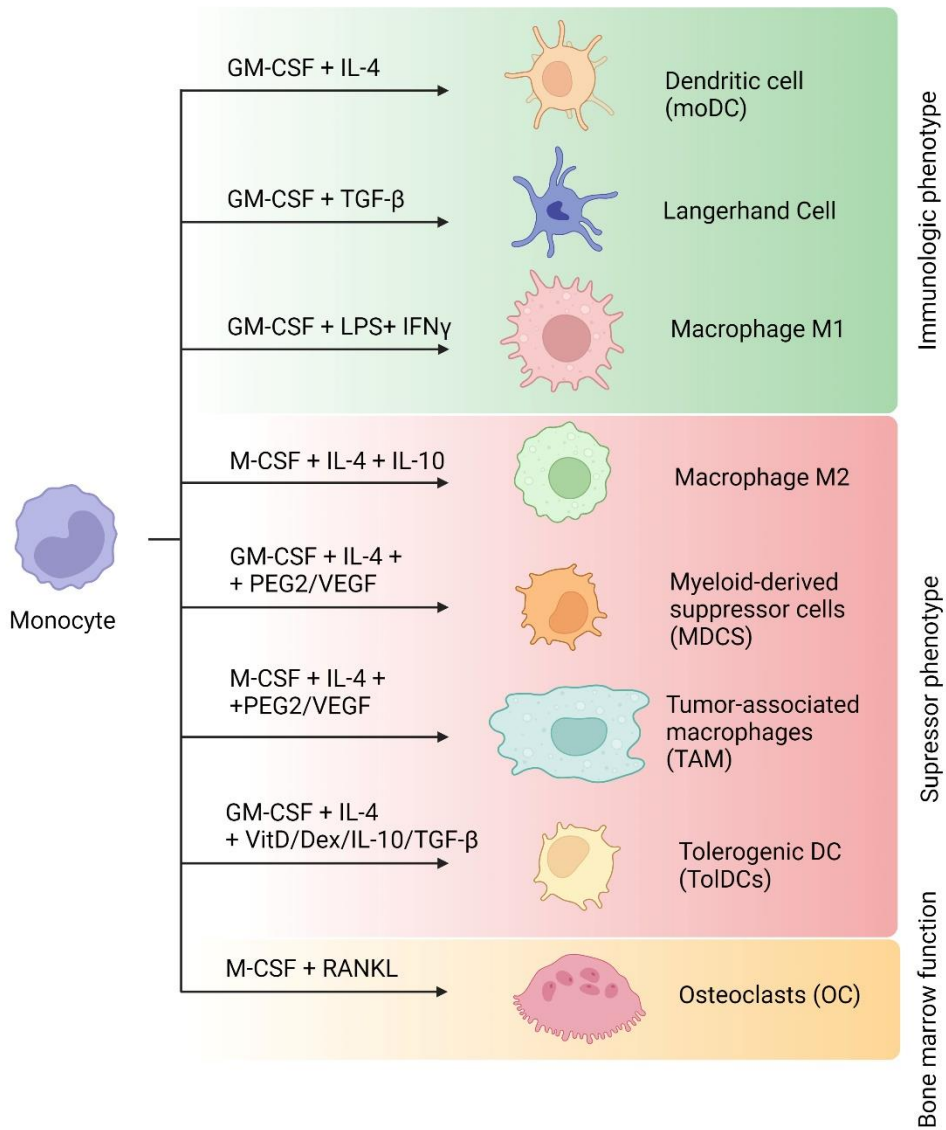


Figure 2. *In vitro* monocytes possess the capacity to differentiate into various terminally differentiated cells, each with distinct immunogenic or immunosuppressive roles. This differentiation process is facilitated by employing specific combinations of cytokines, steroids such as vitamin D₃ and dexamethasone, or factors derived from tumors such as TGF-β, VEGF, or PEG-2. Adapted from (56).

1.2. Mechanisms of immune suppression

The immune system can recognize and react to various antigens, necessitating tolerance mechanism to prevent immune reactions against endogenous molecules. Immunogenic tolerance is defined as unresponsiveness to an antigen induced after its exposure. Self-tolerance can occur either by deleting immature self-reactive lymphocytes within the generative lymphoid organs (**central tolerance**) or in mature lymphocytes within peripheral sites (**peripheral tolerance**) (70).

On one hand, **central tolerance** involves a mechanism that eliminates and deactivates lymphocytes expressing high-affinity receptors for self-antigens. This process is antigen-specific and occurs through the recognition of antigens by specific clones of lymphocytes. Tolerance to self-antigens is so called self-tolerance. The failure of the maturation phase and clonal selection of the T cell on the thymus can give rise to an error on this fundamental property and produce an **autoimmune disease** leading to organ destruction or dysfunction. Autoimmune diseases are one of the leading causes of death among young and middle-aged women (71). Various factors, such as genetic predispositions, environmental influences, and immune dysregulation, including infections, often converge to initiate autoimmune diseases. There are almost 100 identified autoimmune diseases and the most common include systemic lupus erythematosus (SLE), rheumatoid arthritis (Ra), multiple sclerosis (MS), type 1 diabetes mellitus (TD₁), Graves' disease, inflammatory bowel disease (IBD) and psoriasis (Ps) (72, 73).

On the other hand, when self-reactive lymphocytes escape into the periphery, **peripheral tolerance** ensures that they are deleted. The main mechanism of peripheral tolerance are suppression by anergy (functional un-

Introduction

responsiveness), clonal deletion (cell death) and development of "induced" Treg. As it has been mentioned before, T cells undergo activation upon receiving both a signal from the TCR and a costimulatory signal facilitated by CD28 binding. **Anergy** consists of the exposure of mature CD4⁺ T cells to an antigen in the absence of co-stimulation or innate immunity and this makes the cells incapable of responding to that antigen. In anergy, there is an active suppression of TCR signaling and IL-2 production (74). Some examples of molecules inducing anergy are cytotoxic T-lymphocyte associated protein 4 (**CTLA-4**) and programmed cell death protein -1 (**PD-1**). CTLA4 is a receptor expressed by activated T cells and Tregs and can bind CD80 and CD86 on DCs, resulting in the removal of these molecules and a reduced availability of CD80/CD86 for CD28-mediated co-stimulation. In the case of PD-1, it is normally expressed on T cells and recognizes a ligand called PD-L1. This PD-1 promotes the recruitment of phosphatases SHP-1 and SHP-2 and inhibits the TCR and CD28 signaling pathway, subsequently promoting tolerance via induction of clonal anergy and Treg differentiation. (75).

Cell **deletion** consists of self-reactive lymphocytes eliminated in both the thymus and the periphery through apoptotic cell death, with the involvement of crucial pathways such as Fas- or TRAIL-mediated apoptosis by APCs (76, 77).

Tregs, which are naïve CD4⁺ T cells activated in the presence of TGF- β and/or IL-10, are characterized by the expression of FOXP3, and have an immunosuppressive phenotype (78). These cells inhibit immune responses through various mechanisms, including the secretion of anti-inflammatory cytokines, direct cell-to-cell interaction, and modulation of the activation status and function of APCs, including DCs. This includes CTLA-4 mediated inhibition of co-stimulation, expression of PD-1, production of the

immunosuppressive cytokines like IL-10 and TGF- β , and consumption of IL-2, by the expression of **IL2RA** (CD25). In addition, some B lymphocytes subsets have also been defined as IL-10-secreting cells, promoting a suppressor role. DCs, NKs, epithelial cells, macrophages and glial cells also express suppressor cytokines such as IL-10 and TGF- β . Various types of cells, including myeloid cells, play also roles in maintaining peripheral tolerance.

This process of peripheral suppression can occur under normal conditions, such as in the elimination of self-reactive T lymphocytes or in maintaining the integrity of the **epithelial barrier** to prevent immune reactions against commensal microorganisms or food antigens. However, it can also be observed in diseases, including **tumors** or severe viral infections such as **SARS-CoV-2** infection, which can impact the response against the threats, affecting the progression of the disease.

1.2.1. Immune suppression on epithelial barrier immunity, the role of Retinoic Acid

The immune system also relies on physical and anatomical barriers to exert its functions. For instance, the connective tissue, such as the dermis in the skin and the lamina propria in the gut, contains numerous lymphocytes, DCs, macrophages, and other cells that mediate innate immune response and the effector phase of adaptive immune response. The sampling of antigens in the gut and their transport to secondary lymphoid organs rely on distinct cell types and routes of lymphatic drainage, differing somewhat from processes observed in other organs (2).

To avoid immune responses against food antigens or non-pathogenic commensal organisms that colonize the surfaces of skin and the lumens of mucosal organisms the immune system has evolved specialized properties. One

Introduction

of the most classic strategies in immune suppression in the gut-associated lymphoid tissue (GALT) is the accumulation of Tregs. It is estimated that the proportion of FOXP3⁺ Tregs among CD4⁺ cells is bigger in this tissue than in others (2, 79). Many of these Tregs are induced in the gut in response to antigen encountered locally and thus belong to the category of peripheral Tregs. However, myeloid cells can also contribute through the expression of several cytokines, including TGF- β , IL-10 and IL-2 that play a crucial role in maintaining homeostasis in the gut immune system, and deficiencies in these cytokines result in pathological bowel inflammation.

One of the factors that contribute the most to the generation of immune suppression is the induced local production of all-trans retinoic acid (ATRA), also known as **retinoic acid (RA)**, a metabolite derived from dietary **Vitamin A**, by CD103⁺ DCs and lamina propria macrophages. The synthesis of RA by various types of cells within the intestine relies on their capability to activate aldehyde dehydrogenases (ALDHs). Notably, an increase of ALDH1a is predominantly observed in DCs of the small intestine, where cells that produce RA are found in higher concentrations (80). Basically, RA produced in the lamina propria induces the generation of CCR7⁺ DCs, prompting their migration to the mesenteric lymph nodes. Within the lymph node, CD103⁺ DCs are responsible for presenting food or microbiota antigens and promoting the differentiation of T cells into Treg cells in the presence of RA and TGF- β . Finally, antigen-specific Treg cells migrate to the intestinal mucosa, where they establish tolerance within the intestinal lamina propria (81, 82) (**Figure 3**).

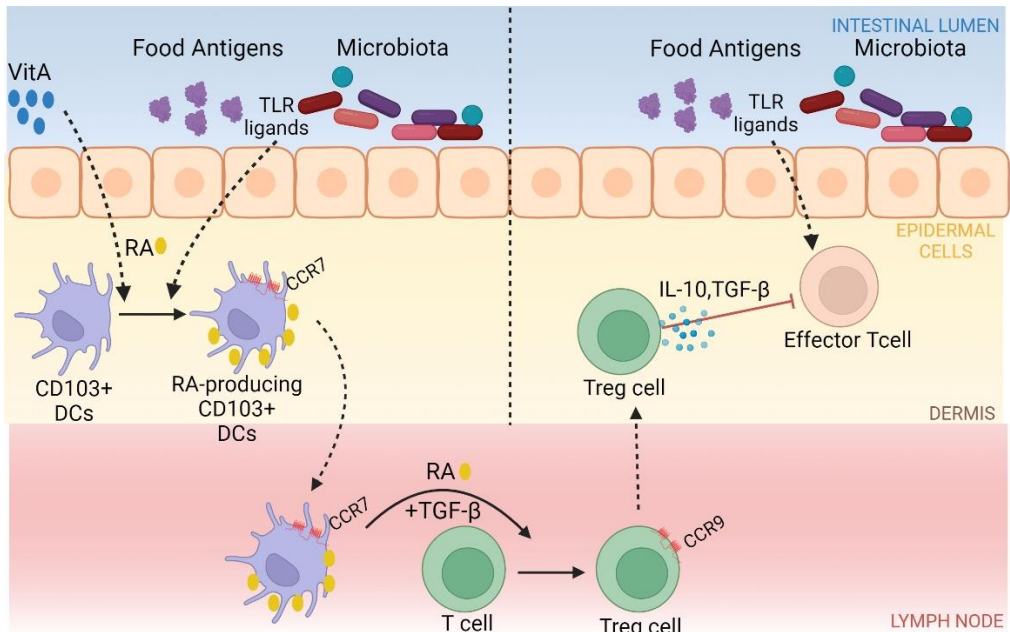


Figure 3. The role of RA in modulating intestinal DC differentiation, maturation, and function is crucial in establishing gut immunological tolerance. CD103⁺ DCs are located below the epithelial layer. Various molecules, including TLR ligands and RA itself, induce the production of RA from Vitamin A promoted by CCR7⁺ DCs, enabling their migration to the mesenteric lymph nodes (MLN). Within the MLN, CD103⁺ DCs facilitate antigen presentation and the differentiation of regulatory T cells in the presence of RA and TGF-β. Additionally, DC-derived RA is essential for inducing gut-homing receptor expression in T cells. Subsequently, Tregs cells migrate to the intestinal mucosa, gaining the ability to produce IL-10 and becoming IL-10 producing Tregs cells, which is crucial for establishing gut tolerance in the intestinal lamina propria.

During steady-state conditions, RA generated by DCs plays a crucial role in suppressing the differentiation of naive T cells into Th17 (83). This suppression is achieved by inhibiting the signaling pathways of IL-6, IL-21, and IL-23 in naive T cells (84–86). RA also blocks the production of IL-4, IL-21, and IFN-γ in CD4⁺ CD44^{high} cells. Since these cytokines prevent the formation of Tregs, RA promotes the shift of naive T cells towards becoming Tregs (87, 88). Moreover, RA is also capable of directly enhancing the conversion of naive T cells into Tregs (89). Numerous studies have indicated that RA not only

Introduction

enhances the differentiation, stability, and functionality of murine and human Tregs but also induces the expression of gut-homing receptors in these cells, including $\alpha 4\beta 7$ and CCR9 (90–93). Finally, RA is also capable of priming human dendritic cells to induce gut-homing, IL-10-producing regulatory T cells (94).

Collectively, RA plays a vital role in the function of DCs, ensuring tolerance towards food and microbial antigens and fostering tissue homeostasis. Simultaneously, it was observed that DC nearest to the intestine exhibited a more immature phenotype, a condition attributed to the local production of RA, showing that ATRA is required to maintain CD103⁺ CD11b⁺ cDC2s in the small intestine (95). Nevertheless, the effector functions of RA are determined by many different factors such as local RA concentrations, TLR signalling, the presence of additional cytokines, the cellular and molecular composition of the microenvironment and the on the presence of inflammatory conditions (86). It has been demonstrated that various inflammatory triggers can boost the production of RA, leading to increased responses from Th1 cells (96, 97), as well as promoting the release of proinflammatory cytokines IL-12 and IL-23 by DCs (98).

RA uses different nuclear receptors to perform its effects, known as retinoic acid receptors, which that are categorized into two main groups: the retinoic acid receptor (RAR) and the retinoid X receptor (RXR). Each group contains three variants, namely RAR $\alpha/\beta/\gamma$ and RXR $\alpha/\beta/\gamma$ (99). Both ATRA and 9-cis-retinoic acid (9-cis-RA) can bind to and activate RAR, which then pairs with RXR to form a heterodimer. This complex plays a crucial role in the regulation of gene expression by attaching to retinoic acid response elements (RARE) in DNA. RAR antagonists (LE540 and LE135) have been shown to suppress the formation of Foxp3⁺ Treg cells, indicating that RA operates via

RA/RAR signaling on the generation of tolerance (100). Furthermore, the interplay between RA and RAR hampers the transcriptional activity of AP-1, known to impede the consistent expression of Foxp3 (101). Conversely, RXR is specifically activated by 9-cis-RA, but it has the unique ability to interact with various other nuclear receptors, including the liver X receptor (LXR) and peroxisome proliferator-activated receptor gamma (PPAR γ), influencing gene expression in the process (102).

In summary, myeloid cells together with RA, can also orchestrate peripheral immune tolerance, particularly in the gut, through the modulation of Tregs and gene expression via RARs.

1.2.2. Tumor immune-suppression

Several studies have pointed out that T cells are major players to the antitumor response when a tumor develops. At least, the evaluation of T lymphocyte density, spatial localization, cell types and functional immune orientation stimuli within the tumor could predict survival in colorectal cancer. The composition of T cells within the tumor microenvironment (**TME**) is influenced by the tumor's mutational landscape. Oncogene activation can promote the **secretion of factors** that modulate the TME, facilitating T cell migration and localization within the tumor core. Indeed, there's a parameter known as the *Immunoscore* that serves to gauge the adaptive immune makeup within the TME. Using this parameter tumors are categorized into four principal groups (103):

- i. **Cold tumors:** termed immune deserts, exhibit a lack of T cell infiltration due to deficient priming or activation mechanisms, often

associated with low tumor mutational burden and inadequate antigen presentation (104).

- ii. **Altered-excluded immune tumors:** T cell exclusion within the tumor core driven by aberrant vasculature and fibrotic networks.
- iii. **Immunosuppressed tumors:** an intermediate presence of exhausted T cells, such as those expressing T cell immunoglobulin and mucin domain-containing protein 3 (TIM3), together with high levels of inhibitory mediators like IL-10 and immune-suppressive cells like Tregs.
- iv. **Hot tumors:** characterized by substantial infiltration of cytotoxic T lymphocytes (CTLs) expressing **PD-1** or **CTLA4**, alongside tumor cells expressing molecules such as PD-L1, which alter T cell functionality. Remarkably, hot tumors also exhibit local inflammation and demonstrate responsiveness to immunotherapy (105).

Nevertheless, other immune cells can also have a role in promoting the immunosuppression typically found on the TME. A general activation of signaling pathways such as mitogen-activated protein kinase (MAPK), phosphoinositide 3-kinase (PI3K), signal transducer and activator of transcription 3 (STAT3), and NF- κ B pathways occurs. Subsequently, they promote the expression of IL-6, IL-10, GM-CSF and TGF- β , among others factors. This may assist some of the infiltrated immune cells, especially DCs and NK cells, to lose their ability to present antigens and their cytotoxic function, respectively (106, 107). One of the most affected cell types by these factors are the immature cells from both granulocytic and monocytic lineages that can evolve into **MDSCs**, whose presence is often linked with unfavorable outcomes across various cancer types (108). One example of this myeloid cell polarization is seen in the expression of IL-10 in the tumor, which reduces the expression of

MHC-II and CD40 in DCs (109). This reduction affects their capacity to mature and to present antigens, and therefore, the antitumor response (110). Nevertheless, cytokines are not the only ones influencing the formation of MDSCs as there is increasing recognition of how metabolic regulation also plays a significant role in affecting myeloid cells, as they primarily utilize glycolytic and pentose phosphate pathways. Within the TME characterized by nutrient scarcity, hypoxia and acidity, there is a shift towards reliance on oxidative phosphorylation, fatty acid oxidation, and arginine metabolism (111–113). This together with the number of metabolites prevalent in the TME, such as adenosine, kynurenines, lactate, VEGF, PEG₂ and the peptides S_{100A8} and S_{100A9}, affects MDSCs formation (106).

MDSCs exert their suppressive effects on T cells in TME TME through different mechanisms including (**Figure 4**):

- i. The production of anti-inflammatory cytokines or expression of PD-L1 or CTLA4 (114–116).
- ii. Promoting T cell anergy and accelerating T cell removal via apoptosis.
- iii. Induction of immune suppressor cells such as Treg cells.
- iv. Non-specifically, by employing processes related to the generation of reactive oxygen species (ROS) or nitrogen oxygen species (NOS) (117).
- v. Draining metabolites essential for T cell activities.
- vi. Altering the expression of chemotactic molecules and ligands that direct T-cell migration.
- vii. Affecting adenosine metabolism through the upregulation of ectoenzymes (116).

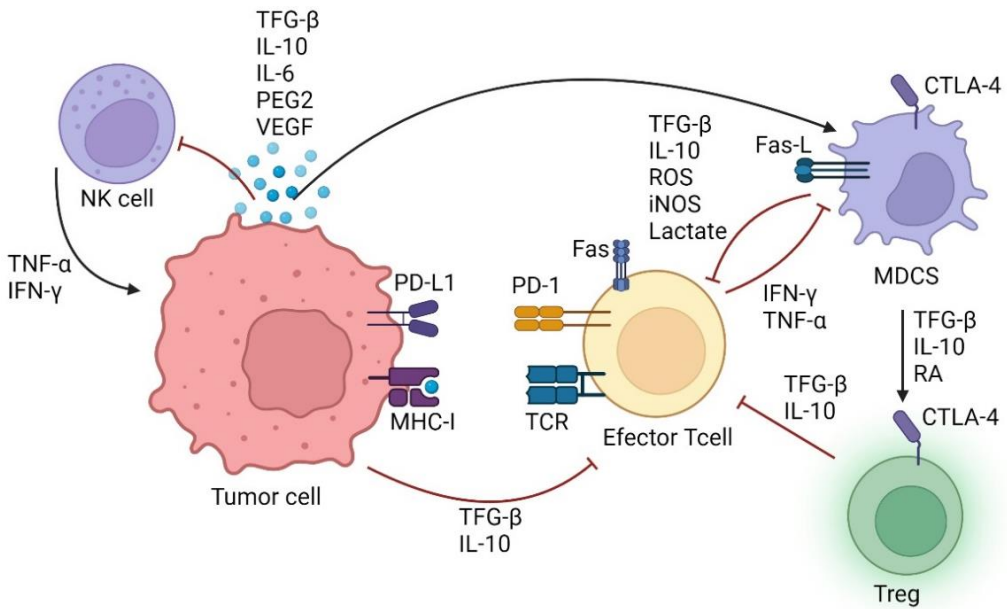


Figure 4. Cancer cells employ strategies to block the immune system, particularly by affecting DCs' antigen presentation capabilities and diminishing NK cells' cytotoxic abilities. Additionally, cancer cells facilitate the differentiation of MDSCs, enhancing their ability to suppress the immune system. MDSCs interfere with the anti-tumor immune response through various means, including the release of anti-inflammatory cytokines, emission of non-specific metabolic molecules that contribute to a suppressive environment, expression of CTLA-4 to inhibit T-cell activation, and the promotion of T cell conversion into Tregs. Tregs further suppress the activity of effector cells crucial for combating cancer cells.

Another molecule that can be added to the list of molecules promoting the formation of MDSCs is RA. In a recent study, it has been shown that the accumulation of RA in the TME is one of the factors that inhibits the correct differentiation of from monocytes to moDCs, producing cells with suppressive capabilities (118, 119). Moreover, it has been observed that RA promotes the generation of PGE2 (120). Nevertheless, the processes that control both the polarization and mechanism used to promote immune suppression remain unclear.

1.2.3. COVID-19-associated Immune-suppression

In December 2019, the first cases of pneumonia produced by a new virus were reported. Initially called 2019-nCoV (for 2019 novel coronavirus), the virus was renamed severe acute respiratory syndrome coronavirus 2 (SARS-CoV-2) and the disease caused by the virus, coronavirus disease 2019 (COVID-19). COVID-19 manifests with symptoms ranging from fully asymptomatic to severe disease and death.

The virus enters the host cell by using its viral spike (S) glycoprotein to interact with angiotensin-converting enzyme 2 (ACE2) and transmembrane protease serine 2 (TMPRSS2), a host receptor proteins (121). TLR2 has been shown to promote an inflammatory response to SARS-CoV-2, suggesting that TLR2 is one of the PRRs that recognize the virus (122). The innate immune cells activated by PRR signaling respond by activating effector cells like T and B cells to eliminate the virus. B cells are responsible for the production of antibodies targeting protein S. Neutralizing antibody responses, likely directed against protein S, start to emerge by the second week, with the majority of patients developing neutralizing antibodies by the third week (123). CD8+ T cells play a crucial role in directly targeting and eliminating virus-infected cells, while CD4+ T cells are essential for priming both types of cells. Moreover, CD4+ T cells play a pivotal role in generating cytokines to orchestrate the recruitment of other immune cells and expressing IFN γ , TNF- α , and IL-2, indicating that individuals with SARS-CoV infection present a Th1 cell response, predominantly relying on cellular immunity to combat the infection (123).

Importantly, some patients develop dysregulated immune responses against SARS-CoV-2 upon detection by PRRs. Some immune cells such as macrophages, DCs, monocytes and NK cells release IFNs and proinflammatory

Introduction

cytokines including IL-1 β , IL-6, TNF- α , IL-12, and IFN- γ , which in turn stimulates further proinflammatory cytokine release, that can give rise to a cytokine storm that produces organ damage and respiratory failure (124) (**Figure 5**). Even though some clinical aspects of the patients have been associated with this dysregulated immune response like age, obesity or hypertension, it is still not possible to predict when it will occur.

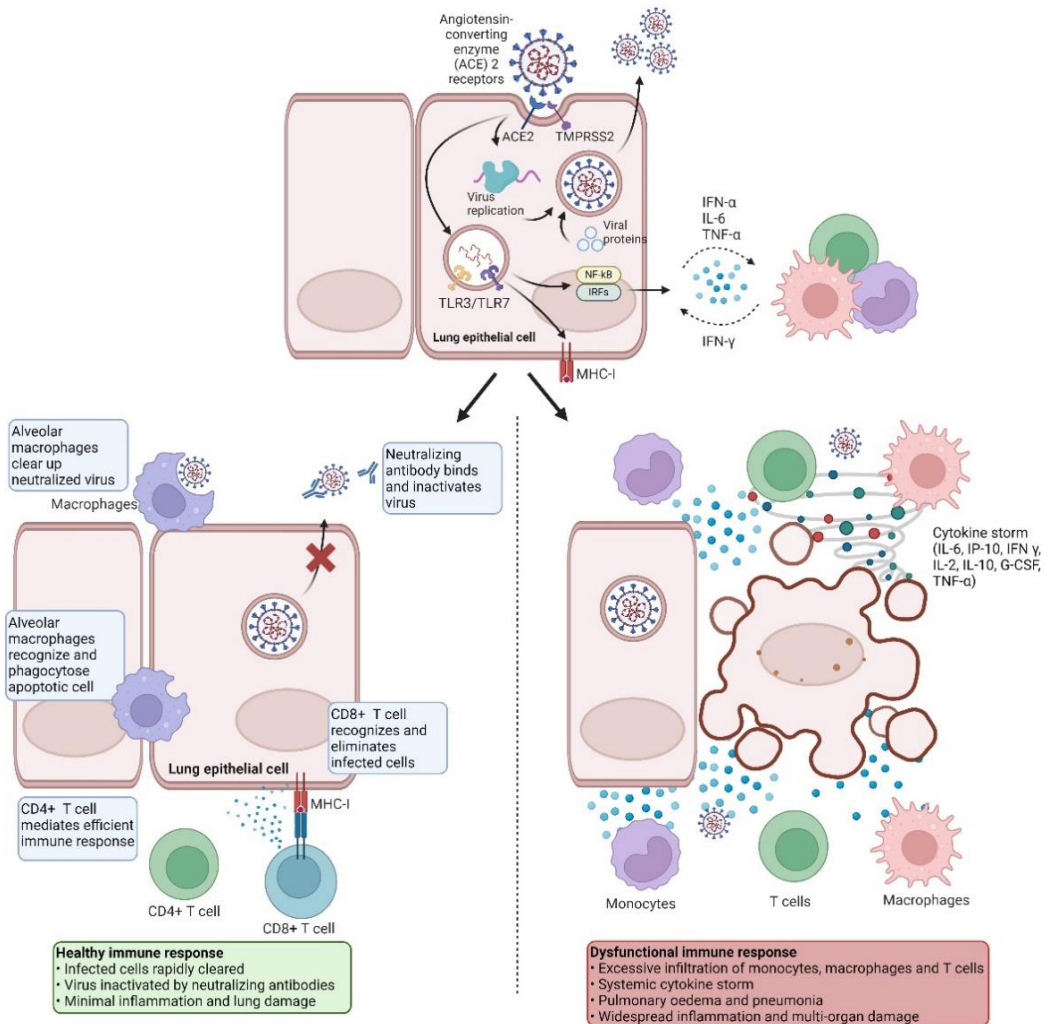


Figure 5. (See figure legend on the next page.)

Figure 5. When SARS-CoV-2 infiltrates cells expressing surface receptors such as angiotensin-converting enzyme 2 (ACE2) and TMPRSS2, it triggers active replication and subsequent release of the virus. This process drives the release of DAMPs detected by neighboring epithelial cells, endothelial cells, and alveolar macrophages, initiating the production of pro-inflammatory cytokines and chemokines such as IL-6, IFN- α or TNF- α . These cytokines attract monocytes, macrophages, and T cells to the infection site, intensifying inflammation and establishing a pro-inflammatory feedback loop, further aggravated by IFN γ produced by T cells. In a normal immune response (on the left side) the initial inflammation attracts virus-specific T cells to the infection site, facilitating the elimination of infected cells before viral spread. Neutralizing antibodies in these individuals can impede viral infection, and alveolar macrophages recognize neutralized viruses and apoptotic cells, clearing them through phagocytosis. Together, these mechanisms result in viral clearance with minimal lung damage, leading to recovery. In an impaired immune response (on the right side), this can result in excessive accumulation of immune cells in the lungs, leading to the overproduction of pro-inflammatory cytokines, ultimately causing lung damage. The ensuing cytokine storm can spread to other organs, causing multi-organ damage. Adapted from (123).

Severe COVID-19, much like sepsis, triggers a multifaceted response characterized by the simultaneous presence of pro-inflammatory and anti-inflammatory features, although with compromised homeostasis (125). The initial hyperinflammatory reaction is linked to tissue damage and organ dysfunction, while a subsequent or delayed anti-inflammatory response significantly promotes prolonged immunosuppression. Consequently, this phenomenon increases susceptibility to nosocomial infections, heightened rates of rehospitalization, and potentially elevated mortality (126) (**Figure 6**).

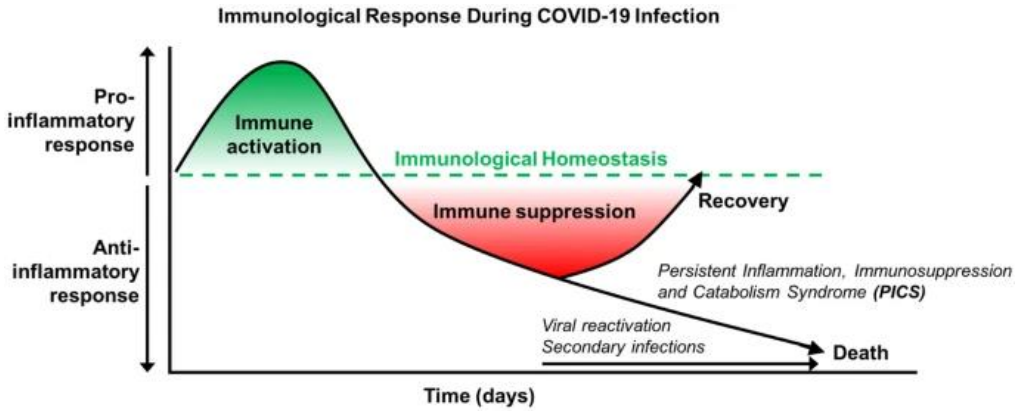


Figure 6. Initially, COVID-19 triggers a strong proinflammatory response; to counter this, anti-inflammatory cytokines are released, aiming to mitigate the cytokine storm. Over time, chronic immunosuppression can lead to persistent inflammation, immunosuppression, and catabolism syndrome. Early fatalities often result from the cytokine storm, whereas later deaths may occur due to secondary infections during the anti-inflammatory phase (127).

This immunosuppression in the more severe cases of the disease was defined by different phenomena. For instance, NK cells play a crucial role in identifying and eliminating cells infected with the virus. However, in severe cases of COVID-19, NK cells are depleted from the bloodstream and lose functionality due to the TGF- β , hindering their ability to combat the virus (128). Alveolar macrophages, which are pivotal in the lungs by detecting and initiating antiviral immunity, are notably diminished in severe COVID-19 patients (129, 130). Conversely, while early antiviral defense mediated by IFN-I is compromised, in severe cases of COVID-19, it displays impaired type I IFN signaling (131). Additionally, T cells are significantly reduced in severe COVID-19 cases compared to moderate ones, suggesting a potential impairment in generating adaptive effector T cells essential for clearing infected cells (132–135). Decreased DCs numbers and profound T-cell lymphopenia, driven by proinflammatory cytokines, are also common features in severe cases (134). In addition, several studies have indicated an increase in neutrophils and a

decrease in nonclassical (CD14_{low}CD16_{hi}) monocytes in severe COVID-19 patients (131, 136, 137).

Furthermore, the excessive circulation of immature monocytes, neutrophils, and myeloid progenitors, known as emergency myelopoiesis, is common on severe cases. This phenomenon is triggered early in infection, likely due to delayed viral clearance, particularly in conditions with preexisting alterations in myelopoiesis (138, 139). Finally, it has also been shown that monocytes from severe COVID-19 patients are characterized by a tolerogenic phenotype with reduced expression of class MHC-II antigens (138, 140, 141) and increased activation of apoptotic pathways (142), given that these monocytes are characterized by displaying an immunosuppressive phenotype (143, 144). This suggests that in the most severe cases of SARS-CoV-2 infection, immunosuppression takes place, although through mechanisms distinct from the most described ones.

1.3. DNA methylation as a major epigenetic mechanism in myeloid cells

1.3.1. Overview

Every cell type within an organism possesses identical DNA to the rest and needs to utilize a specific set of genes different from those required for another cell type. Organisms have developed mechanism to specify the genes that will be expressed in different cell types operates under the same genetic expression mechanisms. Some of these mechanisms are comprised by the concept known as "Epigenetics". This encompasses the array of chemical modifications occurring on DNA itself or on the associated histone proteins that package it. These modifications enable a single cell to adopt distinct properties, setting it apart from others, all without altering its nucleotide sequence.

In 1925, *Johnson and Coghill* aimed to uncover the pathogenic determinants of *Mycobacterium tuberculosis* by isolating and crystallizing nucleic acids. Among their findings was 5-methylcytosine (5mC), a nucleotide previously hypothesized to exist naturally in living organisms. Examination of their hydrolyzed nucleic acid picrate crystals under polarized light effectively differentiated cytosine from 5mC (145). This modification was termed **DNA methylation**. *Sinsheimer* later observed that 5mC is not distributed randomly within DNA but is instead predominantly located within the CpG dinucleotide context (146, 147). DNA methylation is particularly relevant when taking place in CpG dense regions which are present at many gene promoters termed CpG islands (CGIs). Nevertheless, 5mC can be also present in intergenic regions, gene body or enhancer regions (148).

It is widely known that 5mC can play a significant role in regulating gene expression. Generally, it is associate with transcriptional repression, and when

methylation is lost, it tends to associate with transcriptional activation (149). It is pivotal in long-term gene silencing, X-chromosome inactivation and pre-mRNA alternative splicing (150). DNA methylation can directly impede transcription by affecting transcription factor binding in specific instances, including those in which a CpG site is present within a transcription factor binding motif (151).

This epigenetic mark has been highly studied in cancer, given the frequent occurrence of hypermethylation in transcriptional regulatory elements such as gene promoters and enhancers, notably those of tumor suppressor genes (TSGs) (152). The initial discovery of DNA methylation in the promoter region of the retinoblastoma tumor suppressor gene (RB1) among retinoblastoma patients marked a significant milestone (153), with subsequent identification of numerous cancer suppressor genes exhibiting silenced gene expression due to DNA hypermethylation in tumor tissues (154).

However, DNA methylation can be also associated with an increase in expression, for example when present within intergenic regions, often recruits specific histone modification enzymes and chromatin remodelling complexes that can cause increased transcription (155). In the case of gene bodies, which are considered gene regions past the first exon, their methylation can lead to silencing, like in the case of promoters. However, evidence suggests that DNA methylation of the gene body is associated with a higher level of gene expression in dividing cells (156).

Histone post-translational modifications are the second main group of epigenetic marks. There are several types of post-translational modification, including acetylation of Lys, methylation of Lys and Arg, phosphorylation of

Ser and Thr, and others. These chemical modifications not only have direct effects on chromatin structure, but also facilitate the binding of other factors and promote or repress transcription. The nature of the chemical modification and the position of the amino acid residue in the protein sequence yield different functional outcomes. Generally, histone H₃ trimethylation at Lys9 (H₃K₉me₃) and Lys27 (H₃K₂₇me₃) are considered repressive modifications, whereas histone acetylation at the same positions (H₃K₉ac and H₃K₂₇ac) in promoters and enhancers, respectively, are generally associated with transcriptional activation, and the removal of these acetyl marks is linked to gene repression. Conversely, H₃ trimethylation at Lys4 (H₃K₄me₃) and Lys36 (H₃K₃₆me₃) is also associated with active transcription (157).

1.3.2. Regulation of DNA methylation

While DNA methylation typically remains stable, multiple pathways of demethylation and hypermethylation exist and they play an important role in various biological contexts. First, the *de novo* methylation at CpG sites is primarily guided by the *de novo* methyltransferases DNA cytosine-5-methyltransferase 3A (DNMT3A) and DNMT3B (158). Both DNMT3A and DNMT3B contain a Pro-Trp-Trp-Pro (PWWP) domain in the N-terminal region, an ATRX-DNMT3A-DNMT3L (ADD) domain in the central region, and an enzymatic domain in the C-terminal region (159). The PWWP and ADD domains play crucial roles in localizing DNMT3A and DNMT3B to their binding sites and regulating enzymatic activity. Specifically, the PWWP domain facilitates proper binding to chromatin and acts as a reader module, recognizing and binding histones H₃K₃₆me₂ and H₃K₃₆me₃ (160). On the other hand, during DNA replication, DNMT1 is responsible for maintaining methyl groups. Proper localization and activation of DNMT1 at DNA

methylation sites require several regulatory factors. Ubiquitin-like containing PHD and RING finger domains 1 (UHRF1), also known as ICPB90 in humans, also play a critical role in maintaining DNA methylation (161, 162).

During development, the DNA methylation patterns dynamically fluctuate through genome-wide DNA demethylation and *de novo* methylation (163, 164). Also, DNA methylation profiles in cell change in relation to many biological processes including their differentiation or activation in response to different stimuli. **DNA demethylation** is particularly crucial in immune cell differentiation and activation (165) and primarily occurs through two pathways:

- i. DNA replication-dependent demethylation, also known as passive demethylation, through inhibition of DNMTs (166).
- ii. DNA replication-independent demethylation, or active demethylation, mediated by Ten-eleven translocation (TET) methylcytosine dioxygenases (167).

TET enzymes catalyze the oxidation of 5mC to 5-hydroxymethylcytosine (5hmC). In non-proliferative cells, TET further oxidizes 5hmC to 5-formylcytosine (5fC) and 5-carboxylcytosine (5caC) (168). Both 5fC and 5caC are removed generating an abasic sites through the activity of Thymine DNA Glycosylase (TDG). Unmodified cytosines are then restored by the base excision repair (BER) mechanisms (169, 170) (**Figure 7A**). TET-mediated oxidation can target 5mC, 5hmC, and 5fC, with varying affinity or catalytic efficiency of the three members of the TET family for these substrates. Biochemical and structural analyses indicate a preference of TET enzymes for 5mC over 5hmC or 5fC (171). Kinetic studies of enzyme activity have shown that the conversion of 5mC to 5hmC by human TET₁ or TET₂ occurs more rapidly

Introduction

than the conversion of 5hmC to 5fC, and 5fC to 5caC. At a mechanistic level, even though human TET2 binds 5mC, 5hmC, and 5fC with similar affinities, 5hmC and 5fC are the less preferred (172, 173).

TET enzymes are iron(II)/ α -ketoglutarate (Fe(II)/ α -KG)-dependent dioxygenases. Their catalytic activity is primarily located within the carboxyl-terminal core, which consists of a double-stranded β -helix (DSBH) domain alongside a cysteine-rich domain. This DSBH domain facilitates the convergence of Fe(II), α -KG, and 5mC for the oxidation process. Concurrently, the cysteine-rich domain encircles the DSBH core, enhancing the structural integrity and the interaction between TET and DNA. It is important to note that the interaction with DNA does not involve the methyl group. Full-length TET1 and TET3 have a CXXC domain at their amino termini, whereas the putative CXXC domain of TET2 is separated from the protein. These CXXC domains are present in several chromatin-associated proteins, including MLL, DNMT1, MBD1 and are essential for binding nonmethylated CpG-containing DNA, making TET2 TFs-dependent recruitment to perform their function (174) (**Figure 7B**).

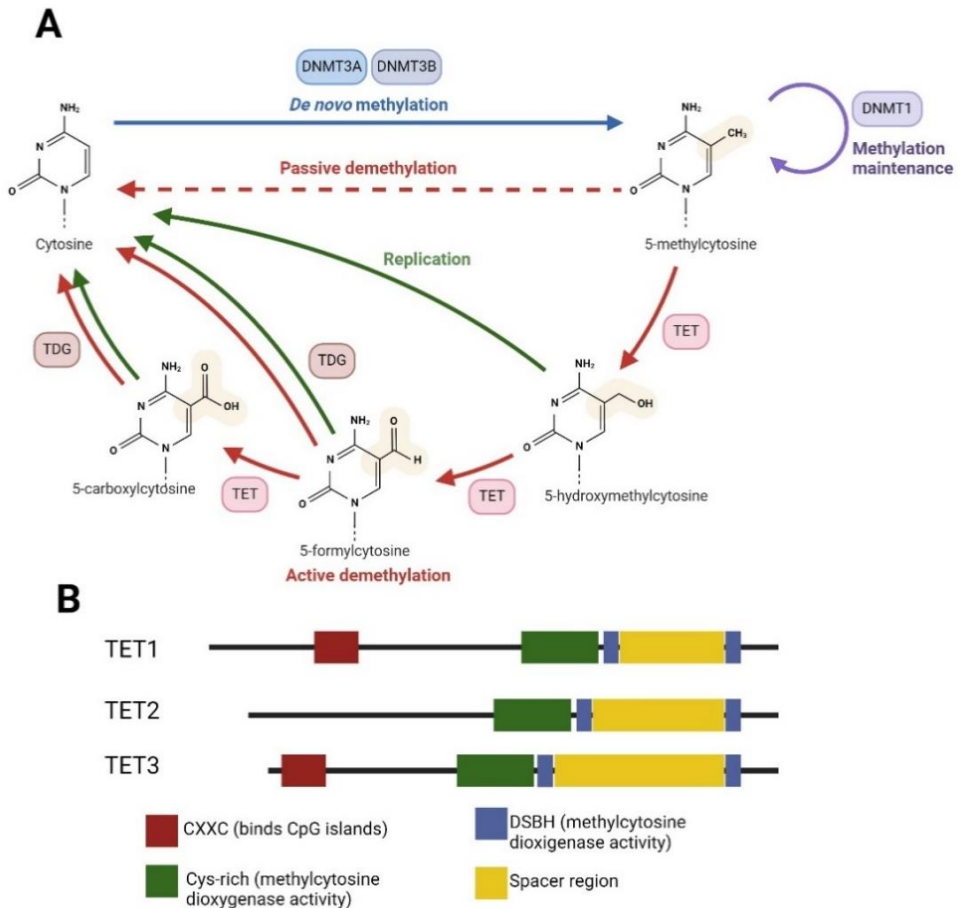


Figure 6. (A) Process of active DNA demethylation involves a cyclical mechanism. Initially, DNMTs catalyze the conversion of unmodified cytosine into 5-methylcytosine (5mC). Subsequently, 5mC can undergo a reversal process mediated by TET enzymes, leading to the generation of 5-hydroxymethylcytosine (5hmC), 5-formylcytosine (5fC), and 5-carboxylcytosine (5caC). Thymine DNA glycosylase (TDG) facilitates the excision of 5fC or 5caC, coupled with base excision repair (BER), in a mechanism termed active modification–active removal (AM–AR). Alternatively, the dilution of 5hmC, 5fC, or 5caC can occur during DNA replication, known as active modification–passive dilution (AM–PD). (B) TET proteins exhibit a domain structure crucial for their function. Catalytic activity is conferred by cysteine-rich and double-stranded β -helix (DSBH) domains located at the carboxyl terminus. While full-length TET₁ and TET₃ possess an amino-terminal CXXC domain, TET₂ lacks this domain.

1.3.3. Transcription factors as mediators of DNA methylation changes

TFs are proteins capable of binding to DNA, influencing gene expression. Most TFs present a DNA-binding domain and a transactivator domain, which interacts with other proteins to mediate activating or repressive functions. TFs recognize specific short DNA sequence motifs for binding, although epigenetic regulation can further modulate their access to DNA (175). However, there are specific TFs, called **pioneer TFs**, that can bind to inaccessible chromatin by remodelling the structure and facilitating the context-specific TF binding (176).

Certain TFs can recruit DNMTs to promote DNA methylation at specific sites. For instance, the leukemia-promoting PML-RAR fusion protein was shown to induce DNA methylation in the RAR β promoter (177). Similarly, MYC, PU.1, E2F6, DNMT1-PAS1-PH20, and p65 (RELA) have been implicated in promoting DNA methylation in different contexts (178–182).

TFs can also induce active demethylation by recruiting TET enzymes. This was observed with CTCF and REST using stable insertions of methylated reporters, where these proteins could bind and trigger local demethylation (183). Subsequently, similar mechanisms were identified for PU.1 through motif analysis in differentially methylated regions (184), and for RUNX1, RUNX3, GATA2, CEBPB, MAFB, NR4A2, MYOD1, CEBPA, and TBX5 via methylation array studies (185). Once a region becomes unmethylated, TFs have been also shown to protect it from DNA methylation. CXXC zinc finger proteins like CXXC1/CFP1 and FBXL19 bind to unmethylated CpGs within CpG islands, recruiting chromatin remodelers to maintain these regions unmethylated (186, 187).

Finally, it is worth mentioning that there is a specific subtype of TFs, named **nuclear receptors**, that are a family of ligand-regulated TFs that are activated by steroid hormones, such as estrogen and progesterone, and other lipid-soluble signals, including retinoic acid, oxysterols, and thyroid hormone (188). One example is RAR that has been also associated with the recruitment of TET to modified DNA methylation its binding site (189). This suggests that external factors can activated nuclear receptors, functioning as TFs, that can perform DNA methylation changes through the recruitment of the different epigenetic enzymes, and finally affecting the cell phenotype.

1.3.4. DNA methylation alterations in immune mediated diseases

Aberrant DNA methylation has been widely studied in most cancer types, including solid cancers such as colon, breast, liver, bladder, and bone cancers as well as hematological malignancies, such as leukemias and lymphomas. In relation to DNA methylation, DNMT mutations, different expression levels of DNMTs, as well as dysregulation of TETs are frequently observed in cancer (190, 191) Also, similarities in the DNA methylation signature have been observed between primary tumor and distant metastases in the same individual (192). All of this evidence supports a strong connection between alterations in DNA methylation and cancer. However, the exploration of DNA methylation changes extends beyond cancer research. Another biological context where DNA methylation has been widely studies is in the context of genomic imprinting (193).

DNA methylation has been also used in genetically complex autoimmune diseases, shering light on the implication of DNA methylation on disease phenotypes. Low concordance rates among monozygotic twins in

Introduction

diseases like Ra (194), SLE (195), and MS (196) suggest potential roles for environmental factors or epigenetics in disease etiology. Given that immune cells are primary targets in autoimmune diseases and are readily accessible from blood samples, they serve as an appropriate model for studying the link between DNA methylation and disease.

Ra is a chronic autoimmune inflammatory disease affecting small and large joints, with a global prevalence estimated between 0.3% to 1.0% (197). Genome-wide DNA methylation analysis of peripheral blood mononuclear cells has revealed altered DNA methylation patterns at the HLA-class II locus, implicating its role in mediating the genetic risk of developing Ra (198). Furthermore, significant changes and increased variability in the DNA methylomes of peripheral blood monocytes have been observed in Ra patients compared to those from healthy controls, with correlations identified between these alterations and the expression of inflammatory cytokines, shedding light on the interplay between DNA methylation changes and external factors (199). DNA methylation alterations in peripheral blood monocytes also appear to reflect prognosis, disease evolution, and treatment response in the early stages of Ra (200).

In **SLE**, blood genome-wide studies have identified differential DNA methylation in genes involved in autoantibody production (201). A specific hypomethylation was also observed in the promoter region of the IL-6 gene in peripheral blood (202). Recently, the analysis of monocytes from SLE patients has revealed DNA methylation and transcriptomic alterations associated with an interferon signature and monocyte subset-specific changes, providing insights into their impact of SLE on monocyte differentiation (203).

MS, the leading cause of neurological disability in young adults, exhibits DNA methylation changes across various immune cell types, including CD4+ T cells, CD8+ T cells, and CD44+ encephalitogenic T cells (204).

Moreover, DNA methylation studies have also expanded to metabolic disorders such as type 2 diabetes mellitus (**T2DM**), where altered methylation levels at specific genomic sites correlate with differential gene expression in pancreatic islets (205). Additionally, shortened leukocyte telomere length has been implicated in affecting LINE-1 methylation levels, potentially increasing T2DM risk in certain populations (206).

Neurological disorders, including autism spectrum disorder (**ASD**) and Rett Syndrome, exhibit frequent mutations in the Methyl-CpG-binding protein 2 (MeCP2) gene, suggesting an implication of DNA methylation alteration in disease pathogenesis (207, 208). Changes in the DNA methylation profiles were associated with differential expression of genes involved in synaptic activity, indicating a potential mechanism underlying these disorders (209, 210). Additionally, DNA methylation changes in epilepsy patients have been correlated with disease duration, particularly affecting inflammation-related genes in both cortex and hippocampus (211).

Finally, DNA methylation studies have been conducted in infectious diseases, such as **sepsis**, revealing altered DNA methylomes in tolerized monocytes from sepsis patients compared to healthy controls. These changes affect critical monocyte-related genes and correlate with increased levels of IL-10 and IL-6 (212).

1.3.5. Role of DNA methylation in monocyte differentiation and suppression

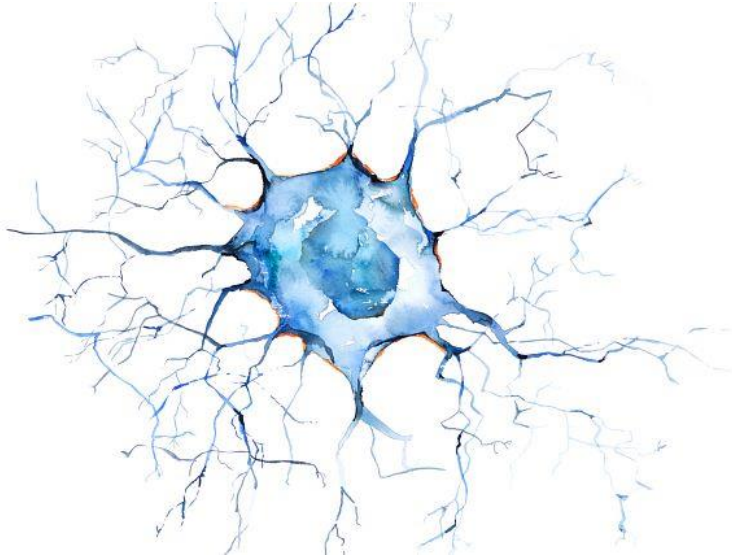
DNA methylation is crucial in the early stages of immune cell development and differentiation; however, it also plays a role in their terminal differentiation. In fact, the differentiation of monocytes into various effector cell types derived from MO is influenced by factors such as cytokines, growth factors, or environmental cues, which have an influence on the epigenetic profiles (55, 213, 214). Specifically, it has been reported that TET2-dependent demethylation is vital for the development of the identity and function of DCs and macrophages. In the differentiation to DCs from monocytes, a key process involves the activation of the JAK3-STAT6 pathway by IL-4, which is necessary for DCs-specific demethylation and expression (215). Another example is represented in the differentiation to osteoclasts from monocytes, where the binding of PU.1 to both DNMT3A and TET2 leads to DNA methylation changes essential for monocyte differentiation into osteoclasts (184).

External factors added during *in vitro* differentiation from monocytes can also induce the acquisition of new phenotypes, where DNA methylation plays a significant role. The addition of Vitamin D and glucocorticoids has been shown to promote TolDCs, where not only their respective receptors VDR and GR, but also other TFs, such as STAT3 and MAFB, in conjunction with TET2 drive these changes (216, 217). For MDSCs differentiated in the presence of PEG2, an increase in DNMT3A promotes hypermethylation, defining their immunosuppressive phenotype (218).

Furthermore, the immune response to infection involves active demethylation of thousands of CpG sites at distal enhancer elements associated with NF- κ B/Rel (p65) (219). Vitamin C is known to enhance TET enzymes'

enzymatic activity, likely acting as a cofactor (220, 221), by directly interacting with the catalytic domain of TET proteins to increase their function (222). Exposure to Vitamin C during the activation of moDCs promotes enhanced demethylation and upregulation of many genes regulated by NF- κ B, enhancing the DC ability to stimulate the proliferation of autologous antigen-specific T cells in a p65-TET2 interaction manner (222).

In summary, there is abundant evidence that the significant morphological, transcriptional, and epigenetic shifts occur during *in vitro* culture of moDC are associated with site-specific TET2-dependent active DNA demethylation. However, the mechanism of TET2 recruitment to demethylated sites remains unclear. Research has shown that while IRF4 is a hallmark of DC functions it have minimal impact on DNA methylation, early growth response 2 (EGR2) is critical for MO differentiation and DNA methylation turnover at its binding sites (223).



HYPOTHESIS
and
OBJECTIVES

2. HYPOTHESIS

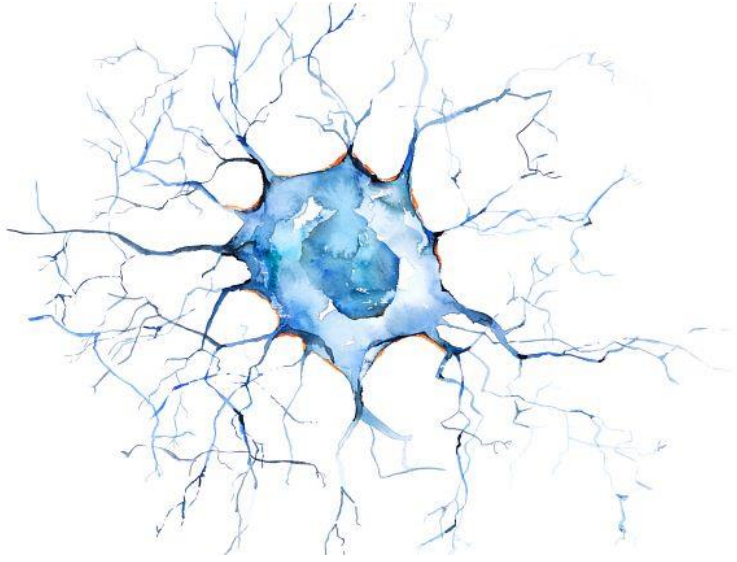
Given the intricate nature of the innate immune response and the various components involved in maintaining homeostasis, gaining a deeper understanding is crucial. To date, numerous immunosuppressive mechanisms have been identified, with most being linked to lymphoid cells. However, recent research has emphasized the significant role that myeloid cells, particularly monocytes and monocyte-derived dendritic cells, may play in these processes. These cells can transition from a pro-inflammatory state to a more tolerance-inducing one based on their environment or the specific molecules they interact with. These transitions to a more immunosuppressive capability have been observed in various scenarios, including epithelial barrier immunity and within tumor microenvironments -where RA is a major player in both cases- or in infections, such as severe COVID-19. Despite these insights, the regulatory mechanisms underlying such phenotypic changes on myeloid cells remain poorly understood. In this regard, epigenetics, particularly DNA methylation, could be a critical factor driving these adjustments. This research hypothesizes that specific given epigenetic, specifically DNA methylation, and transcriptomic modifications within myeloid cells, produced by the external factors, can significantly influence their immunosuppressive functions.

In COVID-19, the effectiveness of immune cells to respond to the SARS-CoV-2 virus could be significantly influenced by whether individuals have impairments in central tolerance, leading to autoimmunity. There further remains a need for knowledge about the specific antiviral immune responses mounted by such patients. In this regard, it was hypothesized that the response to viral infection can vary in the context of different autoimmune diseases.

3. OBJECTIVES

The main objective of this doctoral thesis is to shed light into some of intricate mechanisms that regulate myeloid cell-mediated immunosuppression through the lens of epigenetic and transcriptional regulation. The specific objectives of this doctoral thesis can be divided into the following points:

1. To investigate the immunological, epigenomic and transcriptomic changes associated with the exposure to RA during monocyte to DC differentiation.
2. To characterize the epigenomic and transcriptomic reprogramming of monocytes in severe COVID-19, given the central role of these cells in inflammatory responses, to understand the specific dysregulated pathways involved in the dramatic immune dysregulation in these patients.
3. To investigate the impact of SARS-CoV-2 infection on different immune cell populations in patients with autoimmune diseases, focusing on three representative conditions: rheumatoid arthritis (Ra), psoriasis (Ps), and multiple sclerosis (MS).



ARTICLES

3. ARTICLES

Director's report

I certify that the PhD student Gerard Godoy-Tena will defend his Doctoral Thesis by article publication compendium, two of which have already been published. His contribution to each article is specified below:

ARTICLE 1. Retinoic Acid-Induced Epigenetic Modulation of VSIG4 via LXR α in Dendritic Cells Promotes Immunosuppression

Gerard Godoy-Tena, Celia L. Calvillo, Lucía Link, Laura Ciudad, Nikolas Valencia, Antonio Castrillo, Annabel F. Valledor, Ángel L. Corbí, Esteban Ballestar

Journal: Nucleic Acids Research (**under revision**)

IF 2023: 14.9

In this paper, currently under revision, Gerard has optimized the retinoic acid differentiation model and generated the samples to perform DNA methylation and expression analysis. Moreover, he conducted CD8+ proliferation assays, qPCR, flow cytometry, ELISAs, Western Blots, Chromatin Immunoprecipitation assays (ChIPs) and treatments with the nuclear receptors' agonists/antagonists. He was in charge of all bioinformatics analyses performed in the paper, including raw reads alignments, processing, and plotting of methylation, expression, and scRNA-seq data. Finally, Gerard, along with me, interpreted all the results. He assembled figures and wrote the article, along with me.

ARTICLE 2. Epigenetic and transcriptomic reprogramming in monocytes of severe COVID-19 patients reflects alterations in myeloid differentiation and the influence of inflammatory cytokines

Gerard Godoy-Tena, Anis Barmada, Octavio Morante-Palacios, Carlos de la Calle-Fabregat, Ricardo Martins-Ferreira, Anna G. Ferreté-Bonastre, Laura Ciudad, Adolfo Ruiz-Sanmartín, Mónica Martínez-Gallo, Ricard Ferrer, Juan Carlos Ruiz-Rodríguez, Javier Rodríguez-Ubreva, Roser Vento-Tormo, Esteban Ballestar¹.

Journal: *Genome Medicine* (2022); 14(1): 134

IF 2021: 15.266

In this article, Gerard Godoy-Tena was the main person responsible for the patient sample processing and subsequent data generation (methylation bead arrays and scRNAseq). In addition, he conducted all the bioinformatics analyses performed in the paper, including reads alignments, processing, and plotting of methylation and expression data. Finally, Gerard, along with me, interpreted all the results obtained and wrote the paper.

ARTICLE 3. Single-cell multi-omics analysis of COVID-19 patients with pre-existing autoimmune diseases shows aberrant immune responses to infection

Anis Barmada, **Louis-François Handfield***, **Gerard Godoy-Tena***, **Carlos de la Calle-Fabregat***, Laura Ciudad, Anna Arutyunyan, Eduardo Andrés-León, Regina Hoo, Tarryn Porter, Agnes Oszlanczi, Laura Richardson, Fernando J. Calero-Nieto, Nicola K. Wilson, Domenica Marchese, Carmen Sancho-Serra, Jorge Carrillo, Silvia Presas-Rodríguez, Cristina Ramo-Tello, Adolfo Ruiz-Sanmartin, Ricard Ferrer, Juan Carlos Ruiz-Rodriguez, Mónica Martínez-Gallo, Mónica Munera-Campos, Jose Manuel Carrascosa, Berthold Göttgens, Holger Heyn, Elena Prigmore, Ivette Casafont-Solé, Xavier Solanich, Ildefonso Sánchez-Cerrillo, Isidoro González-Álvaro, Maria Gabriella Raimondo, Andreas Ramming, Javier Martin, Eva Martínez-Cáceres, Esteban Ballestar, Roser Vento-Tormo and Javier Rodríguez-Ubreva³

*Equal contribution

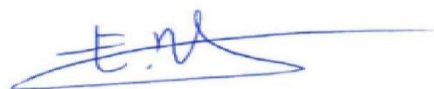
Journal: *European Journal of Immunology* (2024); 54(1): e2350633

IF 2020: 5.532

In this article, Gerard prepared and processed all samples included in the study. Gerard was involved in data generation and performed some bioinformatics analyses. Gerard assembled the figures together with Anis Barmada and Javier Rodriguez-Ubreva and participated in the writing of the manuscript. Anis Barmada was a master student so he will not use this article as part of his doctoral thesis.

In witness whereof, I hereby sign the present doctoral thesis, 12th April 2024,
Badalona (Barcelona)

Esteban Ballestar,
Ph.D. Epigenetics and Immune Disease Group,
Leader Josep Carreras Research Institute (IJC)
Ctra de Can Ruti, Camí de les Escoles s/n
08916 Badalona, Barcelona, Spain
Tel: +34 935572800
ext. 4250
E-mail: eballestar@carrerasresearch.org

A handwritten signature in blue ink, appearing to read 'E. Ballestar', with a long horizontal line extending to the right.

3.1 ARTICLE 1. Retinoic Acid-Induced Epigenetic Modulation of VSIG4 via LXR α in Dendritic Cells Promotes Immunosuppression

Retinoic Acid-Induced Epigenetic Activation of VSIG4 via LXR α in Dendritic Cells Promotes Immunosuppression

Gerard Godoy-Tena¹, Celia L. Calvillo¹, Lucía Link¹, Laura Ciudad¹, Nikolas Valencia¹, Antonio Castrillo^{2,3}, Annabel F. Valledor^{4,5}, Ángel L. Corbí⁶, Esteban Ballestar^{1,7}

1. Epigenetics and Immune Disease Group, Josep Carreras Research Institute (IJC), 08916, Badalona, Barcelona, Spain
2. Instituto de Investigaciones Biomédicas Sols-Morreale, Centro Mixto Consejo Superior de Investigaciones Científicas CSIC-Universidad Autónoma de Madrid, Madrid, Spain.
3. Unidad de Biomedicina (Unidad Asociada al CSIC), Instituto Universitario de Investigaciones Biomédicas y Sanitarias (IUIBS) de la Universidad de Las Palmas de Gran Canaria, Las Palmas, Spain.
4. Nuclear Receptor Group, Department of Cell Biology, Physiology and Immunology, School of Biology, University of Barcelona, Barcelona 08028, Spain
5. Institute of Biomedicine of the University of Barcelona (IBUB), Barcelona, Spain.
6. Myeloid Cell Laboratory, Centro de Investigaciones Biológicas, Consejo Superior de Investigaciones Científicas (CSIC), Madrid, Spain
7. Epigenetics in Inflammatory and Metabolic Diseases Laboratory, Health Science Center (HSC), East China Normal University (ECNU), Shanghai, 200241, China

ABSTRACT

Dendritic cells (DCs) play a pivotal role in immune responses. Understanding the factors influencing their function is critical for therapeutic interventions. In this study, we investigate the impact of retinoic acid (RA) on the immunological, epigenomic and transcriptomic features of monocyte-derived DCs (moDCs) and reveal a multifaceted role of RA in inducing immunosuppressive properties. Specifically, RA promotes the acquisition of a macrophage-like phenotype in moDCs, which undergo increased expression of macrophage markers and develop immunosuppressive functions. We identify that genes governing immunosuppression undergo specific DNA methylation changes in response to RA, emphasizing the implication of epigenetics in the observed phenotype. Additionally, we uncover the involvement of the nuclear receptor Liver X Receptor alpha ($LXR\alpha$) as an important mediator of the immunosuppressive effects of RA on moDCs. $LXR\alpha$ expression is upregulated during RA treatment, and its activation is linked to the epigenetic reprogramming and expression of immunosuppressive factors like VSIG4, which directly binds. We also show that the direct targeting of VSIG4 revert partially the immunosuppressive properties. RA-mediated downregulation of retinoid X receptor alpha ($RXR\alpha$) expression is also essential for $LXR\alpha$ to exert its immunomodulatory function. Finally, we determine that *in vivo* colon and tumor-associated macrophages co-express $LXR\alpha$ and VSIG4. These findings provide valuable insights into the intricate regulatory mechanisms governing the immunomodulatory effects of RA on DCs.

INTRODUCTION

Dendritic cells (DCs) serve as professional antigen-presenting cells (APCs) that are needed to stimulate T cell-driven immunity and enhancing their robustness. The phenotypically and functionally different subsets of DCs, together with their developmental origins, have been thoroughly studied. They play a pivotal role in controlling immune responses under both physiological and pathological conditions, making them valuable therapeutic targets [1]. There are three main DC subtypes: conventional DCs (cDCs), plasmacytoid DCs (pDCs) and monocyte-derived DCs (moDCs). Most tissue-infiltrating DCs primarily derive from the local differentiation of recruited monocytes (MO) into moDCs at inflammatory tissues [2]. What makes moDCs particularly interesting for investigating regulatory mechanisms is their ability to be differentiated from monocytes *in vitro* in the presence of granulocyte macrophage colony-stimulating factor (GM-CSF) and interleukin (IL-4). These *in vitro* differentiated DCs do not only share gene expression patterns with *in vivo* inflammatory moDCs but also with blood cDCs [3].

The plasticity of myeloid cells, including DCs, is underscored by their sensitivity to extracellular factors. Their immunological properties are subject to variation influenced by environmental cues. At the epigenetic level, studies reveal dynamic DNA methylation changes in DCs, among others, in response to diverse external influences [4]. DNA methylation involves the addition of methyl groups to the 5' position of cytosines (5mC) at CpG dinucleotides and is generally associated with transcriptional repression [5, 6]. Alterations in DNA methylation may result from upstream environmental influences connecting cell membrane receptors, signaling pathways, and transcription factors (TFs). These factors can either directly recruit DNA methyltransferases (DNMT) and

ten–eleven translocation (TET) methylcytosine dioxygenases or indirectly modulate their binding to specific genomic sites [7].

In recent years, it has become evident that the nutritional status impacts metabolism and function of immune cells. One example is the all-trans retinoic acid (ATRA), generically known as retinoic acid (RA), a vitamin A metabolite that is an important determinant of intestinal immunity [8–12]. Classically, RA has been shown to play a role in cell development [13], including macrophage development [9]. The immunological effector functions of RA are determined by many different factors such as local RA concentrations, TLR signalling, the presence of additional cytokines, and the cellular and molecular composition of the microenvironment [12]. RA is generally thought to promote tolerance via multiple immune cell types [14]. Specifically, it induces Foxp3⁺ T regulatory cells [15, 16], promotes a shift from an M₁ to an M₂ phenotype and inhibits macrophage-mediated immunity [17]. Recently, it has been demonstrated that food-derived RA confers immature features to intraepithelial cDCs, low surface expression of CCR7 and costimulatory molecule, and decreased antigen presentation capacity that promote T cell hyporesponsiveness [18]. Nevertheless, some groups have reported that at low doses, RA favours Th₁ or Th₁₇ T cell responses [19]. For example, Takahashi and collaborators have shown that RA promotes Th₁₇ cell differentiation *in vitro* at physiological doses (1nM) [20].

The biological effects of RAs are mainly mediated through retinoic acid receptors (RARs) [21]. As type II nuclear receptors, RARs form heterodimers with retinoid X receptors (RXRs) and bind to retinoic acid response elements (RAREs) in the regulatory regions of their target genes, including promoter or enhancers, that regulate their expression. RXRs can also form homodimers or

heterodimers with other nuclear receptors and regulate gene expression [22]. However, it has been described that RA can induce degradation of its receptors [23,24]. RAR-RXR heterodimers are non-permissive as they activate transcription only in response to RAR agonists. In contrast, other class II nuclear receptors, including peroxisome proliferator-activated receptors (PPARs), liver X receptors (LXRs), and farnesoid X receptors (FXRs), form heterodimers with RXR that are permissive to RXR agonists. LXRs are probably best known as oxysterol receptors and physiological master regulators of sterol metabolism. LXR α and LXR β (encoded by the NR1H3 and NR1H2 genes, respectively) are TFs classically involved in cellular cholesterol metabolism [25–27]. LXRs are also involved in the proliferation and differentiation of keratinocytes and the inhibition of tumor cell proliferation [26]. However, this is a controversial topic as LXRs also display anti-inflammatory activities [28–31]. In cancer immunology, LXRs suppress the proliferation of a variety of human cancer cells, which in turn produce LXR agonists (oxysterols) that inhibit immune responses as a mechanism of tumor escape from immune surveillance [32].

Recently, it has been shown that the accumulation of RA in the tumor microenvironment (TME) promotes immunosuppression, preventing immunotherapy efficacy [33]. Specifically, in the presence of RA, monocytes reaching the TME preferentially differentiate into immunosuppressive macrophages, although the transcriptomic and epigenetic mechanisms regulating these changes and how the immunosuppression is produced remain unclear.

The present study sheds light on the intricate regulatory mechanisms underlying the immunomodulatory effects of RA on moDCs, unveiling novel specific molecular pathways that drive the acquisition of immunosuppressive properties.

MATERIALS AND METHODS

CD14⁺ monocyte purification and culture

CD14⁺ monocytes were obtained with magnetic CD14 MicroBeads (Miltenyi Biotec) from PBMCs previously isolated by density-gradient centrifugation using lymphocyte-isolation solution (Rafer). Blood was obtained from anonymous donors via the Catalan Blood and Tissue Bank (CBTB). The CBTB follows the principles of the World Medical Association (WMA) Declaration of Helsinki.

MOs were resuspended in Roswell Park Memorial Institute (RPMI) containing 10% fetal bovine serum (Gibco, ThermoFisher), 100 units/ml penicillin/streptomycin (Gibco, ThermoFisher), 10 ng/ml human GM-CSF (PeproTech), 10 ng/ml human IL-4 (PeproTech) and 1 μ M of RA (Sigma Aldrich) (DMSO diluted) was added to the treated cells. Cells non treated with RA, the same volume of DMSO was added. 1 μ M of GW3965 (Sigma), LG268 [34] and GSK2033 (#HY-108688) were used as LXR and RXR agonists and LXR antagonist, respectively. For DCs maturation, LPS (10 ng/ml) was added to the cell culture on day 5 and the cells were collected after 48h. On day 7, we therefore collected immature dendritic cells (iDC/iDC_{RA}) and mature dendritic cells, with LPS stimulus (mDC/mDC_{RA}).

CD8⁺ cell proliferation assay

Allogenic CD8⁺ T-cells isolated using negative selection with the human CD8 T Cells Kit (Invitrogen) and were labeled with carboxy fluorescein succinimidyl ester (CFSE) CellTrace™ (Invitrogen) in according with the manufacturer's instructions. T-cells were seeded in 96-well plates at 200,000 cells/well, with

iDC or iDC_{RA} at different ratios (DC:CD8⁺ T-cell ratios: 1:2, 1:3 and 1:4), previously collected using Versene, a non-enzymatic dissociation buffer (ThermoFisher). CD8⁺ cells were then stimulated with 5 μ L/mL of anti-CD3/CD28 Dynabeads (Invitrogen) and cultured for 4 days. AntibodyS against VSIG4 (Ab_VSIG4_1(#MAB46462), Ab_VSIG4_2(#:MAB4646)) and IgG (#CS200581) were added at day 0 when corresponding. CD8⁺ T-cell proliferation was analyzed by FACS and determined by considering the proliferating CD8⁺ T-cells those where CFSE staining had decreased compared to unstimulated CD8⁺ T-cells. CD8⁺ T-cells without and only with anti-CD3/CD28 Dynabeads were used as negative control (C-) and positive control (C+) respectively.

T cell clonal expansion and proliferation assay

PBMCs from healthy donors were purified from blood by density gradient centrifugation. The PBMCs (1 ml; 3×10^6 cells per well) were cultured in the presence of SARSCoV-2- S (9pmol) (PepTivator) in 24-well plates and maintained in IMDM medium (Gibco) supplemented with penicillin (100 units/ml), streptomycin (100 mg/ml) and human serum (10%) (Millipore) in the absence of IL-2 for 3 days. After 3 days, 1 ml of medium with 80 U/ml of recombinant human IL-2 (PeproTech) was added to the wells, with a final concentration of 1.5×10^6 cell/ml and 40 U/ml of IL-2. After 7–10 days of culture, T cells were expanded in the presence of 30-Gy irradiated autologous PBMCs (3×10^6 cells/well) previously pulsed with 9pmol of SARS-CoV-2-S (PepTivator). Antigen-specific T cells (mix of CD4⁺ and CD8⁺ T cells) were selected by performing the same protocols two times to have a positive selection.

After 5 days of differentiation and activation, moDCs were washed to remove RA and were co-cultured with antigen-specific autologous CFSE-stained T cells at a DC: T cell ratio of 1:2, 1:3 and 1:4 in 200 µl of RPMI 1640 medium containing 10% FBS, penicillin (100 units/ml), streptomycin (100 mg/ml) in round bottom 96-well plates (ThermoFisher). Co-culture was performed in the presence of SARS-CoV-2-S antigen or SARS-CoV-2-N control antigen (PepTivator). T cell proliferation was analyzed by FACS and determined by considering the proliferating of those where CFSE staining had decreased compared to not co-cultured T cells. T cells stimulated with anti-CD3/CD28 microbeads 5 µg/ml (eBioscience) were used as a positive control (C+).

Flow cytometry

For the study of surface cell markers, cells were collected using Versene, and harvested after differentiation culture and washed once with PBS. Cell staining was performed in a staining buffer (PBS with 4% fetal bovine serum and 0.4% ethylenediaminetetraacetic acid (EDTA)) after blocking for non-specific binding with Fc block (BD Pharmingen) for 5 minutes on ice. Cells were stained for 20 minutes on ice. Antibodies used included: CD14 (APC) (#130-110-520, Miltenyi Biotec), CD16 (APC) (#130-113-389, Miltenyi Biotec), CD163 (FITC) (#33618, BioLegend), CD1a (PE) (#300106, BioLegend), CD86 (APC) (#130-113-569, Miltenyi Biotec), HLA-DR (PE) (#12-9956-42, eBioScience), CD206 (FITC) (#551132, BD pharmgen), CD25 (#12-0251-82, eBioscience), VSIG4 (#17-5757-42, eBioscience). After staining, cells were fixed with PBS + 4% paraformaldehyde (Electron Microscopy Sciences) and analyzed using a BD FACSCanto™ II Cell Analyzer (BD Biosciences). Data were analyzed with the FlowJo v10 software.

Quantification of cytokine production

Cell culture supernatants were collected after 7 days and diluted appropriately. Enzyme-linked immunosorbent assays (ELISA) were performed to detect IL-10, IL-12 and TNF- α from BioLegend and IL-1 β from ThermoFisher following the manufacturer's instructions.

Real-time quantitative Polymerase Chain Reaction (RT-qPCR)

RNA was extracted using the Maxwell RSC simplyRNA Cells kit (Promega) following the manufacturer's instructions. 250 ng of total RNA were converted to cDNA with Transcriptor First Strand cDNA Synthesis Kit (Roche), following manufacturer's instructions. RT-qPCR primers were designed with Primer3 software. RT-qPCR reactions were prepared with LightCycler 480 SYBR Green I Master according to manufacturer instructions and analyzed with a LightCycler 480 instrument (Roche). The average value from each technical replicate was obtained. Then, the standard double-delta Ct method was used to determine the relative quantities of target genes, and values were normalized against the control gene RPL38. Custom primers were designed to analyse genes of interest (Supp. Table 1).

Chip-qPCR

After 3 days of differentiation 10 million of iDC and iDC_{RA} were fixed with Pierce™ fresh methanol-free formaldehyde (ThermoFisher) for 10 min and prepared for sonication with the truChIP Chromatin Shearing Kit (Covaris), following the manufacturer's instructions. Chromatin was sonicated 15 min with the Covaris M220 in 1 ml milliTubes (Covaris). The size distribution of the sonicated chromatin was checked by electrophoresis to ensure an appropriate

sonication, with a size around 150-200 bp. Magna Beads Protein A+G (Millipore) were incubated for 4h with the correspondence antibody in a buffer with 1% Triton X-100, 150 mM NaCl and 0.15% SDS. Chromatin was precleared with 10000g centrifugation and were incubated overnight with each antibody: 10 ul Anti-LXR alpha antibody (ab41902) and RXRA antibody (21218-1-AP), in the same buffer as the antibody+beads. Then, three washes were performed with the Low Salt Wash Buffer (0.1% SDS, 1% Triton X-100, 2 mM EDTA, pH 8.0, 20 mM Tris-HCl pH 8.0, 150 mM NaCl), the High Salt Wash Buffer (0.1% SDS, 1% Triton X-100, 2 mM EDTA, pH 8.0, 20 mM Tris-HCl pH 8, 500 mM NaCl) and the LiCl Wash Buffer (0.25 M LiCl, 1% Nonidet P-40, 1% deoxycholate, 1 mM EDTA pH 8, 10 mM Tris-HCl), followed by a last wash with TE buffer (pH 8.0, 10 mM Tris-HCl, 1 mM EDTA). Chromatin was eluted for 45 min 65°C with 100 ul of elution buffer (10 mM Tris-Cl, 1 mM EDTA, 1% SDS) and decrosslinked adding 5 ul 1M NaCl and 5 ul 1M NaHCO₃ (2 h 65°C). Next, 1 ul of 10mg/ml proteinase K (Invitrogen) was added, and samples were incubated at 37°C for 1 h. For DNA purification, iPure kit v2 (Diagenode) was used, following the manufacturer's instructions. 1% of the chromatin input from each sample was purified by the same method. For ChIP-qPCR, samples were diluted 1/10, and 4 ul and specific primers (Supp. Table 1) were used for each reaction. qRT-PCR was performed in technical triplicates for each biological replicate, using LightCycler® 480 SYBR Green Mix (Roche). The relative amount of immunoprecipitated DNA compared to input was calculated with the following formula: $2^{((Ct_{input} - 3) - Ct_{sample})} \times 100\%$.

Western blot

Protein expression was visualized by western blotting, performed using standard Western blot. The following antibodies were used: anti-pStat6 Y641

(Cell Signaling Technology), anti-Stat6 #9362 (Cell Signaling Technology), anti-Lamin B1 ab65986 (Abcam), anti-p65 C15310256 (Diagenode), anti-pp65 (Ser536) 93H1 (Cell Signaling Technology), anti-TET2 ab94580 (Abcam), anti-DNMT3b ab2851 (Abcam), anti-DNMT3a D23G1 (Cell Signaling Technology), anti-RAR α C15310155 (Diagenode), anti-RAR γ OT13G1 (TrueMAB), anti-RXR α 21218-1-AP (Proteintech), anti-PPAR γ D69 (Cell Signaling Technology) and anti-LXR α ab41902 (Abcam).

DNA methylation profiling, quality control and statistical analysis of DMPs

Genomic DNA extraction was carried out utilizing the DNA precipitation protocol. Bisulfite (BS) conversion was performed employing the EZ-96 DNA Methylation™ Kit (Zymo Research, CA, USA) as per the manufacturer's guidelines. Subsequently, 500 nanograms of BS-converted DNA were subjected to hybridization on Infinium Methylation EPIC BeadChip arrays (Illumina, Inc., San Diego, CA, USA). These arrays facilitated the analysis of DNA methylation, enabling the assessment of >850,000 methylation sites per sample at single-nucleotide resolution, encompassing 99% of the reference sequence (RefSeq) genes. Each methylation data point was derived from the combined Cy3 and Cy5 fluorescent intensities representing methylated and unmethylated alleles, respectively. Background intensity was subtracted from each data point using a computed value obtained from a set of negative controls. Beta (β) and M values were utilized for representation and further analysis. Beta denotes the ratio of methylated probe intensity to overall intensity (sum of methylated and unmethylated probe intensities), while M is computed as the log₂ ratio of methylated and unmethylated probe intensities. For statistical purposes, the use of M values is deemed more appropriate due to the severe

heteroscedasticity of β -values observed for highly methylated and unmethylated CpG sites. Raw DNA methylation data are accessible via the Gene Expression Omnibus (GEO) database under accession number GSE255789.

Quality control, data normalization, and statistical analysis of DMPs

Quality control and analysis of EPIC arrays were performed utilizing ShinyÉPICo, a graphical pipeline incorporating minf (v1.36) for normalization and limma (v3.46) for differential methylation analysis. The BS conversion control probe test integrated within ShinyÉPICo was employed to assess whether the conversion rate surpassed the quality threshold of 2 established by Illumina, computed from the information of the BS conversion control probes present on the EPIC arrays. CpH and SNP loci were eliminated utilizing the Noob method, followed by quantile normalization. Analysis excluded sex chromosomes (X and Y) to prevent discordant information across samples. This sex exclusion was not performed to study VSIG4 related CpGs. Despite data generation occurring within a single batch and being randomized, batch effect correction was applied. The Trend and Robust options were utilized in the eBayes moderated t-test analysis. Differential methylation between treated and non-treated moDCs was determined using t-tests and a method with defined empirical array weights from the limma package [35], with CpGs selected based on a false discovery rate (FDR) < 0.05 and an absolute differential methylation ($\Delta\beta$) exceeding 10% (> 0.1).

RNA-seq

RNA-seq libraries were generated and sequenced by Novogene (Cambridge), in 150-bp paired-end, with the Illumina NovaSeq 6000 platform, using four biological replicates for each group. More than 40 million reads were obtained

for each sample. Fastq files were aligned to the hg38 transcriptome using kallisto package [36]. Reads were assigned to genes with featureCounts [37]. Differentially expressed genes were detected with DESeq2 [38]. The donor was used as a covariate in the model. The Ashrshrinkage algorithm was applied and only protein-coding genes with an absolute logFC >0.5 and an FDR < 0.05 were selected as differentially expressed gene (DEG). Raw expression data are accessible via the Gene Expression Omnibus (GEO) database under accession number GSE255925.

Single cell analysis

Two publicly available single-cell RNA sequencing datasets were acquired for a validation analysis in an *in vivo* context [39, 40]. After selecting the myeloid cell population clusters of interest, integration and reclustering was performed independently for each one of the datasets.

Both were normalized, top 2000 highest variable genes were selected, and data was scaled, following the Seurat pipeline. Cell clustering was performed using Louvain's algorithm (FindNeighbors and FindClusters). The Uniform Manifold Approximation and Projection (UMAP) algorithm was then applied for visualisation, selecting the top 30 dimensions.

Gene ontology, transcription factor enrichment, chromatin state discovery and representation

Statistical analyses were performed in R 4.0.3. The GREAT online tool was used for gene ontology (GO) analysis with DNA methylation analysis. GO analysis of DEGs was carried out using the online Enricher gene ontology analysis tool [41]. FindMotifsGenome.pt tool from the Hypergeometric Optimization of Motif

EnRichment (HOMER) motif discovery software to analyze motif enrichment was used. A flanking window of ± 250 bp from each CpG was applied, and CpGs annotated in the EPIC array were used as background. Transcription factor (TF) enrichment of DEGs was carried out using the Discriminant Regulon Expression Analysis (DoRoThEA) tool. Chromatin functional state enrichment of DMPs was analyzed using public PBMC data from the Roadmap Epigenomics Project generated with ChromHMM. CHIP-seq peaks files of histone marks from MO and iDCs were downloaded from the BLUEprint webpage (<http://dcc.blueprint-epigenome.eu>). Consensus peaks of the different replicates were obtained with the MSPC algorithm [42], using the options ‘-r Biological -w 1E-4 -s 1E-8 -c 3’. Public DNase-seq bigwigs were aggregated using wiggletools to obtain the mean value of several replicates. Heatmaps of DMPs were generated with functions available in the ComplexHeatmap and gplots R packages. PCA projection matrices were calculated with R’s prcomp function and visual representations. All statistical analyses were done in R v3.5.1. Normally distributed data were tested using two-tailed unpaired Student's t-tests; non-normal data were analyzed with the appropriate non-parametric statistical test. Levels of significance are indicated as: *, $P < 0.05$; **, $P < 0.01$; ***, $P < 0.005$; ****, $P < 0.001$.

Data access

DNA methylation and RNA-seq data for this publication have been deposited in the NCBI Gene Expression Omnibus and are accessible through GEO Series accession numbers GSE255789 and GSE255925 (Superseries).

RESULTS

Retinoic acid induces the acquisition of immunosuppressive properties in DCs

To investigate the effects of RA in the phenotype of moDCs, from now on referred to as DCs, we first differentiated *in vitro* peripheral blood monocytes from healthy donors to iDCs for 5 days using GM-CSF and IL-4 in the absence and presence of RA (iDC and iDC_{RA}), followed by two days of activation using lipopolysaccharide (LPS), obtaining mature DCs (mDC and mDC_{RA}) (Figure 1A). We first observed that iDC_{RA} were able to inhibit CD8⁺T cell proliferation *in vitro*, in contrast to iDCs, indicating the acquisition of immunosuppressive properties in the presence of RA (Figure 1B). Previously, it has been proposed a dual role for RA in the polarization of DCs, one inducing tolerogenic properties in a steady state, and the other potentiating the production of pro-inflammatory cytokines in an inflammatory context [43]. To test whether a complex milieu modulates the acquisition of the immunosuppressive phenotype, we differentiated monocytes to iDCs in the presence of RA and medium derived from culturing Caco2 cancer cells. We observed that the presence of the soluble factors produced by cancer cells increases the immunosuppressive capacities induced by RA (Supp. Figure 1A). In standard conditions, ELISA assays showed that LPS stimulated the production of IL-1 β , IL-6, and TNF- α , but the production of these cytokines was partially impaired in the presence of RA (Figure 1C). However, the expression of the classical immunosuppressive cytokine IL-10 was also downregulated, suggesting a global downregulation of NF- κ B activation.

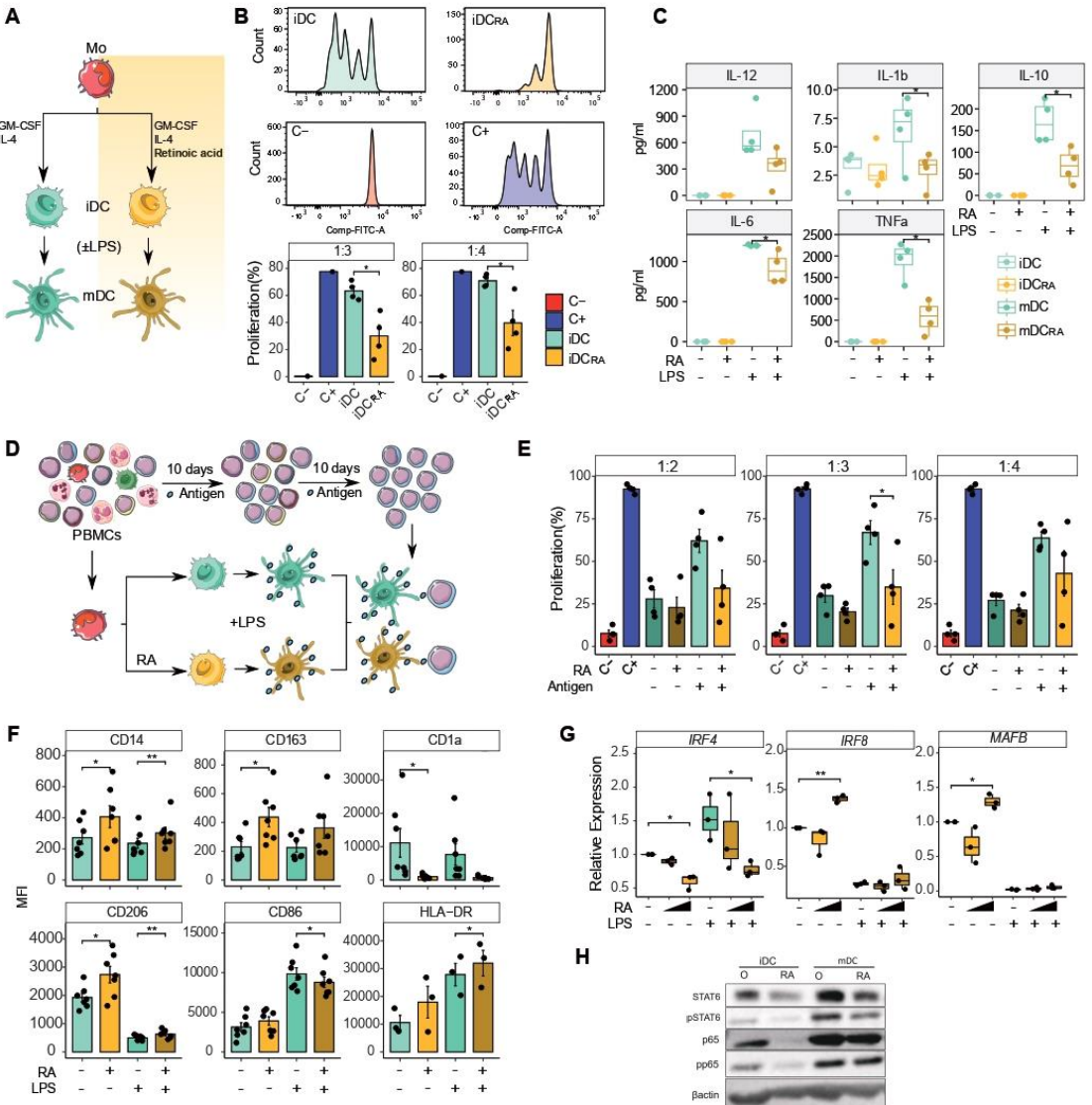
To further characterize the effects of RA on DCs regarding their T cell stimulation and antigen-presenting capabilities, we conducted antigen presentation assays using clonally expanded T cells (see Methods) (Figure 1D). We observed that co-culturing T cells with mDCs loaded with no antigen did not result in proliferation, whereas co-culturing with mDCs loaded with the antigen led to significant proliferation, indicating antigen-specific T cell proliferation. However, when mDCs were differentiated in the presence of RA, T cell proliferation did not occur (Figure 1E).

At the cell surface level, we observed that exposure to RA during DC differentiation increased the expression of macrophage markers like CD14, CD163 and CD206, together with a decrease in the expression of CD1a, a DC marker, in a dose-dependent manner (Figure 1F and Supp. Figure 1B,1C). Nevertheless, when we compared the CD163 expression in DC_{RA} with GM-CSF-induced macrophages, we observed much higher levels in the latter (Supp. Figure 1C). We also observed decreased expression of the costimulatory molecule CD86 and an increase of antigen-presenting molecules like HLA-DR (Figure 1F). In parallel, we determined that *IRF4*, a TF relevant for DC differentiation, decreased in the presence of RA, as previously described [33]. Conversely, *IRF8* and *MAFB*, important for macrophage differentiation [44], displayed a significant increase in relation to RA exposure (Figure 1G).

Finally, we detected a decrease in the expression and phosphorylation of STAT6, which is needed for the acquisition of the DC phenotype, as we and others have previously reported [45]. We also observed a drastic decrease in the protein levels of p65 NF- κ B under the treatment of RA, which is needed for proinflammatory gene expression (Figure 1H). Collectively, these results support the idea that DCs acquire immunosuppressive capacities under RA

treatment, with the differentiation from monocytes to DCs partially blocked, and giving rise to a more macrophage-like phenotype.

Figure 1



(See figure legend on the next page.)

Figure 1. (A) Schematic overview of the differentiation model, including monocytes (Mo), immature dendritic cells (iDC) and mature dendritic cells (mDC), treated and untreated with retinoic acid (RA). (B) iDC and iDC_{RA} were co-cultured with CD8⁺ cells for 4 days. The final CFSE signal of CD8⁺ cells is shown (bottom panels). CD8⁺ with only CD3/CD28 T-activator beads (C+) or alone (C-) are also shown (n=3). (C) Box-plot representation of IL-6, TNF- α , IL-12p70, IL-1 β and IL-10 production by each cell type, after 48h treatment with LPS. (D) Scheme depicting the T cell proliferation assay. PBMCs were obtained from healthy donors. T cell clones reacting to the specific antigen (SARS-CoV-2 protein S) were selected through several rounds of clonal expansion. On the other hand, mDCs and mDC_{RA} were obtained from the same donor and charged with the specific antigen. Finally, the Carboxyfluorescein succinimidyl ester (CFSE)-stained T cells were cocultured with mDCs/mDCvitC for 5 days. (E) The proliferation of T cells cocultured with moDC (2:1, 3:1 and 4:1 proportion), with or without the loading with a specific SARA-CoV-2 antigen. Non activated T cells from each donor was used as negative control (C-) and T cells with CD3/CD28 were used as positive control (C+) (n = 4) (F) Bar-plots of surface marker expression (Median Fluorescence Intensity) in DCs in steady-state (n=6). (G) Box-plot representation of gene expression obtained from qRT-PCR in treated and untreated iDCs and mDCs with increasing concentration of RA (n=3). (H) Western blot of phosphorylated and total of STAT6 and p65 proteins in whole-cell lysates of iDCs and mDCs, treated and untreated with RA. β -actin was used as a loading control. (* P < 0.05, **P<0.01).

DNA methylation reprogramming of DCs in response to RA

As indicated above, the immunological properties of DCs have been linked to TET-mediated DNA demethylation [4]. We therefore obtained and compared the DNA methylation profiles of Mos and DCs in relation to the exposure to RA, in both iDCs and mDCs. Hierarchical clustering of differentially methylated CpGs between iDC and iDC_{RA} and between mDC and mDC_{RA} (FDR < 0.05 and absolute differential beta $\Delta\beta$ > 0.1) revealed four main clusters of CpG sites (Figure 2A): a cluster of CpGs that underwent specific demethylation in both iDC and mDC and whose demethylation is impaired in iDC_{RA} and mDC_{RA} (Cluster 1, 1126 CpGs); a second cluster that undergoes enhanced hypermethylation in both iDC_{RA} and mDC_{RA} (Cluster 2, 325 CpGs); a third cluster that is specifically demethylated upon activation only in mDCs and not in mDC_{RA} (Cluster 3, 135 CpGs); and, finally, a cluster of CpGs with RA-specific DNA demethylation (Cluster 4, 104 CpGs) (Supp. Table 2). Examples of each

cluster include *IRF4* and *RXRA* in Cluster 1, *CXCR4* and *IL10* in Cluster 2, *IL6* and *TNF* in Cluster 3 and the *JUN* and the Hypermethylated in Cancer 1 (*HIC1*) genes in Cluster 4 (Supp. Figure 2A). Previous work has identified the gene *HIC1* as a RAR direct target gene [46], which we found to be specifically demethylated under the treatment with RA (Supp. Table 2).

Principal component analysis (PCA) showed that most of the variability observed at the DNA methylation level can be explained by events common to differentiation and activation processes. We found that iDC_{RA} and mDC_{RA} are closer to monocytes in the principal component 1 (PC1), whereas the PC2 clusters together iDC and mDC , on the one hand, and iDC_{RA} and mDC_{RA} on the other. We also observed that the activation produces more changes in mDC than in mDC_{RA} (Figure 2B).

All clusters, except Cluster 2, were enriched in introns and depleted in promoters (Supp. Figure 2B). Looking at the enrichment in active enhancer histone marks ($H3K4me1$ and $H3K27ac$) in DCs and MOs, an increase in the signal of these marks was noted in $moDC$ differentiation, especially in Cluster 1 and Cluster 3, which became specifically demethylated in DCs (Supp. Figure 2C). All DNA methylation clusters were enriched in monocytic enhancers and regions flanking active transcription start sites (Figure 2C). Employing the average signal of public MO DNase-seq (Blueprint database) we found that Cluster 2 and Cluster 4, the ones presenting a RA-specific hyper- and hypomethylation, had greater accessibility in DCs, demonstrating a correlation between chromatin accessibility and DNA methylation changes (Figure 2D).

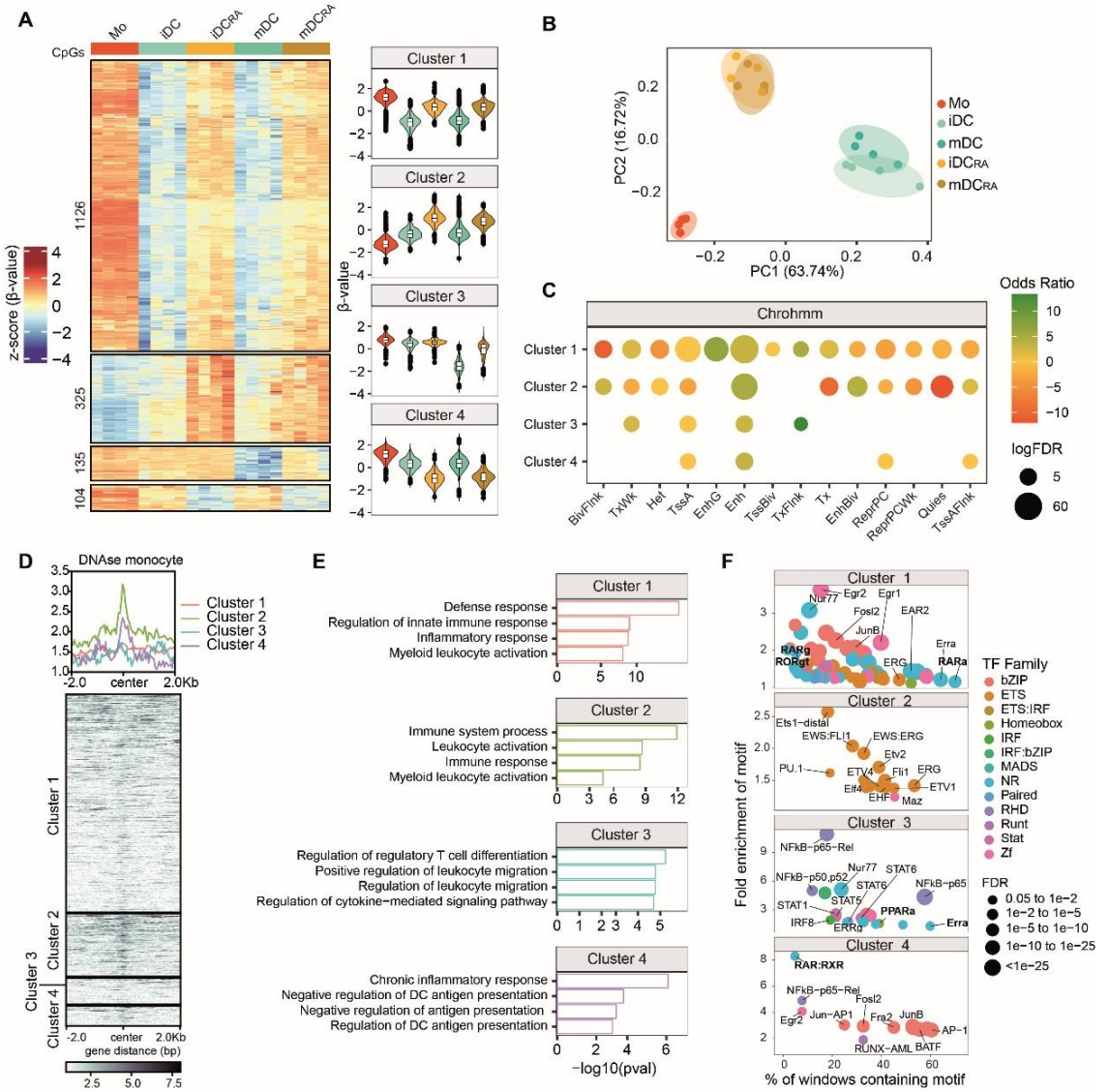
We correlated each CpG with the nearby gene and performed GO enrichment analysis using GREAT program. We observed that Cluster 1 is

associated with categories related to defense response and myeloid differentiation. Cluster 2 and Cluster 3 are enriched in categories related to leukocyte activation and differentiation. In contrast, Cluster 4 is enriched in chronic inflammatory response and negative regulation of DC antigen presentation (Figure 2E). These functions are consistent with the phenotype previously observed.

To identify TFs potentially involved in the DNA methylation dynamics, we performed TF motif enrichment analysis using FindMotifsGenome tool from HOMER motif discovery software. In Cluster 1 we observed enrichment of the consensus binding motifs of transcription factors associated with DC differentiation, such as EGR2 [47], together with TF related with RA response like RAR α or RAR γ , also present in Cluster 4. In Cluster 2 we observed the enrichment of ETS family transcription factors like PU.1 or Ets1 [48]. Finally, in Cluster 3 there was enrichment in consensus binding motifs of NF- κ B, AP-1 and IRF, together with Erra and PPAR α (Figure 2F).

Finally, we analysed the protein levels of the enzymes catalysing DNA methylation changes (DNMTs and TETs) and determined that RA treatment results in both a decrease of TET2 and an increase of DNMT3A (Supp. Figure 2D). The latter is consistent with our previous report of increased levels of DNMT3A in association with the acquisition of an immunosuppressive phenotype [49]. These changes in TET2 and DNMT3A are compatible with the impaired demethylation in response to RA in clusters 1 and 3, as well as the hypermethylation in cluster 2.

Figure 2



(See figure legend on the next page.)

Figure 2. (A) Scaled DNA methylation (z-score) heatmap of DMPs and box and violin plots summarizing the distribution of DNA methylation levels per cell type and cluster. Differentially methylated CpGs were calculated comparing iDC with iDC_{RA} and mDC with mDC_{RA} ($\Delta\beta \geq 0.1$, FDR<0.05) (n=4). DNA methylation values of the precursor cell type (MO) are also shown. (B) Principal-component analysis of differentially methylated CpGs. (C) Enrichment of each DMPs cluster in ChromHMM 15-states categories of MOs (Roadmap Epigenomics Project). Fisher's exact tests of DMPs cluster were calculated using all the CpGs annotated in the EPIC array as background. The relative enrichment is represented as Odds Ratio. Analysis include TssA, Active TSS; TssBiv, Bivalent/Poised TSS; BivFlnk, Flanking Bivalent TSS/Enh; EnhBiv, Bivalent Enhancer; ReprPC, Repressed PolyComb; ReprPCWk, Weak Repressed PolyComb; Quies, Quiescent/Low; TssAFlnk, Flanking Active TSS; TxFlnk, Transcr. at gene 5' and 3'; Tx, Strong transcription; TxWk, Weak transcription; EnhG, Genic enhancers; Enh, Enhancers; ZNF/Rpts, ZNF genes & repeats; Het, Heterochromatin. (D) DNAase data of CD14⁺ monocytes from the BLUEPRINT database. Odds ratios of histone marks enrichment were calculated for bins of 10bp, 200bp upstream and downstream in relation DNA methylation clusters. CpGs annotated in the EPIC array were used as background. (E) GO over-represented categories in each cluster. Fold change in comparison with background (EPIC array CpGs) and $-\log_{10}$ (FDR). Selected significant functional categories are shown (*p*-value). (F) Bubble scatter-plot of TF-binding motif enrichment for each methylation cluster. The x-axis shows the percentage of windows containing the motif and the y-axis shows the factor of enrichment of the motif over the EPIC background. Bubble sare colored according to the TF family. FDR is indicated by bubble size.

RA-induces expression changes leading to immunosuppression

In parallel, we performed RNAseq on the same samples used for DNA methylation profiling and examined differences in their transcriptomes. Since the samples were collected on day 7, without or with LPS-mediated activation, for iDC/iDC_{RA} and for mDC/mDC_{RA} respectively, different comparisons to test the effects of RA can be performed. In the first comparison (iDC_{RA} vs. iDC), we observed a total of 510 genes that were upregulated, and 285 genes downregulated (FDR<0.05 and logFC>0.5) (Supp. Figure 3A and Supp. Table 3). We observed the upregulation of genes related with a macrophage-like phenotype such as *CD163*, *CD14* or *MAFB* together with some chemokines like *CCL2* and *CCL5*. We also observed the downregulation of the *CD1a* gene together with a marked downregulation of the IL-1 receptors (*IL1R1* and *IL1R2*)

and *STAT6*. We also noticed the upregulation of *NR1H3*, encoding LXR α , which interacts with RXR α [50] that is downregulated. In the second comparison (mDC_{RA} vs. mDC), we observed a total of 1020 genes that were upregulated, including *CEBPA*, *CD68*, *HLA-DRA* or the gene coding for the immunosuppressive cytokine *TGFBI*. Among the downregulated genes, we observed a total of 330 genes including some proinflammatory-related genes like *IL6*, *NFKB1* and *TNF*. In both comparisons, we observed *VSIG4* as one of the most differentially expressed genes (Figure 3A). *VSIG4* is a type I transmembrane receptor exclusively expressed in a subset of tissue-resident macrophages that maintains immune homeostasis by suppressing the activation of T cells and inducing Treg differentiation [51, 52], thereby inhibiting the development of immune-mediated inflammatory diseases.

In contrast with the DNA methylation data, transcriptome variance of PC1 and PC2 are mainly explained by the maturation of DCs and the differentiation of MO to iDCs, respectively. However, differences between mDC and mDC_{RA} can also be observed in the PCA (Supp. Figure 3B). GO terms were calculated for each comparison (Figure 3B). For instance, iDC_{RA} present a positive regulation of categories related to the negative regulation of the immune response and a downregulation of myeloid differentiation.

Since RA induces downregulation of IL-10 (Figure 1C), an archetypical immunosuppressive cytokine, we hypothesized that another cytokine could be involved in the acquisition of immunosuppressive capacities. To explore this possibility, we adapted a tool initially designed to explore intercellular communication in bulk and single-cell expression data to test autocrine/paracrine signal activation [53]. With this approach, we inferred potential ligands that may regulate these processes. Some of the two most

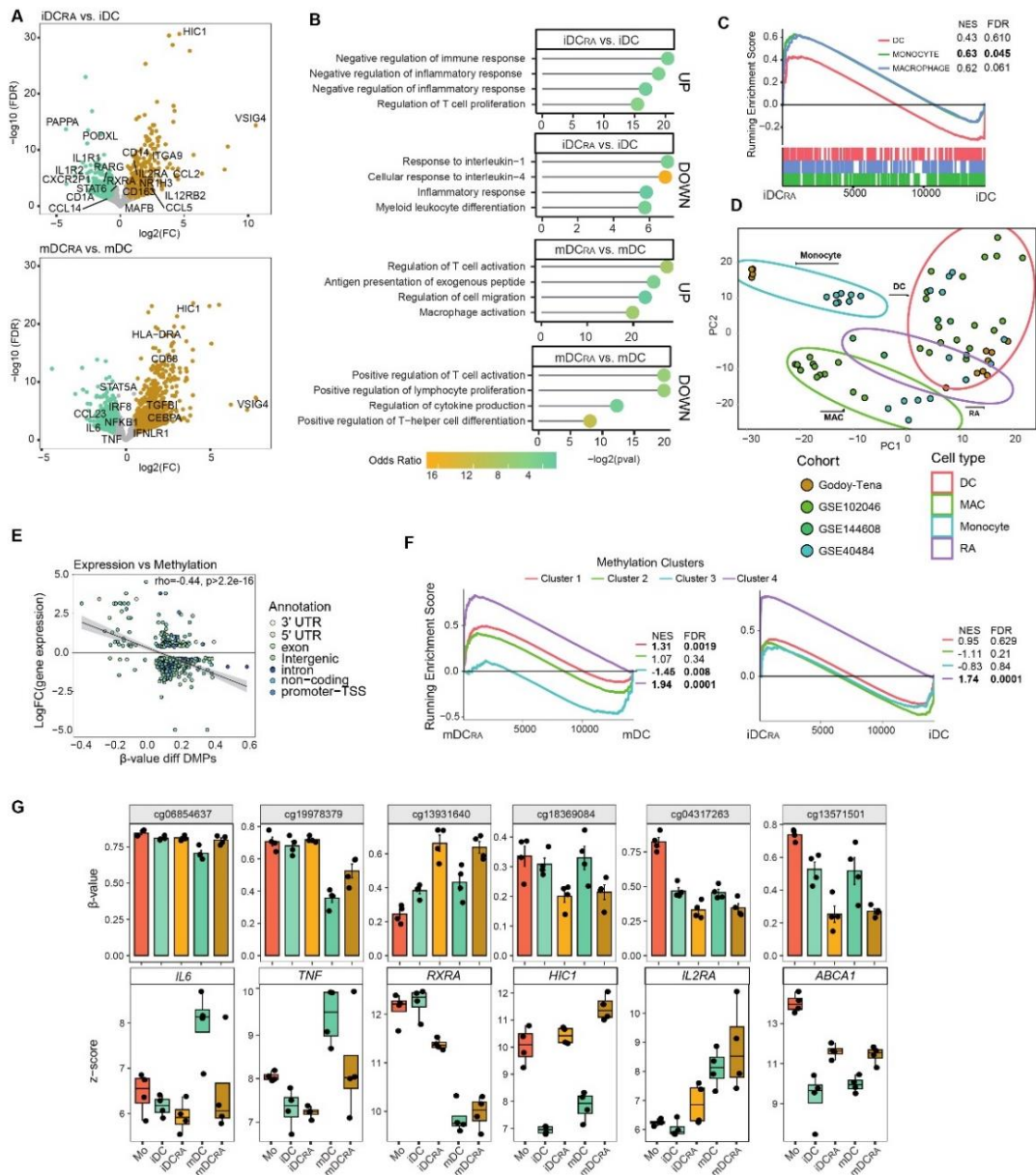
interesting ligands that we observed enriched were the BMP8A and BMP8B encoding genes (Supp. Figure 3C-F), which are members of the TGF β superfamily. Interestingly, we observed upregulation of the *TGFBI* gene in our RNAseq data and previous studies have defined the expression of TGF- β by DCs [54]. We also observed the enrichment of INHBA (Supp. Figure 3C), which is upregulated by GM-CSF and also encodes another TGF β family member. TGF- β expression could explain their immunosuppressive capacities. However, we were unable to detect TGF β in the supernatants.

We performed Gene Set Enrichment Analysis (GSEA) of the genes associated with DC, monocytes and macrophages [55, 56] to determine the phenotype acquired by DC under the treatment with RA. With this analysis, we observed that the genes related with monocytes and macrophages are enriched on iDC_{RA} (Figure 3C). Interestingly, we observed that only mDC_{RA} present significant/high enrichment of alveolar macrophage-associated genes, obtained from different studies [57-59] (Supp. Figure 3G). We integrated our data with public datasets of these cell types and observed that iDC_{RA} acquire a phenotype that is intermediate between macrophages, including inflammatory and non-inflammatory macrophages, and DCs [33, 44, 60] (Figure 3D), as also observed at the protein cell surface level (Figure 1F).

To integrate the previously observed DNA methylation changes with gene expression, we correlated each CpG with the closest gene and observed a significant inverse correlation between DNA methylation and gene expression changes ($\rho = -0.44$; $p = 2.2e-16$) (Figure 3E). To conduct a more detailed examination of the observed correlation, we conducted GSEA focusing on the genes associated with the previously defined CpG clusters. Various comparative analyses were employed, including mDC_{RA} vs. mDC, revealing an upregulation

of Cluster 3 in mDC. Additionally, comparisons such as iDC_{RA} vs iDCs indicated an upregulation of Cluster 4 in iDC_{RA} (Figure 3F). This inverse correlation between DNA methylation and gene expression is exemplified by different genes including proinflammatory genes like *IL6* and *TNF*, anti-inflammatory genes like *IL2RA*, the nuclear receptor *RXRA* or specific targets of RAR α like *HIC1* [61, 62] (Figure 3G). These results support the epigenetic importance on the observed transcriptomic changes.

Figure 3



(See figure legend on the next page.)

Figure 3. (A) Volcano plots of gene expression in the iDC_{RA} vs. iDC and the mDC_{RA} vs. mDC comparisons. The binary logarithm of the fold change is represented on the x-axis, whereas the negative decimal logarithm of the FDR is represented on the y-axis. Downregulated genes are shown in blue (FDR < 0.05, Fold Change < -0.5) and upregulated genes are shown in yellow (FDR < 0.05, Fold Change > 0.5). (B) GO over-representation of GO Biological Process of iDC_{RA} vs. iDC and the mDC_{RA} vs. mDC comparisons. Selected significant functional categories are shown. Fold Change of genes over the background and $-\log_{10}$ (FDR) of the Fisher's exact tests are shown. (C) Gene set enrichment analysis (GSEA) of the RA treated versus untreated iDC, using public datasets of Monocytes, DC and Macrophages as gene sets [54, 55]. The running enrichment score and the normalized enrichment score (NES) are shown above the graph. (D) Principal-component analysis plot of the aggregated and batch-corrected gene expression data from our study (Monocytes, DC and RA) and 3 additional public datasets. The four different groups obtained using k-means clustering are represented with ellipses of multivariate t-distributions. (E) Correlation of average DNA methylation levels of DMPs with average gene expression of DEGs in the iDC vs iDC_{RA} comparison. $\log_2(\text{FC})$ of expression is plotted on the y-axis. DNA methylation is depicted on the x-axis as $\Delta\beta$. Points are colored according to their genomic context. Points are colored according to their genomic context. A significant negative correlation between methylation and expression is observed ($R=-0.44$, $P<2.2e-16$). (F) DMPs were associated with the nearest gene. The resulting gene set from each methylation cluster was used in the GSEA of iDC vs iDC_{RA} and mDC vs mDC_{RA} comparisons. The running enrichment score and the normalized enrichment score (NES) are shown. (G) Bar-plot representation the DNA methylation levels (β -values) of a specific CpG with the nearby gene expression (z-score) below ($n = 4$).

RA induces the expression of LXR α and downregulation of RXR α to promote immunosuppression

To identify the implication of TFs in leading the observed transcriptomic changes, we performed Discriminant Regulon Expression Analysis (DoRotheA) in two comparisons iDC_{RA} vs. iDC and mDC_{RA} vs. mDC. This analysis highlighted enriched TF regulons in both comparisons, including MAF and VDR. Interestingly, MAFB and VDR have been previously identified as implicated in the epigenetic reprogramming toward tolerogenic DCs [63, 64]. In both comparisons, we observed an enrichment of *NR1H3*, encoding LXR α , which interacts with RXRs [50], as mentioned above (Figure 4A and Supp. Figure 4A). LXR α also showed greater enrichment compared to other nuclear

receptors, including LXR β (Supp. Figure 4B). We confirmed by both RNAseq data and western blot the increased expression of this TF, together with a decreased expression of its partner RXR α (Figure 4B-C and Supp. Figure 4C).

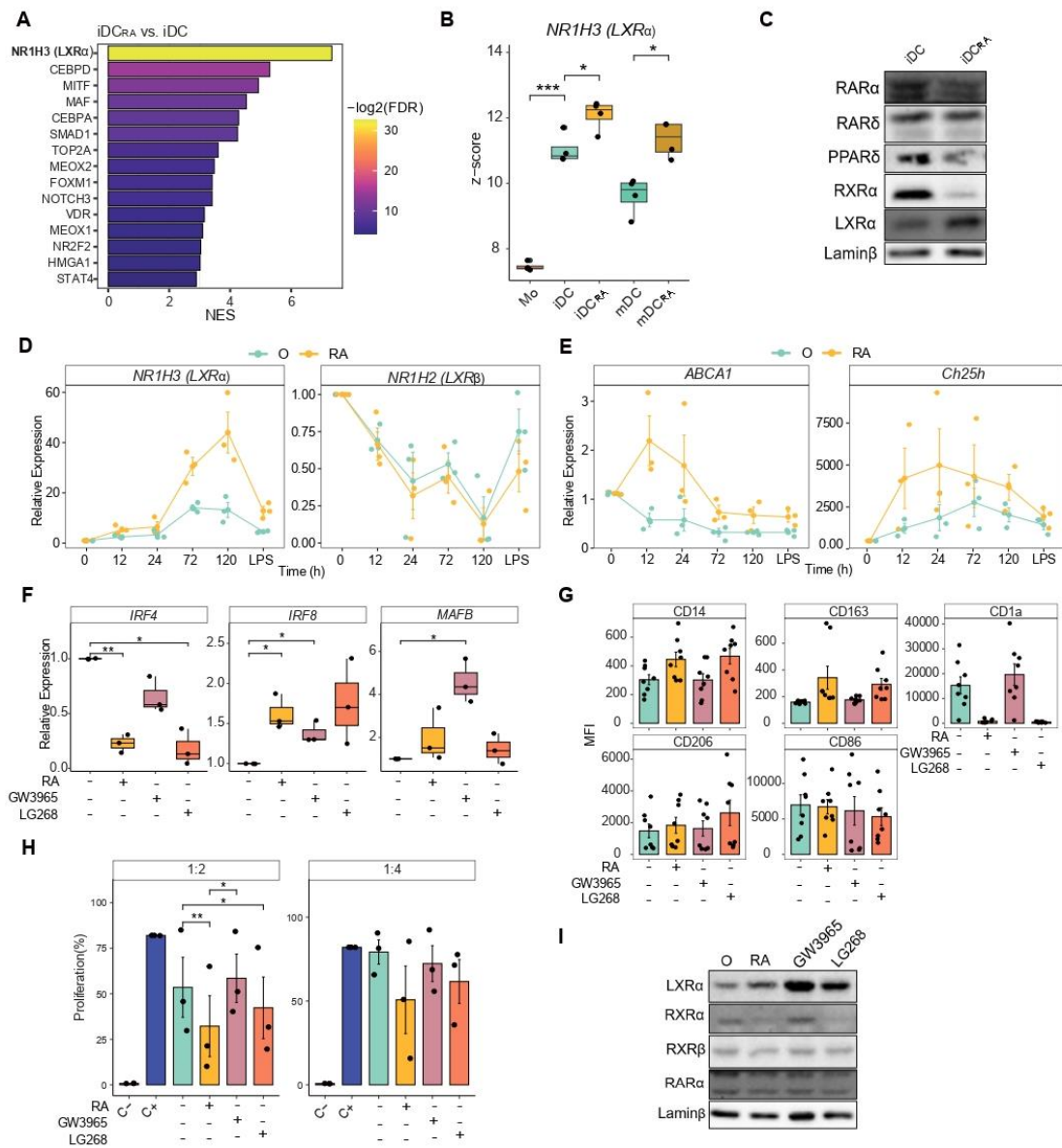
Additionally, we noted an elevated expression of *NR1H3* (LXR α) throughout DC differentiation in the presence of RA, while *NR1H2* (LXR β) exhibited no such increase (Figure 4D). LXR α increased expression along the differentiation process was also validated at the protein level (Supp. Figure 4D). One possible explanation is the NR1H3 hnRNA stabilization by RA treatment.

To explore when LXR is producing changes at the transcriptional level, we analysed the expression of *ABCA1*, as a classical target of LXRs [65] (Figure 4E), which also presents difference at the DNA methylation and expression levels (Figure 3G). We observed an increase in the expression of *ABCA1* at 12h. LXR is an agonist-activated factor [66], therefore we also checked the expression of the enzyme cholesterol 25-hydroxylase (*CH25H*), as being the one that metabolizes cholesterol into 25HC, an endogenous LXR agonist [67]. Again, at 12h there was already increased expression of this enzyme and, therefore potential accumulation of the endogenous LXR agonist (Figure 4E).

To further investigate whether the RA-driven changes are LXR mediated, we differentiated MOs into DC in the presence of a specific LXR agonist (GW3965). We confirm efficacy of this agonist by the expression of different LXR targets (Supp. Figure 4E). We also used an RXR agonist (LG268), as RXR agonist has been shown to repress inflammatory genes. Transcriptional analysis of *IRF4*, *IRF8*, and *MAFB* revealed that the RXR agonism mimics the changes induced by RA, downregulating *IRF4* and upregulating *IRF8* and *MAFB* (Figure 4F). At the cell surface marker level, the RXR agonist, in contrast to the

LXR agonist alone, replicated RA-induced changes, including increased expression of macrophage markers (CD14, CD163, and CD206) and decreased expression of DC markers (CD1a) (Figure 4G). Importantly, DC differentiated with the RXR agonist exhibited an immunosuppressive phenotype, akin to RA treatment, whereas the LXR agonist alone did not induce such effects (Figure 4H). Interestingly, the RXR agonist elicited similar effects on DC at the TF level, leading to RXR α downregulation and increased LXR α expression, and has no effects on RXR β (Figure 4I). These results suggest that the pharmacological activation of LXR alone is not capable of mimicking the immunosuppressive effects of RA, and that both simultaneous RXR α downregulation and LXR induction are important for the immunosuppressive effect, suggesting a preference for LXR α to bind RXR β , forming an alternative heterodimer to promote different changes.

Figure 4



(See figure legend on the next page.)

Figure 4. (A) Discriminant regulon expression analysis (DoRothEA) of iDC_{RA} vs iDC comparison. Only transcription factors with FDR<0.05 are shown. NES of transcription factor expression are depicted. (B) Normalized expression (z-score) of NR1H3 (LXR α) from the RNAseq data (n=4). (C) Western blot of retinoic acid receptor (RAR), retinoic X receptor (RXR), peroxisome proliferative activated receptor, gamma (PPAR γ) and liver X receptor (LXR). β actin proteins were used as loading controls. (D, E) mRNA kinetics expression of LXR α , LXR β , ABCA1 and Ch25h genes (n=3) obtained from RT-pPCR. (F) Box-plot representation of gene expression obtained from qRT-PCR and (G) bar-plots of surface marker expression represented as Median Fluorescence Intensity (MFI) on iDC differentiated under the treatment with retinoic acid (RA), agonist of LXR (GW3965) and agonist of RXR (LG268) (n=3). (H) iDC differentiated under the treatment with RA, GW3965 and LG268, were co-cultured with CD8+ cells for 4 days. The final CFSE signal of CD8+ cells is shown. CD8+ with only CD3/CD28 T-activator beads (C+) or alone (C-) are also shown (n=3). (I) Western blot of LXR α , RXR α , RXR β and RAR α differentiated under the treatment with RA, GW3965 and LG268. Lamin β proteins were used as loading controls. (* P < 0.05, **P<0.01, ***P<0.005).

LXR α regulates the expression of VSIG4, promoting immunosuppression

Our initial attempts to solely activate LXR with a synthetic agonist failed to replicate the effects observed with RA alone. To further elucidate the dual impact of RA and LXR activation, we employed an LXR antagonist (GSK2033) to inhibit LXR functionality. The addition of the LXR antagonist led to a decrease in the expression of ABCA1, a well-established LXR target and LXR α (NR1H3) itself (Figure 5A). Interestingly, the use of the LXR antagonist reversed the suppressive phenotype induced by RA (Figure 5B), unlike the combined addition of RA and the LXR agonist, which maintained the suppressive phenotype (Supp. Figure 5A).

With these conditions, we performed RNAseq and observed that most of the genes that were upregulated under the treatment with RA were not upregulated by only adding the agonist of LXR (DC+Ag). However, they underwent a more marked upregulation when the agonist was added together with RA (RA+Ag). In parallel, these genes were downregulated when the antagonist was added together with RA (RA+Ant). For other retinoic acid

related receptors ($RAR\alpha$, $RAR\beta$, $RAR\gamma$, $RXR\alpha$, $RXR\beta$, $PPAR\gamma$), they were still downregulated when the antagonist was added together with RA (Supp. Figure 5B). We noticed that one of the genes downregulated in the RA+Ant vs. RA comparison was *VSIG4* (Supp. Figure 5C, Supp. Table 4), being one of the genes more upregulated in response to RA exposure (Figure 3A).

As shown above, both *VSIG4* and *IL2RA* (CD25) were upregulated under RA treatment, and they caught our attention due to their involvement in immune tolerance regulation through the control of regulatory T cells (68, 69). Furthermore, a recent paper describes a $IL2RA^+ VSIG4^+$ tumor-associated macrophage as key subpopulation of the immunosuppressive microenvironment [39]. To assess whether the suppression was mediated by *VSIG4*, two different anti-*VSIG4* antibody were introduced during the suppression assay. Intriguingly, the inclusion of the antibody (Ab) decrease the suppression capabilities of iDC_{RA} (Supp. Figure 5D). These result supported a positive relationship between *VSIG4* expression and the acquisition of immunosuppressive capabilities.

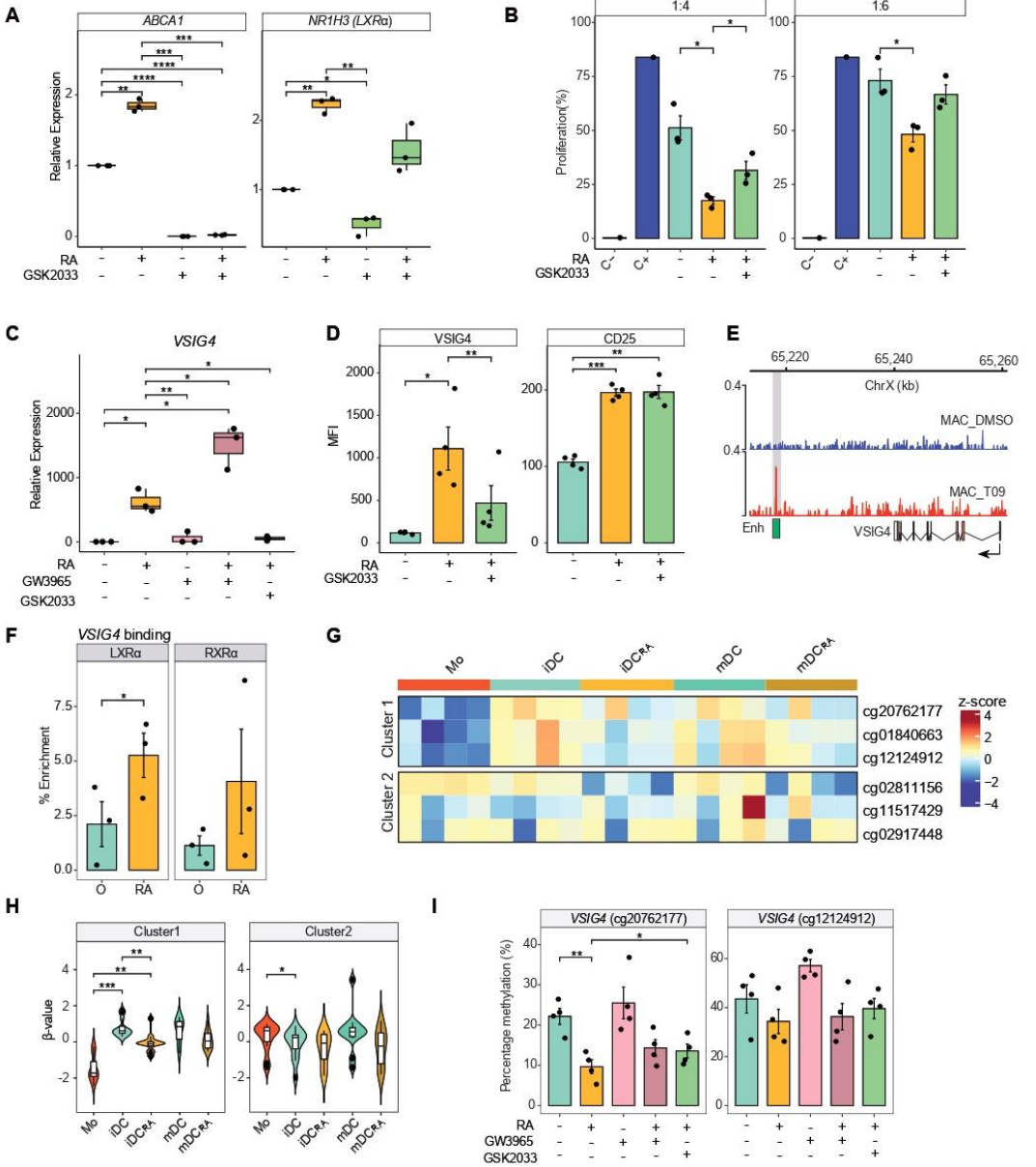
We then examined the relationship between $LXR\alpha$ and *VSIG4* in relation to immune suppression. Notably, *VSIG4* was specifically upregulated over time in the presence of RA, with expression levels being noticeable as early as 12h (Supp. Figure 5E). Subsequent RT-qPCR analysis of *VSIG4* expression under treatment with LXR agonist and antagonist confirmed the pattern observed in the RNAseq. The LXR agonist alone failed to induce *VSIG4* and *IL2RA* (CD25) production, but in combination with RA, it led to greater expression compared to RA alone. Conversely, the LXR antagonist, combined with RA, abolished *VSIG4* and *IL2RA* (CD25) expression (Figure 5C, Supp. Figure 5F). These trends were further corroborated at the protein level,

however, the addition of the antagonist failed to revert the expression of IL2RA (CD25), although the simultaneous addition of RA and the LXR agonist also induced a higher expression (Figure 5D and Supp. Figure 5G).

In addition, to investigate into the regulatory mechanisms of LXR α , we used public CHIP-seq datasets to analyse LXR α binding on human macrophages differentiated in the presence of a pan-LXR agonist To901317 [70]. Our analysis identified a binding motif for LXR α in a proximal zone of the *VSIG4* gene (Figure 5E). Subsequently, qPCR primers were designed, and our CHIP-qPCR experiments confirmed increased LXR α binding to this region in iDC_{RA} (Figure 5F).

To further characterize whether *VSIG4* expression is epigenetically regulated, we analyzed the DNA methylation status of the identified CpG sites annotated to the *VSIG4* gene. We determined that three CpGs were specifically unmethylated in DC_{RA} (Figure 5G and 5H). Finally, we performed pyrosequencing to assess the impact of LXR agonist or antagonist addition on these CpGs. A decrease in the DNA methylation levels was observed in DC differentiated in the presence of RA and this was partially reverted by the addition of the LXR antagonist, however, an increase in DNA methylation was not observed for the treatment with the LXR agonist (Figure 5I). These data support the relevance of LXR on the epigenetic *VSIG4* regulation.

Figure 5



(See figure legend on the next page.)

Figure 5. (A) Box-plot representation of mRNA expression of ABCA1 and NR1H3 (LXR α) on iDC differentiated under the treatment with retinoic acid (RA), agonist of LXR (GW3965) and antagonist of LXR (GSK2033) (n=3). (B) iDC differentiated under the treatment with RA and antagonist of LXR (GSK2033) were co-cultured with CD8+ cells for 4 days. The final CFSE signal of CD8+ cells is shown. CD8+ with only CD3/CD28 T-activator beads (C+) or alone (C-) are also shown (n=3). (C) Box-plot representation of VSIG4 expression obtained from qRT-PCR on iDC differentiated under the treatment with RA, GW3965 and GSK2033. (D) Bar-plots of surface marker expression represented as Median Fluorescence Intensity (MFI) on iDCs differentiated under the treatment with RA and GSK2033. (E) Representation of the LXR α ChIP-seq signal (BPMs), obtained from public data base (71) close to the VSIG4 genes. Data was generated on macrophages (MAC) differentiated under the treatment or not with another LXR α agonist, To901317 (MAC_DMSO and MAC_To9 respectively). (F) ChIP signal of LXR α binding on a region associated with VSIG4 on iDC differentiated under the treatment or not treated with RA. The RT-qPCR signal relative to the ChIP input is shown (n = 3). (G, H) Scaled DNA methylation (z-score) heatmap and violin plot of DMPs associated with VSIG4 summarizing the distribution of DNA methylation levels per cell type and cluster. (I) DNA methylation measured by bisulfite pyrosequencing on RA, GW3965 and GSK2033 treated iDCs. (* P < 0.05, **P<0.01, ***P<0.005).

LXR α and VSIG4 are co-expressed on tumor resident and colon macrophages

To investigate the potential LXR-mediated regulation of VSIG4 in an *in vivo* context, particularly within the TME, a reanalysis of a single-cell RNAseq (scRNAseq) anaplastic thyroid cancer (ATC) dataset was performed. Notably, in such study, it was described a VSIG4+ tumor-associated macrophage as a key subpopulation of the immunosuppressive microenvironment [39]. An initial general clustering gave us diverse cellular populations within the TME, including monocytes, macrophages, and DC (Supp. Figure 6A). Given the specific interest in the myeloid component, a subsequent reanalysis of this population was performed obtaining a more refined myeloid clustering that includes the cells that are only present in ATC patients (ATAM). (Figure 6A). Within these clusters, macrophages emerged as the primary cell type expressing VSIG4 and IL2RA. Concurrently, an analysis of LXR α (NR1H3) expression in this myeloid population revealed that, once again, macrophages

were the predominant cell type expressing this gene. Furthermore, the LXR target, *ABCA1* was also co-expressed on cells expressing *VSIG4*. (Figure 6B). The identification of cells expressing *VSIG4* revealed their predominant presence in ATC patients (Figure 6C). Interestingly, we observed an enrichment on the macrophages in co-expressing of both *VSIG4* and *LXR α* , suggesting a potential role of *LXR α* in the regulation of *VSIG4* expression within this specific TME context (Figure 6D).

Moreover, to elucidate the context in which RA promotes LXR-mediated *VSIG4* expression, we conducted a reanalysis of another scRNAseq dataset comprising diverse myeloid cell data from various studies [40]. We selected only myeloid cells derived from barrier tissues such as the colon, skin, stomach, and liver, including both healthy and cancerous states, with a particular emphasis on the biological role of RA [12]. The resulting clustering revealed a total of 14 clusters, each representing distinct myeloid cell subpopulations (Figure 6E). We then examined the expression profiles of *VSIG4*, *NR1H3*, *ABCA1*, and *IL2RA* within each cluster, identifying two macrophage subtypes characterized by elevated expression of all those genes and concurrent downregulation of *RXR α* (*RXRA*) (Figure 6F). Our analysis delineates the role of RA in mediating the immunosuppressive effects of LXR, where *RXR α* downregulation is one of the outcomes of the RA treatment. Lastly, we observed an enrichment of these specific macrophage clusters in both healthy and cancer colon tissues, underscoring the notion that vitamin A mediated immunosuppression in barrier tissues is orchestrated through the *VSIG4* pathway (Supp. Figure 6B).

Figure 6

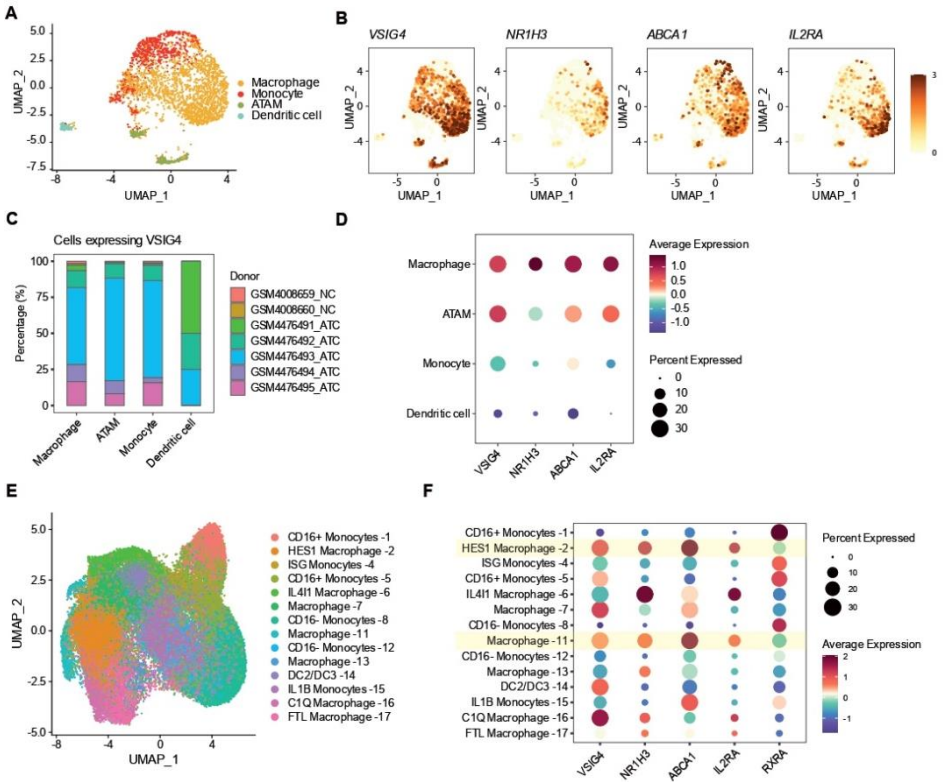


Figure 6. (A, E) UMAP visualization showing the immune cell populations identified from Louvain clustering and cell-specific marker gene expression. (B) Feature plots of expression distribution for selected genes, including VSIG4, NR1H3, ABCA1 and IL2RA. (C) Bar-plot plot representing the percentage of each cell types in the different tissues. (D, F) Dot plot representing the expression of selected genes on each cell population.

DISCUSSION

In this study, we demonstrate that RA induces an immunosuppressive phenotype in DCs together with the acquisition of macrophage-like features. Previous work has already defined that RA accumulation is implicated in the generation of an immunosuppressive milieu in the TME [33], where monocytes preferentially differentiate into immunosuppressive macrophages. We also show that the DNA methylation changes promoted by RA are associated with gene expression changes related to the establishment of this new phenotype. Furthermore, this study demonstrates that the immunosuppressive effects of RA are mediated, at least in part, by LXR α and the degradation of RXR α [23, 24, 71]. The distinct responses observed with LXR and RXR agonists suggest a nuanced interplay between these receptors and the necessity of RXR α downregulation, among other things, for LXR α to exert its immunomodulatory function. Since LXR α needs to promote transcription of specific target genes, it is feasible that LXR α preferentially heterodimerizes with RXR β upon RA treatment, since we did not observe the downregulation of this RXR subtype. Specifically, this study provides some insights into how LXR α epigenetically regulates VSIG4 expression that promotes immunosuppression. One possible explanation is that LXR α -RXR β dimer positively regulates VSIG4 and when RA-mediated downregulation of RXR α occurs, the LXR α -RXR β dimer is favoured and therefore the transactivation of VSIG4 is produced. This provides a novel insight into the molecular mechanisms governing RA-mediated immunosuppression.

Consistent with our findings, previous studies have shown that vitamin A mediates the conversion of monocyte-derived macrophages into tissue-resident macrophages during alternative activation [9, 33], or the expression of

anti-inflammatory cytokines like TGF- β [72, 73]. Nevertheless, none of these studies have addressed the gene regulatory mechanisms governing these observed alterations. In this study, we have determined that RA suppresses the expression of key TFs, including IRF4, STAT6, and NF- κ B(p-65), which play pivotal roles in cDC differentiation [74], moDC polarization [44], and the regulation of proinflammatory gene expression [75], respectively. These changes were also observed at DNA methylation level, confirming the key play of epigenetics in the blockade of the differentiation process and inflammation.

The functional correlation between DNA demethylation and gene expression has undergone comprehensive investigation across diverse biological contexts [6, 76]. In the present study, a notable observation was the enhanced expression of DNMT3A as a result of the treatment with RA. DNMT3A holds a pivotal position among epigenetic enzymes, being responsible for the de novo methylation [77]. This enzyme plays a critical role in hematopoietic differentiation and anti-inflammatory processes [49, 78]. The intricate involvement of DNMT3A in both responses underscores its significance in modulating immune responses and highlights its potential as a key player in the observed alterations in DNA methylation regulation. This association suggests that the observed increase in DNMT3A expression in our study may potentially shift the immune function from a promoting inflammation to an immunosuppressive phenotype. Further investigations into the specific impact of DNMT3A upregulation on immune cell phenotypes and functions are warranted to elucidate its precise role in the context of the observed changes in DNA methylation patterns.

One of the effects that we observed in DCs differentiated in the presence of RA was the decrease of the RAR and RXR protein levels, which could be

attributed in part to degradation, as described in previous studies [24, 79, 80]. One of our key findings is the upregulation of LXR under the treatment with RA [81]. It is likely that treatment with RA results in the production of endogenous oxysterols, such as 25-HC. We propose that 25-HC acts as an endogenous LXR agonist, given that RA induces the expression of the enzyme that produce this oxysterol, CH₂₅H [82]. Further studies in this regard are needed to better understand this RA-induced LXR expression.

LXR activity is crucially involved in cellular cholesterol metabolism in most tissues [83] as well as controlling inflammation in diverse cell types such as macrophages [84], however the resulting response may vary from anti-inflammatory to pro-inflammatory. In some studies, it was defined that LXRs promote an anti-inflammatory response or inhibits inflammation, as we have observed in this study [85–90]. Nevertheless, it has also been reported that the activation of LXR exacerbates inflammatory responses in human monocytes, DC and in a mouse arthritis model [30, 91], and that agonist induced LXR activation elicits antitumor immune activity [31]. It has been described the high activity of LXR on triple-negative breast cancer and that the inhibition of LXR induces immune-mediated tumour clearance through stimulation of cytotoxic T cells [92]. However, neither the specific effects of LXR α or the associated epigenetic changes have been previously defined on DCs. Nevertheless, it is complicated to discriminate whether the effects are driven by LXR α or LXR β as they both share target genes. We observed the RA-dependent downregulation of pro-inflammatory cytokines like IL-6 and TNF- α , as some studies have demonstrated the ability of LXRs to inhibit the signal-dependent activation of NF- κ B. LXR also inhibits the signal dependent activation of TFs such as STATs and AP1 family members, as we have determined in DCs differentiated in the

presence of RA [28, 93, 94]. Similar to other TFs, like glucocorticoid receptors (GR) and PPAR, LXR ligands can inhibit the expression of genes induced by LPS/TLR₄ signaling in macrophages [95]. Moreover, a recent study has reported that the administration of an LXR agonist promotes remodelling of atherosclerotic lesions in murine inflammatory arthritis, partly by decreasing the expression of these cytokines [96]. In other studies, it has been demonstrated that the TME promoted the expression of LXR α , and this inhibited the expression of CCR7, important for DC migration, dampening the antitumor response [18, 97, 98].

There are several ways in which DC could promote immunosuppression, including the expression of anti-inflammatory cytokines like IL-10 or TGF- β , upregulation of PD-L1 or induction of anergic T cells by downregulating co-stimulatory molecules and MHCII, among others. In this regard, previous investigations have delineated diverse mechanisms through which RA-treated DCs facilitate immunosuppression. These mechanisms include the induction of a more immature phenotype [99], the upregulation of TGF- β expression [100], and the enhancement of IL-10 expression by T cells [54]. However, in this study we have focused on a recently identified membrane protein, VSIG4, known to induce immunosuppression through direct cell contact [101, 102]. We have described that RA, accumulated in the TME, promotes the expression of VSIG4, as do other molecules like IL-10, IL-6, dexamethasone or Vitamin D (103–105). Notably, in our lab, we have previously described the epigenetic regulation of DC differentiation into tolerogenic phenotypes by dexamethasone [63] and Vitamin D [64]. Furthermore, we observed the LXR-dependent regulation of IL2RA (CD25), a surface protein expressed at high levels by Treg cells. The CD25 protein is used by Treg to

preferentially capture IL-2, preventing binding to conventional CD8⁺ T cells, thus preventing their proliferation. However, the effects on myeloid cells are poorly understood.

VSIG4 has been previously reported to be exclusively expressed on the surface of a specific subset of tissue-resident macrophages [106–108]. The predominant expression of VSIG4 on tissue-resident macrophages aligns with the observed shift towards an alveolar macrophage phenotype induced by RA treatment in our study. This correlation is noteworthy, as we also observed that VSIG4-expressing macrophages have been implicated in suppressing anti-tumor immune responses [39, 109, 110]. Hence, the upregulation of LXR α expression by RA, and its subsequent regulation of VSIG4, suggests a potential mechanism by which RA contributes to immunosuppression in the microenvironment, thus facilitating cancer progression. Additionally, previous investigations into the expression of VSIG4 in tissue-resident macrophages have revealed postnatal environmental influences [52]. This emphasizes the dynamic interplay between environmental factors, epigenetic regulation, and VSIG4-mediated immunosuppression in the tumor microenvironment.

In conclusion, our study elucidates the intricate interplay among RA, LXR α , classical RARs, and VSIG4, providing insight into the molecular mechanisms underlying the immunosuppressive properties of DCs mediated by RA. Further investigations into the crosstalk between RA signaling, epigenetic remodelling, and immune regulation are necessary for a comprehensive understanding of these complex processes.

ACKNOWLEDGEMENTS

We thank CERCA Programme/Generalitat de Catalunya and the Josep Carreras Foundation for institutional support. E.B. was funded by the Spanish Ministry of Science and Innovation (PID2020-117212RB-I00; AEI/10.13039/501100011033).

AUTHOR CONTRIBUTIONS

G.G-T. and E.B. conceived and designed the study; G.G.-T., L-L, L-C. and N.V. performed experiments; G. G-T. and C.L.C. performed the bioinformatic analyses; A.C. and A.F.V. provided some reagents; G.G-T., E.B., A.C., A.F.V. and A.L.C. participated in discussions and interpreting the results; G.G-T and E.B. wrote the manuscript.

Declaration of generative AI and AI-assisted technologies in the writing process

During the preparation of this work the author(s) used ChatGPT in order to check grammar. After using this tool/service, the author(s) reviewed and edited the content as needed and take(s) full responsibility for the content of the publication.

DECLARATION OF INTERESTS

There are no conflicts of interests.

REFERENCES

1. Wculek,S.K., Cueto,F.J., Mujal,A.M., Melero,I., Krummel,M.F. and Sancho,D. (2020) Dendritic cells in cancer immunology and immunotherapy. *Nat. Rev. Immunol.*, 20, 7–24.
2. Morante-Palacios,O., Fondelli,F., Ballestar,E. and Martínez-Cáceres,E.M. (2021) Tolerogenic Dendritic Cells in Autoimmunity and Inflammatory Diseases. *Trends Immunol.*, 42, 59–75.
3. Zanna,M.Y., Yasmin,A.R., Omar,A.R., Arshad,S.S., Mariatulqabtiah,A.R., Nur-Fazila,S.H. and Mahiza,M.I.N. (2021) Review of Dendritic Cells, Their Role in Clinical Immunology, and Distribution in Various Animal Species. *Int. J. Mol. Sci.*, 22.
4. Álvarez-Errico,D., Vento-Tormo,R., Sieweke,M. and Ballestar,E. (2015) Epigenetic control of myeloid cell differentiation, identity and function. *Nat. Rev. Immunol.*, 15, 7–17.
5. Luo,C., Hajkova,P. and Ecker,J.R. (2018) Dynamic DNA methylation: In the right place at the right time. *Science*, 361, 1336–1340.
6. Moore,L.D., Le,T. and Fan,G. (2013) DNA methylation and its basic function. *Neuropsychopharmacology*, 38, 23–38.
7. Zhang,X., Su,J., Jeong,M., Ko,M., Huang,Y., Park,H.J., Guzman,A., Lei,Y., Huang,Y.-H., Rao,A., et al. (2016) DNMT3A and TET2 compete and cooperate to repress lineage-specific transcription factors in hematopoietic stem cells. *Nat. Genet.*, 48, 1014–23.
8. Sun,C.-M., Hall,J.A., Blank,R.B., Bouladoux,N., Oukka,M., Mora,J.R. and Belkaid,Y. (2007) Small intestine lamina propria dendritic cells promote de novo generation of Foxp3 T reg cells via retinoic acid. *J. Exp. Med.*, 204, 1775–85.
9. Gundra,U.M., Girgis,N.M., Gonzalez,M.A., San Tang,M., Van Der Zande,H.J.P., Lin,J.-D., Ouimet,M., Ma,L.J., Poles,J., Vozhilla,N., et al. (2017) Vitamin A mediates conversion of monocyte-derived macrophages into tissue-resident macrophages during alternative activation. *Nat. Immunol.*, 18, 642–653.
10. Johansson-Lindbom,B. and Agace,W.W. (2004) Vitamin A helps gut T cells find their way in the dark. *Nat. Med.*, 10, 1300–1.
11. Iwata,M. (2009) Retinoic acid production by intestinal dendritic cells and its role in T-cell trafficking. *Semin. Immunol.*, 21, 8–13.
12. Erkelens,M.N. and Mebius,R.E. (2017) Retinoic Acid and Immune Homeostasis: A Balancing Act. *Trends Immunol.*, 38, 168–180.
13. Ghyselinck,N.B. and Duester,G. (2019) Retinoic acid signaling pathways. *Development*, 146.
14. Nefedova,Y., Fishman,M., Sherman,S., Wang,X., Beg,A.A. and Gibrilovich,D.I. (2007) Mechanism of all-trans retinoic acid effect on tumor-associated myeloid-derived suppressor cells. *Cancer Res.*, 67, 11021–8.
15. Martínez-Blanco,M., Lozano-Ojalvo,D., Pérez-Rodríguez,L., Benedé,S., Molina,E. and López-Fandiño,R. (2021) Retinoic Acid Induces Functionally Suppressive Foxp3+RORγt+ T Cells In Vitro. *Front. Immunol.*, 12, 675733.
16. Hill,J.A., Hall,J.A., Sun,C.-M., Cai,Q., Ghyselinck,N., Chambon,P., Belkaid,Y., Mathis,D. and Benoist,C. (2008) Retinoic acid enhances Foxp3 induction indirectly by relieving inhibition from CD4+CD44hi Cells. *Immunity*, 29, 758–70.
17. Vellozo,N.S., Pereira-Marques,S.T., Cabral-Piccin,M.P., Filardey,A.A., Ribeiro-Gomes,F.L., Rigoni,T.S., DosReis,G.A. and Lopes,M.F. (2017) All-Trans Retinoic Acid

- Promotes an M1- to M2-Phenotype Shift and Inhibits Macrophage-Mediated Immunity to *Leishmania major*. *Front. Immunol.*, 8, 1560.
18. Rivera,C.A., Randrian,V., Richer,W., Gerber-Ferder,Y., Delgado,M.-G., Chikina,A.S., Frede,A., Sorini,C., Maurin,M., Kammoun-Chaari,H., et al. (2022) Epithelial colonization by gut dendritic cells promotes their functional diversification. *Immunity*, 55, 129-144.e8.
 19. Bhattacharya,N., Yuan,R., Prestwood,T.R., Penny,H.L., DiMaio,M.A., Reticker-Flynn,N.E., Krois,C.R., Kenkel,J.A., Pham,T.D., Carmi,Y., et al. (2016) Normalizing Microbiota-Induced Retinoic Acid Deficiency Stimulates Protective CD8(+) T Cell-Mediated Immunity in Colorectal Cancer. *Immunity*, 45, 641-655.
 20. Takahashi,H., Kanno,T., Nakayamada,S., Hirahara,K., Sciumè,G., Muljo,S.A., Kuchen,S., Casellas,R., Wei,L., Kanno,Y., et al. (2012) TGF- β and retinoic acid induce the microRNA miR-10a, which targets Bcl-6 and constrains the plasticity of helper T cells. *Nat. Immunol.*, 13, 587-95.
 21. le Maire,A., Alvarez,S., Shankaranarayanan,P., Lera,A.R. de, Bourguet,W. and Gronemeyer,H. (2012) Retinoid receptors and therapeutic applications of RAR/RXR modulators. *Curr. Top. Med. Chem.*, 12, 505-27.
 22. le Maire,A., Teyssier,C., Balaguer,P., Bourguet,W. and Germain,P. (2019) Regulation of RXR-RAR Heterodimers by RXR- and RAR-Specific Ligands and Their Combinations. *Cells*, 8.
 23. Zhu,J., Gianni,M., Kopf,E., Honoré,N., Chelbi-Alix,M., Koken,M., Quignon,F., Rochette-Egly,C. and de Thé,H. (1999) Retinoic acid induces proteasome-dependent degradation of retinoic acid receptor alpha (RARalpha) and oncogenic RARalpha fusion proteins. *Proc. Natl. Acad. Sci. U. S. A.*, 96, 14807-12.
 24. Tsai,J.M., Aguirre,J.D., Li,Y.-D., Brown,J., Focht,V., Kater,L., Kempf,G., Sandoval,B., Schmitt,S., Rutter,J.C., et al. (2023) UBR5 forms ligand-dependent complexes on chromatin to regulate nuclear hormone receptor stability. *Mol. Cell*, 83, 2753-2767.e10.
 25. Lee,S.D. and Tontonoz,P. (2015) Liver X receptors at the intersection of lipid metabolism and atherogenesis. *Atherosclerosis*, 242, 29-36.
 26. El-Hajjaji,F.-Z., Oumeddour,A., Pommier,A.J.C., Ouvrier,A., Viennois,E., Dufour,J., Caira,F., Drevet,J.R., Volle,D.H., Baron,S., et al. (2011) Liver X receptors, lipids and their reproductive secrets in the male. *Biochim. Biophys. Acta*, 1812, 974-81.
 27. Schultz,J.R., Tu,H., Luk,A., Repa,J.J., Medina,J.C., Li,L., Schwendner,S., Wang,S., Thoolen,M., Mangelsdorf,D.J., et al. (2000) Role of LXRs in control of lipogenesis. *Genes Dev.*, 14, 2831-8.
 28. Jakobsson,T., Treuter,E., Gustafsson,J.-Å. and Steffensen,K.R. (2012) Liver X receptor biology and pharmacology: new pathways, challenges and opportunities. *Trends Pharmacol. Sci.*, 33, 394-404.
 29. Kiss,M., Czimmerer,Z. and Nagy,L. (2013) The role of lipid-activated nuclear receptors in shaping macrophage and dendritic cell function: From physiology to pathology. *J. Allergy Clin. Immunol.*, 132, 264-86.
 30. González de la Aleja,A., Herrero,C., Torres-Torresano,M., de la Rosa,J.V., Alonso,B., Capa-Sardón,E., Muller,I.B., Jansen,G., Puig-Kröger,A., Vega,M.A., et al. (2022) Activation of LXR Nuclear Receptors Impairs the Anti-Inflammatory Gene and Functional Profile of M-CSF-Dependent Human Monocyte-Derived Macrophages. *Front. Immunol.*, 13, 835478.

31. Tavazoie,M.F., Pollack,I., Tanqueco,R., Ostendorf,B.N., Reis,B.S., Gonsalves,F.C., Kurth,I., Andreu-Agullo,C., Derbyshire,M.L., Posada,J., et al. (2018) LXR/ApoE Activation Restricts Innate Immune Suppression in Cancer. *Cell*, 172, 825-840.e18.
32. Nazih,H. and Bard,J.M. (2020) Cholesterol, Oxysterols and LXRs in Breast Cancer Pathophysiology. *Int. J. Mol. Sci.*, 21.
33. Devalaraja,S., To,T.K.J., Folkert,I.W., Natesan,R., Alam,M.Z., Li,M., Tada,Y., Budagyan,K., Dang,M.T., Zhai,L., et al. (2020) Tumor-Derived Retinoic Acid Regulates Intratumoral Monocyte Differentiation to Promote Immune Suppression. *Cell*, 180, 1098-1114.e16.
34. Faul,M.M., Ratz,A.M., Sullivan,K.A., Trankle,W.G. and Winneroski,L.L. (2001) Synthesis of novel retinoid X receptor-selective retinoids. *J. Org. Chem.*, 66, 5772-82.
35. Carvalho,B.S. and Irizarry,R.A. (2010) A framework for oligonucleotide microarray preprocessing. *Bioinformatics*, 26, 2363-7.
36. Bray,N.L., Pimentel,H., Melsted,P. and Pachter,L. (2016) Near-optimal probabilistic RNA-seq quantification. *Nat. Biotechnol.*, 34, 525-7.
37. Liao,Y., Smyth,G.K. and Shi,W. (2014) featureCounts: an efficient general purpose program for assigning sequence reads to genomic features. *Bioinformatics*, 30, 923-30.
38. Love,M.I., Huber,W. and Anders,S. (2014) Moderated estimation of fold change and dispersion for RNA-seq data with DESeq2. *Genome Biol.*, 15, 550.
39. Pan,Z., Bao,L., Lu,X., Hu,X., Li,L., Chen,J., Jin,T., Zhang,Y., Tan,Z., Huang,P., et al. (2023) IL2RA+VSIG4+ tumor-associated macrophage is a key subpopulation of the immunosuppressive microenvironment in anaplastic thyroid cancer. *Biochim. Biophys. acta. Mol. basis Dis.*, 1869, 166591.
40. Mulder,K., Patel,A.A., Kong,W.T., Piot,C., Halitzki,E., Dunsmore,G., Khalilnezhad,S., Irac,S.E., Dubuisson,A., Chevrier,M., et al. (2021) Cross-tissue single-cell landscape of human monocytes and macrophages in health and disease. *Immunity*, 54, 1883-1900.e5.
41. Hur,J., Danes,L., Hsieh,J.-H., McGregor,B., Krout,D. and Auerbach,S. (2018) Tox21 Enricher: Web-based Chemical/Biological Functional Annotation Analysis Tool Based on Tox21 Toxicity Screening Platform. *Mol. Inform.*, 37, e1700129.
42. Jalili,V., Matteucci,M., Masseroli,M. and Morelli,M.J. (2015) Using combined evidence from replicates to evaluate ChIP-seq peaks. *Bioinformatics*, 31, 2761-9.
43. Hall,J.A., Grainger,J.R., Spencer,S.P. and Belkaid,Y. (2011) The role of retinoic acid in tolerance and immunity. *Immunity*, 35, 13-22.
44. Goudot,C., Coillard,A., Villani,A.-C., Gueguen,P., Cros,A., Sarkizova,S., Tang-Huau,T.-L., Bohec,M., Baulande,S., Hacoheh,N., et al. (2017) Aryl Hydrocarbon Receptor Controls Monocyte Differentiation into Dendritic Cells versus Macrophages. *Immunity*, 47, 582-596.e6.
45. Vento-Tormo,R., Company,C., Rodríguez-Ubreva,J., de la Rica,L., Urquiza,J.M., Javierre,B.M., Sabarinathan,R., Luque,A., Esteller,M., Aran,J.M., et al. (2016) IL-4 orchestrates STAT6-mediated DNA demethylation leading to dendritic cell differentiation. *Genome Biol.*, 17, 4.
46. Hassan,H.M., Kolendowski,B., Isovich,M., Bose,K., Dranse,H.J., Sampaio,A. V., Underhill,T.M. and Torchia,J. (2017) Regulation of Active DNA Demethylation through RAR-Mediated Recruitment of a TET/TDG Complex. *Cell Rep.*, 19, 1685-1697.
47. Mendes,K., Schmidhofer,S., Minderjahn,J., Glatz,D., Kiesewetter,C., Raithel,J., Wimmer,J., Gebhard,C. and Rehli,M. (2021) The epigenetic pioneer EGR2 initiates DNA demethylation in differentiating monocytes at both stable and transient binding sites. *Nat. Commun.*, 12, 1556.

48. de la Rica,L., Rodríguez-Ubrevia,J., García,M., Islam,A.B.M.M.K., Urquiza,J.M., Hernando,H., Christensen,J., Helin,K., Gómez-Vaquero,C. and Ballestar,E. (2013) PU.1 target genes undergo Tet2-coupled demethylation and DNMT3b-mediated methylation in monocyte-to-osteoclast differentiation. *Genome Biol.*, 14, 1–21.
49. Rodríguez-Ubrevia,J., Català-Moll,F., Obermajer,N., Álvarez-Errico,D., Ramirez,R.N., Company,C., Vento-Tormo,R., Moreno-Bueno,G., Edwards,R.P., Mortazavi,A., et al. (2017) Prostaglandin E2 Leads to the Acquisition of DNMT3A-Dependent Tolerogenic Functions in Human Myeloid-Derived Suppressor Cells. *Cell Rep.*, 21, 154–167.
50. Mangelsdorf,D.J. and Evans,R.M. (1995) The RXR heterodimers and orphan receptors. *Cell*, 83, 841–50.
51. Vogt,L., Schmitz,N., Kurrer,M.O., Bauer,M., Hinton,H.I., Behnke,S., Gatto,D., Sebbel,P., Beerli,R.R., Sonderegger,I., et al. (2006) VSIG4, a B7 family-related protein, is a negative regulator of T cell activation. *J. Clin. Invest.*, 116, 2817–26.
52. Yuan,X., Yang,B.-H., Dong,Y., Yamamura,A. and Fu,W. (2017) CRIg, a tissue-resident macrophage specific immune checkpoint molecule, promotes immunological tolerance in NOD mice, via a dual role in effector and regulatory T cells. *Elife*, 6.
53. Browaeys,R., Saelens,W. and Saeys,Y. (2020) NicheNet: modeling intercellular communication by linking ligands to target genes. *Nat. Methods*, 17, 159–162.
54. Bakdash,G., Vogelpoel,L.T.C., van Capel,T.M.M., Kapsenberg,M.L. and de Jong,E.C. (2015) Retinoic acid primes human dendritic cells to induce gut-homing, IL-10-producing regulatory T cells. *Mucosal Immunol.*, 8, 265–78.
55. Saini,Y., Dang,H., Livraghi-Buttrico,A., Kelly,E.J., Jones,L.C., O’Neal,W.K. and Boucher,R.C. (2014) Gene expression in whole lung and pulmonary macrophages reflects the dynamic pathology associated with airway surface dehydration. *BMC Genomics*, 15, 726.
56. Hay,S.B., Ferchen,K., Chetal,K., Grimes,H.L. and Salomonis,N. (2018) The Human Cell Atlas bone marrow single-cell interactive web portal. *Exp. Hematol.*, 68, 51–61.
57. Melms,J.C., Biermann,J., Huang,H., Wang,Y., Nair,A., Tagore,S., Katsyv,I., Rendeiro,A.F., Amin,A.D., Schapiro,D., et al. (2021) A molecular single-cell lung atlas of lethal COVID-19. *Nature*, 595, 114–119.
58. Wendisch,D., Dietrich,O., Mari,T., von Stillfried,S., Ibarra,I.L., Mittermaier,M., Mache,C., Chua,R.L., Knoll,R., Timm,S., et al. (2021) SARS-CoV-2 infection triggers profibrotic macrophage responses and lung fibrosis. *Cell*, 184, 6243–6261.e27.
59. Grant,R.A., Morales-Nebreda,L., Markov,N.S., Swaminathan,S., Querrey,M., Guzman,E.R., Abbott,D.A., Donnelly,H.K., Donayre,A., Goldberg,I.A., et al. (2021) Circuits between infected macrophages and T cells in SARS-CoV-2 pneumonia. *Nature*, 590, 635–641.
60. Segura,E., Touzot,M., Bohineust,A., Cappuccio,A., Chiocchia,G., Hosmalin,A., Dalod,M., Soumelis,V. and Amigorena,S. (2013) Human inflammatory dendritic cells induce Th17 cell differentiation. *Immunity*, 38, 336–48.
61. Chatagnon,A., Veber,P., Morin,V., Bedo,J., Triqueneaux,G., Sémon,M., Laudet,V., D’Alché-Buc,F. and Benoit,G. (2015) RAR/RXR binding dynamics distinguish pluripotency from differentiation associated cis-regulatory elements. *Nucleic Acids Res.*, 43, 4833–54.
62. Costet,P., Lalanne,F., Gerbod-Giannone,M.C., Molina,J.R., Fu,X., Lund,E.G., Gudas,L.J. and Tall,A.R. (2003) Retinoic acid receptor-mediated induction of ABCA1 in macrophages. *Mol. Cell. Biol.*, 23, 7756–66.

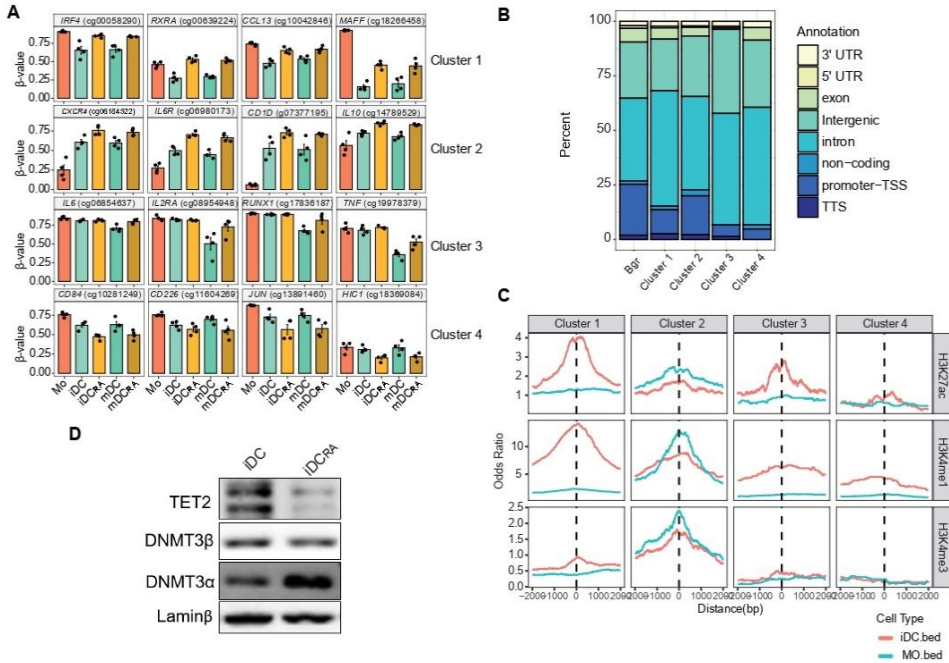
63. Morante-Palacios,O., Ciudad,L., Micheroli,R., de la Calle-Fabregat,C., Li,T., Barbisan,G., Houtman,M., Edalat,S.G., Frank-Bertoncelj,M., Ospelt,C., et al. (2022) Coordinated glucocorticoid receptor and MAFB action induces tolerogenesis and epigenome remodeling in dendritic cells. *Nucleic Acids Res.*, 50, 108–126.
64. Català-Moll,F., Ferreté-Bonastre,A.G., Godoy-Tena,G., Morante-Palacios,O., Ciudad,L., Barberà,L., Fondelli,F., Martínez-Cáceres,E.M., Rodríguez-Ubreva,J., Li,T., et al. (2022) Vitamin D receptor, STAT3, and TET2 cooperate to establish tolerogenesis. *Cell Rep.*, 38, 10244.
65. Matsuo,M. (2022) ABCA1 and ABCG1 as potential therapeutic targets for the prevention of atherosclerosis. *J. Pharmacol. Sci.*, 148, 197–203.
66. Michael,L.F., Schkeryantz,J.M. and Burris,T.P. (2005) The pharmacology of LXR. *Mini Rev. Med. Chem.*, 5, 729–40.
67. Saito,H., Tachiura,W., Nishimura,M., Shimizu,M., Sato,R. and Yamauchi,Y. (2023) Hydroxylation site-specific and production-dependent effects of endogenous oxysterols on cholesterol homeostasis: Implications for SREBP-2 and LXR. *J. Biol. Chem.*, 299, 102733.
68. Liu,B., Cheng,L., Gao,H., Zhang,J., Dong,Y., Gao,W., Yuan,S., Gong,T. and Huang,W. (2023) The biology of VSIG4: Implications for the treatment of immune-mediated inflammatory diseases and cancer. *Cancer Lett.*, 553, 215996.
69. Ohue,Y. and Nishikawa,H. (2019) Regulatory T (Treg) cells in cancer: Can Treg cells be a new therapeutic target? *Cancer Sci.*, 110, 2080–2089.
70. Feldmann,R., Fischer,C., Kodelja,V., Behrens,S., Haas,S., Vingron,M., Timmermann,B., Geikowski,A. and Sauer,S. (2013) Genome-wide analysis of LXR α activation reveals new transcriptional networks in human atherosclerotic foam cells. *Nucleic Acids Res.*, 41, 3518–31.
71. Osburn,D.L., Shao,G., Seidel,H.M. and Schulman,I.G. (2001) Ligand-dependent degradation of retinoid X receptors does not require transcriptional activity or coactivator interactions. *Mol. Cell. Biol.*, 21, 4909–18.
72. Kang,S.G., Lim,H.W., Andrisani,O.M., Broxmeyer,H.E. and Kim,C.H. (2007) Vitamin A metabolites induce gut-homing FoxP3⁺ regulatory T cells. *J. Immunol.*, 179, 3724–33.
73. Xu,Q. and Kopp,J.B. (2012) Retinoid and TGF- β families: crosstalk in development, neoplasia, immunity, and tissue repair. *Semin. Nephrol.*, 32, 287–94.
74. Ainsua-Enrich,E., Hatipoglu,I., Kadel,S., Turner,S., Paul,J., Singh,S., Bagavant,H. and Kovats,S. (2019) IRF4-dependent dendritic cells regulate CD8⁺ T-cell differentiation and memory responses in influenza infection. *Mucosal Immunol.*, 12, 1025–1037.
75. Taniguchi,K. and Karin,M. (2018) NF- κ B, inflammation, immunity and cancer: coming of age. *Nat. Rev. Immunol.*, 18, 309–324.
76. Pacis,A., Mailhot-Léonard,F., Tailleux,L., Randolph,H.E., Yotova,V., Dumaine,A., Grenier,J.-C. and Barreiro,L.B. (2019) Gene activation precedes DNA demethylation in response to infection in human dendritic cells. *Proc. Natl. Acad. Sci. U. S. A.*, 116, 6938–6943.
77. Ramabadran,R., Wang,J.H., Reyes,J.M., Guzman,A.G., Gupta,S., Rosas,C., Brunetti,L., Gundry,M.C., Tovy,A., Long,H., et al. (2023) DNMT3A-coordinated splicing governs the stem state switch towards differentiation in embryonic and haematopoietic stem cells. *Nat. Cell Biol.*, 25, 528–539.
78. Challen,G.A., Sun,D., Jeong,M., Luo,M., Jelinek,J., Berg,J.S., Bock,C., Vasanthakumar,A., Gu,H., Xi,Y., et al. (2011) Dnmt3a is essential for hematopoietic stem cell differentiation. *Nat. Genet.*, 44, 23–31.

79. Rodriguez,V., Bailey,R., Larion,M. and Gilbert,M.R. (2019) Retinoid receptor turnover mediated by sumoylation, ubiquitination and the valosin-containing protein is disrupted in glioblastoma. *Sci. Rep.*, 9, 16250.
80. Nomura,Y., Nagaya,T., Hayashi,Y., Kambe,F. and Seo,H. (1999) 9-cis-retinoic acid decreases the level of its cognate receptor, retinoid X receptor, through acceleration of the turnover. *Biochem. Biophys. Res. Commun.*, 260, 729–33.
81. Diaz,O.E., Xue,S., Luo,X., Nava,J., Appelblom,A., Morales,R.A., Das,S. and Villablanca,E.J. (2020) Retinoic acid induced cytokines are selectively modulated by liver X receptor activation in zebrafish. *Reprod. Toxicol.*, 93, 163–168.
82. Abrams,M.E., Johnson,K.A., Perelman,S.S., Zhang,L.-S., Endapally,S., Mar,K.B., Thompson,B.M., McDonald,J.G., Schoggins,J.W., Radhakrishnan,A., et al. (2020) Oxysterols provide innate immunity to bacterial infection by mobilizing cell surface accessible cholesterol. *Nat. Microbiol.*, 5, 929–942.
83. Wang,B. and Tontonoz,P. (2018) Liver X receptors in lipid signalling and membrane homeostasis. *Nat. Rev. Endocrinol.*, 14, 452–463.
84. Schulman,I.G. (2017) Liver X receptors link lipid metabolism and inflammation. *FEBS Lett.*, 591, 2978–2991.
85. A-González,N. and Castrillo,A. (2011) Liver X receptors as regulators of macrophage inflammatory and metabolic pathways. *Biochim. Biophys. Acta*, 1812, 982–94.
86. Endo-Umeda,K., Kim,E., Thomas,D.G., Liu,W., Dou,H., Yalcinkaya,M., Abramowicz,S., Xiao,T., Antonson,P., Gustafsson,J.-Å., et al. (2022) Myeloid LXR (Liver X Receptor) Deficiency Induces Inflammatory Gene Expression in Foamy Macrophages and Accelerates Atherosclerosis. *Arterioscler. Thromb. Vasc. Biol.*, 42, 719–731.
87. Thomas,D.G., Doran,A.C., Fotakis,P., Westerterp,M., Antonson,P., Jiang,H., Jiang,X.-C., Gustafsson,J.-Å., Tabas,I. and Tall,A.R. (2018) LXR Suppresses Inflammatory Gene Expression and Neutrophil Migration through cis-Repression and Cholesterol Efflux. *Cell Rep.*, 25, 3774–3785.e4.
88. Marathe,C., Bradley,M.N., Hong,C., Lopez,F., Ruiz de Galarreta,C.M., Tontonoz,P. and Castrillo,A. (2006) The arginase II gene is an anti-inflammatory target of liver X receptor in macrophages. *J. Biol. Chem.*, 281, 32197–206.
89. Li,N., Li,Y., Han,X., Zhang,J., Han,J., Jiang,X., Wang,W., Xu,Y., Xu,Y., Fu,Y., et al. (2022) LXR agonist inhibits inflammation through regulating MyD88 mRNA alternative splicing. *Front. Pharmacol.*, 13, 973612.
90. Ito,A., Hong,C., Rong,X., Zhu,X., Tarling,E.J., Hedde,P.N., Gratton,E., Parks,J. and Tontonoz,P. (2015) LXRs link metabolism to inflammation through Abca1-dependent regulation of membrane composition and TLR signaling. *Elife*, 4, e08009.
91. Fontaine,C., Rigamonti,E., Nohara,A., Gervois,P., Teissier,E., Fruchart,J.-C., Staels,B. and Chinetti-Gbaguidi,G. (2007) Liver X receptor activation potentiates the lipopolysaccharide response in human macrophages. *Circ. Res.*, 101, 40–9.
92. Carpenter,K.J., Valfort,A.-C., Steinauer,N., Chatterjee,A., Abuirqeba,S., Majidi,S., Sengupta,M., Di Paolo,R.J., Shornick,L.P., Zhang,J., et al. (2019) LXR-inverse agonism stimulates immune-mediated tumor destruction by enhancing CD8 T-cell activity in triple negative breast cancer. *Sci. Rep.*, 9, 19530.
93. Ghisletti,S., Huang,W., Ogawa,S., Pascual,G., Lin,M.-E., Willson,T.M., Rosenfeld,M.G. and Glass,C.K. (2007) Parallel SUMOylation-dependent pathways mediate gene- and signal-specific transrepression by LXRs and PPARgamma. *Mol. Cell*, 25, 57–70.
94. Pascual-García,M., Rué,L., León,T., Julve,J., Carbó,J.M., Matalonga,J., Auer,H., Celada,A., Escolà-Gil,J.C., Steffensen,K.R., et al. (2013) Reciprocal negative cross-talk

- between liver X receptors (LXRs) and STAT1: effects on IFN- γ -induced inflammatory responses and LXR-dependent gene expression. *J. Immunol.*, 190, 6520–32.
95. Ogawa,S., Lozach,J., Benner,C., Pascual,G., Tangirala,R.K., Westin,S., Hoffmann,A., Subramaniam,S., David,M., Rosenfeld,M.G., et al. (2005) Molecular determinants of crosstalk between nuclear receptors and toll-like receptors. *Cell*, 122, 707–21.
 96. Dragoljevic,D., Lee,M.K.S., Pernes,G., Morgan,P.K., Louis,C., Shihata,W., Huynh,K., Kochetkova,A.A., Bell,P.W., Mellett,N.A., et al. (2023) Administration of an LXR agonist promotes atherosclerotic lesion remodelling in murine inflammatory arthritis. *Clin. Transl. Immunol.*, 12, e1446.
 97. Villablanca,E.J., Raccosta,L., Zhou,D., Fontana,R., Maggioni,D., Negro,A., Sanvito,F., Ponzoni,M., Valentini,B., Bregni,M., et al. (2010) Tumor-mediated liver X receptor- α activation inhibits CC chemokine receptor-7 expression on dendritic cells and dampens antitumor responses. *Nat. Med.*, 16, 98–105.
 98. Hanley,T.M., Blay Puryear,W., Gummuluru,S. and Viglianti,G.A. (2010) PPAR γ and LXR signaling inhibit dendritic cell-mediated HIV-1 capture and trans-infection. *PLoS Pathog.*, 6, e1000981.
 99. Jin,C.-J., Hong,C.Y., Takei,M., Chung,S.-Y., Park,J.-S., Pham,T.-N.N., Choi,S.-J.-N., Nam,J.-H., Chung,I.-J., Kim,H.-J., et al. (2010) All-trans retinoic acid inhibits the differentiation, maturation, and function of human monocyte-derived dendritic cells. *Leuk. Res.*, 34, 513–20.
 100. Hoover,L.L., Burton,E.G., O'Neill,M.L., Brooks,B.A., Sreedharan,S., Dawson,N.A. and Kubalak,S.W. (2008) Retinoids regulate TGF β signaling at the level of Smad2 phosphorylation and nuclear accumulation. *Biochim. Biophys. Acta*, 1783, 2279–86.
 101. Li,J., Diao,B., Guo,S., Huang,X., Yang,C., Feng,Z., Yan,W., Ning,Q., Zheng,L., Chen,Y., et al. (2017) VSIG4 inhibits proinflammatory macrophage activation by reprogramming mitochondrial pyruvate metabolism. *Nat. Commun.*, 8, 1322.
 102. Lee,S.-W. (2021) VISTA Stimulation of VSIG4-Positive Macrophages Strongly Suppresses T Cell Proliferation via Excessive Nitric Oxide Production in Sepsis. *Biol. Pharm. Bull.*, 44, 1645–1652.
 103. Gorgani,N.N., Thathaisong,U., Mukaro,V.R.S., Pongpair,O., Tirimacco,A., Hii,C.S.T. and Ferrante,A. (2011) Regulation of CR1g expression and phagocytosis in human macrophages by arachidonate, dexamethasone, and cytokines. *Am. J. Pathol.*, 179, 1310–8.
 104. Small,A.G., Harvey,S., Kaur,J., Putty,T., Quach,A., Munawara,U., Perveen,K., McPhee,A., Hii,C.S. and Ferrante,A. (2021) Vitamin D upregulates the macrophage complement receptor immunoglobulin in innate immunity to microbial pathogens. *Commun. Biol.*, 4, 401.
 105. Lyu,Q., Pang,X., Zhang,Z., Wei,Y., Hong,J. and Chen,H. (2020) Microglial V-set and immunoglobulin domain-containing 4 protects against ischemic stroke in mice by suppressing TLR4-regulated inflammatory response. *Biochem. Biophys. Res. Commun.*, 522, 560–567.
 106. Helmy,K.Y., Katschke,K.J., Gorgani,N.N., Kljavin,N.M., Elliott,J.M., Diehl,L., Scales,S.J., Ghilardi,N. and van Lookeren Campagne,M. (2006) CR1g: a macrophage complement receptor required for phagocytosis of circulating pathogens. *Cell*, 124, 915–27.
 107. Gao,H., Luo,Z., Ji,Y., Tang,K., Jin,Z., Ly,C., Sears,D.D., Mahata,S. and Ying,W. (2022) Accumulation of microbial DNAs promotes to islet inflammation and β cell abnormalities in obesity in mice. *Nat. Commun.*, 13, 565.

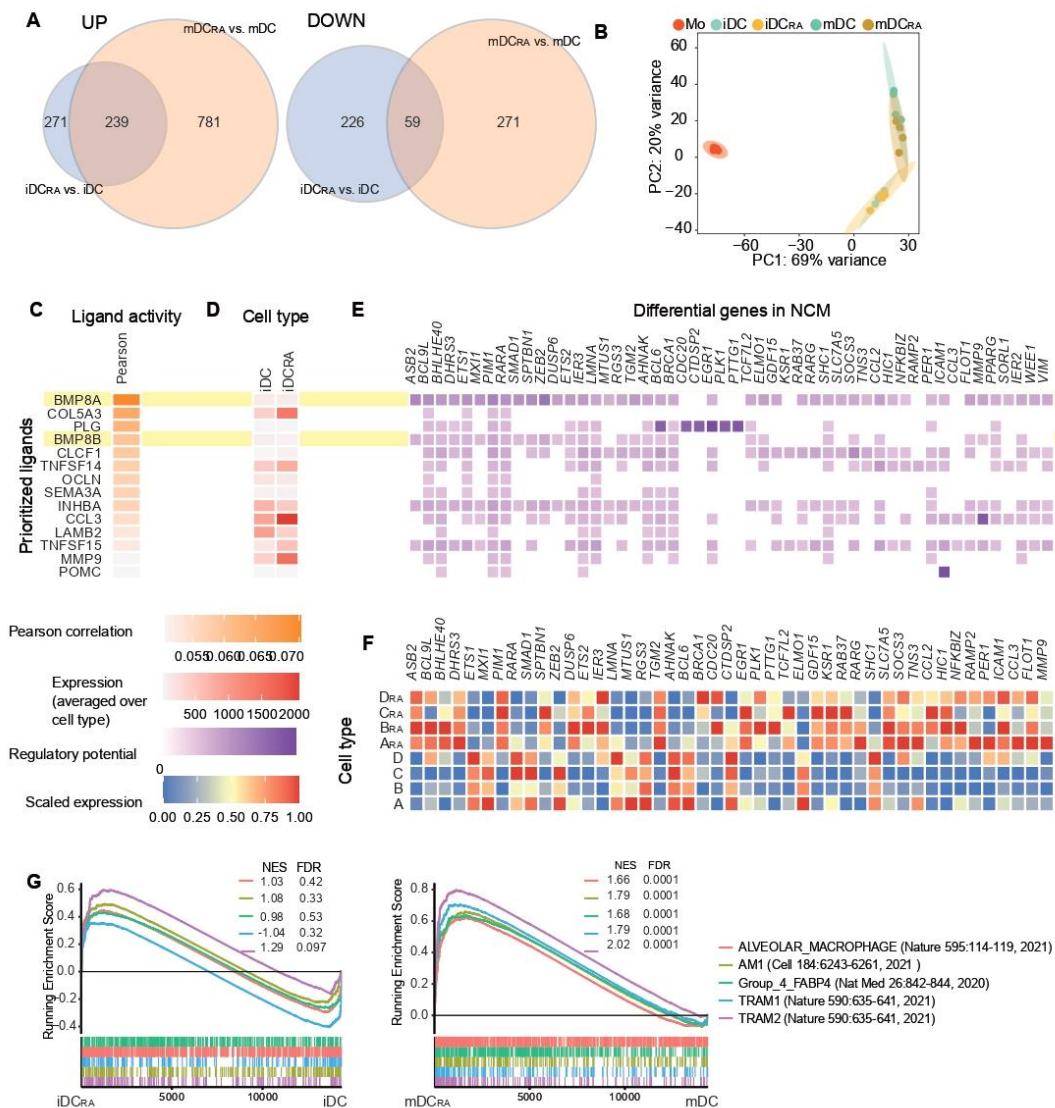
108. Lee, M.-Y., Kim, W.-J., Kang, Y.-J., Jung, Y.-M., Kang, Y.-M., Suk, K., Park, J.-E., Choi, E.-M., Choi, B.-K., Kwon, B.S., et al. (2006) Z39Ig is expressed on macrophages and may mediate inflammatory reactions in arthritis and atherosclerosis. *J. Leukoc. Biol.*, 80, 922–8.
109. Small, A.G., Al-Baghdadi, M., Quach, A., Hii, C. and Ferrante, A. (2016) Complement receptor immunoglobulin: a control point in infection and immunity, inflammation and cancer. *Swiss Med. Wkly.*, 146, w14301.
110. Chow, A., Schad, S., Green, M.D., Hellmann, M.D., Allaj, V., Ceglia, N., Zago, G., Shah, N.S., Sharma, S.K., Mattar, M., et al. (2021) Tim-4⁺ cavity-resident macrophages impair anti-tumor CD8⁺ T cell immunity. *Cancer Cell*, 39, 973–988.e9.

Supp. Figure 2



Supp. Figure 2. (A) Box-plot representation of selected CpGs (β value) from each cluster together with the nearby gene. (B) Location proportion of CpGs from each cluster in the context of CpG islands (CGIs). (C) ChIP-seq data of H3K27ac, H3K4me1 and H3K4me3 of CD14⁺ monocytes and DCs was downloaded from the BLUEPRINT database. Odds ratios of histone marks enrichment were calculated for bins of 10bp, 200bp upstream and downstream in relation to each methylation cluster. CpGs annotated in the EPIC array were used as background. (D) Western blot of DNA methylation enzymes, including DNA methyltransferase 3 alpha and beta (DNMT3A and DNMT3B) and Tet methylcytosine dioxygenase 2 (TET2). Lamin β proteins were used as loading controls.

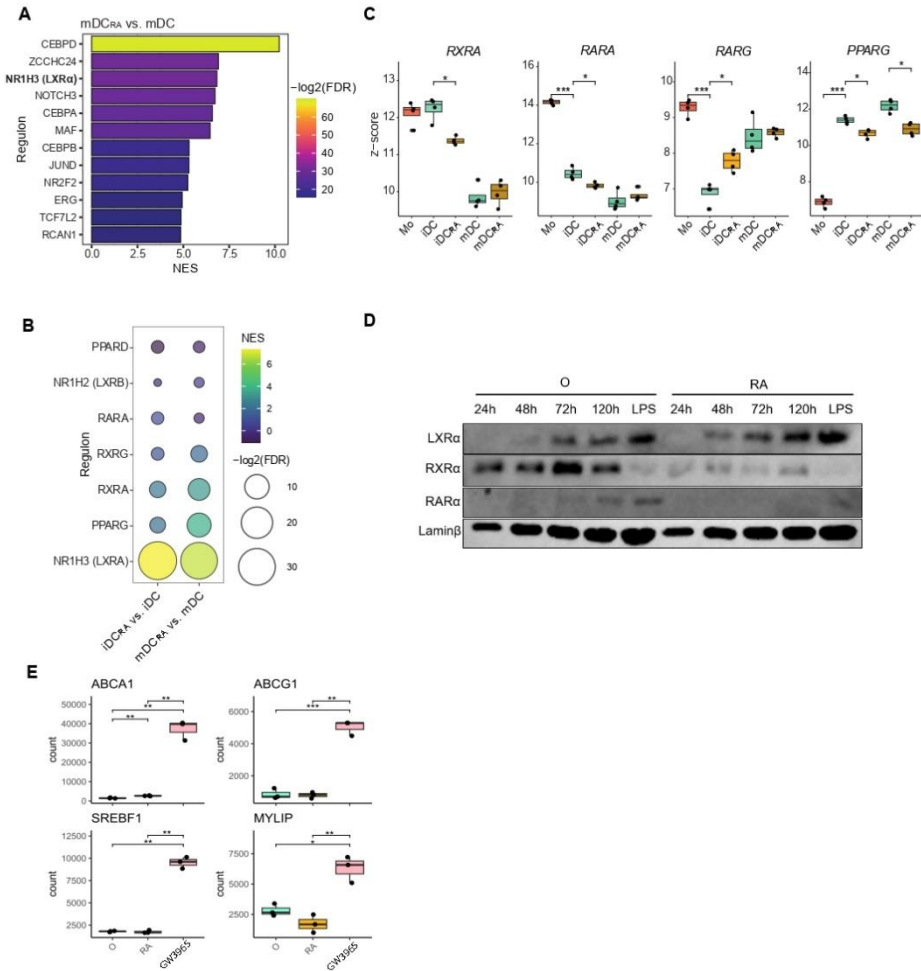
Supp. Figure 3



(See figure legend on next page.)

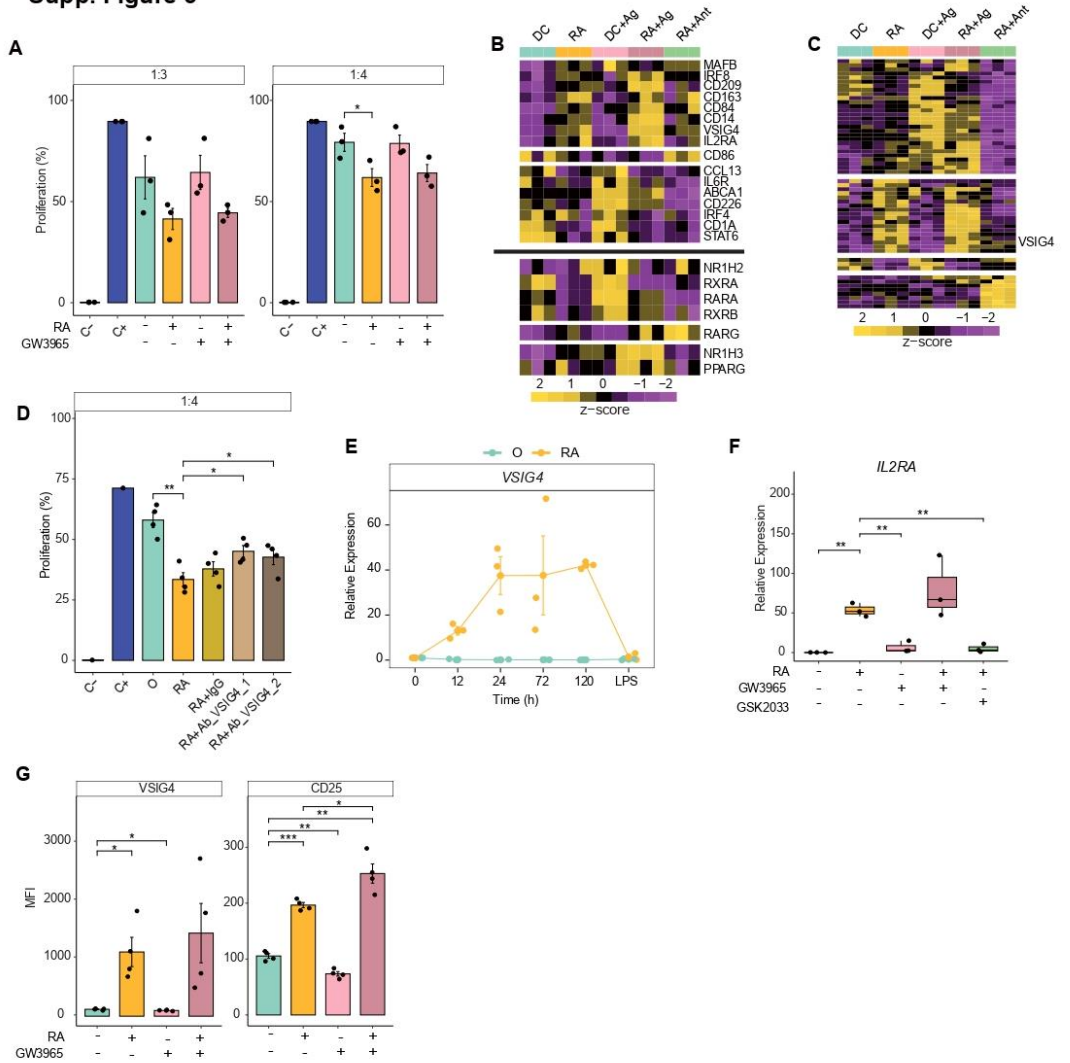
Supp. Figure 3. (A) Overlap of the UP and DOWN regulated genes ($\log Fc > 0.5$ and $FDR < 0.05$) in the different comparison. (B) Principal Component Analysis (PCA) of gene expression. Principal component 1 and principal component 2 are represented on the x- and y-axis, respectively. (C) Heatmap showing ligand activity prediction based on the Pearson correlation with its target genes. (D) Heatmap displaying average gene expression of ligands for iDCs and iDC_{RA} on day 7. (E, F) Heatmap showing the regulatory potential of each ligand on the target genes based on nichenetr package database (upper panel) and the expression level of these target genes in each sample (lower panel). (G) Gene set enrichment analysis (GSEA) of the RA treated versus untreated iDC and mDC, using public datasets of alveolar macrophages obtained from different studies (56–58). The running enrichment score and the normalized enrichment score (NES) are shown.

Supp. Figure 4



Supp. Figure 4. (A, B) Discriminant Regulon Expression Analysis (DoRothea) of mDC_{RA} vs mDC comparison. (C) Boxplot of the gene expression of retinoic acid receptors (z-score). (D) Western blot of retinoic acid receptors during differentiation. Laminβ proteins were used as loading controls. (E) Boxplot of the gene expression of LXR targets obtained from RNAseq (z-score) (* P < 0.05, **P<0.01, ***P<0.005).

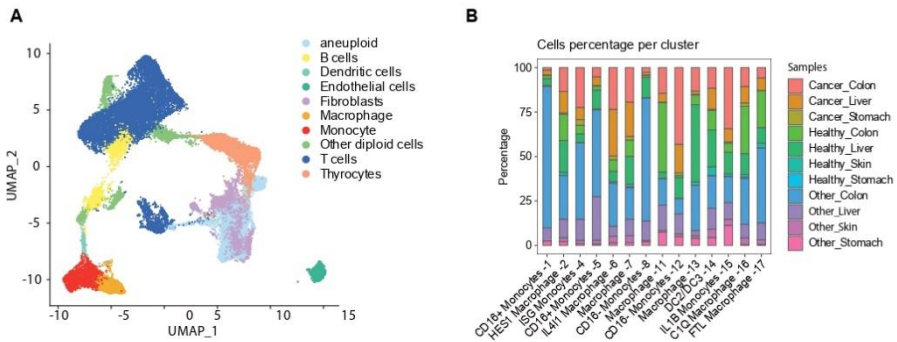
Supp. Figure 5



(See figure legend on next page.)

Supp. Figure 5. (A) iDC differentiated under the treatment with retinoic acid (RA) and agonist of LXR (GW3965) were co-cultured with CD8+ cells for 4 days. The final CFSE signal of CD8 + cells are shown. CD8+ with only CD3/CD28 T-activator beads (C+) or alone (C-) are also shown (n=3). (B) Heatmap representing the expression level (z-score) of selected genes. (C) Heatmap representing differentially expressed genes (DEGs) with a $\log_2(\text{FC}) > 1$ and a $\text{FDR} < 0.05$ on the RA+Ant vs. RA comparison. (D) iDC differentiated under the treatment with retinoic acid (RA) were co-cultured with CD8+ cells for 5 days. During the co-culture, two different antibody against VSIG4 (Ab_VSIG4_1(# MAB46462), Ab_VSIG4_2(#: MAB4646)) were added. IgG was used as a control (#CS200581). The final CFSE signal of CD8 + cells are shown. CD8+ with only CD3/CD28 T-activator beads (C+) or alone (C-) are also shown (n=4). (E) mRNA expression kinetics of VSIG4 gene. (F) Box-plot representation of IL2RA expression obtained from qRT-PCR in iDC differentiated under the treatment with RA, agonista of LXR (GW3965) and GSK2033. (G) Bar-plots of surface marker expression represented as Median Fluorescence Intensity (MFI) in DCs differentiated under the treatment with RA and GW3965. (* $P < 0.05$, ** $P < 0.01$, *** $P < 0.005$).

Supp. Figure 6



Supp. Figure 6. (A) UMAP visualization showing the immune cell populations identified from Louvain clustering and cell-specific marker gene expression. (B) Barplot plot representing the percentage of each cell type in the different tissues and conditions.

3.2 ARTICLE 2. Epigenetic and transcriptomic reprogramming in monocytes of severe COVID-19 patients reflects alterations in myeloid differentiation and the influence of inflammatory cytokines

Epigenetic and transcriptomic reprogramming in monocytes of severe COVID-19 patients reflects alterations in myeloid differentiation and the influence of inflammatory cytokines

Gerard Godoy-Tena¹, Anis Barmada^{2,3}, Octavio Morante-Palacios¹, Carlos de la Calle-Fabregat¹, Ricardo Martins-Ferreira¹, Anna G. Ferreté-Bonastre¹, Laura Ciudad¹, Adolfo Ruiz-Sanmartín⁴, Mónica Martínez-Gallo⁵, Ricard Ferrer⁴, Juan Carlos Ruiz-Rodríguez⁴, Javier Rodríguez-Ubreva¹, Roser Vento-Tormo², Esteban Ballestar^{1,6}

1. Epigenetics and Immune Disease Group, Josep Carreras Research Institute (IJC), 08916 Badalona, Barcelona, Spain
2. Wellcome Sanger Institute, Wellcome Genome Campus, Hinxton CB10 1RQ, United Kingdom
3. Department of Medical Genetics, University of Cambridge, Cambridge CB2 0QQ, United Kingdom
4. Intensive Care Department, Vall d'Hebron University Hospital, Shock, Organ Dysfunction and Resuscitation (SODIR) Research Group, Vall d'Hebron Research Institute (VHIR), Universitat Autònoma de Barcelona, 08035 Barcelona, Spain
5. Immunology Division, Vall d'Hebron University Hospital and Diagnostic Immunology Research Group, Vall d'Hebron Research Institute (VHIR), 08035 Barcelona, Spain
6. Epigenetics in Inflammatory and Metabolic Diseases Laboratory, Health Science Center (HSC), East China Normal University (ECNU), Shanghai, 200241, China

ABSTRACT

COVID-19 manifests with a wide spectrum of clinical phenotypes, ranging from asymptomatic and mild to severe and critical. Severe and critical COVID-19 patients are characterized by marked changes in the myeloid compartment, especially monocytes. However, little is known about the epigenetic alterations that occur in these cells during hyperinflammatory responses in severe COVID-19 patients. In this study, we obtained the DNA methylome and transcriptome of peripheral blood monocytes from severe COVID-19 patients. DNA samples extracted from CD14⁺CD15⁻ monocytes of 48 severe COVID-19 patients and 11 healthy controls were hybridized on MethylationEPIC BeadChip arrays. In parallel, single-cell transcriptomics of 10 severe COVID-19 patients were generated. CellPhoneDB was used to infer changes in the crosstalk between monocytes and other immune cell types. We observed DNA methylation changes in CpG sites associated with interferon-related genes and genes associated with antigen presentation, concordant with gene expression changes. These changes significantly overlapped with those occurring in bacterial sepsis, although specific DNA methylation alterations in genes specific to viral infection were also identified. We also found these alterations to comprise some of the DNA methylation changes occurring during myeloid differentiation and under the influence of inflammatory cytokines. A progression of DNA methylation alterations in relation to the Sequential Organ Failure Assessment (SOFA) score was found to be related to interferon-related genes and T-helper 1 cell cytokine production. CellPhoneDB analysis of the single-cell transcriptomes of other immune cell types suggested the existence of altered crosstalk between monocytes and other cell types like NK cells and regulatory T cells. Our findings show the occurrence of an epigenetic and

transcriptional reprogramming of peripheral blood monocytes, which could be associated with the release of aberrant immature monocytes, increased systemic levels of pro-inflammatory cytokines, and changes in immune cell crosstalk in these patients.

Keywords: COVID-19, monocytes, epigenomics, DNA methylation, single-cell transcriptomics, immune cell cross-talk.

INTRODUCTION

Severe acute respiratory syndrome coronavirus 2 (SARSCoV-2) causes the well-known Coronavirus disease 2019 (COVID-19), which has become a major global health burden. SARS-CoV-2 infection occurs through the nasopharyngeal mucosa [1]. Subsequent immune responses occur at the local mucosa and at a systemic level. An effective response to SARS-CoV-2 infection requires coordination between the innate and adaptive immune systems, including granulocytes, monocytes, macrophages, and T and B cells [2, 3]. The range of immune responses to SARS-CoV-2 infection is diverse, from asymptomatic or mild upperrespiratory illness to severe viral pneumonia, acute respiratory distress syndrome, and death [4]. The most severe forms of COVID19 are caused by dysregulation of immune homeostasis, which leads to hyperinflammation in the lungs [5]. This has been shown to be more pronounced in the elderly and in individuals with pre-existing comorbidities [6, 7]. Nevertheless, despite the numerous studies performed in the field, the impact of exacerbated immune responses associated with severe COVID-19 at the systemic level remains unclear.

Various studies have demonstrated that peripheral pathogenic T cells and inflammatory monocytes can induce a cytokine storm in severe COVID-19 patients [8]. This takes the form of excessive production of inflammatory mediators, specifically, interleukin (IL)-6, IL-1 β , granulocyte-macrophage colony-stimulating factor (GM-CSF), tumor necrosis factor-alpha (TNF- α), and interferon gamma (IFN γ) [8–11]. IFN is essential for inducing the innate immune response during viral infection through different interferon regulatory factors (IRFs) [12]. Further, in COVID-19 patients, type I IFN deficiency appears

to be a hallmark of severe cases [13–19] in association with persistent blood viral load and an exacerbated inflammatory response [14].

Single-cell omics studies have identified specific transcriptional features in monocytes, natural killer (NK) cells, dendritic cells (DCs), and T cells associated with the severity of COVID-19 [13, 20–22]. These studies have revealed that severe COVID-19 is marked by a dysregulated myeloid cell compartment [13]. It has also been shown that monocytes from severe COVID-19 patients are characterized by a tolerogenic phenotype with reduced expression of class II major histocompatibility complex (MHC-II) antigens [23] and increased activation of apoptotic pathways [24].

Differentiation and activation of monocytes and other myeloid cells are directly associated with epigenetic mechanisms [25]. The functional plasticity of these cells is also reflected at the epigenetic level, and several studies have shown that DNA methylation profiles, among other epigenetic marks, vary in response to inflammatory cytokines, hormones, and other factors [26, 27], depending on their functionality. Cytosine methylation (5mC) occurs at CpG dinucleotides and is generally associated with transcriptional repression [28], although its relationship with transcription depends on the genomic location of the affected CpG sites [29]. In some cases, DNA methylation changes occur as a result of upstream environmental effects that link cell membrane receptors, signaling pathways, and transcription factors (TFs) that can either directly recruit DNA methyl transferases (DNMT) and ten–eleven translocation (TET) enzymes, or indirectly influence their binding to specific genomic sites.

The characterization of the epigenetic and transcriptomic reprogramming in monocytes, given their central role in inflammatory

responses, is essential if we are to understand the specific dysregulated pathways involved in severe forms of COVID-19. In this study, we obtained the DNA methylation profiles of peripheral blood monocytes of severe COVID-19 patients and studied their relationship with transcriptomic changes, obtained by generating droplet-based single-cell RNA sequencing (scRNA-seq) data from peripheral blood.

MATERIALS AND METHODS

Human samples

Our study included a selection of 58 severe COVID₁₉ patients from the intensive care unit (ICU) of Vall d'Hebron University Hospital (Barcelona) recruited during the second wave of infection in Spain (October to November 2020). Peripheral blood samples were taken at different times following admission of the patient to the ICU, as specified in Additional file 1. Table S1 (Days in ICU). Ninetyfour percent of the patients required intubation and all enrolled cases were confirmed to be infected with SARS-CoV-2 using realtime RT-PCR at the time of collection. For all enrolled patients, the date of enrolment, clinical classification, or treatment was obtained from the clinical records. From all these patients, 48 of the 58 patients were selected for DNA methylation analysis (Table 1) and peripheral blood mononuclear cells (PBMCs) from 10 of the 58 patients were used for droplet-based scRNA-seq analysis (Additional file 2. Table S2). The control population for the DNA methylation analysis comprised 11 healthy donors (HDs) recruited at the Blood Bank of Vall d'Hebron University Hospital. Table 1 summarizes the characteristics and clinical data from patients included in the DNA methylation analysis. We included an additional group of 14 patients from the same hospital for DNA methylation and expression validation, including 9 severe COVID-19 patients and 5 mild COVID-19 patients, together with an additional group of 6 HDs. The validation cohort was collected during February 2022, applying the same selection criteria as for the discovery cohort. For the validation cohort, we only included non-vaccinated patients, to match the vaccination status with that of the patients collected in the initial phase of the study. Clinical information corresponding to the new cohort is also included in Additional

file 1. Table S1 (validation cohort). This study was approved by the Clinical Research Ethics Committees of Hospital Universitari Germans Trias i Pujol (PI-20–129) and Vall d’Hebron University Hospital (PR(AG)282/2020), both of which adhered to the principles set out in the WMA Declaration of Helsinki. Informed consent was obtained from all patients before their inclusion.

Table 1 Summary of patient cohort for DNA methylation analysis

	Healthy controls	COVID19 severe patients	p value
Number	11	48	-
Age (mean ± SD)	50 ± 11.16	60 ± 11.96	0.0042
Sex (% female)	36.4	25	0.710
SOFA	0	5 ± 2.97	2.4e−07
IL-6 (pg/ml) (mean ± SD)	NA	316.94 ± 1238.82	-
Days in ICU (mean ± SD)	NA	6 ± 5.93	-
Treated with dexamethasone (%)	NA	52.08	-
Obesity (%)	NA	27.03	-
Hypertension (%)	NA	56.25	-
Death (%)	NA	33.33	-
Mechanical ventilation (%)	NA	93.75	-

Monocyte purification and DNA isolation

PBMCs were obtained from peripheral blood by Ficoll gradient using Lymphocyte Isolation Solution (Rafer, Zaragoza, Spain) from 48 of the severe COVID-19 patients and 11 HDs. Once PBMCs were isolated, all samples were stored at −150 °C in 10% DMSO in fetal bovine serum (FBS) until monocyte purification. The monocyte population was isolated by flow cytometry (FacsAria Fusion, BD, Beckton Dickinson, San Jose, CA, USA). PBMCs were stained with CD14-APC-Vio770 (Miltenyi Biotec) and CD15-FITC (Miltenyi Biotec) in staining buffer (MACS) for 20 min. A gating strategy was employed to eliminate cell debris, doublets, and DAPI+ cells. CD14 and CD15 antibodies were used to isolate CD14+CD15−. Purified cells were pelleted and stored at −80 °C. After monocyte isolation, DNA was isolated using the AllPrep

DNA/RNA/miRNA Universal Kit (Qiagen) following the manufacturer's instructions.

DNA methylation profiling

Bisulfite (BS) conversion was performed using EZ-96 DNA Methylation™ Kit (Zymo Research, CA, USA) according to the manufacturer's instructions. Five hundred nanograms of BS-converted DNA was hybridized on Infinium Methylation EPIC BeadChip arrays (Illumina, Inc., San Diego, CA, USA). These were used to analyse DNA methylation. They enable >850,000 methylation sites per sample to be assessed at single-nucleotide resolution, which corresponds to 99% of the reference sequence (RefSeq) genes.

Each methylation data point was obtained from a combination of the Cy3 and Cy5 fluorescent intensities from the methylated and unmethylated alleles. Background intensity computed from a set of negative controls was subtracted from each data point. For representation and further analysis, we used beta (β) and M values. Beta is the ratio of methylated probe intensity to overall intensity (the sum of the methylated and unmethylated probe intensities). M is calculated as the log₂ ratio of the intensities of the methylated and unmethylated probes. For statistical purposes, the use of M is more appropriate since β -values are severely heteroscedastic for highly methylated and unmethylated CpG sites. Raw DNA methylation data are available at GEO, with accession number GSE188573 [30].

Quality control, data normalization, and statistical analysis of DMPs

Quality control and analysis of EPIC arrays were performed using ShinyÉPICo [31], a graphical pipeline that uses *minf* (v1.36) [32] for normalization, and *limma*

(v3.46) [33] for analysing differentially methylated positions. ShinyÉPICO is available as an R package at the Bioconductor and GitHub sites. We used the BS conversion control probe test included in ShinyÉPICO to determine whether the conversion rate was above the quality threshold of 2 established by Illumina. The threshold was calculated from the information of the BS conversion control probes of the EPIC arrays. When the BS conversion reaction is successful, control probes display strong signal in the red channel, whereas if the sample has unconverted DNA, control probes have a strong signal in the green channel. The red/green ratio for each control position was calculated for each sample. CpH and SNP loci were removed by the Noob method, followed by quantile normalization. Sex chromosomes (X and Y) were also excluded from the analysis to avoid discordant information among samples. Even when data were generated in a single batch and randomized, we applied the batch effect correction. Sex and age of the donors were included as covariates, to minimize confounding effects due to differences between the median age of the patient and control cohorts, and the Trend and Robust options were implemented in the eBayes moderated *t*-test analysis. To compare healthy donors with the entire severe COVID-19 patient cohort, we identified differentially methylated CpG sites by using *t*-tests and a method with defined empirical array weights, included in the *limma* package [33], and selecting CpGs with a false discovery rate (FDR) of <0.05 and a $\Delta\beta > 0.15$. To test the effects of potential changes in monocyte subset proportions, we also included this information as a covariate, and performed the same analysis as above, but including only those samples for which such information was available. We used the iEVORA package (v1.9.1) [34] to identify differentially variable positions (DVPs). This algorithm identifies differences in variance using

Bartlett's test ($FDR < 0.05$) to regularize the variability test, which is overly sensitive to single outliers. For the analysis in Fig. 2, we calculated Spearman's correlation coefficient (ρ) to measure the association of two variables and thereby identify CpG sites in which DNA methylation was correlated with SOFA in patients with severe COVID-19. We selected the CpG sites for which Spearman's ρ was greater than 0.4 and had an associated value of $p < 0.01$. Principal component analysis (PCA) of β -values from ShinyÉPICo was used to determine the correlations of PCs with clinical variables such as dexamethasone treatment, obesity, and hypertension. Pearson correlation coefficient between numerical variables and PCs were calculated. Categorical variables were entered in a linear model together with the PCs, which were considered as a function of the variable.

Gene ontology, transcription factor enrichment, and chromatin state discovery and characterization

The GREAT (v3.0.0) online tool was used for gene ontology (GO) analysis, in which genomic regions were annotated by applying adapted basal and extension settings (5 kb upstream, 5 kb downstream, 1000 kb plus distal). GRCh37 (UCSC hg19, Feb. 2009) was used as the alignment genome reference. Annotated CpGs in the EPIC array were used as background. GO terms were considered significant for a > twofold change and an $FDR < 0.05$. Enrichment is represented as $-\log_2(FDR)$. GO categories with $p < 0.05$ were considered significantly enriched. GO analysis of differentially expressed genes (DEGs) was carried out using the online Enricher gene ontology analysis tool. GO categories with a > twofold change and an $FDR < 0.05$ were considered significantly enriched.

We used the *findMotifsGenome.pt* tool from the motif discovery HOMER software (v4.10.3) to analyze motif enrichment [35]. A flanking window of ± 250 bp from each CpG was applied, and CpGs annotated in the EPIC array were used as background. To determine the location relative to a CpG island (CGI), we used “hg19_cpGs” annotation in the *annotatr* (v1.8) R package. The statistical test used for the enrichment in these analyses was Fisher’s exact test. Chromatin functional state enrichment of DMPs was measured using public PBMC data from the Roadmap Epigenomics Project generated with ChromHMM (v1.23) [36]. Enrichments were calculated with Fisher’s exact test using array annotation as background regions. Only significantly enriched states are shown.

Heatmaps and PCA plots

Heatmaps of DMPs were generated with functions available in the *ComplexHeatmap* (v2.11.1) and *gplots* (v3.1.3) R packages. We used PCA for the low-dimensional analyses. PCA projection matrices were calculated with R’s *prcomp* function, and visual representations of PCs were plotted with the *ggfortify* package (v4.1.4). Whole genome bisulfite sequencing (WGBS) analysis DNA methylation values of Ensembl Regulatory Build regions of progenitor cells such as hematopoietic stem cell (HSC), multipotent progenitor (MPP), common myeloid progenitor (CMP), granulocyte macrophage progenitor (GMP), and control monocytes were extracted from public whole genome bisulfite sequencing (WGBS) (GSE87197) [37]. Using *GenomicRanges* (v1.42.0) and based on genomic location, the overlap of the hypermethylated DMPs observed in COVID-19 compared with HD was determined with the Ensembl Regulatory Regions from the hematopoietic precursors and monocytes. For this

analysis, all DNA methylation data were annotated with respect to the GRCh38 human genome reference.

Single-cell capture

PBMCs from 10 ICU patients were used to generate single-cell gel beads-in-emulsion (GEMs) (Additional file 2. Table S2). Cells were then washed three times and counted. For samples with low viability (<90%), we performed Ficoll separation in an Eppendorf tube to eliminate dead cells and increase cell viability. For samples with greater than 90% viability, we filtered using a Flowmi strainer and counted the cells before loading into 10X chromium to generate single-cell GEMs, following the manufacturer's instructions. We loaded 50,000 cells per pool, including a total of 4 patients per pool. Datasets from patients and HDs are available as h5ad files (<https://www.COVID-19cellatlas.org/index.patient.html>) (Additional file 2. Table S2). In parallel, genomic DNA was isolated from the same 10 PBMCs for genotyping and subsequent donor deconvolution (as described in [38]) using a Maxwell® 16 Blood DNA Purification Kit from Promega following the manufacturer's instructions.

scRNA-seq cell type identification and annotation

Single-cell transcriptome data from COVID-19 patients were quantified and aligned using Cell Ranger (v3.1) with the GRCh38 genome concatenated to SARS-Cov-2 genome as a reference. Thereafter, cells from pooled samples were deconvolved and demultiplexed using *Soupor-cell* (v3.0) [39], yielding a genotype variant that allows donor identity to be matched across different samples. This additionally enabled the removal of doublet cells that could not be explained by any single genotype. *Scrublet* (vo.2.3) [40] was subsequently

employed to further filter out other doublets based on computed doublet scores. Specifically, Student's *t*-test ($p < 0.01$) after Bonferroni correction was used within finegrained sub-clustering of each initial cluster produced by the Leiden algorithm. Data were not denoised because no significant contamination or ambient RNA was present. Previously described scRNA-seq datasets of HDs [41] were then integrated for comparison using single-cell variational inference (scVI) [42] with a generative model of 64 latent variables and 500 iterations. More specifically, scVI employs a negative binomial model using raw counts, selecting 5000 highly variable genes to produce the latent variables. Defined cell-cycle phase specific genes in the Seurat package (v4.1.0) [43] were excluded from these to reduce the dependence of clustering on cell-cycle effects. Data were subsequently analysed using Scanpy (v1.9.1) [44] following the recommended standard practices. For quality control, genes expressed in fewer than three cells, and cells with fewer than 200 genes or more than 20% mitochondrial gene content, were removed prior to downstream analysis. Data were normalized (`scanpy.pp.normalize_per_cell`, scaling factor = 10,000) and log₂-transformed (`scanpy.pp.log1p`). For gene expression visualization (e.g., heat maps), data were further scaled (`scanpy.pp.scale`, maximum value = 10).

Cell type clustering and annotation

The resulting latent representation from the integrated datasets was used to compute the neighbourhood graph (`scanpy.pp.neighbors`), then the Louvain clustering algorithm (`scanpy.tl.louvain`, resolution = 3) and Uniform Manifold Approximation and Projection (UMAP) visualization (`scanpy.tl.umap`) were employed. Cell type annotations were manually refined using literature-driven,

cell-specific marker genes. Identified residual RBCs from incomplete PBMC isolation were excluded before further analysis, as recommended [45].

Differential gene expression and transcription factor enrichment analysis

Differential gene expression between COVID-19 patients and healthy individuals (FDR < 0.05) was analysed using the *limma* package [46]. To predict transcription factor (TF) involvement in transcriptomic changes, we used DoRothEA (Discriminant Regulon Expression Analysis) v2 tool [47]. Regulons with a confidence score of A–C were analysed, and cases with $p < 0.05$ and a normalized enrichment score (NES) of ± 2 were considered significantly enriched.

Cell-cell communication

Based on the differential expression analysis, Cell-PhoneDB [48] v3 ([www. CellPhoneDB.org](http://www.CellPhoneDB.org)) was used to infer changes in ligand/receptor interactions between the identified cell types in COVID-19 versus HD. Specifically, instead of random shuffling, as used in the previously described statistical method, differentially expressed genes (FDR < 0.05) were used to select interactions that were significantly enriched in either severe COVID-19 patients or healthy individuals relative to the other group. An interaction was considered enriched if at least one of the two partners (ligand or receptor) was differentially expressed, and if both partners were expressed by at least 10% of the interacting cells.

Bisulfite pyrosequencing

EZ DNA Methylation-Gold kit (Zymo Research) was used to BS-converted 500 ng of genomic DNA following the manufacturer's instructions. BS-treated DNA

was PCR-amplified using IMMOLASE DNA polymerase kit (Bioline). Primers used for the PCR were designed with PyroMark Assay Design 2.0 software (Qiagen) (Additional file 3. Table S3). PCR amplicons were pyrosequencing with the PyroMark Q24 system and analysed with PyroMark Q48 Autoprep (Qiagen).

Real-time quantitative polymerase chain reaction (RT-qPCR)

The Transcription First Strand cDNA Synthesis Kit (Roche) was used to convert 250 ng of total RNA to cDNA following the manufacturer's instructions. RT-qPCR primers were designed with Primer3 software [49] (Additional file 3. Table S3). RT-qPCR reactions were prepared with LightCycler 480 SYBR Green I Master (Roche) according to the manufacturer's instructions and analysed with a LightCycler 480 instrument (Roche).

Flow cytometry

To study the surface cell markers on monocytes (CD14 +), PBMCs from the 10 patients used for single-cell analysis and 10 HDs were defrosted and washed once with PBS. After blocking for non-specific binding with Fc block (BD Pharmingen) for 5 min on ice, cells were incubated for 20 min on ice using staining buffer (PBS with 4% fetal bovine serum and 0.4% EDTA). Antibodies used included the following: CD14-FitC (Miltenyi Biotec), CD85-PEviolet770 (Miltenyi Biotec), CD172a-APC (Miltenyi Biotec), CD97-PEviolet770 (Miltenyi Biotec), CD31-PE (Miltenyi Biotec), CD366-PEviolet615 (Miltenyi Biotec), CD62L-APC (Miltenyi Biotec), CD58-PE (Miltenyi Bio-tec), CD191-PEviolet770 (Miltenyi Biotec), CD52-PEviolet615 (Miltenyi Biotec), CD48-APC (Miltenyi Biotec). Cells were analyzed in a BD FACSCanto-II flow cytometer.

Statistical analysis

All statistical analyses were done with R v4.0.2. Box, bar, violin, bubble, and line plots were generated using functions from the ggplot2 (v3.3.6) and ggpubr (v4.0) packages. Mean normalized DNA methylation values were compared using two-tailed test. Multivariate frequency distributions were calculated using Fisher's exact test. The levels of significance are indicated as: * $p < 0.05$, ** $p < 0.01$, *** $p < 0.001$, and **** $p < 0.0001$.

RESULTS

DNA methylome remodeling in peripheral blood monocytes of severe COVID-19 patients

To directly inspect epigenetic alterations in peripheral blood monocytes in severe COVID-19, we isolated CD14⁺ CD15⁻ cells from 59 blood samples, comprising 48 severe COVID-19 patients and 11 healthy donors (HDs), and performed DNA methylation profiling (Figure 1A, Table 1, and Additional file 1. Table S1). For cell sorting, we first separated live cells from debris, then extracted singlets and isolated CD14⁺ CD15⁻ cells to avoid neutrophil contamination (Figure 1B) [50]. Since we selected CD14⁺ cells, the purification procedure only included classical (CM) (CD14⁺ CD16⁻) and intermediate monocytes (IM) (CD14⁺ CD16⁺), excluding the non-classical monocyte (NCM) (CD14^{low}CD16⁺) subpopulation, which in healthy individuals corresponds to around 5% of the total monocyte compartment [51]. Negative selection using CD15 was necessary, as there is a significant increase in the frequency of neutrophils in severe COVID-19 patients, as activated neutrophils are not separated in the Ficoll step [52] (Additional file 4. Supp. Figure 1A-S1C). To confirm the purity of our monocytes, we performed FACS analysis and obtained an average purity of 98% (example in Additional file 4 Figure S1D). Studies in various other inflammatory diseases have shown that the proportions of monocytes can shift between the three major subsets, i.e., CM, IM, and NCM. For instance, it has been shown that severe COVID-19 patients feature reduced NCM and IM populations [53]. The analysis of monocyte subpopulations in our cohort showed a significant increase in the CM population and a decrease in the NCM population (Additional file 4. Figure S1E-S1F). Since we purified CD14⁺ monocytes, our study only included CM and IM.

We performed DNA methylation profiling of isolated monocytes and identified 2211 differentially methylated positions (DMPs) of CpGs in severe COVID-19 patients compared with HDs (FDR < 0.05 and absolute $\Delta\beta$ > 0.15). Of these, 1773 were hypermethylated (hypermethylated cluster) and 438 were hypomethylated (hypomethylated cluster) (Figure 1C and Additional file 5. Table S4). PCA of these DMPs showed that the two groups of monocytes (COVID-19 and HD) separated along the first principal component axis (Figure 1D). We obtained similar results when we included monocyte subpopulation proportions as a covariate in the analysis (overlap, $p < 0.0001$) (Additional file 6. Supp. Figure 2A). No significant differences (FDR < 0.05) were observed within COVID-19 patients separated by their condition (obesity, hypertension, days admitted to the ICU, and exitus/death) or treatment with dexamethasone (Additional file 1. Table S1). None of the abovementioned conditions was significantly correlated with the DNA methylation changes (Additional file 6. Supp. Figure 2B). This was also apparent from the PCA showing the overlap of patients with different clinical parameters (Additional file 6. Supp. Figure 2C).

The analysis of the genomic functional features of the DMPs in the hypermethylated and hypomethylated clusters (Additional file 6. Supp. Figure 2D) using public data from monocytes [36] revealed an enrichment in promoters and enhancers. This is consistent with their proposed roles for DNA methylation in regulatory elements [54].

Gene ontology analysis (GO) of the two DMP clusters revealed several functional categories associated with the immune response to viral infection (Figure 1E). In the hypermethylated cluster, we observed enrichment of categories such as natural killer-mediated immunity, leukocyte migration, adaptive immune response, and positive regulation of interferon gamma

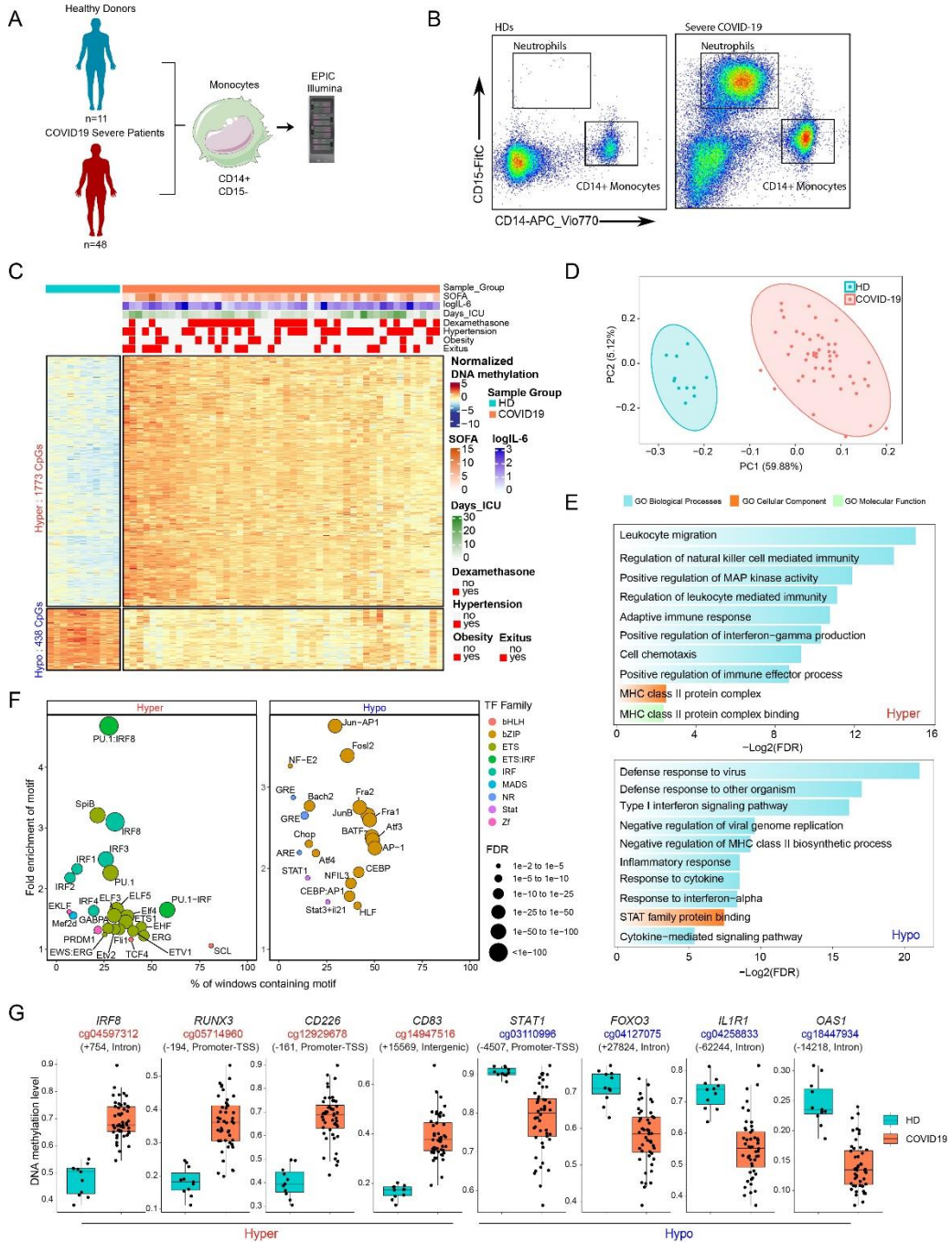
production. We also observed hypermethylation in the MHC-II protein complex that was related to antigen presentation. In addition, we found an enrichment of the positive regulation of MAP kinase activity category (Figure 1E, top panel). In the hypomethylated cluster, we observed enrichment of functional categories relevant to viral infection, including defense response to virus and negative regulation of viral genome replication. Importantly, the hypomethylated cluster also featured enrichment of functional categories related to type I interferons (IFN) signalling and MHC class II (Figure 1E, bottom panel).

Transcription factor (TF) binding motif enrichment analysis, in 250-bp windows surrounding DMPs, revealed overrepresentation of TFs of significance to the immune response. The hypermethylated cluster CpGs displayed enrichment of binding motifs of IRFs and ETS TF families, which are linked to IFN changes (Figure 1F, left panel). Motifs of the bZIP TF family like AP-1, Jun, Fos12, Fra1, and Fra2 were enriched in the hypomethylated cluster. DMPs of the hypomethylated cluster were also enriched in motifs of the signal transducer factor and activator of transcription factor (STAT) members STAT1 and STAT3. We also detected enrichment of the glucocorticoid response element (GRE) in the hypomethylated cluster (Figure 1F, right panel). Given these results, we hypothesized that pharmacological treatment with glucocorticoids (GCs) in severe COVID-19 patients in the intensive care unit (ICU) might influence DNA methylation in monocytes. To test this possibility, we performed *limma* analysis and subsequent binding motif enrichment after separating COVID-19 patients into two groups, with and without GC treatment. Both groups of patients exhibited significant enrichment of GRE motifs in the hypomethylated cluster (Additional file 6. Supp. Figure 2E), suggesting that the endogenous production

of GCs in severe COVID-19 patients could participate in the hypomethylation through GRE. However, given the size of the cohort, we cannot rule out the possibility that pharmacological treatment could also influence DNA methylation changes and therefore remains as a potential confounder factor.

Inspection of the individual genes within or in the vicinity of the DMPs revealed several genes with functions essential to the viral immune response. The list of relevant genes included *IRF8*, *RUNX3*, *CD226*, and *CD83* in the hypermethylated cluster, and *STAT1*, *FOXO3*, *IL1R1*, and *OAS1* in the hypomethylated cluster (Figure 1G). We validated these results using bisulfite pyrosequencing in a new cohort of severe COVID-19 patients (Additional file 6. Supp. Figure 2F). Interestingly, these changes were also observed in mild COVID-19 patients (Additional file 6. Supp. Figure 2F). *IRF8*, *IL1R1*, and *CD83* are associated with the IFN response. *CD226* encodes a glycoprotein related to monocyte, NK, and T cell adhesion. This glycoprotein has been shown to be involved in the cytotoxicity of these cells and is known to be altered in COVID-19 patients [13]. *STAT1* is associated with the cytokine response, which, in turn, is related to *IL1R1*. The latter is the receptor of interleukin-1, which participates in the inflammatory response and is strongly expressed in severe COVID-19 patients [14]. *OAS1* is induced by interferons and activates latent RNase, causing viral RNA degradation, which could be related to the identification of the category negative regulation of viral genome replication in the GO analysis.

Figure 1



(See figure legend on the next page.)

Figure 1. Analysis of DNA methylation in blood monocytes of severe COVID-19 patients. (A) Scheme depicting the cohort and workflow for monocyte purification of severe COVID-19 patients and controls and DNA methylation analysis. (B) Representative flow cytometry profile, indicating sorting gates used to purify monocytes from HD and COVID-19 patients' peripheral blood. (C) Scaled DNA methylation (z-score) heatmap of differentially methylated positions (DMPs) between HDs (blue bar above) and COVID-19 patients (red bar above). Significant DMPs were obtained by applying a filter of $FDR > 0.05$ and a differential of beta value ($\Delta\beta > 0.15$). A scale is shown on the right, in which blue and red indicate lower and higher levels of methylation, respectively. Clinical and treatment data of COVID-19 patients are represented above the heatmap. SOFA, IL-6 level, and days in the ICU scales are shown on the right of the panel. (D) Principal component analysis (PCA) of the DMPs. HDs and severe COVID-19 patients are illustrated as blue and red dots, respectively. (E) Gene ontology of hypermethylated and hypomethylated DMPs. Selected significant functional categories ($FDR < 0.05$) are shown. (F) Bubble plot of TF motifs enriched on hypermethylated and hypomethylated DMPs. Bubbles are colored according to their TF family; their size corresponds to the FDR rank. (G) Box plot of individual DNA methylation values of CpG from hypermethylated and hypomethylated clusters (β -values), with the name of the closest gene and the position relative to the transcription start site.

Monocytes from severe COVID-19 patients display increased DNA methylation variability

Overall, our DNA methylation analysis showed greater heterogeneity (different variable positions, DVPs) in the profiles from COVID-19 patient monocytes than in those from HDs (Additional file 6. Supp. Figure 2G). We then examined the relationship between the DNA methylation profiles and the Sequential Organ Failure Assessment (SOFA) score, which is used in ICUs to calculate organ damage. The score ranges from 0 to 24, with values greater than 6 being associated with a significant increase in the risk of mortality [55]. Using Spearman's correlation coefficient to assess specific hypermethylated or hypomethylated CpGs with SOFA, we identified 1375 CpG sites whose methylation levels positively correlated with SOFA (increased methylation) ($\rho < 0.4$ and $p < 0.01$) and 1497 CpG sites with an inverse correlation with SOFA (decreased methylation) ($\rho < -0.4$ and $p < 0.01$) (Figure 2A and Additional file 7. Table

S5). The mean normalization DNA methylation profiles of increased and decreased methylation CpG sites were similar in patients with low SOFA (< 6) and in healthy controls in an unsupervised representation but differed between the low and high SOFA score groups (Figure 2B). These results suggest that changes in DNA methylation are concomitantly exacerbated for higher SOFA scores, which is associated with bad prognosis. Several CpGs correlating with SOFA were associated with genes, such as *IL17R*, *SOCS5*, and *PCDHA5*, that are involved in T cell-mediated inflammatory responses (Figure 2C). Others, like *FOXP1* and *CDC20B*, are associated with DNA damage. GO analysis revealed that changes in DNA methylation that are concomitant with SOFA show an overrepresentation of terms associated with IFN γ , production of the molecular mediator involved in inflammatory response, viral gene expression, the B cell proliferation involved in immune response, and Th1 cell cytokine production (Figure 2D).

Figure 2

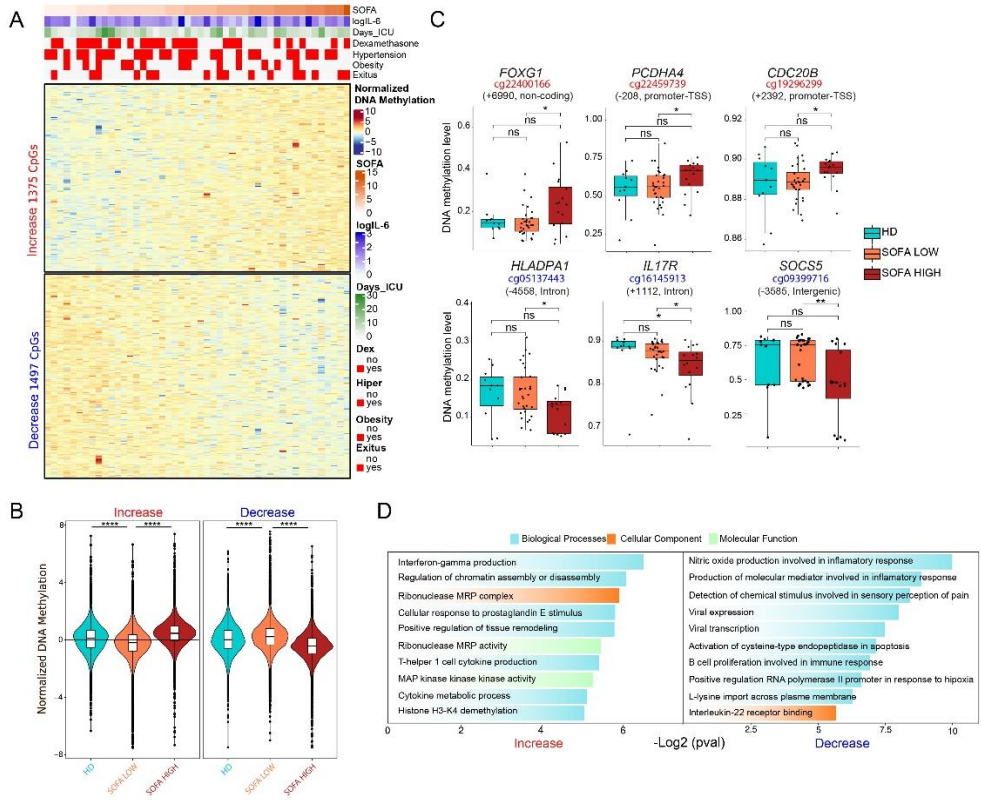


Figure 2. DNA methylation changes in COVID-19 monocytes parallel organ damage. (A) Heatmap of severe COVID-19 patients with DNA methylation ordered by SOFA score, including all CpG-containing probes significantly correlated with the SOFA score (Spearman correlation coefficient $\rho > 0.4$, $p < 0.01$). Clinical and treatment data of COVID-19 patients are shown above the heatmap. SOFA, IL-6 level, and days in the ICU scales are shown on the right of the panel. (B) Normalized methylation values from heatmap showing overall group methylation of HD. Patients with $SOFA \leq 6$ are indicated as SOFA LOW; those with $SOFA > 6$ are indicated as SOFA HIGH. (C) DNA methylation levels (β -values) of selected individual CpGs (and closest genes) in hypermethylated and hypomethylated sets and their position relative to the transcription start site. (D) Gene ontology (GO) analysis of hypermethylated and hypomethylated DMPs, analyzed with the GREAT online tool, in which CpG annotation in the EPIC array was used as background. Statistical significance: * $p < 0.05$, ** $p < 0.01$, *** $p < 0.0005$, **** $p < 0.0001$.

DNA methylation alterations in monocytes of severe COVID-19 patients significantly associate with those derived from patients with bacterial sepsis, myeloid differentiation, and the influence of inflammatory cytokines

To better characterize the impact of DNA methylation changes in COVID-19, we compared the DMPs from severe COVID-19 patients with those obtained from monocytes derived from patients with bacterial sepsis in a previous study by our team [27], given that severe COVID-19 can be considered a form of sepsis [56]. To this end, we first estimated the DNA methylation values of DMPs corresponding to the sepsis relative to the HD comparison from our previous sepsis study (accession number GSE138074) [27] using the data from the severe COVID-19 methylation dataset. Overall, we found significant enrichment in the hypermethylation and hypomethylation clusters (Figure 3A). We also calculated the odds ratio of the overlap between these two datasets and found a strong enrichment of the hyper-DMPs in COVID-19 relative to those in sepsis ($FDR \leq 2.22 \cdot 10^{-16}$) and in the hypo-DMPs ($FDR \leq 2.22 \cdot 10^{-16}$) (Figure 3B). We also confirmed an enrichment in introns and depletion in promoters relative to the background when testing the genomic location of the DMPs common to both COVID-19 and sepsis (Figure 3C and Supp. Figure 3A). DMPs located in introns are often localized in enhancer regions involved in long-distance regulation [54].

We then determined that the two datasets had 362 hypermethylated and 92 hypomethylated CpGs in common (Figure 3D), corresponding to 51% of the total DMPs of the sepsis patients (Additional file 8. Supp. Figure 3B). GO analysis of the shared DMPs revealed significant enrichment in functional terms related to host response, including regulation of NK cells, inflammatory

response, and leukocyte chemotaxis (Additional file 8. Supp. Figure 3C). Shared hypermethylated CpGs were enriched in functional categories related to cell signaling, such as the JAK-STAT and MAPK pathways, that could be involved in the reduction of the inflammatory response and the IL15- and IL12-mediated signaling pathways, which are related to cytokine production and Th1 proliferation (Figure 3E, left panel). Shared hypomethylated CpGs were enriched in functional categories responsible for regulating the inflammatory response, such as negative regulation of IL-1 production and positive regulation of macrophage activation. In concordance with the hypermethylated cluster, we also observed negative regulation of IFN α production (Figure 3E, right panel). It is of note that severe COVID-19-specific DMPs were enriched in functional categories related to virus infection, such as the defense response to virus, and impairment of the antigen-presenting process, which seems to be specific to COVID-19 infection [13, 23] (Additional file 8. Supp. Figure 3D).

Inspection of TF binding motifs corresponding to the DMPs shared between the two groups, separating the shared hypermethylated and hypomethylated CpG sets revealed IRF family transcription factors like IRF1, IRF2, IRF3, and IRF8 in the shared hypermethylated CpG set, which are well established regulators of the type I IFN system, being common in viral and bacterial infections [57]. We also detected enrichment of the ETS transcription factors that are regulated by MAPK proteins, which were enriched in the GO analysis (Figure 3F). In the shared hypomethylated set, we noted enrichment of STAT3 and TFs from bZIP AP-1, like Jun, and other bZIPs, like CEBP. Interestingly, GRE was also present in the shared hypomethylated cluster (Figure 3F). This suggests the influence of GC in the acquisition of aberrant methylation profiles in COVID-19 and sepsis. Individual genes associated with

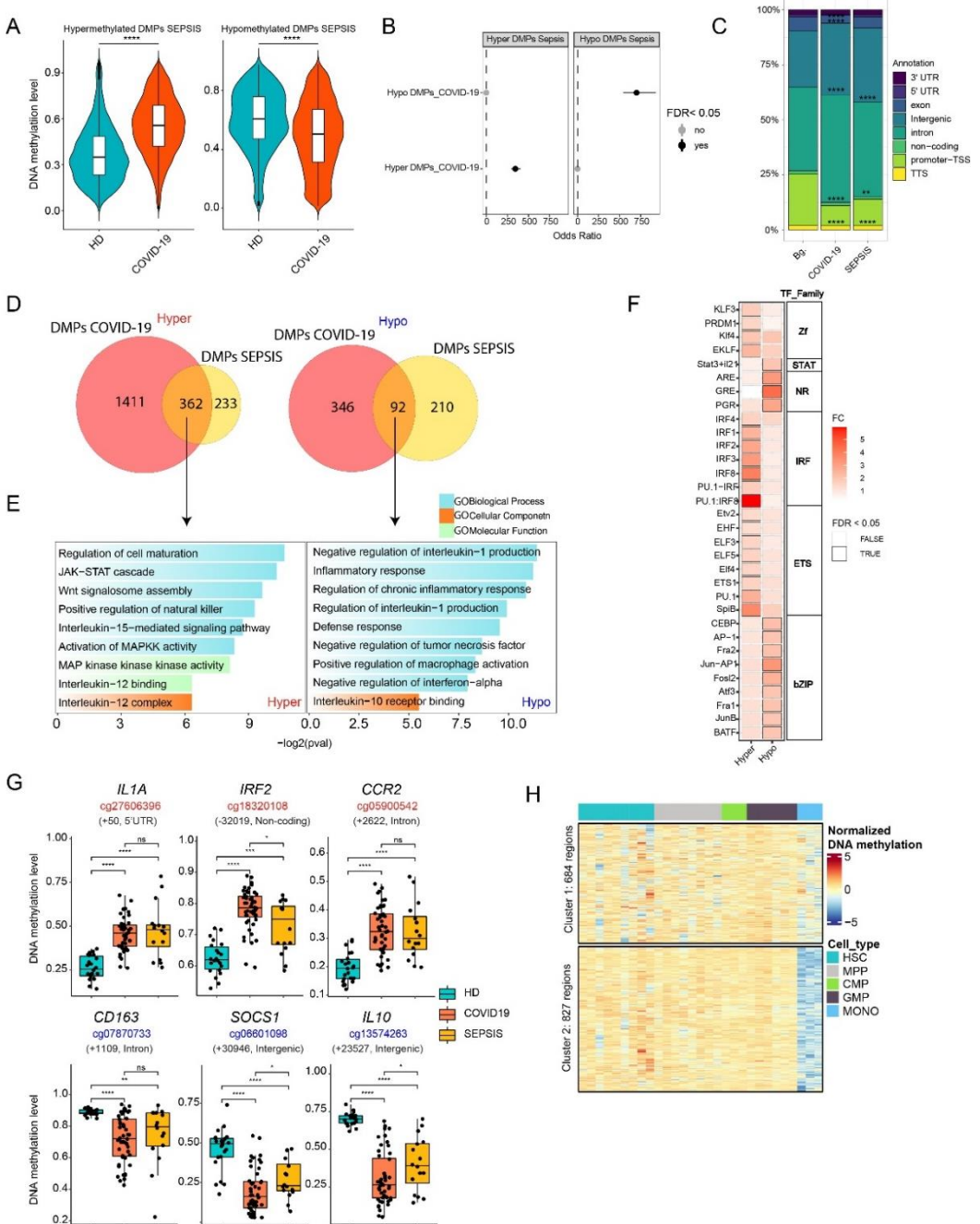
the COVID-19/sepsis shared hypermethylated and hypomethylated CpG genes include type I IFN-related genes, like *IRF2*, and others, such as *IL1A* and *CCR2*, that are involved in inflammatory processes and monocyte chemotaxis, respectively (Figure 3G). We also identified several genes among the shared hypomethylated set, like *CD163*, *SOCS1*, and *IL10*, that have been associated with the acquisition of tolerogenic properties in monocytes [58] (Figure 3G).

In both infections, systemic inflammation could be responsible for part of the DNA methylation changes that arise in monocytes. To address this possibility, we examined the DNA methylation levels of the hypomethylated and hypermethylated CpGs of severe COVID-19 and sepsis patients in monocytes isolated from healthy donor PBMCs that had been treated *in vitro* with inflammatory cytokines like IFN- α , IFN- γ , and TNF- α [26] (accession number GSE134425). This analysis revealed several significant changes following the trends for both COVID-19 and sepsis (Additional file 8. Supp. Figure 3E), suggesting that these inflammatory cytokines, which are elevated in these patients, could influence the monocyte DNA methylomes.

An alternative explanation for the observed changes in severe COVID-19 monocyte methylomes could be that DNA methylation changes reflect alterations during myeloid/monocyte differentiation or the release of immature or aberrant monocytes. This has been described in severe COVID-19 cases [13, 59–62]. It is worth noting that immature cells are also released from the bone marrow in sepsis [63]. To test this hypothesis, we used public whole-genome bisulfite sequencing (WGBS) data (GSE87197) of progenitor cells including HSC, MPP, CMP, and GMP cells and monocytes as references. We compared the 1773 hypermethylated CpGs based on their genomic location and obtained 1511 unique Ensembl Regions, which grouped in two clusters. Cluster 1 showed

low-level demethylation in monocytes compared with all hematopoietic precursor cell types, whereas cluster 2 showed clear demethylation in monocytes (Figure 3H). These results are compatible with the possibility that a proportion of the DMPs in severe COVID-19 result from aberrant myeloid differentiation or the release of immature monocytes, which display high methylation levels, and are not demethylated to the extent they are during normal differentiation.

Figure 3



(See figure legend on the next page.)

Figure 3. Comparative analysis of DNA methylation in blood monocytes of severe COVID-19 and bacterial sepsis patients. (A) Violin plot representing the mean methylation state of the DMPs found in the comparison between HDs and sepsis patients with β -values obtained from severe COVID-19 patients. (B) Fisher's exact test showing the odds ratio \pm 95% confidence interval of the overlap between DMPs found in monocytes from bacterial sepsis patients and DMPs in monocytes from COVID-19 patients. (C) Proportions of the genomic locations (in relation to genes) of DMPs in COVID-19 and sepsis; Bg., background, EPIC probes. D Venn diagram of the overlap of COVID-19 DMPs identified by the comparison of HDs and severe COVID-19 patients with DMPs identified by the comparison between HDs and sepsis patients, separating hypermethylated and hypomethylated DMPs. (E) Gene ontology analysis of hypermethylated and hypomethylated overlapping DMPs identified in the previous comparison. Selected significant categories ($p < 0.05$) are shown. (F) TF binding motif analysis of shared hypermethylated and hypomethylated DMPs comparing HDs and COVID-19 patients, and by HDs and sepsis patients. The panel shows the fold change (FC), TF family. Boxes with black outlines indicate TF binding motifs with $FDR < 0.05$. (G) Box-plot showing the DNA methylation values of individual CpGs (together with the name of the closest gene and its position relative to the transcription start site) from the hypermethylated and hypomethylated clusters from both COVID-19 and sepsis. (H) Scaled DNA methylation heatmap of regions from the whole-genome bisulfite sequencing (WGBS) data of hematopoietic stem cells (HSCs), multipotent progenitors (MPPs), common myeloid progenitors (CMPs), and granulocyte macrophage progenitors (GMPs) that overlap with the genomic location of the 1772 hypermethylated DMPs identified in the COVID-19 vs. HDs comparison. Statistical significance: * $p < 0.05$, ** $p < 0.01$, *** $p < 0.005$, **** $p < 0.001$

Aberrant DNA methylation is associated with changes in gene expression of COVID-19 patient monocytes

To study the relationship between the DNA methylation changes and aberrant gene expression of monocytes derived from severe COVID-19 patients, we obtained single-cell (sc) RNA-seq data of peripheral blood mononuclear cells (PBMCs) from 10 additional severe COVID-19 patients from the same hospital and compared them with those of 10 HDs from a public dataset [41] (Additional file 2. Table S2 and Additional file 9. Supp. Figure 4A-B). This analysis enabled us to identify 24 cell populations based on specific markers (Figure 4A and Additional file 9. Supp. Figure 4C-D), and thereby not only to determine the alterations in gene expression in monocytes, but also to inspect alterations in

additional immune cell subsets. Strikingly, the monocyte fraction comprised solely CD14⁺ cells (CD14 mono: CD14) (Figure 4B).

In the CD14⁺ monocyte cluster, we identified 10,440 differentially expressed genes (DEGs) between COVID-19 patients and HDs (Additional file 10. Table S6). The top DEGs (based on the fold change (FC)) included pro-inflammatory molecules (*IL1B*, *CCL3*), surface markers (*CD163*, *CD63*, *AREG*, *CD74*, *S100A12*, *S100A8*, *S100A9*), and transcription factors (*JUN*, *MAFB*, *NF-κB*) (Figure 4C). We observed upregulation of monocyte-derived cell markers like *S100A12*, *S100A8*, and *S100A9*. *S100A8* is already known to contribute to the cytokine storm in severe COVID-19 [41, 64]. Pro-inflammatory genes like *IL1B* of IRF1 were downregulated, as well as *HLA* genes, in agreement with previous studies, suggesting decreased antigen presentation in severe COVID-19 patients. Finally, we observed downregulation of the NF-κB inhibitor zeta-encoding gene (*NFKBIZ*), consistent with activation of this pro-inflammatory pathway [65]. Since type I IFNs are essential for antiviral immunity, and the DNA methylation analysis had indicated the potential occurrence of epigenetic alterations in IFN-stimulated genes (ISGs), we checked the expression levels of genes regulated by type I IFNs and found downregulation of several ISGs, such as *STAT1*, *BST2*, *PTPN6*, and *IRF1* (Additional file 11. Supp. Figure 5A). In addition, given that some of the observed DNA methylation changes were associated with genes involved in antigen presentation, we inspected *HLA* genes in our expression data and found this gene set to be significantly downregulated, consistent with dysfunction in antigen processing and presentation (Additional file 11. Supp. Figure 5B).

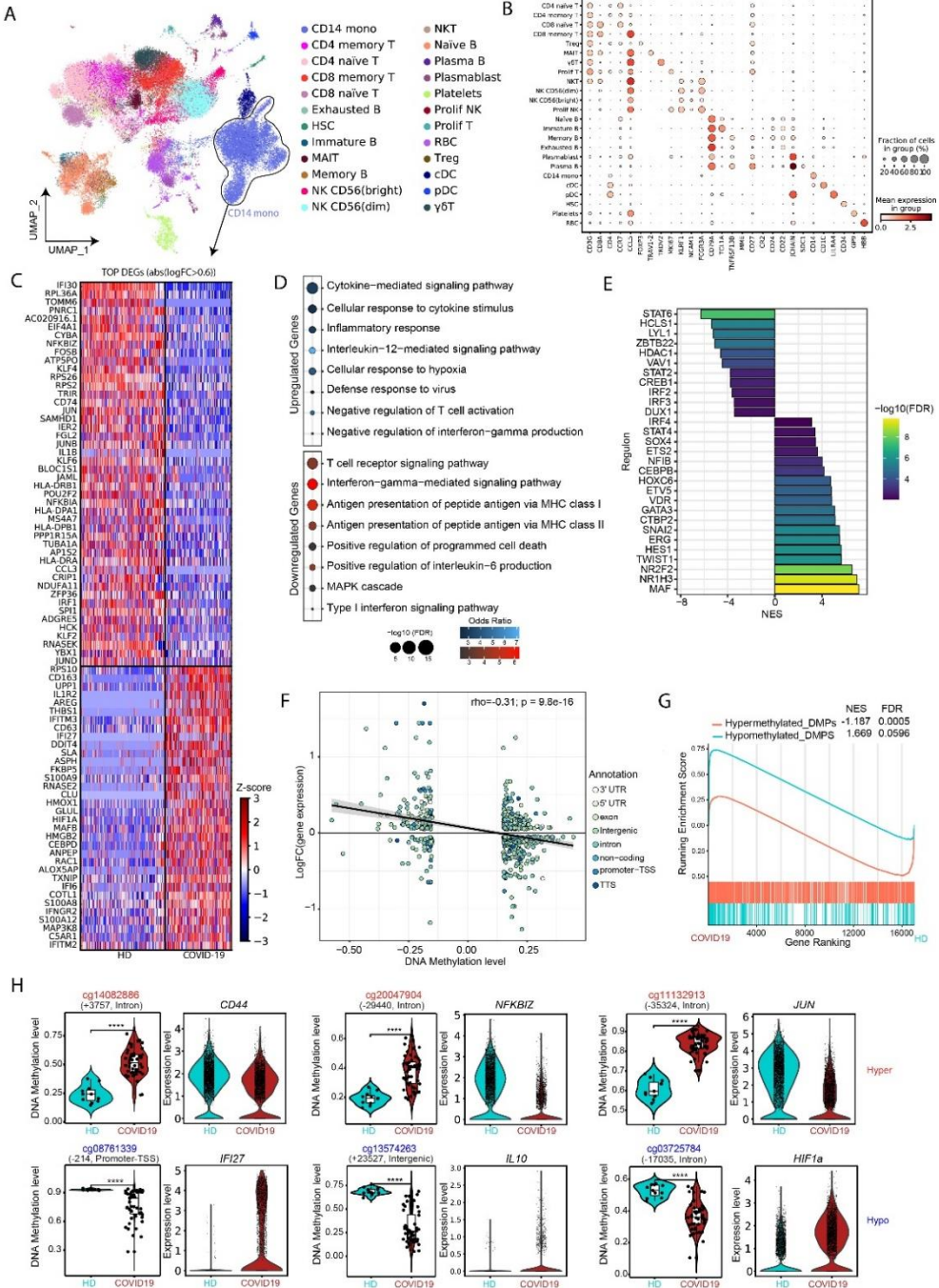
GO analysis of both DEG sets revealed enrichment in functional terms coincident with those from DNA methylation analysis. We observed functional

categories such as cytokine-mediated signaling, IL-12-mediated signaling, negative regulation of T cell activation, negative regulation of IFN γ production, and defense response to the virus in the upregulated cluster genes (Figure 4D). Conversely, functional categories such as antigen processing and presentation by MHC-I and MHC-II and IFN γ -mediated signaling were enriched among the downregulated gene set (Figure 4D). We then studied TFs potentially involved in the transcriptomic changes observed in COVID-19 monocytes, using Discriminant Regulon Expression Analysis (DoRothEA), and found that MAF family members, GATA3, STAT4, and IRF4, were associated with upregulated genes in severe COVID-19 (Figure 4E). Conversely, STAT6, STAT2, IRF2, IRF3, and LYL1 were associated with downregulated genes (Figure 4E). TF enrichment of upregulated and downregulated genes was also consistent with the results from DNA methylation analysis, in which binding motifs for several of these TFs were overrepresented among the regions neighboring the DMPs.

We determined the significance of a negative correlation between DMPs and the expression levels of their closest genes ($\rho = -0.31$; $p = 9.8e - 16$) (Figure 4F). To study the relationship between DNA methylation and expression changes further, we performed Gene Set Enrichment Analysis (GSEA) of the genes associated with hypermethylated and hypomethylated CpG clusters. Genes associated with hypermethylated CpGs were generally downregulated (NES = -1.187; FDR = 0.0005), whereas those associated with hypomethylated CpGs were upregulated (NES = 1.669; FDR = 0.0596) in COVID-19 patients (Figure 4G). GO analysis of genes with an inverse relationship between methylation and expression levels showed enrichment of functional categories like negative regulation of T cells, IFN α , and antigen presentation (Additional file 11. Supp. Figure 5C-D). This analysis reinforced the relationship

between DNA methylation changes and expression changes related to the acquisition of a more tolerogenic phenotype in monocytes in COVID-19 patients. Some examples include *IL10*, a tolerogenic cytokine whose expression is increased in COVID-19, and *NFKB1z*, whose level of expression is decreased (Figure 3H). We validated these results using bisulfite pyrosequencing and qRT-PCR with a new cohort of severe COVID-19 patients (Additional file 11. Supp. Figure 5E-F). The analysis also included mild COVID-19 that showed partial or total DNA methylation changes to the extent seen in severe COVID-19 cases (Additional file 11. Supp. Figure 5E-F).

Figure 4



(See figure legend on next page.)

Figure 4. Correlation between DNA methylation and gene expression. (A) UMAP visualization showing the immune cell populations identified from Louvain clustering and cell-specific marker gene expression. (B) Dot plot representing the expression of selected marker genes identified in the cell population. The scale represents the mean gene expression level in the cell subset and the circle size represents the percentage of cells in the subset of expressing cells. (C) Heatmap representing differentially expressed genes (DEGs) with a $\log_2(\text{FC}) > 0.6$, above, and $\log_2(\text{FC}) < -0.6$, below. Genes overexpressed and downregulated in COVID-19 patients in relation to HDs are depicted in red and blue, respectively. (D) Gene ontology (GO) overrepresentation of GO Biological Process categories comprising the upregulated and downregulated DEGs. The odds ratios for each group and the $-\log_2(\text{FC})$ are shown. Selected significant categories ($\text{FDR} < 0.05$) are shown. (E) Discriminant Regulon Expression Analysis (DoRothEA) of COVID-19 severe patients compared with HDs. Normalized enrichment score (NES) and $\log_2(\text{FC})$ of transcription factor expression are depicted. (F) Correlation of average DNA methylation levels of DMPs with average gene expression of DEGs in the HDs vs. COVID-19 severe patients. $\log_2(\text{FC})$ of expression is plotted on the y-axis, higher numbers representing a higher level of expression in COVID-19 and lower numbers a higher level of expression in HDs. DNA methylation is depicted on the x-axis as $\Delta\beta$, lower numbers representing a lower level of methylation in COVID-19 monocytes, and higher numbers a lower level of methylation in HDs. Points are colored according to their genomic context. (G) Gene set enrichment analysis (GSEA) of HD vs. COVID-19, using hypomethylated-associated genes and hypermethylated-associated genes as genesets. The running enrichment score is represented, and the normalized enrichment score (NES) is shown above ($\text{FDR} < 0.01$). (H) Representation of individual DNA methylation values of DMPs from the hypermethylated and hypomethylated clusters (beta values), the position in respect to the transcription start site, and the relative expression of the closely related DEGs. Statistical significance: * $p < 0.05$, ** $p < 0.01$, *** $p < 0.0005$, **** $p < 0.0001$.

Potential relationship between transcriptional and epigenetic reprogramming and altered immune cell-cell communication

Given the overrepresentation of genes associated with cytokine activity, MHC-II-mediated antigen presentation among the observed DNA methylation, and gene expression alterations in severe COVID-19, we explored the potential correlation of these changes in monocytes with their pattern of communication with other immune cell types. To systematically analyze the effect of cell-cell communication on monocytes, we used CellPhoneDB (www.cellphonedb.org), a repository of ligands, receptors, and their interactions integrated within a statistical framework that predicts enriched cellular interactions between two

cell types using scRNA-seq datasets. This allowed us to infer potentially altered interactions between monocytes and other immune cell subsets in severe COVID-19. In particular, we inspected cell–cell communication alterations between CD14⁺ and CD4⁺ memory, CD4⁺ naïve, CD8⁺ memory, and CD8⁺ naïve T cells; B cell subsets including memory, naïve, and plasma B cells; natural killer cells (NK CD56^{dim}: NK CD56^{bright}) (Figure 5 A,B). Our analysis revealed 4483 ligand/receptor pairs, in which the expression levels of ligands and receptors of CD14⁺ and/or interacting partners in the aforementioned cell types were significantly different between severe COVID-19 patients and HDs, suggesting changes in the interaction of the corresponding immune cells (Additional file 12. Table S7). The aberrant levels of the proteins encoded by these genes in monocytes were validated by flow cytometry (Supp. Figure 5G), supporting a potential impact on cell–cell communication.

Figure 5A illustrates the significant ligand-receptor interactions that may be affected when the expression of receptor in monocytes is altered, revealing their potential impact on other cell types. In general, there was a high frequency of interactions involving different types of NK cells, consistent with the terms observed in the GO analysis performed with DMPs (Figure 1E). *PILRA*, *LILRB1*, *LILRB2*, and *PECAM1* (CD31), the products of which are involved in the inhibition of immune response, were downregulated in monocytes. Their corresponding ligand-encoding genes, *CD99*, *HLA-F*, and *CD38*, were expressed in all the analyzed cell types, except for *CD38*, which is only expressed in NK and plasma B cells. Additionally, the gene encoding for receptor LAIR1, which inhibits IL-2 expression, was upregulated in monocytes [66], which might influence the interaction with cells expressing its corresponding ligand, i.e., plasma B cells and monocytes. Our analysis also revealed changes in the

expression of TNF receptor genes (*TNFRSF14*, *TNFRSF1B*, *TNFRSF1A*) in monocytes, which could affect the interaction with T cells through the ligands encoded by TNF and LTA. This is compatible with the possibility that TNF-associated DNA methylation alterations in monocytes could arise from altered interactions with T cells through these ligand-receptor pairs. We also noted downregulation of the receptor *TNFRSF14*, which interacts with CD160 in NK cells. Some studies have argued that CD160 is essential for NK-mediated IFN γ production [67], a conclusion that is consistent with the results obtained in our gene ontology analysis of the DNA methylation data. *ADGRE5* (CD97) was downregulated in monocytes. This receptor interacts with CD55, which is expressed in all the analyzed cell types. This interaction is involved in leukocyte migration [68]. The potential alteration of this interaction could be linked to the observed hypomethylation of CpGs close to genes related to leukocyte migration (Figure 1E, top).

We also examined DEGs corresponding to ligands expressed in all immune cell types, whose corresponding receptors are expressed in monocytes, to identify potential cell–cell communication alterations that might affect monocytes (Figure 5B). In general, we detected upregulation of ligands in regulatory T cells (Treg) and downregulation of ligands in plasma B cells. We also observed increased levels of *CCL5* and *CCL3*, expressed in NK cells, that interact with the CD191 receptor (*CCR1*), and whose inhibition potentially suppresses immune hyper-activation in critical COVID-19 patients [69]. In the context of antigen presentation, there was upregulation of *HLA-F* from Treg and NKT, which interacts with *LILRB1* in monocytes. Recent studies have associated *LILRB1* with the development of tolerance [70]. Our analysis also revealed low levels of CD99, expressed in CD4+ memory and naïve T cells, Treg

and memory B cells, and the receptor PILRA, which is expressed in monocytes. The opposite occurs with CD8 memory and naïve T cells and NK CD56(bright), which enhances T cell migration [71]. There was a similar trend between CD74 and the receptor APP expressed in monocytes, which is involved in antigen processing and presentation. This could be related to the impaired antigen presentation previously highlighted in our data. In brief, the potential alteration of cell–cell communication events, through increased or decreased levels of ligands and receptors involving inflammatory cytokines, antigen presentation-related factors, and cell activation regulators, in severe COVID-19 patients could affect downstream cell-signaling pathways and TFs and perhaps influence DNA methylation profiles in monocytes, thereby perpetuating aberrant immune responses.

Figure 5

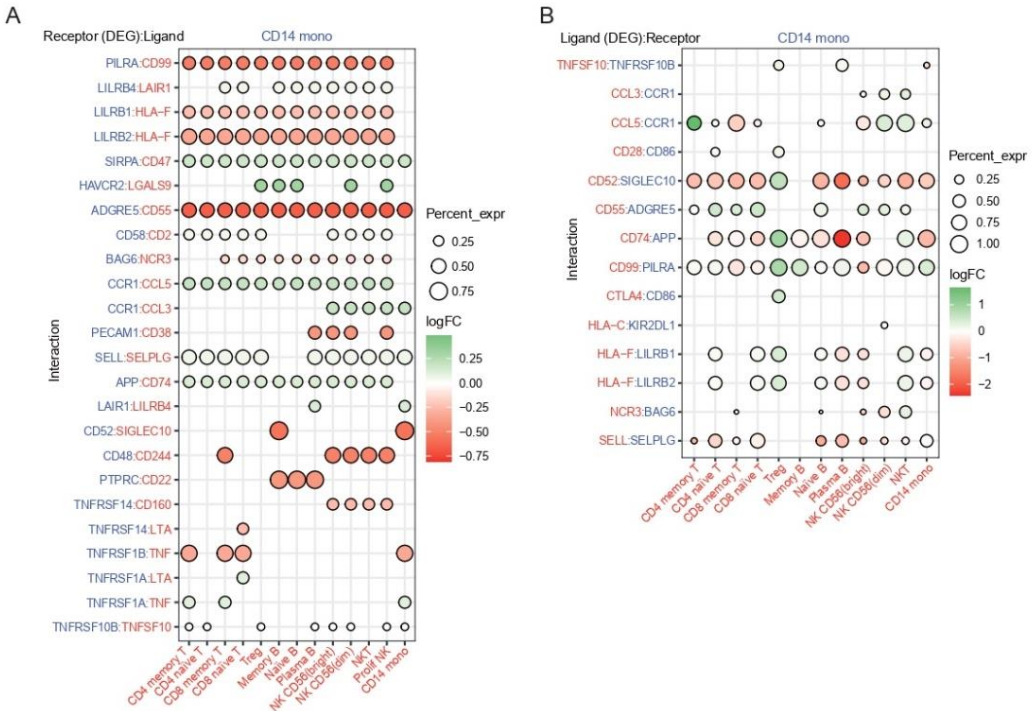


Figure 5. Cell-cell communication analysis. Dot plot of selected receptor/ligand pair (A) and ligand/receptor (B) interactions between CD14 +monocytes and other cell components in the COVID-19 patient group. Gene expression is indicated as log₂(FC) for differentially expressed genes (FDR < 0.05), which, in both cases (A and B), are the molecules presented on the left. The percentage expression of the differentially expressed genes in each cell type is indicated by the circle size. Molecules shown in blue are those expressed in CD14 + monocytes. Molecules expressed in the immune cell partner are shown in red.

DISCUSSION

Our results reveal that peripheral blood monocytes from severe COVID-19 patients display aberrant DNA methylomes and transcriptomes associated with functions related to IFN type I signaling and antigen presentation, among others. The changes are significantly associated with organ damage and with DNA methylation changes occurring in bacterial sepsis. Finally, our analysis suggests that pro-inflammatory cytokines, the release of immature or aberrant monocytes, and specific dysregulated immune cell–cell communication events may be responsible for some epigenetic changes. To date, there have been very few DNA methylation studies addressing the involvement of COVID-19 DNA methylation in regulating the angiotensin-converting enzyme 2 (ACE2) type I membrane receptor gene [72], which is present in arterial, lung type II alveolar cells, where it acts as a SARS-CoV-2 receptor. There is a suggestion that the host epigenome may represent a risk factor for COVID-19 infection. Very few studies have reported alterations in DNA methylation in relation to immune responses [73–75]. Our study aimed to explore the involvement of DNA methylation in relation to a severe COVID-19 outcome in the myeloid compartment, which is directly related to systemic inflammation. We specifically studied monocytes because it is the cell type that undergoes the most dramatic transcriptomic reprogramming during COVID-19 infection [13, 21, 23, 76]. In this regard, our study provides the first instance of DNA methylome profiling in a specific immune cell type in COVID-19 patients.

Our data revealed that most DNA methylation changes in monocytes derived from severe COVID-19 patients occurred in genomic sites enriched in PU.1 binding motifs, consistent with earlier studies showing its role as a pioneer TF directly recruiting TET2 and DNMT3b [77]. In our case, most DNA

methylation changes occurred in genes related to cytokines, MHC class II proteins, and IFN signaling. Similar results about the defective function of MHC-II molecules and activation of apoptosis pathways were obtained in single-cell atlas studies of PBMCs from severe COVID-19 patients [6, 21, 78, 79] and in sepsis [80, 81].

We found that DNA methylation changes in severe COVID-19 patients share some features with sepsis, especially those associated with the expression of tolerogenic cytokines like IL-10 [82]. The acute phase of these infections suggests a dysregulated inflammatory host response, resulting in an imbalance between pro-inflammatory and anti-inflammatory mediators [14]. Some studies have suggested that viral components induce STAT₁ dysfunction and compensatory hyper-activation of STAT₃ in SARS-CoV-2-infected cells [83]. We noted the involvement of kinases like JNK, and earlier studies had shown that COVID-19 infection activates the JNK and ERK pathways that end in the AP-1-dependent gene expression of pro-inflammatory cytokines [84]. One of the most strongly affected TFs is STAT₂, together with STAT₆, which could be linked to the aberrant IFN signaling in monocytes in COVID-19 [83]. The presence of STAT₂ downregulation also suggests a deficiency in the ability to cross-present to CD8⁺ T cells [85].

We also identified GRE binding sites in association with DNA methylation changes. Generally, the glucocorticoid receptor (GR) is activated when patients are treated with GC. However, we also noted significant GRE enrichment in patients who were not treated with GC, suggesting that endogenous production of GC in COVID-19 patients could regulate GR and affect DNA methylation at its genomic binding sites. GC is also produced endogenously in sepsis patients in whom cytokines like IL-1 β , TNF- α , and IL-6

induce its production from the adrenal cortex using cholesterol as a substrate to reduce inflammatory responses [86, 87]. These cytokines were hypomethylated and overexpressed in our dataset, consistent with the results of other studies that have reported increased levels in the serum of COVID-19 patients [88, 89]. GRE binding sites are enriched in the DMPs common to COVID-19 and sepsis. GR is a nuclear receptor expressed in most cell types that can trigger the expression of anti-inflammatory genes through direct DNA binding. Furthermore, GRE represses the action of other inflammation-related TFs, including members of the NF- κ B and AP-1 families [90, 91], which are also known to be downregulated in our cohort. Taken together, our results suggest the existence of a relationship between extracellular factors associated with the cytokine storm occurring in severe COVID-19 and DNA methylation changes. Several studies have shown an increase in the levels of inflammatory cytokines in severe COVID-19, which may contribute to the severity of the disease [92].

However, it is also possible that the DNA methylation changes are partly due to the release of immature or altered monocytes from myelopoiesis, as reported for severe COVID-19 [13, 20, 93, 94] and sepsis [63]. Release of immature myeloid cells from the bone marrow in severe COVID-19 is reminiscent of emergency myelopoiesis [95]. This is a well-known phenomenon, characterized by the mobilization of immature myeloid cells to restore functional immune cells, and by its contribution to the dysfunction of innate immunity [96]. In fact, a proportion of the hypermethylated CpGs in monocytes from severe COVID-19 patients overlap with regions that become demethylated during myeloid differentiation. This suggests that part of the hypermethylated CpG sites in isolated peripheral blood CD14⁺ might be associated with aberrantly differentiated monocytes released into the

bloodstream in severe COVID-19 patients. However, the small numbers of CD34+ cells in the PBMC fraction of COVID-19 patients and the lack of CD14+ cells in this subset suggest no interference with our results for CD14+ CD15- cells, isolated with our method.

The relationship between DNA methylation and gene expression is complex. DNA methylation patterns are cell-type-specific and are established during dynamic differentiation events by sitespecific remodeling at regulatory regions [97]. In general, methylation of CpGs located in gene promoters, first exons, and introns is negatively correlated with gene expression [98]. The analysis of our data shows that there is an inverse correlation between the CpG methylation changes and the expression levels of the closest genes. The comparison of the inferred TFs associated with DNA methylation changes and gene expression changes shows common factors like IRF2 and IRF3, which regulate downregulated genes and hypermethylated CpGs. In this context, it is possible that reduced levels of IFN regulatory factor IRF3 or defective IRF7 function reduces the level of IFN α/β gene expression, increasing the sensitivity to viral infection [12, 99].

Finally, analysis of cell-cell communication has revealed potential relationships between DNA methylation changes and altered communication of monocytes and other immune cells (e.g., T, plasma B and NK cells). Our data suggest the potential reduction of interactions between monocytes and NK cells through CD160, which mediates the antibody-dependent cell-mediated cytotoxicity that it is essential for IFN γ production [67]. The potentially greater interaction between monocytes and Treg through multiple ligand and receptor pairs is an interesting finding, since Tregs are immunosuppressive cells responsible for maintaining immune homeostasis [100]. In any case, the use of

CellPhone DB is useful for inferring cell–cell communications events; however, additional validation experiments would be necessary to validate interactions and activation of downstream signaling pathways.

In our study, we could not determine whether the observed DNA methylation alterations in COVID-19 were the cause or the consequence of the changes in gene expression. The analysis of mild COVID-19 cases, in which the DNA methylation and expression level of a few genes showed differences in their similarities with severe COVID-19 cases, suggests that there are cases where expression changes might anticipate DNA methylation changes. In any case, it is reasonable to propose that some DNA methylation changes help perpetuate dysregulated immune responses.

Some limitations of our study include the size of the cohort, and the unequal numbers of individuals administered particular drugs in the different patient groups, which could have affected the COVID-19 data. However, despite these limitations, we found no significant differences among severe COVID-19 patients with respect to the time they were admitted to the ICU or began to receive treatment. This suggests that DNA methylation is quite a general occurrence in the context of COVID-19. Another limitation concerns the cell population analyzed, since the method for monocyte isolation comprises two populations, CM and IM, one of which (CM) is expanded in the patient group. However, the analysis including the monocyte subsets as a covariate indicates that there are no major differences. Finally, in the comparison with DNA methylation of progenitor cells, it is important to note that the DMPs were overlapped with genomic regions, and not single-base data, and further analyses would be required.

Future studies would benefit from having access to a wider cohort in which it is possible to identify significant links between alterations and drug treatments. Incorporating mild and asymptomatic cases would improve our ability to dissect drug- and severity-related specificity in relation to DNA methylation changes. As is the case for other medical conditions, the analysis of DNA methylation changes would be very likely to help predict disease severity, progression, and recovery.

Our study provides unique insights into the epigenetic alterations of monocytes in severe COVID-19. We have shown that peripheral blood monocytes from severe COVID-19 patients undergo changes in their DNA methylomes, in parallel with changes in expression, and that these significantly overlap with those found in patients with sepsis. We have also shown DNA methylation changes are associated with organ dysfunction. Finally, our results suggest a relationship between DNA methylation changes in COVID-19 patients and changes that occur during myeloid differentiation and others that can be induced by pro-inflammatory cytokines. CellPhoneDB analysis also suggests that alterations in immune cell crosstalk can contribute to transcriptional reprogramming in monocytes, which involves dysregulation of interferon-related genes and genes associated with antigen presentation and chemotaxis.

ACKNOWLEDGEMENTS

We thank the CERCA Programme/Generalitat de Catalunya and the Josep Carreras Foundation for institutional support. We are very grateful to the Cytometry Laboratory and the Scientific and Technological Centers,

University of Barcelona (CCiT-UB), for their help with the gating strategy and cell sorting.

AUTHORS' CONTRIBUTIONS

G.G.-T. and E.B. conceived and designed the study; G.G.-T., A.G.F.-B., and L.C. prepared and purified the samples; G.G.-T., O.M.-P., C.C.-F., and R.M.-F. performed bioinformatic analyses; A.B. analyzed the single-cell datasets; A.R.-S., M.M.G., R.F., and J.C.R.-R. provided the patient samples and analyzed the clinical data; G.G.-T., J.R.-U., R.V.-T., and E.B. analyzed and interpreted the data; G.G.-T. and E.B. wrote the manuscript; all authors read and approved the final manuscript.

FUNDING

This study has been funded by R+D+i project of the Spanish Ministry of Science and Innovation (grant number PID2020-117212RB-I00/MICIN/AEI/10.13039/501100011033). We also thank the Chan Zuckerberg Initiative (grant 2020-216799) and Wellcome Sanger core funding (WT206194). This publication has also been supported by the Unstoppable campaign of the Josep Carreras Leukaemia Foundation. Additional funding comes from Project PI18/00346 (Instituto de Salud Carlos III and co-funded by European Union (ERDF/ESF). A.B. received additional support from a Gates Cambridge Scholarship. Availability of data and materials DNA methylation data for this publication have been deposited in the NCBI Gene Expression Omnibus and are accessible through GEO SuperSeries accession number GSE188573 [30]. Single-cell data generated in this study are available as h5ad files at the European Genome-Phenome Archive (EGA) with Dataset ID EGAD00001007982 [101].

ETHICS APPROVAL AND CONSENT TO PARTICIPATE

This study was approved by the Clinical Research Ethics Committees of Hospital Universitari Germans Trias i Pujol (PI-20-129) and Vall d'Hebron University Hospital (PR(AG)282/2020), which adhered to the principles set out in the WMA Declaration of Helsinki. All samples were managed in compliance with participants' written informed consent to participate in the study.

REFERENCES

1. Lai C-C, Shih T-P, Ko W-C, Tang H-J, Hsueh P-R. Severe acute respiratory syndrome coronavirus 2 (SARS-CoV-2) and coronavirus disease-2019 (COVID-19): The epidemic and the challenges. *Int J Antimicrob Agents*. 2020;55:105924.
2. Schultze JL, Aschenbrenner AC. COVID-19 and the human innate immune system. *Cell*. 2021;184:1671–92.
3. Sette A, Crotty S. Adaptive immunity to SARS-CoV-2 and COVID-19. *Cell*. 2021;184:861–80.
4. Huang C, Wang Y, Li X, Ren L, Zhao J, Hu Y, et al. Clinical features of patients infected with 2019 novel coronavirus in Wuhan, China. *Lancet*. 2020;395:497–506.
5. Tay MZ, Poh CM, Rénia L, MacAry PA, Ng LFP. The trinity of COVID-19: immunity, inflammation and intervention. *Nat Rev Immunol*. 2020;20:363–74.
6. Zhang J-Y, Wang X-M, Xing X, Xu Z, Zhang C, Song J-W, et al. Single-cell landscape of immunological responses in patients with COVID-19. *Nat Immunol*. 2020;21:1107–18.
7. Zhang C, Shi L, Wang F-S. Liver injury in COVID-19: management and challenges. *Lancet Gastroenterol Hepatol*. 2020;5:428–30.
8. Zhou Y, Fu B, Zheng X, Wang D, Zhao C, Qi Y, et al. Pathogenic T-cells and inflammatory monocytes incite inflammatory storms in severe COVID-19 patients. *Natl Sci Rev*. 2020;7:998–1002.
9. Henry BM, de Oliveira MHS, Benoit S, Plebani M, Lippi G. Hematologic, biochemical and immune biomarker abnormalities associated with severe illness and mortality in coronavirus disease 2019 (COVID-19): a meta-analysis. *Clin Chem Lab Med*. 2020;58:1021–8.
10. Lee JS, Park S, Jeong HW, Ahn JY, Choi SJ, Lee H, et al. Immunophenotyping of COVID-19 and influenza highlights the role of type I interferons in development of severe COVID-19. *Sci Immunol*. 2020;5:eabd1554.
11. Gustine JN, Jones D. Immunopathology of hyperinflammation in COVID-19. *Am J Pathol*. 2021;191:4–17.
12. Sato M, Suemori H, Hata N, Asagiri M, Ogasawara K, Nakao K, et al. Distinct and essential roles of transcription factors IRF-3 and IRF-7 in response to viruses for IFN-alpha/beta gene induction. *Immunity*. 2000;13:539–48.
13. Schulte-Schrepping J, Reusch N, Paolik D, Baßler K, Schlickeiser S, Zhang B, et al. Severe COVID-19 is marked by a dysregulated myeloid cell compartment. *Cell*. 2020;182:1419–1440.e23.
14. Hadjadj J, Yatim N, Barnabei L, Corneau A, Boussier J, Smith N, et al. Impaired type I interferon activity and inflammatory responses in severe COVID-19 patients. *Science*. 2020;369:718–24.
15. Blanco-Melo D, Nilsson-Payant BE, Liu W-C, Uhl S, Hoagland D, Møller R, et al. Imbalanced host response to SARS-CoV-2 drives development of COVID-19. *Cell*. 2020;181:1036–1045.e9.
16. Trouillet-Assant S, Viel S, Gaymard A, Pons S, Richard J-C, Perret M, et al. Type I IFN immunoprofiling in COVID-19 patients. *J Allergy Clin Immunol*. 2020;146:206–208.e2.
17. Bastard P, Rosen LB, Zhang Q, Michailidis E, Hoffmann H-H, Zhang Y, et al. Autoantibodies against type I IFNs in patients with life-threatening COVID-19. *Science*. 2020;370:eabd4585.

18. Zhang Q, Bastard P, Liu Z, Le Pen J, Moncada-Velez M, Chen J, et al. Inborn errors of type I IFN immunity in patients with life-threatening COVID-19. *Science*. 2020;370:eabd4570.
19. Arunachalam PS, Wimmers F, Mok CKP, Perera RAPM, Scott M, Hagan T, et al. Systems biological assessment of immunity to mild versus severe COVID-19 infection in humans. *Science*. 2020;369:1210–20.
20. Silvin A, Chapuis N, Dunsmore G, Goubet A-G, Dubuisson A, Derosa L, et al. Elevated Calprotectin and Abnormal Myeloid Cell Subsets Discriminate Severe from Mild COVID-19. *Cell*. 2020;182:1401–1418.e18.
21. Guo C, Li B, Ma H, Wang X, Cai P, Yu Q, et al. Single-cell analysis of two severe COVID-19 patients reveals a monocyte-associated and tocilizumab-responding cytokine storm. *Nat Commun*. 2020;11:3924.
22. Wilk AJ, Rustagi A, Zhao NQ, Roque J, Martínez-Colón GJ, McKechnie JL, et al. A single-cell atlas of the peripheral immune response in patients with severe COVID-19. *Nat Med*. 2020;26:1070–6.
23. Saichi M, Ladjemi MZ, Korniotis S, Rousseau C, Ait Hamou Z, Massenet-Regad L, et al. Single-cell RNA sequencing of blood antigen-presenting cells in severe COVID-19 reveals multi-process defects in antiviral immunity. *Nat Cell Biol*. 2021;23:538–51.
24. Bader SM, Cooney JP, Pellegrini M, Doerflinger M. Programmed cell death: the pathways to severe COVID-19? *Biochem J*. 2022;479:609–28.
25. Álvarez-Errico D, Vento-Tormo R, Sieweke M, Ballestar M, Ballestar E. Epigenetic control of myeloid cell differentiation, identity and function. *Nat Rev Immunol*. 2015;15:7–17.
26. Rodríguez-Ubrea J, de la Calle-Fabregat C, Li T, Ciudad L, Ballestar ML, Català-Moll F, et al. Inflammatory cytokines shape a changing DNA methylome in monocytes mirroring disease activity in rheumatoid arthritis. *Ann Rheum Dis*. 2019;78:1505–16.
27. Lorente-Sorolla C, Garcia-Gomez A, Català-Moll F, Toledano V, Ciudad L, Avendaño-Ortiz J, et al. Inflammatory cytokines and organ dysfunction associate with the aberrant DNA methylome of monocytes in sepsis. *Genome Med*. 2019;11:66.
28. Luo C, Hajkova P, Ecker JR. Dynamic DNA methylation: in the right place at the right time. *Science*. 2018;361:1336–40.
29. Deaton AM, Bird A. CpG islands and the regulation of transcription. *Genes Dev*. 2011;25:1010–22.
30. Godoy-Tena G, Barmada A, Morante-Palacios O, de la Calle-Fabregat C, Ciudad L, Ruiz-Sanmartín A, Martínez-Gallo M, Frank-Bertoncelj M, Ferrer R, Ruiz-Rodríguez JC, Rodríguez-Ubrea J, Vento-Tormo R BE. Epigenetic and transcriptomic remodeling in monocytes of severe COVID-19 patients mirrors systemic changes in cytokines and immune cell crosstalk. *Datasets*. *Gene Expression Omnibus*. 2022. Available from: <https://www.ncbi.nlm.nih.gov/geo/query/acc.cgi?acc=GSE188573>.
31. Morante-Palacios O, Ballestar E. shinyÉPiCo: a graphical pipeline to analyze Illumina DNA methylation arrays. *Bioinformatics*. 2021;37:257–9.
32. Aryee MJ, Jaffe AE, Corrada-Bravo H, Ladd-Acosta C, Feinberg AP, Hansen KD, et al. Minfi: a flexible and comprehensive Bioconductor package for the analysis of Infinium DNA methylation microarrays. *Bioinformatics*. 2014;30:1363–9.
33. Carvalho BS, Irizarry RA. A framework for oligonucleotide microarray preprocessing. *Bioinformatics*. 2010;26:2363–7.
34. Teschendorff AE, Gao Y, Jones A, Ruebner M, Beckmann MW, Wachter DL, et al. DNA methylation outliers in normal breast tissue identify field defects that are enriched in cancer. *Nat Commun*. 2016;7:10478.

35. Heinz S, Benner C, Spann N, Bertolino E, Lin YC, Laslo P, et al. Simple combinations of lineage-determining transcription factors prime cis-regulatory elements required for macrophage and B cell identities. *Mol Cell*. 2010;38:576–89.
36. Bernstein BE, Stamatoyannopoulos JA, Costello JF, Ren B, Milosavljevic A, Meissner A, et al. The NIH Roadmap Epigenomics Mapping Consortium. *Nat Biotechnol*. 2010;28:1045–8.
37. Farlik M, Halbritter F, Müller F, Choudry FA, Ebert P, Klughammer J, et al. DNA methylation dynamics of human hematopoietic stem cell differentiation. *Cell Stem Cell*. 2016;19:808–22.
38. Rodríguez-Ubrea J, Arutyunyan A, Bonder MJ, Del Pino-Molina L, Clark SJ, de la Calle-Fabregat C, et al. Single-cell Atlas of common variable immunodeficiency shows germinal center-associated epigenetic dysregulation in B-cell responses. *Nat Commun*. 2022;13:1779.
39. Heaton H, Talman AM, Knights A, Imaz M, Gaffney DJ, Durbin R, et al. Souporecell: robust clustering of single-cell RNA-seq data by genotype without reference genotypes. *Nat Methods*. 2020;17:615–20.
40. Wolock SL, Lopez R, Klein AM. Scrublet: computational identification of cell doublets in single-cell transcriptomic data. *Cell Syst*. 2019;8:281–291.e9.
41. Stephenson E, Reynolds G, Botting RA, Calero-Nieto FJ, Morgan MD, Tuong ZK, et al. Single-cell multi-omics analysis of the immune response in COVID-19. *Nat Med*. 2021;27:904–16.
42. Lopez R, Regier J, Cole MB, Jordan MI, Yosef N. Deep generative modeling for single-cell transcriptomics. *Nat Methods*. 2018;15:1053–8.
43. Butler A, Hoffman P, Smibert P, Papalexi E, Satija R. Integrating single-cell transcriptomic data across different conditions, technologies, and species. *Nat Biotechnol*. 2018;36:411–20.
44. Wolf FA, Angerer P, Theis FJ. SCANPY: large-scale single-cell gene expression data analysis. *Genome Biol*. 2018;19:15.
45. Yao C, Bora SA, Chen P, Goodridge HS, Gharib SA. Sample processing and single cell RNA-sequencing of peripheral blood immune cells from COVID-19 patients. *STAR Protoc*. 2021;2:100582.
46. Ritchie ME, Phipson B, Wu D, Hu Y, Law CW, Shi W, et al. limma powers differential expression analyses for RNA-sequencing and microarray studies. *Nucleic Acids Res*. 2015;43:e47.
47. Garcia-Alonso L, Holland CH, Ibrahim MM, Turei D, Saez-Rodriguez J. Benchmark and integration of resources for the estimation of human transcription factor activities. *Genome Res*. 2019;29:1363–75.
48. Efremova M, Vento-Tormo M, Teichmann SA, Vento-Tormo R. Cell PhoneDB: inferring cell–cell communication from combined expression of multi-subunit ligand–receptor complexes. *Nat Protoc Springer, US*. 2020;15:1484–506.
49. Koressaar T, Remm M. Enhancements and modifications of primer design program Primer3. *Bioinformatics*. 2007;23:1289–91.
50. Agashe C, Chiang D, Grishin A, Masilamani M, Jones SM, Wood RA, et al. Impact of granulocyte contamination on PBMC integrity of shipped blood samples: Implications for multi-center studies monitoring regulatory T cells. *J Immunol Methods*. 2017;449:23–7.

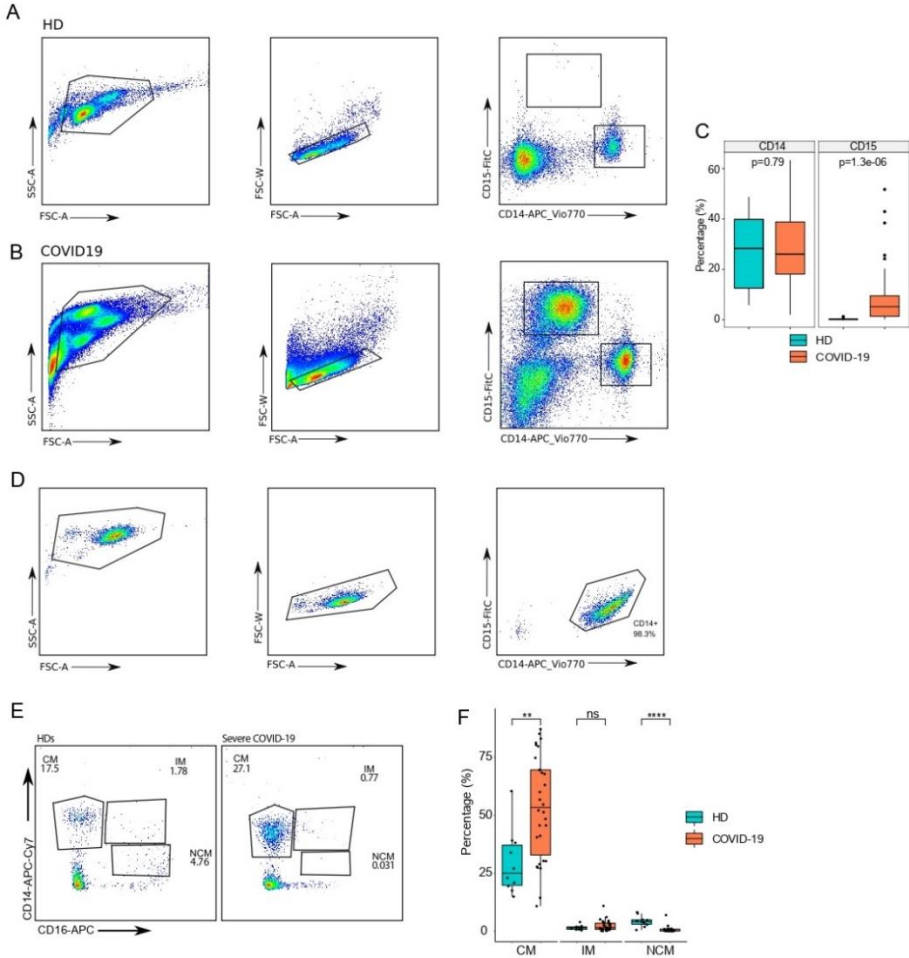
51. Kapellos TS, Bonaguro L, Gemünd I, Reusch N, Saglam A, Hinkley ER, et al. Human monocyte subsets and phenotypes in major chronic inflammatory diseases. *Front Immunol.* 2019;10:2035.
52. Kuhns DB, Priel DAL, Chu J, Zarembek KA. Isolation and functional analysis of human neutrophils. *Curr Protoc Immunol.* 2015;11:7.23.1–7.23.16.
53. Gatti A, Radrizzani D, Viganò P, Mazzone A, Brando B. Decrease of non-classical and intermediate monocyte subsets in severe acute SARS-CoV-2 infection. *Cytometry A.* 2020;97:887–90.
54. Jones PA. Functions of DNA methylation: islands, start sites, gene bodies and beyond. *Nat Rev Genet.* 2012;13:484–92.
55. Ribas VJ, Lopez JC, Ruiz-Rodriguez JC, Ruiz-Sanmartin A, Rello J, Vellido A, On the use of decision trees for ICU outcome prediction in sepsis patients treated with statins. *IEEE Symp Comput Intell Data Min. IEEE.* 2011;2011:37–43.
56. López-Collazo E, Avendaño-Ortiz J, Martín-Quirós A, Aguirre LA. Immune response and COVID-19: a mirror image of sepsis. *Int J Biol Sci.* 2020;16:2479–89.
57. Pietras EM, Saha SK, Cheng G. The interferon response to bacterial and viral infections. *J Endotoxin Res.* 2006;12:246–50.
58. Liu Q, Ou Q, Chen H, Gao Y, Liu Y, Xu Y, et al. Differential expression and predictive value of monocyte scavenger receptor CD163 in populations with different tuberculosis infection statuses. *BMC Infect Dis.* 2019;19:1006.
59. Townsend L, Dyer AH, Naughton A, Imangaliyev S, Dunne J, Kiersey R, et al. Severe COVID-19 is characterised by inflammation and immature myeloid cells early in disease progression. *Heliyon.* 2022;8:e09230.
60. Gibellini L, De Biasi S, Paolini A, Borella R, Boraldi F, Mattioli M, et al. Altered bioenergetics and mitochondrial dysfunction of monocytes in patients with COVID-19 pneumonia. *EMBO Mol Med.* 2020;12:e13001.
61. Brauns E, Azouz A, Grimaldi D, Xiao H, Thomas S, Nguyen M, et al. Functional reprogramming of monocytes in patients with acute and convalescent severe COVID-19. *JCI insight.* 2022;7.
62. Kvedaraitė E, Hertwig L, Sinha I, Ponzetta A, Hed Myrberg I, Lourda M, et al. Major alterations in the mononuclear phagocyte landscape associated with COVID-19 severity. *Proc Natl Acad Sci U S A.* 2021;118:e2018587118.
63. Reyes M, Filbin MR, Bhattacharyya RP, Sonny A, Mehta A, Billman K, et al. Plasma from patients with bacterial sepsis or severe COVID-19 induces suppressive myeloid cell production from hematopoietic progenitors in vitro. *Sci Transl Med.* 2021;13:eabe9599.
64. Ren X, Wen W, Fan X, Hou W, Su B, Cai P, et al. COVID-19 immune features revealed by a large-scale single-cell transcriptome atlas. *Cell.* 2021;184:1895–1913.e19.
65. Hariharan A, Hakeem AR, Radhakrishnan S, Reddy MS, Rela M. The role and therapeutic potential of NF-kappa-B pathway in severe COVID-19 patients. *Inflammopharmacology.* 2021;29:91–100.
66. Spolski R, Li P, Leonard WJ. Biology and regulation of IL-2: from molecular mechanisms to human therapy. *Nat Rev Immunol.* 2018;18:648–59.
67. Tu TC, Brown NK, Kim T-J, Wroblewska J, Yang X, Guo X, et al. CD160 is essential for NK-mediated IFN- γ production. *J Exp Med.* 2015;212:415–29.
68. Safaei M, Clark AJ, Ivan ME, Oh MC, Bloch O, Sun MZ, et al. CD97 is a multifunctional leukocyte receptor with distinct roles in human cancers (Review). *Int J Oncol.* 2013;43:1343–50.

69. Chua RL, Lukassen S, Trump S, Hennig BP, Wendisch D, Pott F, et al. COVID-19 severity correlates with airway epithelium-immune cell inter-actions identified by single-cell analysis. *Nat Biotechnol.* 2020;38:970–9.
70. Nowak I, Malinowski A, Barcz E, Wilczyński JR, Wagner M, Majorczyk E, et al. Possible role of HLA-G, LILRB1 and KIR2DL4 gene polymorphisms in spontaneous miscarriage. *Arch Immunol Ther Exp (Warsz).* 2016;64:505–14.
71. Dufour EM, Deroche A, Bae Y, Muller WA. CD99 is essential for leukocyte diapedesis in vivo. *Cell Commun Adhes.* 2008;15:351–63.
72. Albini A, Di Guardo G, Noonan DM, Lombardo M. The SARS-CoV-2 receptor, ACE-2, is expressed on many different cell types: implications for ACE-inhibitor- and angiotensin II receptor blocker-based cardiovascular therapies. *Intern Emerg Med.* 2020;15:759–66.
73. Corley MJ, Pang APS, Dody K, Mudd PA, Patterson BK, Seethamraju H, et al. Genome-wide DNA methylation profiling of peripheral blood reveals an epigenetic signature associated with severe COVID-19. *J Leukoc Biol.* 2021;110:21–6.
74. Balnis J, Madrid A, Hogan KJ, Drake LA, Chieng HC, Tiwari A, et al. Blood DNA methylation and COVID-19 outcomes. *Clin Epigenetics.* 2021;13:118.
75. Castro de Moura M, Davalos V, Planas-Serra L, Alvarez-Errico D, Arribas C, Ruiz M, et al. Epigenome-wide association study of COVID-19 severity with respiratory failure. *EBioMedicine.* 2021;66:103339.
76. Yao C, Bora SA, Parimon T, Zaman T, Friedman OA, Palatinus JA, et al. Cell-type-specific immune dysregulation in severely ill COVID-19 patients. *Cell Rep.* 2021;34:108590.
77. de la Rica L, Rodríguez-Ubrea J, García M, Islam ABMMK, Urquiza JM, Hernandez H, et al. PU.1 target genes undergo Tet2-coupled demethylation and DNMT3b-mediated methylation in monocyte-to-osteoclast differentiation. *Genome Biol.* 2013;14:1–21.
78. Xu G, Qi F, Li H, Yang Q, Wang H, Wang X, et al. The differential immune responses to COVID-19 in peripheral and lung revealed by single-cell RNA sequencing. *Cell Discov.* 2020;6:73.
79. Villani A-C, Satija R, Reynolds G, Sarkizova S, Shekhar K, Fletcher J, et al. Single-cell RNA-seq reveals new types of human blood dendritic cells, monocytes, and progenitors. *Science.* 2017;356:eaah4573.
80. Delano MJ, Ward PA. Sepsis-induced immune dysfunction: can immune therapies reduce mortality? *J Clin Invest.* 2016;126:23–31.
81. Venet F, Demaret J, Gossez M, Monneret G. Myeloid cells in sepsis-acquired immunodeficiency. *Ann NY Acad Sci.* 2021;1499:3–17.
82. Boks MA, Kager-Groenland JR, Haasjes MSP, Zwaginga JJ, van Ham SM, ten Brinke A. IL-10-generated tolerogenic dendritic cells are optimal for functional regulatory T cell induction—a comparative study of human clinical-applicable DC. *Clin Immunol.* 2012;142:332–42.
83. Matsuyama T, Kubli SP, Yoshinaga SK, Pfeffer K, Mak TW. An aberrant STAT pathway is central to COVID-19. *Cell Death Differ.* 2020;27:3209–25.
84. Varshney B, Agnihotram S, Agnihotram S, Tan Y-J, Baric R, Lal SK. SARS coronavirus 3b accessory protein modulates transcriptional activity of RUNX1b. *PLoS ONE.* 2012;7:e29542.
85. Xu J, Lee MH, Chakhtoura M, Green BL, Kotredes KP, Chain RW, et al. STAT2 is required for TLR-induced murine dendritic cell activation and cross-presentation. *J Immunol.* 2016;197:326–36.
86. Vandewalle J, Libert C. Glucocorticoids in sepsis: to be or not to be. *Front Immunol.* 2020;11:1318.

87. Dantzer R. Neuroimmune interactions: from the brain to the immune system and vice versa. *Physiol Rev.* 2018;98:477–504.
88. Conti P, Ronconi G, Caraffa A, Gallenga C, Ross R, Frydas I, et al. Induction of pro-inflammatory cytokines (IL-1 and IL-6) and lung inflammation by Coronavirus-19 (COVI-19 or SARS-CoV-2): anti-inflammatory strategies. *J Biol Regul Homeost Agents.* 2020;34:327–31.
89. Belfer I, Buzas B, Hipp H, Dean M, Evans C, Lorincz I, et al. Haplotype structure of inflammatory cytokines genes (IL1B, IL6 and TNF/LTA) in US Caucasians and African Americans. *Genes Immun.* 2004;5:505–12.
90. Adcock IM, Nasuhara Y, Stevens DA, Barnes PJ. Ligand-induced differentiation of glucocorticoid receptor (GR) trans-repression and transactivation: preferential targeting of NF-kappaB and lack of I-kappaB involvement. *Br J Pharmacol.* 1999;127:1003–11.
91. Cain DW, Cidlowski JA. After 62 years of regulating immunity, dexamethasone meets COVID-19. *Nat Rev Immunol.* 2020;20:587–8.
92. Vabret N, Britton GJ, Gruber C, Hegde S, Kim J, Kuksin M, et al. Immunology of COVID-19: current state of the science. *Immunity.* 2020;52:910–41.
93. Dress RJ, Ginhoux F. Monocytes and macrophages in severe COVID-19 - friend, foe or both? *Immunol Cell Biol.* 2021;99:561–4.
94. Szabo PA, Dogra P, Gray JI, Wells SB, Connors TJ, Weisberg SP, et al. Longitudinal profiling of respiratory and systemic immune responses reveals myeloid cell-driven lung inflammation in severe COVID-19. *Immunity.* 2021;54:797–814.e6.
95. Schultze JL, Mass E, Schlitzer A. Emerging principles in myelopoiesis at homeostasis and during infection and inflammation. *Immunity.* 2019;50:288–301.
96. Mann ER, Menon M, Knight SB, Konkel JE, Jagger C, Shaw TN, et al. Longitudinal immune profiling reveals key myeloid signatures associated with COVID-19. *Sci Immunol.* 2020;5:eabd6197.
97. Ehrlich M, Lacey M. DNA methylation and differentiation: silencing, upregulation and modulation of gene expression. *Epigenomics.* 2013;5:553–68.
98. Li L, Gao Y, Wu Q, Cheng ASL, Yip KY. New guidelines for DNA methylation studies regarding 5-hydroxymethylcytosine for understanding transcriptional regulation. *Genome Res.* 2019;29:543–53.
99. Salman AA, Waheed MH, Ali-Abdulsahib AA, Atwan ZW. Low type I interferon response in COVID-19 patients: interferon response may be a potential treatment for COVID-19. *Biomed reports.* 2021;14:43.
100. Kondělková K, Vokurková D, Krejsek J, Borská L, Fiala Z, Ctírad A. Regulatory T cells (TREG) and their roles in immune system with respect to immunopathological disorders. *Acta medica (Hradec Kral).* 2010;53:73–7.
101. Single-cell multi-omics analysis of COVID-19 patients with pre-existing autoimmune diseases. Dataset. European Genome-Phenome Archive. 2022. Available from: <https://ega-archi.ve.org/datasets/EGADo0001007982>.

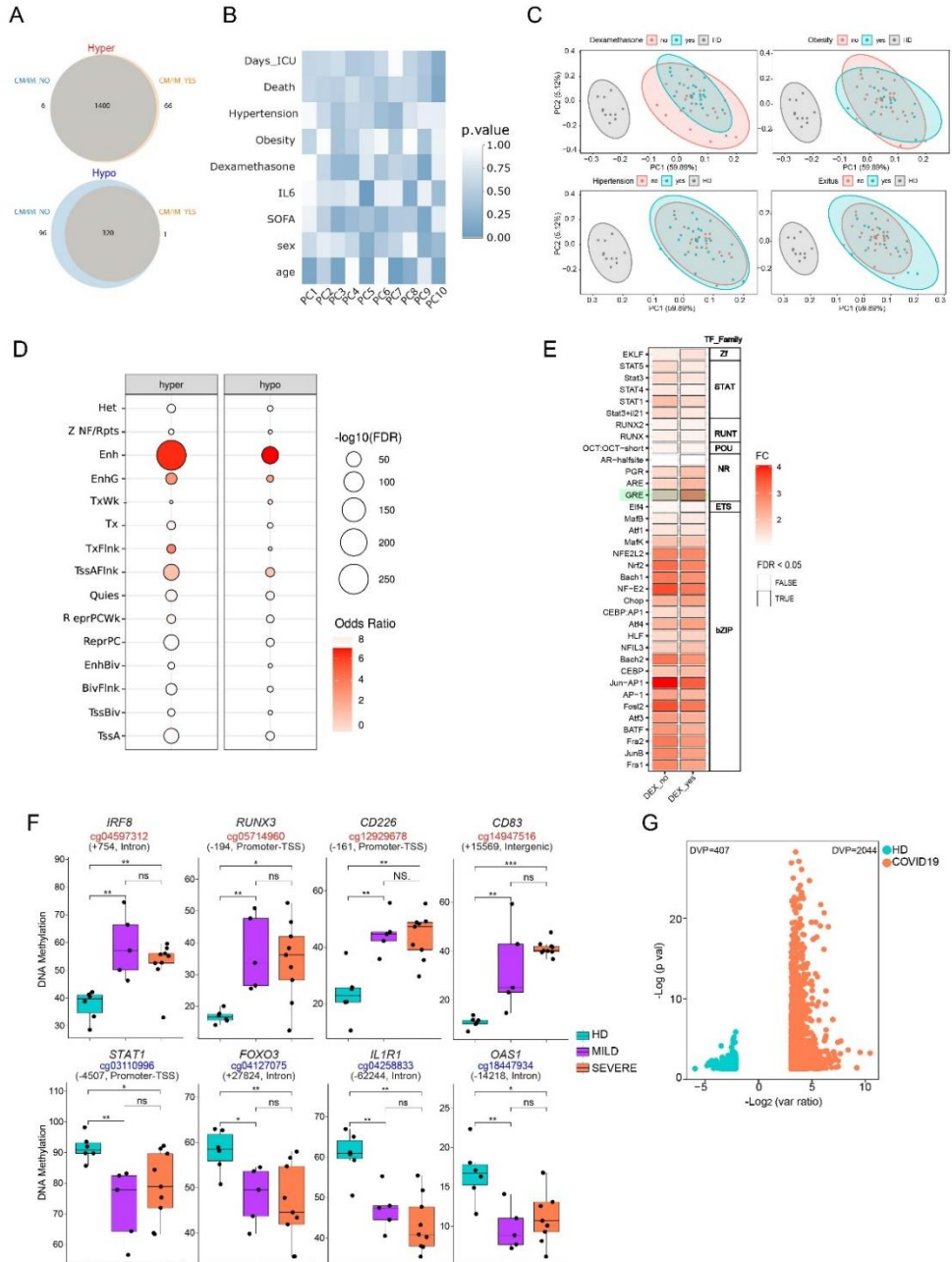
SUPPLEMENTARY FIGURES

Figure S1



Supp. Figure 1. Flow cytometry profiles of a representative sample for each group; HD (A) and COVID-19 (B) indicating the sorting strategy and gates used in the study. (C) Boxplot representing the mean percentage of CD14+ and CD15+ cells in HD and patients. (D) Flow cytometry profile of the CD14+CD15- purified monocytes using the same gates used in the study. (E) HD and COVID-19 indicating the gates used for monocyte subtype analysis (classical monocytes, CM; intermediate monocytes, IM; and non-classical monocytes, NCM) (F) Boxplot representing the mean percentage of CM, IM and NCM in HD and COVID-19 patients.

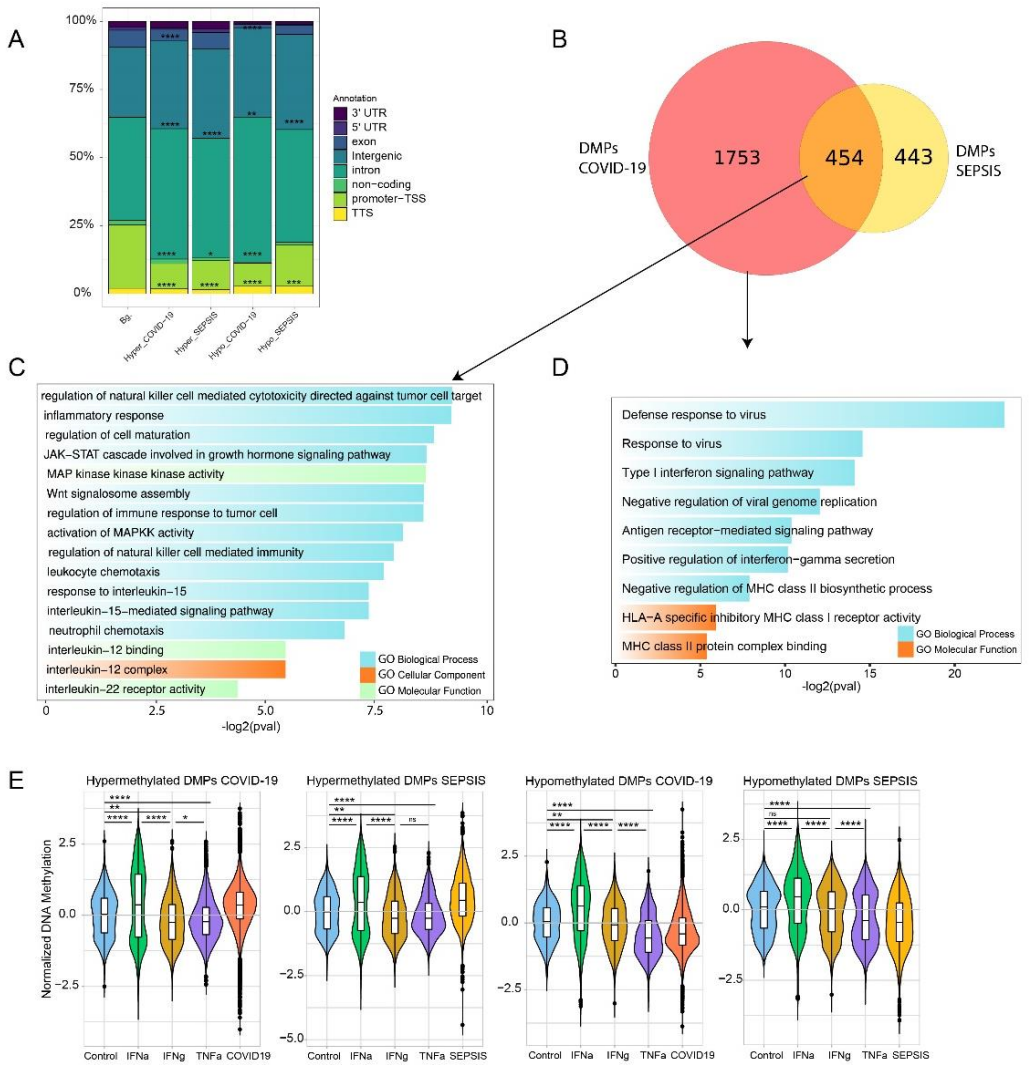
Figure S2



(See figure legend on next page.)

Supp. Figure 2. DNA methylation analysis in blood monocytes of severe COVID-19 patients. (A) Venn diagram of the overlap of hyper- and hypomethylated DMPs identified with a subcluster of samples including (CM/IM_YES) or not (CM/IM_NO) the CM and IM percentage as a covariable in the comparison between HD and severe COVID-19 patients (B) Heatmap representation of beta values of first 10 Principal component (PC) analysis that correlations PCs with different clinical variables. Numerical variables were correlated to PCs using Pearson correlation, whereas categorical variables were entered in a linear model together with the PCs. (C) Principal component analysis (PCA) of the DMPs. The HDs are illustrated in grey, and the severe COVID-19 patients are illustrated as blue and red in function of the clinical parameter or treatment with dexamethasone. (D) Enrichment analysis of different chromatin states for CpGs sites corresponding the Hyper- and Hypomethylated clusters. The FDR is represented with the size of the bubble, as shown. The relative enrichment is represented as Odds Ratio. TssA, Active TSS; TssBiv, Bivalent/Poised TSS; BivFlnk, Flanking Bivalent TSS/Enh; EnhBiv, Bivalent Enhancer; ReprPC, Repressed PolyComb; ReprPCWk, Weak Repressed PolyComb; Quies, Quiescent/Low; TssAFlnk, Flanking Active TSS; TxFlnk, Transcr. at gene 5' and 3'; Tx, Strong transcription; TxWk, Weak transcription; EnhG, Genic enhancers; Enh, Enhancers; ZNF/Rpts, ZNF genes & repeats; Het, Heterochromatin. (E) TF binding motif analysis of hypomethylated DMPs comparing patients no treated with dexamethasone vs. HDs (DEX_no) and patients treated with dexamethasone vs. HDs (DEX_yes). The panel shows the fold change (FC), TF family. Black outlined boxes indicate TF binding motifs with FDR values < 0.05. (F) Box plot of individual DNA methylation values of CpG from the hypermethylated and hypomethylated clusters with the name of the closest gene and the position in respect to the transcription start site calculated using pyrosequencing in the validation cohort that include HD and patients with mild and severe infection of COVID-19. (G) Volcano plot showing the p value vs the variance ratio for HD and COVID-19 associated differentially variable CpG positions (DVPs). DVPs were identified using the algorithm iEVORA. Statistical significance: * $p < 0.05$, ** $p < 0.01$, *** $p < 0.0005$, **** $p < 0.0001$.

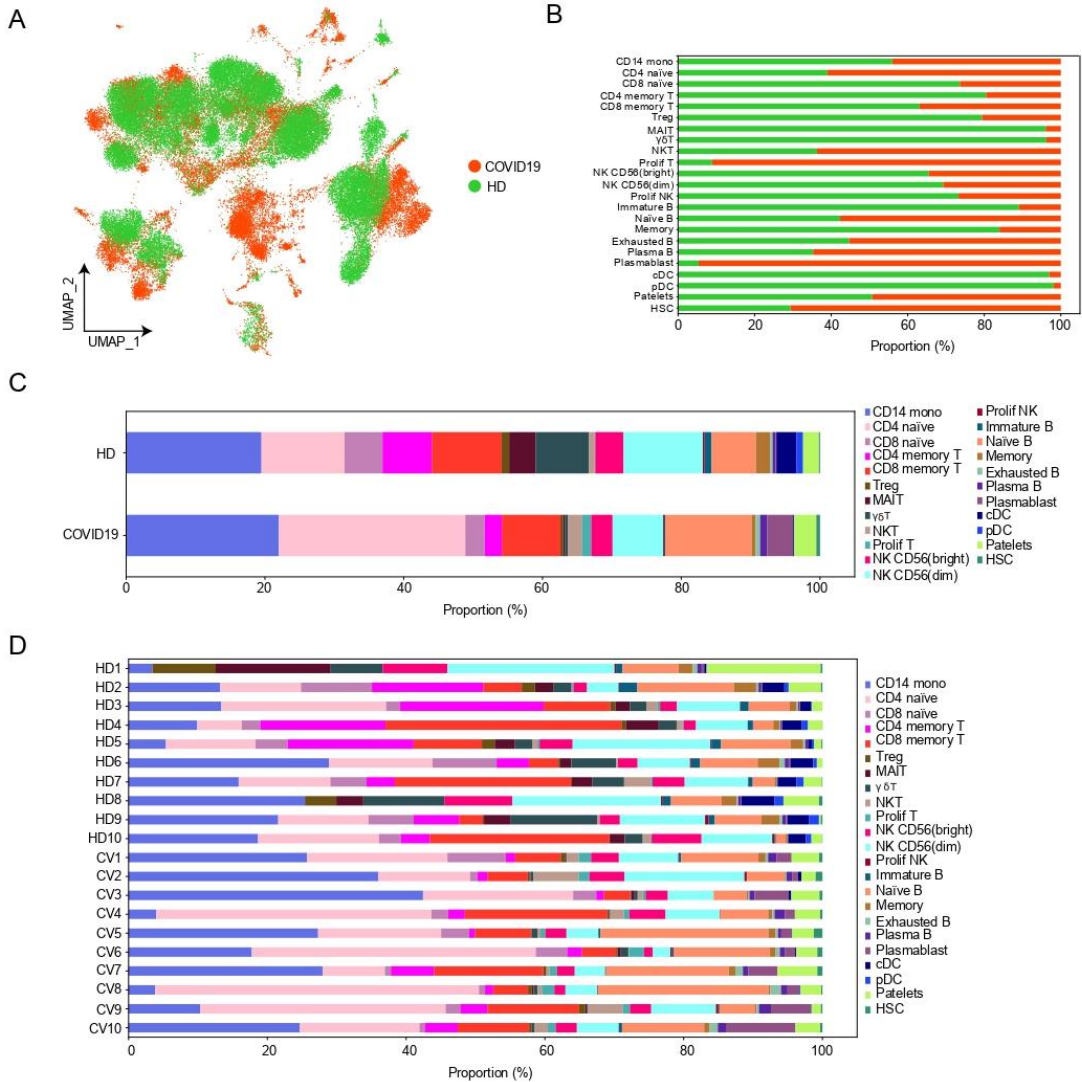
Figure S3



(See figure legend on next page.)

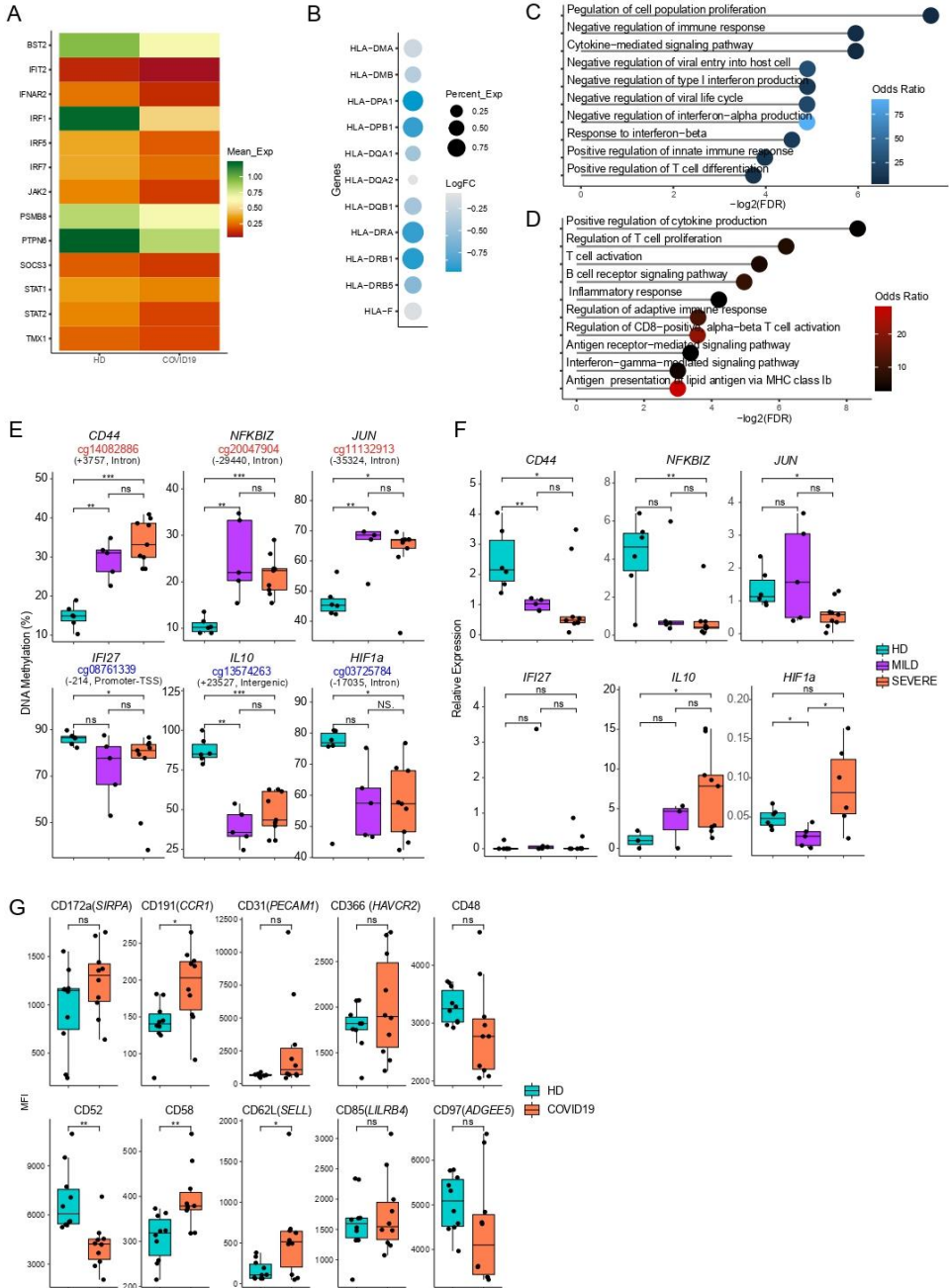
Supp. Figure 3. DNA methylation comparative analysis between blood monocytes of severe COVID-19 patients and bacterial sepsis patients (A) Proportions of the genomic locations (in relation to genes) of hyper- and hypomethylated DMPs in COVID-19 and sepsis; Bg., background, EPIC probes. (B) Venn diagram of the overlap of COVID-19 DMPs identified by the comparison between HD and severe COVID-19 patients with DMPs identified by the comparison between HD and septic patients. Gene ontology (GO) analysis of the shared (C) and not shared (D) DMPs from the previous representation. (E) Violin plot of the mean methylation status of the identified DMPs with β -values obtained from monocytes derived from healthy donor PBMCs exposed *in vitro* for 4 days to interferon-alpha (IFN α) (100ng/mL), interferon gamma (IFN γ) (100ng/mL), tumor necrosis factor-alpha (TNF- α) (10ng/mL) and untreated (Control) (n=3), [26]. Statistical significance: * $p < 0.05$, ** $p < 0.01$, *** $p < 0.0005$, **** $p < 0.0001$.

Figure S4



Supp. Figure 4. (A) UMAP visualization showing the two groups identified from Louvain clustering. (B) Barplot representation of the proportion of the two study groups in the different cell type found. (C) Barplot representation of proportion of each cell type in each study group. (D) Barplot representation of proportion of each cell type in each sample used for the scRNA-seq analysis.

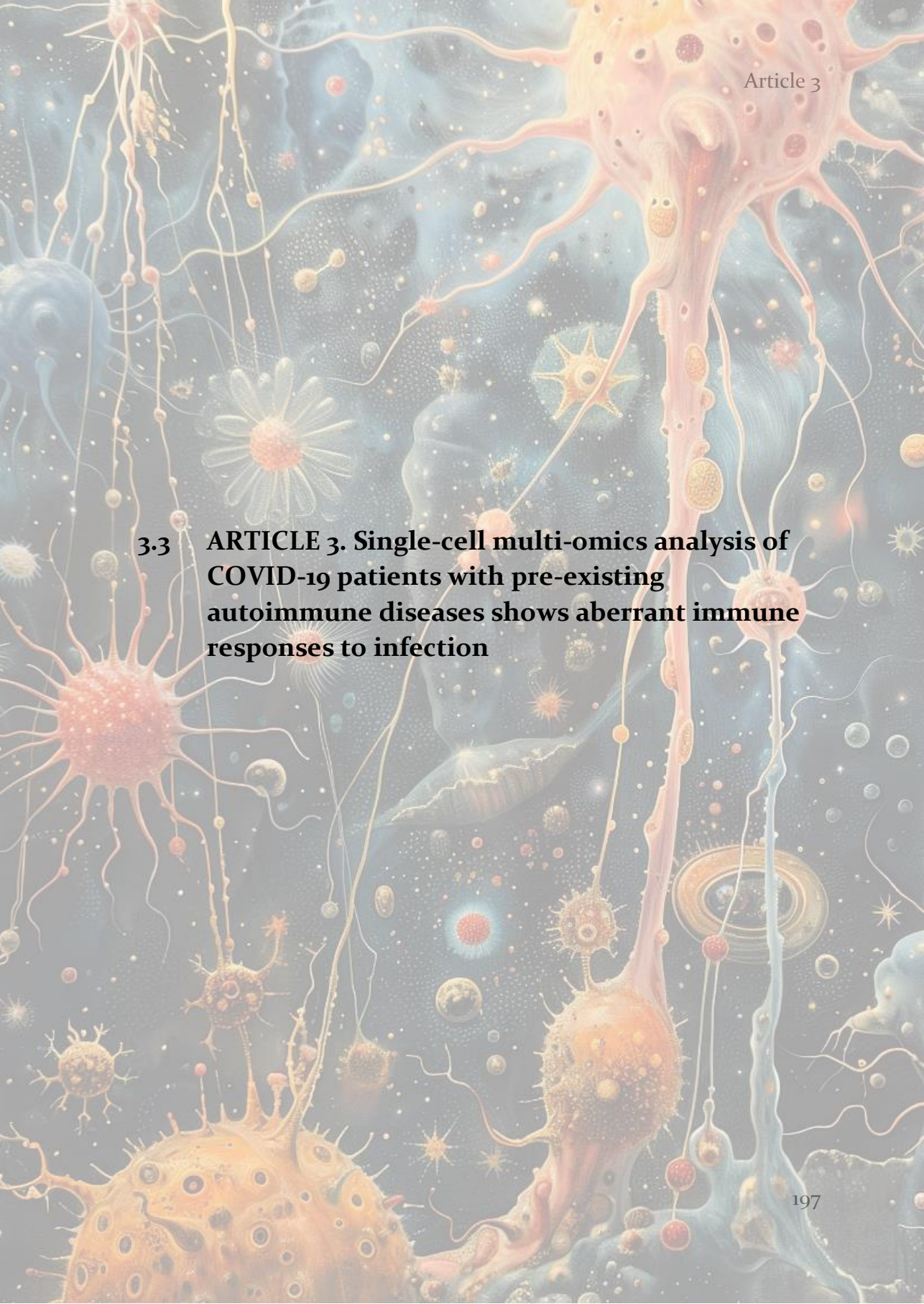
Figure S5



(See figure legend on the next page.)

Supp. Figure 5. Analysis of DEG in monocytes derived from severe COVID-19 patients. (A) Heatmap representation of expression levels of IFN genes (ligands and receptor) in HD and COVID-19 CD14⁺ monocytes. Gene ontology (GO) analysis of the upregulated. (B) Dot plot of major histocompatibility complex (MHC) genes. LogFc and percentage of expression is represented. (C,D) Go of the Up and downregulated DEG that present a negative correlation with their close CpG. (E) Box plot of individual DNA methylation values of CpG from the hypermethylated and hypomethylated clusters with the name of the closest gene and the position in respect to the transcription start site. Calculated using pyrosequencing in the validation cohort that include HD and patients with mild and severe infection of COVID-19. (F) Box plot of relative expression of individual genes performed by real-time quantitative polymerase chain reaction (RT-qPCR) in the validation cohort that include HD and patients with mild and severe infection of COVID-19. (G) Box plot of mean fluorescence intensity (MFI) of cell surface markers in CD14⁺ cells in the cohort used for single cell analysis. Statistical significance: * $p < 0.05$, ** $p < 0.01$, *** $p < 0.0001$, **** $p < 0.00001$.

3.3 ARTICLE 3. Single-cell multi-omics analysis of COVID-19 patients with pre-existing autoimmune diseases shows aberrant immune responses to infection



Single-cell multi-omics analysis of COVID-19 patients with pre-existing autoimmune diseases shows aberrant immune responses to infection

Anis Barmada^{1,2}, Louis-François Handfield^{*1}, **Gerard Godoy-Tena**^{*3}, Carlos de la Calle-Fabregat^{*3}, Laura Ciudad³, Anna Arutyunyan¹, Eduardo Andrés-León⁴, Regina Hooi, Tarryn Porter¹, Agnes Oszlanczi¹, Laura Richardson¹, Fernando J. Calero-Nieto⁵, Nicola K. Wilson⁵, Domenica Marchese⁶, Carmen Sancho-Serra¹, Jorge Carrillo⁷, Silvia Presas-Rodríguez⁸, Cristina Ramo-Tello⁸, Adolfo Ruiz-Sanmartín⁹, Ricard Ferrer⁹, Juan Carlos Ruiz-Rodríguez⁹, Mónica Martínez-Gallo¹⁰, Mónica Munera-Campos¹¹, Jose Manuel Carrascosa¹¹, Berthold Göttgens⁵, Holger Heyn^{6,12}, Elena Prigmore¹, Ivette Casafont-Solé^{13,14}, Xavier Solanich¹⁵, Ildelfonso Sánchez-Cerrillo¹⁶, Isidoro González-Álvaro¹⁷, Maria Gabriella Raimondo^{18,19}, Andreas Ramming^{18,19}, Javier Martín⁴, Eva Martínez-Cáceres^{20,21}, Esteban Ballestar³, Roser Vento-Tormo¹¹ and Javier Rodríguez-Ubreva³

1. Wellcome Sanger Institute, Wellcome Genome Campus, Cambridge, United Kingdom
2. Department of Medical Genetics, University of Cambridge, Cambridge, United Kingdom
3. Epigenetics and Immune Disease Group, Josep Carreras Research Institute (IJC), Barcelona, Spain
4. Instituto de Parasitología y Biomedicina López-Neyra, Consejo Superior de Investigaciones Científicas (IPBLN-CSIC), Granada, Spain
5. Department of Haematology and Wellcome & MRC Cambridge Stem Cell Institute, University of Cambridge, Cambridge, United Kingdom
6. CNAG-CRG, Centre for Genomic Regulation (CRG), Barcelona Institute of Science and Technology (BIST), Barcelona, Spain
7. IrsiCaixa AIDS Research Institute, Hospital Germans Trias i Pujol, Badalona, Spain
8. MS Unit, Department of Neurology, Germans Trias i Pujol University Hospital, Barcelona, Spain
9. Department of Intensive Care, Hospital Universitari Vall d'Hebron, Shock, Organ Dysfunction and Resuscitation Research Group, Vall d'Hebron Research Institute (VHIR), Barcelona, Spain
10. Division of Immunology, Hospital Universitari Vall d'Hebron (HUVH), Vall d'Hebron Research Institute (VHIR), Barcelona, Spain

11. Dermatology Service, Germans Trias i Pujol University Hospital, LCMN, Germans Trias i Pujol Research Institute (IGTP), Barcelona, Spain
12. Universitat Pompeu Fabra (UPF), Barcelona, Spain
13. Department of Rheumatology, Germans Trias i Pujol University Hospital, LCMN, Germans Trias i Pujol Research Institute (IGTP), Barcelona, Spain
14. Department of Infectious Diseases, Germans Trias i Pujol University Hospital, Barcelona, Spain
15. Department of Internal Medicine, Hospital Universitari de Bellvitge, Bellvitge Biomedical Research Institute (IDIBELL), L'Hospitalet de Llobregat, Barcelona, Spain
16. Department of Immunology, Hospital Universitario La Princesa, IIS-IP, Madrid, Spain
17. Rheumatology Service, Hospital Universitario La Princesa, IIS-IP, Madrid, Spain
18. Department of Internal Medicine 3, Friedrich-Alexander-University Erlangen-Nürnberg (FAU) and Universitätsklinikum Erlangen, Erlangen, Germany
19. Deutsches Zentrum Immuntherapie (DZI), Friedrich-Alexander-University Erlangen-Nürnberg and Universitätsklinikum Erlangen, Erlangen, Germany
20. Division of Immunology, Germans Trias i Pujol University Hospital, LCMN, Germans Trias i Pujol Research Institute (IGTP), Barcelona, Spain
21. Department of Cell Biology, Physiology, and Immunology, Universitat Autònoma, Barcelona, Spain

* Equal contribution

ABSTRACT

In COVID-19, hyperinflammatory and dysregulated immune responses contribute to severity. Patients with pre-existing autoimmune conditions can therefore be at increased risk of severe COVID-19 and/or associated sequelae, yet SARS-CoV-2 infection in this group has been little studied. Here, we performed single-cell analysis of peripheral blood mononuclear cells from patients with three major autoimmune diseases (rheumatoid arthritis, psoriasis, or multiple sclerosis) during SARS-CoV-2 infection. We observed compositional differences between the autoimmune disease groups coupled with altered patterns of gene expression, transcription factor activity, and cell-cell communication that substantially shape the immune response under SARS-CoV-2 infection. While enrichment of HLA-DR_{low} CD14⁺ monocytes was observed in all three autoimmune disease groups, type-I interferon signaling as well as inflammatory T cell and monocyte responses varied widely between the three groups of patients. Our results reveal disturbed immune responses to SARS-CoV-2 in patients with pre-existing autoimmunity, highlighting important considerations for disease treatment and follow-up.

KEYWORDS: Autoimmunity, COVID-19, Multiple sclerosis, Psoriasis, Rheumatoid arthritis.

INTRODUCTION

Clinical features of severe acute respiratory syndrome coronavirus 2 (SARS-CoV-2) infection, which causes COVID-19, range from mild or moderate respiratory tract disease to severe disease and respiratory failure. This range of clinical presentations can be dependent on the fitness of the host immune system and the specific immune response mounted against the virus. An effective immune response against SARS-CoV-2 requires coordination between the innate and adaptive immune systems, including the activity of granulocytes, macrophages, and T and B cells [1, 2]. Importantly, some patients develop dysregulated immune responses against SARS-CoV-2 leading to hyperinflammation. This hyperinflammation has been associated with mortality in COVID-19 patients –in whom it is frequently observed in the context of advanced age and comorbidities– suggesting an effect of underlying systemic chronic inflammation [3, 4]. Immune hyperactivation leads to excessive production of inflammatory mediators, either systemic or at the site of infection, that further exacerbate disease symptoms, causing lung tissue destruction and eventual respiratory failure [5]. Specifically, overexpression of IL-6 and IL-1 β has been implicated as a marker of disease severity [6, 7]. Impairment of the type I IFN response has also been identified as a marker of COVID-19 severity, which is further associated with an exacerbated inflammatory response partially driven by NF- κ B and TNF- α activation [7]. This emphasizes the importance of a balanced immune response to the infection.

Single-cell studies have shed light on the underlying immune cell-specific dysregulation in COVID-19-associated hyperinflammation [8-12]. Generally, T cells and inflammatory monocytes are particularly involved in the immune dysregulation and hyperactivation exhibited by COVID-19 patients

[10]. In addition, several studies have indicated an increase in neutrophils and a decrease in nonclassical (CD14_{low}CD16_{hi}) monocytes in severe COVID-19 patients [7, 13]. Further research has demonstrated that transcriptomic profiles of monocytes in COVID-19 reflect defective antigen presentation and IFN responsiveness, which contrasts with the higher responsiveness to IFN signaling noted in lymphocytes [14]. Adaptive immune cells have also been shown to contribute to disease severity, for example through neutrophil recruitment and proinflammatory monocyte/macrophage polarization by Th1 and Th17 responses [2, 15, 16]. Regarding CD4⁺ T cells, previous studies have observed cytopenia in severe COVID-19 patients coupled with substantial heterogeneity of the molecular profile [17, 18].

There is currently only sparse and contradictory evidence regarding the risk of viral infection or evolution to severe COVID-19 forms in individuals with chronic underlying immune pathologies, including autoimmune diseases [19-23]. There further remains a need for knowledge about the specific antiviral immune responses mounted by such patients. To address this matter, we performed single-cell analysis of the transcriptome, surface proteome, and T-cell receptors of peripheral blood mononuclear cells (PBMCs) from COVID-19 patients with three distinct autoimmune diseases – rheumatoid arthritis (RA), psoriasis (Ps), or multiple sclerosis (MS). Our results indicate the existence of highly disturbed immune responses against SARS-CoV-2 that are governed by the specific autoimmune disease context, which may ultimately influence clinical outcomes such as disease severity and the development of sequelae in these patient populations.

MATERIALS AND METHODS

Study participants and sample collection

Human blood samples were collected from patients under SARS-CoV-2 infection with or without pre-existing autoimmune conditions (RA, Ps, MS, and control) as previously diagnosed according to established criteria. COVID-19 individuals categorized as ‘mild’ were those who were located in a ward and did not need oxygen. Those placed outside of the ICU but requiring oxygen were categorized as “moderate”. “Severe” disease was applicable to all patients in the ICU or those requiring noninvasive ventilation. All samples were collected when patients displayed COVID-19 symptoms (with the exception of one patient who was asymptomatic; Supporting information Table S1), thus during the progression of the disease and not at the convalescence stage after recovery. They were collected at Hospital La Princesa, Hospital Vall d’Hebron, Hospital Can Ruti, and Hospital Bellvitge (Spain). All donors received oral and written information about the possibility that their blood would be used for research purposes, and any questions that arose were answered. Patients included in this study were individuals infected with SARS-CoV-2 between March and November of 2020 in Spain. Information about which SARS-CoV-2 lineage was most frequent [24] at the time of infection for each patient (the B.1.177 variant for most patients) can be found in Supporting information Table S1. Prior to sample collection, donors signed a consent form approved by the Ethics Committee of their corresponding hospital, which adhered to the principles set out in the WMA Declaration of Helsinki. PBMCs were obtained from peripheral blood by Ficoll gradient using Lymphocyte Isolation Solution (Rafer). Once PBMCs had been isolated, all samples were stored at -150°C in fetal bovine serum (FBS) + 10% DMSO until analysis.

Single-cell capture

PBMCs were thawed rapidly in a 37°C water bath, then slowly diluted in the prewarmed growth medium, centrifuged, and resuspended in fresh FACS buffer (PBS + 3% FBS) before staining with CITE-seq antibodies (TotalSeq-C 192 antibody panel; Supporting information Table S9) and loading into 10X Chromium. In cases where PBMCs from different donors were pooled, a fraction was taken to isolate genomic DNA for genotyping and the other fraction was used to generate single-cell gel beads-in-emulsion (GEMs). Genomic DNA was isolated from PBMCs for genotyping using a Maxwell® 16 Blood DNA Purification Kit from Promega following the manufacturer's instructions. For the CITE-seq protocol, cells were resuspended in FACS buffer (PBS + 4% FBS), incubated with Fc Block for 10 min, and then with the specific mix of antibodies for 30 min at 4°C. Cells were then washed three times, filtered using a Flowmi strainer, and counted before loading into 10X Chromium to generate single-cell GEMs, following the manufacturer's instructions.

Library generation and sequencing

Libraries were constructed following the manufacturer's protocol for the Chromium Next GEM Single Cell V(D)J Reagent Kits v1.1 with Feature Barcode technology for Cell Surface Protein (10X Genomics Rev E), but with two amendments: the amount of SI primer was doubled, and the number of PCR cycles was set at 7. Samples were sequenced using the Illumina NovaSeq 6000, where cellular gene expression, T-cell clonality, and selected surface proteins in the CITE-seq protocol were simultaneously profiled.

Single-cell data alignment, quantification, and quality control

The single-cell transcriptome data were aligned and quantified by Cell Ranger v3.1 using GRCh38 (Ensembl 93) concatenated to the SARS-Cov-2 genome as a reference. Surface protein data were quantified using a dictionary of tagged antibodies. Pooled donor samples were deconvolved using SoupORcell [25], which yielded a genotype variant that allowed donor identity to be matched across samples. Cells that could not be explained by a single genotype were considered doublets and removed before analysis. Additionally, Scrublet [26] was employed to detect and remove other doublets by computing a doublet score for each cell. Briefly, a Student's *t*-test ($p < 0.01$) was used after Bonferroni correction within fine-grained subclustering of each cluster produced by the Leiden algorithm. Thereafter, SoupX [27] was used to denoise the surface proteome data from ambient RNA. The single-cell data were then integrated and batch effects corrected using total variational inference [28] combining the transcriptome and surface proteome data with a generative model of 64 latent variables and 500 iterations. The resulting latent representation was used to compute a neighborhood graph (`scanpy.pp.neighbors`), which was further used for Louvain clustering (`scanpy.tl.louvain`) and Uniform Manifold Approximation and Projection (UMAP) visualization (`scanpy.tl.umap`), using the Scanpy toolkit [29]. Before downstream analysis, genes expressed in fewer than three cells, and cells with fewer than 200 genes or more than 20% mitochondrial gene content were removed.

Cell type identification and cluster annotation

Scanpy [29] was also used for downstream analysis following the recommended standard practices. Data were first normalized (`scanpy.pp.normalize_per_cell`,

scaling factor 104) and then log-transformed (`scanpy.pp.log1p`). Preliminary annotations were transferred using a logistic regression model from a published large PBMC dataset of COVID-19 patients [30], selecting only highly variable genes (`scanpy.pp.highly_variable_genes`) and then subsetting to shared genes between the datasets. Clustering was thereafter performed using the Louvain algorithm and annotations were manually refined based on the expression of known cell-specific marker genes.

T-cell receptor clonality

Single-cell TCR data were processed with the Cell Ranger v3.1 vdj pipeline using GRCh38 as a reference. Downstream analysis was then performed using Scirpy [31]. In particular, only cells with at least one α -chain and one β -chain but fewer than two full pairs of α/β chains were kept for analysis, and expanded clones were defined when a clonotype was present in more than one cell.

Differential gene expression

The *limma* package [32] was used to perform differential gene expression analysis between the disease groups. Each patient group was compared with all patients from the other three groups combined in order to pinpoint the specific immune responses in each disease condition, and to reduce any bias between individual groups. Simultaneously, differential expression analysis was performed on the published COVID-19 dataset [30] that had been used previously for annotation transfer, comparing male with female COVID-19 patients as well as COVID-19 patients with healthy individuals. This approach enabled us to filter out differentially expressed genes that were influenced by sex (including all Y chromosome genes using a list from Ensembl BioMart [Supporting information Table S10]) and to subset our results to genes

differentially expressed due to COVID-19 (false discovery rate [FDR] < 0.05). Further, given the heterogeneity in COVID-19 disease severity in the autoimmune disease groups owing to the difficulties associated with obtaining such samples, we used the comparison between mild and severe COVID-19 patients with healthy individuals to ensure the immune signatures observed in the autoimmune disease groups are not caused by the differences in COVID-19 severity [33]. For this analysis, the two sets of cells whose expression is to be compared were each partitioned into 4 groups based on the quartile for their total UMI count, such that Wilcoxon tests would be performed on each matching quartile. For each quartile, the group of cells with the higher UMI count per cell had its counts randomly downsampled to better match the other, then the resulting 4 z-scores were combined. This analysis was performed on all identified cell types that were sufficiently represented in the four patient groups. Subsequent downstream analyses then focused on CD14+ monocytes and CD4+ T cells given the highest dysregulation observed in these subsets. Additionally, PBMC datasets of uninfected MS [34], RA [35], and Ps patients were similarly analyzed, in comparison to healthy individuals where annotations were transferred from our dataset using logistic regression as described above, to identify which of the responses observed in the COVID-19 autoimmune disease groups were specific to the infection. Together, these parallel computational analyses allowed us to control for the variability across the autoimmune disease groups and determine the specific immune signatures caused by SARS-CoV-2 infection.

Gene set enrichment analysis

Gene set enrichment analysis was performed with functions from the clusterProfiler R package [36]. Genes were ranked by expression \log_2FC of every

comparison, in every cell cluster, and a normalized enrichment score (NES) was calculated for each gene set. Whole gene set collections C₁ (hallmark) and C₅ (ontology) were included in the analysis. *p*-values were adjusted for FDR across all gene sets.

Transcription factor activity

Discriminant Regulon Expression Analysis [37], a curated resource of TFs and their targets compiled from various sources including the literature, ChIP-Seq peaks, in silico predictions, as well as gene expression data, was used to estimate TF activities from combined expression values of gene targets.

Cell-cell communication

CellPhoneDB [38] (www.CellPhoneDB.org) was used to infer interactions between the identified cell subsets. The previously described statistical method was adjusted to identify ligand/receptor interactions that were significantly enriched between the disease groups. Specifically, differentially expressed genes (FDR < 0.05) obtained within each cell type were used to select relevant interactions instead of random shuffling. Only ligand/receptor pairs expressed by at least 10% of interacting cells were retained, and an interaction was considered enriched if at least one partner was differentially expressed. For the IFN antiviral interactions, given that ligands are produced by cells other than just those of the immune subsets, an interaction was considered to exist if at least one of the receptor subunits was differentially expressed.

Ethics approval and consent to participate

This study was approved by the Clinical Research Ethics Committees of Hospital Universitari Germans Trias i Pujol (PI-20-129), Hospital de Bellvitge

(PI-20-139), Hospital La Princesa (4070), and Vall d'Hebron University Hospital (PR(AG)282/2020), which adhered to the principles set out in the WMA Declaration of Helsinki. All samples were collected in compliance with the written informed consent required to participate in the study.

RESULTS

Cellular compositional and clonal differences in COVID-19 patients with pre-existing autoimmunity

In order to investigate the specific immune responses in patients with pre-existing autoimmune conditions under SARS-CoV-2 infection, we collected peripheral blood samples from a cohort of 5 RA, 4 Ps, and 3 MS COVID-19 patients (positive for SARS-CoV-2 at the time of sample collection), as well as 10 COVID-19 patients without pre-existing autoimmunity who served as controls (Fig. 1A and Supporting information Table S1). These control COVID-19 patients, many of whom suffering from pre-existing conditions associated with a higher risk of severe COVID-19 such as obesity or hypertension, were selected based on their disease severity to test the hypothesis that COVID-19 patients with pre-existing autoimmunity are prone to exhibiting inflammatory responses characteristic of severe COVID-19. As a reference, we also inspected control COVID-19 patients with mild symptoms [33], in order to identify the specific immune responses associated with the pre-existing autoimmunity while controlling for the variable COVID-19 severity status of the autoimmune disease patients at the time of sample collection. Given that most patients involved in this study, including the control group, received immunosuppressant and/or anti-inflammatory treatment during infection, differences in the immune responses observed between the groups will likely be dependent on the pre-existing autoimmune context (including possible intertwined effects of prior immunomodulatory treatments that are typical for such patients). Thus, controlling for the treatment received during COVID-19 between the groups will help separate the likely immune signatures most characteristic of such autoimmune disease patients upon SARS-CoV-2

infection. Additionally, we focused our analysis on the common responses across all patients within each autoimmune disease group that were conserved regardless of the treatment administered. Lastly, we compared the results with uninfected autoimmune disease patients to help identify the signatures unique to these patients under SARS-CoV-2 infection. Although the uninfected MS patients were treatment-naïve, both the uninfected RA and Ps control groups received similar immunomodulatory treatment (Supporting information Table S5) to the SARS-CoV-2-infected RA and Ps patients, further helping dissect the effect of the autoimmune disease from that of the immunomodulatory treatment on the immune responses.

We isolated PBMCs from the aforementioned patient groups and generated a combined single-cell transcriptomic and surface-proteomic (CITE-seq) [39] profile of immune cells. We profiled a total of 97,499 cells, comprising 29,813 cells from COVID-19 patients without pre-existing autoimmunity, 29,477 cells from RA, 19,907 cells from Ps, and 18,302 cells from MS COVID-19 patients. All datasets were integrated into a joint representation considering the transcriptome and surface proteome generated using total variational inference [28].

Our single-cell transcriptomic analysis revealed 28 cell subsets that we annotated based on specific markers (Fig. 1B, C). In particular, we identified distinct populations of T cells (CD3G): CD4 naïve (CD4 and LEF1); CD4 memory (CD4 and CCL5); CD8 naïve (CD8A and LEF1); CD8 memory (CD8A and CCL5); regulatory (Treg: CD4 and FOXP3); mucosal-associated invariant (MAIT: TRAV1-2); gamma-delta ($\gamma\delta$ T: TRDV2); proliferating (Prolif. T: MKI67); and natural killer T cells (NKT: KLRF1 among others). In addition, we identified two subsets of natural killer cells (NK CD56dim: KLRF1, NCAM1, and FCGR3Ahigh;

and NK CD56^{bright}: KLRF1, NCAM1, and FCGR3A_{low}) along with proliferating natural killer cells (Prolif. NK: KLRF1 and MKI67). Captured B cell subsets (CD79A) included naïve (TCL1A); immature (TCL1A and MME); memory (CD27 and TNFRSF13B); exhausted (TNFRSF13B and CR2^{neg}); plasmablast (JCHAIN, SDC1, and MKI67); and plasma B cells (JCHAIN and SDC1). The myeloid fraction comprised two subsets of monocytes (CD14 mono: CD14; and CD16 mono: CD14 and FCGR3A); conventional dendritic cells (FLT3) including cDC1: CLEC9A; cDC2: CD1C; and cDC3: CD1C and CD14; plasmacytoid dendritic cells (pDC: JCHAIN and LILRA4); and neutrophils (FCGR3B). Lastly, we identified precursor hematopoietic stem cells (HSC: CD34); platelets (GP9); and red blood cells (RBC: HBB). We further exploited CITE-seq to validate these cell annotations using markers from the surface proteome data (Fig. 1D).

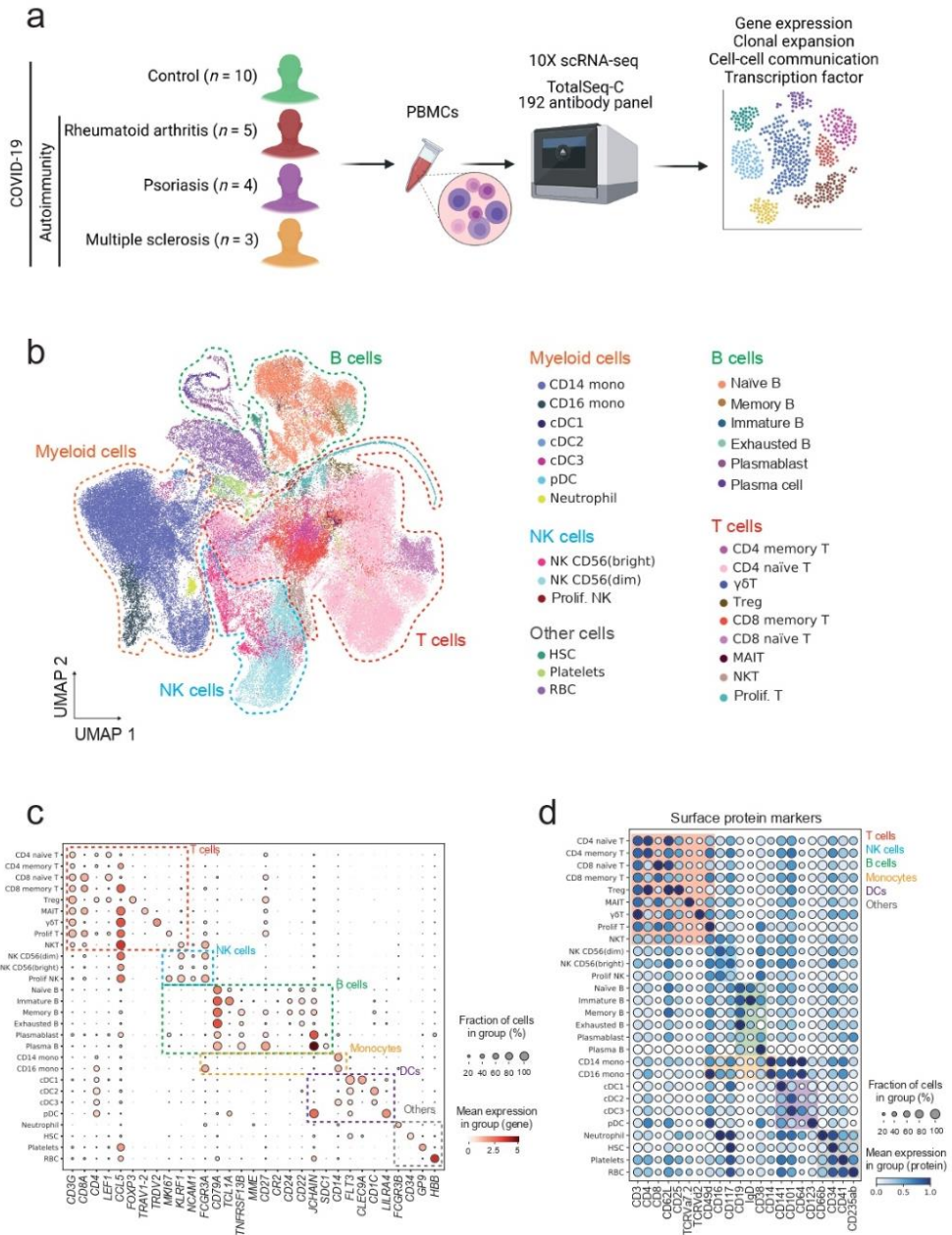
We observed significant differences in cell proportions between the different patient groups (Fig. 2A, B, Supporting information Fig. S1 and Table S2). Within the T-cell compartment, we observed relatively more CD4⁺ memory T cells in RA COVID-19 patients compared with controls (Fig. 2B and Supporting information Fig. S1). In MS COVID-19 patients, we found a higher frequency of circulating MAIT cells than in the other three groups and fewer CD8⁺ memory T cells compared with controls. Higher proportions of MAIT cells in asymptomatic and mild SARS-CoV-2 infections have previously been reported [30]. Within the B-cell compartment, we detected significantly fewer plasmablasts and plasma cells in Ps and RA COVID-19 patients in comparison with controls, although the use of anti-CD20 therapy in some of the RA patients included in the cohort likely influences these observed differences. Control COVID-19 patients also had relatively higher proportions of platelets compared with all three autoimmune COVID-19 groups, and higher proportions of HSCs

compared with the MS COVID-19 group. Relative expansion of HSCs, platelets, and plasmablasts has previously been associated with increased COVID-19 severity [30]. In addition, since monocyte-platelet aggregates have been reported in COVID-19 patients [40], the observed differences in platelet frequencies between controls and autoimmune COVID-19 patients might be caused by a specific subset of monocytes sequestering platelets as previously described [30]. Lastly, differences in some other cell subsets (neutrophils and RBCs) can further be influenced by the sample processing procedure itself.

Within the myeloid compartment, we focused on CD14⁺ monocytes given that dysregulation in this compartment upon SARS-CoV-2 infection is linked to COVID-19 severity [11]. In this regard, we identified a CD14⁺ HLA-DR^{low} subset in our dataset (Fig. 2C, D), whose proportion was significantly higher in all three autoimmune COVID-19 groups compared with controls (Fig. 2E).

Given the altered cellular composition identified in the T-cell compartment, we also analyzed the clonal expansion of the distinct T-cell subsets identified (Fig. 2F and Supporting information Table S3). The MS COVID-19 group had a significantly higher proportion of clonally expanded MAIT cells compared with the other three groups, consistent with the compositional analysis. The RA COVID-19 group instead had a significantly lower proportion of clonally expanded CD8⁺ memory T cells than the COVID-19 Ps and control groups. We also noted a trend toward a higher proportion of clonally expanded CD4⁺ memory T cells compared with the three other groups, consistent with the compositional analysis of this cell type.

Figure 1



(See figure legend on the next page.)

Figure 1. Immune cell subset annotation from single-cell data of COVID-19 patients with pre-existing autoimmunity and controls. (a) Schematic diagram depicting the cohort of control and autoimmune COVID-19 patients included in the study, as well as the single-cell approaches and analyses performed. (b) UMAP visualization showing the different immune cell populations identified from Louvain clustering and cell-specific marker gene expression. The T-cell compartment includes CD4+ naïve, CD4+ memory, CD8+ naïve, and CD8+ memory T cells, as well as regulatory (Treg), mucosal-associated invariant (MAIT), gamma-delta ($\gamma\delta$ T), proliferating (Prolif. T), and natural killer T cells (NKT). The NK cell compartment includes NK CD56^{dim} and NK CD56^{bright} along with proliferating NK cells. The B cell compartment includes naïve, immature, memory, exhausted, plasmablast, and plasma B cells. The myeloid fraction includes CD14+ and CD16+ monocytes, as well as conventional dendritic cells including cDC1, cDC2, and cDC3, plasmacytoid dendritic cells (pDC), and neutrophils. Additionally, we identified precursor hematopoietic stem cells (HSC), platelets, and red blood cells (RBC). (c) Dot plot depicting the expression of selected marker genes in the cell populations identified. The scale represents the mean gene expression in the cell subset; the circle size represents the percentage of cells in the subset expressing the gene. (d) Dot plot depicting the expression of selected protein markers in the cell populations identified. The scale represents the standardized mean protein expression in the cell subset; the circle size represents the percentage of cells in the subset expressing the protein.

Distinct immune gene expression profiles among COVID-19 patients with pre-existing autoimmunity

We next focused on CD14+ monocyte and CD4+ T cell responses due to their compositional and clonal alterations observed in COVID-19 patients with pre-existing autoimmunity, as well as their dysregulated responses under SARS-CoV-2 infection described by others [8, 13, 41, 42]. As such, we performed differential gene expression analysis in the COVID-19 patient groups included in the study, with special emphasis on CD14+ monocytes, as well as CD4+ naïve and memory T cells (Supporting information Table S4). To pinpoint the specific immune responses in each disease condition and reduce any bias between individual groups, cells from each patient group (control, RA, Ps, and MS) within either the CD14+ monocyte, CD4+ naïve T cell, or CD4+ memory T-cell clusters were compared with the other cells within that cluster (including cells from the three other groups combined). We further made use of a publicly

available large PBMC dataset [30] to select those genes showing the most significant transcriptional changes in COVID-19 patients compared with healthy individuals (Supporting information Tables S5 and S6).

Gene set enrichment analysis revealed that multiple immune-related categories are uniquely dysregulated in COVID-19 patients with pre-existing autoimmunity (Fig. 3A). In particular, CD14⁺ monocytes from MS COVID-19 patients were characterized by increased responses to inflammatory cytokines such as IL-1 β , IL-6, type I IFNs, and IFN γ , as well as increased innate and adaptive immune responses (Fig. 3A). This subset of CD14⁺ monocytes displayed significant upregulation of genes of the type I IFN pathway, including members of the IFN-induced protein with tetratricopeptide repeats (IFIT) family (e.g., IFIT2), members of the IFN-induced transmembrane protein (IFITM) family, such as IFITM1, as well as IFN-stimulated genes like ISG15 (Fig. 3B and Supporting information Table S4). Additionally, CD14⁺ monocytes showed significant upregulation of genes of the inflammasome pathway such as NAIP, NLRC4, CASP1, and CASP4, as well as IL-6 production-related genes such as CD36, LGALS9, STAT3, and IL17RA, among others (Fig. 3B and Supporting information Table S4). In Ps COVID-19 patients, CD14⁺ monocytes displayed greater enrichment of the hypoxia and TNF- α /NF- κ B pathways (Fig. 3A). Consistently, CD14⁺ monocytes from Ps COVID-19 patients displayed upregulation of hypoxia-related genes including HIF1A, HK2, and MAFF in comparison with MS and, to a lower extent, RA COVID-19 patients (Fig. 3B).

In the case of CD4⁺ T cells, we also found alterations in the expression of multiple relevant genes for all three groups of patients with pre-existing autoimmunity upon SARS-CoV-2 infection. MS COVID-19 individuals showed significant enrichment of the type I IFN response category in both CD4⁺ naïve

and memory T cells (Fig. 3A). In this regard, we observed upregulation of type I IFN-related genes such as IFI35, IFNAR2, and IFITM2 among others in CD4+ naïve T cells (Fig. 3C). It is of note that lymphocyte antigen 6 complex, locus E (LY6E), a previously described ISG [43] that has recently been found to impair coronavirus fusion and restrict its entry into cells [44, 45], was also upregulated in MS COVID-19 patients in CD14+ monocytes and CD4+ naïve T cells (Supporting information Table S4). Remarkably, the specific IFN signature observed in CD14+ monocytes and CD4+ naïve T cells of MS COVID-19 patients is likely specific to the autoimmune condition under infection, as no differences in sampling time relative to COVID-19 onset are seen compared with controls. Similarly, no significant differences were observed in sampling time relative to COVID-19 onset in the Ps and RA groups compared with controls (Supporting information Table S1). In Ps COVID-19 patients, CD4+ naïve T cells displayed enrichment of the TNF- α /NF- κ B signaling pathway, as well as a pronounced hypoxia signature. Consistent with these results, we observed upregulation of TNF- α /NF- κ B signaling pathway genes such as NFKB1, CEBPD, and CD83 (Fig. 3C). In RA COVID-19 patients, CD4+ memory T cells displayed enrichment of the TNF- α /NF- κ B signaling pathway, as well as higher levels of hypoxia, IL-12, and IFN- γ responses (Fig. 3A). Additionally, this cell compartment displayed upregulation of several TNF- α /NF- κ B signaling-related genes, including RELA, RELB, and ICAM1, among others, as well as upregulation of several genes related to the IFN- γ response, such as IRF1, TRIM21, and PIAS1 (Fig. 3C).

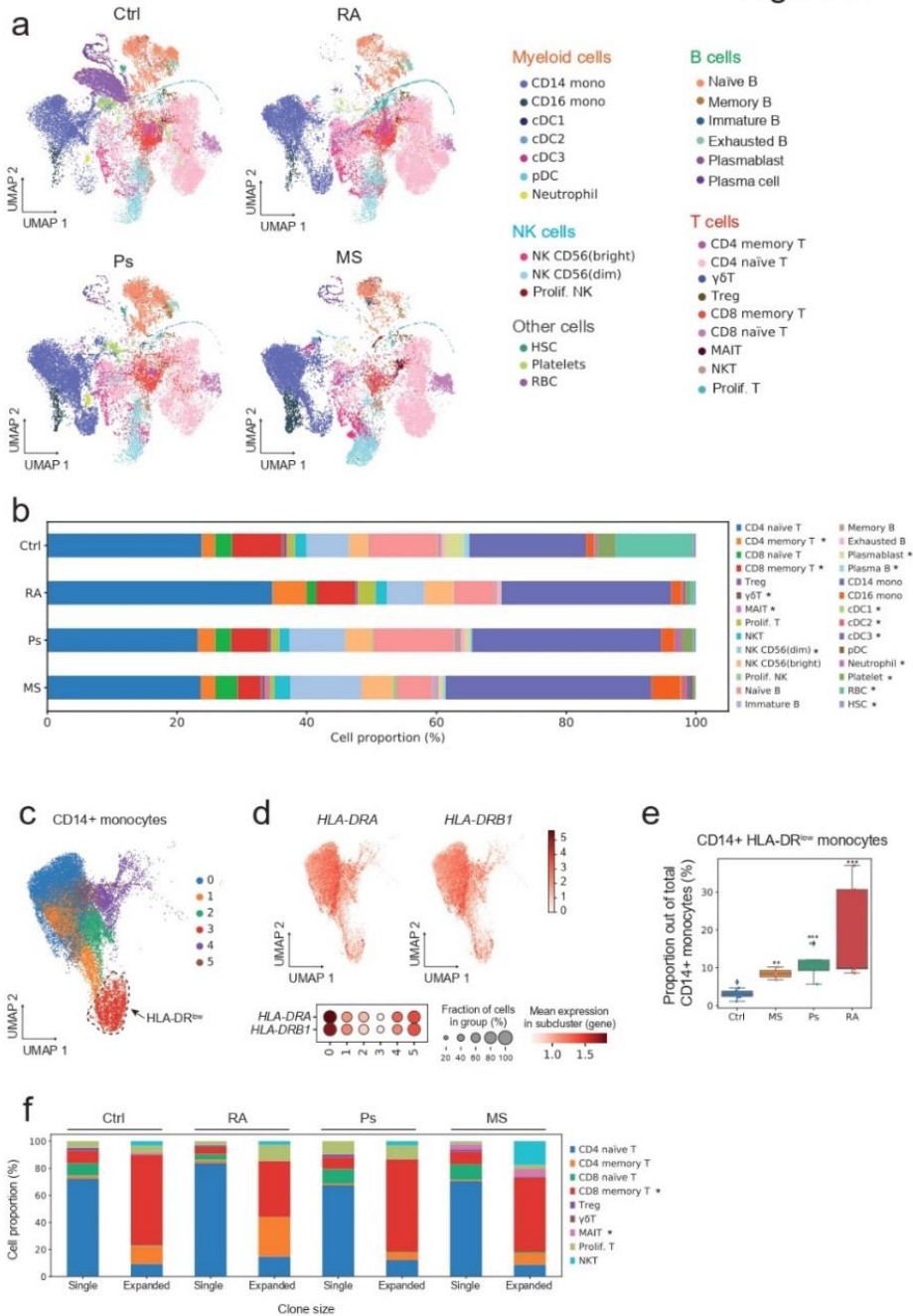
Importantly, the upregulation of the aforementioned genes was not observed in CD14+ monocytes or CD4+ T cells of uninfected RA, Ps, or MS patients compared with healthy donors (Supporting information Tables S5 and S6), suggesting that the observed gene signatures specifically originate in

response to SARS-CoV-2 infection. Moreover, many of these upregulated genes in COVID-19 with pre-existing autoimmunity (many of whom displayed mild COVID-19 at the time of sample collection compared with COVID-19 controls) were shown to be less expressed in mild compared with severe COVID-19 controls (Supporting information Fig. S2A, B), suggesting that such responses are unique to the autoimmune disease patients under infection regardless of COVID-19 severity.

Some of the autoimmune disease patients included in this study received rituximab treatment (anti-CD20 monoclonal antibody) before SARS-CoV-2 infection. To gain further insights into the possible effects of this immunotherapy on the immune response to SARS-CoV2 infection, we compared those rituximab-treated patients in our cohort (3 RA and 1 MS) versus patients from the same disease groups who did not receive rituximab as controls (2 RA and 2 MS). Our results indicate that several genes involved in IFN and antiviral immune responses that are upregulated in monocytes during SARS-CoV-2 infection such as IFITM1, IFI16, IRF1, ISG15, OAS1, and MX2, together with genes involved in inflammasome activation and IL-1 β production such as NAIP, CASP1, and PYCARD, had significantly reduced expression in monocytes from rituximab-treated patients compared with the controls (Supporting information Table S6).

Overall, CD14⁺ monocytes and CD4⁺ T cells show altered immune signatures associated with inflammation, hypoxia, as well as IFNs and TNF responses for all three autoimmune disease patients under SARS-CoV-2 infection that might condition the function and polarization of these cells to specific phenotypes.

Figure 2



(See figure legend on the next page.)

Figure 2. Alterations in cell composition and T cell receptor clonality in patients with pre-existing autoimmunity under SARS-CoV-2 infection. **(a)** UMAP visualization shows the distribution of the immune cell populations in the patient groups and controls included. **(b)** Bar plot depicting the average cell proportions of the immune cell types in each patient group. Significant differences in cell proportions between any two groups are marked with an asterisk next to the cell type (unpaired, two-sided Wilcoxon rank-sum test; see Supporting information Table S2 for statistically significant p-values between each pair of groups). **(c)** UMAP visualization depicting the sub-clustering of the CD14+ monocyte compartment, where subcluster 3 corresponding to CD14+ HLA-DR_{low} monocytes is shown in red. **(d)** UMAP visualization showing the gene expression of HLA-DR subunits (HLA-DRA and HLA-DRB1) in CD14+ monocytes. The dot plot depicts the gene expression of the two HLA-DR subunits in the subclusters identified within CD14+ monocytes. **(e)** Box plot depicting the average proportion of HLA-DR_{low} cells within CD14+ monocytes between the different groups. Boxes represent the interquartile range (IQR), horizontal bars depict the median, whiskers extend to $1.5 \times$ IQR, and dots denote the values for each donor where outliers are additionally marked with grey labels. Statistical significance was determined using the unpaired, two-sided Wilcoxon rank-sum test of comparisons with controls ($p = 2.20 \times 10^{-3}$ vs. RA, $p = 1.12 \times 10^{-2}$ vs. MS, $p = 7.21 \times 10^{-3}$ vs. Ps). **(f)** Bar plot of the average proportions of the T cell subsets corresponding to single or expanded clones in the different groups. Significant differences in cell proportions of expanded clones between the groups by the unpaired, two-sided Wilcoxon rank-sum test are marked with an asterisk (increased MAIT in MS: $p = 2.53 \times 10^{-2}$ vs. RA, $p = 3.39 \times 10^{-2}$ vs. Ps, $p = 4.25 \times 10^{-2}$ vs. control; reduced CD8+ memory T cells in RA: $p = 1.43 \times 10^{-2}$ vs. Ps, $p = 7.05 \times 10^{-3}$ vs. control).

Altered transcription factor activity in autoimmune patients supports diverging responses to SARS-CoV-2

We next analyzed transcription factor (TF) activities in the different COVID-19 patient groups using Discriminant Regulon Expression Analysis, a comprehensive resource of curated TFs and their gene targets [37].

In MS COVID-19 patients, both CD14+ monocytes and CD4+ T cells displayed stronger activation of type I IFN-associated TFs – namely STAT1, STAT2, IRF9, and IRF1 – compared with Ps, RA, and control COVID-19 patients, in line with our previous differential gene expression analysis (Fig. 4A, B). This signature was only observed in MS patients under SARS-CoV-2 infection and not in uninfected MS patients (analysis performed on published dataset [34];

Supporting information Fig. S2C and Tables S5 and S6), supporting that the observed IFN signature specifically originates in response to infection. Additionally, CD14⁺ monocytes of Ps COVID-19 individuals displayed a significantly lower level of activity of several regulatory factor X (RFX) TFs, particularly in comparison to the MS COVID-19 group (Fig. 4A). RFX TFs are involved in the transcriptional regulation of HLA genes [46], including HLA-DR, which is known to be downregulated in dysfunctional HLA-DR_{low}CD163_{high} and HLA-DR_{low}S100A_{high} CD14⁺ monocytes in severe COVID-19 [11]. We also inspected hypoxia-associated TFs such as hypoxia-inducible factor 1-alpha (HIF-1 α) and EPAS1 (HIF-2 α), as they have been related to tolerogenic phenotype in monocytes [47] and with an increase in glycolysis involved in the acquisition of trained immunity in myeloid cells during inflammation [48]. We detected predominant and significant hyperactivation of these two TFs in CD14⁺ monocytes of Ps COVID-19 patients compared with the other patient groups (Fig. 4A). These signatures for HIF-1 α and EPAS1, but not for RFX TFs, only occurred in Ps patients under SARS-CoV-2 infection and not in uninfected ones (Supporting information Fig. S2C and Tables S5 and S6), supporting that the observed hypoxia signature in Ps patients specifically originates in response to the infection.

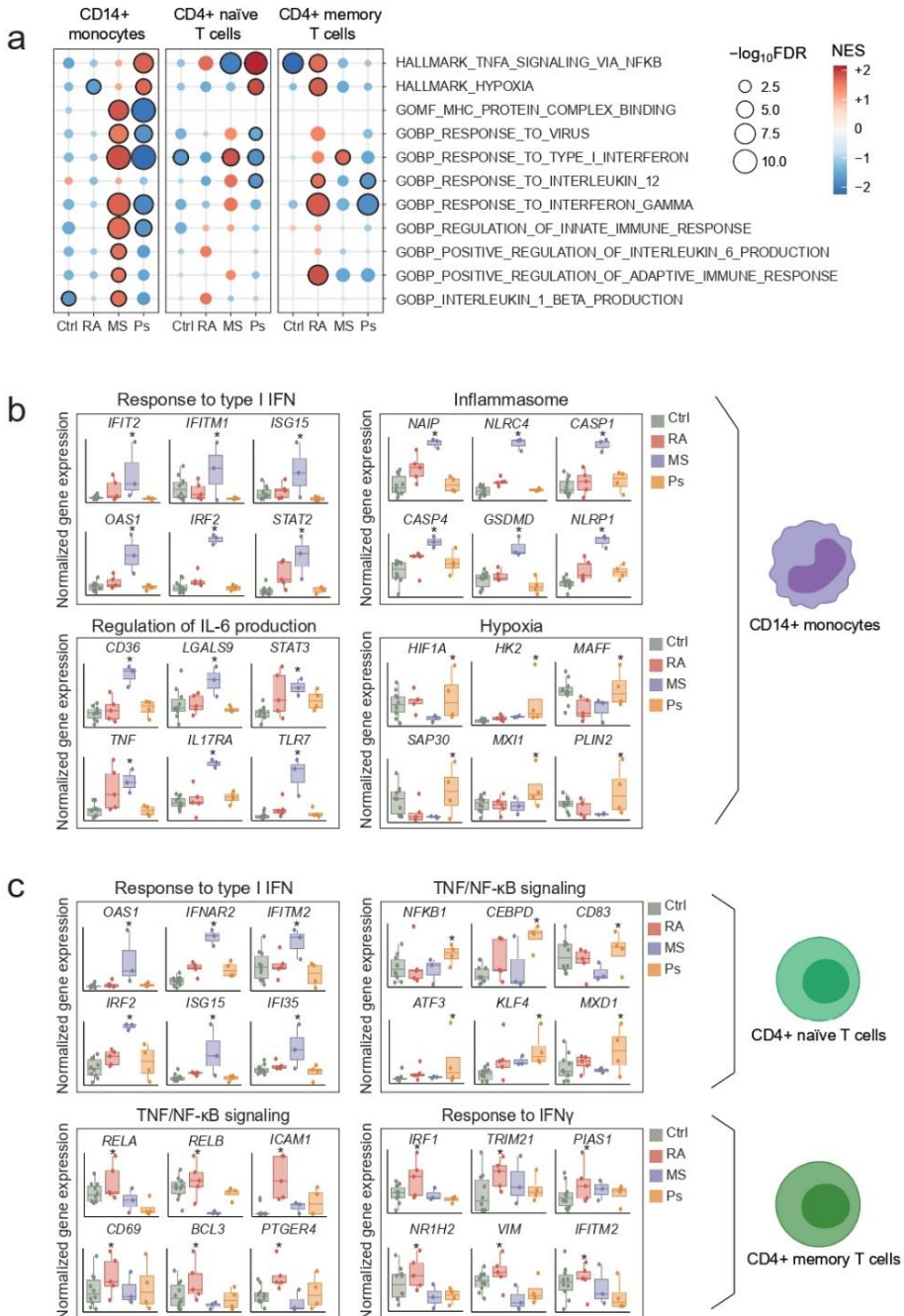
In Ps COVID-19 patients, both CD4⁺ naïve and memory T cells presented a specific activation of the GATA3 pathway (Fig. 4B), which might be associated with higher polarization toward a Th2 response. In the MS COVID-19 group, GATA3 pathway TFs were only modestly upregulated in CD4⁺ memory T cells. Notably, CD4⁺ naïve T cells of Ps COVID-19 patients showed significant protein upregulation of CD124 (Supporting information Table S7), the IL-4 receptor, which is involved in Th2 polarization of CD4⁺ T cells [49].

We also noted significant protein upregulation of the IL-21 receptor (CD360) (Supporting information Table S7), whose ligand IL-21 is known to impair Th1 polarization and amplify the Th2 response [50].

We also detected higher levels of activity of the AP-1 subunits JUND and FOS, and NF- κ B pathway TFs in CD4⁺ naïve T cells of Ps COVID-19 patients (Fig. 4B). Both of these TF pathways are downstream of TNF signaling [51], consistent with the enrichment of the TNF- α signaling category observed earlier in the same cell compartment of Ps COVID-19 patients. Instead, the activation of NF- κ B in the RA group was seen in CD4⁺ memory T cells (Fig. 4B), which was also the cell subset displaying TNF- α signaling enrichment as observed earlier. In contrast to the GATA3 signature that was already detectable in uninfected Ps individuals (which may likely be the consequence of immunomodulatory treatment in such patients [52]), the signatures for AP-1 in Ps patients and NF- κ B in Ps and RA patients were only observed under SARS-CoV-2 infection and not in uninfected individuals (RA analysis performed on published dataset [35]; Supporting information Fig. S1D and Tables S5 and S6), suggesting that they originate specifically in response to the infection.

Overall, these results reveal altered TF activities associated with IL-4, type I IFN, TNF, and hypoxia pathway unique to the autoimmune conditions under SARS-CoV-2 infection.

Figure 3



(See figure legend on next page.)

Figure 3. Genes differentially expressed in patients with pre-existing autoimmunity under SARS-CoV-2 infection. **(a)** Dot plots depicting the gene set enrichment analysis (GSEA) in CD14+ monocytes, CD4+ naïve T cells, and CD4+ memory T cells of differentially expressed genes between the COVID-19 patient groups (control, RA, MS, and Ps). The scale represents the normalized enrichment score (NES); the circle size indicates the $-\log_{10}$ FDR value, where the circle edge represents the statistical significance of the enrichment (black: significant; no edge: not significant). **(b)** Box plots depicting the normalized mean expression of differentially expressed genes (false discovery rate [FDR] < 0.05) between the four COVID19 patient groups that are involved in pathways implicated in (a) in CD14+ monocytes (see Supporting information Table S4 for FDR values). The asterisk indicates the significantly different patient group. **(c)** Box plots depicting the normalized mean expression of genes differentially expressed (FDR < 0.05) between the four COVID-19 patient groups involved in the pathways implicated in (A) in CD4+ naïve and memory T cells (see Supporting information Table S4 for FDR values). Similarly, the asterisk indicates a significantly different patient group.

Defects in cell-cell communication in COVID-19 patients with pre-existing autoimmunity

To systematically analyze the effect of cell-cell communication on immune responses upon SARS-CoV-2 infection, we used CellPhoneDB [38, 53], which infers specific cell-cell interactions based on the expression of ligands and receptors. We identified alterations in several ligand-receptor pairs involved in the immune and inflammatory responses (Fig. 4C and Supporting information Table S8). For instance, in MS COVID-19 patients, we detected a dysregulated higher interaction between TRAIL (TNFSF10), expressed in CD14+ monocytes and CD4+ naïve T cells, and its receptor TNFRSF10B, expressed in monocytes and memory B cells (Fig. 4C), which is probably a consequence of the upstream IFN activation [54]. A similar dysregulated interaction pattern in the same cell subsets was observed with respect to LFA-1 integrin (consisting of ITGB2 and ITGAL subunits) and its ligand CD54 (ICAM1) (Fig. 4C). Enhanced interaction between the CCL5 ligand, expressed in all the immune cells inspected, and the CD191 (CCR1) receptor, whose inhibition potentially suppresses immune hyperactivation in critical COVID-19 [55], was noted in the MS and RA COVID-

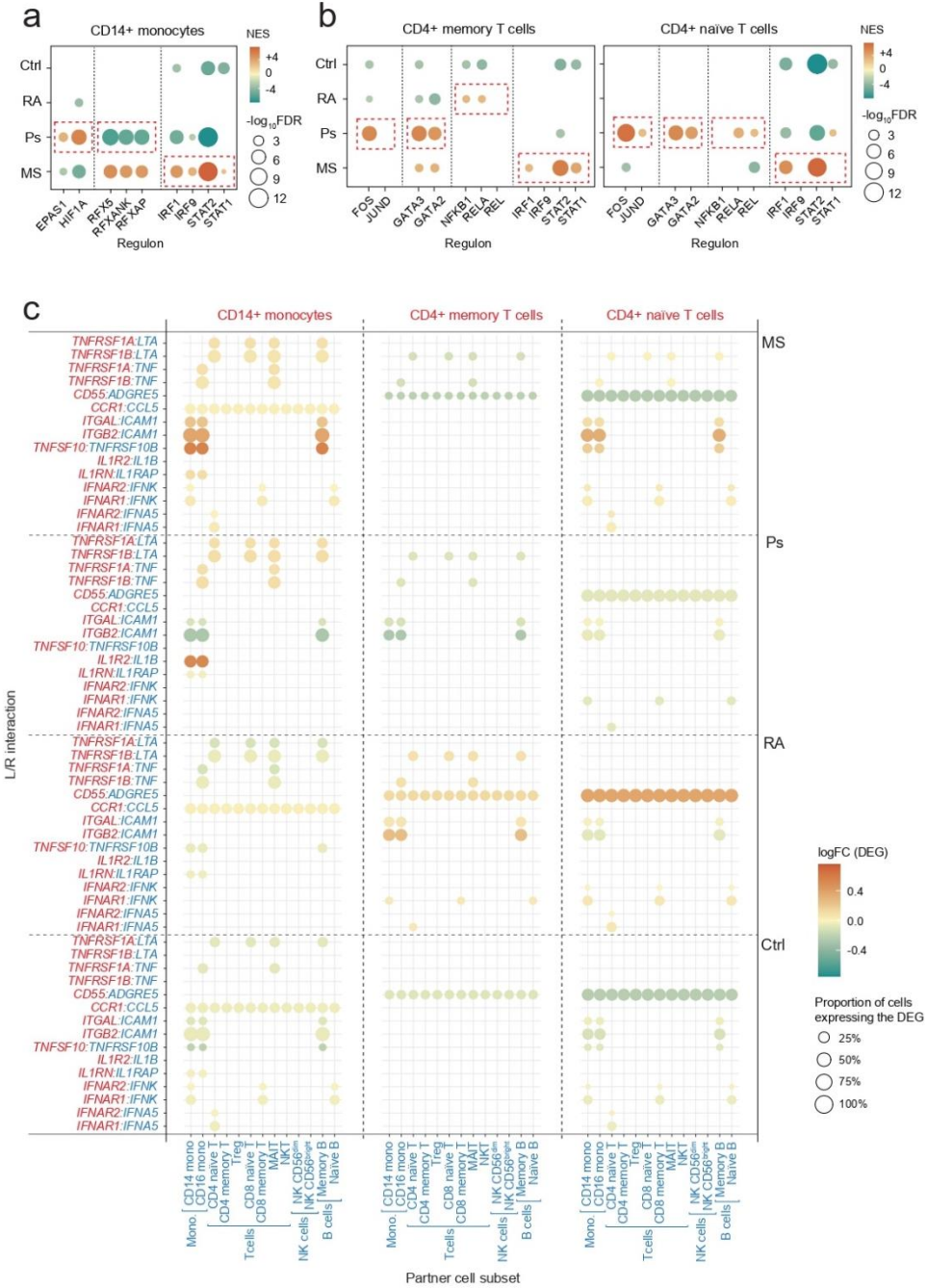
19 groups for CD14⁺ monocytes. Our analysis also revealed, in RA COVID-19 patients, a stronger interaction between CD55, expressed in CD4⁺ T cells, and its ligand CD97 (ADGRE5) (Fig. 4C), which has been described to enhance T cell activation [56]. While a stronger TNF/TNFR interaction was observed in the CD14⁺ monocyte subset of MS and Ps COVID-19 patients, such interaction predominated in the CD4⁺ memory T cells of the RA group (Fig. 4C), which is consistent with the previously observed downstream activation of NF- κ B in the same cell type. Additionally, in Ps COVID-19 patients, we observed a stronger autocrine/paracrine interaction between IL-1 β , expressed in CD14⁺ and CD16⁺ monocytes, and its inhibitory receptor (IL1R2), expressed in CD14⁺ monocytes (Fig. 4C).

Consistent with the overarching immune pattern revealed in this study, we also found stronger interactions with type I IFN receptors (IFNAR₁ and IFNAR₂) in the CD4⁺ T cell subsets for MS and RA COVID-19 patients, as well as in CD14⁺ monocytes predominantly for the MS COVID-19 group (Fig. 4C), which most likely explains the general type I IFN signature seen.

In summary, we found a dysregulated network of cell-cell communication events in autoimmune disease patients in response to infection involving inflammatory cytokines, cell adhesion molecules, and cell activation regulators, which likely modulate the downstream TFs pathways and may impact the antiviral immune responses triggered in these patients.

(See figure legend on next page.)

Figure 4



(See figure legend on the next page.)

Figure 4. Transcription factor activity and cell–cell communication alterations in patients with pre-existing autoimmunity under SARS-CoV-2 infection. (a) Dot plot showing selected transcription factor activities of different regulons in CD14+ monocytes from the different COVID-19 patient groups (control, RA, Ps, and MS). The scale represents the normalized enrichment score (NES); the circle size indicates the $-\log_{10}$ FDR value. (b) Dot plots showing selected transcription factor activities of different regulons in CD4+ naïve and memory T cells from each patient group. The scale represents the normalized enrichment score (NES); the circle size indicates the $-\log_{10}$ FDR value. (c) Dot plot of selected dysregulated ligand/receptor (L/R) interactions between CD14+ monocytes or CD4+ T cells (naïve and memory) and other immune cell compartments in the COVID-19 patient groups. The scale indicates the \log_2 (FC) in gene expression of differentially expressed genes (FDR < 0.05); the circle size represents the percentage of cells expressing the differentially expressed gene. Molecules of the L/R pairs expressed in the inspected immune subset (CD14+ monocyte, CD4+ naïve T cell, or CD4+ memory T cell) are shown in red, and molecules of the L/R pairs expressed in the immune cell partner are shown in blue. Assays were performed at the mRNA level, but results were extrapolated to protein interactions.

DISCUSSION

Here, we analyzed the immune response changes in the peripheral blood of three groups of autoimmune disease patients during the course of COVID-19 by combining single-cell transcriptome and surface proteome profiles. Our study revealed that these patients display aberrant immune responses to SARS-CoV-2 infection that are most likely dependent on the context of the autoimmune disease.

Very few studies have addressed the implications of chronic underlying inflammatory conditions in relation to the severity of COVID-19, focusing on clinical or epidemiological analyses rather than immunological insights. A meta-analysis of 62 observational studies, covering more than 300,000 patients with autoimmune diseases, suggested that these patients had an increased risk of COVID-19 [21]. More recently, another study has shown that patients with immune-mediated inflammatory diseases were at higher risk of being hospitalized with COVID-19 [23]. Conversely, another study suggested that patients with autoimmunity who required hospital admission owing to SARS-CoV-2 infection had a lower risk of developing severe disease and were less likely to require a stay in the intensive care unit or mechanical ventilation [22]. It has been shown that MS patients with advanced age and disease, as well as those with greater disability, are at an increased likelihood of developing severe and even fatal COVID-19 [57]. In addition, as viral respiratory infections are recognized to increase the risk of relapse in MS patients [58], there is a concern that COVID-19 might exacerbate symptoms in MS individuals, though this remains an open question [59]. For RA patients, it has also been described that such patients face an increased risk of severe COVID-19, particularly those with related interstitial lung disease [60]. Furthermore, several studies have

consistently revealed that unvaccinated individuals with RA show an elevated risk of COVID-19 hospitalization and mortality [61-63]. For Ps patients, it has been suggested that although individuals can have an increased risk of contracting SARS-CoV-2 infection, they may not exhibit increased susceptibility to the complications of COVID-19 [64]. Given such divergent scenarios, our study aimed at exploring the particular immune signatures to SARS-CoV-2 infection in individuals with pre-existing autoimmune diseases.

Our analysis of cell proportions revealed that COVID-19 patients with pre-existing autoimmunity do not display features characterizing severity, such as expanded HSCs, platelets, or plasmablasts [30]. However, the three autoimmune groups studied showed a marked expansion of HLA-DR_{low} CD14⁺ monocytes. Expansion of these dysfunctional HLA-DR_{low} monocytes has recently been described in patients with severe COVID-19 [8, 11]. Regardless of whether this subset of monocytes is already present at baseline in autoimmune disease patients or if instead it is expanded under SARS-CoV-2 infection, the high proportion of HLA-DR_{low} CD14⁺ monocytes in COVID-19 with pre-existing autoimmunity might interfere with a proper antiviral response, given that these monocytes are characterized by displaying an immunosuppressive phenotype [65-68]. Remarkably, MS COVID-19 patients had higher proportions, as well as clonal expansion, of circulating MAIT cells. Higher proportions of MAIT cells have been reported in asymptomatic and mild infections [30], and their expansion may enhance the antiviral immune response in these patients [69].

We also identified a predominant upregulation of the type I IFN pathway along with its downstream transcription factors (i.e. STAT1, STAT2, and IRF9) in CD14⁺ monocytes and CD4⁺ T cells of MS COVID-19 patients. This signature most likely stems from a stronger ligand/receptor (IFNAR₁ and

IFNAR2) interaction, as identified in our cell–cell communication analysis. Whether this feature may be beneficial or detrimental to these patients in the context of SARS-CoV-2 infection remains unclear. Several studies have identified impaired type I IFN activity in patients with severe COVID-19 [7, 70–74], and COVID-19 patients treated with inhaled nebulized IFN beta-1a (SNG001) showed greater odds of improvement and recovered more rapidly from SARS-CoV-2 infection [75]. On the other hand, it has been suggested that such a robust type I IFN response potentially exacerbates hyperinflammation, facilitating the development of severe COVID-19 [76, 77]. This predominant IFN signature in MS COVID-19 patients may therefore be a double-edged sword, simultaneously promoting antiviral immune responses and exacerbating immune hyperactivation in these patients. Angiotensin-converting enzyme 2 (ACE2), whose protein product binds to the SARS-CoV-2 spike (S) protein and promotes cellular entry of the virus, was initially described as a human ISG [78], but these results were challenged shortly after [79, 80]. Indeed, increased SARS-CoV-2 cell entry leading to higher viral loads is ultimately associated with increased COVID-19 severity and mortality [81, 82]. In this regard, the ISG LY6E, which has been reported to impair coronavirus fusion and restrict its entry into cells [44, 45], was upregulated in MS COVID-19 patients relative to the other patient groups in both CD14+ monocytes and CD4+ naïve T cells. Notably, our analysis of uninfected MS patients did not show this predominant IFN signature, suggesting that it originates specifically in response to the infection.

In Ps COVID-19 patients, we found a higher level of GATA3 pathway activity in the CD4+ T-cell compartment. GATA3 is a crucial TF involved in Th2 polarization [83], which is induced by IL-4. In this regard, we have also detected a higher level of the IL-4 receptor protein (CD124) in the CD4+ T cells of these

patients, which likely explains the observed greater activity of GATA3. The Th2 immune response has been linked to a fatal outcome of COVID-19 [16]. Higher proportions of Th2 cells have been further detected in poor-prognosis COVID-19 patients [84], with cytological signals of the Th2 immune response in peripheral blood from COVID-19 patients who required intensive care [85]. As such, a high Th2 polarization in Ps patients during SARS-CoV-2 infection, which might be caused or enhanced by the specific treatments received and/or the underlying immune condition (86), might represent an adverse immunological feature in these patients.

Beyond CD4+ T cells, we identified altered immune responses in the myeloid compartment of Ps COVID-19 patients. For instance, the CD14+ monocytes of Ps COVID-19 individuals showed a higher level of activation of the HIF pathway. HIF factors are upregulated at low oxygen concentrations and are involved in the regulation of immune responses [87]. Although control COVID-19 patients also showed activation of the HIF pathway, Ps COVID-19 patients displayed significantly higher levels of activity in this HIF pathway, predominantly in CD14+ monocytes. This pathway has been associated with the acquisition of an immunosuppressive phenotype in contexts characterized by altered immune responses such as sepsis [47]. Taken together, these results suggest that Ps patients may confront a SARS-CoV-2 infection with inefficient responses in several immune compartments that affect their innate and adaptive immune systems.

For RA COVID-19 patients, in addition to increased proportions and a trend toward clonal expansion of CD4+ memory T cells, this immune subset displayed the highest level of dysregulation in this patient group. In particular, we observed significant activation of TNF- α /NF- κ B signaling as well as

upregulation of the IL-12 and IFN- γ responses. Synergistic activation of these cytokines occurs in CD4⁺ T cells and is associated with the exacerbated inflammatory response in severe and critical COVID-19 [7, 88]. Additionally, inhibition of NF- κ B and TNF- α is thought to have a therapeutic potential for alleviating the cytokine storm and COVID-19 severity [89].

The appearance of sequelae in some COVID-19 patients after the acute phase of infection is a paramount clinical aspect that has become apparent during the pandemic. Such sequelae include manifestations like pulmonary damage, thromboembolism, and neuroinflammation among others [90]. Pulmonary sequelae, ranging from dyspnea to fibrotic damage and persistent oxygen requirement, might be a consequence of elevated inflammatory cytokine production and lung invasion by neutrophils and monocytes [90]. In this regard, our results indicate that the IL-6 pathway is significantly upregulated in CD14⁺ monocytes of MS COVID-19 patients, which may ultimately facilitate a fibrotic state [91]. Furthermore, LFA-1 was upregulated in the CD14⁺ monocytes of MS COVID-19 patients, potentially favoring monocyte extravasation into the alveolar space [92]. Conversely, CD14⁺ monocytes of Ps COVID-19 patients and CD4⁺ memory T cells of RA COVID-19 patients displayed hypoxia features, which are related to thrombotic complications in COVID-19 patients [93].

The limited number of patients included in this study reflects the difficulty in collecting samples from such patient populations at the time of infection, especially given that patients classified as at-risk, including autoimmune disease patients, significantly reduced their frequency of medical visits during the COVID-19 pandemic [94, 95]. Additionally, although we perform several analyses to control for the inherent heterogeneity between

groups (accounting for differences in COVID-19 disease course and severity, sex, treatment, timing, and infection status; see Methods), such differences should be considered for broad conclusions. Nevertheless, our cohort is unique and valuable by including COVID-19 patients with pre-existing autoimmunity in a prevaccination state, and it allowed us to explore unresolved questions in the field of immunology and virology. One of the unique strengths of our work is the validation of the immune responses observed across separate computational analyses and tools, particularly from immune ligand/receptor interactions and downstream pathway activity, providing consistent and complementary evidence of immune dysregulation.

While our analysis focused on identifying shared responses among all patients within each autoimmune disease group to minimize the influence of specific prior immunomodulatory treatments on the observed transcriptional changes upon SARS-CoV-2 infection, this is a limitation that could potentially impact the findings. Nevertheless, it is worth noting that individuals with autoimmune diseases often have a history of immunomodulatory treatments whose effects become intertwined with the chronic autoimmune state in these patients. These combined factors together can then shape how these patients respond to SARS-CoV-2 infection. Therefore, our study provides valuable insights into the immune responses to infection in patients with pre-existing autoimmunity on immunomodulatory treatment, which is most representative of typical autoimmune disease patients.

In our cohort of patients with pre-existing autoimmune conditions, some patients received rituximab prior to SARS-CoV-2 infection. Published evidence suggested that such rituximab treatment may be linked to unfavorable COVID-19 outcomes [96, 97]. Our analysis may be consistent with this

hypothesis revealing that monocytes from such rituximab-treated patients have reduced expression of several genes involved in the antiviral response and inflammasome activation during SARS-CoV-2 infection. Nonetheless, patients on anti-CD20 treatment are still able to generate robust T-cell responses following COVID-19 vaccination, including CD8+ T-cell responses linked to milder COVID-19 outcomes, despite the impaired humoral responses, which may be important in reducing the risk of complications associated with severe COVID-19 [98, 99].

Our results highlight the presence of altered and diverging immune responses in autoimmune disease patients that are specific to SARS-CoV-2 infection, and that may affect the course of the disease. Future molecular and clinical studies building on our work, including expanded cohorts, will shed light on the ultimate consequences of the range of altered immune responses observed, including whether they are ultimately beneficial or harmful for these patients. The influence of these specific immune responses on the risk of evolution to severe forms of COVID-19 and/or clinical sequelae after the acute phase of SARS-CoV-2 infection, which may help find tailored treatments for different autoimmune patient populations, is particularly important to consider. This study presents a substantial and critical step toward that end. Notably, given the overlapping features of immunopathology between COVID-19 and other infections, such as influenza [100, 101], the implications of the altered immune responses observed here may further extend the study on how autoimmune disease patients cope with other viral infections.

ACKNOWLEDGEMENTS

This publication is part of the Human Cell Atlas (<https://www.humancellatlas.org/publications/>). The authors gratefully acknowledge the Sanger Cellular Genetics Informatics team, particularly A. Predeus and S. Murray for their assistance with aligning the published raw data from uninfected MS patients, as well as S. van Dongen, M. Prete, and Q. Lin for their help with online data hosting. We acknowledge the members of the Vento-Tormo and Ballestar groups for useful discussions. A.B. received additional support from a Gates Cambridge Scholarship. This research was funded/supported by the R+D+i project of the Spanish Ministry of Science and Innovation (grant number PID2020-117212RB-I00/MICIN/AEI/10.13039/501100011033), the Chan Zuckerberg Initiative (grant 2020-216799) and Wellcome Sanger core funding (WT206194). This publication has been supported by the Unstoppable campaign of the Josep Carreras Leukaemia Foundation. B.G., F.J.C.-N., and N.K.W. were funded by Wellcome (206328/Z/17/Z), the MRC (MR/S036113/1), and the Aging Biology Foundation.

CONFLICT OF INTEREST

I.G.-A. has received research support from Sanofi, Roche, and Lilly. H.H. is a co-founder and shareholder of Omniscope. The remaining authors declare no conflicts of interest.

AUTHOR CONTRIBUTIONS

Esteban Ballestar, Roser Vento-Tormo, and Javier Rodríguez-Ubrea conceived and designed the study; Gerard Godoy-Tena, Laura Ciudad, Tarryn Porter, Laura Richardson, Carmen Sancho-Serra, and Javier Rodríguez-Ubrea

performed sample preparation and 10x experiments; Regina Hoo, Tarryn Porter, Agnes Oszlanczi, Laura Richardson, Carmen Sancho-Serra, and Elena Prigmore generated libraries and performed the sequencing; Eduardo Andrés-León and Javier Martin performed patient genotyping; Anis Barmada, Louis-François Handfield, Carlos de la Calle-Fabregat, Anna Arutyunyan, Eduardo Andrés-León, and Javier Rodríguez-Ubreva performed the computational analyses; Fernando J. Calero-Nieto, Nicola K. Wilson and Berthold Göttgens optimized the CITE-seq protocol; Domenica Marchese and Holger Heyn provided support with the 10x experiments; Jorge Carrillo, Silvia Presas-Rodríguez, Cristina Ramo-Tello, Adolfo Ruiz-Sanmartin, Ricard Ferrer, Juan Carlos Ruiz-Rodríguez, Mónica Martínez-Gallo, Mónica Munera-Campos, Jose Manuel Carrascosa, Ivette Casafont-Solé, Xavier Solanich, Ildefonso Sánchez-Cerrillo, Isidoro González-Álvaro, Maria Gabriella Raimondo, Andreas Ramming, and Eva Martínez-Cáceres provided patient samples and analyzed clinical data; Anis Barmada, Louis-François Handfield, Gerard Godoy-Tena, Carlos de la Calle-Fabregat, Regina Hoo, Javier Martin, Esteban Ballestar, Roser Vento-Tormo, and Javier Rodríguez-Ubreva analyzed and interpreted the data; Anis Barmada and Javier Rodríguez-Ubreva wrote the manuscript with contributions from Gerard Godoy-Tena, Carlos de la Calle-Fabregat, Esteban Ballestar, and Roser Vento-Tormo; Esteban Ballestar, Roser Vento-Tormo and Javier Rodríguez-Ubreva supervised the study; all authors read and approved the final manuscript.

REFERENCES

1. Schultze, J. L. and Aschenbrenner, A. C., COVID-19 and the human innate immune system. *Cell*. 2021. 184: 1671–1692.
2. Sette, A. and Crotty, S., Adaptive immunity to SARS-CoV-2 and COVID19. *Cell*. 2021. 184: 861–880.
3. Wang, C., Xie, J., Zhao, L., Fei, X., Zhang, H., Tan, Y., Nie, X. et al., Alveolar macrophage dysfunction and cytokine storm in the pathogenesis of two severe COVID-19 patients. *EBioMedicine*. 2020. 57: 102833.
4. Furman, D., Campisi, J., Verdin, E., Carrera-Bastos, P., Targ, S., Franceschi, C., Ferrucci, L. et al., Chronic inflammation in the etiology of disease across the life span. *Nat. Med.* 2019. 25: 1822–1832.
5. Tay, M. Z., Poh, C. M., Rénia, L., Macary, P. A. and Ng, L. F. P., The trinity of COVID-19: immunity, inflammation and intervention. *Nat. Rev. Immunol.* 2020. 20: 363–374.
6. Henry, B. M., De Oliveira, M. H. S., Benoit, S., Plebani, M. and Lippi, G., Hematologic, biochemical and immune biomarker abnormalities associated with severe illness and mortality in coronavirus disease 2019 (COVID-19): a meta-analysis. *Clin. Chem. Lab. Med.* 2020. 58: 1021–1028.
7. Hadjadj, J., Yatim, N., Barnabei, L., Corneau, A., Boussier, J., Smith, N., Péré, H. et al., Impaired type I interferon activity and inflammatory responses in severe COVID-19 patients. *Science*. 2020. 369: 718–724.
8. Silvin, A., Chapuis, N., Dunsmore, G., Goubet, A.-G., Dubuisson, A., Derosa, L., Almiere, C. et al., Elevated calprotectin and abnormal myeloid cell subsets discriminate severe from mild COVID-19. *Cell*. 2020. 182: 1401–1418.e18.e18.
9. Guo, C., Li, B., Ma, H., Wang, X., Cai, P., Yu, Q., Zhu, L. et al., Single-cell analysis of two severe COVID-19 patients reveals a monocyte-associated and tocilizumab-responding cytokine storm. *Nat Commun*. 2020. 11().
10. Zhou, Y., Fu, B., Zheng, X., Wang, D., Zhao, C., Qi, Y., Sun, R. et al., Pathogenic T-cells and inflammatory monocytes incite inflammatory storms in severe COVID-19 patients. *Natl. Sci. Rev.* 2020. 7: 998–1002.
11. Schulte-Schrepping, J., Reusch, N., Paclik, D., Baßler, K., Schlickeiser, S., Zhang, B., Krämer, B. et al., Severe COVID-19 is marked by a dysregulated myeloid cell compartment. *Cell*. 2020. 182: 1419–1440.e23.e23.
12. Tian, Y., Carpp, L. N., Miller, H. E. R., Zager, M., Newell, E.W. and Gottardo, R., Single-cell immunology of SARS-CoV-2 infection. *Nat. Biotechnol.* 2022. 40: 30–41.
13. Sánchez-Cerrillo, I., Landete, P., Aldave, B., Sánchez-Alonso, S., SánchezAzofra, A., Marcos-Jiménez, A., Ávalos, E. et al., COVID-19 severity associates with pulmonary redistribution of CD1c+ DCs and inflammatory transitional and nonclassical monocytes. *J Clin Invest*. 2020. 130: 6290–6300.
14. Yao, C., Bora, S. A., Parimon, T., Zaman, T., Friedman, O. A., Palatinus, J. A., Surapaneni, N. S. et al., Cell-type-specific immune dysregulation in severely ill COVID-19 patients. *Cell Rep*. 2021. 34: 108590.
15. Wong, J. J. M., Leong, J. Y., Lee, J. H., Albani, S. and Yeo, J. G., Insights into the immunopathogenesis of acute respiratory distress syndrome. *Ann. Transl. Med.* 2019. 7: 504–504.
16. Gil-Etayo F. J., Suárez-Fernández P., Cabrera-Marante O., Arroyo D., Garcinuño S., Naranjo L., Pleguezuelo D. E. et al., T-helper cell subset response is a determining factor in COVID-19 progression. *Front. Cell Infect. Microbiol.* 2021. 11: 624483.

17. Giamarellos-Bourboulis, E. J., Netea, M. G., Rovina, N., Akinosoglou, K., Antoniadou, A., Antonakos, N., Damoraki, G. et al., Complex immune dysregulation in COVID-19 patients with severe respiratory failure. *Cell Host Microbe*. 2020. 27: 992–1000.e3.e3.
18. Meckiff, B. J., Ramírez-Suástegui, C., Fajardo, V., Chee, S. J., Kusnadi, A., Simon, H., Eschweiler, S. et al., Imbalance of regulatory and cytotoxic SARS-CoV-2-reactive CD4⁺ T cells in COVID-19. *Cell*. 2020;183: 1340–1353.e16.e16.
19. Freitas Nuñez, D. D., Leon, L., Mucientes, A., Rodriguez-Rodriguez, L., Font Urgelles, J., Madrid García, A., Colomer, J. I. et al., Risk factors for hospital admissions related to COVID-19 in patients with autoimmune inflammatory rheumatic diseases. *Ann. Rheum. Dis*. 2020;79: 1393–1399.
20. Willis, M. D. and Robertson, N. P., Multiple sclerosis and the risk of infection: considerations in the threat of the novel coronavirus, COVID19/SARS-CoV-2. *J. Neurol*. 2020. 267: 1567–1569.
21. Akiyama, S., Hamdeh, S., Micic, D. and Sakuraba, A., Prevalence and clinical outcomes of COVID-19 in patients with autoimmune diseases: a systematic review and meta-analysis. *Ann. Rheum. Dis*. 2021. 80: 384–391.
22. Sarmiento-Monroy, J. C., Espinosa, G., Londoño, M. C., Meira, F., Caballol, B., Llufrui, S., Carrasco, J. L. et al., A multidisciplinary registry of patients with autoimmune and immune-mediated diseases with symptomatic COVID-19 from a single center. *J. Autoimmun*. 2021. 117: 102580.
23. Eder, L., Croxford, R., Drucker, A. M., Mendel, A., Kuriya, B., Touma, Z., Johnson, S. R. et al., COVID-19 hospitalizations, intensive care unit stays, ventilation, and death among patients with immune-mediated inflammatory diseases compared to controls. *J. Rheumatol*. 2022. 49: 523–530. Available from: <http://www.jrheum.org/content/49/5/523.abstract>
24. Troyano-Hernández, P., Reinoso, R. and Holguín, Á., Evolution of SARSCoV-2 in Spain during the first two years of the pandemic: circulating variants, amino acid conservation, and genetic variability in structural, non-structural, and accessory proteins. *Int. J. Mol. Sci*. 2022. 23: 6394.
25. Heaton, H., Talman, A. M., Knights, A., Imaz, M., Gaffney, D. J., Durbin, R., Hemberg, M. et al., Souporecell: robust clustering of single-cell RNAseq data by genotype without reference genotypes. *Nat. Methods*. 2020. 17: 615–620.
26. Wolock, S. L., Lopez, R. and Klein, A. M., Scrublet: Computational identification of cell doublets in single-cell transcriptomic data. *Cell Syst*. 2019. 8: 281–291.e9.
27. Young, M. D. and Behjati, S., SoupX removes ambient RNA contamination from droplet-based single-cell RNA sequencing data. *Gigascience*. 2020. 9: gaa151.
28. Gayoso, A., Steier, Z., Lopez, R., Regier, J., Nazor, K. L., Streets, A. and Yosef, N., Joint probabilistic modeling of single-cell multi-omic data with totalVI. *Nat. Methods*. 2021. 18: 272–282.
29. Wolf, F. A., Angerer, P. and Theis, F. J., SCANPY: Large-scale single-cell gene expression data analysis. *Genome Biol*. 2018. 19.
30. Stephenson, E., Reynolds, G., Botting, R. A., Calero-Nieto, F. J., Morgan, M. D., Tuong, Z. K., Bach, K. et al., Single-cell multi-omics analysis of the immune response in COVID-19. *Nat. Med*. 2021: 904–916.
31. Sturm, G., Szabo, T., Fotakis, G., Haider, M., Rieder, D., Trajanoski, Z. and Finotello, F., Scirpy: a Scanpy extension for analyzing single-cell T-cell receptor-sequencing data. *Bioinformatics*. 2020. 36: 4817–4818.

32. Ritchie, M. E., Phipson, B., Wu, D., Hu, Y., Law, C.W., Shi, W. and Smyth, G. K., Limma powers differential expression analyses for RNA-sequencing and microarray studies. *Nucleic Acids Res.* 2015. 43: e47.
33. Ren, X., Wen, W., Fan, X., Hou, W., Su, B., Cai, P., Li, J. et al., COVID19 immune features revealed by a large-scale single-cell transcriptome atlas. *Cell.* 2021. 184: 1895–1913.e19.e19.
34. Schafflick, D., Xu, C. A., Hartlehnert, M., Cole, M., Schulte-Mecklenbeck, A., Lautwein, T., Wolbert, J. et al., Integrated single cell analysis of blood and cerebrospinal fluid leukocytes in multiple sclerosis. *Nat. Commun.* 2020. 11: 247.
35. Ranjan, B., Sun, W., Park, J., Mishra, K., Schmidt, F., Xie, R., Alipour, F. et al., DUBStepR is a scalable correlation-based feature selection method for accurately clustering single-cell data. *Nat. Commun.* 2021. 12: 5849.
36. Yu, G., Wang, L. G., Han, Y. and He, Q. Y., ClusterProfiler: an R package for comparing biological themes among gene clusters. *OMICS: J. Integr. Biol.* 2012. 16: 284–287.
37. Garcia-Alonso, L., Holland, C. H., Ibrahim, M. M., Turei, D. and SaezRodriguez, J., Benchmark and integration of resources for the estimation of human transcription factor activities. *Genome Res.* 2019. 29: 1363–1375.
38. Efremova, M., Vento-Tormo, M., Teichmann, S. A. and Vento-Tormo, R., CellPhoneDB: inferring cell-cell communication from combined expression of multi-subunit ligand-receptor complexes. *Nat. Protoc.* 2020. 15: 1484–1506.
39. Stoeckius, M., Hafemeister, C., Stephenson, W., Houck-Loomis, B., Chattopadhyay, P. K., Swerdlow, H., Satija, R. et al., Simultaneous epitope and transcriptome measurement in single cells. *Nat. Methods.* 2017. 14: 865–868.
40. Hottz, E. D., Azevedo-Quintanilha, I. G., Palhinha, L., Teixeira, L., Barreto, E. A., Pão, C. R. R., Righy, C. et al., Platelet activation and platelet-monocyte aggregate formation trigger tissue factor expression in patients with severe COVID-19. *Blood.* 2020. 136: 1330–1341.
41. Grifoni, A., Weiskopf, D., Ramirez, S. I., Mateus, J., Dan, J. M., Moderbacher, C. R., Rawlings, S. A. et al., Targets of T cell responses to SARS-CoV-2 coronavirus in humans with COVID-19 disease and unexposed individuals. *Cell.* 2020. 181: 1489–1501.e15.e15.
42. Sekine, T., Perez-Potti, A., Rivera-Ballesteros, O., Strålin, K., Gorin, J. B., Olsson, A., Llewellyn-Lacey, S. et al., Robust T cell immunity in convalescent individuals with asymptomatic or mild COVID-19. *Cell.* 2020. 183:158–168.e14.e14.
43. Xu, X., Qiu, C., Zhu, L., Huang, J., Li, L., Fu, W., Zhang, L. et al., IFNs stimulated gene LY6E in monocytes regulates the CD14/TLR4 pathway but inadequately restrains the hyperactivation of monocytes during chronic HIV-1 infection. *J. Immunol.* 2014. 193: 4125–4136. 44 Pfaender, S., Mar, K. B., Michailidis, E., Kratzel, A., Boys, I. N., V'kovski, P., Fan, W. et al., LY6E impairs coronavirus fusion and confers immune control of viral disease. *Nat. Microbiol.* 2020. 5: 1330–1339.
44. Zhao, X., Zheng, S., Chen, D., Zheng, M., Li, X., Li, G., Lin, H. et al, LY6E restricts entry of human coronaviruses, including currently pandemic SARS-CoV-2. *J. Virol.* 2020. 94: e00562–20.
45. Johnson, J. K., Wright, P. W., Li, H. and Anderson, S K., Identification of trophoblast-specific elements in the HLA-C core promoter. *HLA.* 2018. 92: 288–297.
46. Shalova, I. N., Lim, J. Y., Chittechath, M., Zinkernagel, A. S., Beasley, F., Hernández-Jiménez, E., Toledano, V. et al., Human monocytes undergo functional re-programming during sepsis mediated by hypoxia-inducible factor-1 α . *Immunity.* 2015. 42: 484–498.

47. Cheng, S. C., Quintin, J., Cramer, R. A., Shephardson, K. M., Saeed, S., Kumar, V. et al., MTOR- and HIF- α -mediated aerobic glycolysis as metabolic basis for trained immunity. *Science* (80-). 2014. 345.
48. Swain, S. L., Weinberg, A. D., English, M. and Huston, G., IL-4 directs the development of Th2-like helper effectors. *J. Immunol.* 1990. 145: 3796– 3806. Available from: <http://www.ncbi.nlm.nih.gov/pubmed/2147202>
49. Wurster, A. L., Rodgers, V. L., Satoskar, A. R., Whitters, M. J., Young, D. A., Collins, M. and Grusby, M. J., Interleukin 21 is a T helper (Th) cell 2 cytokine that specifically inhibits the differentiation of naive Th cells into interferon γ -producing Th1 cells. *J. Exp. Med.* 2002. 196: 969–977.
50. Hayden, M. S. and Ghosh, S., Regulation of NF- κ B by TNF family cytokines. *Semin. Immunol.* 2014. 26: 253–266.
51. Quaglino, P., Bergallo, M., Ponti, R., Barberio, E., Cicchelli, S., Buffa, E., Comessatti, A. et al., Th1, Th2, Th17 and regulatory T cell pattern in psoriatic patients: Modulation of cytokines and gene targets induced by etanercept treatment and correlation with clinical response. *Dermatology.* 2011. 223: 57–67.
52. Vento-Tormo, R., Efremova, M., Botting, R. A., Turco, M. Y., Vento-Tormo, M., Meyer, K. B., Park, J. E. et al., Single-cell reconstruction of the early maternal–fetal interface in humans. *Nature.* 2018. 563: 347–353.
53. Peteranderl, C. and Herold, S., The impact of the interferon/TNF-related apoptosis-inducing ligand signaling axis on disease progression in respiratory viral infection and beyond. *Front. Immunol.* 2017. 8: 313.
54. Chua, R. L., Lukassen, S., Trump, S., Hennig, B. P., Wendisch, D., Pott, F., Debnath, O. et al., COVID-19 severity correlates with airway epithelium– immune cell interactions identified by single-cell analysis. *Nat. Biotechnol.* 2020. 38: 970–979.
55. Capasso, M., Durrant, L. G., Stacey, M., Gordon, S., Ramage, J. and Spendlove, I., Costimulation via CD55 on human CD4 + T cells mediated by CD97. *J. Immunol.* 2006. 177: 1070–1077.
56. Arrambide, G., Llanea-González, M. Á., Costa-Frossard França, L., Meca-Lallana, V., Díaz, E. F., Moreno-Torres, I., García-Domínguez, J. M. et al., SARS-CoV-2 infection in multiple sclerosis: results of the Spanish neurology society registry. *Neurol. Neuroimmunol.* 2021. 8: e1024.
57. Barzegar, M., Vaheb, S., Mirmosayyeb, O., Afshari-Safavi, A., Nehzat, N. and Shaygannejad, V., Can coronavirus disease 2019 (COVID-19) trigger exacerbation of multiple sclerosis? A retrospective study. *Mult. Scler. Relat. Disord.* 2021. 52: 102947.
58. Muñoz-Jurado, A., Escribano, B M., Agüera, E., Caballero-Villarraso, J., Galván, A. and Túnez, I., SARS-CoV-2 infection in multiple sclerosis patients: interaction with treatments, adjuvant therapies, and vaccines against COVID-19. *J. Neurol.* 2022. 269: 4581–4603.
59. Figueroa-Parra, G., Gilbert, E. L., Valenzuela-Almada, M. O., Vallejo, S., Neville, M. R., Patel, N. J., Cook, C. et al., Risk of severe COVID-19 outcomes associated with rheumatoid arthritis and phenotypic subgroups: a retrospective, comparative, multicentre cohort study. *Lancet Rheumatol.* 2022. 4: e765–e774.
60. Bournia, V. K., Fragoulis, G. E., Mitrou, P., Mathioudakis, K., Tsolakidis, A., Konstantonis, G., Tseti, I. et al., Different COVID-19 outcomes among systemic rheumatic diseases: a nation-wide cohort study. *Rheumatology (Oxford).* 2023. 62: 1047–1056.

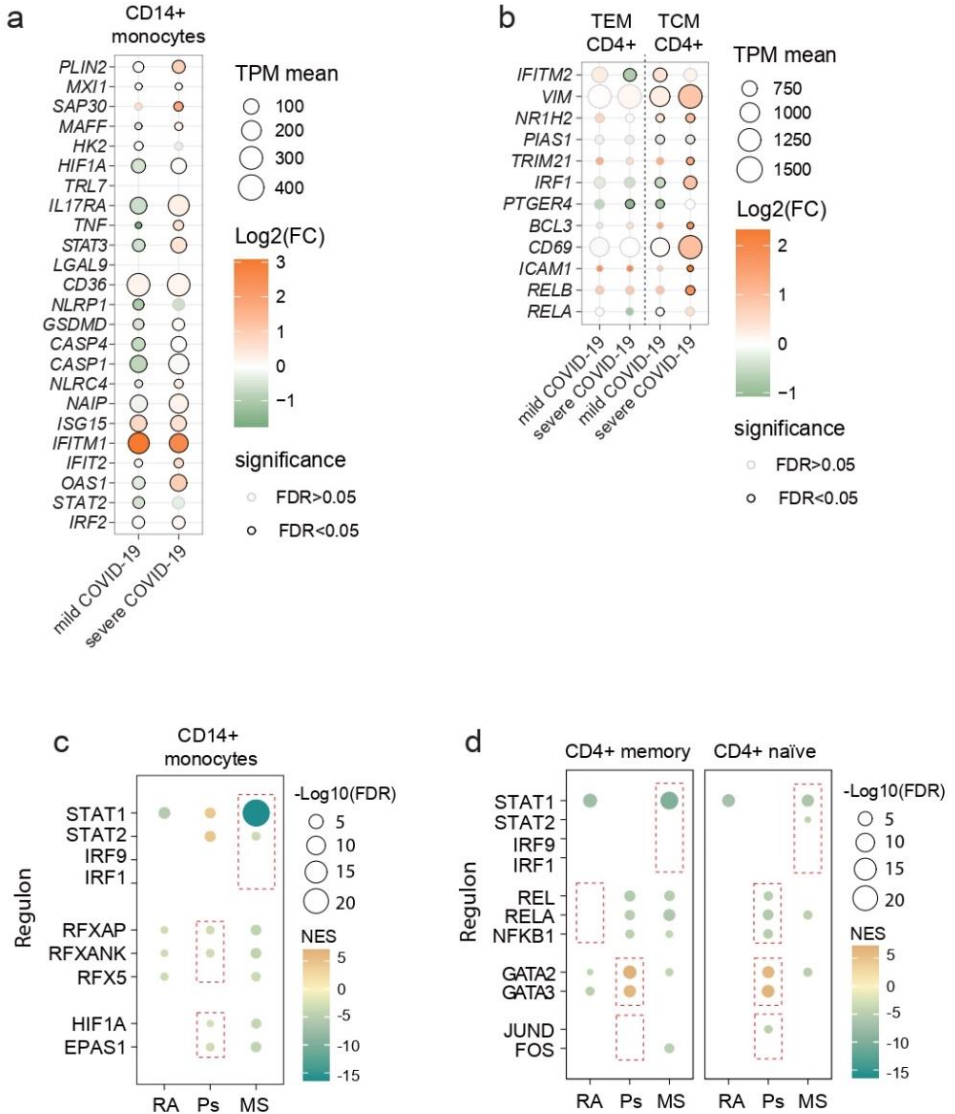
61. Bower, H., Frisell, T., Di Giuseppe, D., Delcoigne, B., Ahlenius, G. M., Baecklund, E., Chatzidionysiou, K. et al., Impact of the COVID-19 pandemic on morbidity and mortality in patients with inflammatory joint diseases and in the general population: a nationwide Swedish cohort study. *Ann. Rheum. Dis.* 2021. 80: 1086–1093.
62. Shin, Y Ho, Shin, J Il, Moon, S. Y., Jin, H. Y., Kim, So Y, Yang, J. M., Cho, S Ho et al., Autoimmune inflammatory rheumatic diseases and COVID-19 outcomes in South Korea: a nationwide cohort study. *Lancet Rheumatol.* 2021. 3: e698–e706.
63. Kridin, K., Schonmann, Y., Onn, E., Bitan, D. T., Weinstein, O., Shavit, E. and Cohen, A. D., Nineteen months into the pandemic, what have we learned about COVID-19-related outcomes in patients with psoriasis? *J. Cosmet. Dermatol.* 2022. 21: 6549–6553.
64. Lin, Yi, Gustafson, M. P., Bulur, P. A., Gastineau, D. A., Witzig, T. E. and Dietz, A. B., Immunosuppressive CD14+HLA-DRlow/- monocytes in Bcell non-Hodgkin lymphoma. *Blood.* 2011. 117: 872–881.
65. Mengos, A. E., Gastineau, D. A. and Gustafson, M P., The CD14+HLADrIO/NEG monocyte: an immunosuppressive phenotype that restrains responses to cancer immunotherapy. *Front. Immunol.* 2019. 10: 1147.
66. Reyes, M., Filbin, M. R., Bhattacharyya, R. P., Sonny, A., Mehta, A., Billman, K., Kays, K. R. et al., Plasma from patients with bacterial sepsis or severe COVID-19 induces suppressive myeloid cell production from hematopoietic progenitors in vitro. *Sci Transl Med.* 2021. 13: eab9599.
67. Wilk, A. J., Lee, M. J., Wei, B., Parks, B., Pi, R., Martínez-Colón, G. J., Ranganath, T. et al., Multi-omic profiling reveals widespread dysregulation of innate immunity and hematopoiesis in COVID-19. *J. Exp. Med.* 2021. 218: e20210582.
68. Parrot, T., Gorin, J-B., Ponzetta, A., Maleki, K. T., Kammann, T., Emgård, J., Perez-Potti, A. et al., MAIT cell activation and dynamics associated with COVID-19 disease severity. *Sci. Immunol.* 2020. 5: eabe1670.
69. Trouillet-Assant, S., Viel, S., Gaymard, A., Pons, S., Richard, J. C., Perret, M., Villard, M. et al., Type I IFN immunoprofiling in COVID-19 patients. *J. Allergy. Clin. Immunol.* 2020. 146: 206–208.e2.e2.
70. Bastard, P., Rosen, L. B., Zhang, Q., Michailidis, E., Hoffmann, H. H., Zhang, Y., Dorgham, K. et al., Autoantibodies against type I IFNs in patients with life-threatening COVID-19. *Science.* 2020. 370: eabd4585.
71. Zhang, Q., Bastard, P., Liu, Z., Le Pen, J., Moncada-Velez, M., Chen, J., Ogishi, M. et al., Inborn errors of type I IFN immunity in patients with life-threatening COVID-19. *Science.* 2020. 370: eabd4570.
72. Arunachalam, P. S., Wimmers, F., Mok, C. K. P., Perera, R A. P. M., Scott, M., Hagan, T., Sigal, N. et al., Systems biological assessment of immunity to mild versus severe COVID-19 infection in humans. *Science.* 2020. 369: 1210–1220.
73. Combes, A. J., Courau, T., Kuhn, N. F., Hu, K. H., Ray, A., Chen, W. S., Chew, N. W. et al., Global absence and targeting of protective immune states in severe COVID-19. *Nature.* 2021. 591: 124–130.
74. Monk, P. D., Marsden, R. J., Tear, V. J., Brookes, J., Batten, T. N., Mankowski, M., Gabbay, F. J. et al., Safety and efficacy of inhaled nebulised interferón beta-1a (SNG001) for treatment of SARS-CoV-2 infection: a randomised, double-blind, placebo-controlled, phase 2 trial. *Lancet Respir. Med.* 2021. 9: 196–206.
75. Lee, J. S. and Shin, E. C., The type I interferon response in COVID19: implications for treatment. *Nat. Rev. Immunol.* 2020. 20: 585–586.

76. King, C. and Sprent, J., Dual nature of type I interferons in SARS-CoV-2-induced inflammation. *Trends Immunol.* 2021. 42: 312–322.
77. Ziegler, C. G.K., Allon, S. J., Nyquist, S. K., Mbanjo, I M., Miao, V. N., Tzouanas, C. N., Cao, Y. et al., SARS-CoV-2 receptor ACE2 is an interferonstimulated gene in human airway epithelial cells and is detected in specific cell subsets across tissues. *Cell.* 2020. 181: 1016–1035.e19.e19.
78. Onabajo, O. O., Banday, A. R, Stanifer, M. L., Yan,W., Obajemu, A., Santer, D. M., Florez-Vargas, O. et al., Interferons and viruses induce a novel truncated ACE2 isoform and not the full-length SARS-CoV-2 receptor. *Nat Genet.* 2020. 52: 1283–1293. 80 Saffern, M., ACE2 is not induced by interferon. *Nat Rev Immunol.* 2020. 20: 521.
79. Fajnzylber, J.,Regan, J.,Coxen, K.,Corry, H.,Wong, C.,Rosenthal, A.,Worrall, D. et al., SARS-CoV-2 viral load is associated with increased disease severity and mortality. *Nat Commun.* 2020. 11: 5493.
80. Liu, Y., Yan, L. M.,Wan, L., Xiang, T. X., Le, A., Liu, J. M. et al., Viral dynamics in mild and severe cases of COVID-19. *Lancet Infect. Dis.* 2020. 20. 656–657.
81. Zhu, J., Yamane, H., Cote-Sierra, J., Guo, L. and Paul, W. E., GATA-3 promotes Th2 responses through three different mechanisms: Induction of Th2 cytokine production, selective growth of Th2 cells and inhibition of Th1 cell-specific factors. *Cell Res.* 2006. 16: 3–10.
82. Lin, W. L., Jing, W. W., Xi, C. D. and Xu, B., Dysregulation of the immune response affects the outcome of critical COVID-19 patients. *J. Med. Virol.* 2020. 92: 2768–2776.
83. Roncati, L., Nasillo, V., Lusenti, B. and Riva, G., Signals of Th2 immune response from COVID-19 patients requiring intensive care. *Ann. Hematol.* 2020. 99: 1419–1420.
84. Ghoreschi, K.,Thomas, P.,Breit, S.,Dugas, M.,Mailhammer, R., Van Eden, W., Van Der Zee, R. et al., Interleukin-4 therapy of psoriasis induces Th2 responses and improves human autoimmune disease. *Nat Med.* 2003. 9: 40–46.
85. Palazon, A., Goldrath, A. W., Nizet, V. and Johnson, R. S., HIF transcription factors, inflammation, and immunity. *Immunity.* 2014. 41: 518–528.
86. Fara, A., Mitrev, Z., Rosalia, R. A. and Assas, B. M., Cytokine storm and COVID-19: a chronicle of pro-inflammatory cytokines: cytokine storm: the elements of rage!. *Open Biol.* 2020. 10: 200160.
87. Hariharan, A., Hakeem, A. R., Radhakrishnan, S., Reddy, M. S. and Rela, M., The role and therapeutic potential of NF-kappa-B pathway in severe COVID-19 patients. *Inflammopharmacology.* 2021. 29: 91–100.
88. Nalbandian, A., Sehgal, K., Gupta, A., Madhavan, M. V., Mcgroder, C., Stevens, J. S., Cook, J. R. et al., Post-acute COVID-19 syndrome. *Nat. Med.* 2021. 27: 601–615.
89. Le, T-T. T., Karmouty-Quintana, H., Melicoff, E., Le, T-T. T., Weng, T., Chen, N. Y., Pedroza, M. et al., Blockade of IL-6 trans signaling attenuates pulmonary fibrosis. *J. Immunol.* 2014. 193: 3755–3768
90. Teh, Y. C, Ding, J. L., Ng, L. G. and Chong, S. Z., Capturing the fantastic voyage of monocytes through time and space. *Front. Immunol.* 2019. 10: 3389.
91. Thachil, J., Hypoxia—An overlooked trigger for thrombosis in COVID-19 and other critically ill patients. *J. Thromb. Haemost.* 2020. 18: 3109–3110.
92. Chuah, S. L., Teh, C. L., Wan Mohd Akbar, S. A., Cheong, Y. K. and Sachdev Manjit Singh, B., Impact of COVID-19 pandemic on hospitalisation of patients with systemic lupus erythematosus (SLE): report from a tertiary hospital during the peak of the pandemic. *Ann. Rheum. Dis.* 2020. 81: e144.

93. George, M. D., Venkatachalam, S., Banerjee, S., Baker, J. F., Merkel, P. A., Gavigan, K., Curtis, D. et al., Concerns, healthcare use, and treatment interruptions in patients with common autoimmune rheumatic diseases during the COVID-19 pandemic. *J. Rheumatol.* 2021. 48: 603–607.
94. Avouac, J., Drumez, E., Hachulla, E., Seror, R., Geogin-Lavialle, S. and El Mahou, S., COVID-19 outcomes in patients with inflammatory rheumatic and musculoskeletal diseases treated with rituximab: a cohort study. *Lancet Rheumatol.* 2021. 3: e419–e426.
95. Burgener, S., Rochat, P., Dollenmaier, G., Benz, G., Kistler, A. D., Fulchini, R. et al., Progression of COVID-19 in a patient on anti-CD20 antibody treatment: case report and literature review. *Case Rep. Infect. Dis.* 2022. 2022: 1–5.
96. Verstegen, N. J., Hagen, R. R., van den Dijssel, J., Kuijper, L. H., Kreher, C., Ashhurst, T. et al., Immune dynamics in SARS-CoV-2 experienced immunosuppressed rheumatoid arthritis or multiple sclerosis patients vaccinated with mRNA-1273. *eLife.* 2022. 11: e77969.
97. Madelon, N., Lauper, K., Breville, G., Sabater Royo, I., Goldstein, R., Andrey, D. O., Grifoni, A. et al., Robust T-cell responses in anti-CD20- treated patients following COVID-19 vaccination: a prospective cohort study. *Clin. Infect. Dis.* 2022. 75: e1037–e1045.
98. Lee, J. S., Park, S., Jeong, H. W., Ahn, J. Y., Choi, S. J., Lee, H., Choi, B. et al., Immunophenotyping of covid-19 and influenza highlights the role of type I interferons in development of severe covid-19. *Sci. Immunol.* 2020.5: eabd1554.
99. Alon, R., Sportiello, M., Kozlovski, S., Kumar, A., Reilly, E C., Zarbock, A. et al., Leukocyte trafficking to the lungs and beyond: lessons from influenza for COVID-19. *Nat. Rev. Immunol.* 2021. 21: 49–64.

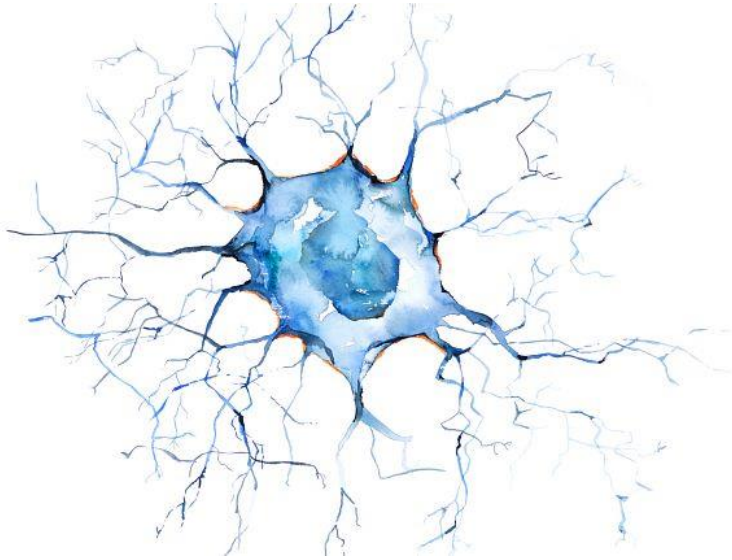
SUPPLEMENTARY FIGURE

Supp. Figure 1



(See figure legend on the next page.)

Supp. Figure 1. Gene expression in mild and severe COVID-19 controls and transcription factor activity in uninfected patients with autoimmune disease. **(a)** Circle plot representing the expression of selected genes in CD14⁺ monocytes of mild or severe COVID-19 controls during infection over uninfected individuals. Circle size indicates TPM mean and scale indicates Log₂ of the gene expression fold change during infection over uninfected individuals. Significance is also indicated by a black (FDR < 0.05) or gray (FDR > 0.05) line. **(b)** Circle plot representing the expression of selected genes in CD4⁺ T cells (TEM: T effector memory; TCM: T central memory) of mild or severe COVID-19 controls during infection over uninfected individuals. Circle size indicates TPM mean and scale indicates Log₂ of the gene expression fold change during infection over uninfected individuals. Significance is also indicated by a black (FDR < 0.05) or gray (FDR > 0.05) line. **(c)** Dot plot showing selected transcription factor activities of different regulons in CD14⁺ monocytes from uninfected autoimmune disease patients (RA, Ps, and MS) compared with healthy controls. The scale represents the normalized enrichment score (NES); the circle size indicates the -log₁₀FDR value. **(d)** Dot plot showing selected transcription factor activities of different regulons in CD4⁺ naïve and memory T cells from uninfected autoimmune disease patients (RA, Ps, and MS) compared with healthy controls. The scale represents the normalized enrichment score (NES); the circle size indicates the -log₁₀FDR value.



GLOBAL RESULTS
and
DISCUSSION

5. GLOBAL RESULTS

Article 1. Retinoic Acid-Induced Epigenetic Modulation of VSIG4 via LXR α in Dendritic Cells Promotes Immunosuppression

To investigate the mechanisms underlying the RA-mediated phenotypic reprogramming of DCs, monocytes isolated from the peripheral blood of healthy donors were differentiated to DCs for 5 days *in vitro* using GM-CSF and IL-4, in the absence and presence of RA and activated them LPS for 2 days.

We found that RA resulted in the acquisition of immunosuppressive properties by DCs, which now were able to inhibit CD8⁺ T cell proliferation. RA also resulted in the downregulation of pro-inflammatory cytokines such as IL-1 β , IL-6, and TNF- α while also reducing the expression of IL-10, suggesting a global downregulation of NF- κ B-mediated activation. RA-treated DCs also exhibited a macrophage-like phenotype with increased expression of macrophage markers (CD14, CD163, CD206) and decreased expression of the DC marker CD1a.

DNA methylation profiles revealed distinct patterns in response to RA treatment, with different specific demethylation and hypermethylation clusters. These changes were associated with differentiation and activation processes, affecting genes involved in myeloid differentiation, leukocyte activation, and immune response. TF motif enrichment analysis suggested the involvement of transcription factors such as EGR2, RARs, and NF- κ B in regulating DNA methylation dynamics.

RNA sequencing analysis showed upregulation of genes associated with a macrophage-like phenotype and immunosuppression in RA-treated DCs. VSIG4, associated with immune homeostasis, was among the most

differentially expressed genes. Gene set enrichment analysis indicated enrichment of monocyte and macrophage-related genes in RA-treated DCs, with an intermediate phenotype observed between macrophages and DCs. The analysis also revealed an inverse correlation between DNA methylation and gene expression changes.

Interestingly we found that RA induces the expression of LXR α and downregulates its partner RXR α . The sole activation of LXR with a synthetic agonist does not replicate the effects of RA. RXR agonist replicate the effects of RA, producing the same LXR α upregulation and RXR α downregulation. Conversely, inhibiting LXR functionality with an antagonist reverses the suppressive phenotype induced by RA.

Binding motifs for LXR α were identified near the VSIG4 gene, and LXR α shows increased binding to this region in RA-treated DCs. Furthermore, DNA methylation analysis suggests that LXR α epigenetically regulates VSIG4 expression.

Analysis of single-cell RNA sequencing data from ATC patients reveals co-expression of LXR α and VSIG4 in tumor-associated macrophages within the TME. This suggests a potential role for LXR α in regulating VSIG4 expression in the TME, contributing to immunosuppression.

Integration of the data from our in vitro model with single-cell RNA sequencing dataset from myeloid cells from barrier tissues such as the colon, skin, stomach, and liver, demonstrates that RA treatment leads to the upregulation of VSIG4 and LXR α in specific macrophage subtypes. This suggests a broader role for RA-mediated immunosuppression via the VSIG4 pathway in various tissues (**Figure 7**).

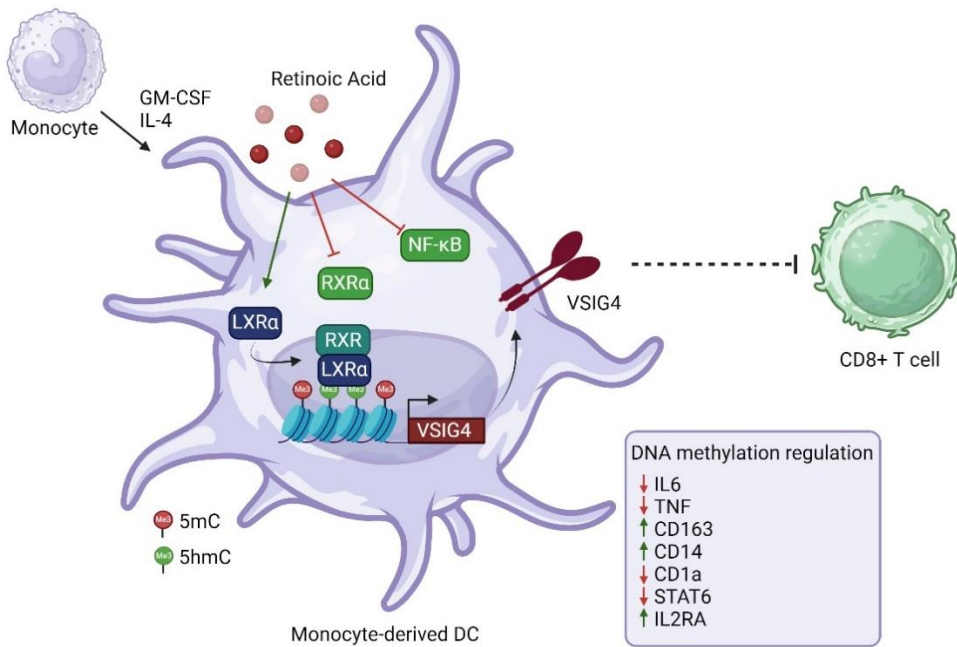


Figure 7. Scheme depicting the relevance of LXR activation by RA to promote the demethylation and expression of the immunosuppressive protein VSIG4.

ARTICLE 2. Epigenetic and transcriptomic reprogramming in monocytes of severe COVID-19 patients reflects alterations in myeloid differentiation and the influence of inflammatory cytokines

We isolated CD14⁺ monocytes from severe COVID-19 patients and HDs and performed DNA methylation profiling. We identified 221 DMPs between severe COVID-19 patients and HDs, with 1773 hypermethylated and 438 hypomethylated positions.

We found that hypermethylated regions were enriched in functional categories related to immune responses such as natural killer-mediated immunity, leukocyte migration, and antigen presentation. On the other hand, hypomethylated regions were associated with defense response to viruses, type

I interferon signalling, and MHC class II. Enrichment analysis revealed overrepresentation of transcription factor binding motifs associated with immune response regulation. Hypermethylated DMPs showed enrichment of IRFs and ETS TF families, while hypomethylated DMPs were enriched in bZIP TF family motifs and STAT binding motifs.

We investigated the relationship between DNA methylation profiles and the SOFA score, a measure of organ damage and a predictor of mortality in ICU patients. We found that higher SOFA scores, indicative of a more severe organ dysfunction, are associated with specific patterns of DNA methylation changes.

To further characterise the DNA methylation profiles acquired by monocytes of severe COVID-19 patients, we compared them to those from patients with bacterial sepsis. This comparison revealed significant overlap in DMPs. Shared hypermethylated CpGs were associated with pathways related to cell signaling and cytokine production, while hypomethylated CpGs were associated with the regulation of inflammatory responses. Additionally, examination of DNA methylation changes in monocytes treated with inflammatory cytokines *in vitro* supported the hypothesis that systemic inflammation contributes to observed DNA methylation alterations in severe COVID-19. Analysis of progenitor cell DNA methylation patterns suggested that some methylation changes observed in severe COVID-19 monocytes may arise from aberrant myeloid differentiation or the release of immature monocytes from the bone marrow to peripheral blood.

scRNA-seq data analysis showed significant differential gene expression between COVID-19 patients and HDs. Genes related to pro-inflammatory

responses, surface markers, and transcription factors were upregulated, while those associated with antigen presentation and type I interferon responses were downregulated. Integration of DNA methylation and gene expression data showed a negative correlation between DNA methylation levels and gene expression, with hypermethylated genes generally downregulated and hypomethylated genes upregulated in COVID-19 patients.

Finally, analysis of ligand-receptor interactions using CellPhoneDB revealed potential alterations in cell-cell communication between monocytes and other immune cell subsets in severe COVID-19. Changes were observed in interactions involving NK cells, T cells, B cells, and Tregs.

The observed DNA methylation and gene expression changes suggest a shift towards a more tolerogenic phenotype in monocytes from severe COVID-19 patients. Alterations in cell-cell communication may further contribute to dysregulated immune responses in COVID-19 (**Figure 8**).

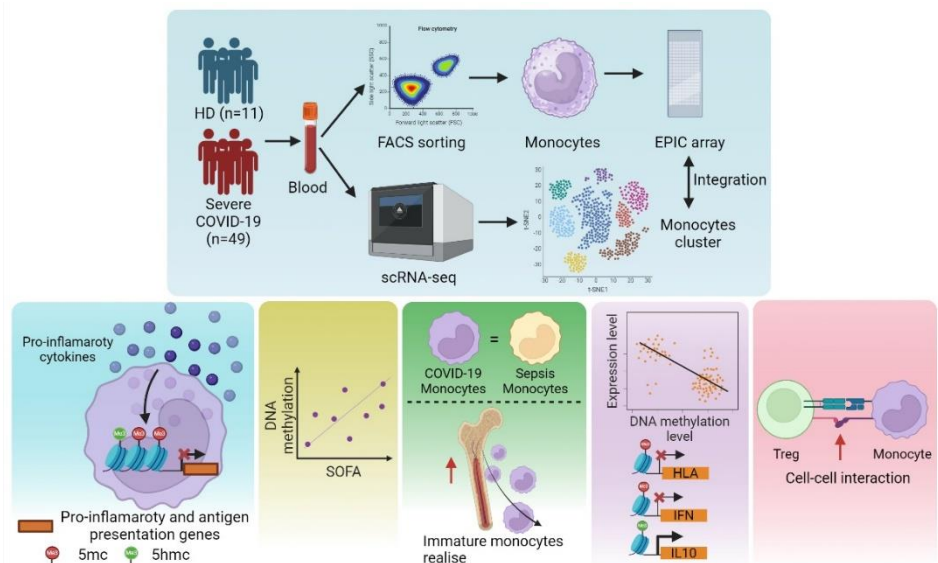


Figure 8. Monocytes from severe COVID-19 cases exhibit an immunosuppressive phenotype that is regulated by DNA methylation.

ARTICLE 3. Single-cell multi-omics analysis of COVID-19 patients with pre-existing autoimmune diseases shows aberrant immune responses to infection

Peripheral blood samples were collected from COVID-19 patients with Ra (5 patients), Ps (4 patients), and MS (3 patients), as well as from 10 COVID-19 patients without pre-existing autoimmunity who served as controls. PBMCs were isolated and subjected to single-cell transcriptomic and surface-proteomic profiling. The analysis revealed distinct immune cell populations, including T cells, B cells, myeloid cells, and hematopoietic stem cells, along with their subsets.

Notable findings included higher frequencies of CD4⁺ memory T cells in Ra COVID-19 patients, increased circulating MAIT cells in MS COVID-19 patients, and fewer plasmablasts and plasma cells in Ps and Ra COVID-19 patients compared to controls. The CD14⁺ monocytes with low HLA-DR expression were significantly increased in all autoimmune COVID-19 patients compared to controls, which is associated with COVID-19 severity.

Clonal expansion analysis revealed higher proportions of clonally expanded MAIT cells in MS COVID-19 patients and lower proportions of clonally expanded CD8⁺ memory T cells in Ra COVID-19 patients. Ra COVID-19 patients also showed a trend towards higher proportions of clonally expanded CD4⁺ memory T cells.

By performing differential gene expression analysis, the results highlighted the dysregulation of unique immune-related pathways in COVID-19 patients with pre-existing autoimmunity. Some examples include CD14⁺ monocytes from MS COVID-19 patients that showed upregulation of type I IFN-

related genes, inflammasome pathway genes, and IL-6 production-related genes. Ps COVID-19 patients exhibited enrichment of hypoxia and TNF- α /NF- κ B pathways in CD14⁺ monocytes, along with upregulation of hypoxia-related genes. Ra COVID-19 patients displayed enrichment of TNF- α /NF- κ B signaling pathway and IFN- γ response genes in CD4⁺ memory T cells.

Aiming to study how these changes were regulated we performed transcription factor activity analysis that revealed unique signatures associated with IL-4, type I IFN, TNF, and hypoxia pathways in autoimmune COVID-19 patients.

Finally, dysregulated interactions between immune cells were observed, involving inflammatory cytokines, cell adhesion molecules, and cell activation regulators. For instance, we observed stronger TNF/TNFR interaction in monocyte subsets of MS and Ps COVID-19 patients. In Ps COVID-19 patients, we noted a heightened autocrine/paracrine interaction between IL-1 β , expressed in CD14⁺ and CD16⁺ monocytes. Additionally, we identified stronger interactions with secreted cytokines such as type I IFN, as its receptors exhibited higher expression in CD4⁺ T cell subsets for MS and Ra COVID-19 patients, and predominantly in CD14⁺ monocytes for the MS COVID-19 group (**Figure 9**).

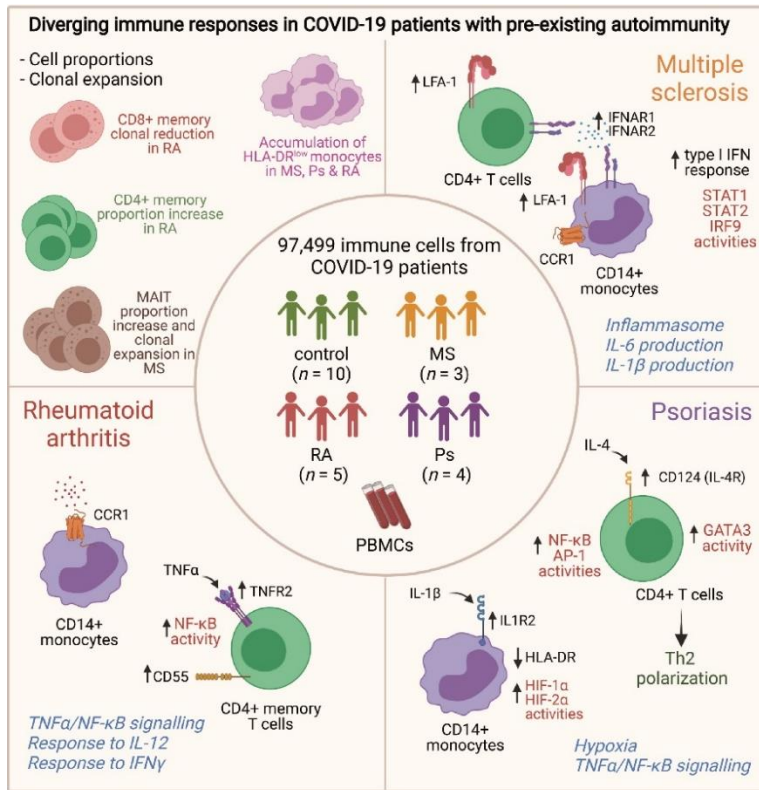


Figure 9. Diverging immune responses in COVID-19 patients with pre-existing autoimmunity.

6. GLOBAL DISCUSSION

The complexity of immune responses is evident, requiring a delicate balance between activation to combat pathogens or cancer cells and mechanisms to repress this response when it is not necessary. Lymphoid cells are primarily responsible for immunosuppression, although myeloid cells can also contribute to regulate this process. In various environments where immunosuppression occurs, such as barrier tissues, RA plays a pivotal role in suppressing responses to commensal bacteria. Additionally, RA has been implicated in the immunosuppressive environment of the TME, particularly impacting the differentiation of monocytes into DCs. Another situation where immunosuppression occurs is in the most severe cases of infection, such as those caused in the context of COVID-19 or sepsis. In these instances, monocytes exhibit a more immunosuppressive phenotype which can lead to a reduction in hyperinflammation or may also result in a lack of response to a secondary pathogen, potentially leading to death (126). However, the mechanisms driving this transition from pro-inflammatory to anti-inflammatory states on myeloid cells remain poorly understood. One potential mechanism, that we speculate to be involved in all these processes is DNA methylation, due to its major role in myeloid differentiation and function.

In the present thesis, we have studied how myeloid cells acquire their suppressive phenotype and explore whether DNA methylation is implicated in this process. Firstly, we have examined how the treatment with RA during the differentiation of monocytes into DCs promotes epigenetic changes that facilitate the acquisition of the suppressive phenotype, along with the mechanisms by which this is promoted (**Article 1**). In another study, we have analysed *ex vivo* monocytes from patients with severe COVID-19 and

determined the relationship between DNA methylation and the suppressive phenotype acquired by monocytes in these patients. We have also established the relationship between these alterations and both external factors and contacts with other immune cells (**Article 2**). Finally, we have analysed the phenotype that different immune populations acquire when reacting against the SARS-CoV-2 virus in patients who presented a deficit in suppression mechanisms, that is, with patients with pre-existing autoimmunity prior to infection (**Article 3**). Despite the significant differences that each study, they present several common points.

Overview

In the first study (**Article 1**), we investigated the impact of RA on monocyte to DCs differentiation and subsequent activation by LPS. We first found that RA induces immunosuppressive properties in DCs. Through *in vitro* experiments, we showed that RA-treated immature DCs (iDC_{RA}) inhibit CD8⁺ T cell proliferation and display reduced production of pro-inflammatory cytokines upon activation. RA-treated DCs also exhibited altered surface marker expression, resembling a macrophage-like phenotype with decreased expression of DC markers, as previously shown (118, 224). However, none of these previous studies have investigated the relationship of these changes in the phenotype with DNA methylation. Overall, we primarily found a blockage in the demethylation process, affecting genes not only associated with the differentiation process, like *IRF4*, but also to the acquisition of this immune suppressive phenotype. Interestingly, in the case of the second study (**Article 2**), where we analyzed the methylation profiles of monocytes from severe COVID-19 patients, we also observed a blockage in the demethylation process. We also observed the demethylation of CpGs associated with anti-

inflammatory response like *IL10* or genes associated with suppressive macrophages like *CD163*. This suggests that in both cases, whether in polarization during suppression induced by a tumor through RA or in hyperinflammation, similar methylation changes are promoted. This demonstrates how the suppression profiles presented in both studies are extensively regulated by DNA methylation.

In reference to the two COVID-19 studies presented (**Article 2** and **Article 3**), it has been seen how myeloid cells can play a role in the response to the virus, as several immune-related functions are affected. This is consistent with the proposed roles of monocytes in blood, beyond those related to tissue homeostasis, including antigen presentation or cytokine production (31, 36, 38). In the case of **Article 2**, where we observed this suppressive profile, mainly driven by DNA methylation, we also detected a notable increase in the percentage of classical monocytes, which, as mentioned in the Introduction, tend to present a more suppressive profile, either through cytokines produced or surface markers (36, 37). This was in concordance with previous work (225). Concurrently, we observed a reduction in the percentage of nonclassical monocytes, which are more pro-inflammatory (34) in concordance with other studies that showed a reduction of the intermediate subpopulation (226) or expansion of classical monocytes in severe SARS-CoV-2 infections (227). This suggests that this hyperinflammation maintains the state of classical monocyte in blood, preserving its anti-inflammatory function on blood (228).

In the case of **Article 3**, autoimmune diseases prior to infection in patients can modulate the immune response in front of the virus. Is important to understand the different immune responses that patients can have, as is still not clear whether a patient will present a balanced or imbalanced immune

response (124). We observed that particularly, CD14⁺ monocytes from MS COVID-19 patients were characterized by increased responses to inflammatory cytokines such as IL-1 β , IL-6, type I IFN, and IFN γ , as well as by enhanced innate and adaptive immune responses. In these same patients, we saw that both CD14⁺ monocytes and CD4⁺ T cells exhibited a stronger activation of TFs associated with type I IFN compared to patients with Ps, Ra and control COVID-19 patients. In the case of monocytes from patients with Ps, they showed a significantly lower level of activity of various RFX TFs, particularly in comparison with the MS COVID-19 group. These findings underscore the variation and deviation in immune responses among patients with autoimmune diseases when faced with SARS-CoV-2 infection, potentially influencing disease progression.

DNA methylation and transcriptomic regulation

In this work, we have been extensively interested in how these changes observed are regulated at the epigenetic level, specifically at DNA methylation level. This epigenetic mark plays a key role during monocyte differentiation, not only from precursor cells to final monocytes, but also from monocytes to other cell types (229, 230). Our DNA methylation analysis on **Article 1** reveals distinct clusters of CpG sites affected by RA, suggesting epigenetic reprogramming that promotes macrophage differentiation. We determined that RA suppresses the expression of key TFs, including IRF4, STAT6, and NF- κ B (p-65), which play pivotal roles in cDC differentiation (231), moDC polarization (215), and the regulation of proinflammatory gene expression (232), respectively. These changes were also observed at DNA methylation level, confirming the key play of epigenetics in the blockade of the differentiation process and inflammation. Indeed, some studies that highlight the relevance of

DNA methylation to acquiring the macrophage phenotype (233, 234). Some studies mainly noted demethylation in the transition from monocytes to macrophages (215, 235), however, others show an increase in DNA methylation during this process (230). Considering that it may be factors in the environment can promote these changes by activating their nuclear receptors, which, through binding to an epigenetic enzyme such as DNMT3A or TET2, can produce some of the changes that lead to the acquisition of the immunosuppressive phenotype (236). Connecting how external factors can, through producing epigenetic changes, modulate the phenotype of myeloid cells.

In **Article 1**, we investigated the effects of a RA, a metabolite of Vitamin A. Other studies have shown that significant changes in vitamin intake can affect the DNA methylation patterns in the loci of DNMT1, DNMT3A and DNMT3B, leading to increased expression of all DNMTs (237). This is in line with the observed changes in DNMT3Aa upon RA treatment, where we determined an increase on its expression. This association suggests that the observed increase in DNMT3A expression in our study may potentially shift the immune function from a promoting inflammation to an immunosuppressive phenotype, as previously observed (218).

In the Introduction, it has been mentioned how nuclear receptors can recruit epigenetic enzymes to promote changes in DNA methylation at their binding sites. One of the classical nuclear receptors for RA is RAR. Its role in recruiting TET2 to promote the demethylation of a specific CpG has already been described (189). However, in our study, we have observed that both TET2 and RAR were downregulated when monocytes were treated with RA, suggesting that perhaps there are alternative mechanisms for the observed

immunosuppressive phenotype. By performing RNA sequencing we demonstrated differential gene expression in RA-treated DCs, including upregulation of immunosuppressive genes like *VSIG4* and downregulation of pro-inflammatory genes like *IL6* or *TNF*. When we analysed the potential TFs regulating the observed changes, we noted LXR α to be a major player. Interestingly, this RNAseq revealed that RA upregulates LXR α and downregulates RXR α , another classic receptor for RA, which interacts with LXR α (238). We found that activating LXR α alone using an agonist does not reproduce the immune suppression. However, inducing LXR α while simultaneously reducing RXR α levels by RXR agonist does trigger the suppression. Given the interaction between LXR α and RXR α , it is plausible to propose that LXR α , when in the presence of RA, prefers to interact with RXR β , leading to the observed suppression. This is plausible as RXR proteasomal degradation is selective, since RXR β is resistant to proteasome-mediated degradation in human embryonic kidney (HEK) cells (239). A similar thing was observed with PPAR γ , where the degradation of RXR reprogrammed its transcriptional activity (240).

To explain this switch on heterodimer formation, in a murine macrophage cell line stably expressing LXR α , ligands for the RXR receptor such as the 9-cis-retinoic acid and bexarotene inhibited Ser198 phosphorylation, leading to changes in LXR/RXR-regulated gene expression, particularly on genes sensitive to changes in LXR α phosphorylation at this residue, such as *Ccl24* (241, 242). The RXR degradation can be explained by phosphorylation as Ser260 residue is phosphorylated by c-jun N-terminal kinase in response to IL-1 β , which leads to the rapid nuclear export and subsequent degradation of RXR α (243). Another possibility is that LXR α is affected by RA and this changes its

target. For example, when LXR α is not phosphorylated at Ser198, there is a significant increase in the expression of CCR7 in macrophages. This increase is linked to reduced chromatin repression markers (H3K9me3 and H3K27me3) at the *Ccr7* gene site in cells with the unphosphorylated form of the receptor (244).

As described, the role of LXR, similar to that of RA, can vary, producing both anti-inflammatory and pro-inflammatory phenotypes (245, 246). Although there are several papers emphasizing the suppression effects of RA and its pro-tumoral effects (94, 247–249), there is a study that has prompted that RA increases the induction of inflammatory macrophages and IFN- γ -producing CD4⁺ and CD8⁺ T cells within tumors (250). In the case of LXR α , it is suggested that its activation can be used as a novel therapeutic strategy to stimulate antitumor activity (251). However, LXR agonist is also able to inhibit inflammation through regulating MyD88 mRNA alternative splicing (252). This suggests that the effect of both RA and LXR α may largely depend on the environment in which they are found (253). In our case, we observed how treatment with RA increases LXR α expression, which promotes the suppressive phenotype. More specifically, we determined that this suppression is mediated by VSIG4 and its expression is highly coordinated by LXR α . Some studies show how the therapeutic agonism reduced MDSC abundance in murine models and in patients treated in a first-in-human dose escalation phase 1 trial (254). It is important to mention that the effects of the agonism of LXR α alone did not replicate the suppressive capacities of iDC_{RA}, which does not discard what other studies have provided in reference to the activation of LXR α on MDSCs. We could only revert the effects of the RA when cells were treated with an antagonist of LXR, in line with other studies (255, 256). Furthermore,

oxysterols, the natural agonists of LXR α , can also inhibit the expression of *CCR7* on DCs, a chemokine receptor critical for the migration of DCs to tumor-draining lymph nodes (257). More post-transcriptional studies are needed to better understand this switch on LXR α function.

A notable link between our findings on the effects of RA in monocyte-to-DC differentiation and those in monocytes in severe COVID-19 patients related to methylation (**Article 1** and **Article 2**) is the involvement of LXR α . When we performed regulon analysis using DoRothEA in monocytes from severe COVID-19 patients we also observed an enrichment for LXR α . This finding suggests that the functions of LXR α in facilitating immune suppression in myeloid cells might be more general than initially anticipated (258).

In relation to the roles of DNA methylation-mediated regulation in the suppressive phenotype of monocytes from severe COVID-19 patients (**Article 2**), our results indicate that it might not be direct and they could just reflect other mechanisms. It is possible that it involves various extracellular molecules that may be playing a role. We determined that several of the DNA methylation changes identified were due to the increase in IFN, as we observed enrichment of binding sites of IRF family members in our TF binding motif analysis, which are downstream to IFN. This finding leads us to consider that, similar to the case of RA, external factors to myeloid cells can activate transcription factors that move into the nucleus and, along with binding to epigenetic enzymes, promote the changes observed.

The notion that DNA methylation patterns are highly influenced by environmental factors has received a high level of attention as a potential pathway linking environmental exposures to downstream phenotypic variation

(259, 260). Recent advancements in epigenomic editing of DNA methylation marks have been shown to alter the activity of TFs important in disease and development *in vivo* (261, 262). While some studies suggest that DNA methylation could disrupt TFs binding and other gene expression mechanisms, contrasting evidence suggests a minimal impact on the activity of most regulatory elements (263). These conflicting results highlight the need to closely examine which type of impact methylation may have on various regulatory sites (264). In this regard, *Johnston et al.* investigated whether the existing DNA methylation status predisposed cells to respond differently to external stimuli. They analyzed immune cells exposed to molecules known to modulate inflammation and stress responses. Their study, which simulated immune system activation and stress reactions, unveiled numerous regulatory regions exhibiting distinct responses to these compounds based on their initial DNA methylation status. Subsequent experiments utilizing macrophages from human donors corroborated these findings, demonstrating that variances in pre-existing methylation patterns could predict responses to viral infection (265).

In the Introduction, it has been mentioned how the study of monocyte methylation from various autoimmune diseases has allowed a better understanding of the disease (192-210). In this regard, in **Article 2**, we were not able to identify differences in DNA methylation patterns when comparing patients depending on their clinical outcomes, supporting the idea that the profile acquired is specific for severe infection. Some articles propose that severe adaptive immune suppression may be the reason why patients with severe COVID-19 cannot be discharged from the ICU even after negative viral tests (266). We also noted that a significant part of the methylation profiles on

monocytes derived from severe COVID-19 patients, specifically the hypermethylated CpGs, were due to the monocytes presenting a more “immature” profile. We hypothesize this as seen in cancer or inflammation, there is an accumulation of monocytes that deviate from the conventional MDP-cMoP-monocyte developmental pathway and develop characteristics akin to neutrophils. For instance, the neutrophil-like Ly6Chi monocytes originating from GMPs exhibit notable similarities (19). This was observed when analyzing the state of the CpGs that we found hypermethylated with the methylation profile of monocyte progenitor cells such as HSCs, MPPs, CMPs, and GMPs. This indicates that the suppressive phenotype observed in both the RA study and severe COVID-19 cases is promoted by a block in differentiation due to inhibited demethylation.

Nevertheless, a new actively discussed hypothesis has emerged where DNA methylation could be a consequence rather than a cause of TF binding and transcriptional activity (267). In this regard, there are certain limitations to our correlations between gene expression and DNA methylation that merit discussion. Firstly, we have linked each DMP with its nearest gene. While this method is convenient due to its simplicity, it overlooks potential confounding factors such as modifications in histone marks, remodeling of DNA accessibility, and other pertinent variables like chromatin 3D structure and context within CpG genomics. Also, as mentioned in the Introduction, DNA methylation can affect on the nearby gene depending on the region of the genome where is located. Additionally, our studies (**Article 1** and **Article 2**) solely focus on 5mC, but we are not excluding the possibility that rapid increases in 5hmC or other demethylation intermediates might directly impact gene expression. Notably, 5hmC has been proposed as a legitimate epigenetic

mark, and correlations have been observed between its presence and the positive regulation of genes across various contexts (150, 268, 269). Lastly, the sample sizes employed in our DNA methylation analysis may not be sufficient to detect subtle methylation changes that could precede alterations in gene expression.

Mechanisms of immune suppression

As mentioned in the Introduction, there are several mechanisms by which a myeloid cell can promote suppression, including anergy, cell deletion or the production of anti-inflammatory cytokines. This last one was observed in **Article 2** where we detected a DNA methylation-dependent *IL10* expression. In the case of **Article 1**, we observed IL-10 downregulation and therefore speculated that TGF- β can be also produced, as previously described (270–272). Through the adaptation of a bioinformatic pipeline, we identified that certain transcriptional changes observed are influenced by TGF- β downstream signaling. Nevertheless, we were unable to detect this cytokine in the medium. In the same article, we also observed the LXR-dependent regulation of IL2RA (CD25), a surface protein expressed at high levels by Treg cells. The CD25 protein is used by Treg to preferentially capture IL-2, preventing binding to conventional CD8+ T cells, thus preventing their proliferation. However, the effects on myeloid cells are poorly understood.

Another mechanism to promote immunosuppression is through a reduction of the pro-inflammatory response. In our case, we have observed how in both cases, in the treatment with RA and in the severe cases of COVID-19, a reduction in the expression of the majority of pro-inflammatory genes (**Article 1** and **Article 2**), as previously described in alveolar macrophages. In this study, it is also described the reduction of the NF- κ B pathway, together with a TLR4

decrease (273). In addition, we have observed how RA promotes differentiation into an alveolar macrophage phenotype, cells that are capable of promoting tolerance in the lungs by inducing FoxP3⁺ in naïve T cells (274, 275). This ability to polarize Tregs has been associated with the production of TGF- β and RA by alveolar macrophages(275).

In our first study, we further described an alternative immune-suppression mechanism not previously reported; the cell-cell interaction through VSIG4. This protein is essential for maintaining immune tolerance, host defense, and immune regulation. Studies have demonstrated its specific correlation with various inflammatory diseases, highlighting its role in the early response to adenoviral infection and anti-infective processes (276, 277).

VSIG4 signaling acts as an anti-immune evasion mechanism against bacterial growth in macrophages by binding activated complement protein C3 (276–278). Additionally, VSIG4 suppresses specific helper T cells and cytotoxic T lymphocytes, inhibiting their IL-2 production by binding to co-inhibitory receptors on T lymphocyte membranes (279). Recent research has shed light on the immune suppression capacities of macrophages that express this protein, which has been linked to facilitating lung cancer development (280), while also inhibiting pro-inflammatory macrophage activation by reprogramming mitochondrial pyruvate metabolism (281). This protein has been externally found on anti-inflammatory macrophages together with CD163, and HMOX1 (282). VSIG4 has been implicated in mediating transcriptional inhibition of Nlrp3 and IL-1 β in macrophages, emphasizing its regulatory role in inflammation (283). Importantly, targeting VSIG4 was identified as a novel macrophage checkpoint and showed promise in repolarizing macrophages, inducing inflammatory responses *in vitro* and inhibiting tumor growth *in vivo*.

Finally, other works have pointed out the DNA methylation regulation on the expression of this gene on moDCs (284). Our DNA methylation analysis implicates LXR-mediated epigenetic regulation of VSIG4 expression. These findings elucidate RA-induced immunosuppressive mechanisms in DCs mediated through LXR α and epigenetic modifications that promote not only the expression of an immunosuppressive protein but also the acquisition of less reactive phenotype, shedding light on potential therapeutic targets for immune modulation.

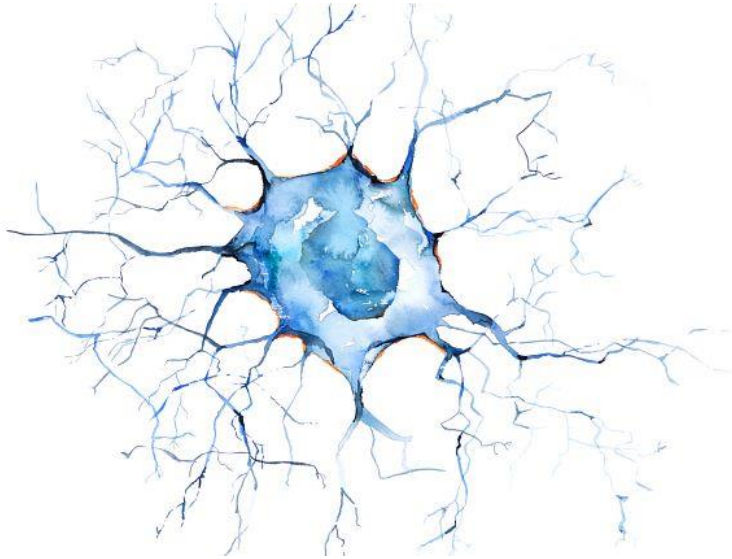
Another characteristic suppressive mechanism observed in **Article 2**, as previously described, is the reduced expression of MHC-II by monocytes (138, 140, 141, 285), as well as by the low expression of other stimulatory molecules such as CD40 and CD86 (286). In the case of **Article 3** we found that CD14⁺ HLA-DR_{low} cells were also significantly increased in all three autoimmune COVID-19 groups compared with controls. Interestingly, this reduction of MHC-II in classical monocytes has been associated with a higher mortality rate in SARS-CoV-2 young patients (141). The reduction of HLA-DR within monocytes is consistently linked with heightened susceptibility to bacterial infections in critically ill individuals (287). This suggests that the loss in antigen presentation capacity is another way to promote immunosuppression. This loss can be acquired by the excessive cytokine production during COVID-19. For example, IL-10 has the capability to inhibit the activity of JAK2 enzyme, crucial for initiating the JAK-STAT signaling pathway, and therefore reduce the expression of HLA-DR (288). This can also affect the ability of human dendritic cells to activate specific CD4⁺ T cells via a reduction in MHC-II (289). Taking this together, high levels of IL-10 and IL-6 during cytokine storm could be a

possible cause of decreased expression of monocyte HLA-DR in patients with severe COVID-19, affecting their immune response.

Cell-cell communication

An important point to highlight in the present study is the investigation of interactions between immune cells. In **Article 1**, we observed that suppression was mediated by VSIG4, which requires cell-to-cell interaction to carry out its function. In **Article 2**, many of the affected pathways were related to antigen presentation, so when this suppressive phenotype occurred, the ability of monocytes to present antigens was partially lost. In more detail, we studied the expression of various ligand-receptor pairs between the different analyzed cells and observed how the monocytes analyzed showed increased interaction with NK cells and, notably, an increase in the interaction with Treg cells. This could suggest that the observed phenotype is partly mediated by interactions with other cells and not only by cytokines expressed in the environment. In **Article 3**, we found various altered interactions depending on the diseases and cell type. Overall, our findings unveil a dysregulated network of cell-cell communication events in autoimmune disease patients in response to infection.

These interactions, alongside external factors including inflammatory cytokines, cell adhesion molecules, and cell activation regulators probably influence downstream transcription factor pathways and affect DNA methylation patterns, thereby impacting the phenotype of the cells being studied.



CONCLUSIONS

7. CONCLUSIONS

The conclusions obtained during this doctoral thesis can be summarized as follows:

Article 1

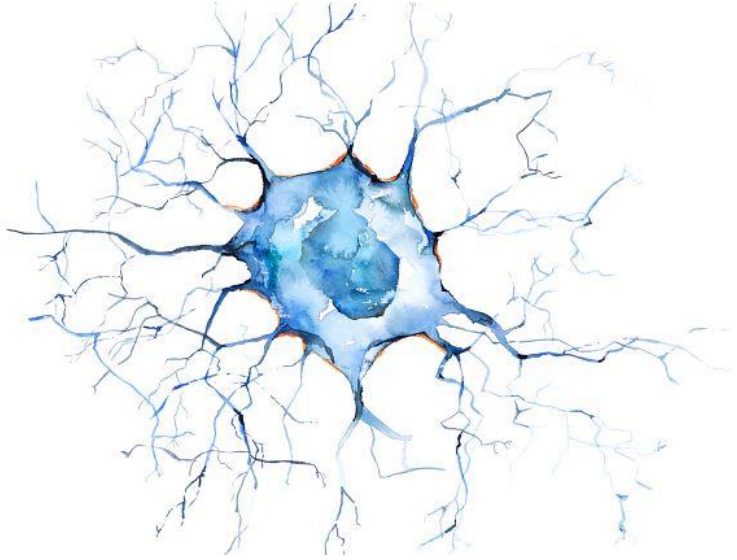
1. RA promotes the acquisition of a macrophage-like phenotype during the differentiation from monocytes to DCs, which develop immunosuppressive functions.
2. RA reduces the expression of pro-inflammatory cytokines on moDCs.
3. Various genes governing immunosuppression and moDC phenotype undergo specific DNA methylation changes in response to RA.
4. DNA methylation changes of RA-treated moDCs in comparison with non-treated moDCs are inversely correlated with gene expression.
5. RA promotes the expression of LXR α , and its inhibition reverts the suppressive properties of RA treated moDCs.
6. LXR α expression on moDCs, together with RA-mediated downregulation of RXR α expression, are essential for LXR α to exert its immunosuppressive functions.
7. LXR α activation and binding is associated with the epigenetic reprogramming and expression of VSIG4 that mediates immunosuppression.
8. *In vivo* tumor and colon-associated macrophages co-express LXR α and VSIG4.

Article 2

9. Peripheral blood monocytes display aberrant DNA methylomes and transcriptomes in severe COVID-19 patients, showing associations with functions linked to type I IFN signaling and antigen presentation.
10. DNA methylation alterations in monocytes from severe COVID-19 patients occur in genomic sites enriched for PU.1 and IRFs binding sites which are linked to DNA methylation reprogramming and IFN response, respectively.
11. The observed DNA methylation changes are remarkably associated with organ damage and are partially overlapping with those observed in monocytes of patients with bacterial sepsis.
12. Most of the shared DNA methylation changes between patients with severe COVID-19 and bacterial sepsis involve genes associated with the acquisition of an immune-suppressive phenotype.
13. *In vitro* experiments with inflammatory cytokines lead to the acquisition of DNA methylation changes similar to those observed in severe COVID-19 and sepsis patients.
14. Certain DNA methylation changes occurring in monocytes of severe COVID-19 patients may arise from abnormal myeloid differentiation or the release of immature monocytes.
15. Many DNA methylation changes in monocytes from severe COVID-19 patients are inversely correlated to the closest gene.
16. Alterations in immune cell communication in severe COVID-19 may contribute to transcriptional reprogramming in monocytes, and involve dysregulation of interferon-related genes, antigen presentation, and chemotaxis-associated genes.

Article 3

17. Infection of SARS-CoV-2 in patients with autoimmune disease patients such as those with Rheumatoid Arthritis (Ra), Psoriasis (Ps), and Multiple Sclerosis (MS) results in distinct variations in immune cell composition and responses to the virus.
18. In individuals with autoimmune diseases, SARS-CoV-2 infection leads to modifications in the immune signatures of CD14⁺ monocytes and CD4⁺ T cells. These alterations are manifested as heightened inflammation, hypoxia, and responses involving IFNs and TNF, potentially influencing the functionality and polarization of these cells towards specific phenotypes.
19. Patients with autoimmune diseases exhibit changes in TF activities linked to IL-4, type I IFNs, TNF, and hypoxia pathways, which are distinctive to their autoimmune conditions under SARS-CoV-2 infection.
20. There is a disrupted network of cell-to-cell communication in autoimmune disease patients following SARS-CoV-2 infection, involving inflammatory cytokines, cell adhesion molecules, and regulators of cell activation.



REFERENCES

8. REFERENCES

1. Vivier,E. and Malissen,B. (2005) Innate and adaptive immunity: specificities and signaling hierarchies revisited. *Nat. Immunol.*, **6**, 17–21.
2. Abbas MBBS, Abul K.; Lichtman MD PhD, Andrew H.; Pillai MBBS PhD,S. (2021) Cellular and Molecular Immunology. *Elsevier*.
3. Rhodes,J., Zipfel,C., Jones,J.D.G. and Ngou,B.P.M. (2022) Concerted actions of PRR- and NLR-mediated immunity. *Essays Biochem.*, **66**, 501–511.
4. Akira,S. and Takeda,K. (2004) Toll-like receptor signalling. *Nat. Rev. Immunol.*, **4**, 499–511.
5. Kawai,T. and Akira,S. (2011) Toll-like receptors and their crosstalk with other innate receptors in infection and immunity. *Immunity*, **34**, 637–50.
6. Akira,S., Uematsu,S. and Takeuchi,O. (2006) Pathogen recognition and innate immunity. *Cell*, **124**, 783–801.
7. Iwasaki,A. and Medzhitov,R. (2004) Toll-like receptor control of the adaptive immune responses. *Nat. Immunol.*, **5**, 987–95.
8. Vyas,J.M., Van der Veen,A.G. and Ploegh,H.L. (2008) The known unknowns of antigen processing and presentation. *Nat. Rev. Immunol.*, **8**, 607–18.
9. Blees,A., Janulienė,D., Hofmann,T., Koller,N., Schmidt,C., Trowitzsch,S., Moeller,A. and Tampé,R. (2017) Structure of the human MHC-I peptide-loading complex. *Nature*, **551**, 525–528.
10. Trowitzsch,S. and Tampé,R. (2020) Multifunctional Chaperone and Quality Control Complexes in Adaptive Immunity. *Annu. Rev. Biophys.*, **49**, 135–161.
11. Bowdish,D.M.E., Loffredo,M.S., Mukhopadhyay,S., Mantovani,A. and Gordon,S. (2007) Macrophage receptors implicated in the ‘adaptive’ form of innate immunity. *Microbes Infect.*, **9**, 1680–7.
12. Quintin,J., Cheng,S.-C., van der Meer,J.W.M. and Netea,M.G. (2014) Innate immune memory: towards a better understanding of host defense mechanisms. *Curr. Opin. Immunol.*, **29**, 1–7.
13. Ochando,J., Mulder,W.J.M., Madsen,J.C., Netea,M.G. and Duivenvoorden,R. (2023) Trained immunity - basic concepts and contributions to immunopathology. *Nat. Rev. Nephrol.*, **19**, 23–37.
14. Netea,M.G., Joosten,L.A.B., Latz,E., Mills,K.H.G., Natoli,G., Stunnenberg,H.G.,

References

- O'Neill,L.A.J. and Xavier,R.J. (2016) Trained immunity: A program of innate immune memory in health and disease. *Science*, **352**, aafio98.
15. Slukvin,I.I. (2013) Deciphering the hierarchy of angiohematopoietic progenitors from human pluripotent stem cells. *Cell Cycle*, **12**, 720–7.
 16. Busch,K., Klapproth,K., Barile,M., Flossdorf,M., Holland-Letz,T., Schlenner,S.M., Reth,M., Höfer,T. and Rodewald,H.-R. (2015) Fundamental properties of unperturbed haematopoiesis from stem cells in vivo. *Nature*, **518**, 542–6.
 17. Akashi,K., Traver,D., Miyamoto,T. and Weissman,I.L. (2000) A clonogenic common myeloid progenitor that gives rise to all myeloid lineages. *Nature*, **404**, 193–7.
 18. Kondo,M., Weissman,I.L. and Akashi,K. (1997) Identification of clonogenic common lymphoid progenitors in mouse bone marrow. *Cell*, **91**, 661–72.
 19. Yáñez,A., Coetzee,S.G., Olsson,A., Muench,D.E., Berman,B.P., Hazelett,D.J., Salomonis,N., Grimes,H.L. and Goodridge,H.S. (2017) Granulocyte-Monocyte Progenitors and Monocyte-Dendritic Cell Progenitors Independently Produce Functionally Distinct Monocytes. *Immunity*, **47**, 890-902.e4.
 20. Kawamura,S., Onai,N., Miya,F., Sato,T., Tsunoda,T., Kurabayashi,K., Yotsumoto,S., Kuroda,S., Takenaka,K., Akashi,K., *et al.* (2017) Identification of a Human Clonogenic Progenitor with Strict Monocyte Differentiation Potential: A Counterpart of Mouse cMoPs. *Immunity*, **46**, 835-848.e4.
 21. Notta,F., Zandi,S., Takayama,N., Dobson,S., Gan,O.I., Wilson,G., Kaufmann,K.B., McLeod,J., Laurenti,E., Dunant,C.F., *et al.* (2016) Distinct routes of lineage development reshape the human blood hierarchy across ontogeny. *Science*, **351**, aab2116.
 22. Zhang,Z., Bossila,E.A., Li,L., Hu,S. and Zhao,Y. (2022) Central gene transcriptional regulatory networks shaping monocyte development in bone marrow. *Front. Immunol.*, **13**, 1011279.
 23. Cytlak,U., Resteu,A., Pagan,S., Green,K., Milne,P., Maisuria,S., McDonald,D., Hulme,G., Filby,A., Carpenter,B., *et al.* (2020) Differential IRF8 Transcription Factor Requirement Defines Two Pathways of Dendritic Cell Development in Humans. *Immunity*, **53**, 353-370.e8.
 24. Guilliams,M., Mildner,A. and Yona,S. (2018) Developmental and Functional Heterogeneity of Monocytes. *Immunity*, **49**, 595–613.
 25. Tak,T., Drylewicz,J., Conemans,L., de Boer,R.J., Koenderman,L., Borghans,J.A.M. and Tesselaar,K. (2017) Circulatory and maturation kinetics of human monocyte subsets in vivo. *Blood*, **130**, 1474–1477.
 26. Shi,C., Jia,T., Mendez-Ferrer,S., Hohl,T.M., Serbina,N. V, Lipuma,L., Leiner,I.,

- Li,M.O., Frenette,P.S. and Pamer,E.G. (2011) Bone marrow mesenchymal stem and progenitor cells induce monocyte emigration in response to circulating toll-like receptor ligands. *Immunity*, **34**, 590–601.
27. Coillard,A. and Segura,E. (2019) In vivo Differentiation of Human Monocytes. *Front. Immunol.*, **10**, 1907.
28. Narasimhan,P.B., Marcovecchio,P., Hamers,A.A.J. and Hedrick,C.C. (2019) Nonclassical Monocytes in Health and Disease. *Annu. Rev. Immunol.*, **37**, 439–456.
29. Villani,A.-C., Satija,R., Reynolds,G., Sarkizova,S., Shekhar,K., Fletcher,J., Griesbeck,M., Butler,A., Zheng,S., Lazo,S., *et al.* (2017) Single-cell RNA-seq reveals new types of human blood dendritic cells, monocytes, and progenitors. *Science*, **356**.
30. Goudot,C., Coillard,A., Villani,A.-C., Gueguen,P., Cros,A., Sarkizova,S., Tang-Huau,T.-L., Bohec,M., Baulande,S., Hacoheh,N., *et al.* (2017) Aryl Hydrocarbon Receptor Controls Monocyte Differentiation into Dendritic Cells versus Macrophages. *Immunity*, **47**, 582-596.e6.
31. Wong,K.L., Yeap,W.H., Tai,J.J.Y., Ong,S.M., Dang,T.M. and Wong,S.C. (2012) The three human monocyte subsets: implications for health and disease. *Immunol. Res.*, **53**, 41–57.
32. Zawada,A.M., Rogacev,K.S., Rotter,B., Winter,P., Marell,R.-R., Fliser,D. and Heine,G.H. (2011) SuperSAGE evidence for CD14⁺⁺CD16⁺ monocytes as a third monocyte subset. *Blood*, **118**, e50-61.
33. Patel,V.K., Williams,H., Li,S.C.H., Fletcher,J.P. and Medbury,H.J. (2017) Monocyte inflammatory profile is specific for individuals and associated with altered blood lipid levels. *Atherosclerosis*, **263**, 15–23.
34. Shapouri-Moghaddam,A., Mohammadian,S., Vazini,H., Taghadosi,M., Esmaeili,S.-A., Mardani,F., Seifi,B., Mohammadi,A., Afshari,J.T. and Sahebkar,A. (2018) Macrophage plasticity, polarization, and function in health and disease. *J. Cell. Physiol.*, **233**, 6425–6440.
35. Haschka,D., Petzer,V., Burkert,F.R., Fritsche,G., Wildner,S., Bellmann-Weiler,R., Tymoszuk,P. and Weiss,G. (2022) Alterations of blood monocyte subset distribution and surface phenotype are linked to infection severity in COVID-19 inpatients. *Eur. J. Immunol.*, **52**, 1285–1296.
36. Cros,J., Cagnard,N., Woollard,K., Patey,N., Zhang,S.-Y., Senechal,B., Puel,A., Biswas,S.K., Moshous,D., Picard,C., *et al.* (2010) Human CD14^{dim} monocytes patrol and sense nucleic acids and viruses via TLR7 and TLR8 receptors. *Immunity*, **33**, 375–86.

References

37. Skrzeczyńska-Moncznik,J., Bzowska,M., Loseke,S., Grage-Griebenow,E., Zembala,M. and Pryjma,J. (2008) Peripheral blood CD14^{high} CD16⁺ monocytes are main producers of IL-10. *Scand. J. Immunol.*, **67**, 152–9.
38. Wong,K.L., Tai,J.J.-Y., Wong,W.-C., Han,H., Sem,X., Yeap,W.-H., Kourilsky,P. and Wong,S.-C. (2011) Gene expression profiling reveals the defining features of the classical, intermediate, and nonclassical human monocyte subsets. *Blood*, **118**, e16–31.
39. Balan,S., Saxena,M. and Bhardwaj,N. (2019) Dendritic cell subsets and locations. *Int. Rev. Cell Mol. Biol.*, **348**, 1–68.
40. Collin,M. and Bigley,V. (2018) Human dendritic cell subsets: an update. *Immunology*, **154**, 3–20.
41. Ferris,S.T., Durai,V., Wu,R., Theisen,D.J., Ward,J.P., Bern,M.D., Davidson,J.T., Bagadia,P., Liu,T., Briseño,C.G., *et al.* (2020) cDC1 prime and are licensed by CD4⁺ T cells to induce anti-tumour immunity. *Nature*, **584**, 624–629.
42. Rodrigues,P.F., Alberti-Servera,L., Eremin,A., Grajales-Reyes,G.E., Ivanek,R. and Tussiwand,R. (2018) Distinct progenitor lineages contribute to the heterogeneity of plasmacytoid dendritic cells. *Nat. Immunol.*, **19**, 711–722.
43. Dress,R.J., Dutertre,C.-A., Giladi,A., Schlitzer,A., Low,I., Shadan,N.B., Tay,A., Lum,J., Kairi,M.F.B.M., Hwang,Y.Y., *et al.* (2019) Plasmacytoid dendritic cells develop from Ly6D⁺ lymphoid progenitors distinct from the myeloid lineage. *Nat. Immunol.*, **20**, 852–864.
44. Reizis,B. (2019) Plasmacytoid Dendritic Cells: Development, Regulation, and Function. *Immunity*, **50**, 37–50.
45. Liu,Y.-J. (2005) IPC: professional type 1 interferon-producing cells and plasmacytoid dendritic cell precursors. *Annu. Rev. Immunol.*, **23**, 275–306.
46. Jego,G., Palucka,A.K., Blanck,J.-P., Chalouni,C., Pascual,V. and Banchereau,J. (2003) Plasmacytoid dendritic cells induce plasma cell differentiation through type I interferon and interleukin 6. *Immunity*, **19**, 225–34.
47. Schlitzer,A., McGovern,N. and Ginhoux,F. (2015) Dendritic cells and monocyte-derived cells: Two complementary and integrated functional systems. *Semin. Cell Dev. Biol.*, **41**, 9–22.
48. Mildner,A., Yona,S. and Jung,S. (2013) A close encounter of the third kind: monocyte-derived cells. *Adv. Immunol.*, **120**, 69–103.
49. Bosteels,C., Neyt,K., Vanheerswynghels,M., van Helden,M.J., Sichien,D., Debeuf,N., De Prijck,S., Bosteels,V., Vandamme,N., Martens,L., *et al.* (2020) Inflammatory Type 2 cDCs Acquire Features of cDC1s and Macrophages to Orchestrate

- Immunity to Respiratory Virus Infection. *Immunity*, **52**, 1039-1056.e9.
50. Coillard,A. and Segura,E. (2021) Antigen presentation by mouse monocyte-derived cells: Re-evaluating the concept of monocyte-derived dendritic cells. *Mol. Immunol.*, **135**, 165-169.
 51. Kuhn,S., Yang,J. and Ronchese,F. (2015) Monocyte-Derived Dendritic Cells Are Essential for CD8(+) T Cell Activation and Antitumor Responses After Local Immunotherapy. *Front. Immunol.*, **6**, 584.
 52. Davison,G.M., Novitzky,N. and Abdulla,R. (2013) Monocyte derived dendritic cells have reduced expression of co-stimulatory molecules but are able to stimulate autologous T-cells in patients with MDS. *Hematol. Oncol. Stem Cell Ther.*, **6**, 49-57.
 53. Dalod,M., Chelbi,R., Malissen,B. and Lawrence,T. (2014) Dendritic cell maturation: functional specialization through signaling specificity and transcriptional programming. *EMBO J.*, **33**, 1104-16.
 54. Sánchez-Sánchez,N., Riol-Blanco,L. and Rodríguez-Fernández,J.L. (2006) The multiple personalities of the chemokine receptor CCR7 in dendritic cells. *J. Immunol.*, **176**, 5153-9.
 55. Sallusto,F. and Lanzavecchia,A. (1994) Efficient presentation of soluble antigen by cultured human dendritic cells is maintained by granulocyte/macrophage colony-stimulating factor plus interleukin 4 and downregulated by tumor necrosis factor alpha. *J. Exp. Med.*, **179**, 1109-18.
 56. Garcia-Gomez,A., Rodríguez-Ubreva,J. and Ballestar,E. (2018) Epigenetic interplay between immune, stromal and cancer cells in the tumor microenvironment. *Clin. Immunol.*, **196**, 64-71.
 57. Russell,D.G., Huang,L. and VanderVen,B.C. (2019) Immunometabolism at the interface between macrophages and pathogens. *Nat. Rev. Immunol.*, **19**, 291-304.
 58. Bujko,A., Atlasy,N., Landsverk,O.J.B., Richter,L., Yaqub,S., Horneland,R., Øyen,O., Aandahl,E.M., Aabakken,L., Stunnenberg,H.G., *et al.* (2018) Transcriptional and functional profiling defines human small intestinal macrophage subsets. *J. Exp. Med.*, **215**, 441-458.
 59. Kamada,N., Hisamatsu,T., Okamoto,S., Chinen,H., Kobayashi,T., Sato,T., Sakuraba,A., Kitazume,M.T., Sugita,A., Koganei,K., *et al.* (2008) Unique CD14 intestinal macrophages contribute to the pathogenesis of Crohn disease via IL-23/IFN-gamma axis. *J. Clin. Invest.*, **118**, 2269-80.
 60. Bajpai,G., Schneider,C., Wong,N., Bredemeyer,A., Hulsmans,M., Nahrendorf,M., Epelman,S., Kreisel,D., Liu,Y., Itoh,A., *et al.* (2018) The human heart contains

References

- distinct macrophage subsets with divergent origins and functions. *Nat. Med.*, **24**, 1234–1245.
61. Tang-Huau,T.-L., Gueguen,P., Goudot,C., Durand,M., Bohec,M., Baulande,S., Pasquier,B., Amigorena,S. and Segura,E. (2018) Human in vivo-generated monocyte-derived dendritic cells and macrophages cross-present antigens through a vacuolar pathway. *Nat. Commun.*, **9**, 2570.
 62. González-Domínguez,É., Samaniego,R., Flores-Sevilla,J.L., Campos-Campos,S.F., Gómez-Campos,G., Salas,A., Campos-Peña,V., Corbí,Á.L., Sánchez-Mateos,P. and Sánchez-Torres,C. (2015) CD163L1 and CLEC5A discriminate subsets of human resident and inflammatory macrophages in vivo. *J. Leukoc. Biol.*, **98**, 453–66.
 63. Moret,F.M., Hack,C.E., van der Wurff-Jacobs,K.M.G., de Jager,W., Radstake,T.R.D.J., Lafeber,F.P.J.G. and van Roon,J.A.G. (2013) Intra-articular CD1c-expressing myeloid dendritic cells from rheumatoid arthritis patients express a unique set of T cell-attracting chemokines and spontaneously induce Th1, Th17 and Th2 cell activity. *Arthritis Res. Ther.*, **15**, R155.
 64. Veglia,F., Sanseviero,E. and Gabrilovich,D.I. (2021) Myeloid-derived suppressor cells in the era of increasing myeloid cell diversity. *Nat. Rev. Immunol.*, **21**, 485–498.
 65. Udagawa,N., Koide,M., Nakamura,M., Nakamichi,Y., Yamashita,T., Uehara,S., Kobayashi,Y., Furuya,Y., Yasuda,H., Fukuda,C., *et al.* (2021) Osteoclast differentiation by RANKL and OPG signaling pathways. *J. Bone Miner. Metab.*, **39**, 19–26.
 66. Lutz,M.B., Strobl,H., Schuler,G. and Romani,N. (2017) GM-CSF Monocyte-Derived Cells and Langerhans Cells As Part of the Dendritic Cell Family. *Front. Immunol.*, **8**, 1388.
 67. Morante-Palacios,O., Fondelli,F., Ballestar,E. and Martínez-Cáceres,E.M. (2021) Tolerogenic Dendritic Cells in Autoimmunity and Inflammatory Diseases. *Trends Immunol.*, **42**, 59–75.
 68. Švajger,U. and Rožman,P.J. (2020) Recent discoveries in dendritic cell tolerance-inducing pharmacological molecules. *Int. Immunopharmacol.*, **81**, 106275.
 69. Cauwels,A. and Tavernier,J. (2020) Tolerizing Strategies for the Treatment of Autoimmune Diseases: From ex vivo to in vivo Strategies. *Front. Immunol.*, **11**, 674.
 70. Yu,H., Cai,Y., Zhong,A., Zhang,Y., Zhang,J. and Xu,S. (2021) The ‘Dialogue’ Between Central and Peripheral Immunity After Ischemic Stroke: Focus on Spleen. *Front. Immunol.*, **12**, 792522.
 71. Walsh,S.J. and Rau,L.M. (2000) Autoimmune diseases: a leading cause of death among young and middle-aged women in the United States. *Am. J. Public Health*,

- 90, 1463–6.
72. Mané-Damas,M., Hoffmann,C., Zong,S., Tan,A., Molenaar,P.C., Losen,M. and Martinez-Martinez,P. (2019) Autoimmunity in psychotic disorders. Where we stand, challenges and opportunities. *Autoimmun. Rev.*, **18**, 102348.
 73. Xiao,Z.X., Miller,J.S. and Zheng,S.G. (2021) An updated advance of autoantibodies in autoimmune diseases. *Autoimmun. Rev.*, **20**, 102743.
 74. Xing,Y. and Hogquist,K.A. (2012) T-cell tolerance: central and peripheral. *Cold Spring Harb. Perspect. Biol.*, **4**.
 75. Patsoukis,N., Wang,Q., Strauss,L. and Boussiotis,V.A. (2020) Revisiting the PD-1 pathway. *Sci. Adv.*, **6**.
 76. Fanger,N.A., Maliszewski,C.R., Schooley,K. and Griffith,T.S. (1999) Human dendritic cells mediate cellular apoptosis via tumor necrosis factor-related apoptosis-inducing ligand (TRAIL). *J. Exp. Med.*, **190**, 1155–64.
 77. Süss,G. and Shortman,K. (1996) A subclass of dendritic cells kills CD4 T cells via Fas/Fas-ligand-induced apoptosis. *J. Exp. Med.*, **183**, 1789–96.
 78. Sisirak,V., Vey,N., Goutagny,N., Renaudineau,S., Malfroy,M., Thys,S., Treilleux,I., Labidi-Galy,S.I., Bachelot,T., Dezutter-Dambuyant,C., *et al.* (2013) Breast cancer-derived transforming growth factor- β and tumor necrosis factor- α compromise interferon- α production by tumor-associated plasmacytoid dendritic cells. *Int. J. cancer*, **133**, 771–8.
 79. Lyu,M., Suzuki,H., Kang,L., Gaspal,F., Zhou,W., Goc,J., Zhou,L., Zhou,J., Zhang,W., JRI Live Cell Bank, *et al.* (2022) ILC3s select microbiota-specific regulatory T cells to establish tolerance in the gut. *Nature*, **610**, 744–751.
 80. Chassot,A.-A., Le Rolle,M., Jolivet,G., Stevant,I., Guignonis,J.-M., Da Silva,F., Nef,S., Pailhoux,E., Schedl,A., Ghyselinck,N.B., *et al.* (2020) Retinoic acid synthesis by ALDH1A proteins is dispensable for meiosis initiation in the mouse fetal ovary. *Sci. Adv.*, **6**, eaaz1261.
 81. Czarnewski,P., Das,S., Parigi,S.M. and Villablanca,E.J. (2017) Retinoic Acid and Its Role in Modulating Intestinal Innate Immunity. *Nutrients*, **9**.
 82. Kang,S.G., Park,J., Cho,J.Y., Ulrich,B. and Kim,C.H. (2011) Complementary roles of retinoic acid and TGF- β 1 in coordinated expression of mucosal integrins by T cells. *Mucosal Immunol.*, **4**, 66–82.
 83. Nagy,N.A., Hafkamp,F.M.J., Sparrius,R., Bas,R., Lozano Vigario,F., van Capel,T.M.M., van Ree,R., Geijtenbeek,T.B.H., Slütter,B., Tas,S.W., *et al.* (2024) Retinoic acid-loaded liposomes induce human mucosal CD103+ dendritic cells that inhibit Th17 cells and drive regulatory T-cell development in vitro. *Eur. J.*

References

- Immunol.*, 10.1002/eji.202350839.
84. Bettelli,E., Carrier,Y., Gao,W., Korn,T., Strom,T.B., Oukka,M., Weiner,H.L. and Kuchroo,V.K. (2006) Reciprocal developmental pathways for the generation of pathogenic effector TH17 and regulatory T cells. *Nature*, **441**, 235–8.
 85. Xiao,S., Jin,H., Korn,T., Liu,S.M., Oukka,M., Lim,B. and Kuchroo,V.K. (2008) Retinoic acid increases Foxp3+ regulatory T cells and inhibits development of Th17 cells by enhancing TGF-beta-driven Smad3 signaling and inhibiting IL-6 and IL-23 receptor expression. *J. Immunol.*, **181**, 2277–84.
 86. Erkelens,M.N. and Mebius,R.E. (2017) Retinoic Acid and Immune Homeostasis: A Balancing Act. *Trends Immunol.*, **38**, 168–180.
 87. Hill,J.A., Hall,J.A., Sun,C.-M., Cai,Q., Ghyselinck,N., Chambon,P., Belkaid,Y., Mathis,D. and Benoist,C. (2008) Retinoic acid enhances Foxp3 induction indirectly by relieving inhibition from CD4+CD44hi Cells. *Immunity*, **29**, 758–70.
 88. Sun,C.-M., Hall,J.A., Blank,R.B., Bouladoux,N., Oukka,M., Mora,J.R. and Belkaid,Y. (2007) Small intestine lamina propria dendritic cells promote de novo generation of Foxp3 T reg cells via retinoic acid. *J. Exp. Med.*, **204**, 1775–85.
 89. Mucida,D., Pino-Lagos,K., Kim,G., Nowak,E., Benson,M.J., Kronenberg,M., Noelle,R.J. and Cheroutre,H. (2009) Retinoic acid can directly promote TGF-beta-mediated Foxp3(+) Treg cell conversion of naive T cells. *Immunity*, **30**, 471–2; author reply 472–3.
 90. Moore,C., Tejon,G., Fuentes,C., Hidalgo,Y., Bono,M.R., Maldonado,P., Fernandez,R., Wood,K.J., Fierro,J.A., Roseblatt,M., *et al.* (2015) Alloreactive regulatory T cells generated with retinoic acid prevent skin allograft rejection. *Eur. J. Immunol.*, **45**, 452–63.
 91. Lu,L., Zhou,X., Wang,J., Zheng,S.G. and Horwitz,D.A. (2010) Characterization of protective human CD4CD25 FOXP3 regulatory T cells generated with IL-2, TGF- β and retinoic acid. *PLoS One*, **5**, e15150.
 92. Moore,C., Sauma,D., Morales,J., Bono,M.R., Roseblatt,M. and Fierro,J.A. (2009) Transforming growth factor-beta and all-trans retinoic acid generate ex vivo transgenic regulatory T cells with intestinal homing receptors. *Transplant. Proc.*, **41**, 2670–2.
 93. Scottà,C., Esposito,M., Fazekasova,H., Fanelli,G., Edozie,F.C., Ali,N., Xiao,F., Peakman,M., Afzali,B., Sagoo,P., *et al.* (2013) Differential effects of rapamycin and retinoic acid on expansion, stability and suppressive qualities of human CD4(+)/CD25(+)/FOXP3(+) T regulatory cell subpopulations. *Haematologica*, **98**, 1291–9.

94. Bakdash,G., Vogelpoel,L.T.C., van Capel,T.M.M., Kapsenberg,M.L. and de Jong,E.C. (2015) Retinoic acid primes human dendritic cells to induce gut-homing, IL-10-producing regulatory T cells. *Mucosal Immunol.*, **8**, 265–78.
95. Rivera,C.A., Randrian,V., Richer,W., Gerber-Ferder,Y., Delgado,M.-G., Chikina,A.S., Frede,A., Sorini,C., Maurin,M., Kammoun-Chaari,H., *et al.* (2022) Epithelial colonization by gut dendritic cells promotes their functional diversification. *Immunity*, **55**, 129-144.e8.
96. Hall,J.A., Cannons,J.L., Grainger,J.R., Dos Santos,L.M., Hand,T.W., Naik,S., Wohlfert,E.A., Chou,D.B., Oldenhove,G., Robinson,M., *et al.* (2011) Essential role for retinoic acid in the promotion of CD4(+) T cell effector responses via retinoic acid receptor alpha. *Immunity*, **34**, 435-47.
97. Morales,R.A., Campos-Mora,M., Gajardo,T., Pérez,F., Campos,J., Aguillón,J.C. and Pino-Lagos,K. (2015) Retinaldehyde dehydrogenase activity is triggered during allograft rejection and it drives Th1/Th17 cytokine production. *Immunobiology*, **220**, 769–74.
98. DePaolo,R.W., Abadie,V., Tang,F., Fehlner-Peach,H., Hall,J.A., Wang,W., Marietta,E. V, Kasarda,D.D., Waldmann,T.A., Murray,J.A., *et al.* (2011) Co-adjuvant effects of retinoic acid and IL-15 induce inflammatory immunity to dietary antigens. *Nature*, **471**, 220–4.
99. Larange,A. and Cheroutre,H. (2016) Retinoic Acid and Retinoic Acid Receptors as Pleiotropic Modulators of the Immune System. *Annu. Rev. Immunol.*, **34**, 369–94.
100. Coombes,J.L., Siddiqui,K.R.R., Arancibia-Cárcamo,C. V, Hall,J., Sun,C.-M., Belkaid,Y. and Powrie,F. (2007) A functionally specialized population of mucosal CD103+ DCs induces Foxp3+ regulatory T cells via a TGF-beta and retinoic acid-dependent mechanism. *J. Exp. Med.*, **204**, 1757–64.
101. von Boehmer,H. (2007) Oral tolerance: is it all retinoic acid? *J. Exp. Med.*, **204**, 1737–9.
102. Kam,R.K.T., Deng,Y., Chen,Y. and Zhao,H. (2012) Retinoic acid synthesis and functions in early embryonic development. *Cell Biosci.*, **2**, 11.
103. Ugel,S., Canè,S., De Sanctis,F. and Bronte,V. (2021) Monocytes in the Tumor Microenvironment. *Annu. Rev. Pathol.*, **16**, 93–122.
104. Galon,J. and Bruni,D. (2019) Approaches to treat immune hot, altered and cold tumours with combination immunotherapies. *Nat. Rev. Drug Discov.*, **18**, 197–218.
105. Chen,D.S. and Mellman,I. (2017) Elements of cancer immunity and the cancer-immune set point. *Nature*, **541**, 321–330.
106. Godoy-Tena,G. and Ballestar,E. (2022) Epigenetics of Dendritic Cells in Tumor

References

- Immunology. *Cancers (Basel)*, **14**.
107. Obermajer,N., Muthuswamy,R., Lesnock,J., Edwards,R.P. and Kalinski,P. (2011) Positive feedback between PGE₂ and COX₂ redirects the differentiation of human dendritic cells toward stable myeloid-derived suppressor cells. *Blood*, **118**, 5498–505.
 108. Wang,P.-F., Song,S.-Y., Wang,T.-J., Ji,W.-J., Li,S.-W., Liu,N. and Yan,C.-X. (2018) Prognostic role of pretreatment circulating MDSCs in patients with solid malignancies: A meta-analysis of 40 studies. *Oncoimmunology*, **7**, e1494113.
 109. Ruffell,B., Chang-Strachan,D., Chan,V., Rosenbusch,A., Ho,C.M.T., Pryer,N., Daniel,D., Hwang,E.S., Rugo,H.S. and Coussens,L.M. (2014) Macrophage IL-10 blocks CD8⁺ T cell-dependent responses to chemotherapy by suppressing IL-12 expression in intratumoral dendritic cells. *Cancer Cell*, **26**, 623–37.
 110. Luo,N., Nixon,M.J., Gonzalez-Ericsson,P.I., Sanchez,V., Opalenik,S.R., Li,H., Zahnow,C.A., Nickels,M.L., Liu,F., Tantawy,M.N., *et al.* (2018) DNA methyltransferase inhibition upregulates MHC-I to potentiate cytotoxic T lymphocyte responses in breast cancer. *Nat. Commun.*, **9**, 248.
 111. Labani-Motlagh,A., Ashja-Mahdavi,M. and Loskog,A. (2020) The Tumor Microenvironment: A Milieu Hindering and Obstructing Antitumor Immune Responses. *Front. Immunol.*, **11**, 940.
 112. Vitale,I., Manic,G., Coussens,L.M., Kroemer,G. and Galluzzi,L. (2019) Macrophages and Metabolism in the Tumor Microenvironment. *Cell Metab.*, **30**, 36–50.
 113. Kumar,V., Patel,S., Tcyganov,E. and Gabrilovich,D.I. (2016) The Nature of Myeloid-Derived Suppressor Cells in the Tumor Microenvironment. *Trends Immunol.*, **37**, 208–220.
 114. Gabrilovich,D.I., Bronte,V., Chen,S.-H., Colombo,M.P., Ochoa,A., Ostrand-Rosenberg,S. and Schreiber,H. (2007) The terminology issue for myeloid-derived suppressor cells. *Cancer Res.*, **67**, 425; author reply 426.
 115. Laurent,S., Carrega,P., Saverino,D., Piccioli,P., Camoriano,M., Morabito,A., Dozin,B., Fontana,V., Simone,R., Mortara,L., *et al.* (2010) CTLA-4 is expressed by human monocyte-derived dendritic cells and regulates their functions. *Hum. Immunol.*, **71**, 934–41.
 116. Yaseen,M.M., Abuharfeil,N.M., Darmani,H. and Daoud,A. (2020) Mechanisms of immune suppression by myeloid-derived suppressor cells: the role of interleukin-10 as a key immunoregulatory cytokine. *Open Biol.*, **10**, 200111.
 117. Gabrilovich,D.I. (2017) Myeloid-Derived Suppressor Cells. *Cancer Immunol. Res.*, **5**, 3–8.

118. Devalaraja,S., To,T.K.J., Folkert,I.W., Natesan,R., Alam,M.Z., Li,M., Tada,Y., Budagyan,K., Dang,M.T., Zhai,L., *et al.* (2020) Tumor-Derived Retinoic Acid Regulates Intratumoral Monocyte Differentiation to Promote Immune Suppression. *Cell*, **180**, 1098-1114.e16.
119. Retinoic Acid Mediates Monocyte Differentiation and Immune Response. (2020) *Cancer Discov.*, **10**, OF7.
120. Mamidi,S., Hofer,T.P.J., Hoffmann,R., Ziegler-Heitbrock,L. and Frankenberger,M. (2012) All-trans retinoic acid up-regulates Prostaglandin-E Synthase expression in human macrophages. *Immunobiology*, **217**, 593-600.
121. Zhou,P., Yang,X.-L., Wang,X.-G., Hu,B., Zhang,L., Zhang,W., Si,H.-R., Zhu,Y., Li,B., Huang,C.-L., *et al.* (2020) A pneumonia outbreak associated with a new coronavirus of probable bat origin. *Nature*, **579**, 270-273.
122. Zheng,M., Karki,R., Williams,E.P., Yang,D., Fitzpatrick,E., Vogel,P., Jonsson,C.B. and Kanneganti,T.-D. (2021) TLR2 senses the SARS-CoV-2 envelope protein to produce inflammatory cytokines. *Nat. Immunol.*, **22**, 829-838.
123. Tay,M.Z., Poh,C.M., Rénia,L., MacAry,P.A. and Ng,L.F.P. (2020) The trinity of COVID-19: immunity, inflammation and intervention. *Nat. Rev. Immunol.*, **20**, 363-374.
124. Karki,R., Sharma,B.R., Tuladhar,S., Williams,E.P., Zalduondo,L., Samir,P., Zheng,M., Sundaram,B., Banoth,B., Malireddi,R.K.S., *et al.* (2021) Synergism of TNF- α and IFN- γ Triggers Inflammatory Cell Death, Tissue Damage, and Mortality in SARS-CoV-2 Infection and Cytokine Shock Syndromes. *Cell*, **184**, 149-168.e17.
125. Koçak Tufan,Z., Kayaaslan,B. and Mer,M. (2021) COVID-19 and Sepsis. *Turkish J. Med. Sci.*, **51**, 3301-3311.
126. Torres,L.K., Pickkers,P. and van der Poll,T. (2022) Sepsis-Induced Immunosuppression. *Annu. Rev. Physiol.*, **84**, 157-181.
127. Oronsky,B., Larson,C., Hammond,T.C., Oronsky,A., Kesari,S., Lybeck,M. and Reid,T.R. (2023) A Review of Persistent Post-COVID Syndrome (PPCS). *Clin. Rev. Allergy Immunol.*, **64**, 66-74.
128. Witkowski,M., Tizian,C., Ferreira-Gomes,M., Niemeyer,D., Jones,T.C., Heinrich,F., Frischbutter,S., Angermair,S., Hohnstein,T., Mattiola,I., *et al.* (2021) Untimely TGF β responses in COVID-19 limit antiviral functions of NK cells. *Nature*, **600**, 295-301.
129. Liao,M., Liu,Y., Yuan,J., Wen,Y., Xu,G., Zhao,J., Cheng,L., Li,J., Wang,X., Wang,F., *et al.* (2020) Single-cell landscape of bronchoalveolar immune cells in patients

References

- with COVID-19. *Nat. Med.*, **26**, 842–844.
130. Delorey, T.M., Ziegler, C.G.K., Heimberg, G., Normand, R., Yang, Y., Segerstolpe, Å., Abbondanza, D., Fleming, S.J., Subramanian, A., Montoro, D.T., *et al.* (2021) COVID-19 tissue atlases reveal SARS-CoV-2 pathology and cellular targets. *Nature*, **595**, 107–113.
 131. Hadjadj, J., Yatim, N., Barnabei, L., Corneau, A., Boussier, J., Smith, N., Péré, H., Charbit, B., Bondet, V., Chenevier-Gobeaux, C., *et al.* (2020) Impaired type I interferon activity and inflammatory responses in severe COVID-19 patients. *Science*, **369**, 718–724.
 132. Lucas, C., Wong, P., Klein, J., Castro, T.B.R., Silva, J., Sundaram, M., Ellingson, M.K., Mao, T., Oh, J.E., Israelow, B., *et al.* (2020) Longitudinal analyses reveal immunological misfiring in severe COVID-19. *Nature*, **584**, 463–469.
 133. Wilk, A.J., Rustagi, A., Zhao, N.Q., Roque, J., Martínez-Colón, G.J., McKechnie, J.L., Ivison, G.T., Ranganath, T., Vergara, R., Hollis, T., *et al.* (2020) A single-cell atlas of the peripheral immune response in patients with severe COVID-19. *Nat. Med.*, **26**, 1070–1076.
 134. Zhou, R., To, K.K.-W., Wong, Y.-C., Liu, L., Zhou, B., Li, X., Huang, H., Mo, Y., Luk, T.-Y., Lau, T.T.-K., *et al.* (2020) Acute SARS-CoV-2 Infection Impairs Dendritic Cell and T Cell Responses. *Immunity*, **53**, 864–877.e5.
 135. Wilk, A.J., Lee, M.J., Wei, B., Parks, B., Pi, R., Martínez-Colón, G.J., Ranganath, T., Zhao, N.Q., Taylor, S., Becker, W., *et al.* (2021) Multi-omic profiling reveals widespread dysregulation of innate immunity and hematopoiesis in COVID-19. *J. Exp. Med.*, **218**.
 136. Sánchez-Cerrillo, I., Landete, P., Aldave, B., Sánchez-Alonso, S., Sánchez-Azofra, A., Marcos-Jiménez, A., Ávalos, E., Alcaraz-Serna, A., de Los Santos, I., Mateu-Albero, T., *et al.* (2020) COVID-19 severity associates with pulmonary redistribution of CD1c+ DCs and inflammatory transitional and nonclassical monocytes. *J. Clin. Invest.*, **130**, 6290–6300.
 137. Qin, S., Jiang, Y., Wei, X., Liu, X., Guan, J., Chen, Y., Lu, H., Qian, J., Wang, Z. and Lin, X. (2021) Dynamic changes in monocytes subsets in COVID-19 patients. *Hum. Immunol.*, **82**, 170–176.
 138. Schulte-Schrepping, J., Reusch, N., Paclik, D., Baßler, K., Schlickeiser, S., Zhang, B., Krämer, B., Krammer, T., Brumhard, S., Bonaguro, L., *et al.* (2020) Severe COVID-19 Is Marked by a Dysregulated Myeloid Cell Compartment. *Cell*, **182**, 1419–1440.e23.
 139. Silvin, A., Chapuis, N., Dunsmore, G., Goubet, A.G., Dubuisson, A., Derosa, L., Almire, C., Hénon, C., Kosmider, O., Droin, N., *et al.* (2020) Elevated Calprotectin and Abnormal Myeloid Cell Subsets Discriminate Severe from Mild COVID-19.

- Cell*, **182**, 1401-1418.e18.
140. Saichi,M., Ladjemi,M.Z., Korniotis,S., Rousseau,C., Ait Hamou,Z., Massenet-Regad,L., Amblard,E., Noel,F., Marie,Y., Bouteiller,D., *et al.* (2021) Single-cell RNA sequencing of blood antigen-presenting cells in severe COVID-19 reveals multi-process defects in antiviral immunity. *Nat. Cell Biol.*, **23**, 538–551.
 141. Hena0-Agudelo,J.S., Ayala,S., Badiel,M., Zea-Vera,A.F. and Matta Cortes,L. (2024) Classical monocytes-low expressing HLA-DR is associated with higher mortality rate in SARS-CoV-2+ young patients with severe pneumonia. *Heliyon*, **10**, e24099.
 142. Bader,S.M., Cooney,J.P., Pellegrini,M. and Doerflinger,M. (2022) Programmed cell death: the pathways to severe COVID-19? *Biochem. J.*, **479**, 609–628.
 143. Lin,Y., Gustafson,M.P., Bulur,P.A., Gastineau,D.A., Witzig,T.E. and Dietz,A.B. (2011) Immunosuppressive CD14+HLA-DR(low)/- monocytes in B-cell non-Hodgkin lymphoma. *Blood*, **117**, 872–81.
 144. Mengos,A.E., Gastineau,D.A. and Gustafson,M.P. (2019) The CD14+HLA-DRlo/neg Monocyte: An Immunosuppressive Phenotype That Restrains Responses to Cancer Immunotherapy. *Front. Immunol.*, **10**, 1147.
 145. Johnson,T.B. and Coghill,R.D. (1925) RESEARCHES ON PYRIMIDINES. CIII. THE DISCOVERY OF 5-METHYL-CYTOSINE IN TUBERCULINIC ACID, THE NUCLEIC ACID OF THE TUBERCLE BACILLUS 1. *J. Am. Chem. Soc.*, **47**, 2838–2844.
 146. SMITH,J.D. and MARKHAM,R. (1952) Polynucleotides from deoxyribonucleic acids. *Nature*, **170**, 120–1.
 147. SINSHEIMER,R.L. (1954) The action of pancreatic desoxyribonuclease. I. Isolation of mono- and dinucleotides. *J. Biol. Chem.*, **208**, 445–59.
 148. Moore,L.D., Le,T. and Fan,G. (2013) DNA methylation and its basic function. *Neuropsychopharmacology*, **38**, 23–38.
 149. Cedar,H. (1988) DNA methylation and gene activity. *Cell*, **53**, 3–4.
 150. Branco,M.R., Ficz,G. and Reik,W. (2011) Uncovering the role of 5-hydroxymethylcytosine in the epigenome. *Nat. Rev. Genet.*, **13**, 7–13.
 151. Ehrlich,M. and Ehrlich,K.C. (1993) Effect of DNA methylation on the binding of vertebrate and plant proteins to DNA. *EXS*, **64**, 145–68.
 152. Jones,P.A. (2012) Functions of DNA methylation: islands, start sites, gene bodies and beyond. *Nat. Rev. Genet.*, **13**, 484–92.
 153. Greger,V., Passarge,E., Höpping,W., Messmer,E. and Horsthemke,B. (1989)

References

- Epigenetic changes may contribute to the formation and spontaneous regression of retinoblastoma. *Hum. Genet.*, **83**, 155–8.
154. Nishiyama,A. and Nakanishi,M. (2021) Navigating the DNA methylation landscape of cancer. *Trends Genet.*, **37**, 1012–1027.
155. Dhar,G.A., Saha,S., Mitra,P. and Nag Chaudhuri,R. (2021) DNA methylation and regulation of gene expression: Guardian of our health. *Nucl. an Int. J. Cytol. allied Top.*, **64**, 259–270.
156. Aran,D., Toperoff,G., Rosenberg,M. and Hellman,A. (2011) Replication timing-related and gene body-specific methylation of active human genes. *Hum. Mol. Genet.*, **20**, 670–80.
157. Bannister,A.J. and Kouzarides,T. (2011) Regulation of chromatin by histone modifications. *Cell Res.*, **21**, 381–95.
158. Okano,M., Bell,D.W., Haber,D.A. and Li,E. (1999) DNA methyltransferases Dnmt3a and Dnmt3b are essential for de novo methylation and mammalian development. *Cell*, **99**, 247–57.
159. Goll,M.G. and Bestor,T.H. (2005) Eukaryotic cytosine methyltransferases. *Annu. Rev. Biochem.*, **74**, 481–514.
160. Dhayalan,A., Rajavelu,A., Rathert,P., Tamas,R., Jurkowska,R.Z., Ragozin,S. and Jeltsch,A. (2010) The Dnmt3a PWWP domain reads histone 3 lysine 36 trimethylation and guides DNA methylation. *J. Biol. Chem.*, **285**, 26114–20.
161. Sharif,J., Muto,M., Takebayashi,S., Suetake,I., Iwamatsu,A., Endo,T.A., Shinga,J., Mizutani-Koseki,Y., Toyoda,T., Okamura,K., *et al.* (2007) The SRA protein Np95 mediates epigenetic inheritance by recruiting Dnmt1 to methylated DNA. *Nature*, **450**, 908–12.
162. Bostick,M., Kim,J.K., Estève,P.-O., Clark,A., Pradhan,S. and Jacobsen,S.E. (2007) UHRF1 plays a role in maintaining DNA methylation in mammalian cells. *Science*, **317**, 1760–4.
163. Guibert,S., Forné,T. and Weber,M. (2012) Global profiling of DNA methylation erasure in mouse primordial germ cells. *Genome Res.*, **22**, 633–41.
164. Hackett,J.A., Sengupta,R., Zyllicz,J.J., Murakami,K., Lee,C., Down,T.A. and Surani,M.A. (2013) Germline DNA demethylation dynamics and imprint erasure through 5-hydroxymethylcytosine. *Science*, **339**, 448–52.
165. Li,J., Li,L., Wang,Y., Huang,G., Li,X., Xie,Z. and Zhou,Z. (2021) Insights Into the Role of DNA Methylation in Immune Cell Development and Autoimmune Disease. *Front. cell Dev. Biol.*, **9**, 757318.

166. Ohno,R., Nakayama,M., Naruse,C., Okashita,N., Takano,O., Tachibana,M., Asano,M., Saitou,M. and Seki,Y. (2013) A replication-dependent passive mechanism modulates DNA demethylation in mouse primordial germ cells. *Development*, **140**, 2892–903.
167. Wu,H. and Zhang,Y. (2014) Reversing DNA methylation: mechanisms, genomics, and biological functions. *Cell*, **156**, 45–68.
168. He,Y.-F., Li,B.-Z., Li,Z., Liu,P., Wang,Y., Tang,Q., Ding,J., Jia,Y., Chen,Z., Li,L., *et al.* (2011) Tet-mediated formation of 5-carboxylcytosine and its excision by TDG in mammalian DNA. *Science*, **333**, 1303–7.
169. Maiti,A. and Drohat,A.C. (2011) Thymine DNA glycosylase can rapidly excise 5-formylcytosine and 5-carboxylcytosine: potential implications for active demethylation of CpG sites. *J. Biol. Chem.*, **286**, 35334–35338.
170. Ito,S., Shen,L., Dai,Q., Wu,S.C., Collins,L.B., Swenberg,J.A., He,C. and Zhang,Y. (2011) Tet proteins can convert 5-methylcytosine to 5-formylcytosine and 5-carboxylcytosine. *Science*, **333**, 1300–3.
171. Weber,A.R., Krawczyk,C., Robertson,A.B., Kuśnierczyk,A., Vågbo,C.B., Schuermann,D., Klungland,A. and Schär,P. (2016) Biochemical reconstitution of TET1-TDG-BER-dependent active DNA demethylation reveals a highly coordinated mechanism. *Nat. Commun.*, **7**, 10806.
172. Hu,L., Lu,J., Cheng,J., Rao,Q., Li,Z., Hou,H., Lou,Z., Zhang,L., Li,W., Gong,W., *et al.* (2015) Structural insight into substrate preference for TET-mediated oxidation. *Nature*, **527**, 118–22.
173. Wu,X. and Zhang,Y. (2017) TET-mediated active DNA demethylation: mechanism, function and beyond. *Nat. Rev. Genet.*, **18**, 517–534.
174. Ko,M., An,J., Bandukwala,H.S., Chavez,L., Aijö,T., Pastor,W.A., Segal,M.F., Li,H., Koh,K.P., Lähdesmäki,H., *et al.* (2013) Modulation of TET2 expression and 5-methylcytosine oxidation by the CXXC domain protein IDAX. *Nature*, **497**, 122–6.
175. Héberlé,É. and Bardet,A.F. (2019) Sensitivity of transcription factors to DNA methylation. *Essays Biochem.*, **63**, 727–741.
176. Iwafuchi-Doi,M. and Zaret,K.S. (2014) Pioneer transcription factors in cell reprogramming. *Genes Dev.*, **28**, 2679–92.
177. Di Croce,L., Raker,V.A., Corsaro,M., Fazi,F., Fanelli,M., Faretta,M., Fuks,F., Lo Coco,F., Kouzarides,T., Nervi,C., *et al.* (2002) Methyltransferase recruitment and DNA hypermethylation of target promoters by an oncogenic transcription factor. *Science*, **295**, 1079–82.
178. Brenner,C., Deplus,R., Didelot,C., Lorient,A., Viré,E., De Smet,C., Gutierrez,A.,

References

- Danovi,D., Bernard,D., Boon,T., *et al.* (2005) Myc represses transcription through recruitment of DNA methyltransferase corepressor. *EMBO J.*, **24**, 336–46.
179. Suzuki,M., Yamada,T., Kihara-Negishi,F., Sakurai,T., Hara,E., Tenen,D.G., Hozumi,N. and Oikawa,T. (2006) Site-specific DNA methylation by a complex of PU.1 and Dnmt3a/b. *Oncogene*, **25**, 2477–88.
180. Velasco,G., Hubé,F., Rollin,J., Neuillet,D., Philippe,C., Bouzinba-Segard,H., Galvani,A., Viegas-Péquignot,E. and Francastel,C. (2010) Dnmt3b recruitment through E2F6 transcriptional repressor mediates germ-line gene silencing in murine somatic tissues. *Proc. Natl. Acad. Sci. U. S. A.*, **107**, 9281–6.
181. Fu,Y., Zhang,X., Liu,X., Wang,P., Chu,W., Zhao,W., Wang,Y., Zhou,G., Yu,Y. and Zhang,H. (2022) The DNMT1-PAS1-PH20 axis drives breast cancer growth and metastasis. *Signal Transduct. Target. Ther.*, **7**, 81.
182. Xie,M., Tang,Q., Nie,J., Zhang,C., Zhou,X., Yu,S., Sun,J., Cheng,X., Dong,N., Hu,Y., *et al.* (2020) BMAL1-Downregulation Aggravates Porphyromonas Gingivalis-Induced Atherosclerosis by Encouraging Oxidative Stress. *Circ. Res.*, **126**, e15–e29.
183. Stadler,M.B., Murr,R., Burger,L., Ivanek,R., Lienert,F., Schöler,A., van Nimwegen,E., Wirbelauer,C., Oakeley,E.J., Gaidatzis,D., *et al.* (2011) DNA-binding factors shape the mouse methylome at distal regulatory regions. *Nature*, **480**, 490–5.
184. de la Rica,L., Rodríguez-Ubreva,J., García,M., Islam,A.B.M.M.K., Urquiza,J.M., Hernando,H., Christensen,J., Helin,K., Gómez-Vaquero,C. and Ballestar,E. (2013) PU.1 target genes undergo Tet2-coupled demethylation and DNMT3b-mediated methylation in monocyte-to-osteoclast differentiation. *Genome Biol.*, **14**, R99.
185. Suzuki,T., Maeda,S., Furuhashi,E., Shimizu,Y., Nishimura,H., Kishima,M. and Suzuki,H. (2017) A screening system to identify transcription factors that induce binding site-directed DNA demethylation. *Epigenetics Chromatin*, **10**, 60.
186. Boulard,M., Edwards,J.R. and Bestor,T.H. (2015) FBXL10 protects Polycomb-bound genes from hypermethylation. *Nat. Genet.*, **47**, 479–85.
187. Long,H.K., Blackledge,N.P. and Klose,R.J. (2013) ZF-CxxC domain-containing proteins, CpG islands and the chromatin connection. *Biochem. Soc. Trans.*, **41**, 727–40.
188. Sever,R. and Glass,C.K. (2013) Signaling by nuclear receptors. *Cold Spring Harb. Perspect. Biol.*, **5**, a016709.
189. Hassan,H.M., Kolendowski,B., Isovici,M., Bose,K., Dranse,H.J., Sampaio,A. V., Underhill,T.M. and Torchia,J. (2017) Regulation of Active DNA Demethylation through RAR-Mediated Recruitment of a TET/TDG Complex. *Cell Rep.*, **19**, 1685–

- 1697.
190. Feinberg,A.P., Koldobskiy,M.A. and Göndör,A. (2016) Epigenetic modulators, modifiers and mediators in cancer aetiology and progression. *Nat. Rev. Genet.*, **17**, 284–99.
 191. Timp,W. and Feinberg,A.P. (2013) Cancer as a dysregulated epigenome allowing cellular growth advantage at the expense of the host. *Nat. Rev. Cancer*, **13**, 497–510.
 192. McDonald,O.G., Li,X., Saunders,T., Tryggvadottir,R., Mentch,S.J., Warmoes,M.O., Word,A.E., Carrer,A., Salz,T.H., Natsume,S., *et al.* (2017) Epigenomic reprogramming during pancreatic cancer progression links anabolic glucose metabolism to distant metastasis. *Nat. Genet.*, **49**, 367–376.
 193. Jin,Z. and Liu,Y. (2018) DNA methylation in human diseases. *Genes Dis.*, **5**, 1–8.
 194. Aho,K., Koskenvuo,M., Tuominen,J. and Kaprio,J. (1986) Occurrence of rheumatoid arthritis in a nationwide series of twins. *J. Rheumatol.*, **13**, 899–902.
 195. Deapen,D., Escalante,A., Weinrib,L., Horwitz,D., Bachman,B., Roy-Burman,P., Walker,A. and Mack,T.M. (1992) A revised estimate of twin concordance in systemic lupus erythematosus. *Arthritis Rheum.*, **35**, 311–8.
 196. BAMMER,H., SCHALTENBRAND,G. and SOLCHER,H. (1960) [Examinations of twins in multiple sclerosis]. *Dtsch. Z. Nervenheilkd.*, **181**, 261–79.
 197. Murphy,D. and Hutchinson,D. (2017) Is Male Rheumatoid Arthritis an Occupational Disease? A Review. *Open Rheumatol. J.*, **11**, 88–105.
 198. Liu,Y., Aryee,M.J., Padyukov,L., Fallin,M.D., Hesselberg,E., Runarsson,A., Reinius,L., Acevedo,N., Taub,M., Ronninger,M., *et al.* (2013) Epigenome-wide association data implicate DNA methylation as an intermediary of genetic risk in rheumatoid arthritis. *Nat. Biotechnol.*, **31**, 142–7.
 199. Rodríguez-Ubrea,J., de la Calle-Fabregat,C., Li,T., Ciudad,L., Ballestar,M.L., Català-Moll,F., Morante-Palacios,O., Garcia-Gomez,A., Celis,R., Humby,F., *et al.* (2019) Inflammatory cytokines shape a changing DNA methylome in monocytes mirroring disease activity in rheumatoid arthritis. *Ann. Rheum. Dis.*, **78**, 1505–1516.
 200. de la Calle-Fabregat,C., Rodríguez-Ubrea,J., Ciudad,L., Ramírez,J., Celis,R., Azuaga,A.B., Cuervo,A., Graell,E., Pérez-García,C., Díaz-Torné,C., *et al.* (2022) The synovial and blood monocyte DNA methylomes mirror prognosis, evolution, and treatment in early arthritis. *JCI insight*, **7**.
 201. Chung,S.A., Nititham,J., Elboudwarej,E., Quach,H.L., Taylor,K.E., Barcellos,L.F. and Criswell,L.A. (2015) Genome-Wide Assessment of Differential DNA Methylation Associated with Autoantibody Production in Systemic Lupus

References

- Erythematosus. *PLoS One*, **10**, e0129813.
202. Cai,X.Y., Lu,Y., Tang,C., Lin,X.J., Ye,J.H., Li,W.N., He,Z.X. and Li,F.F. (2017) [Effect of interleukin-6 promoter DNA methylation on the pathogenesis of systemic lupus erythematosus]. *Zhonghua Yi Xue Za Zhi*, **97**, 1491-1495.
203. Ferreté-Bonastre,A.G., Martínez-Gallo,M., Morante-Palacios,O., Calvillo,C.L., Calafell-Segura,J., Rodríguez-Ubreva,J., Esteller,M., Cortés-Hernández,J. and Ballestar,E. (2024) Disease activity drives divergent epigenetic and transcriptomic reprogramming of monocyte subpopulations in systemic lupus erythematosus. *Ann. Rheum. Dis.*, **10.1136/ard-2023-225433**.
204. Li,X., Xiao,B. and Chen,X.-S. (2017) DNA Methylation: a New Player in Multiple Sclerosis. *Mol. Neurobiol.*, **54**, 4049-4059.
205. Dayeh,T., Volkov,P., Salö,S., Hall,E., Nilsson,E., Olsson,A.H., Kirkpatrick,C.L., Wollheim,C.B., Eliasson,L., Rönn,T., *et al.* (2014) Genome-wide DNA methylation analysis of human pancreatic islets from type 2 diabetic and non-diabetic donors identifies candidate genes that influence insulin secretion. *PLoS Genet.*, **10**, e1004160.
206. Wu,Y., Cui,W., Zhang,D., Wu,W. and Yang,Z. (2017) The shortening of leukocyte telomere length relates to DNA hypermethylation of LINE-1 in type 2 diabetes mellitus. *Oncotarget*, **8**, 73964-73973.
207. Iossifov,I., O’Roak,B.J., Sanders,S.J., Ronemus,M., Krumm,N., Levy,D., Stessman,H.A., Witherspoon,K.T., Vives,L., Patterson,K.E., *et al.* (2014) The contribution of de novo coding mutations to autism spectrum disorder. *Nature*, **515**, 216-21.
208. Amir,R.E., Van den Veyver,I.B., Wan,M., Tran,C.Q., Francke,U. and Zoghbi,H.Y. (1999) Rett syndrome is caused by mutations in X-linked MECP2, encoding methyl-CpG-binding protein 2. *Nat. Genet.*, **23**, 185-8.
209. Fasolino,M. and Zhou,Z. (2017) The Crucial Role of DNA Methylation and MeCP2 in Neuronal Function. *Genes (Basel)*, **8**.
210. Jin,X.-R., Chen,X.-S. and Xiao,L. (2017) MeCP2 Deficiency in Neuroglia: New Progress in the Pathogenesis of Rett Syndrome. *Front. Mol. Neurosci.*, **10**, 316.
211. Martins-Ferreira,R., Leal,B., Chaves,J., Li,T., Ciudad,L., Rangel,R., Santos,A., Martins da Silva,A., Pinho Costa,P. and Ballestar,E. (2022) Epilepsy progression is associated with cumulative DNA methylation changes in inflammatory genes. *Prog. Neurobiol.*, **209**, 102207.
212. Lorente-Sorolla,C., Garcia-Gomez,A., Català-Moll,F., Toledano,V., Ciudad,L., Avendaño-Ortiz,J., Maroun-Eid,C., Martín-Quirós,A., Martínez-Gallo,M., Ruiz-

- Sanmartín,A., *et al.* (2019) Inflammatory cytokines and organ dysfunction associate with the aberrant DNA methylome of monocytes in sepsis. *Genome Med.*, **11**, 66.
213. Akagawa,K.S., Komuro,I., Kanazawa,H., Yamazaki,T., Mochida,K. and Kishi,F. (2006) Functional heterogeneity of colony-stimulating factor-induced human monocyte-derived macrophages. *Respirology*, **11 Suppl**, S32-6.
214. Nicholson,G.C., Malakellis,M., Collier,F.M., Cameron,P.U., Holloway,W.R., Gough,T.J., Gregorio-King,C., Kirkland,M.A. and Myers,D.E. (2000) Induction of osteoclasts from CD14-positive human peripheral blood mononuclear cells by receptor activator of nuclear factor kappaB ligand (RANKL). *Clin. Sci. (Lond.)*, **99**, 133-40.
215. Vento-Tormo,R., Company,C., Rodríguez-Ubreva,J., de la Rica,L., Urquiza,J.M., Javierre,B.M., Sabarinathan,R., Luque,A., Esteller,M., Aran,J.M., *et al.* (2016) IL-4 orchestrates STAT6-mediated DNA demethylation leading to dendritic cell differentiation. *Genome Biol.*, **17**, 4.
216. Català-Moll,F., Ferreté-Bonastre,A.G., Godoy-Tena,G., Morante-Palacios,O., Ciudad,L., Barberà,L., Fondelli,F., Martínez-Cáceres,E.M., Rodríguez-Ubreva,J., Li,T., *et al.* (2022) Vitamin D receptor, STAT3, and TET2 cooperate to establish tolerogenesis. *Cell Rep.*, **38**, 110244.
217. Morante-Palacios,O., Ciudad,L., Micheroli,R., de la Calle-Fabregat,C., Li,T., Barbisan,G., Houtman,M., Edalat,S.G., Frank-Bertoncelj,M., Ospelt,C., *et al.* (2022) Coordinated glucocorticoid receptor and MAFB action induces tolerogenesis and epigenome remodeling in dendritic cells. *Nucleic Acids Res.*, **50**, 108-126.
218. Rodríguez-Ubreva,J., Català-Moll,F., Obermajer,N., Álvarez-Errico,D., Ramirez,R.N., Company,C., Vento-Tormo,R., Moreno-Bueno,G., Edwards,R.P., Mortazavi,A., *et al.* (2017) Prostaglandin E2 Leads to the Acquisition of DNMT3A-Dependent Tolerogenic Functions in Human Myeloid-Derived Suppressor Cells. *Cell Rep.*, **21**, 154-167.
219. Pacis,A., Mailhot-Léonard,F., Tailleux,L., Randolph,H.E., Yotova,V., Dumaine,A., Grenier,J.-C. and Barreiro,L.B. (2019) Gene activation precedes DNA demethylation in response to infection in human dendritic cells. *Proc. Natl. Acad. Sci. U. S. A.*, **116**, 6938-6943.
220. Blaschke,K., Ebata,K.T., Karimi,M.M., Zepeda-Martínez,J.A., Goyal,P., Mahapatra,S., Tam,A., Laird,D.J., Hirst,M., Rao,A., *et al.* (2013) Vitamin C induces Tet-dependent DNA demethylation and a blastocyst-like state in ES cells. *Nature*, **500**, 222-6.
221. Yin,R., Mao,S.-Q., Zhao,B., Chong,Z., Yang,Y., Zhao,C., Zhang,D., Huang,H., Gao,J.,

References

- Li,Z., *et al.* (2013) Ascorbic acid enhances Tet-mediated 5-methylcytosine oxidation and promotes DNA demethylation in mammals. *J. Am. Chem. Soc.*, **135**, 10396–403.
222. Morante-Palacios,O., Godoy-Tena,G., Calafell-Segura,J., Ciudad,L., Martínez-Cáceres,E.M., Sardina,J.L. and Ballestar,E. (2022) Vitamin C enhances NF-κB-driven epigenomic reprogramming and boosts the immunogenic properties of dendritic cells. *Nucleic Acids Res.*, **50**, 10981–10994.
223. Mendes,K., Schmidhofer,S., Minderjahn,J., Glatz,D., Kiewewetter,C., Raithel,J., Wimmer,J., Gebhard,C. and Rehli,M. (2021) The epigenetic pioneer EGR2 initiates DNA demethylation in differentiating monocytes at both stable and transient binding sites. *Nat. Commun.*, **12**, 1556.
224. Gundra,U.M., Girgis,N.M., Gonzalez,M.A., San Tang,M., Van Der Zande,H.J.P., Lin,J.-D., Ouimet,M., Ma,L.J., Poles,J., Vozhilla,N., *et al.* (2017) Vitamin A mediates conversion of monocyte-derived macrophages into tissue-resident macrophages during alternative activation. *Nat. Immunol.*, **18**, 642–653.
225. Yao,R.-Q., Zhao,P.-Y., Li,Z.-X., Liu,Y.-Y., Zheng,L.-Y., Duan,Y., Wang,L., Yang,R.-L., Kang,H.-J., Hao,J.-W., *et al.* (2023) Single-cell transcriptome profiling of sepsis identifies HLA-DR^{low}SI00A^{high} monocytes with immunosuppressive function. *Mil. Med. Res.*, **10**, 27.
226. Utrero-Rico,A., González-Cuadrado,C., Chivite-Lacaba,M., Cabrera-Marante,O., Laguna-Goya,R., Almendro-Vazquez,P., Díaz-Pedroche,C., Ruiz-Ruigómez,M., Lalueza,A., Folgueira,M.D., *et al.* (2021) Alterations in Circulating Monocytes Predict COVID-19 Severity and Include Chromatin Modifications Still Detectable Six Months after Recovery. *Biomedicines*, **9**.
227. Knoll,R., Schultze,J.L. and Schulte-Schrepping,J. (2021) Monocytes and Macrophages in COVID-19. *Front. Immunol.*, **12**, 720109.
228. Miyake,K., Ito,J., Takahashi,K., Nakabayashi,J., Brombacher,F., Shichino,S., Yoshikawa,S., Miyake,S. and Karasuyama,H. (2024) Single-cell transcriptomics identifies the differentiation trajectory from inflammatory monocytes to pro-resolving macrophages in a mouse skin allergy model. *Nat. Commun.*, **15**, 1666.
229. Calle-Fabregat,C. de la, Morante-Palacios,O. and Ballestar,E. (2020) Understanding the Relevance of DNA Methylation Changes in Immune Differentiation and Disease. *Genes (Basel)*, **11**.
230. Dekkers,K.F., Neele,A.E., Jukema,J.W., Heijmans,B.T. and de Winther,M.P.J. (2019) Human monocyte-to-macrophage differentiation involves highly localized gain and loss of DNA methylation at transcription factor binding sites. *Epigenetics Chromatin*, **12**, 34.

231. Ainsua-Enrich,E., Hatipoglu,I., Kadel,S., Turner,S., Paul,J., Singh,S., Bagavant,H. and Kovats,S. (2019) IRF4-dependent dendritic cells regulate CD8+ T-cell differentiation and memory responses in influenza infection. *Mucosal Immunol.*, **12**, 1025–1037.
232. Taniguchi,K. and Karin,M. (2018) NF- κ B, inflammation, immunity and cancer: coming of age. *Nat. Rev. Immunol.*, **18**, 309–324.
233. Armstrong,D.A., Chen,Y., Dessaint,J.A., Aridgides,D.S., Channon,J.Y., Mellinger,D.L., Christensen,B.C. and Ashare,A. (2019) DNA Methylation Changes in Regional Lung Macrophages Are Associated with Metabolic Differences. *ImmunoHorizons*, **3**, 274–281.
234. Hey,J., Paulsen,M., Toth,R., Weichenhan,D., Butz,S., Schatterny,J., Liebers,R., Lutsik,P., Plass,C. and Mall,M.A. (2021) Epigenetic reprogramming of airway macrophages promotes polarization and inflammation in muco-obstructive lung disease. *Nat. Commun.*, **12**, 6520.
235. Wallner,S., Schröder,C., Leitão,E., Berulava,T., Haak,C., Beißer,D., Rahmann,S., Richter,A.S., Manke,T., Bönisch,U., *et al.* (2016) Epigenetic dynamics of monocyte-to-macrophage differentiation. *Epigenetics Chromatin*, **9**, 33.
236. Zhu,H., Wang,G. and Qian,J. (2016) Transcription factors as readers and effectors of DNA methylation. *Nat. Rev. Genet.*, **17**, 551–65.
237. Ghoshal,K., Li,X., Datta,J., Bai,S., Pogribny,I., Pogribny,M., Huang,Y., Young,D. and Jacob,S.T. (2006) A folate- and methyl-deficient diet alters the expression of DNA methyltransferases and methyl CpG binding proteins involved in epigenetic gene silencing in livers of F344 rats. *J. Nutr.*, **136**, 1522–7.
238. Shen,Q., Bai,Y., Chang,K.C.N., Wang,Y., Burris,T.P., Freedman,L.P., Thompson,C.C. and Nagpal,S. (2011) Liver X receptor-retinoid X receptor (LXR-RXR) heterodimer cistrome reveals coordination of LXR and AP1 signaling in keratinocytes. *J. Biol. Chem.*, **286**, 14554–63.
239. Tsao,W.-C., Wu,H.-M., Chi,K.-H., Chang,Y.-H. and Lin,W.-W. (2005) Proteasome inhibitors induce peroxisome proliferator-activated receptor transactivation through RXR accumulation and a protein kinase C-dependent pathway. *Exp. Cell Res.*, **304**, 234–43.
240. Lefebvre,B., Benomar,Y., Guédin,A., Langlois,A., Hennuyer,N., Dumont,J., Bouchaert,E., Dacquet,C., Pénicaud,L., Casteilla,L., *et al.* (2010) Proteasomal degradation of retinoid X receptor alpha reprograms transcriptional activity of PPARgamma in obese mice and humans. *J. Clin. Invest.*, **120**, 1454–68.
241. Torra,I.P., Ismaili,N., Feig,J.E., Xu,C.-F., Cavasotto,C., Pancratov,R., Rogatsky,I., Neubert,T.A., Fisher,E.A. and Garabedian,M.J. (2008) Phosphorylation of liver X

References

- receptor alpha selectively regulates target gene expression in macrophages. *Mol. Cell. Biol.*, **28**, 2626–36.
242. Becares,N., Gage,M.C. and Pineda-Torra,I. (2017) Posttranslational Modifications of Lipid-Activated Nuclear Receptors: Focus on Metabolism. *Endocrinology*, **158**, 213–225.
243. Zimmerman,T.L., Thevananther,S., Ghose,R., Burns,A.R. and Karpen,S.J. (2006) Nuclear export of retinoid X receptor alpha in response to interleukin-1beta-mediated cell signaling: roles for JNK and SER260. *J. Biol. Chem.*, **281**, 15434–40.
244. Wu,C., Hussein,M.A., Shrestha,E., Leone,S., Aiyegbo,M.S., Lambert,W.M., Pourcet,B., Cardozo,T., Gustafson,J.-A., Fisher,E.A., *et al.* (2015) Modulation of Macrophage Gene Expression via Liver X Receptor α Serine 198 Phosphorylation. *Mol. Cell. Biol.*, **35**, 2024–34.
245. González de la Aleja,A., Herrero,C., Torres-Torresano,M., de la Rosa,J.V., Alonso,B., Capa-Sardón,E., Muller,I.B., Jansen,G., Puig-Kröger,A., Vega,M.A., *et al.* (2022) Activation of LXR Nuclear Receptors Impairs the Anti-Inflammatory Gene and Functional Profile of M-CSF-Dependent Human Monocyte-Derived Macrophages. *Front. Immunol.*, **13**, 835478.
246. Fontaine,C., Rigamonti,E., Nohara,A., Gervois,P., Teissier,E., Fruchart,J.-C., Staels,B. and Chinetti-Gbaguidi,G. (2007) Liver X receptor activation potentiates the lipopolysaccharide response in human macrophages. *Circ. Res.*, **101**, 40–9.
247. Jin,C.-J., Hong,C.Y., Takei,M., Chung,S.-Y., Park,J.-S., Pham,T.-N.N., Choi,S.-J.-N., Nam,J.-H., Chung,I.-J., Kim,H.-J., *et al.* (2010) All-trans retinoic acid inhibits the differentiation, maturation, and function of human monocyte-derived dendritic cells. *Leuk. Res.*, **34**, 513–20.
248. Hoover,L.L., Burton,E.G., O'Neill,M.L., Brooks,B.A., Sreedharan,S., Dawson,N.A. and Kubalak,S.W. (2008) Retinoids regulate TGFbeta signaling at the level of Smad2 phosphorylation and nuclear accumulation. *Biochim. Biophys. Acta*, **1783**, 2279–86.
249. Ma,Z.-L., Ding,Y.-L., Jing,J., Du,L.-N., Zhang,X.-Y., Liu,H.-M. and He,P.-X. (2022) ATRA promotes PD-L1 expression to control gastric cancer immune surveillance. *Eur. J. Pharmacol.*, **920**, 174822.
250. Rao,E., Hou,Y., Huang,X., Wang,L., Wang,J., Zheng,W., Yang,H., Yu,X., Yang,K., Bugno,J., *et al.* (2021) All-trans retinoic acid overcomes solid tumor radioresistance by inducing inflammatory macrophages. *Sci. Immunol.*, **6**.
251. Carbó,J.M., León,T.E., Font-Díaz,J., De la Rosa,J.V., Castrillo,A., Picard,F.R., Staudenraus,D., Huber,M., Cedó,L., Escolà-Gil,J.C., *et al.* (2021) Pharmacologic Activation of LXR Alters the Expression Profile of Tumor-Associated

- Macrophages and the Abundance of Regulatory T Cells in the Tumor Microenvironment. *Cancer Res.*, **81**, 968–985.
252. Li,N., Li,Y., Han,X., Zhang,J., Han,J., Jiang,X., Wang,W., Xu,Y., Xu,Y., Fu,Y., *et al.* (2022) LXR agonist inhibits inflammation through regulating MyD88 mRNA alternative splicing. *Front. Pharmacol.*, **13**, 973612.
253. Caricasulo,M.A., Zanetti,A., Terao,M., Garattini,E. and Paroni,G. (2024) Cellular and micro-environmental responses influencing the antitumor activity of all-trans retinoic acid in breast cancer. *Cell Commun. Signal.*, **22**, 127.
254. Tavazoie,M.F., Pollack,I., Tanqueco,R., Ostendorf,B.N., Reis,B.S., Gonsalves,F.C., Kurth,I., Andreu-Agullo,C., Derbyshire,M.L., Posada,J., *et al.* (2018) LXR/ApoE Activation Restricts Innate Immune Suppression in Cancer. *Cell*, **172**, 825-840.e18.
255. Carpenter,K.J., Valfort,A.-C., Steinauer,N., Chatterjee,A., Abuirqeba,S., Majidi,S., Sengupta,M., Di Paolo,R.J., Shornick,L.P., Zhang,J., *et al.* (2019) LXR-inverse agonism stimulates immune-mediated tumor destruction by enhancing CD8 T-cell activity in triple negative breast cancer. *Sci. Rep.*, **9**, 19530.
256. Thomas,D.G., Doran,A.C., Fotakis,P., Westerterp,M., Antonson,P., Jiang,H., Jiang,X.-C., Gustafsson,J.-Å., Tabas,I. and Tall,A.R. (2018) LXR Suppresses Inflammatory Gene Expression and Neutrophil Migration through cis-Repression and Cholesterol Efflux. *Cell Rep.*, **25**, 3774-3785.e4.
257. Villablanca,E.J., Raccosta,L., Zhou,D., Fontana,R., Maggioni,D., Negro,A., Sanvito,F., Ponzoni,M., Valentinis,B., Bregni,M., *et al.* (2010) Tumor-mediated liver X receptor-alpha activation inhibits CC chemokine receptor-7 expression on dendritic cells and dampens antitumor responses. *Nat. Med.*, **16**, 98–105.
258. Bilotta,M.T., Petillo,S., Santoni,A. and Cippitelli,M. (2020) Liver X Receptors: Regulators of Cholesterol Metabolism, Inflammation, Autoimmunity, and Cancer. *Front. Immunol.*, **11**, 584303.
259. Hertzman,C. (1999) The biological embedding of early experience and its effects on health in adulthood. *Ann. N. Y. Acad. Sci.*, **896**, 85–95.
260. Hertzman,C. (2012) Putting the concept of biological embedding in historical perspective. *Proc. Natl. Acad. Sci. U. S. A.*, **109 Suppl**, 17160–7.
261. Greenberg,M.V.C. and Bourc’his,D. (2019) The diverse roles of DNA methylation in mammalian development and disease. *Nat. Rev. Mol. Cell Biol.*, **20**, 590–607.
262. Yim,Y.Y., Teague,C.D. and Nestler,E.J. (2020) In vivo locus-specific editing of the neuroepigenome. *Nat. Rev. Neurosci.*, **21**, 471–484.
263. Kreibich,E., Kleinendorst,R., Barzaghi,G., Kaspar,S. and Krebs,A.R. (2023) Single-molecule footprinting identifies context-dependent regulation of enhancers by

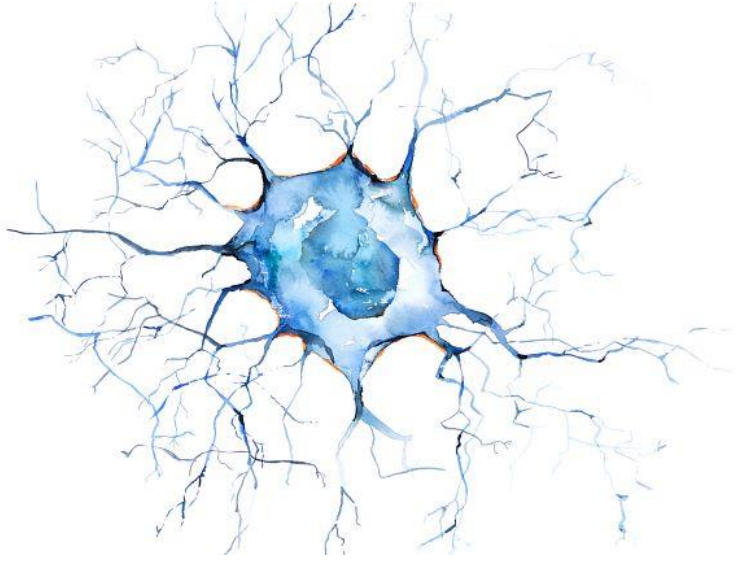
References

- DNA methylation. *Mol. Cell*, **83**, 787-802.e9.
264. Penner-Goeke,S. and Binder,E.B. (2024) Linking environmental factors and gene regulation. *Elife*, **13**.
265. Johnston,R.A., Aracena,K.A., Barreiro,L.B., Lea,A.J. and Tung,J. (2024) DNA methylation-environment interactions in the human genome. *Elife*, **12**.
266. Zhou,Y., Liao,X., Song,X., He,M., Xiao,F., Jin,X., Xie,X., Zhang,Z., Wang,B., Zhou,C., *et al.* (2021) Severe Adaptive Immune Suppression May Be Why Patients With Severe COVID-19 Cannot Be Discharged From the ICU Even After Negative Viral Tests. *Front. Immunol.*, **12**, 755579.
267. Blattler,A. and Farnham,P.J. (2013) Cross-talk between site-specific transcription factors and DNA methylation states. *J. Biol. Chem.*, **288**, 34287-94.
268. Lin,I.-H., Chen,Y.-F. and Hsu,M.-T. (2017) Correlated 5-Hydroxymethylcytosine (5hmC) and Gene Expression Profiles Underpin Gene and Organ-Specific Epigenetic Regulation in Adult Mouse Brain and Liver. *PLoS One*, **12**, e0170779.
269. Johnson,K.C., Houseman,E.A., King,J.E., von Herrmann,K.M., Fadul,C.E. and Christensen,B.C. (2016) 5-Hydroxymethylcytosine localizes to enhancer elements and is associated with survival in glioblastoma patients. *Nat. Commun.*, **7**, 13177.
270. Saboor-Yaraghi,A.A., Harirchian,M.H., Mohammadzadeh Honarvar,N., Bitarafan,S., Abdolahi,M., Siassi,F., Salehi,E., Sahraian,M.A., Eshraghian,M.R., Roostaei,T., *et al.* (2015) The Effect of Vitamin A Supplementation on FoxP3 and TGF- β Gene Expression in Avonex-Treated Multiple Sclerosis Patients. *J. Mol. Neurosci.*, **56**, 608-12.
271. Mucida,D. and Cheroutre,H. (2007) TGFbeta and retinoic acid intersect in immune-regulation. *Cell Adh. Migr.*, **1**, 142-4.
272. Sarper,M., Cortes,E., Lieberthal,T.J. and Del Río Hernández,A. (2016) ATRA modulates mechanical activation of TGF- β by pancreatic stellate cells. *Sci. Rep.*, **6**, 27639.
273. Li,S., Lei,Y., Lei,J. and Li,H. (2021) All-trans retinoic acid promotes macrophage phagocytosis and decreases inflammation via inhibiting CD14/TLR4 in acute lung injury. *Mol. Med. Rep.*, **24**.
274. Coleman,M.M., Ruane,D., Moran,B., Dunne,P.J., Keane,J. and Mills,K.H.G. (2013) Alveolar macrophages contribute to respiratory tolerance by inducing FoxP3 expression in naive T cells. *Am. J. Respir. Cell Mol. Biol.*, **48**, 773-80.
275. Soroosh,P., Doherty,T.A., Duan,W., Mehta,A.K., Choi,H., Adams,Y.F., Mikulski,Z., Khorram,N., Rosenthal,P., Broide,D.H., *et al.* (2013) Lung-resident tissue macrophages generate Foxp3+ regulatory T cells and promote airway tolerance. *J.*

- Exp. Med.*, **210**, 775–88.
276. Helmy,K.Y., Katschke,K.J., Gorgani,N.N., Kljavin,N.M., Elliott,J.M., Diehl,L., Scales,S.J., Ghilardi,N. and van Lookeren Campagne,M. (2006) CRIg: a macrophage complement receptor required for phagocytosis of circulating pathogens. *Cell*, **124**, 915–27.
277. Broadley,S.P., Plaumann,A., Coletti,R., Lehmann,C., Wanisch,A., Seidlmeier,A., Esser,K., Luo,S., Ramer,P.C., Massberg,S., *et al.* (2016) Dual-Track Clearance of Circulating Bacteria Balances Rapid Restoration of Blood Sterility with Induction of Adaptive Immunity. *Cell Host Microbe*, **20**, 36–48.
278. Wiesmann,C., Katschke,K.J., Yin,J., Helmy,K.Y., Steffek,M., Fairbrother,W.J., McCallum,S.A., Embuscado,L., DeForge,L., Hass,P.E., *et al.* (2006) Structure of C3b in complex with CRIg gives insights into regulation of complement activation. *Nature*, **444**, 217–20.
279. Vogt,L., Schmitz,N., Kurrer,M.O., Bauer,M., Hinton,H.I., Behnke,S., Gatto,D., Sebbel,P., Beerli,R.R., Sonderegger,I., *et al.* (2006) VSIG4, a B7 family-related protein, is a negative regulator of T cell activation. *J. Clin. Invest.*, **116**, 2817–26.
280. Liao,Y., Guo,S., Chen,Y., Cao,D., Xu,H., Yang,C., Fei,L., Ni,B. and Ruan,Z. (2014) VSIG4 expression on macrophages facilitates lung cancer development. *Lab. Invest.*, **94**, 706–15.
281. Li,J., Diao,B., Guo,S., Huang,X., Yang,C., Feng,Z., Yan,W., Ning,Q., Zheng,L., Chen,Y., *et al.* (2017) VSIG4 inhibits proinflammatory macrophage activation by reprogramming mitochondrial pyruvate metabolism. *Nat. Commun.*, **8**, 1322.
282. Kulle,A., Thanabalasuriar,A., Cohen,T.S. and Szydlowska,M. (2022) Resident macrophages of the lung and liver: The guardians of our tissues. *Front. Immunol.*, **13**, 1029085.
283. Huang,X., Feng,Z., Jiang,Y., Li,J., Xiang,Q., Guo,S., Yang,C., Fei,L., Guo,G., Zheng,L., *et al.* (2019) VSIG4 mediates transcriptional inhibition of Nlrp3 and Il-1 β in macrophages. *Sci. Adv.*, **5**, eaau7426.
284. Philibert,R.A., Sears,R.A., Powers,L.S., Nash,E., Bair,T., Gerke,A.K., Hassan,I., Thomas,C.P., Gross,T.J. and Monick,M.M. (2012) Coordinated DNA methylation and gene expression changes in smoker alveolar macrophages: specific effects on VEGF receptor 1 expression. *J. Leukoc. Biol.*, **92**, 621–31.
285. Cizmecioglu,A., Emsen,A., Sumer,S., Ergun,D., Akay Cizmecioglu,H., Turk Dagi,H. and Artac,H. (2022) Reduced Monocyte Subsets, Their HLA-DR Expressions, and Relations to Acute Phase Reactants in Severe COVID-19 Cases. *Viral Immunol.*, **35**, 273–282.

References

286. Pirabe,A., Heber,S., Schrottmaier,W.C., Schmuckenschlager,A., Treiber,S., Pereyra,D., Santol,J., Pawelka,E., Traugott,M., Schörgenhofer,C., *et al.* (2021) Age Related Differences in Monocyte Subsets and Cytokine Pattern during Acute COVID-19-A Prospective Observational Longitudinal Study. *Cells*, **10**.
287. Monneret,G., Lepape,A., Voirin,N., Bohé,J., Venet,F., Debard,A.-L., Thizy,H., Biennu,J., Gueyffier,F. and Vanhems,P. (2006) Persisting low monocyte human leukocyte antigen-DR expression predicts mortality in septic shock. *Intensive Care Med.*, **32**, 1175–83.
288. Xiu,B., Lin,Y., Grote,D.M., Ziesmer,S.C., Gustafson,M.P., Maas,M.L., Zhang,Z., Dietz,A.B., Porrata,L.F., Novak,A.J., *et al.* (2015) IL-10 induces the development of immunosuppressive CD14(+)HLA-DR(low/-) monocytes in B-cell non-Hodgkin lymphoma. *Blood Cancer J.*, **5**, e328.
289. Bandola-Simon,J. and Roche,P.A. (2019) Dysfunction of antigen processing and presentation by dendritic cells in cancer. *Mol. Immunol.*, **113**, 31–37.



APPENDIX

9. APPENDIX

1. Barmada A, **Handfield LF***, **Godoy-Tena G***, **de la Calle-Fabregat C***, Ciudad L, Arutyunyan A, Andrés-León E, Hoo R, Porter T, Oszlanczi A, Richardson L, Calero-Nieto FJ, Wilson NK, Marchese D, Sancho-Serra C, Carrillo J, Presas-Rodríguez S, Ramo-Tello C, Ruiz-Sanmartin A, Ferrer R, Ruiz-Rodríguez JC, Martínez-Gallo M, Munera-Campos M, Carrascosa JM, Göttgens B, Heyn H, Prigmore E, Casafont-Solé I, Solanich X, Sánchez-Cerrillo I, González-Álvaro I, Raimondo MG, Ramming A, Martin J, Martínez-Cáceres E, Ballestar E, Vento-Tormo R, Rodríguez-Ubrea J. Single-cell multi-omics analysis of COVID-19 patients with pre-existing autoimmune diseases shows aberrant immune responses to infection. *Eur J Immunol.* **2024** Jan;54(1): e2350633.

* Equal contribution

2. **Godoy-Tena G**, Barmada A, Morante-Palacios O, de la Calle-Fabregat C, Martins-Ferreira R, Ferreté-Bonastre AG, Ciudad L, Ruiz-Sanmartín A, Martínez-Gallo M, Ferrer R, Ruiz-Rodríguez JC, Rodríguez-Ubrea J, Vento-Tormo R, Ballestar E. Epigenetic and transcriptomic reprogramming in monocytes of severe COVID-19 patients reflects alterations in myeloid differentiation and the influence of inflammatory cytokines. *Genome Medicine.* **2022** Nov 29;14(1):134.
3. **Godoy-Tena G**, Ballestar E. Epigenetics of Dendritic Cells in Tumor Immunology. *Cancers.* **2022** Feb 24;14(5):1179.

4. Morante-Palacios O, **Godoy-Tena G**, Calafell-Segura J, Ciudad L, Martínez-Cáceres EM, Sardina JL, Ballestar E. Vitamin C enhances NF- κ B-driven epigenomic reprogramming and boosts the immunogenic properties of dendritic cells. *Nucleic Acids Res.* **2022** Oct 28;50(19):10981-10994.
5. **Català-Moll F***, **Ferreté-Bonastre AG***, **Godoy-Tena G***, Morante-Palacios O, Ciudad L, Barberà L, Fondelli F, Martínez-Cáceres EM, Rodríguez-Ubreva J, Li T, Ballestar E. Vitamin D receptor, STAT3, and TET2 cooperate to establish tolerogenesis. *Cell Rep.* **2022** Jan 18;38(3):110244.
* Equal contribution
6. Garcia-Gomez A, Li T, de la Calle-Fabregat C, Rodríguez-Ubreva J, Ciudad L, Català-Moll F, **Godoy-Tena G**, Martín-Sánchez M, San-Segundo L, Muntión S, Morales X, Ortiz-de-Solórzano C, Oyarzabal J, San José-Enériz E, Esteller M, Agirre X, Prosper F, Garayoa M, Ballestar E. Targeting aberrant DNA methylation in mesenchymal stromal cells as a treatment for myeloma bone disease. *Nat Commun.* **2021** Jan 18;12(1):421.

Review

Epigenetics of Dendritic Cells in Tumor Immunology

Gerard Godoy-Tena ¹ and Esteban Ballestar ^{1,2,*}

- ¹ Epigenetics and Immune Disease Group, Josep Carreras Research Institute (IJC), 08916 Barcelona, Spain; ggodoy@carrerasresearch.org
- ² Epigenetics in Inflammatory and Metabolic Diseases Laboratory, Health Science Center (HSC), East China Normal University (ECNU), Shanghai 200241, China
- * Correspondence: eballestar@carrerasresearch.org

Simple Summary: Dendritic cells (DCs) are an important type of immune cell present in the blood and tissues, capable of detecting potential threats and displaying them to lymphocytes in the lymph nodes, therefore initiating lymphocyte-mediated responses. DCs not only recognize pathogens but also damaged or altered cells from our own bodies, such as cancer cells, and contribute to the immune response to cancer. However, the tumor microenvironment, the environment that surrounds cancer cells, produces a number of factors that can modulate the function of DCs, which can acquire an immunosuppressive phenotype that allows tumor growth. This acquisition is also tightly regulated by epigenetics, the set of mechanisms that impact gene function without altering the DNA sequence. In this review, we discuss epigenetic mechanisms that influence the development of functional DCs and their altered function in the tumor microenvironment. We propose how this knowledge can be used both to epigenetically modulate these cells, and for the development of DC-based vaccine therapies.

Abstract: Dendritic cells (DCs) are professional antigen-presenting cells with the distinctive property of inducing the priming and differentiation of naïve CD4+ and CD8+ T cells into helper and cytotoxic effector T cells to develop efficient tumor-immune responses. DCs display pathogenic and tumorigenic antigens on their surface through major histocompatibility complexes to directly influence the differentiation of T cells. Cells in the tumor microenvironment (TME), including cancer cells and other immune-infiltrated cells, can lead DCs to acquire an immune-tolerogenic phenotype that facilitates tumor progression. Epigenetic alterations contribute to cancer development, not only by directly affecting cancer cells, but also by their fundamental role in the differentiation of DCs that acquire a tolerogenic phenotype that, in turn, suppresses T cell-mediated responses. In this review, we focus on the epigenetic regulation of DCs that have infiltrated the TME and discuss how knowledge of the epigenetic control of DCs can be used to improve DC-based vaccines for cancer immunotherapy.

Keywords: dendritic cells; tumor microenvironment; epigenetics; DNA methylation; tolerogenesis; cancer epigenetics; histone modification; tumor immunology



Citation: Godoy-Tena, G.; Ballestar, E. Epigenetics of Dendritic Cells in Tumor Immunology. *Cancers* **2022**, *14*, 1179. <https://doi.org/10.3390/cancers14051179>

Academic Editors:
Armand Bensussan and Luis Franco

Received: 25 January 2022
Accepted: 23 February 2022
Published: 24 February 2022

Publisher's Note: MDPI stays neutral with regard to jurisdictional claims in published maps and institutional affiliations.



Copyright: © 2022 by the authors. Licensee MDPI, Basel, Switzerland. This article is an open access article distributed under the terms and conditions of the Creative Commons Attribution (CC BY) license (<https://creativecommons.org/licenses/by/4.0/>).

1. Introduction

Efficient immune responses to threats involve a wide range of cell types within the adaptive and innate immune systems. These threats include pathogens, self-antigens in autoimmune conditions, and damaged or aberrant cells in cancer. Cancer cells display aberrant phenotypes and behavior as genetic mutations and epigenetic alterations accumulate, resulting in malignant transformation of cells [1].

To achieve a correct immune response to cancer cells, it is critical that antigen-presenting cells (APCs) activate T cells by cross-presenting antigens from the tumor. Dendritic cells (DCs) are specialized APCs that are needed to stimulate T cell-driven anticancer immunity and make it more robust. Recent studies have expanded our knowledge about the role of the different DC subtypes in the immune antitumor response. However, in most cases, tumor-infiltrating DCs develop an immune-tolerant phenotype that favors tumor

growth [2,3]. This is in part due to the effects that cancer cells exert on different immune cell types through cell-to-cell contacts, secretion of soluble factors and exosome release, which influence their epigenetic and gene expression profiles. In recent years, the tumor microenvironment (TME), i.e., the environment around a tumor, including the surrounding blood vessels, the infiltrating immune cells, fibroblasts, and extracellular matrix, has been recognized as a major player in tumor progression.

Epigenetic dysregulation provides several mechanisms for cancer development and progression due to its effects on the aberrant activation of oncogenes and repression of tumor suppressor genes. Epigenetics is also relevant in this context as it links extracellular signals with changes in gene expression. Most cancer epigenetic studies have focused on cancer cells, which display aberrant changes in DNA methylation and histone modifications. However, epigenetic alterations are involucrate in numerous processes in the DC development and recruitment and might also play a crucial role in the switch from an immunogenic to a tolerogenic phenotype in DCs. The potential role of epigenetic dysregulation in tumor-infiltrated DCs is also highly relevant as a result of the potential pharmacological reversion of epigenetic alterations and immunogenic phenotype, as well as in the context of using these mechanisms for improving DC-based vaccines.

2. Mechanisms Underlying Epigenetic Dysregulation

Epigenetic mechanisms, in conjunction with transcription factors (TFs), define the transcriptional status of different gene sets, and those that are transcribed in a given cell type and in a particular situation ultimately determine cell function. In cancer cells, epigenetic alterations profoundly disrupt their transcriptome. In relation to DCs, it is well established that epigenetics plays a crucial role in the control of immune cell differentiation, identity, and function. The role of epigenetics in the differentiation of the myeloid lineage, which is particularly relevant to most DC subtypes, has been thoroughly described [4,5]. In addition, recent studies have revealed strong connections between epigenetics and cytokine production by tumor cells [6].

Epigenetic alterations mainly involve changes in DNA methylation, histone modifications and non-coding RNAs. Methylation of the 5' position of cytosines (5meC) followed by guanines (CpG dinucleotides) is the best studied epigenetic modification. This chemical modification can influence the binding and recruitment of numerous proteins, including TFs and chromatin-modifying regulators. DNA methylation is catalyzed by DNA methyltransferases (DNMTs). These enzymes are classified in two main types: maintenance DNMTs, such as DNMT1, which are responsible for copying the DNA methylation patterns from the parental DNA strands during DNA replication; and de novo DNMTs, such as DNMT3A and DNMT3B [7]. The removal of methyl groups can be passive, by the inefficient action of DNMT1 during replication, or active. Active DNA demethylation is mediated by the concerted activity of the enzymes of the ten-eleven translocation (TET) family, thymine DNA glycosylase (TDG), and the base-excision repair (BER) machinery [8]. Alterations in the methylation patterns of DNA are responsible for cell differentiation, and their dysregulation leads to diseases, including cancer [9].

Histone post-translational modifications are the second main group of epigenetic marks. They may be associated with transcriptional activation or repression. There are several types of post-translational modification, including acetylation of Lys, methylation of Lys and Arg, phosphorylation of Ser and Thr, and others. These chemical modifications not only have direct effects on chromatin structure, but also facilitate the binding of other factors. Different enzymes are responsible for the deposition and removal of these post-translational modifications, including histone acetyltransferases (HATs), histone deacetylases (HDACs), histone methyltransferases (HMTs), and histone demethylases (HDMs), among others. The nature of the chemical modification and the position of the amino acid residue in the protein sequence yield different functional outcomes. Generally, histone H3 trimethylation at Lys9 (H3K9me3) and Lys27 (H3K27me3) are considered repressive modifications [10], whereas histone acetylation at the same positions (H3K9ac and H3K27ac) in promoters and

enhancers, respectively, are generally associated with transcriptional activation, and the removal of these acetyl marks is linked to gene repression. Conversely, H3 trimethylation at Lys4 (H3K4me3) and Lys36 (H3K36me3) are also associated with active transcription [10].

Non-coding RNAs (ncRNAs) are also considered a type of epigenetic mechanism, although, in this case, it does not involve any chemical modification. Specifically, it consists of RNA molecules that do not encode proteins, yet have functions after being spliced and/or processed into smaller products. ncRNAs include microRNAs (miRNAs), small nucleolar RNAs (snoRNAs) as well as tens of thousands of longer transcripts, such as long non-coding RNAs (lncRNAs), most of the functions of which are still unknown [11]. For instance, miRNAs primarily act at a post-transcriptional level by base-pairing with their complementary mRNA targets to alter mRNA stability and/or translation into protein [12]. mRNA destabilization explains the vast majority of miRNA-mediated repression [13].

3. Dendritic Cell Subtypes and Epigenetic Regulation

DCs are professional APCs with the distinctive property of inducing priming and differentiation of naïve T cells like CD4⁺ and CD8⁺ T cells into helper and cytotoxic effector T cells, respectively. This role has been confirmed by the study of DC-deficient animals, obtained by, for instance, knocking out *Batf3*, an essential TF for several DC subtypes [14,15]. DCs mature following the detection of pathogen-associated molecular patterns (PAMPs) from viruses and bacteria, and of damage-associated molecular patterns (DAMPs), in the case of cancer cells, through binding to pattern recognition receptors such as Toll-like receptors (TLRs). During maturation, major histocompatibility complex (MHC) molecules move to the DC plasma membrane, upregulation of CD80/CD86 molecules and IL-12 is produced [16]. This maturation can also be accompanied by loss of DNA methylation followed by de novo methylation. This has been attributed to modulation of the expression of DNMT1, DNMT3A, and DNMT3B [17]. DC maturation is also accompanied by changes in histone modifications. A recent study has demonstrated that the intracellular heat shock protein 70-like protein (HSP70L1) inhibits human DC maturation. Intracellular HSP70L1 inhibits the recruitment of Ash1l and maintains repressive H3K27me3 and H2AK119Ub1 modifications on the promoter regions of the MHC and STAT3 genes [18]. Another study has shown that Polycomb group factor 6 (PCGF6) is associated with the H3K4me3 demethylase JARID1c, and together, they negatively regulate H3K4me3 levels in DCs, which are necessary for DC activation [19].

DCs are not only required to stimulate T cell-driven anticancer immunity, but also to make it more robust. Antigens from tumor cells are internalized and loaded through MHC molecules. This process activates DCs that then migrate towards draining lymph nodes, where they can induce an adaptive immune response by presenting these antigens to T cells [20]. Antigen presentation by DCs occurs through the T-cell receptor (TCR), which is expressed in naïve T cells and can recognize these antigens. Once the TCR-MHC interaction has occurred, T cells initiate the process of activation and differentiation, known as T-cell priming. During this process, there is also a global remodeling of the epigenome, including changes in DNA methylation [21,22] and histone modification [23,24] in T cells. Subsequently, primed T cells migrate to the tumor, where they exert cytotoxic anti-tumor effects.

One of the characteristics that makes DCs so important is their ability to present antigens by both MHC-I and MHC-II molecules [25,26]. The unconventional presentation of antigens loaded onto MHCs by DCs relies on “cross-presentation” [27], which is needed to ensure immunity to viruses, intracellular bacteria, and cancer cells. Antigens loaded onto MHC-II molecules can be recognized by antigen-specific CD4⁺ T helper cells. In addition, MHC-I molecules can be recognized by antigen-specific CD8⁺ T cells, leading to their proliferation and the activation of their cytotoxic capabilities [27].

Phenotypic and functional criteria have customarily been used to define three main DC subtypes, namely, conventional DCs (cDCs), plasmacytoid DCs (pDCs) and monocyte-derived DCs (moDCs). cDCs, characterized by the expression of CD11c, derive from common DC precursors (CDPs) in the bone marrow (BM). cDCs can be further split into

two main lineages: cDC1 and cDC2. cDC1s have an enhanced ability to cross-present exogenous antigens on MHC-I and to activate CD8+ T cells. This subtype is characterized by the expression of CD141 in humans [28,29] and XCR1 in mice. In comparison, cDC2s, characterized by the expression of CD1c in humans [26] and CD11b in mice, represent a heterogeneous population with enhanced MHC-II antigen presentation [28,29]. However, a recent study has shown that cDC1 DCs are also capable of activating CD4+ T cells. In this study, they selectively removed MHC-II from cDC1 DCs, and this resulted in a reduction in CD4+ T cell-mediated responses [30]. A recent model suggests that CD4+ T cells are first primed by cDC2 and then reconnect with cDC1, to empower CD4+ T cells and enhance CD8+ T cell responses [31].

DC subsets are classified by their origin and function; they also differ with respect to the set of specific transcription factors (TFs) required for their development. Interferon regulatory factor 8 (IRF8) and IRF4 are necessary for the development of cDC1 and cDC2, respectively [32–35], accompanied by increased DNA accessibility [36]. These factors act in collaboration with PU.1, ID2, E2-2, ZEB2, Flt3 and BATF3, which have different degrees of specificity for DCs [29,33] (see Figure 1). For instance, the combination of whole-genome mapping of PU.1 binding and gene expression analysis has revealed a key role for this TF in maintaining cDC identity by inducing the transcriptional regulator DC-SCRIPT [37]. In this regard, the coordinated participation of transcription factors and histone modifications is critical. A good example of this is histone H2A deubiquitinase Mym1, which mediates PU.1 recruitment in cDC differentiation [38]. Analysis of PU.1 and H3K4me1 shows an increasing overlap of PU.1 binding and H3K4me1 during cDCs differentiation [39].

Another DC subtype is exemplified by plasmacytoid DCs (pDCs), which differentiate from both the common dendritic cell precursor (CDP) and lymphoid progenitors [40,41]. Similar to cDCs, pDC express cytokine receptor Flt3 and are strictly dependent on its ligand Flt3L for their development [42]. Human pDCs were customarily defined as being those that express CD123, CD303 (BDCA2), CD304 (BDCA4), and immunoglobulin-like transcript 7 (ILT7) [43]. pDCs are mainly found circulating in the peripheral blood, however, are also present in peripheral organs. They have a characteristic surface phenotype and morphology that includes a highly developed secretory compartment [44]. This DC subset requires high levels of expression of IRF8, TCF4 (also known as E2-2) and BCL11A for their development, functional specification, and maintenance [45]. The TF E2-2 is essential for maintaining pDC identity as the loss of E2-2 in mouse pDCs causes them to differentiate into cDCs [46]. Some studies have observed that IRF8 does not play a key role in regulating pDC functions, although it is important for their development [47]. HDACs may also influence the differentiation of this subtype since, for example, the inhibition of HDAC reduces the expression of PU.1 and suppresses the recruitment of PU.1 to FLT3 and IRF8, which are fundamental TFs for the differentiation of pDCs [48].

Inflammatory conditions can lead to the recruitment of monocytes from blood, in a CC-chemokine receptor 2 (CCR2) dependent manner, and prompt them to differentiate to monocyte-derived DCs (moDCs) in peripheral tissues [49]. Mildner and colleagues regarded this subset as activated effector monocytes rather than cDC-like cells [50], on the basis of the pronounced proinflammatory signature. These cells have a similar phenotype to cDC2, however, can be distinguished by the absence of expression of CD26 [51]. Another special characteristic is the fact that they do not need the growth factor Flt3L for their development and they express low levels of Zbtb46, which are specific to the development of the other DC subsets [52,53]. This DC subset has been extensively studied using an in vitro model consisting of monocytes differentiating to DC-like cells in the presence of granulocyte-macrophage colony-stimulating factor (GM-CSF) and IL-4 [54]. Our group demonstrated that DNA demethylation plays a fundamental role in the differentiation from monocytes to moDCs, which depends on the JAK3-STAT6 pathway and TET2 [55]. Another example of epigenetic control in relation to DC differentiation comes from a study, in which the differentiation of monocytes to DC was blocked by pharmacological inhibition of HDACs [56].

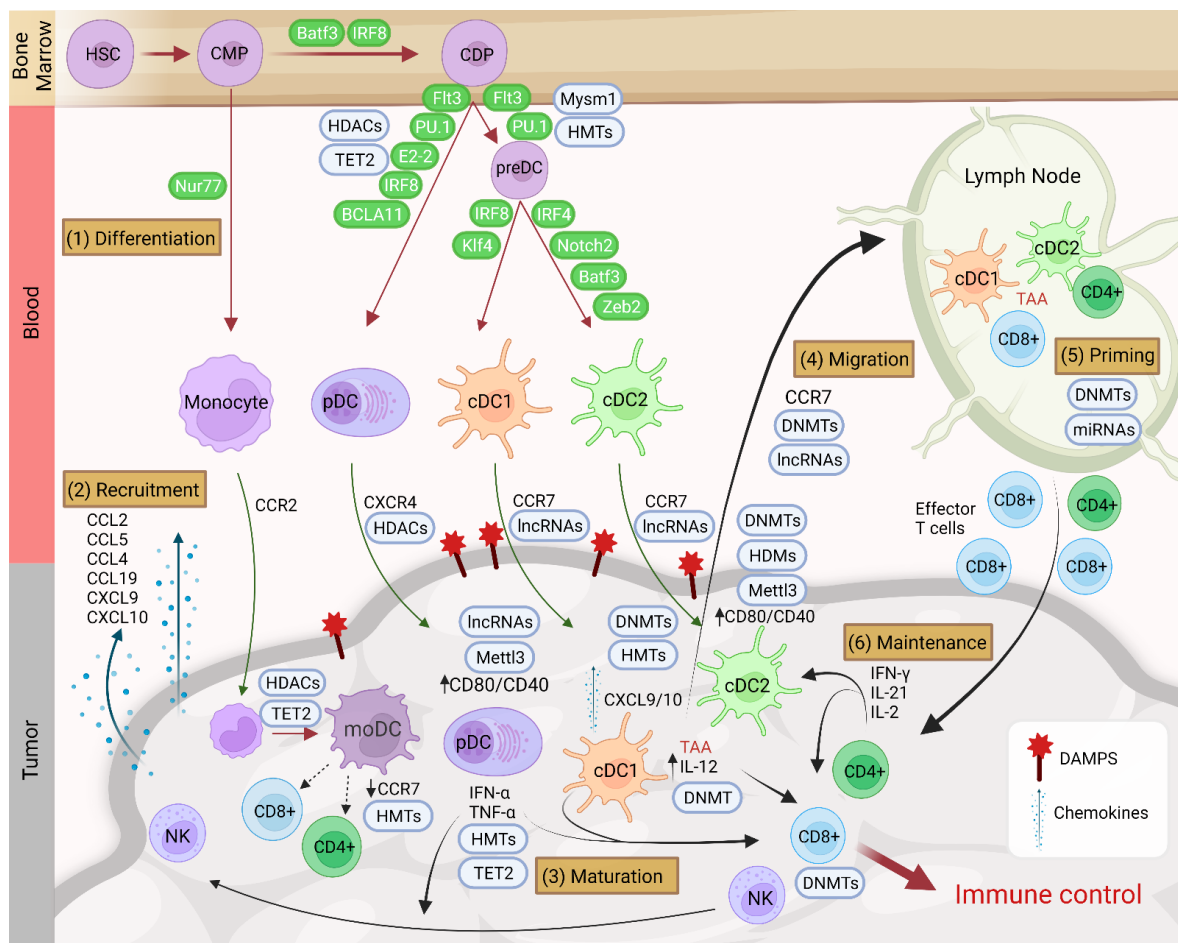


Figure 1. (1) Dendritic cells are originated from hematopoietic stem cells (HSC), which differentiate (represented with red arrows) into common myeloid progenitor (MDP) in the bone marrow. MDP can originate monocytes under the regulation of TF Nur77 or differentiate into common dendritic progenitor (CDP) under the TFs Batf3 and IRF8. Conventional type 1 DC (cDC1), conventional type 2 DC (cDC2), and plasmacytoid DC (pDC) subsets come from CDPs, under the influence of critical TFs and growth factors (shown next to each red arrow). (2) Under the expression of damage-associated molecular patterns (DAMPs) and chemokines like CCL2, CCL5 or CCL19 from the tumor the different DCs and monocytes are recruited in the tumor (represented with green arrows). This recruitment is guided by the expression of CCR2, CXCR4 and CCR7 in myeloid cells. (3) Once in the TME, DCs mature. This involves the upregulation of CD80/CD40 and the release of interleukin-12 (IL-12). In the case of cDC1, maturation processes also involve the expression of additional chemokines like CXCL9/10. Monocytes can further differentiate into monocyte-derived DCs (moDCs) in the tumor conditions. These cells have low expression of CCR7, which reduce their migration capacity. However, these cells are capable of activating CD4+ and CD8+ T cells within the tumor. (4) After tumor associated-antigen recognition (TAA), DCs migrate (represented with black arrows) to lymph nodes and (5) prime naïve CD4+ and CD8+ T cells. (6) After T cell activation, T cells migrate to the tumor and a constant cross-talk is produced between DCs and T cells to produce a correct immune control and maintenance. This maintenance consists in the expression of cytokines like interferon- α (IFN- α), tumor necrosis factor (TNF)- α from pDC or IL-12 from cDC that, in turn, is amplified by T- and natural killer (NK) cell-derived cytokines such as IFN- γ , IL-2 and IL-21. NKs can also be implicated in the release of chemokines, which will attract more DCs. During all these processes different epigenetic enzymes are implicated like ten-eleven translocation (TET)-2, DNA methyltransferases (DNMTs), histone deacetylases (HDACs), histone methyltransferases (HMTs), long noncoding RNAs (lncRNAs) or Mym1 and the RNA methyltransferase Mettl3, represented in blue circles. Created with [BioRender.com](https://www.biorender.com) (accessed on 24 January 2022).

4. Recruitment of Dendritic Cells in the TME and Involvement of Epigenetics

Analysis of the TME in patients with a variety of solid tumors has revealed immune cell infiltration, with two major phenotypes, based on the presence of infiltrating T cells: one has a broad chemokine profile and a type I interferon signature, while the other lacks this T cell-inflamed phenotype [57]. Not only solid tumors present immune cell infiltration. In fact, tumor-draining lymph nodes (TDLNs) are typically comprised of distinct subsets of immune cells [28]. Single-cell RNA sequencing studies have revealed a great complexity of immune cells in the TME [58–60]. Myeloid cells are a key cellular component among the immune cells that infiltrate into tumors and play important roles in modulating tumor inflammation and angiogenesis [61]. Immature DCs can be recruited into the TME, attracted by tumor-secreted factors such as CCL2, CCL20/MIP3a, CCL25, CCL5, CXCL12, CXCL1, and CXCL5, while mature DCs reside in areas surrounding the tumor [2,62,63]. The expression of the C-C chemokine receptor 7 (CCR7), the chemokine receptor for CCL19/CCL21, by DCs is important to facilitate their trafficking between the lymph nodes and the tumor [64,65]. Tumor-derived liver X- α receptor (LXR α) agonists in the TME can affect CCR7 expression in DCs since inhibition of LXR α increases protection against tumor growth [66].

Some specific treatments, like low-doses of CpG-B and GM-CSF, could result in the accumulation of cDC1 in the lymph nodes. An *in vivo* study has demonstrated that these treatments lead to the accumulation of cDC1 cells and recruitment in the lymph node by secreting type I interferon (IFN) [67]. It has been shown that non-coding RNAs, specifically lncRNAs, expressed exclusively in human cDCs, play a fundamental role in the differentiation and activation of DCs by directly binding to cytoplasmic signal transducer and activator of transcription 3 (STAT3) [68]. According to a recent study, lncRNAs may also affect DC migration, as they found that lnc-Dpf3 binds directly to the transcription factor HIF-1 α and suppresses the HIF-1 α -dependent transcription of the glycolytic gene *Ldha*, thereby inhibiting the glycolytic metabolism of DC and its migratory capacity [69].

pDCs are recruited to the specific target tissues from the bone marrow by the chemokine CXCR4. The NAD⁺ dependent deacetylase Sirtuin 6 (SIRT6) helps CXCR4⁺ DCs migrate to the afferent lymph nodes through its effects on histone H3K9 acetylation [70]. For moDCs, CCR2 seems to be necessary to ensure the correct migration of monocytes from blood to inflammatory tissue as there are fewer cells of this type in the inflammatory tissues of CCR2^{-/-} mice [71]. After differentiation, moDCs display a limited capacity to migrate to the lymph node [72,73], which is related with the low expression of *ccr7*. This is epigenetically regulated as significant differences between migratory cDCs and non-migratory moDCs have been noted in the repressive levels of histone H3K27me₃ in the locus of the *ccr7* gene [74].

The TME contains a set of factors that inhibit the infiltration of DCs and reduce their immunosuppressive activity. Among them, a low level of expression of the chemokine CCL4 by tumor cells reduces the degree of DC infiltration [75]. Tumors can also limit DC infiltration indirectly by decreasing the viability of natural killer cells (NKs), which produce CCL5 [76]. The extent of infiltration is influenced by changes in DCs and possibly by DNA methylation changes in other infiltrated cells. For instance, Shi et al. reported a strong interaction between DNMTs and immune genes associated with the infiltration of neutrophils and DCs in colorectal carcinoma (CRC), suggesting that the TME was largely influenced by the methylation of related genes like *ALOX5AP* and *CSF3R* [77].

Cancer cells use a variety of epigenetically regulated pathways to avoid the immune system, which gives rise to a low level of migration of DCs. These include the downregulation of tumor-associated antigens (TAA), the loss of the antigen processing and presentation machinery, and the expression of Programmed Cell Death Protein 1 (PD-1) [78]. PD-1 is essential for inhibiting immune responses and promoting self-tolerance by modulating the activity of T-cells, activating apoptosis in antigen-specific T cells, and inhibiting it in regulatory T cells [79].

In general, the conditions found in the TME can promote, or not, the recruitment of certain subtypes of DCs, whereupon they can exercise a variety of functions (see Figure 1).

5. Functions of Dendritic Cells in the TME

Several studies have demonstrated the crucial role of DCs in anti-tumor responses [65,80–82]. One of the main functions of DCs in cancer immunity is the acquisition, processing and cross-presentation of TAAs, as well as the release of co-stimulatory and soluble factors to increase T cell response. In the TME, cancer cells induce expression of MHC-II, CD40, CD80, and CD86 on DCs, together with the release of inflammatory cytokines like IL-12, type I IFN, IL-1 β , IL-6 and tumor necrosis factor (TNF) [83]. However, tumor cells can silence antigenic genes related to antigen presentation in DCs using epigenetic mechanisms that in turn impact antigen presentation by DCs [84–87].

One of the most efficient functions of DCs within the TME is the expression of IL-12, which polarizes naïve CD4⁺ T cells to T helper 1 (Th1), which enables them to express IFN α , and prime CD8⁺ T cells [88]. CD4⁺ T cells also help eliminate tumor cells through the production of IL-21 and IL-2, which are needed to adequately establish long-term memory T cells [89,90]. At the same time, IFN- α production increases the production of IL-12 by cDC1 and potentiates their antigen cross-presentation. This crosstalk proves to be even more complex since NKs and CD8⁺ T cells produce several factors that promote the recruitment of more cDC1 [91]. DCs also generate type I IFN, for example, when stimulated by anti-PD-1, a cancer immune therapy. In this context, stimulation of antitumor T cells by anti-PD-1 is not direct, but instead involves T cell:DC crosstalk, which is licensed by INF- γ and IL-12 [92]. Interferon expression is also epigenetically regulated by HMT KMT3A (SETD2) through the methylation of Lys 525 of STAT1 [93].

Each specific DC subtype has a different function in the TME. The crucial role of DCs in cancer immune response has been additionally demonstrated as cancer patients with more infiltration of cDC1 have a lower incidence of metastasis in oral, head and neck tumors [94]. This could be related to the association of tumor-infiltrated cDC1 with the abundance of CD8⁺ T cells in the TME [64,95]. In addition, the presence of cDC1 in the tumor is associated with a better immune response to tumors [81]. cDC1 can also secrete CXCL9 or CXCL10 in the TME, which attracts CXCR3⁺ effector cells other than T cells, such as NK cells and group 1 innate lymphoid cells (ILC1) [96]. CXCL9/10 expression is not constitutive in cDC1, and it requires the expression of type I IFN or IFN- γ by T cells. One study demonstrated that the combined inhibition of DNMT1-mediated DNA methylation and EZH2-mediated trimethylation of H3K27 in a murine ovarian cancer model increased tumor infiltration of effector T cells by restoring levels of CXCL9 and CXCL10 production by Th1 [97]. The expression of these chemokines is important for more cDCs to infiltrate the TME, however, their expression can be suppressed by epigenetic enzymes such as KMT6A (EZH2), one of the DNMTs [97].

Initially, it seemed that cDC1 was the only DC subset involved in tumor immunity, however a more extensive analysis revealed the presence of other DC subsets [98] and the limited prevalence of cDC1 in human tumors [99]. Additionally, CD8⁺ T cells are not the only lymphocyte population involved in tumor immunity, and CD4⁺ T cells are known to be required in many tumor models [31,100–104]. It has been shown that cDC1 are not capable of activating CD4⁺ T cells *ex vivo* [99], and that the antigenic presentation of cDC2 to CD4⁺ T cells regulates multiple aspects of tumor immune response. Duong and colleagues reported an activation state of infiltrated cDC2s that was characterized by the expression of IFN-stimulated genes (ISG + DCs) and the ability to acquire and present intact tumor-derived peptide MHC class I complexes. These ISG + DCs can activate CD8⁺ T cells and promote protective anti-tumor immunity in the absence of cDC1 [105]. The same researchers subsequently found that this ISG + DC gene signature could be detected in human tumors.

pDCs are recognized by their main function of producing high levels of IFN- α in response to viruses and pathogens [106]. In addition, pDCs promote both innate and adap-

tive immune responses through induction of NK cell migration, macrophage and dendritic cell maturation, T cell response and antigen presentation [107]. IFN expression in pDCs is influenced by HMTs. For example, H3K9me2 levels are correlated with IFN expression levels, and the inactivation of the lysine methyltransferase G9a, which is essential for generating H3K9me2, consequently inhibits IFN production [108]. Type I IFN expression may also be influenced by DNA methylation since its induction requires TET2-dependent DNA demethylation of the IRF8 gene in pDCs [109]. Some models of breast cancer in mice have shown that pDCs alone can kill tumor cells through the expression of TNF, as well as promoting the activation of NKs [110]. Furthermore, pDCs occur in ovarian cancers, where they are essential for immunosuppression through their expression of indoleamine 2,3-dioxygenase 1 (IDO1) and inducible T cell costimulatory ligand (ICOSL) [111]. In addition, the enrichment of a specific subset of pDCs expressing high levels of TNF receptor (TNFR) superfamily member OX40 (CD134) in the TME has been reported. These pDCs can be discriminated by their distinct immunostimulatory phenotype, cytolytic function, and ability to synergize with cDCs to generate powerful tumor antigen-specific CD8+ T cell responses [112], thereby revealing another important facet of the involvement of pDCs in the TME. However, unlike with cDCs, tumor infiltration of pDCs is correlated with a poor prognosis in cancer patients. This is mainly due to pDC accumulation being associated with an increase in regulatory T cells (Tregs), which are naïve CD4+ T cells activated in the presence of transforming growth factor (TGF)- β and/or IL10 that have an immunosuppressive phenotype, resulting in decreased overall survival of the patients [113].

Once monocytes have reached the TME and have correctly differentiated to moDCs, they are capable of antigen presentation. Several studies have reported the presence of moDCs in the TME [82,114]. moDCs can also be found in the drainage from lymph nodes of mice with tumors that were treated locally with a combination of monosodium urate crystals and *Mycobacterium smegmatis* [114]. It has been established that moDCs are essential for CD8+ T cell activation and antitumor responses following local immunotherapy [114]. Even though different studies have also demonstrated the ability of these cells to present to CD4+ T cells [115]. Furthermore, moDCs differentiated for eight days in culture expressed CD141 and were able to capture dead cells and became mature when stimulated with TLR3 [116]. Finally, CD4+ and CD8+ T cells can be stimulated simultaneously if moDCs express MHC [117], although moDCs are scarce in lymph nodes [72,118]. The presence of this cell type in tumors is positively associated with cancer prognosis. Even though these cells may be present in tumors, their proportions are very low, and there is evidence that some tumors appear to exclude them actively [81] (see Figure 1).

6. Epigenetic Impact of the TME on Dendritic Cells

DC subtypes have the potential to promote correct immune responses. However, the TME contains immunosuppressive factors that limit the immunostimulatory properties of DCs. In the TME, tumor and immune cells acquire different characteristics that allow them to produce cytokines, chemokines, and growth factors. In cancer cells, a general activation of signaling pathways such as mitogen-activated protein kinase (MAPK), phosphoinositide 3-kinase (PI3K), STAT3, and nuclear factor κ B (NF- κ B) pathways happens, whereupon they promote the expression of IL-6, IL-10, GM-CSF and TGF- β , among others. This may help some of the infiltrated immune cells, especially DCs and NK cells, to lose their ability to present antigens and their cytotoxic function, respectively.

Various epigenetic modifications play a fundamental role in the differentiation and activation of DCs [4]. Together with the factors that are released by cancer cells, epigenetics may also have a main role in the transition to a tolerogenic phenotype of DCs. The relevance of epigenetics is exemplified by the pharmacological inhibitors of HDACs that block monocyte-to-DC differentiation, giving rise to a less immunogenic phenotype [56]. It has also been shown that TET2 represses the expression of the pro-inflammatory cytokine IL-6 by recruiting HDAC2 in order to resolve inflammation in innate myeloid cells [119]. Furthermore, the aberrant

expression of miRNAs such as miR-22, miR-146a, and miR-146b inhibits the maturation and antigen presentation function of DCs, impairing their antitumor activity [120].

IL-10 expression in the tumor, which is mainly produced by macrophages [121], reduces the expression of MHC-II and CD40 in DCs [122], affecting their capacity to mature and to present antigens and this is epigenetically regulated by DNMTs and HDACs [85,86]. In this regard, repression in mature DCs of CIITA, a protein that acts as a positive regulator of MHC-II, is known to involve changes in histone acetylation across the whole gene locus and specific binding of positive regulatory domain 1 (PRDM1) to the promoters [123]. The expression of IL-10, together with GM-CSF, in the TME markedly increases the acetylation of histones H3 and H4 at the CIITA gene type I promoter locus during DC differentiation [124]. Recent studies have demonstrated that, under IL-10 expression, HDAC3, a class I HDAC, regulates the expression of proinflammatory cytokine like IL-12 in alveolar macrophages [125,126]. At the same time, HDAC11 negatively regulates the expression of the IL-10 gene in DCs in humans and mice [127].

IL-6 overproduction in the TME is associated with a functional defect in DCs in cancer patients [128]. In a different context, we have recently associated this cytokine with the acquisition of a tolerogenic phenotype. Specifically, vitamin D3 induces the *in vitro* acquisition of specific DNA demethylation and expression changes in DCs associated with tolerogenesis, and this is associated with direct vitamin D receptor (VDR) binding to genomic sites and the direct recruitment of TET2. This acquired tolerogenesis can be reverted by inhibiting JAK2/pSTAT3 [129].

Tumor-derived gangliosides and prostaglandin E2 (PGE2) are also produced in the TME, thereby altering the differentiation of cDCs and monocytes [130]. The expression of PGE2 by cancer cells also impairs the survival of NK cells by inhibiting the production of cytokines that attract cDC1 [76]. For instance, PGE2 levels are elevated in patients with colon cancer and are correlated with tumor size and patient survival [131], and are responsible for the reduced differentiation of DCs [132]. Another study also showed that PGE2 induces the upregulation of DNMTs and DNA hypermethylation of several genes [133].

More examples of secreted factors affecting the maturation and function of DCs, leading to the acquisition of a tolerogenic phenotype, include vascular endothelial growth factor (VEGF) and TGF- β , which inhibit normal DC maturation [134], and RANKL, a TNF family member that downregulates and upregulates the expression of IL-12 and IL-10, respectively [135]. VEGF is a protein responsible for the formation of tumor neovasculature and for tumor development [136,137]. This factor regulates DC migration and targeting by recruiting immature myeloid cells and immature DCs from the bone marrow [138]. After the inhibition of VEGF receptor 2, an increased cDC2 infiltration occurs, together with increased production of IL-1 β and IL-6, showing the relevance of this molecule in inhibiting DC infiltration and action in the TME [139].

TGF- β expressed by the tumor cells lowers the expression of DCs maturation markers like CD83, CD80, CD86, and MHC II molecules [140], and inhibits the expression of pro-inflammatory cytokines that induce the maturation of DCs, such as TNF- α , IL-1, IL-12, and IFN- α , while promoting the release of regulatory cytokines, including TGF- β itself [113,141]. TGF- β induces changes in histone H3K4me3 and H3K27me3 levels that cause the upregulation of costimulatory molecules and cytokines/chemokines and, in turn, the downregulation of differentiation markers [142].

Another study showed that the treatment of cell lines with two pro-inflammatory mediators found in TME, nitric oxide and IL-1 β , increases the activity of DNMTs and leads to hypermethylation of a vast number of CpG islands [143]. DNA methylation can additionally silence endogenous retroviruses (ERVs), thereby activating the MDA5 pattern-recognition receptor, which normally detects viral infection by recognizing double-stranded (ds) viral RNAs. MDA5 induces signaling cascades that result in the secretion of type I interferon. HDAC and H3K4me1/2 have similar roles in ERV suppression and ERV-induced activation of the interferon pathway [144]. The cytokine-2 suppressor protein (SOCS2), a conserved program transcript, is another factor found in the TME. In primary

melanoma, SOCS2 is expressed by mononuclear phagocytes that infiltrate these cells and is induced by IFN- γ . SOCS2 limits adaptive anti-tumor immunity and DC-based T-cell priming *in vivo*, indicating a critical regulatory role [145].

Other metabolites of the TME, such as lactic acid or reactive oxygen species (ROS), can reduce DC function. Lactic acid is a metabolic product that alters the differentiation and activation of moDCs, for example, by reducing the expression of IL-12 [146]. Several studies have shown that the production of ROS in the TME is associated with epigenetic changes. In one such study, treatment of a colorectal cancer cell line with hydrogen peroxide induced hypermethylation and subsequent silencing of potential tumor suppressor genes such as RUNX3 and CDX1 [147,148]. In another, oxidative damage was found to induce formation and relocalization of a silencing complex, which might explain cancer-specific aberrant DNA methylation and transcriptional silencing [149].

The production of factors released into the TME, such as VEGF, PGE₂, and GM-CSF, pro-inflammatory cytokines such as IL-1 β , IL-6, and TNF, and the peptides S100A8 and S100A9, can influence the differentiation of monocytes that arrive in the TME, where they accumulate and bestow a powerful immunosuppressive capacity, which affects their differentiation into moDCs [150]. These cells are typically defined as myeloid-derived suppressor cells (MDSCs) [151], and may serve as a protective mechanism to prevent excessive tissue damage caused by unresolved immune responses [152]. MDSCs are a heterogeneous population of immature myeloid cells, characterized by the absence of surface markers associated with fully differentiated myeloid cells and by their morphological resemblance to granulocytic and monocytic cells [152]. These cells participate in many aspects of tumor progression, including immune evasion, angiogenesis, pre-metastatic niche formation, and epithelial-mesenchymal transition (EMT). It has been demonstrated that artificial TMEs, made with organotypic skin melanoma cultures (OMCs), prompts the transformation of normal immunostimulatory cDC2s into CD141⁺ DCs, with a phenotype matching their *in vivo* counterparts, and an impaired ability to stimulate T-cell proliferation, which is phenotypically similar to MDSCs [153].

MDSCs extracted from tumors produce secondary products such as ARG1, inducible nitric oxide synthase (iNOS), and ROS, that suppress the antitumor T response [154–156]. Additionally, it has been recently described that HMT SETD1B, which methylates histone H3 at Lys4, is responsible for iNOS upregulation in MDSCs [157]. Furthermore, pathways involved in cell trafficking and immunosuppression, including Wnt signaling, IL-6, and MAPK, are upregulated in MDSCs [158]. MDSCs also participate in tumor immune tolerance by generating Tregs through the secretion of TGF- β and IL-10 [159]. Cancer cells can also change the epigenome of MDSCs with respect to the expression of IL-6, whereby Krüppel-like factor 4, a transcription factor with zinc fingers, regulates the production of IL-6 in DCs through the acetylation of histones [160], thereby modifying the pattern of Treg accumulation.

Tetrahydrocannabinol, an exogenous cannabinoid, mediates epigenetic changes to promote MDSC differentiation and function, by a process in which S100A8 is closely involved [161]. miRNAs are other epigenetic marks that can regulate differentiation to MDSCs. For instance, the expression of STAT3 in MDSCs is modulated by miR-17-5p and miR-20a, which are usually negatively regulated [162].

Furthermore, our group has shown that the generation of monocytic MDSCs mediated by PGE₂ depends on the upregulation of DNMT3A [163]. Comparison of the MDSC and DC DNA methylomes reveals specific gains in DNA methylation and repression of immunogenic-associated genes in MDSCs. Downregulation of DNMT3A in MDSCs abrogates the specific MDSC-specific hypermethylation and abolishes its immunosuppressive activity [163]. HDAC11 has been shown to regulate IL-10 gene expression in myeloid cells, [164]. This was demonstrated as tumor-bearing HDAC11-knockout mice presented an increased number of MDSCs compared to wild-type (WT) tumor-bearing control mice [164]. Finally, the use of DNMT3A-specific siRNAs can also restore the suppressor phenotype of MDSCs, demonstrating the influence of methylation on the acquisition of an immunosuppressed phenotype in a tumor environment [163].

7. Epigenetic Modifications in Dendritic Cells in Cancer Immunotherapy

DCs have properties that make them good candidates for generating tumor vaccines. Among the mechanisms most commonly used to produce cancer vaccines are the exposure of DCs to TAAs from cancer cell lysates [165]. Sipuleucel-T (Provenge) is the only DC-based vaccine to have been approved for use so far [166]. It consists of autologous blood DCs loaded with a recombinant fusion TAA composed of prostatic acid phosphatase and GM-CSF.

It might be possible to exploit the knowledge acquired regarding the effects of tumor cells on the epigenetic profiles of DCs to improve them for use in tumor immunotherapy. One of the most important properties of DCs that enables them to exhibit an anti-tumorigenic phenotype is their migration capacity, which arises from the expression of the CCR7 gene, along with the expression of IL-12. As explained earlier, cDC1 plays an integral role in tumor immunity and is a promising cell type for the development of DC-based vaccines. However, no clinical trials have used ex vivo-derived cDC1 for adoptive cell transfer, largely as they are very scarce in blood, accounting for fewer than 1% of PBMCs, and also as they are difficult to obtain ex vivo in such a way as to maintain their functional phenotype. The latter problem can be attributed to several factors, including the different patterns of antigen expression arising from the heterogeneity of the tumor, the low levels of tumor-infiltrated lymphocytes (TILs), and the evolution of different immunosuppressive mechanisms as the tumor develops [167].

Many attempts have been made to apply the use of cDC1 cells to design strategies to fight tumors. One of the strategies used involves differentiating precursor cells, such as those in BM culture treated with Flt3L, to develop a mixture of cells that resemble pDCs, cDC1, and cDC2 DCs [168]. A consideration of epigenetics is important for acquiring these DCs from BM, since stimulation with GM-CSF increases the expression of the *Pdcd11g2* gene, which is accompanied by increases in PU.1 binding and histone acetylation. The participation of PU.1, IRF4, and p300 in mouse splenic DCs has also been noted [169]. However, the DCs obtained do not express the typical cDC1 markers. Kirkling et al. treated monolayer murine BM precursor cells for three days with FLT3L, OP9-DL1 resulting in cells expressing typical cDC1 markers such as CD103, CD24, DEC205, and CD8a. The transcriptome of the derived cells has a similar pattern to that of cDC1 purified from the spleen. These cells led to better vaccination outcomes since, when loaded with ovalbumin, they improve survival. These results may be partially attributed to the better migration of the resulting cDC1 to the lymphatic ganglia, as these also have a higher expression level of the *ccr7* gene, the encoding protein of which guides DCs to the lymph nodes [170,171] (Figure 2A).

In recent years, epigenetic therapies have been considered a promising option in the fight against cancer, where they can be used to improve cancer vaccines. For example, during the activation of DCs with LPS, HDMs such as KDM6B (JMJD3) and KDM4D (JMJD2D) eliminate the repressive marks H3K27me3 and H3K9me3, thereby regulating pro-inflammatory genes and stimulating inflammation. [172,173]. In this fashion, the intratumoral activation of HMT KDM6B or HDM KDM4D could be considered important for promoting local DC activity. Another example is the use of EPZ004777, which reduces the levels of H3K79me2, to improve the function of DCs in TME. This causes a drop in the level of expression of the Forkhead box M1 transcription factor (FOXM1), which is a proliferation-associated transcription factor involved in tumorigenesis through the transcriptional regulation of its target genes in various cells, including DCs. In the case of pancreatic and colon cancers, FOXM1 has an immunosuppressive role through impaired DC maturation [174]. One study reported that the low-dose combination of two FDA-approved epipharmaeaceuticals, the DNMT inhibitor (DNMTi) 5-azacytidine and the HDAC inhibitor (HDACi) romidepsin, with IFN- α limits the aggressiveness of colorectal cancer stem and metastatic cells in vivo and triggers immunogenic cell death signals that stimulate DCs function and increase their migratory capacity [175].

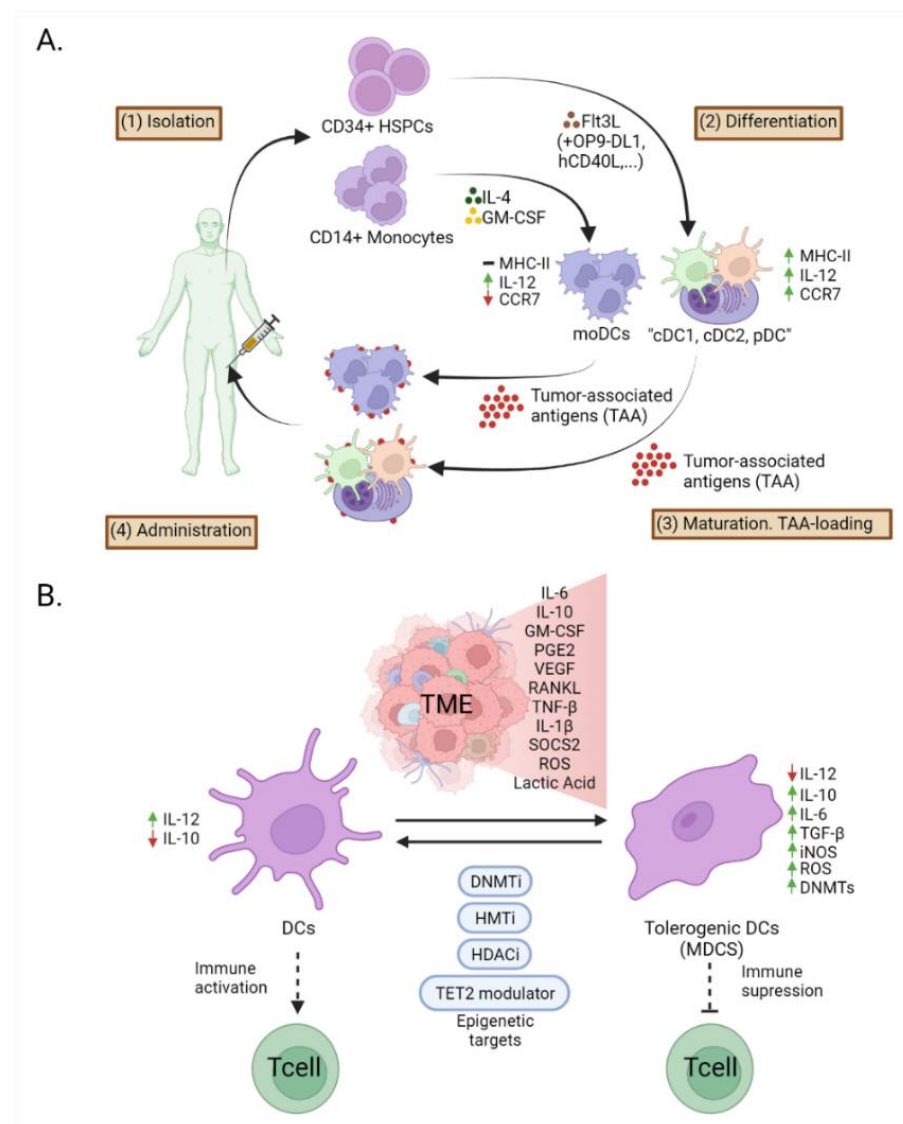


Figure 2. (A). Methods used for DC-based cancer vaccines. Black arrows indicate conventional manufacturing steps. CD34+ haematopoietic stem progenitor cells (HSPCs) are isolated from cancer patients and differentiated into and conventional type 1 DC (cDC1), conventional type 2 DC (cDC2), and plasmacytoid DC (pDC) like cells with Flt3L together with other to improve the resulting DCs. CD14+ monocytes are isolated and differentiated and monocyte-derived dendritic cells (moDCs) with IL-4 and GM-CSF. moDC presents low antigen presentation and low migration capacity, together with the expression of interleukine-12 (IL-12) and the cDC1, cDC2 and pDC like cells present better migration capacity, antigen presentation and produce cytokine like IL-12 and interferon (IFN)- α . DCs are then loaded with tumor-associated antigens (TAAs) and administrated again to the cancer patient. (B). Soluble factor and exosomes secreted in the tumor microenvironment (TME), including IL-6, IL-10, granulocyte-macrophage colony-stimulating factor (GM-CSF), prostaglandin E2 (PGE2), vascular endothelial growth factor (VEGF), RANKL, tumor necrosis factor (TNF)- β , IL-1 β , cytokine-2 suppressor protein (SOCS2), reactive oxygen species (ROS) and lactic acid, dendritic cells acquire an immune tolerance phenotype. The resultant cells, present low expression of IL-12 but increase expression of IL-10, IL-6, TGF- β , nitric oxide synthase (iNOS), ROS and also present more expression of DNA methyltransferases (DNMTs). This process can be reverted by targeting epigenetic enzymes like ten-eleven translocation (TET)-2, DNA methyltransferases (DNMTs), histone deacetylases (HDACs), histone methyltransferases (HMTs). Created with [BioRender.com](https://www.biorender.com) (accessed on 24 January 2022).

One of the most common strategies aims to improve migration capacity through the expression of *CCR7*. This emerged from a study, in which the overexpression of *CCR7* improved accumulation in the lymph nodes that drain tumors [176]. An attempt has recently been made to improve the bone marrow-derived DCs (BM-DCs) by targeting $\beta 2$ -integrin. The latter are a family of heterodimeric adhesion receptors with a common $\beta 2$ chain (CD18). $\beta 2$ -integrins are expressed by leukocytes and are involved in immune synapse formation, phagocytosis, and adhesion. BM-DCs that express dysfunctional $\beta 2$ -integrin have enhanced tumor rejection capabilities in B16.OVA and B16-F10 melanoma models and higher levels of expression of CD86, *Il12*, *CCR7*, and *Fcscn1*, which are indicative of improved co-stimulation and migration capacity. These changes were associated with epigenetic changes such as overall increases in both chromatin accessibility and levels of histone H3K4me3/H3K27me3 methylation. These changes were in turn related to transcription factors such as *Ikaros* and *RelA* [177]. Deletion of microRNA-155 (miR-155) in BM-derived moDCs in mice increases H3K27me3 levels, leading to transcriptional repression of *CCR7* [178]. This also impairs DC maturation and IL-12 secretion [178], with miR-155 proving to be a possible target with which to improve moDC therapies. However, the role of miR-155 has not been studied in cDC1; addressing this would open a new area of study. Finally, it has recently been reported that once cDCs have performed antigen presentation, they increase the expression of *CCR7* and their capacity to migrate to the lymph nodes, thereby also increasing their antigenic capacity [179]. The same study also noted that the upregulated genes in these so-called post-synaptic DCs were epigenetically regulated as their accessibility increased. The authors describe a previously unknown population of DCs whose transcriptomics, epigenomics, and migratory capacity change in response to their cognate contact with T cells [179].

Another possible strategy to improve DC-based vaccines is to improve their antigen presentation capacity. In this regard, it has been seen that vitamin C (VitC) modulates anticancer immune responses and, in turn, is a cofactor of TET2 [180]. In a recent study, it was shown that VitC treatment not only enhances the cytotoxic activity of adoptively transferred CD8⁺ T cells, but also cooperates with immune checkpoint therapy (ICT) in various types of cancer [181]. A possible field of study would be to study the effects of VitC on DCs since this could improve the ability of DCs to present tumor antigens to CD8⁺ T cells through the specific demethylation of certain genes.

As previously mentioned, the biggest concern is the scarcity of cDCs in BM-derived cells. In this context, a therapy based on moDCs is a promising alternative. One property that makes the moDC type special is that GM-CSF-induced moDCs can also be used as a vaccine when they are matured *ex vivo* with CD40 ligand, IFN- γ , and/or TLR agonists. moDCs have a limited capacity to cross-present antigens or to migrate to the lymph nodes. Some phase III clinical trials of the use of moDCs in treating uveal melanoma (NCT01983748), castration-resistant prostate cancer (NCT02111577), and metastatic colorectal cancer (NCT02503150), are currently underway. Preliminary results from a large trial (NCT00045968) of a moDC-based vaccine loaded with autologous tumor lysates have shown that this treatment is feasible and safe in glioblastoma patients. Similarly, intratumoral and intranodal administration is known to induce an equivalent immune response and efficacy in breast cancer patients treated with moDCs [182] (Figure 2A).

Finally, epigenetics can also be used to improve the immune response of cells that are already affected by TME-like MDSCs, which are a potential target for cancer therapy. However, the low TLR-mediated activation capacity of MDSCs makes their use in immunotherapy challenging. Several clinical trials that use MDSCs as a target in a variety of cancer types including leukemia, breast cancer, melanoma, and glioblastoma, are underway. These therapies involve targets like *Arg1*, *iNOS*, *STAT3*, *CD36*, and *CXCR2* [159]. There are also therapies undergoing phase I/II clinical trials targeting MDSCs that indirectly inhibit HDACs by using atezolizumab (NCT03024437). HAT CBP/P300 promotes the suppressor function of MDSCs by increasing the levels of H3K27Ac in promoters and enhancers of proto-tumor genes. Its inhibition hampers its suppressive activity in the

colon carcinoma model [183]. In addition, HDACi entinostat class I is reported to have antitumoral properties since it has been shown to neutralize MDSCs through epigenetic reprogramming in mouse models of breast, pancreatic, and renal cell cancer [184,185]. Liu et al. reported a deregulated miR-148a/DNMT1/SOCS1 axis as being a unique mechanism for stimulating buffered TLR in MDSCs. They determined that miR-148a was elevated in MDSC polyinosinic-polycytidylic acid (poly I: C) or that DC maturation was induced by LPS by the direct suppression of the DNMT1 gene, which consequently led to hypomethylation and thereby upregulation of SOCS1, the suppressor of TLR signaling [186]. Finally, Orillion et al. found that the application of the HDACi entinostat reduces the levels of MDSC-associated chemoattractants and MDSC suppressive activity, and enhanced the efficacy of anti-PD-1 therapy [184] (Figure 2B).

Although several studies have demonstrated the value of DC and MDSC epigenetics in improving cancer vaccines, this is still a matter that warrants further exploration.

8. Conclusions

DCs play a fundamental role in the response to tumors. However, the TME produces a number of factors that can modulate DCs immune response, thereby acquiring an immunosuppressive phenotype that allows tumor growth. Recent evidence has shown the fundamental role of epigenetics in the regulation of DCs, both in their differentiation and in their recruitment in the TME, as well as in the response against cancer cells in the TME. It is important to note that there are different types of DCs, including cDC1, cDC2, pDC and moDCs, and each one has a different role in the immune response against the tumor, either by migrating to the lymph node and activating the effective T cells, or in the maintenance of the immune response within the tumor. Epigenetic regulation in the various DC subtypes by itself may elicit more robust antitumor immunity as an interventional approach. However, the different factors secreted by the tumor can cause these DCs to acquire a tolerogenic phenotype, allowing tumor growth. In this case, epigenetics is also playing a fundamental role in this transition. Therefore, a rational strategy to further increase immunotherapeutic efficacy is to combine certain epigenetic regulators to improve DC-based vaccines for cancer or drugs that reverse the tolerogenic phenotype acquired by DCs under the influence of the tumor microenvironment.

Author Contributions: G.G.-T. and E.B. conceived and wrote the article. All authors have read and agreed to the published version of the manuscript.

Funding: Our research is funded by the Spanish Ministry of Science and Innovation (MICINN; grant number PID2020-117212RB-I00; AEI/10.13038/501100011033).

Acknowledgments: We thank the CERCA Programme/Generalitat de Catalunya and the Josep Carreras Foundation for institutional support.

Conflicts of Interest: The authors declare no conflict of interest.

References

1. Quail, D.F.; Joyce, J.A. Microenvironmental regulation of tumor progression and metastasis. *Nat. Med.* **2013**, *19*, 1423–1437. [[CrossRef](#)] [[PubMed](#)]
2. Janco, J.M.T.; Lamichhane, P.; Karyampudi, L.; Knutson, K.L. Tumor-Infiltrating Dendritic Cells in Cancer Pathogenesis. *J. Immunol.* **2015**, *194*, 2985–2991. [[CrossRef](#)]
3. Ugel, S.; De Sanctis, F.; Mandruzzato, S.; Bronte, V. Tumor-induced myeloid deviation: When myeloid-derived suppressor cells meet tumor-associated macrophages. *J. Clin. Investig.* **2015**, *125*, 3365–3376. [[CrossRef](#)]
4. Alvarez-Errico, D.; Vento-Tormo, R.; Sieweke, M.; Ballestar, E. Epigenetic control of myeloid cell differentiation, identity and function. *Nat. Rev. Immunol.* **2015**, *15*, 7–17. [[CrossRef](#)] [[PubMed](#)]
5. Ivashkiv, L.B.; Park, S.H. Epigenetic Regulation of Myeloid Cells. *Microbiol. Spectr.* **2016**, *4*, 571–590. [[CrossRef](#)]
6. Roulois, D.; Loo Yau, H.; Singhanian, R.; Wang, Y.; Danesh, A.; Shen, S.Y.; Han, H.; Liang, G.; Jones, P.A.; Pugh, T.J.; et al. DNA-Demethylating Agents Target Colorectal Cancer Cells by Inducing Viral Mimicry by Endogenous Transcripts. *Cell* **2015**, *162*, 961–973. [[CrossRef](#)] [[PubMed](#)]
7. Okano, M.; Bell, D.W.; Haber, D.A.; Li, E. DNA Methyltransferases Dnmt3a and Dnmt3b Are Essential for De Novo Methylation and Mammalian Development. *Cell* **1999**, *99*, 247–257. [[CrossRef](#)]

8. Shen, L.; Wu, H.; Diep, D.; Yamaguchi, S.; D'Alessio, A.C.; Fung, H.-L.; Zhang, K.; Zhang, Y. Genome-wide Analysis Reveals TET- and TDG-Dependent 5-Methylcytosine Oxidation Dynamics. *Cell* **2013**, *153*, 692–706. [[CrossRef](#)]
9. Wajed, S.A.; Laird, P.W.; Demeester, T.R. DNA Methylation: An Alternative Pathway to Cancer. *Ann. Surg.* **2001**, *234*, 10–20. [[CrossRef](#)]
10. Bannister, A.J.; Kouzarides, T. Regulation of chromatin by histone modifications. *Cell Res.* **2011**, *21*, 381–395. [[CrossRef](#)]
11. Mattick, J.S.; Makunin, I.V. Non-coding RNA. *Hum. Mol. Genet.* **2006**, *15*, R17–R29. [[CrossRef](#)] [[PubMed](#)]
12. Bartel, D.P. MicroRNAs: Genomics, Biogenesis, Mechanism, and Function. *Cell* **2004**, *116*, 281–297. [[CrossRef](#)]
13. Eichhorn, S.W.; Guo, H.; McGeary, S.E.; Rodriguez-Mias, R.A.; Shin, C.; Baek, D.; Hsu, S.-H.; Ghoshal, K.; Villén, J.; Bartel, D.P. mRNA Destabilization Is the Dominant Effect of Mammalian MicroRNAs by the Time Substantial Repression Ensues. *Mol. Cell* **2014**, *56*, 104–115. [[CrossRef](#)] [[PubMed](#)]
14. Birnberg, T.; Bar-On, L.; Sapozhnikov, A.; Caton, M.L.; Cervantes-Barragán, L.; Makia, D.; Krauthgamer, R.; Brenner, O.; Ludewig, B.; Brockschneider, D.; et al. Lack of Conventional Dendritic Cells Is Compatible with Normal Development and T Cell Homeostasis, but Causes Myeloid Proliferative Syndrome. *Immunity* **2008**, *29*, 986–997. [[CrossRef](#)]
15. Hildner, K.; Edelson, B.T.; Purtha, W.E.; Diamond, M.; Matsushita, H.; Kohyama, M.; Calderon, B.; Schraml, B.U.; Unanue, E.R.; Diamond, M.S.; et al. Batf3 Deficiency Reveals a Critical Role for CD8 α + Dendritic Cells in Cytotoxic T Cell Immunity. *Science* **2008**, *322*, 1097–1100. [[CrossRef](#)]
16. Cella, M.; Salio, M.; Sakakibara, Y.; Langen, H.; Julkunen, I.; Lanzavecchia, A. Maturation, Activation, and Protection of Dendritic Cells Induced by Double-stranded RNA. *J. Exp. Med.* **1999**, *189*, 821–829. [[CrossRef](#)]
17. Zhang, X.; Ulm, A.; Sominen, H.K.; Oh, S.; Weirauch, M.T.; Zhang, H.-X.; Chen, X.; Lehn, A.M.; Janssen, E.M.; Ji, H. DNA methylation dynamics during ex vivo differentiation and maturation of human dendritic cells. *Epigenet. Chromatin* **2014**, *7*, 21. [[CrossRef](#)]
18. Yi, L.; Li, Z.; Hu, T.; Liu, J.; Li, N.; Cao, X.; Liu, S. Intracellular HSP70L1 inhibits human dendritic cell maturation by promoting suppressive H3K27me3 and H2AK119Ub1 histone modifications. *Cell. Mol. Immunol.* **2019**, *17*, 85–94. [[CrossRef](#)]
19. Boukhaled, G.M.; Cordeiro, B.; Deblois, G.; Dimitrov, V.; Bailey, S.D.; Holowka, T.; Domi, A.; Guak, H.; Chiu, H.-H.; Everts, B.; et al. The Transcriptional Repressor Polycomb Group Factor 6, PCGF6, Negatively Regulates Dendritic Cell Activation and Promotes Quiescence. *Cell Rep.* **2016**, *16*, 1829–1837. [[CrossRef](#)]
20. Reis e Sousa, C. Toll-like receptors and dendritic cells: For whom the bug tolls. *Semin. Immunol.* **2004**, *16*, 27–34. [[CrossRef](#)]
21. Scharer, C.; Barwick, B.; Youngblood, B.; Ahmed, R.; Boss, J.M. Global DNA Methylation Remodeling Accompanies CD8 T Cell Effector Function. *J. Immunol.* **2013**, *191*, 3419–3429. [[CrossRef](#)] [[PubMed](#)]
22. Ladle, B.H.; Li, K.-P.; Phillips, M.J.; Pucsek, A.B.; Haile, A.; Powell, J.D.; Jaffee, E.M.; Hildeman, D.A.; Gamper, C.J. De novo DNA methylation by DNA methyltransferase 3a controls early effector CD8+ T-cell fate decisions following activation. *Proc. Natl. Acad. Sci. USA* **2016**, *113*, 10631–10636. [[CrossRef](#)] [[PubMed](#)]
23. Russ, B.E.; Olshanksky, M.; Smallwood, H.S.; Li, J.; Denton, A.; Prier, J.; Stock, A.T.; Croom, H.A.; Cullen, J.G.; Nguyen, M.L.; et al. Distinct Epigenetic Signatures Delineate Transcriptional Programs during Virus-Specific CD8+ T Cell Differentiation. *Immunity* **2014**, *41*, 853–865. [[CrossRef](#)] [[PubMed](#)]
24. Araki, Y.; Wang, Z.; Zang, C.; Wood, W.H.; Schones, D.; Cui, K.; Roh, T.-Y.; Lhotsky, B.; Wersto, R.P.; Peng, W.; et al. Genome-wide Analysis of Histone Methylation Reveals Chromatin State-Based Regulation of Gene Transcription and Function of Memory CD8+ T Cells. *Immunity* **2009**, *30*, 912–925. [[CrossRef](#)] [[PubMed](#)]
25. Nussenzweig, M.C.; Steinman, R.M.; Gutchinov, B.; Cohn, A.Z. Dendritic cells are accessory cells for the development of anti-trinitrophenyl cytotoxic T lymphocytes. *J. Exp. Med.* **1980**, *152*, 1070–1084. [[CrossRef](#)]
26. Mildner, A.; Jung, S. Development and Function of Dendritic Cell Subsets. *Immunity* **2014**, *40*, 642–656. [[CrossRef](#)]
27. Joffre, O.; Segura, E.; Savina, A.; Amigorena, S. Cross-presentation by dendritic cells. *Nat. Rev. Immunol.* **2012**, *12*, 557–569. [[CrossRef](#)]
28. Merad, M.; Sathe, P.; Helft, J.; Miller, J.; Mortha, A. The Dendritic Cell Lineage: Ontogeny and Function of Dendritic Cells and Their Subsets in the Steady State and the Inflamed Setting. *Annu. Rev. Immunol.* **2013**, *31*, 563–604. [[CrossRef](#)]
29. Collin, M.; Bigley, V. Human dendritic cell subsets: An update. *Immunology* **2018**, *154*, 3–20. [[CrossRef](#)]
30. Ferris, S.T.; Durai, V.; Wu, R.; Theisen, D.J.; Ward, J.; Bern, M.D.; Iv, J.T.D.; Bagadia, P.; Liu, T.; Briseño, C.G.; et al. cDC1 prime and are licensed by CD4+ T cells to induce anti-tumour immunity. *Nature* **2020**, *584*, 624–629. [[CrossRef](#)]
31. Binnewies, M.; Mujal, A.M.; Pollack, J.L.; Combes, A.J.; Hardison, E.A.; Barry, K.C.; Tsui, J.; Ruhland, M.K.; Kersten, K.; Abushawish, M.A.; et al. Unleashing Type-2 Dendritic Cells to Drive Protective Antitumor CD4+ T Cell Immunity. *Cell* **2019**, *177*, 556–571. [[CrossRef](#)] [[PubMed](#)]
32. Grajales-Reyes, G.E.; Iwata, A.; Albring, J.C.; Wumesh, K.C.; Tussiwand, R.; Kc, W.; Kretzer, N.M.; Brisenno, C.; Durai, V.; Bagadia, P.; et al. Batf3 maintains autoactivation of Irf8 for commitment of a CD8 α + conventional DC clonogenic progenitor. *Nat. Immunol.* **2015**, *16*, 708–717. [[CrossRef](#)] [[PubMed](#)]
33. Murphy, T.L.; Grajales-Reyes, G.E.; Wu, X.; Tussiwand, R.; Briseño, C.G.; Iwata, A.; Kretzer, N.M.; Durai, V.; Murphy, K.M. Transcriptional Control of Dendritic Cell Development. *Annu. Rev. Immunol.* **2016**, *34*, 93–119. [[CrossRef](#)] [[PubMed](#)]
34. Schlitzer, A.; McGovern, N.; Teo, P.; Zelante, T.; Atarashi, K.; Low, D.; Ho, A.W.S.; See, P.; Shin, A.; Wasan, P.S.; et al. IRF4 Transcription Factor-Dependent CD11b+ Dendritic Cells in Human and Mouse Control Mucosal IL-17 Cytokine Responses. *Immunity* **2013**, *38*, 970–983. [[CrossRef](#)] [[PubMed](#)]

35. Williams, J.W.; Tjota, M.Y.; Clay, B.S.; Vander Lugt, B.; Bandukwala, H.S.; Hrusch, C.L.; Decker, D.C.; Blaine, K.M.; Fixsen, B.R.; Singh, H.; et al. Transcription factor IRF4 drives dendritic cells to promote Th2 differentiation. *Nat. Commun.* **2013**, *4*, 2990. [[CrossRef](#)]
36. Kurotaki, D.; Kawase, W.; Sasaki, H.; Nakabayashi, J.; Nishiyama, A.; Morse, H.C.; Ozato, K.; Suzuki, Y.; Tamura, T. Epigenetic control of early dendritic cell lineage specification by the transcription factor IRF8 in mice. *Blood* **2019**, *133*, 1803–1813. [[CrossRef](#)] [[PubMed](#)]
37. Chopin, M.; Lun, A.T.; Zhan, Y.; Schreuder, J.; Coughlan, H.; D’Amico, A.; Mielke, L.; Almeida, F.F.; Kueh, A.J.; Dickins, R.; et al. Transcription Factor PU.1 Promotes Conventional Dendritic Cell Identity and Function via Induction of Transcriptional Regulator DC-SCRIPT. *Immunity* **2019**, *50*, 77–90. [[CrossRef](#)]
38. Won, H.; Nandakumar, V.; Yates, P.; Sanchez, S.; Jones, L.; Huang, X.F.; Chen, S.-Y. Epigenetic control of dendritic cell development and fate determination of common myeloid progenitor by Mysz1. *Blood* **2014**, *124*, 2647–2656. [[CrossRef](#)] [[PubMed](#)]
39. Lin, Q.; Chauvistré, H.; Costa, I.G.; Gusmao, E.G.; Mitzka, S.; Hänzelmann, S.; Baying, B.; Klisch, T.; Moriggl, R.; Hennuy, B.; et al. Epigenetic program and transcription factor circuitry of dendritic cell development. *Nucleic Acids Res.* **2015**, *43*, 9680–9693. [[CrossRef](#)]
40. Rodrigues, P.; Alberti-Servera, L.; Eremin, A.; Grajales-Reyes, G.E.; Ivanek, R.; Tussiwand, R. Distinct progenitor lineages contribute to the heterogeneity of plasmacytoid dendritic cells. *Nat. Immunol.* **2018**, *19*, 711–722. [[CrossRef](#)]
41. Dress, R.J.; Dutertre, C.-A.; Giladi, A.; Schlitzer, A.; Low, I.; Shadan, N.B.; Tay, A.; Lum, J.; Kairi, M.F.B.M.; Hwang, Y.Y.; et al. Plasmacytoid dendritic cells develop from Ly6D+ lymphoid progenitors distinct from the myeloid lineage. *Nat. Immunol.* **2019**, *20*, 852–864. [[CrossRef](#)] [[PubMed](#)]
42. Reizis, B. Plasmacytoid Dendritic Cells: Development, Regulation, and Function. *Immunity* **2019**, *50*, 37–50. [[CrossRef](#)] [[PubMed](#)]
43. Ye, Y.; Gaugler, B.; Mohty, M.; Malard, F. Plasmacytoid dendritic cell biology and its role in immune-mediated diseases. *Clin. Transl. Immunol.* **2020**, *9*, 1139. [[CrossRef](#)]
44. Musumeci, A.; Lutz, K.; Winheim, E.; Krug, A.B. What Makes a pDC: Recent Advances in Understanding Plasmacytoid DC Development and Heterogeneity. *Front. Immunol.* **2019**, *10*, 1222. [[CrossRef](#)] [[PubMed](#)]
45. Sichien, D.; Scott, C.; Martens, L.; Vanderkerken, M.; Van Gassen, S.; Plantinga, M.; Joeris, T.; De Prijck, S.; Vanhoutte, L.; Vanheerswynghels, M.; et al. IRF8 Transcription Factor Controls Survival and Function of Terminally Differentiated Conventional and Plasmacytoid Dendritic Cells, Respectively. *Immunity* **2016**, *45*, 626–640. [[CrossRef](#)] [[PubMed](#)]
46. Ghosh, H.S.; Cisse, B.; Bunin, A.; Lewis, K.L.; Reizis, B. Continuous Expression of the Transcription Factor E2-2 Maintains the Cell Fate of Mature Plasmacytoid Dendritic Cells. *Immunity* **2010**, *33*, 905–916. [[CrossRef](#)]
47. Schiavoni, G.; Mattei, F.; Sestili, P.; Borghi, P.; Venditti, M.; Morse, H.; Belardelli, F.; Gabriele, L. ICSBP Is Essential for the Development of Mouse Type I Interferon-producing Cells and for the Generation and Activation of CD8 α + Dendritic Cells. *J. Exp. Med.* **2002**, *196*, 1415–1425. [[CrossRef](#)]
48. Chauvistré, H.; Küstermann, C.; Rehage, N.; Klisch, T.; Mitzka, S.; Felker, P.; Rose-John, S.; Zenke, M.; Seré, K.M. Dendritic cell development requires histone deacetylase activity. *Eur. J. Immunol.* **2014**, *44*, 2478–2488. [[CrossRef](#)]
49. Schlitzer, A.; McGovern, N.; Ginhoux, F. Dendritic cells and monocyte-derived cells: Two complementary and integrated functional systems. *Semin. Cell Dev. Biol.* **2015**, *41*, 9–22. [[CrossRef](#)]
50. Mildner, A.; Yona, S.; Jung, S. A Close Encounter of the Third Kind. *Adv. Immunol.* **2013**, *120*, 69–103. [[CrossRef](#)]
51. Bosteels, C.; Neyt, K.; Vanheerswynghels, M.; van Helden, M.J.; Sichien, D.; Debeuf, N.; De Prijck, S.; Bosteels, V.; Vandamme, N.; Martens, L.; et al. Inflammatory Type 2 cDCs Acquire Features of cDC1s and Macrophages to Orchestrate Immunity to Respiratory Virus Infection. *Immunity* **2020**, *52*, 1039–1056. [[CrossRef](#)]
52. Naik, S.H.; Sathe, P.; Park, H.-Y.; Metcalf, D.; Proietto, I.A.; Dakic, A.; Carotta, S.; O’Keeffe, M.; Bahlo, M.; Papenfuss, A.; et al. Development of plasmacytoid and conventional dendritic cell subtypes from single precursor cells derived in vitro and in vivo. *Nat. Immunol.* **2007**, *8*, 1217–1226. [[CrossRef](#)] [[PubMed](#)]
53. Meredith, M.M.; Liu, K.; Darrasse-Jeze, G.; Kamphorst, A.O.; Schreiber, H.A.; Guermonprez, P.; Idoyaga, J.; Cheong, C.; Yao, K.-H.; Niec, R.; et al. Expression of the zinc finger transcription factor zDC (Zbtb46, Btbd4) defines the classical dendritic cell lineage. *J. Exp. Med.* **2012**, *209*, 1153–1165. [[CrossRef](#)] [[PubMed](#)]
54. Sallusto, F.; Lanzavecchia, A. Efficient presentation of soluble antigen by cultured human dendritic cells is maintained by granulocyte/macrophage colony-stimulating factor plus interleukin 4 and downregulated by tumor necrosis factor alpha. *J. Exp. Med.* **1994**, *179*, 1109–1118. [[CrossRef](#)]
55. Vento-Tormo, R.; Company, C.; Rodríguez-Ubrevia, J.; De La Rica, L.; Urquiza, J.M.; Javierre, B.M.; Sabarinathan, R.; Luque, A.; Esteller, M.; Aran, J.M.; et al. IL-4 orchestrates STAT6-mediated DNA demethylation leading to dendritic cell differentiation. *Genome Biol.* **2016**, *17*, 4. [[CrossRef](#)]
56. Nencioni, A.; Beck, J.; Werth, D.; Grünebach, F.; Patrone, F.; Ballestrero, A.; Brossart, P. Histone Deacetylase Inhibitors Affect Dendritic Cell Differentiation and Immunogenicity. *Clin. Cancer Res.* **2007**, *13*, 3933–3941. [[CrossRef](#)] [[PubMed](#)]
57. Gajewski, T.F.; Schreiber, H.; Fu, Y.-X. Innate and adaptive immune cells in the tumor microenvironment. *Nat. Immunol.* **2013**, *14*, 1014–1022. [[CrossRef](#)]
58. Jerby-Aron, L.; Shah, P.; Cuoco, M.; Rodman, C.; Su, M.-J.; Melms, J.; Leeson, R.; Kanodia, A.; Mei, S.; Lin, J.-R.; et al. A Cancer Cell Program Promotes T Cell Exclusion and Resistance to Checkpoint Blockade. *Cell* **2018**, *175*, 984–997. [[CrossRef](#)]

59. Kumar, V.; Ramnarayanan, K.; Sundar, R.; Padmanbhan, N.; Srivastava, S.; Koiwa, M.; Yasuda, T.; Koh, V.; Huang, K.K.; Tay, S.T.; et al. Single-cell atlas of lineage states, tumor microenvironment and subtype-specific expression programs in gastric cancer. *Cancer Discov.* **2021**. [[CrossRef](#)]
60. Massalha, H.; Halpern, K.B.; Abu-Gazala, S.; Jana, T.; Massasa, E.E.; Moor, E.A.; Buchauer, L.; Rozenberg, M.; Pikarsky, E.; Amit, I.; et al. A single cell atlas of the human liver tumor microenvironment. *Mol. Syst. Biol.* **2020**, *16*, e9682. [[CrossRef](#)]
61. Engblom, C.; Pflirschke, C.; Pittet, M.J. The role of myeloid cells in cancer therapies. *Nat. Rev. Cancer* **2016**, *16*, 447–462. [[CrossRef](#)] [[PubMed](#)]
62. Garris, C.S.; Luke, J.J. Dendritic Cells, the T-cell-inflamed Tumor Microenvironment, and Immunotherapy Treatment Response. *Clin. Cancer Res.* **2020**, *26*, 3901–3907. [[CrossRef](#)]
63. Perrot, I.; Blanchard, D.; Freymond, N.; Isaac, S.; Guibert, B.; Pacheco, Y.; Lebecque, S. Dendritic Cells Infiltrating Human Non-Small Cell Lung Cancer Are Blocked at Immature Stage. *J. Immunol.* **2007**, *178*, 2763–2769. [[CrossRef](#)]
64. Roberts, E.W.; Broz, M.L.; Binnewies, M.; Headley, M.B.; Nelson, A.E.; Wolf, D.M.; Kaisho, T.; Bogunovic, D.; Bhardwaj, N.; Krummel, M.F. Critical Role for CD103⁺/CD141⁺ Dendritic Cells Bearing CCR7 for Tumor Antigen Trafficking and Priming of T Cell Immunity in Melanoma. *Cancer Cell* **2016**, *30*, 324–336. [[CrossRef](#)] [[PubMed](#)]
65. Salmon, H.; Idoyaga, J.; Rahman, A.; Leboeuf, M.; Remark, R.; Jordan, S.; Casanova-Acebes, M.; Khudoynazarova, M.; Agudo, J.; Tung, N.; et al. Expansion and Activation of CD103⁺ Dendritic Cell Progenitors at the Tumor Site Enhances Tumor Responses to Therapeutic PD-L1 and BRAF Inhibition. *Immunity* **2016**, *44*, 924–938. [[CrossRef](#)] [[PubMed](#)]
66. Villablanca, E.; Raccosta, L.; Zhou, D.; Fontana, R.; Maggioni, D.; Negro, A.; Sanvito, F.; Ponzoni, M.; Valentinis, B.; Bregni, M.; et al. Tumor-mediated liver X receptor- α activation inhibits CC chemokine receptor-7 expression on dendritic cells and dampens antitumor responses. *Nat. Med.* **2010**, *16*, 98–105. [[CrossRef](#)]
67. Sluijter, B.J.; Hout, M.F.V.D.; Koster, B.; Van Leeuwen, P.A.; Schneiders, F.L.; Van De Ven, R.; Molenkamp, B.G.; Vosslamber, S.; Verweij, C.L.; Tol, M.P.V.D.; et al. Arming the Melanoma Sentinel Lymph Node through Local Administration of CpG-B and GM-CSF: Recruitment and Activation of BDCA3/CD141⁺ Dendritic Cells and Enhanced Cross-Presentation. *Cancer Immunol. Res.* **2015**, *3*, 495–505. [[CrossRef](#)] [[PubMed](#)]
68. Wang, P.; Xue, Y.; Han, Y.; Lin, L.; Wu, C.; Xu, S.; Jiang, Z.; Xu, J.; Liu, Q.; Cao, X. The STAT3-Binding Long Noncoding RNA lnc-DC Controls Human Dendritic Cell Differentiation. *Science* **2014**, *344*, 310–313. [[CrossRef](#)]
69. Liu, J.; Zhang, X.; Chen, K.; Cheng, Y.; Liu, S.; Xia, M.; Chen, Y.; Zhu, H.; Li, Z.; Cao, X. CCR7 Chemokine Receptor-Inducible lnc-Dpf3 Restrains Dendritic Cell Migration by Inhibiting HIF-1 α -Mediated Glycolysis. *Immunity* **2019**, *50*, 600–615. [[CrossRef](#)]
70. Ferrara, G.; Benzi, A.; Sturla, L.; Marubbi, D.; Frumento, D.; Spinelli, S.; Abbotto, E.; Ivaldi, F.; Von Holtey, M.; Murone, M.; et al. Sirt6 inhibition delays the onset of experimental autoimmune encephalomyelitis by reducing dendritic cell migration. *J. Neuroinflamm.* **2020**, *17*, 228. [[CrossRef](#)]
71. Tsou, C.-L.; Peters, W.; Si, Y.; Slaymaker, S.; Aslanian, A.M.; Weisberg, S.; Mack, M.; Charo, I.F. Critical roles for CCR2 and MCP-3 in monocyte mobilization from bone marrow and recruitment to inflammatory sites. *J. Clin. Investig.* **2007**, *117*, 902–909. [[CrossRef](#)]
72. Morse, M.A.; Coleman, R.E.; Akabani, G.; Niehaus, N.; Coleman, D.; Lyerly, H.K. Migration of human dendritic cells after injection in patients with metastatic malignancies. *Cancer Res.* **1999**, *59*, 56–58.
73. Shinde, P.; Fernandes, S.; Melinkeri, S.; Kale, V.; Limaye, L. Compromised functionality of monocyte-derived dendritic cells in multiple myeloma patients may limit their use in cancer immunotherapy. *Sci. Rep.* **2018**, *8*, 5705. [[CrossRef](#)] [[PubMed](#)]
74. Moran, T.P.; Nakano, H.; Kondilis-Mangum, H.D.; Wade, P.A.; Cook, N.N. Epigenetic control of Ccr7 expression in distinct lineages of lung dendritic cells. *J. Immunol.* **2014**, *193*, 4904–4913. [[CrossRef](#)] [[PubMed](#)]
75. Williford, J.-M.; Ishihara, J.; Ishihara, A.; Mansurov, A.; Hosseinchi, P.; Marchell, T.M.; Potin, L.; Swartz, M.A.; Hubbell, J.A. Recruitment of CD103⁺ dendritic cells via tumor-targeted chemokine delivery enhances efficacy of checkpoint inhibitor immunotherapy. *Sci. Adv.* **2019**, *5*, eaay1357. [[CrossRef](#)] [[PubMed](#)]
76. Böttcher, J.P.; Bonavita, E.; Chakravarty, P.; Blees, H.; Cabeza-Cabrero, M.; Sammicheli, S.; Rogers, N.C.; Sahai, E.; Zelenay, S.; Reis e Sousa, C. NK Cells Stimulate Recruitment of cDC1 into the Tumor Microenvironment Promoting Cancer Immune Control. *Cell* **2018**, *172*, 1022–1037. [[CrossRef](#)] [[PubMed](#)]
77. Shi, Q.; Shen, L.; Gan, J.; He, L.; Lin, J.; Guo, S.; Xiong, Z.; Lin, J.; Zhang, S. Integrative analysis identifies DNMTs against immune-infiltrating neutrophils and dendritic cells in colorectal cancer. *Epigenetics* **2019**, *14*, 392–404. [[CrossRef](#)]
78. Lodewijk, I.; Nunes, S.P.; Henrique, R.; Jerónimo, C.; Dueñas, M.; Paramio, J.M. Tackling tumor microenvironment through epigenetic tools to improve cancer immunotherapy. *Clin. Epigenet.* **2021**, *13*, 1–24. [[CrossRef](#)]
79. Han, Y.; Liu, D.; Li, L. PD-1/PD-L1 pathway: Current researches in cancer. *Am. J. Cancer Res.* **2020**, *10*, 727–742.
80. Pflirschke, C.; Engblom, C.; Rickelt, S.; Cortez-Retamozo, V.; Garris, C.; Pucci, F.; Yamazaki, T.; Poirier-Colame, V.; Newton, A.; Redouane, Y.; et al. Immunogenic Chemotherapy Sensitizes Tumors to Checkpoint Blockade Therapy. *Immunity* **2016**, *44*, 343–354. [[CrossRef](#)]
81. Spranger, S.; Dai, D.; Horton, B.; Gajewski, T.F. Tumor-Residing Batf3 Dendritic Cells Are Required for Effector T Cell Trafficking and Adoptive T Cell Therapy. *Cancer Cell* **2017**, *31*, 711–723. [[CrossRef](#)] [[PubMed](#)]
82. Sharma, M.D.; Rodriguez, P.C.; Koehn, B.H.; Baban, B.; Cui, Y.; Guo, G.; Shimoda, M.; Pacholczyk, R.; Shi, H.; Lee, E.-J.; et al. Activation of p53 in Immature Myeloid Precursor Cells Controls Differentiation into Ly6c⁺CD103⁺ Monocytic Antigen-Presenting Cells in Tumors. *Immunity* **2018**, *48*, 91–106. [[CrossRef](#)]

83. Noubade, R.; Majri-Morrison, S.; Tarbell, K.V. Beyond cDC1: Emerging Roles of DC Crosstalk in Cancer Immunity. *Front. Immunol.* **2019**, *10*, 1014. [[CrossRef](#)] [[PubMed](#)]
84. Leone, P.; Shin, E.-C.; Perosa, F.; Vacca, A.; Dammacco, F.; Racanelli, V. MHC Class I Antigen Processing and Presenting Machinery: Organization, Function, and Defects in Tumor Cells. *J. Natl. Cancer Inst.* **2013**, *105*, 1172–1187. [[CrossRef](#)] [[PubMed](#)]
85. Luo, N.; Nixon, M.J.; Gonzalez-Ericsson, P.I.; Sanchez, V.; Opalenik, S.R.; Li, H.; Zahnow, C.A.; Nickels, M.L.; Liu, F.; Tantawy, M.N.; et al. DNA methyltransferase inhibition upregulates MHC-I to potentiate cytotoxic T lymphocyte responses in breast cancer. *Nat. Commun.* **2018**, *9*, 1–11. [[CrossRef](#)] [[PubMed](#)]
86. Magner, W.J.; Kazim, A.L.; Stewart, C.; Romano, M.A.; Catalano, G.; Grande, C.; Keiser, N.; Santaniello, F.; Tomasi, T.B. Activation of MHC Class I, II, and CD40 Gene Expression by Histone Deacetylase Inhibitors. *J. Immunol.* **2000**, *165*, 7017–7024. [[CrossRef](#)] [[PubMed](#)]
87. Kortenhorst, M.S.; Wissing, M.D.; Rodriguez, R.; Kachhap, S.K.; Jans, J.; Van Der Groep, P.; Verheul, H.; Gupta, A.; Aiyetan, O.P.; Van Der Wall, E.; et al. Analysis of the genomic response of human prostate cancer cells to histone deacetylase inhibitors. *Epigenetics* **2013**, *8*, 907–920. [[CrossRef](#)] [[PubMed](#)]
88. Gardner, A.; Ruffell, B. Dendritic Cells and Cancer Immunity. *Trends Immunol.* **2016**, *37*, 855–865. [[CrossRef](#)]
89. Antony, P.A.; Piccirillo, C.A.; Akpınarlı, A.; Finkelstein, S.E.; Speiss, P.J.; Surman, D.R.; Palmer, D.; Chan, C.-C.; Klebanoff, C.; Overwijk, W.W.; et al. CD8+T Cell Immunity against a Tumor/Self-Antigen Is Augmented by CD4+T Helper Cells and Hindered by Naturally Occurring T Regulatory Cells. *J. Immunol.* **2005**, *174*, 2591–2601. [[CrossRef](#)]
90. Sun, J.C.; Bevan, M.J. Defective CD8 T Cell Memory Following Acute Infection Without CD4 T Cell Help. *Science* **2003**, *300*, 339–342. [[CrossRef](#)]
91. Ferlazzo, G.; Morandi, B. Cross-Talks between Natural Killer Cells and Distinct Subsets of Dendritic Cells. *Front. Immunol.* **2014**, *5*, 159. [[CrossRef](#)] [[PubMed](#)]
92. Garris, C.S.; Arlauckas, S.P.; Kohler, R.H.; Trefny, M.P.; Garren, S.; Piot, C.; Engblom, C.; Pfirschke, C.; Siwicki, M.; Gungabeesoon, J.; et al. Successful Anti-PD-1 Cancer Immunotherapy Requires T Cell-Dendritic Cell Crosstalk Involving the Cytokines IFN- γ and IL-12. *Immunity* **2018**, *49*, 1148–1161. [[CrossRef](#)] [[PubMed](#)]
93. Chen, K.; Liu, J.; Liu, S.; Xia, M.; Zhang, X.; Han, D.; Jiang, Y.; Wang, C.; Cao, X. Methyltransferase SETD2-Mediated Methylation of STAT1 Is Critical for Interferon Antiviral Activity. *Cell* **2017**, *170*, 492–506. [[CrossRef](#)]
94. Lotze, M.T. Getting to the Source: Dendritic Cells as Therapeutic Reagents for the Treatment of Patients with Cancer. *Ann. Surg.* **1997**, *226*, 1–5. [[CrossRef](#)] [[PubMed](#)]
95. Mattiuz, R.; Brousse, C.; Ambrosini, M.; Cancel, J.; Bessou, G.; Mussard, J.; Sanlaville, A.; Caux, C.; Bendriss-Vermare, N.; Valladeau-Guilemond, J.; et al. Type 1 conventional dendritic cells and interferons are required for spontaneous CD4+ and CD8+ T-cell protective responses to breast cancer. *Clin. Transl. Immunol.* **2021**, *10*, 1305. [[CrossRef](#)]
96. Mikucki, M.E.; Fisher, D.T.; Matsuzaki, J.; Skitzki, J.J.; Gaulin, N.B.; Muhitch, J.B.; Ku, A.W.; Frelinger, J.G.; Odunsi, K.; Gajewski, T.F.; et al. Non-redundant requirement for CXCR3 signalling during tumoricidal T-cell trafficking across tumour vascular checkpoints. *Nat. Commun.* **2015**, *6*, 7458. [[CrossRef](#)]
97. Peng, D.; Kryczek, I.; Nagarsheth, N.; Zhao, L.; Wei, S.; Wang, W.; Sun, Y.; Zhao, E.; Vatan, L.; Szeliga, W.; et al. Epigenetic silencing of TH1-type chemokines shapes tumour immunity and immunotherapy. *Nature* **2015**, *527*, 249–253. [[CrossRef](#)]
98. Bischoff, P.; Trinks, A.; Obermayer, B.; Pett, J.P.; Wiederspahn, J.; Uhlitz, F.; Liang, X.; Lehmann, A.; Jurmeister, P.; Elsner, A.; et al. Single-cell RNA sequencing reveals distinct tumor microenvironmental patterns in lung adenocarcinoma. *Oncogene* **2021**, *40*, 6748–6758. [[CrossRef](#)]
99. Broz, M.L.; Binnewies, M.; Boldajipour, B.; Nelson, A.E.; Pollack, J.L.; Erle, D.J.; Barczak, A.; Rosenblum, M.D.; Daud, A.; Barber, D.L.; et al. Dissecting the Tumor Myeloid Compartment Reveals Rare Activating Antigen-Presenting Cells Critical for T Cell Immunity. *Cancer Cell* **2014**, *26*, 638–652. [[CrossRef](#)]
100. Cachot, A.; Bilous, M.; Liu, Y.-C.; Li, X.; Saillard, M.; Cenerenti, M.; Rockinger, G.A.; Wyss, T.; Guillaume, P.; Schmidt, J.; et al. Tumor-specific cytolytic CD4 T cells mediate immunity against human cancer. *Sci. Adv.* **2021**, *7*, eabe3348. [[CrossRef](#)]
101. Sommermeyer, D.; Hudecek, M.; Kosasih, P.L.; Gogishvili, T.; Maloney, D.G.; Turtle, C.J.; Riddell, S.R. Chimeric antigen receptor-modified T cells derived from defined CD8+ and CD4+ subsets confer superior antitumor reactivity in vivo. *Leukemia* **2016**, *30*, 492–500. [[CrossRef](#)] [[PubMed](#)]
102. Gerner, M.Y.; Casey, K.A.; Mescher, M.F. Defective MHC Class II Presentation by Dendritic Cells Limits CD4 T Cell Help for Antitumor CD8 T Cell Responses. *J. Immunol.* **2008**, *181*, 155–164. [[CrossRef](#)] [[PubMed](#)]
103. Bos, R.; Sherman, L.A. CD4+ T-Cell Help in the Tumor Milieu Is Required for Recruitment and Cytolytic Function of CD8+ T Lymphocytes. *Cancer Res.* **2010**, *70*, 8368–8377. [[CrossRef](#)] [[PubMed](#)]
104. Xie, Y.; Akpınarlı, A.; Maris, C.; Hipkiss, E.L.; Lane, M.; Kwon, E.-K.M.; Muranski, P.; Restifo, N.P.; Antony, P.A. Naive tumor-specific CD4+ T cells differentiated in vivo eradicate established melanoma. *J. Exp. Med.* **2010**, *207*, 651–667. [[CrossRef](#)]
105. Duong, E.; Fessenden, T.B.; Lutz, E.; Dinter, T.; Yim, L.; Blatt, S.; Bhutkar, A.; Wittrup, K.D.; Spranger, S. Type I interferon activates MHC class I-dressed CD11b+ conventional dendritic cells to promote protective anti-tumor CD8+ T cell immunity. *Immunity* **2021**, *55*, 308–323. [[CrossRef](#)] [[PubMed](#)]
106. Liu, Y.-J. IPC: Professional Type 1 Interferon-Producing Cells and Plasmacytoid Dendritic Cell Precursors. *Annu. Rev. Immunol.* **2005**, *23*, 275–306. [[CrossRef](#)] [[PubMed](#)]

107. Jego, G.; Palucka, A.; Blanck, J.-P.; Chalouni, C.; Pascual, V.; Banchereau, J. Plasmacytoid Dendritic Cells Induce Plasma Cell Differentiation through Type I Interferon and Interleukin 6. *Immunity* **2003**, *19*, 225–234. [[CrossRef](#)]
108. Fang, T.C.; Schaefer, U.; Mecklenbrauker, I.; Stienen, A.; Dewell, S.; Chen, M.S.; Rioja, I.; Parravicini, V.; Prinjha, R.K.; Chandwani, R.; et al. Histone H3 lysine 9 di-methylation as an epigenetic signature of the interferon response. *J. Exp. Med.* **2012**, *209*, 661–669. [[CrossRef](#)] [[PubMed](#)]
109. Ma, S.; Wan, X.; Deng, Z.; Shi, L.; Hao, C.; Zhou, Z.; Zhou, C.; Fang, Y.; Liu, J.; Yang, J.; et al. Epigenetic regulator CXXC5 recruits DNA demethylase Tet2 to regulate TLR7/9-elicited IFN response in pDCs. *J. Exp. Med.* **2017**, *214*, 1471–1491. [[CrossRef](#)] [[PubMed](#)]
110. Wu, J.; Li, S.; Yang, Y.; Zhu, S.; Zhang, M.; Qiao, Y.; Liu, Y.-J.; Chen, J. TLR-activated plasmacytoid dendritic cells inhibit breast cancer cell growth in vitro and in vivo. *Oncotarget* **2016**, *8*, 11708–11718. [[CrossRef](#)]
111. Conrad, C.; Gregorio, J.; Wang, Y.-H.; Ito, T.; Meller, S.; Hanabuchi, S.; Anderson, S.; Atkinson, N.; Ramirez, P.T.; Liu, Y.-J.; et al. Plasmacytoid Dendritic Cells Promote Immunosuppression in Ovarian Cancer via ICOS Costimulation of Foxp3+ T-Regulatory Cells. *Cancer Res.* **2012**, *72*, 5240–5249. [[CrossRef](#)] [[PubMed](#)]
112. Poropatich, K.; Dominguez, D.; Chan, W.-C.; Andrade, J.; Zha, Y.; Wray, B.; Miska, J.; Qin, L.; Cole, L.; Coates, S.; et al. OX40+ plasmacytoid dendritic cells in the tumor microenvironment promote antitumor immunity. *J. Clin. Investig.* **2020**, *130*, 3528–3542. [[CrossRef](#)] [[PubMed](#)]
113. Sisirak, V.; Vey, N.; Goutagny, N.; Renaudineau, S.; Malfroy, M.; Thys, S.; Treilleux, I.; Labidi-Galy, S.I.; Bachelot, T.; Dezutter-Dambuyant, C.; et al. Breast cancer-derived transforming growth factor- β and tumor necrosis factor- α compromise interferon- α production by tumor-associated plasmacytoid dendritic cells. *Int. J. Cancer* **2013**, *133*, 771–778. [[CrossRef](#)]
114. Kuhn, S.; Yang, J.; Ronchese, F. Monocyte-Derived Dendritic Cells Are Essential for CD8+ T Cell Activation and Antitumor Responses After Local Immunotherapy. *Front. Immunol.* **2015**, *6*, 584. [[CrossRef](#)] [[PubMed](#)]
115. Davison, G.M.; Novitzky, N.; Abdulla, R. Monocyte derived dendritic cells have reduced expression of co-stimulatory molecules but are able to stimulate autologous T-cells in patients with MDS. *Hematol. Stem Cell Ther.* **2013**, *6*, 49–57. [[CrossRef](#)] [[PubMed](#)]
116. Kim, S.J.; Kim, G.; Kim, N.; Chu, H.; Park, B.-C.; Yang, J.S.; Han, S.H.; Yun, C.-H. Human CD141+ dendritic cells generated from adult peripheral blood monocytes. *Cytotherapy* **2019**, *21*, 1049–1063. [[CrossRef](#)]
117. Wakim, L.M.; Waithman, J.; van Rooijen, N.; Heath, W.R.; Carbone, F.R. Dendritic Cell-Induced Memory T Cell Activation in Nonlymphoid Tissues. *Science* **2008**, *319*, 198–202. [[CrossRef](#)]
118. De Vries, I.J.M.; Krooshoop, D.J.E.B.; Scharenborg, N.M.; Lesterhuis, W.J.; Diepstra, J.H.S.; Van Muijen, G.N.P.; Strijk, S.P.; Ruers, T.J.; Boerman, O.C.; Oyen, W.J.G.; et al. Effective migration of antigen-pulsed dendritic cells to lymph nodes in melanoma patients is determined by their maturation state. *Cancer Res.* **2003**, *63*, 12–17.
119. Zhang, Q.; Zhao, K.; Shen, Q.; Han, Y.; Gu, Y.; Li, X.; Zhao, D.; Liu, Y.; Wang, C.; Zhang, X.; et al. Tet2 is required to resolve inflammation by recruiting Hdac2 to specifically repress IL-6. *Nature* **2015**, *525*, 389–393. [[CrossRef](#)]
120. Liang, X.; Liu, Y.; Mei, S.; Zhang, M.; Xin, J.; Zhang, Y.; Yang, R. MicroRNA-22 Impairs Anti-Tumor Ability of Dendritic Cells by Targeting p38. *PLoS ONE* **2015**, *10*, e0121510. [[CrossRef](#)]
121. Ruffell, B.; Chang-Strachan, D.; Chan, V.; Rosenbusch, A.; Ho, C.M.; Pryer, N.; Daniel, D.; Hwang, E.S.; Rugo, H.S.; Coussens, L.M. Macrophage IL-10 Blocks CD8+ T Cell-Dependent Responses to Chemotherapy by Suppressing IL-12 Expression in Intratumoral Dendritic Cells. *Cancer Cell* **2014**, *26*, 623–637. [[CrossRef](#)]
122. De Smedt, T.; van Mechelen, M.; De Becker, G.; Urbain, J.; Leo, O.; Moser, M. Effect of interleukin-10 on dendritic cell maturation and function. *Eur. J. Immunol.* **1997**, *27*, 1229–1235. [[CrossRef](#)] [[PubMed](#)]
123. Pan, H.; O'Brien, T.F.; Wright, G.; Yang, J.; Shin, J.; Wright, K.L.; Zhong, X.-P. Critical Role of the Tumor Suppressor Tuberous Sclerosis Complex 1 in Dendritic Cell Activation of CD4 T Cells by Promoting MHC Class II Expression via IRF4 and CIITA. *J. Immunol.* **2013**, *191*, 699–707. [[CrossRef](#)]
124. Choi, Y.-E.; Yu, H.-N.; Yoon, C.-H.; Bae, Y.-S. Tumor-mediated down-regulation of MHC class II in DC development is attributable to the epigenetic control of the CIITA type I promoter. *Eur. J. Immunol.* **2009**, *39*, 858–868. [[CrossRef](#)] [[PubMed](#)]
125. Stanfield, B.A.; Purves, T.; Palmer, S.; Sullenger, B.; Welty-Wolf, K.; Haines, K.; Agarwal, S.; Kasotakis, G. IL-10 and class 1 histone deacetylases act synergistically and independently on the secretion of proinflammatory mediators in alveolar macrophages. *PLoS ONE* **2021**, *16*, e0245169. [[CrossRef](#)] [[PubMed](#)]
126. Kobayashi, T.; Matsuoka, K.; Sheikh, S.Z.; Russo, S.M.; Mishima, Y.; Collins, C.; Dezoeten, E.F.; Karp, C.; Ting, J.P.Y.; Sartor, R.B.; et al. IL-10 Regulates IL12b Expression via Histone Deacetylation: Implications for Intestinal Macrophage Homeostasis. *J. Immunol.* **2012**, *189*, 1792–1799. [[CrossRef](#)]
127. Villagra, A.; Cheng, F.; Wang, H.-W.; Suarez, I.; Glozak, M.; Maurin, M.; Nguyen, D.; Wright, K.L.; Atadja, P.W.; Bhalla, K.; et al. The histone deacetylase HDAC11 regulates the expression of interleukin 10 and immune tolerance. *Nat. Immunol.* **2008**, *10*, 92–100. [[CrossRef](#)]
128. Kitamura, H.; Ohno, Y.; Toyoshima, Y.; Ohtake, J.; Homma, S.; Kawamura, H.; Takahashi, N.; Taketomi, A. Interleukin-6/STAT3 signaling as a promising target to improve the efficacy of cancer immunotherapy. *Cancer Sci.* **2017**, *108*, 1947–1952. [[CrossRef](#)]
129. Català-Moll, F.; Ferraté-Bonastre, A.G.; Godoy-Tena, G.; Morante-Palacios, O.; Ciudad, L.; Barberà, L.; Fondelli, F.; Martínez-Cáceres, E.M.; Rodríguez-Ubreva, J.; Li, T.; et al. Vitamin D receptor, STAT3, and TET2 cooperate to establish tolerogenesis. *Cell Rep.* **2022**, *38*, 110244. [[CrossRef](#)] [[PubMed](#)]

130. Zong, J.; Keskinov, A.A.; Shurin, G.V.; Shurin, M. Tumor-derived factors modulating dendritic cell function. *Cancer Immunol. Immunother.* **2016**, *65*, 821–833. [[CrossRef](#)] [[PubMed](#)]
131. Pugh, S.; Thomas, A.G. Patients with adenomatous polyps and carcinomas have increased colonic mucosal prostaglandin E2. *Gut* **1994**, *35*, 675–678. [[CrossRef](#)] [[PubMed](#)]
132. Sombroek, C.C.; Stam, A.G.M.; Masterson, A.J.; Lougheed, S.M.; Schakel, M.J.A.G.; Meijer, C.J.L.M.; Pinedo, H.M.; Eertwegh, A.J.M.V.D.; Scheper, R.J.; De Gruijl, T.D. Prostanoids Play a Major Role in the Primary Tumor-Induced Inhibition of Dendritic Cell Differentiation. *J. Immunol.* **2002**, *168*, 4333–4343. [[CrossRef](#)] [[PubMed](#)]
133. Xia, D.; Wang, D.; Kim, S.-H.; Katoh, H.; Dubois, R.N. Prostaglandin E2 promotes intestinal tumor growth via DNA methylation. *Nat. Med.* **2012**, *18*, 224–226. [[CrossRef](#)] [[PubMed](#)]
134. Gabrilovich, D.; Ishida, T.; Oyama, T.; Ran, S.; Kravtsov, V.; Nadaf, S.; Carbone, D.P. Vascular endothelial growth factor inhibits the development of dendritic cells and dramatically affects the differentiation of multiple hematopoietic lineages in vivo. *Blood* **1998**, *92*, 4150–4166. [[CrossRef](#)] [[PubMed](#)]
135. Demoulin, A.S.; Somja, J.; Duray, A.; Guénin, S.; Roncarati, P.; Delvenne, O.P.; Herfs, M.F.; Hubert, P.M. Cervical (pre)neoplastic microenvironment promotes the emergence of tolerogenic dendritic cells via RANKL secretion. *OncolImmunology* **2015**, *4*, e1008334. [[CrossRef](#)]
136. Ferrara, N.; Gerber, H.-P.; LeCouter, J. The biology of VEGF and its receptors. *Nat. Med.* **2003**, *9*, 669–676. [[CrossRef](#)]
137. Gabrilovich, D.I.; Chen, H.L.; Girgis, K.R.; Cunningham, H.T.; Meny, G.M.; Nadaf, S.; Kavanaugh, D.; Carbone, D.P. Production of vascular endothelial growth factor by human tumors inhibits the functional maturation of dendritic cells. *Nat. Med.* **1996**, *2*, 1096–1103. [[CrossRef](#)]
138. Kim, R.; Emi, M.; Tanabe, K.; Arihiro, K. Tumor-Driven Evolution of Immunosuppressive Networks during Malignant Progression. *Cancer Res.* **2006**, *66*, 5527–5536. [[CrossRef](#)]
139. Roland, C.L.; Lynn, K.D.; Toombs, J.E.; Dineen, S.; Udugamasooriya, D.G.; Brekken, R.A. Cytokine Levels Correlate with Immune Cell Infiltration after Anti-VEGF Therapy in Preclinical Mouse Models of Breast Cancer. *PLoS ONE* **2009**, *4*, e7669. [[CrossRef](#)]
140. Kel, J.M.; Girard-Madoux, M.J.H.; Reizis, B.; Clausen, B.E.; Van De Laar, L.; Buitenhuis, M.; Wensveen, F.M.; Janssen, H.L.; Coffey, P.J.; Woltman, A.M. TGF- β Is Required to Maintain the Pool of Immature Langerhans Cells in the Epidermis. *J. Immunol.* **2010**, *185*, 3248–3255. [[CrossRef](#)]
141. Lievens, D.; Habets, K.L.; Robertson, A.-K.; Laouar, Y.; Winkels, H.; Rademakers, T.; Beckers, L.; Wijnands, E.; Boon, L.; Mosaheb, M.; et al. Abrogated transforming growth factor beta receptor II (TGF β RII) signalling in dendritic cells promotes immune reactivity of T cells resulting in enhanced atherosclerosis. *Eur. Heart J.* **2013**, *34*, 3717–3727. [[CrossRef](#)] [[PubMed](#)]
142. Huang, Y.; Min, S.; Lui, Y.; Sun, J.; Su, X.; Liu, Y.; Zhang, Y.; Han, D.; Che, Y.; Zhao, C.; et al. Global mapping of H3K4me3 and H3K27me3 reveals chromatin state-based regulation of human monocyte-derived dendritic cells in different environments. *Genes Immun.* **2012**, *13*, 311–320. [[CrossRef](#)] [[PubMed](#)]
143. Hmadcha, A.; Bedoya, F.; Sobrino, F.; Pintado, E. Methylation-Dependent Gene Silencing Induced by Interleukin 1 β via Nitric Oxide Production. *J. Exp. Med.* **1999**, *190*, 1595–1604. [[CrossRef](#)] [[PubMed](#)]
144. Topper, M.J.; Vaz, M.; Chiappinelli, K.B.; Shields, C.E.D.; Niknafs, N.; Yen, R.-W.C.; Wenzel, A.; Hicks, J.; Ballew, M.; Stone, M.; et al. Epigenetic Therapy Ties MYC Depletion to Reversing Immune Evasion and Treating Lung Cancer. *Cell* **2017**, *171*, 1284–1300. [[CrossRef](#)]
145. Nirschl, C.J.; Suárez-Fariñas, M.; Izar, B.; Prakadan, S.; Dannenfelser, R.; Tirosh, I.; Liu, Y.; Zhu, Q.; Devi, K.S.P.; Carroll, S.L.; et al. IFN γ -Dependent Tissue-Immune Homeostasis Is Co-opted in the Tumor Microenvironment. *Cell* **2017**, *170*, 127–141. [[CrossRef](#)]
146. Gottfried, E.; Kunz-Schughart, L.; Ebner, S.; Mueller-Klieser, W.; Hoves, S.; Andreesen, R.; Mackensen, A.; Kreutz, M. Tumor-derived lactic acid modulates dendritic cell activation and antigen expression. *Blood* **2006**, *107*, 2013–2021. [[CrossRef](#)]
147. Kang, K.A.; Zhang, R.; Kim, G.Y.; Bae, S.C.; Hyun, J.W. Epigenetic changes induced by oxidative stress in colorectal cancer cells: Methylation of tumor suppressor RUNX3. *Tumor Biol.* **2012**, *33*, 403–412. [[CrossRef](#)]
148. Zhang, R.; Kang, K.A.; Kim, K.C.; Na, S.-Y.; Chang, W.Y.; Kim, G.Y.; Kim, H.S.; Hyun, J.W. Oxidative stress causes epigenetic alteration of CDX1 expression in colorectal cancer cells. *Gene* **2013**, *524*, 214–219. [[CrossRef](#)]
149. O’Hagan, H.; Wang, W.; Sen, S.; Shields, C.D.; Lee, S.; Zhang, Y.W.; Clements, E.G.; Cai, Y.; Van Neste, L.; Easwaran, H.; et al. Oxidative Damage Targets Complexes Containing DNA Methyltransferases, SIRT1, and Polycomb Members to Promoter CpG Islands. *Cancer Cell* **2011**, *20*, 606–619. [[CrossRef](#)]
150. Obermajer, N.; Muthuswamy, R.; Lesnock, J.; Edwards, R.P.; Kalinski, P. Positive feedback between PGE2 and COX2 redirects the differentiation of human dendritic cells toward stable myeloid-derived suppressor cells. *Blood* **2011**, *118*, 5498–5505. [[CrossRef](#)]
151. Gabrilovich, D.I.; Bronte, V.; Chen, S.-H.; Colombo, M.P.; Ochoa, A.; Ostrand-Rosenberg, S.; Schreiber, H. The Terminology Issue for Myeloid-Derived Suppressor Cells. *Cancer Res.* **2007**, *67*, 425. [[CrossRef](#)] [[PubMed](#)]
152. Yang, Y.; Li, C.; Liu, T.; Dai, X.; Bazhin, A.V. Myeloid-Derived Suppressor Cells in Tumors: From Mechanisms to Antigen Specificity and Microenvironmental Regulation. *Front. Immunol.* **2020**, *11*, 1371. [[CrossRef](#)] [[PubMed](#)]
153. Di Blasio, S.; Van Wigcheren, G.F.; Becker, A.; Van Duffelen, A.; Gorris, M.; Verrijp, K.; Stefanini, I.; Bakker, G.J.; Bloemendal, M.; Halilovic, A.; et al. The tumour microenvironment shapes dendritic cell plasticity in a human organotypic melanoma culture. *Nat. Commun.* **2020**, *11*, 2749. [[CrossRef](#)] [[PubMed](#)]
154. Ohl, K.; Tenbrock, K. Reactive Oxygen Species as Regulators of MDSC-Mediated Immune Suppression. *Front. Immunol.* **2018**, *9*, 2499. [[CrossRef](#)] [[PubMed](#)]

155. Sacchi, A.; Tumino, N.; Sabatini, A.; Cimini, E.; Casetti, R.; Bordoni, V.; Grassi, G.; Agrati, C. Myeloid-Derived Suppressor Cells Specifically Suppress IFN- γ Production and Antitumor Cytotoxic Activity of V δ 2 T Cells. *Front. Immunol.* **2018**, *9*, 1271. [CrossRef]
156. Zhang, Y.; Xu, B.; Luan, B.; Zhang, Y.; Li, Y.; Xiong, X.; Shi, H. Myeloid-derived suppressor cells (MDSCs) and mechanistic target of rapamycin (mTOR) signaling pathway interact through inducible nitric oxide synthase (iNOS) and nitric oxide (NO) in asthma. *Am. J. Transl. Res.* **2019**, *11*, 6170–6184.
157. Redd, P.S.; Ibrahim, M.L.; Klement, J.D.; Sharman, S.K.; Paschall, A.V.; Yang, D.; Nayak-Kapoor, A.; Liu, K. SETD1B Activates iNOS Expression in Myeloid-Derived Suppressor Cells. *Cancer Res.* **2017**, *77*, 2834–2843. [CrossRef]
158. Nair, V.S.; Saleh, R.; Toor, S.M.; Taha, R.Z.; Ahmed, A.A.; Kurer, M.A.; Murshed, K.; Alajez, N.M.; Abu Nada, M.; Elkord, E. Transcriptomic profiling disclosed the role of DNA methylation and histone modifications in tumor-infiltrating myeloid-derived suppressor cell subsets in colorectal cancer. *Clin. Epigenet.* **2020**, *12*, 13. [CrossRef]
159. Fleming, V.; Hu, X.; Weber, R.; Nagibin, V.; Groth, C.; Altevogt, P.; Utikal, J.; Umansky, V. Targeting Myeloid-Derived Suppressor Cells to Bypass Tumor-Induced Immunosuppression. *Front. Immunol.* **2018**, *9*, 398. [CrossRef]
160. Rosenzweig, J.M.; Glenn, J.D.; Calabresi, P.A.; Whartenby, K.A. KLF4 Modulates Expression of IL-6 in Dendritic Cells via Both Promoter Activation and Epigenetic Modification. *J. Biol. Chem.* **2013**, *288*, 23868–23874. [CrossRef]
161. Sido, J.M.; Yang, X.; Nagarkatti, P.S.; Nagarkatti, M. Δ^9 -Tetrahydrocannabinol-mediated epigenetic modifications elicit myeloid-derived suppressor cell activation via STAT3/S100A8. *J. Leukoc. Biol.* **2015**, *97*, 677–688. [CrossRef] [PubMed]
162. Zhang, M.; Liu, Q.; Mi, S.; Liang, X.; Zhang, Z.; Su, X.; Liu, J.; Chen, Y.; Wang, M.; Zhang, Y.; et al. Both miR-17-5p and miR-20a Alleviate Suppressive Potential of Myeloid-Derived Suppressor Cells by Modulating STAT3 Expression. *J. Immunol.* **2011**, *186*, 4716–4724. [CrossRef]
163. Rodríguez-Ubreva, J.; Català-Moll, F.; Obermajer, N.; Álvarez-Errico, D.; Ramirez, R.N.; Company, C.; Vento-Tormo, R.; Moreno-Bueno, G.; Edwards, R.P.; Mortazavi, A.; et al. Prostaglandin E2 Leads to the Acquisition of DNMT3A-Dependent Tolerogenic Functions in Human Myeloid-Derived Suppressor Cells. *Cell Rep.* **2017**, *21*, 154–167. [CrossRef] [PubMed]
164. Sahakian, E.; Powers, J.; Chen, J.; Deng, S.L.; Cheng, F.; Distler, A.; Woods, D.M.; Rock-Klotz, J.; Sodre, A.L.; Youn, J.-I.; et al. Histone deacetylase 11: A novel epigenetic regulator of myeloid derived suppressor cell expansion and function. *Mol. Immunol.* **2015**, *63*, 579–585. [CrossRef] [PubMed]
165. Wculek, S.K.; Cueto, F.J.; Mujal, A.M.; Melero, I.; Krummel, M.F.; Sancho, D. Dendritic cells in cancer immunology and immunotherapy. *Nat. Rev. Immunol.* **2020**, *20*, 7–24. [CrossRef] [PubMed]
166. Graff, J.N.; Chamberlain, E.D. Sipuleucel-T in the treatment of prostate cancer: An evidence-based review of its place in therapy. *Core Evid.* **2014**, *10*, 1–10. [CrossRef] [PubMed]
167. Mougel, A.; Terme, M.; Tanchot, C. Therapeutic Cancer Vaccine and Combinations with Antiangiogenic Therapies and Immune Checkpoint Blockade. *Front. Immunol.* **2019**, *10*, 467. [CrossRef] [PubMed]
168. Lau-Kilby, A.; Kretz, C.C.; Pechhold, S.; Price, J.D.; Dorta, S.; Ramos, H.; Trinchieri, G.; Tarbell, K.V. Interleukin-2 inhibits FMS-like tyrosine kinase 3 receptor ligand (flt3L)-dependent development and function of conventional and plasmacytoid dendritic cells. *Proc. Natl. Acad. Sci. USA* **2011**, *108*, 2408–2413. [CrossRef] [PubMed]
169. Inaba, K.; Yashiro, T.; Hiroki, I.; Watanabe, R.; Kasakura, K.; Nishiyama, C. Dual Roles of PU.1 in the Expression of PD-L2: Direct Transactivation with IRF4 and Indirect Epigenetic Regulation. *J. Immunol.* **2020**, *205*, j1901008. [CrossRef]
170. Kirkling, M.E.; Cytlak, U.; Lau, C.M.; Lewis, K.L.; Resteu, A.; Khodadadi-Jamayran, A.; Siebel, C.W.; Salmon, H.; Merad, M.; Tsigos, A.; et al. Notch Signaling Facilitates In Vitro Generation of Cross-Presenting Classical Dendritic Cells. *Cell Rep.* **2018**, *23*, 3658–3672. [CrossRef]
171. Riol-Blanco, L.; Sánchez-Sánchez, N.; Torres, A.; Tejedor, A.; Narumiya, S.; Corbí, A.L.; Sánchez-Mateos, P.; Fernandez, J.L.R. The Chemokine Receptor CCR7 Activates in Dendritic Cells Two Signaling Modules That Independently Regulate Chemotaxis and Migratory Speed. *J. Immunol.* **2005**, *174*, 4070–4080. [CrossRef] [PubMed]
172. Doñas, C.; Carrasco, M.; Fritz, M.; Prado, C.; Tejón, G.; Osorio-Barrios, F.; Manríquez, V.; Reyes, P.; Pacheco, R.; Bono, M.R.; et al. The histone demethylase inhibitor GSK-J4 limits inflammation through the induction of a tolerogenic phenotype on DCs. *J. Autoimmun.* **2016**, *75*, 105–117. [CrossRef] [PubMed]
173. Jin, J.; Xie, X.; Xiao, Y.; Hu, H.; Zou, Q.; Cheng, X.; Sun, S.-C. Epigenetic regulation of the expression of Il12 and Il23 and autoimmune inflammation by the deubiquitinase Trubid. *Nat. Immunol.* **2016**, *17*, 259–268. [CrossRef]
174. Zhou, Z.; Chen, H.; Xie, R.; Wang, H.; Li, S.; Xu, Q.; Xu, N.; Cheng, Q.; Qian, Y.; Huang, R.; et al. Epigenetically modulated FOXM1 suppresses dendritic cell maturation in pancreatic cancer and colon cancer. *Mol. Oncol.* **2019**, *13*, 873–893. [CrossRef] [PubMed]
175. Fragale, A.; Romagnoli, G.; Licursi, V.; Buoncervello, M.; Del Vecchio, G.; Giuliani, C.; Parlato, S.; Leone, C.; De Angelis, M.; Canini, I.; et al. Antitumor Effects of Epidrug/IFN α Combination Driven by Modulated Gene Signatures in Both Colorectal Cancer and Dendritic Cells. *Cancer Immunol. Res.* **2017**, *5*, 604–616. [CrossRef] [PubMed]
176. Okada, N.; Mori, N.; Koretomo, R.; Okada, Y.; Nakayama, T.; Yoshie, O.; Mizuguchi, H.; Hayakawa, T.; Nakagawa, S.; Mayumi, T.; et al. Augmentation of the migratory ability of DC-based vaccine into regional lymph nodes by efficient CCR7 gene transduction. *Gene Ther.* **2004**, *12*, 129–139. [CrossRef]
177. Guenther, C.; Faisal, I.; Fuscillo, M.; Sokolova, M.; Harjunpää, H.; Ilander, M.; Tallberg, R.; Vartiainen, M.K.; Alon, R.; Gonzalez-Granado, J.-M.; et al. β 2-Integrin Adhesion Regulates Dendritic Cell Epigenetic and Transcriptional Landscapes to Restrict Dendritic Cell Maturation and Tumor Rejection. *Cancer Immunol. Res.* **2021**, *9*, 1354–1369. [CrossRef]

178. Wang, J.; Iwanowycz, S.; Yu, F.; Jia, X.; Leng, S.; Wang, Y.; Li, W.; Huang, S.; Ai, W.; Fan, D. microRNA-155 deficiency impairs dendritic cell function in breast cancer. *Oncol Immunology* **2016**, *5*, e1232223. [[CrossRef](#)]
179. Alcaraz-Serna, A.; Bustos-Morán, E.; Fernández-Delgado, I.; Calzada-Fraile, D.; Torralba, D.; Marina-Zárate, E.; Lorenzo-Vivas, E.; Vázquez, E.; de Alburquerque, J.B.; Ruef, N.; et al. Immune synapse instructs epigenomic and transcriptomic functional reprogramming in dendritic cells. *Sci. Adv.* **2021**, *7*, eabb9965. [[CrossRef](#)]
180. Blaschke, K.; Ebata, K.; Karimi, M.M.; Zepeda-Martínez, J.A.; Goyal, P.; Mahapatra, S.; Tam, A.; Laird, D.J.; Hirst, M.; Rao, A.; et al. Vitamin C induces Tet-dependent DNA demethylation and a blastocyst-like state in ES cells. *Nature* **2013**, *500*, 222–226. [[CrossRef](#)]
181. Magri, A.; Germano, G.; Lorenzato, A.; Lamba, S.; Chilà, R.; Montone, M.; Amodio, V.; Ceruti, T.; Sassi, F.; Arena, S.; et al. High-dose vitamin C enhances cancer immunotherapy. *Sci. Transl. Med.* **2020**, *12*, eaay8707. [[CrossRef](#)]
182. Lowenfeld, L.; Mick, R.; Datta, J.; Xu, S.; Fitzpatrick, E.; Fisher, C.S.; Fox, K.R.; DeMichele, A.; Zhang, P.J.; Weinstein, S.P.; et al. Dendritic Cell Vaccination Enhances Immune Responses and Induces Regression of HER2pos DCIS Independent of Route: Results of Randomized Selection Design Trial. *Clin. Cancer Res.* **2017**, *23*, 2961–2971. [[CrossRef](#)] [[PubMed](#)]
183. De Almeida Nagata, D.E.; Chiang, E.Y.; Jhunjhunwala, S.; Caplazi, P.; Arumugam, V.; Modrusan, Z.; Chan, E.; Merchant, M.; Jin, L.; Arnott, D.; et al. Regulation of Tumor-Associated Myeloid Cell Activity by CBP/EP300 Bromodomain Modulation of H3K27 Acetylation. *Cell Rep.* **2019**, *27*, 269–281. [[CrossRef](#)] [[PubMed](#)]
184. Orillion, A.; Hashimoto, A.; Damayanti, N.; Shen, L.; Adelaiye-Ogala, R.; Arisa, S.; Chintala, S.; Ordentlich, P.; Kao, C.; Elzey, B.; et al. Entinostat Neutralizes Myeloid-Derived Suppressor Cells and Enhances the Antitumor Effect of PD-1 Inhibition in Murine Models of Lung and Renal Cell Carcinoma. *Clin. Cancer Res.* **2017**, *23*, 5187–5201. [[CrossRef](#)] [[PubMed](#)]
185. Christmas, B.J.; Rafie, C.I.; Hopkins, A.C.; Scott, B.A.; Ma, H.S.; Cruz, K.A.; Woolman, S.; Armstrong, T.D.; Connolly, R.M.; Azad, N.A.; et al. Entinostat Converts Immune-Resistant Breast and Pancreatic Cancers into Checkpoint-Responsive Tumors by Reprogramming Tumor-Infiltrating MDSCs. *Cancer Immunol. Res.* **2018**, *6*, 1561–1577. [[CrossRef](#)]
186. Liu, L.; Yi, H.; Wang, C.; He, H.; Li, P.; Pan, H.; Sheng, N.; Ji, M.; Cai, L.; Ma, Y. Integrated Nanovaccine with MicroRNA-148a Inhibition Reprograms Tumor-Associated Dendritic Cells by Modulating miR-148a/DNMT1/SOCS1 Axis. *J. Immunol.* **2016**, *197*, 1231–1241. [[CrossRef](#)]

Vitamin C enhances NF- κ B-driven epigenomic reprogramming and boosts the immunogenic properties of dendritic cells

Octavio Morante-Palacios^{1,2}, Gerard Godoy-Tena¹, Josep Calafell-Segura¹, Laura Ciudad¹, Eva M. Martínez-Cáceres^{3,4}, José Luis Sardina⁵ and Esteban Ballestar^{1,2,6,*}

¹Epigenetics and Immune Disease Group, Josep Carreras Research Institute (IJC), 08916, Badalona, Barcelona, Spain, ²Germans Trias i Pujol Research Institute (IGTP), 08916, Badalona, Barcelona, Spain, ³Division of Immunology, Germans Trias i Pujol Hospital, LCMN, Germans Trias i Pujol Research Institute (IGTP), 08916, Badalona, Barcelona, Spain, ⁴Department of Cell Biology, Physiology, Immunology, Autonomous University of Barcelona, 08193, Bellaterra, Barcelona, Spain, ⁵Epigenetic Control of Haematopoiesis Group, Josep Carreras Research Institute (IJC), 08916, Badalona, Barcelona, Spain and ⁶Epigenetics in Inflammatory and Metabolic Diseases Laboratory, Health Science Center (HSC), East China Normal University (ECNU), Shanghai 200241, China

Received June 22, 2022; Revised September 23, 2022; Editorial Decision October 06, 2022; Accepted October 10, 2022

ABSTRACT

Dendritic cells (DCs), the most potent antigen-presenting cells, are necessary for effective activation of naïve T cells. DCs' immunological properties are modulated in response to various stimuli. Active DNA demethylation is crucial for DC differentiation and function. Vitamin C, a known cofactor of ten-eleven translocation (TET) enzymes, drives active demethylation. Vitamin C has recently emerged as a promising adjuvant for several types of cancer; however, its effects on human immune cells are poorly understood. In this study, we investigate the epigenomic and transcriptomic reprogramming orchestrated by vitamin C in monocyte-derived DC differentiation and maturation. Vitamin C triggers extensive demethylation at NF- κ B/p65 binding sites, together with concordant upregulation of antigen-presentation and immune response-related genes during DC maturation. p65 interacts with TET2 and mediates the aforementioned vitamin C-mediated changes, as demonstrated by pharmacological inhibition. Moreover, vitamin C increases TNF β production in DCs through NF- κ B, in concordance with the upregulation of its coding gene and the demethylation of adjacent CpGs. Finally, vitamin C enhances DC's ability to stimulate the proliferation of autologous antigen-specific T cells. We propose that vitamin C could potentially improve monocyte-derived DC-based cell therapies.

INTRODUCTION

Dendritic cells (DCs) play a central role in the immune system, bridging innate and adaptive immune responses. As innate immune cells, they are able to recognize a plethora of pathogen-associated molecular patterns (PAMPs) and damage-associated molecular patterns (DAMPs) through pattern recognition receptors (PRRs) (1). Moreover, they are very efficient at antigen processing and presentation to T cells and are, therefore, responsible for initiating antigen-specific immune responses.

DCs are highly heterogeneous, and comprise plasmacytoid DCs (pDCs) and conventional DCs (cDCs). Furthermore, monocyte-derived DCs (moDCs) can be differentiated *in vitro* from monocytes (MOs), with GM-CSF and IL-4 (2). moDCs have been classically used as a convenient model that mimics blood DCs, especially cDC2 (3). However, increasing evidence indicates that MOs can extravasate to peripheral tissues and give rise to *bona fide* moDCs *in vivo* (4).

Changes in DNA methylation, mainly active DNA demethylation, are involved in several differentiation processes from MOs, leading to macrophages (5), osteoclasts (6) and DCs (7) and are crucial for immune cell differentiation, identity, and function (8). In general, DNA demethylation is more extensive during MO differentiation than during subsequent maturation/activation (7). Additionally, the maturation of moDCs with live bacteria produces DNA demethylation that follows gene activation, limiting the potential direct regulatory effects of DNA methylation in such a context (9). TET2, a member of the Ten-Eleven Translocation (TET) methylcytosine dioxygenases,

*To whom correspondence should be addressed. Tel: +34 935572800; Fax: +34 934651472; Email: eballestar@carrerasresearch.org

has been pointed out as the main enzyme involved in multi-step active demethylation processes in terminal MO-related differentiation processes (6,10). However, recent data indicate that TET3 might complement TET2-mediated activity during MO differentiation (11). Recently, TET2 has also been implicated in glucocorticoid- and vitamin D-mediated modulation of the immunogenic properties of DCs (12,13).

Vitamin C (L-ascorbic acid) is an essential nutrient with pleiotropic functions. Its deficiency is associated with a disease, namely scurvy, characterized by a plethora of symptoms, including the malfunction of the immune system. For instance, the normal intracellular level of vitamin C in MO cytoplasm is ~ 3 mM, 60 times higher than the plasma level, reflecting a specific function of the molecule in immune cell biology (14). Vitamin C can act as a cofactor of Fe-containing hydroxylases such as TET enzymes and Jumonji C domain-containing histone demethylases (JHMDs), enhancing their catalytic activity (15). Some studies in mice suggest that vitamin C can stimulate DC capacity to produce proinflammatory cytokines and promote differentiation of T cells (16). Moreover, vitamin C intravenous treatment in mice has been shown to abrogate cancer progression through direct TET2 function restoration in cancer cells (17) and immune system modulation (18).

The *in vivo* modulation of DC migration and function, and the administration of DC-based vaccines, are potential strategies to treat different types of cancer (19). In particular, autologous moDCs obtained *ex vivo* from patient-derived blood MOs have been used in several clinical trials with mixed results (20–22). In this regard, the improvement of moDC generation *in vitro*, and the use of molecules to modulate MO differentiation *in vivo* may boost the clinical outcome of cancer patients.

In this work, we have investigated the effects of vitamin C treatment during MO-to-DC *in vitro* differentiation and maturation, identifying extensive DNA demethylation associated with the upregulation of migration, chemotaxis, antigen presentation, and immune response-related genes. Moreover, vitamin C-mediated DNA demethylation, gene upregulation, and increased TNF β production during DC maturation were associated with p65, a component of the NF- κ B complex that interacts with TET2 in this context. We have shown that the modulation of DNA methylation changes during DC differentiation and maturation yields functional and phenotypic changes in these cells, improving their immunogenicity.

MATERIALS AND METHODS

CD14⁺ monocyte purification and culture

Buffy coats were obtained from anonymous donors via the Catalan Blood and Tissue Bank (CBTB). The CBTB follows the principles of the World Medical Association (WMA) Declaration of Helsinki. Before providing blood samples, all donors received detailed oral and written information and signed a consent form at the CBTB.

PBMCs were isolated by density-gradient centrifugation using lymphocyte-isolation solution (Rafer). Pure MOs were then isolated from PBMCs by positive selection with magnetic CD14 MicroBeads (Miltenyi Biotec). Purity was

verified by flow cytometry, which yielded >95% of CD14⁺ cells.

MOs were resuspended in Roswell Park Memorial Institute (RPMI) Medium 1640+ GlutaMAX™ (Gibco, ThermoFisher) and immediately added to cell culture plates. After 20 min, monocytes were attached to the cell culture plates, and the medium was changed with RPMI containing 10% fetal bovine serum (Gibco, ThermoFisher), 100 units/ml penicillin/streptomycin (Gibco, ThermoFisher), 10 ng/ml human GM-CSF (PeproTech) and 10 ng/ml human IL-4 (PeproTech). In the case of the cells treated with vitamin C, 500 μ M (+)-sodium L-ascorbate (Sigma-Aldrich) was also added to the medium. For dendritic cell maturation, LPS (10 ng/ml) was added to cell culture on day 5.

Cells were collected on day 2 (designated as $\emptyset/\emptyset_{vitC}$, given their incomplete differentiation status) and on day 7, including immature dendritic cells (iDC/iDC_{vitC}) and mature dendritic cells, with LPS stimulus (mDC/mDC_{vitC}).

Genomic DNA and total RNA extraction

Genomic DNA and total RNA were extracted using the Maxwell RSC Cultured Cells DNA kit (Promega) and the Maxwell RSC simplyRNA Cells kit (Promega), respectively, following the manufacturer's instructions.

NF- κ B chemical inhibition

Bay 11-7082 (Sigma-Aldrich) was used for NF- κ B inhibition. The compound was diluted in DMSO to 50 mM. Bay 11-7082 at 10 μ M or an equivalent amount of diluent were used as final concentrations.

MOs were differentiated to iDCs/iDC_{vitC} as previously described. On day 5, LPS, Bay 11-7082 or equivalent amounts of diluents were added to the cell culture for 2 days, yielding iDC/iDC_{vitC}, iDC + Bay/iDC_{vitC} + Bay, mDC/mDC_{vitC}, and mDC + Bay/mDC_{vitC} + Bay.

DNA methylation profiling

500 ng of genomic DNA was converted using the EZ DNA Methylation Gold kit (Zymo Research), using 4 biological replicates for each group. Infinium MethylationEPIC BeadChip (Illumina) arrays were used to analyze DNA methylation, following the manufacturer's instructions. This platform allows around 850 000 methylation sites per sample to be interrogated at single-nucleotide resolution, covering 99% of the reference sequence (RefSeq) genes. Raw files (IDAT files) were provided for the Josep Carreras Research Institute Genomics Platform (Barcelona).

Quality control and analysis of EPIC arrays were performed using ShinyEPICo (23) a graphical pipeline that uses minfi (24) for normalization, and limma (25) for differentially methylated positions analysis. CpH and SNP loci were removed and the Noob + Quantile normalization method was used (26,27). After quality control, 831 421 CpGs were preserved for the analysis. Donor ID was used as a covariate, and Trend and Robust options were enabled for the eBayes moderated *t*-test analysis. CpGs were considered differentially methylated when the absolute differential of

methylation was $>30\%$ ($\Delta\beta > 0.3$) and the FDR was <0.05 . Infinium MethylationEPIC BeadChip arrays were designed using the hg19 human genome. For some downstream analysis, the genomic coordinates were converted to hg38 using the LiftOver tool (28).

For the genome-wide DNA methylation study after NF- κ B chemical inhibition, the same experimental approach and normalization pipeline was followed. After quality control, 812 429 CpGs were preserved for the analysis.

RNA-seq

RNA-seq libraries of MOs, $\emptyset/\emptyset_{vitC}$, iDC/iDC $_{vitC}$ and mDC/mDC $_{vitC}$ were generated and sequenced by Novogene (Cambridge), in 150-bp paired-end, with the Illumina NovaSeq 6000 platform, using three biological replicates for each group. More than 40 million reads were obtained for each sample. Fastq files were aligned to the hg38 transcriptome using HISAT2 (29) with standard options. Reads mapped in proper pair and primary alignments were selected with SAMtools (30). Reads were assigned to genes with featureCounts (31).

Differentially expressed genes were detected with DESeq2 (32). The donor was used as a covariate in the model. The Ashr shrinkage algorithm was applied and only protein-coding genes with an absolute logFC >0.5 and an FDR less than 0.05 were selected as differentially expressed. For representation purposes, Variance Stabilizing Transformation (VST) values and normalized counts provided by DESeq2 were used.

Quantification of cytokine production

Cell culture supernatants were collected after 7 days and diluted appropriately. Enzyme-linked immunosorbent assays (ELISA) were performed to detect TNF β , following the manufacturer's instructions (TNF beta Human ELISA Kit, ThermoFisher).

T cell clonal expansion and proliferation assay

PBMCs from healthy donors were purified from blood by density gradient centrifugation. The PBMCs (1 ml; 3×10^6 cells per well) were cultured in the presence of SARS-CoV-2-S (9 pmol) (PepTivator) in 24-well plates and maintained in IMDM medium (Gibco) supplemented with penicillin (100 units/ml), streptomycin (100 mg/ml) and human serum (10%) (Millipore) in the absence of IL-2 for 3 days. After 3 days, 1 ml of medium with 80 U/ml of recombinant human IL-2 (PeproTech) was added to the wells, with a final concentration of 1.5×10^6 cell/ml and 40 U/ml of IL-2. After 7–10 days of culture, T cells were expanded in the presence of 30-Gy irradiated autologous PBMCs (3×10^6 cells/well) previously pulsed with 9 pmol of SARS-CoV-2-S (PepTivator). Antigen-specific T cells (mix of CD4+ and CD8+ T cells) were selected by performing the same protocols two times to have a positive selection.

After 7 days of differentiation and activation, DCs were washed to remove vitamin C and were co-cultured with antigen-specific autologous CFSE-stained T cells at a DC:T cell ratio of 1:2 in 200 μ l of RPMI 1640 medium containing 10% FBS, penicillin (100 units/ml), streptomycin (100

mg/ml) in round bottom 96-well plates (ThermoFisher). Co-culture was performed in the presence of SARS-CoV-2-S antigen or SARS-CoV-2-N control antigen (PepTivator). T cell proliferation was analyzed by FACS and determined by considering the proliferating of those where CFSE staining had decreased compared to not co-cultured T cells. T cells stimulated with anti-CD3/CD28 microbeads 5 μ g/ml (eBioscience) were used as a positive control.

Flow cytometry

To study cell-surface markers, cells were collected using Versene, a non-enzymatic dissociation buffer (ThermoFisher). Cells were resuspended in the staining buffer (PBS with 4% fetal bovine serum and 2 mM ethylenediaminetetraacetic acid (EDTA)). Cells were then incubated on ice with an Fc block reagent (Miltenyi Biotec) for 10 minutes, and stained with the proteins of interest, using the following antibodies: CD8 (FITC) (#21270083, Immunotools), and CD4 (APC) (#555349, BD Biosciences). After staining, cells were analyzed using a BD FACSCanto™ II Cell Analyzer (BD Biosciences). Data were analyzed with the FlowJo v10 software.

Bisulfite pyrosequencing

500 ng of genomic DNA was converted using the EZ DNA Methylation Gold kit (Zymo Research). PCR was performed using the bisulfite-converted DNA as input and primers designed for each amplicon (Supplementary Table 1). These primers were designed using the PyroMark Assay Design 2.0 software (Qiagen). PCR amplicons were pyrosequenced using the PyroMark Q48 system and analyzed with PyroMark Q48 Autoprep software.

Real-time quantitative reverse-transcribed polymerase chain reaction (qRT-PCR)

300 ng of total RNA were reverse-transcribed to cDNA with Transcriptor First Strand cDNA Synthesis Kit (Roche) following the manufacturer's instructions. qRT-PCR was performed in technical triplicates for each biological replicate, using LightCycler® 480 SYBR Green Mix (Roche), and 7.5 ng of cDNA per reaction. The average value from each technical replicate was obtained. Then, the standard double-delta Ct method was used to determine the relative quantities of target genes, and values were normalized against the control genes RPL38 and HPRT1. Custom primers were designed to analyze genes of interest (Supplementary Table 1).

Co-immunoprecipitation (Co-IP)

Co-IP assays were performed using mDCs and mDC $_{vitC}$ after 5 days of differentiation from MOs and 24 h of stimulation with LPS. Cell extracts were prepared in lysis buffer [50 mM Tris-HCl, pH 7.5, 1 mM EDTA, 150 mM NaCl, 1% Triton-X-100, protease inhibitor cocktail (cOmplete™, Merck)] with corresponding units of Benzonase (Sigma) and incubated at 4°C for 4 h. 100 μ l of supernatant was saved as input and diluted with 2 \times Laemmli sample buffer

(5× SDS, 20% glycerol, 1 M Tris-HCl (pH 8.1)). Supernatants were first precleared with PureProteome™ Protein A/G agarose suspension (Merck Millipore) for 1 h. The lysate was then incubated overnight at 4°C with respective crosslinked primary antibodies. The cross-linking was performed in 20 mM dimethyl pimelimidate (DMP) (Pierce, Thermo Fisher Scientific, MA, USA) dissolved in 0.2 M sodium borate (pH 9.0). Subsequently, the beads were quenched with 0.2 M of ethanolamine (pH 8.0) and resuspended at 4°C in PBS until use. Beads were then washed three times with lysis buffer at 4°C. Sample elution was done by acidification using a buffer containing 0.2 M glycine (pH 2.3) and diluted with 2× Laemmli. Samples and inputs were denatured at 95°C in the presence of 1% β-mercaptoethanol. Anti-p65 C15310256 (Diagenode) and control IgG C15410206 (Diagenode) were used for co-IP.

Chromatin immunoprecipitation

On day 6, after 5 days of differentiation and 24h of maturation with LPS or an equivalent amount of diluent, iDC, iDC_{vitC}, mDC and mDC_{vitC} were fixed with Pierce™ fresh methanol-free formaldehyde (ThermoFisher) for 15 min and prepared for sonication with the truChIP Chromatin Shearing Kit (Covaris), following the manufacturer's instructions. We performed chromatin immunoprecipitation assays at 24 h of LPS-mediated maturation to capture the binding occurring before the final time point (48 h). Chromatin was sonicated 18 min with the Covaris M220 in 1 ml milliTubes (Covaris). The size distribution of the sonicated chromatin was checked by electrophoresis to ensure an appropriate sonication, with a size around 200 bp.

Magna Beads Protein A + G (Millipore) were blocked with PBS + BSA (5 mg/ml) for 1 h. Chromatin was precleared with 25 μl of beads for 1.5 h and 10 μg of chromatin were incubated overnight with each antibody: 10 μl Anti-p65 antibody ab16502 (Abcam), in a buffer with 1% Triton X-100, 150 mM NaCl and 0.15% SDS. Then, three washes were performed with the Low Salt Wash Buffer (0.1% SDS, 1% Triton X-100, 2 mM EDTA, pH 8.0, 20 mM Tris-HCl pH 8.0, 150 mM NaCl), the High Salt Wash Buffer (0.1% SDS, 1% Triton X-100, 2 mM EDTA, pH 8.0, 20 mM Tris-HCl pH 8, 500 mM NaCl) and the LiCl Wash Buffer (0.25 M LiCl, 1% Nonidet P-40, 1% deoxycholate, 1 mM EDTA pH 8, 10 mM Tris-HCl), followed by a last wash with TE buffer (pH 8.0, 10 mM Tris-HCl, 1 mM EDTA). Chromatin was eluted for 45 min 65°C with 100 μl of elution buffer (10 mM Tris-Cl, 1 mM EDTA, 1% SDS) and decrosslinked adding 5 μl 5 M NaCl and 5 μl 1 M NaHCO₃ (2 h 65°C). Next, 1 μl of 10mg/ml proteinase K (Invitrogen) was added, and samples were incubated at 37°C for 1 h. For DNA purification, iPure kit v2 (Diagenode) was used, following the manufacturer's instructions. 1% of the chromatin input from each sample was purified by the same method.

For ChIP-qPCR, samples were diluted 1/10, and 4 μl and specific primers (Supplementary Table 1) were used for each reaction. qRT-PCR was performed in technical triplicates for each biological replicate, using LightCycler® 480 SYBR Green Mix (Roche). The relative amount of im-

munoprecipitated DNA compared to input was calculated with the following formula: $2^{(C_{input} - 6.64) - C_{sample}} \times 100\%$

Western blotting

Cytoplasmic and nuclear protein fractions were obtained using hypotonic lysis buffer (Buffer A; 10 mM Tris pH 7.9, 1.5 mM MgCl₂, 10 mM KCl supplemented with protease inhibitor cocktail (Complete, Roche) and phosphatase inhibitor cocktail (PhosSTOP, Roche) to lyse the plasma membrane. Cells were visualized in the microscope to assure correct cell lysis. The nuclear pellets were resuspended in Laemmli 1× loading buffer. For whole-cell protein extract, cell pellets were directly resuspended in Laemmli 1× loading buffer.

Proteins were separated by SDS-PAGE electrophoresis. Immunoblotting was performed on polyvinylidene difluoride (PVDF) membranes following standard procedures. Membranes were blocked with 5% Difco™ Skim Milk (BD Biosciences) and blotted with primary antibodies. After overnight incubation, membranes were washed three times for 10 min with TBS-T (50 mM Tris, 150 mM NaCl, 0.1% Tween-20) and incubated for 1 h with HRP-conjugated mouse or rabbit secondary antibody solutions (Thermo Fisher) diluted in 5% milk (diluted 1/10 000). Finally, proteins were detected by chemiluminescence using WesternBright™ ECL (Advanta). The following antibodies were used: Anti-p65 C15310256 (Diagenode), Anti-phosphorylated p65 (Ser536) 93H1 (Cell Signaling), Anti-GAPDH 2275-PC-100 (Trevigen), Anti-TET2 C15200179 (Diagenode), Anti-histone H1 ab4269 (Abcam), Anti-beta Actin ab8227 (Abcam). Protein quantification was performed with ImageJ/Fiji (33).

Data analysis and representation

Statistical analyses were performed in R 4.0.3. Gene expression and DNA methylation heatmaps were created with the heatmap.2 function of the gplots package. The findMotifsGenome.pl function of HOMER (Hypergeometric Optimization of Motif EnRichment) was used to analyze known motif enrichment, using the parameters '-size 200 -cpg'. All EPIC array CpG coordinates were also used as background for the methylation data. GREAT software was used to calculate CpG-associated genes and gene ontology (GO) enrichment (34). GO enrichment of gene expression data was performed using the clusterProfiler package (35). ChIP-seq peaks files of histone marks from MO, iDCs, and mDCs were downloaded from the BLUEprint webpage (<http://dcc.blueprint-epigenome.eu>). Consensus peaks of the different replicates were obtained with the MSPC algorithm (36), using the options '-r Biological -w 1E-4 -s 1E-8 -c 3'.

The chromatin state learning model for CD14+ monocytes was downloaded from the Roadmap Epigenomics Project webpage, and chromatin state enrichments were calculated using Fisher's exact test.

Public DNase-seq and ATAC-seq bigwigs were aggregated using wiggletools (37) to obtain the mean value of several replicates. Heatmaps were generated with deeptools (38).

Proportional Venn diagrams were generated with the Meta-Chart webpage (<https://www.meta-chart.com/>).

RESULTS

Vitamin C drastically enhances DNA demethylation during monocyte to dendritic cell differentiation and maturation

MOs isolated from peripheral blood of healthy donors were differentiated *in vitro* to DCs for 7 days using GM-CSF and IL-4, in the presence or absence of vitamin C (vitC). Samples were collected on day 2, in the middle of the differentiation (designated as $\emptyset/\emptyset_{\text{vitC}}$ given their incomplete differentiation), and on day 7, including immature DCs (iDCs) (iDC/iDC_{vitC}), without further treatment, and mature DCs, exposed the last 48 h to lipopolysaccharide (LPS) (mDC/mDC_{vitC}) (Figure 1A).

DNA methylation was profiled using Illumina Infinium MethylEPIC arrays, which covered 831 421 GpG sites in the human genome, after the quality control. First, overall changes in DNA methylation were calculated between groups pairwise (Supplementary Figure 1A). DNA demethylation was the most prominent change, as previously described (7). We then compared the demethylated positions in MO-to-iDC differentiation, in comparison with MO-to-iDC_{vitC} differentiation, as well as iDC-to-mDC maturation in comparison with iDC_{vitC}-to-mDC_{vitC} maturation. As it can be observed, the positions demethylated in the differentiation and maturation processes in the presence of vitamin C include the majority of CpGs demethylated in the regular differentiation and maturation of DCs, as well as a vast number of additional CpGs (Figure 1B).

Principal component analysis (PCA) revealed that on day 2, most DNA methylation variance of the MO-to-iDC differentiation had already developed (Figure 1C), whereas no differences with the vitamin C stimulus were found. In contrast, on day 7, vast differences were observed for both iDC_{vitC} and mDC_{vitC}, in comparison with their corresponding controls without vitamin C suggesting that the vitamin C-mediated boost in demethylation occurs later in time. The variable that explains most of the variance in DNA methylation resides in the presence/absence of vitamin C during differentiation.

All differentially methylated positions (DMPs) associated with vitamin C (iDC versus iDC_{vitC} and mDC versus mDC_{vitC}) were represented together, revealing two clusters of DMPs (M1 and M2) (Figure 1D and Supplementary Table 2). M1 corresponds with CpGs demethylated during differentiation in the presence of vitamin C whereas M2 are CpGs demethylated during LPS-mediated maturation in the presence of vitamin C. Both clusters were enriched in monocytic enhancers and regions flanking active transcription start sites (Figure 1E). That corresponds with predominant localization in intergenic regions, far from CpG islands (Supplementary Figure 1B and Supplementary Figure 1C). Of note, M1 and M2 DMPs are located in regions with subtle increases in H3K27ac and H3K4me1 histone marks from MOs to iDCs and mDCs, respectively. This suggests that these regions are primed for activation, even in the absence of vitamin C (Supplementary Figure 1D).

Gene Ontology enrichment analysis of M1 DMP-associated genes revealed categories related to positive regulation of myeloid differentiation, regulation of JAK activation, regulation of defense response to virus, and vitamin transport, among others. In contrast, M2 DMPs were enriched in terms related to LPS response and immune activation such as cellular response to molecules of bacterial origin, leukocyte activation, response to bacterium, regulation of IFN γ production, and positive regulation of NF- κ B activity (Figure 1F). These functions are consistent with the respective association of M1 and M2 clusters with the DC differentiation and maturation steps.

Active demethylation in myeloid cells is often mediated by transcription factors that recruit specific epigenetic enzymes. In this regard, M1 DMPs were enriched in the consensus binding motifs of transcription factors previously related to DC differentiation, such as EGR2(11), STAT6(7), and PU.1(11), whereas M2 DMPs were enriched in the consensus binding motifs of NF- κ B, AP-1 and IRF (Figure 1G). Employing the average signal of public MO DNase-seq (Blueprint database) (39) and iDC ATAC-seq triplicates (40), we found that M1 and M2 DMPs present low accessibility in MOs (Supplementary Figure 1E). We also observed that M1 DMPs have greater accessibility than M2 DMPs in iDCs (Supplementary Figure 1F).

Vitamin C drives gene expression remodeling in dendritic cells

Given the extensive differences in DNA methylation mediated by vitamin C, we then performed RNA-seq of MOs, \emptyset , \emptyset_{vitC} , iDC, iDC_{vitC}, mDC and mDC_{vitC} and checked for differences in their transcriptomes. In contrast with DNA methylation, transcriptome variance of principal component (PC)1 and PC2 are mainly explained by the maturation of DCs and the differentiation of MO to DC, respectively. However, differences between iDC and iDC_{vitC} and mDC and mDC_{vitC} can also be observed in the PCA (Figure 2A).

We first checked the expression patterns of the transcription factors related to the motifs enriched in the M1 and M2 DMPs (Figure 1G). We could observe that most of these transcription factors are more expressed than the median gene expression in the dataset, with the exception of WT (WT1), SPIB and Nur77 (NR4A1) which are lowly expressed in dendritic cells (Supplementary Figure 2A).

Since samples were collected on day 2 ($\emptyset/\emptyset_{\text{vitC}}$), and on day 7, without (iDC/iDC_{vitC}) or with (mDC/mDC_{vitC}) LPS-mediated activation, three potential comparisons of vitamin C-treated cells can be performed, in relation to their respective controls. On day 2, very few differences were found between \emptyset and \emptyset_{vitC} (63 downregulated and 75 upregulated genes). On day 7, we found 163 downregulated and 159 upregulated genes between iDC and iDC_{vitC}, whereas most differences were found between mDC and mDC_{vitC} (185 downregulated and 772 upregulated genes) (Figure 2B, Supplementary Table 3). Furthermore, most differentially expressed genes (DEGs) were not shared between comparisons (Figure 2C).

We then joined the differentially expressed genes of the three comparisons. We used hierarchical clustering and the elbow method to decide an appropriate number of clusters

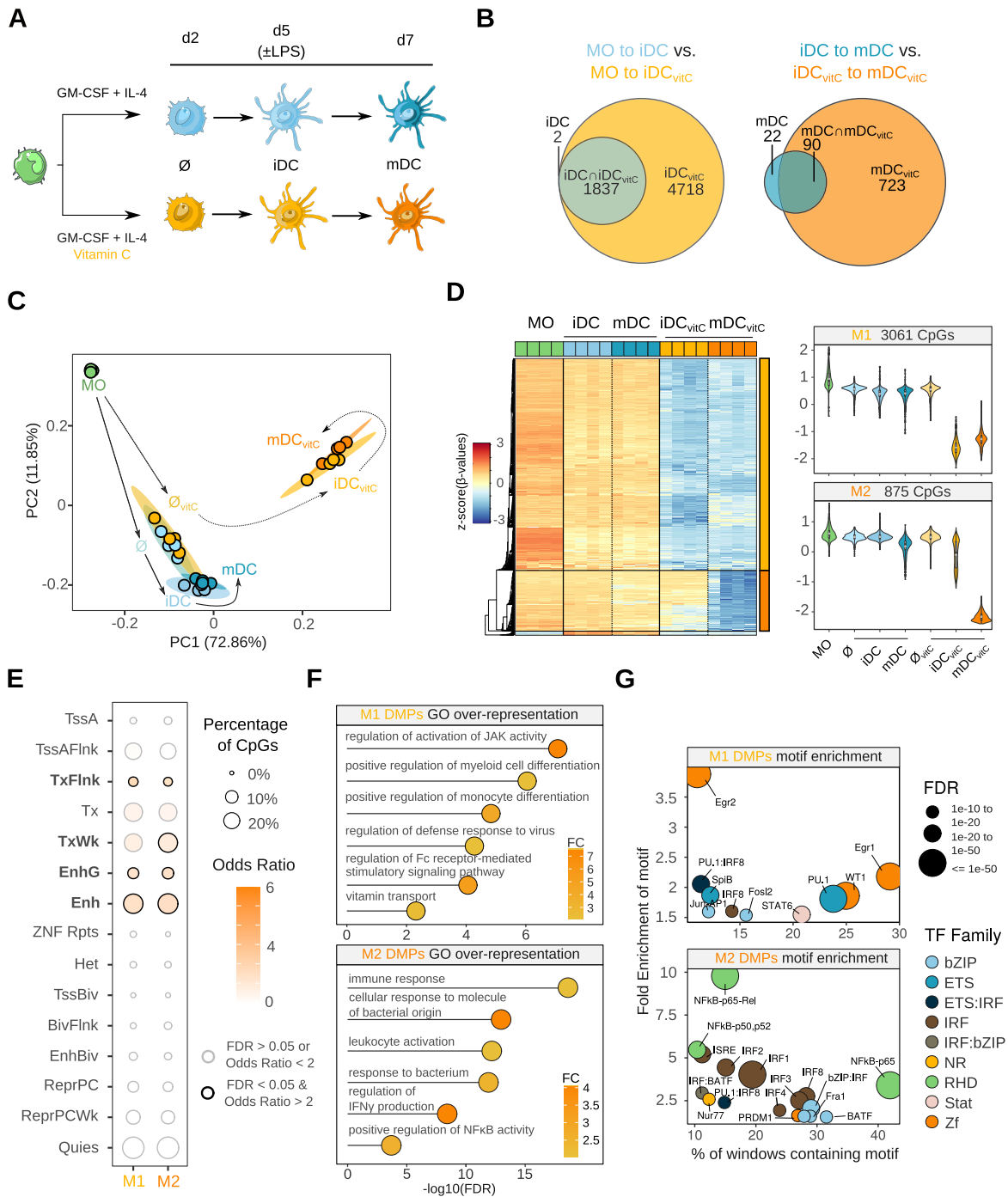


Figure 1. Vitamin C-mediated dendritic cell DNA methylome remodeling. (A) Scheme depicting the experimental setup. Monocytes (MO) were differentiated to dendritic cells (DCs) using GM-CSF and IL-4, in the presence or absence of vitamin C (vitC). Samples were collected on day 2, in the middle of the differentiation, and on day 7, including immature DCs (iDCs) and mature DCs (mDCs), exposed the last 2 days to lipopolysaccharide (LPS). (B) Area-proportional Venn diagrams comparing the demethylated CpG sets of MO-to-iDC versus MO-to-iDC_{vitC}, and iDC-to-mDC versus iDC_{vitC}-to-mDC_{vitC} transitions. (C) Principal Component Analysis (PCA) of differentially methylated positions (DMPs) comparing all groups pairwise. Principal component 1 and principal component 2 are represented on the x- and y-axis, respectively. Solid and dashed lines represent the trajectories across MO-iDC-mDC and MO-iDC_{vitC}-mDC_{vitC} differentiation/maturation respectively, to make the plot easier to follow. (D) DNA methylation heatmap of DMPs comparing iDC to iDC_{vitC}, and mDC to mDC_{vitC} ($\Delta\beta \geq 0.3$, FDR < 0.05). Scaled β -values are shown (lower DNA methylation levels in blue and higher methylation levels in red). On the right side, violin plots of clusters M1 and M2 depict scaled β -values. (E) Enrichment of M1 and M2 DMPs in ChromHMM 15-states categories of MOs (Roadmap Epigenomics Project). Fisher's exact tests of M1 and M2 DMPs were calculated using all the CpGs annotated in the EPIC array as background. Significantly enriched categories (FDR < 0.05 and odds ratio > 2) are depicted with a black stroke, including TxFlnk (Flanking Active TSS), TxWk (Weak Transcription), EnhG (Genic Enhancers), and Enh (Enhancers). (F) GO (Gene Ontology) over-represented categories in M1 and M2 DMPs. Fold Change in comparison with background (EPIC array CpGs) and $-\log_{10}(\text{FDR})$ is represented. (G) Bubble scatterplot of transcription factor binding motif enrichment for M1 and M2 DMPs. The x-axis shows the percentage of windows containing the motif and the y-axis shows the fold enrichment of the motif over the EPIC background. Bubbles are colored according to the transcription factor family. FDR is indicated by bubble size.

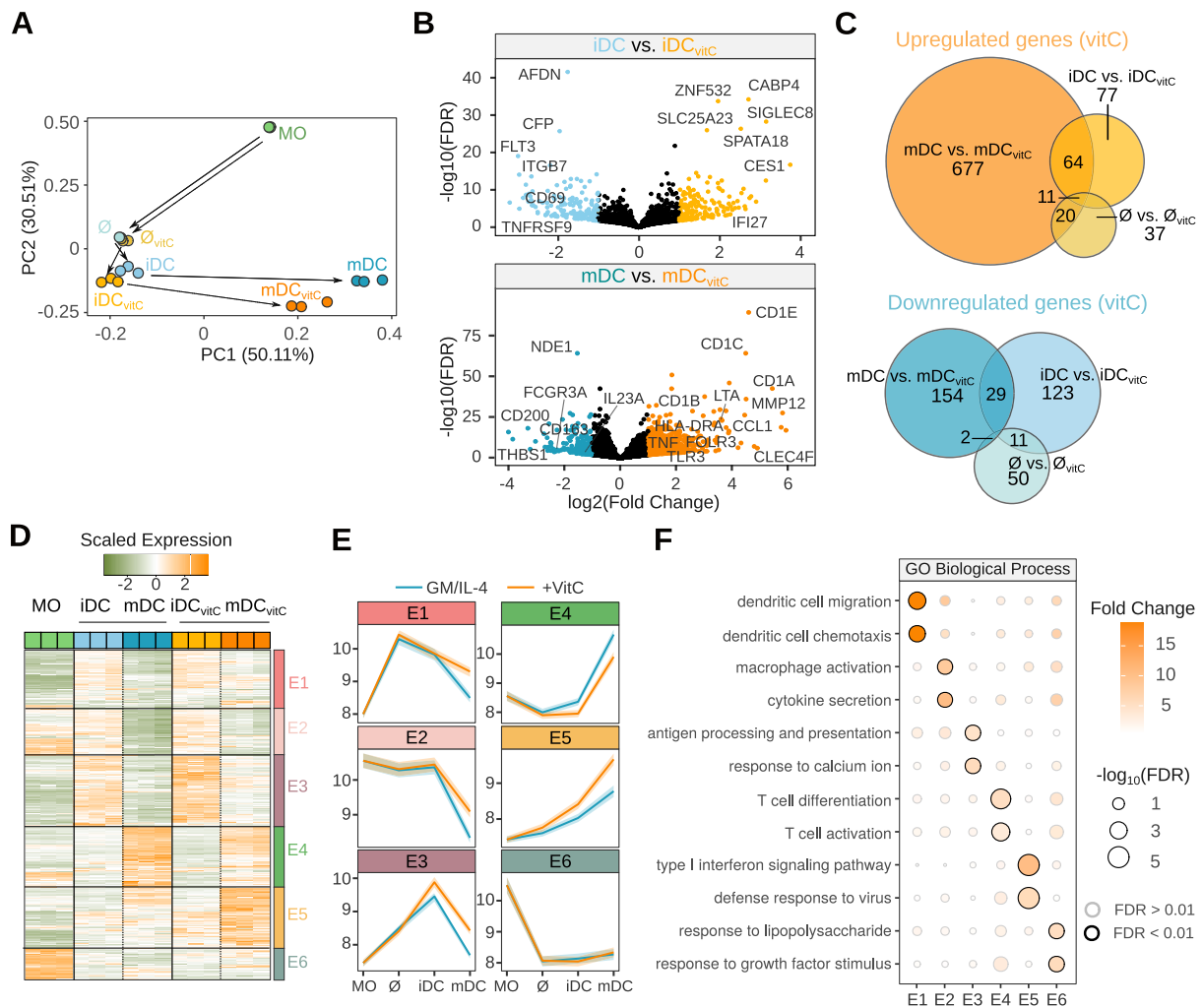


Figure 2. Shifting in gene expression of dendritic cells triggered by vitamin C. (A) Principal Component Analysis (PCA) of gene expression. Principal component 1 and principal component 2 are represented on the x- and y-axis, respectively. Solid and dashed lines represent the trajectories across MO-iDC-mDC and MO-iDC_{vitC}-mDC_{vitC} differentiation/maturation respectively, to make the plot easier to follow. (B) Volcano plots of gene expression in the iDC vs. iDC_{vitC} and the mDC versus mDC_{vitC} comparisons. The binary logarithm of the fold change is represented on the x-axis, whereas the negative decimal logarithm of the FDR is represented on the y-axis. Downregulated genes are shown in blue (FDR < 0.05, Fold Change < -2) and upregulated genes are shown in orange (FDR < 0.05, Fold Change > 2). (C) Area-proportional Venn diagrams comparing the upregulated and downregulated gene sets of the \emptyset versus \emptyset_{vitC} , iDC versus iDC_{vitC} and mDC vs. mDC_{vitC} comparisons. (D) Gene expression heatmap of differentially expressed genes comparing \emptyset to \emptyset_{vitC} , iDC to iDC_{vitC}, and mDC to mDC_{vitC} (absolute log FC > 1, FDR < 0.05). Scaled expression VST values are shown (lower expression levels in green and higher expression values in orange). The division of the dendrogram created with the ward.D2 agglomeration method yielded six different expression clusters (E1–E6). (E) Temporal progression of gene expression of the expression clusters (E1–E6) during the differentiation process with (orange) or without (blue) vitamin C. The y-axis shows VST values, where a higher value means a higher gene expression, and the line ribbons represent the 95% confidence interval. (F) Gene Ontology (GO) over-representation of GO Biological Process categories in the E1–E6 clusters. Fold Change of genes over the background and $-\log_{10}(\text{FDR})$ of the Fisher's exact tests are shown. Significant categories (FDR < 0.01) are depicted with a black stroke.

(Supplementary Figure 2B). We then divided the genes into six clusters (expression clusters E1–E6) with different behaviors (Figure 2D and Supplementary Table 4). E1, E2 and E3 clusters show a diminished downregulation trend in the iDC_{vitC} to mDC_{vitC} transition, in comparison with the iDC to mDC transition, whereas E5 genes are more upregulated in the iDC_{vitC} to mDC_{vitC} transition in comparison with the iDC to mDC transition (Figure 2E).

Gene Ontology Enriched terms were calculated for each expression cluster, obtaining distinctive categories (Figure 2F). For instance, E1 was enriched in dendritic cell migration and chemotaxis, E2 in macrophage activation and cytokine secretion, E3 in antigen processing and presentation

and response to calcium ion, and E5 in type I interferon signaling pathway and defense response to virus.

Vitamin C-mediated demethylation is linked to increased gene expression during dendritic cell maturation

To identify potential functional effects of the vitamin C-mediated demethylation, we linked each DMP with its closest gene. When the global profile of M1 and M2 associated genes was intersected with DEGs from Figure 2D, we found that M1 associated genes are less downregulated in mDCs with vitamin C treatment, whereas M2 associated genes are upregulated in mDCs with vitamin C treatment

(Figure 3A). Concordantly, E1 and E2 clusters are enriched in M1-associated genes, and the E5 cluster is enriched in M2-associated genes (Figure 3B).

Individual DMPs and their associated DEGs illustrate different relationships between DNA methylation/gene expression. M1-associated genes, C1QB and CD1C, which are related to the complement system and antigen presentation respectively, show demethylation with vitamin C treatment in iDCs, conjoined with a lower reduction in expression after activation (Figure 3C). Furthermore, M2-associated genes such as LTA, IKBKE and IRF8 related to TNF β production, NF- κ B pathway regulation, and interferon regulation respectively, depict a decreased methylation in mDC with vitamin C, concomitant with increased gene expression (Figure 3D).

Finally, a database of transcription factor regulation (41) was used to infer potential transcription factors involved in regulating expression clusters (Figure 3E and Supplementary Figure 3A). Interestingly, PU.1 and RELA (p65) were associated with M1/E2 and M2/E5 clusters, respectively.

NF- κ B/p65 orchestrates vitamin C-mediated DNA demethylation, gene upregulation and increased proinflammatory cytokine production

Since p65 was associated with both DNA demethylation (Figure 1G) and gene upregulation (Figure 3E) during mDC_{vitC} maturation, we studied the protein expression and phosphorylation by Western Blot. First, we found that p65 presents similar protein levels in iDCs, mDCs, iDC_{vitC} and mDC_{vitC}. However, phosphorylated p65 (Ser536) (p-p65) is increased in both mDCs and mDC_{vitC} (Figure 4A and Supplementary Figure 4A). Moreover, we also detected p-p65 in the nuclear fraction (NF) of mDCs and mDC_{vitC}, enabling it to act as a transcription factor (Figure 4B and Supplementary Figure 4A).

To further explore the role of NF- κ B/p65 in the mDC_{vitC} transcriptomic and epigenomic reprogramming, we utilized a chemical inhibitor of I κ B degradation (BAY 11-7082, Bay) which reduces the nuclear translocation of p65 (42,43) (Supplementary Figure 4B). MOs were differentiated in DCs as previously described, adding Bay (10 μ M) or Dimethyl Sulfoxide (DMSO) on day 5 (Figure 4C).

We then tested the effect of NF- κ B inhibition on M1 and M2 DMPs. We observed that the NF- κ B inhibitor dampens the demethylation of M2 DMPs, concordantly with their enrichment in NF- κ B motifs. However, this effect is smaller in M1 DMPs (Figure 4D). Specifically, NF- κ B inhibition pervasively prevents the demethylation of most M2 DMPs ($P < 1^{-1}$) (Figure 4E). As a validation, we performed pyrosequencing of selected DMPs from the M2 cluster, observing the blockage of demethylation. Conversely, a DMP from the M1 cluster was not affected (Supplementary Figure 4C).

Secondly, we also tested the expression of M2-associated genes revealing that, inversely to DNA demethylation, gene expression decreases in mDC_{vitC} when NF- κ B is inhibited (Figure 4F and Supplementary Figure 4D). However, the same trend was not found in M1-associated genes (Figure 4F and Supplementary Figure 4E).

We then checked the potential interaction between p65 and TET2, a key mediator of active demethylation in

myeloid cells whose activity is enhanced by vitamin C. The co-immunoprecipitation of p65 revealed its interaction with TET2 in both mDCs and mDC_{vitC} (Figure 4G).

Additionally, we performed a ChIP-qPCR analysis of p65 on day 6, comparing the binding in a negative control amplicon around the *INS* gene with an amplicon around the cg08639424, located close to *LTA* and *TNF* genes. p65 was significantly enriched in mDCs/mDC_{vitC}, but not in iDCs/iDC_{vitC} (Figure 4H).

Since the *LTA* gene, which encodes TNF β , was found upregulated and the adjacent CpGs become demethylated in mDC_{vitC}, we measured the TNF β protein levels secreted by these cells in comparison with mDCs. mDCs produced little amounts of TNF β whereas mDC_{vitC} supernatant contained considerably higher concentrations (Figure 4I). Moreover, Bay treatment damped TNF β production of mDC_{vitC}, consistent with the reversion in the cg08639424 demethylation and *LTA* upregulation (Supplementary Figure 4F).

Vitamin C produces dendritic cells with higher T cell stimulation capabilities

We then characterized the mDC_{vitC} phenotype in comparison with mDCs. In particular, we studied the T cell stimulation capabilities and antigen presentation of mDC_{vitC} in contrast to mDCs. First, we performed a clonal expansion of T cells from healthy donors with a SARS-CoV-2 mix of antigens. After the process, we verified that 95% of the resulting cells were T lymphocytes by staining them with anti-CD4 and anti-CD8 antibodies (Supplementary Figure 5A and Supplementary Figure 5B). We then differentiated autologous MOs *in vitro* to iDC_{vitC}/iDCs. After 48 h of maturation with LPS and 1 h of antigen loading with the same SARS-CoV-2 antigen mix, mDC_{vitC}/mDCs were cocultured with Carboxyfluorescein succinimidyl ester (CFSE)-stained clonal T cells for 5 days (Figure 5A).

In Figure 5B, a selected example of this T cell proliferation assay is shown. The histogram of the CFSE signal of T cells alone (C) or cocultured with mDC/mDC_{vitC} loaded with a control antigen or with the specific set of antigens (An) is depicted.

Overall, we observed a significant increase in T cell proliferation when they are cocultured with mDC_{vitC} loaded with a specific set of antigens, in comparison with mDCs loaded with the same antigens. This can be observed by the increase in the proliferation percentages and the decrease in the median intensity of fluorescence (MFI) of CFSE (Figure 5C and D). However, when T cells were cocultured with mDCs/mDC_{vitC} loaded with a control antigen, no differences in proliferation or MFI were found, indicating that the mDC_{vitC} increased T cell activation capabilities rely on specific antigen presentation and not only indirect stimulation (Figure 5C, D).

DISCUSSION

In this work, we demonstrate a substantial effect of vitamin C supplementation during the MO-to-DC *in vitro* differentiation and maturation. First, we show vast demethylation in DCs treated with vitamin C, consistent with its role as a TET enzyme cofactor, being the number of additional

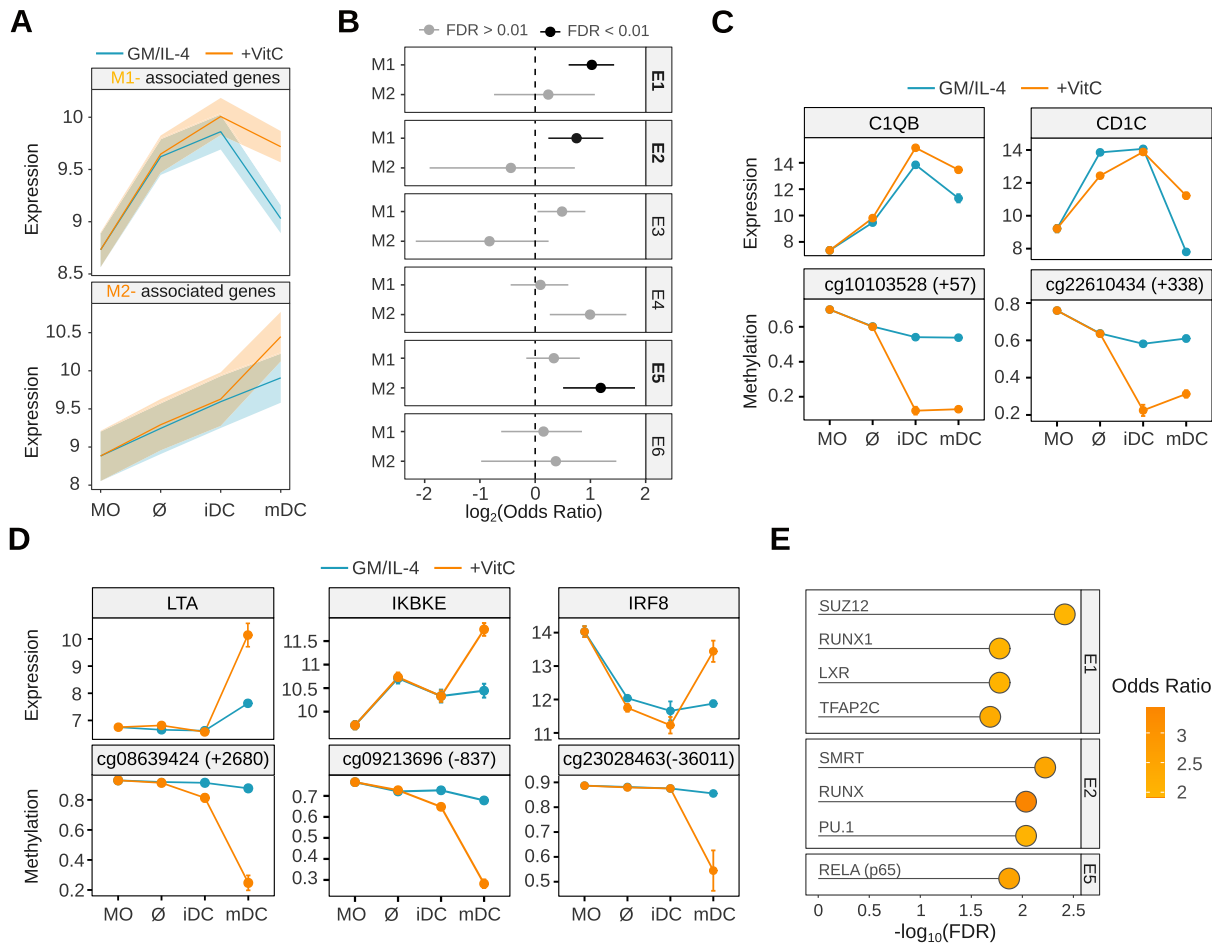


Figure 3. Integration of DNA methylation and gene expression vitamin C-mediated remodeling. (A) M1 and M2 DMPs (from Figure 1D) ($\Delta\beta \geq 0.3$, $FDR < 0.05$), were associated with the nearest transcription start site. Temporal progression of gene expression of the M1- and M2-associated genes intersected with vitamin C-mediated differentially expressed genes (Figure 2D) (absolute log FC > 1, $FDR < 0.05$) with (orange) or without (blue) vitamin C is represented. The y-axis shows VST values, where a higher value means a higher gene expression, and the line ribbons represent the 95% confidence interval. (B) Enrichments of M1- and M2-associated genes over the E1–E6 expression clusters were calculated using Fisher’s exact tests. Odds ratios \pm 95% confidence intervals are shown. Significant enrichments ($FDR < 0.01$) are shown in black. (C) Selected examples of M1 DMPs ($\Delta\beta \geq 0.3$, $FDR < 0.05$) and associated genes (absolute log FC > 1, $FDR < 0.05$). Temporal progression of DNA methylation (β -value) (below) and gene expression (VST) (above) during the differentiation process with (orange) or without (blue) vitamin C is depicted. (D) Selected examples of M2 DMPs and associated genes. Temporal progression of DNA methylation (β -value) (below) and gene expression (VST) (above) during the differentiation process with (orange) or without (blue) vitamin C is depicted. (E) Enrichment of clusters with gene expression/DNA methylation correlation with genesets from CheA 2016 database (REF), containing genes putatively regulated by transcription factors. The odds ratio over the background and $-\log_{10}(FDR)$ of the Fisher’s exact tests are shown.

demethylated CpGs higher than the MO-to-DC demethylation without vitamin C. This epigenomic remodeling correlates with increased expression of genes related to antigen presentation, cytokine secretion, and immune response. Moreover, our analysis indicates that NF- κ B is directly involved in the epigenomic and transcriptomic reprogramming observed during the maturation of DCs in the presence of vitamin C, together with the increase in TNF β production. Finally, vitamin C enhances the capacity of DCs to induce the proliferation of autologous T cells through specific antigen presentation.

Vitamin C is a well-established cofactor of TET proteins, with the ability to enhance TET-mediated oxidation of 5-methylcytosine (5mC) into 5-hydroxymethylcytosine (5hmC) and further oxidized methylcytosine derivatives (44,45). Given the absence of proliferation in the MO-to-DC differentiation process (13), the observed demethyla-

tion should occur through an active mechanism, consistent with previous studies, and be catalyzed by TET enzymes, the activity of which is enhanced by vitamin C. We and others have shown that TET2, the most expressed TET enzyme in MOs, is the major driver of active demethylation in this biological context (7,10,46). In this study, we show the physical interaction between TET2 and p65, one of the NF- κ B subunits, that is associated with the CpGs that become demethylated during DC activation in the presence of vitamin C. However, we cannot discard the participation of other TET enzymes in the demethylation process, whose enzymatic activity could also be enhanced by vitamin C. In fact, TET3 could compensate for TET2 activity during MO differentiation (11).

Of note, the observed effects of vitamin C on DNA methylation occur in the last days of the differentiation process, since no DNA methylation differences were found

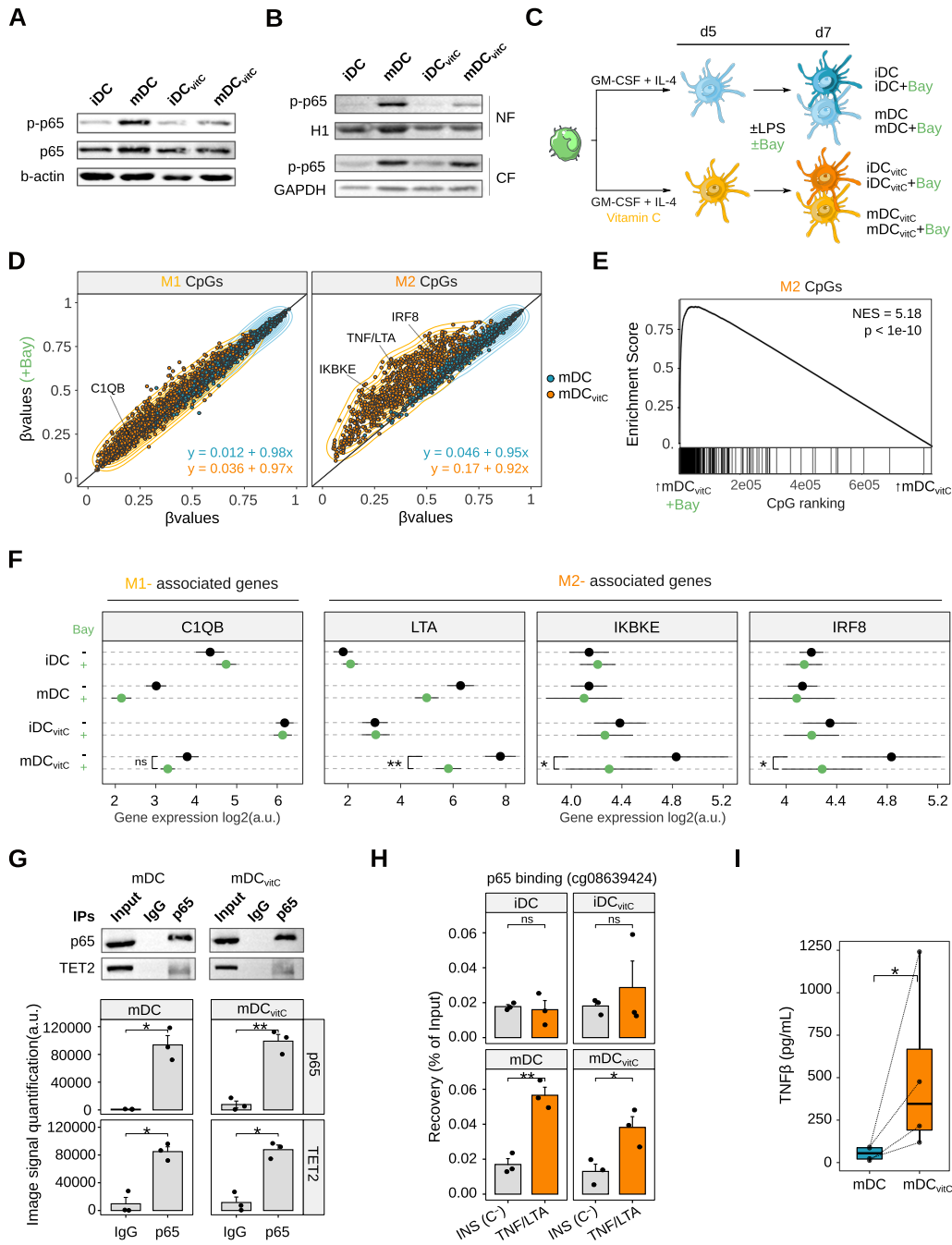


Figure 4. Role of p65 in the transcriptomic and epigenomic remodeling of vitamin C-treated dendritic cells. **(A)** Western blot of phosphorylated p65 (p-p65) (Ser536) and total p65 in whole-cell lysates. β -actin was used as a loading control. **(B)** Western blot of p-p65 in the nuclear (NF) and cytoplasmic fractions (CF). GAPDH and histone H1 proteins were used as loading control for cytoplasm and nuclei, respectively. **(C)** Scheme depicting the inhibition of p65. Monocytes (MO) were differentiated to dendritic cells (DCs) using GM-CSF and IL-4, in the presence or absence of vitamin C (vitC). On day 5, lipopolysaccharide (LPS) and BAY 11-7082 (Bay) or equivalent amounts of dilute were added to the cell culture. On day 7, iDC/iDC_{vitC}, iDC + Bay/iDC_{vitC} + Bay, mDC/mDC_{vitC} and mDC + Bay/mDC_{vitC} + Bay were obtained. **(D)** Scatter plots of M1 and M2 DMPs showing DNA methylation (β -values) of Bay-treated (y-axis) versus untreated mDCs/mDC_{vitC} (x-axis). Contour lines represent a 2D kernel density estimation. Labels with selected examples indicate the DMPs associated with these previously shown genes (Figure 3C, D). **(E)** Methylated CpG set enrichment analysis (mCSEA) of mDC_{vitC} versus mDC_{vitC} + Bay, using M2 DMPs as CpG set. The running enrichment score is represented and the normalized enrichment score (NES) and FDR are shown above. **(F)** The average gene expression of C1QB (M1-associated gene) and M2-associated genes (LTA, IKBKE and IRF8) obtained with RT-qPCR are represented with points, and the black lines indicate the standard error of the mean. P -values of paired t -tests are shown ($n = 6$) (ns: $P > 0.05$, * $P < 0.05$, ** $P < 0.01$). **(G)** Western blot of the co-immunoprecipitation of p65, showing the signal of p65 and TET2 proteins. Below, the image signal quantifications of three independent western blots are shown for each protein. P -values of paired t -tests are shown ($n = 3$) (mean \pm standard error of the mean) (* $P < 0.05$, ** $P < 0.01$). **(H)** Chromatin Immunoprecipitation (ChIP) signal of p65 binding to a negative control locus (*INS*) and around an M2 DMPs (cg08639424) associated with *LTA* and *TNF*. The RT-qPCR signal relative to the ChIP input is shown ($n = 3$). P -values of t -tests are shown ($n = 3$) (mean \pm standard error of the mean) (ns: $P > 0.05$, * $P < 0.05$). **(I)** TNF β production of mDCs and mDC_{vitC}, after 5 days of differentiation and 48h of maturation with LPS. The P -value of a Wilcoxon rank-sum test is shown ($n = 3$)

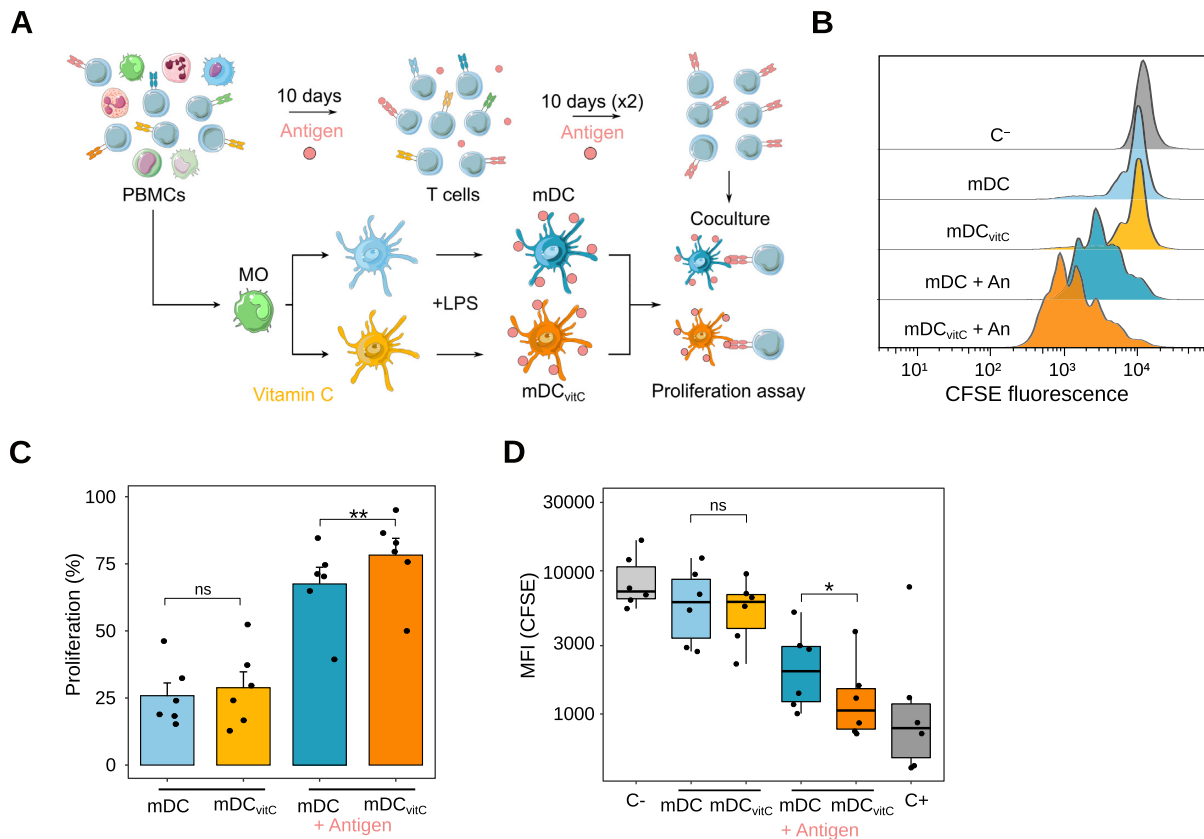


Figure 5. Functional and phenotypic alterations of vitamin C-treated dendritic cells. (A) Scheme depicting the T cell proliferation assay. PBMCs were obtained from healthy donors. T cell clones reacting to the specific antigen (SARS-CoV-2 protein S) were selected through several rounds of clonal expansion. On the other hand, mDCs and mDC_{vitC} were obtained from the same donor and charged with the specific antigen. Finally, the Carboxyfluorescein succinimidyl ester (CFSE)-stained T cells were cocultured with mDCs/mDC_{vitC} for 5 days. (B) Selected example of a histogram of CFSE signal from T cells, alone without stimulation (C⁻) or cocultured with mDC/mDC_{vitC} treated with a control antigen or a specific set of antigens of SARS-CoV-2 (An). When T cells proliferate, the CFSE signal is diminished. The statistical analysis with all the replicates can be observed in panels C and D. (C) The proliferation of T cells cocultured with mDC/mDC_{vitC} (2:1 proportion), with or without the loading with a specific set of antigens of SARS-CoV-2. Negative control from each donor was used to calculate the proliferation percentage. *P*-values from two-tailed paired *t*-tests are shown ($n = 6$) (ns: $P > 0.05$, ** $P < 0.01$). (D) Median Fluorescence Intensity (MFI) of T cells alone (C⁻), cocultured with mDC/mDC_{vitC} (2:1 proportion), with or without the loading with a specific set of antigens of SARS-CoV-2, or stimulated with CD3/CD28 activation beads (C⁺). *P*-values from two-tailed paired *t*-tests are shown ($n = 6$) (ns: $P > 0.05$, * $P < 0.05$).

with vitamin C treatment at day 2 of differentiation. In contrast, most variance in methylation occurring in the MO-to-iDC transition occurs before day 2 suggesting that, without vitamin C, the function of TET enzymes in this model is progressively diminished. Alternative reducing agents present in the culture medium such as glutathione are less efficient as TET cofactors (45,47). Thus, the progressive oxidation of these reducing agents may explain the impairment of TET function over time in the absence of vitamin C.

Vitamin C-mediated demethylation occurs during the differentiation (M1 cluster) or the maturation of DCs (M2 cluster). Interestingly, the sets of transcription factor motifs enriched in the M1 and M2 clusters are equivalent to the transcription factors involved in DC differentiation and LPS-mediated signaling, respectively. This suggests that, overall, vitamin C does not promote the recruitment of TET enzymes through new pathways but boosts the demethylation triggered by preexisting active signaling pathways. In fact, TET2 lacks the CXXC domain that enables di-

rect CpG-binding of the other TETs (TET1 and TET3). In this respect, its targeting depends on transcription factors or their co-factors for locus-specific recruitment (11,48). In addition, the effect of vitamin C of preexisting active signaling pathways is highlighted by the fact that M1 and M2 DMPs are enriched in regions with increasing active chromatin marks (H3K27ac and H3K4me1) in the MO-to-iDC and the iDC-to-mDC transitions, respectively (Supplementary Figure 1D). We cannot rule out that vitamin C produces changes in histone modifications or DNA accessibility that may contribute to the phenotype. In this regard, vitamin C also increases the enzymatic activity of histone demethylases (15).

Since vitamin C can potentiate demethylation triggered by preexisting pathways, we hypothesize that this treatment may have diverse effects depending on the specific context and active transcription factors. In this regard, vitamin C could potentiate demethylation in other models of monocyte differentiation to DCs with clinical use, such as tolerogenic DCs (12,13).

The functional relationship between DNA demethylation and gene expression has been extensively studied in several biological contexts (7,9,12,13). Genes more expressed in mDC_{vitC} than mDC, from E1 and E2 clusters are enriched in M1-associated genes. This establishes a clear temporal relationship, suggesting that prior demethylation could protect some genes from downregulation during DC maturation. On the other hand, genes from the E5 cluster are enriched in M2-associated genes. In this case, demethylation is occurring at the same step as upregulation. Then, we cannot discern whether demethylation or upregulation occurs first. However, since the primary mechanism of action of vitamin C through DNA and histone demethylation is well known, we hypothesize that epigenetic modifications could mediate gene upregulation in mDC_{vitC}. This assumption starts from a different point than other works that established DNA demethylation during DC maturation as a consequence of gene upregulation because in that case, the differential stimulus is live bacteria, that can activate a plethora of signaling pathways not necessarily linked directly to DNA demethylation (9).

NF- κ B mediates both demethylation and upregulation during the maturation of DCs in the presence of vitamin C (Figure 4D and E). Since that pathway is associated with toll-like receptor 4 (TLR4), which recognizes LPS, it is not surprising that it plays a role in the process. Intriguingly, this factor is present in the nucleus in mDCs and mDC_{vitC}, interacts with TET2, and binds in both cases to CpGs that become demethylated only in mDC_{vitC}. We postulate that NF- κ B genomic binding in mDCs and mDC_{vitC} is probably similar, but vitamin C potentiates TET2 function allowing the demethylation of genomic loci, which may condition the expression of the associated genes. Moreover, NF- κ B also drives vitamin C-mediated production of TNF β . This cytokine can signal through tumor necrosis factor receptor (TNFR)I and TNFRII to activate the NF- κ B pathway in both DCs and T cells and has shown anti-carcinogenic properties in animal models (49–51).

Linus Pauling proposed vitamin C as a potential cancer treatment >40 years ago, but the negative results of further clinical trials diminished the enthusiasm (52,53). However, during the last few years, increasing interest has arisen around vitamin C as a treatment or adjuvant for several types of cancer. For instance, intravenous vitamin C treatment in mice abrogates cancer progression through direct TET2 function restoration in cancer cells (17). Moreover, clinical remission following vitamin C treatment was found in a case of acute myeloid leukemia with mutations in *TET2* (54). Furthermore, in mice models of different types of cancer, a fully competent immune system was required to maximize the antiproliferative effects of vitamin C, suggesting an effect of that molecule in the modulation of the immune system (18). Vitamin C has already been reported to play a role in actively demethylating CNS2 in iTregs by activating TET2. Vitamin C treated iTregs could maintain high levels of Foxp3 (55–57). However, those iTregs failed to survive and maintain proper immune responses in complex GvHD models because CpG islands of non-targeted genes, probably pro-apoptotic genes, were also demethylated. Thus, clinical use of those iTregs is impractical. In this regard, in the context of DCs the observation that the implicated TFs are

mainly related to differentiation and activation might confer a better outcome.

Therapies based on autologous DCs (DC vaccines) has been extensively investigated, with >200 completed clinical trials to date (19). Most efforts have been focused on cancer, but some clinical trials have also been initiated to treat infectious diseases such as COVID19 (NCT04685603, NCT05007496) (58). The use of moDCs differentiated *ex vivo* from monocytes of the same donor is a common and straightforward approach to generating DC vaccines, given the relatively high abundance of these cells in the human blood. However, the lower antigen presentation capabilities of moDCs in comparison with blood DCs is a bottleneck for the efficacy of these treatments (59).

Here, we show that mDC_{vitC} loaded with SARS-CoV-2 antigens can stimulate the proliferation of autologous antigen-specific T cells more efficiently than mDCs. This indicates that vitamin C induces an increase of the antigen presentation capabilities of mDCs in an antigen-specific fashion, and could be a promising strategy for generating DC vaccines towards specific tumor antigens. These results can lead to the generation of new *in vitro* protocols for the generation of moDC vaccines with higher performance. However, multiple considerations should be taken into account to consider the viability of these treatments in the cancer context, including the survival of these cells and the maintenance of their enhanced immunogenic responses. Further works using animal models and human *in vivo* moDCs from patients treated with high doses of vitamin C should shed light on the specific clinical implications of these insights.

DATA AVAILABILITY

All DNA methylation and expression datasets for this publication have been deposited in the NCBI Gene Expression Omnibus and are accessible through GEO SuperSeries accession number GSE203463.

SUPPLEMENTARY DATA

Supplementary Data are available at NAR Online.

ACKNOWLEDGEMENTS

We thank CERCA Programme/Generalitat de Catalunya and the Josep Carreras Foundation for institutional support.

Author contributions: O.M.-P. and E.B. conceived and designed the study; O.M.-P., G.G.-T., J.C.-S., L.C., E.M.-C. and J.L.S. performed experiments; O.M.-P. performed the bioinformatic analyses; O.M.-P. and E.B. wrote the manuscript; all authors participated in discussions and interpreting the results.

FUNDING

E.B. was funded by the Spanish Ministry of Science and Innovation [PID2020-117212RB-I00, AEI/10.13039/501100011033] and Instituto de Salud Carlos III (ISCIII), Ref. AC18/00057, associated with

i-PAD project (ERARE European Union program); J.L.S. was funded by Instituto de Salud Carlos III through the project CP19/00176 (co-funded by European Social Fund, ‘Investing in your future’); Spanish Ministry of Science, Innovation and Universities (MICINN) [PID2019-111243RA-I00/AEI/10.13039/501100011033]; E.M.C. is funded by project PI20/01313, integrated in the Plan Nacional de I + D + I and co-supported by the ISCIII-Subdirección General de Evaluación and the Fondo Europeo de Desarrollo Regional (FEDER); O.M.-P. holds an i-PFIS PhD fellowship [IF117/00034] from Acción Estratégica en Salud 2013–2016 ISCIII, co-financed by Fondo Social Europeo. Funding for open access charge: Spanish Ministry of Science and Innovation [PID2020-117212RB-I00, AEI/10.13039/501100011033].

Conflict of interest statement. None declared.

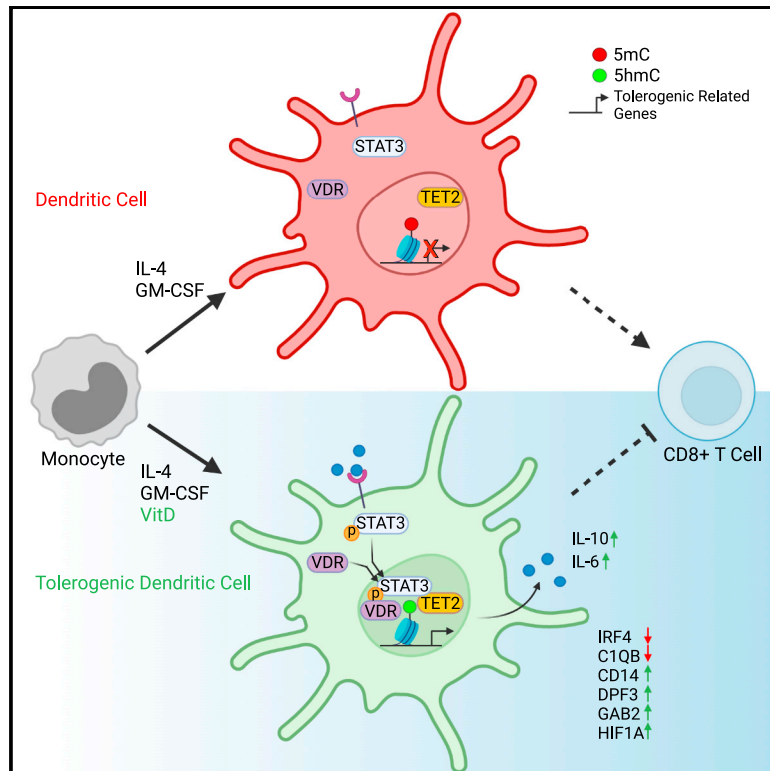
REFERENCES

- Morante-Palacios, O., Fondelli, F., Ballestar, E. and Martínez-Cáceres, E.M. (2021) Tolerogenic dendritic cells in autoimmunity and inflammatory diseases. *Trends Immunol.*, **42**, 59–75.
- Sallusto, F. and Lanzavecchia, A. (1994) Efficient presentation of soluble antigen by cultured human dendritic cells is maintained by granulocyte/macrophage colony-stimulating factor plus interleukin 4 and downregulated by tumor necrosis factor alpha. *J. Exp. Med.*, **179**, 1109–1118.
- Collin, M. and Bigley, V. (2018) Human dendritic cell subsets: an update. *Immunology*, **154**, 3–20.
- Coillard, A. and Segura, E. (2019) In vivo differentiation of human monocytes. *Front. Immunol.*, **10**, 1907.
- Rodríguez, R.M., Suarez-Alvarez, B., Lavín, J.L., Ascensión, A.M., González, M., Lozano, J.J., Raneros, A.B., Bulnes, P.D., Vidal-Castañeira, J.R., Huidobro, C. *et al.* (2019) Signal integration and transcriptional regulation of the inflammatory response mediated by the GM-/M-CSF signaling axis in human monocytes. *Cell Rep.*, **29**, 860–872.
- de la Rica, L., Rodríguez-Ubreva, J., García, M., Islam, A.B.M.M.K., Urquiza, J.M., Hernando, H., Christensen, J., Helin, K., Gómez-Vaquero, C. and Ballestar, E. (2013) PU.1 target genes undergo Tet2-coupled demethylation and DNMT3b-mediated methylation in monocyte-to-osteoclast differentiation. *Genome Biol.*, **14**, R99.
- Vento-Tormo, R., Company, C., Rodríguez-Ubreva, J., de la Rica, L., Urquiza, J.M., Javierre, B.M., Sabarinathan, R., Luque, A., Esteller, M., Aran, J.M. *et al.* (2016) IL-4 orchestrates STAT6-mediated DNA demethylation leading to dendritic cell differentiation. *Genome Biol.*, **17**, 4.
- Álvarez-Errico, D., Vento-Tormo, R., Sieweke, M. and Ballestar, E. (2015) Epigenetic control of myeloid cell differentiation, identity and function. *Nat. Rev. Immunol.*, **15**, 7–17.
- Pacis, A., Mailhot-Léonard, F., Tailleux, L., Randolph, H.E., Yotova, V., Dumaine, A., Grenier, J.-C. and Barreiro, L.B. (2019) Gene activation precedes DNA demethylation in response to infection in human dendritic cells. *Proc. Natl. Acad. Sci. U.S.A.*, **116**, 6938–6943.
- Klug, M., Schmidhofer, S., Gebhard, C., Andreesen, R. and Rehli, M. (2013) 5-Hydroxymethylcytosine is an essential intermediate of active DNA demethylation processes in primary human monocytes. *Genome Biol.*, **14**, R46.
- Mendes, K., Schmidhofer, S., Minderjahn, J., Glatz, D., Kiesewetter, C., Raithe, J., Wimmer, J., Gebhard, C. and Rehli, M. (2021) The epigenetic pioneer EGR2 initiates DNA demethylation in differentiating monocytes at both stable and transient binding sites. *Nat. Commun.*, **12**, 1556.
- Morante-Palacios, O., Ciudad, L., Micheroli, R., de la Calle-Fabregat, C., Li, T., Barbisan, G., Houtman, M., Edalat, S.G., Frank-Bertoncelj, M., Ospelt, C. *et al.* (2022) Coordinated glucocorticoid receptor and MAFB action induces tolerogenesis and epigenome remodeling in dendritic cells. *Nucleic Acids Res.*, **50**, 108–126.
- Català-Moll, F., Ferreté-Bonastre, A.G., Godoy-Tena, G., Morante-Palacios, O., Ciudad, L., Barberà, L., Fondelli, F., Martínez-Cáceres, E.M., Rodríguez-Ubreva, J., Li, T. *et al.* (2022) Vitamin d receptor, STAT3, and TET2 cooperate to establish tolerogenesis. *Cell Rep.*, **38**, 110244.
- Levine, M., Wang, Y., Padayatty, S.J. and Morrow, J. (2001) A new recommended dietary allowance of vitamin c for healthy young women. *Proc. Natl. Acad. Sci. U.S.A.*, **98**, 9842–9846.
- Ang, A., Pullar, J.M., Currie, M.J. and Vissers, M.C.M. (2018) Vitamin c and immune cell function in inflammation and cancer. *Biochem. Soc. Trans.*, **46**, 1147–1159.
- Jeong, Y.-J., Kim, J.-H., Hong, J.-M., Kang, J.S., Kim, H.-R., Lee, W.J. and Hwang, Y. (2014) Vitamin c treatment of mouse bone marrow-derived dendritic cells enhanced CD8(+) memory t cell production capacity of these cells in vivo. *Immunobiology*, **219**, 554–564.
- Cimmino, L., Dolgalev, I., Wang, Y., Yoshimi, A., Martin, G.H., Wang, J., Ng, V., Xia, B., Witkowski, M.T., Mitchell-Flack, M. *et al.* (2017) Restoration of TET2 function blocks aberrant self-renewal and leukemia progression. *Cell*, **170**, 1079–1095.
- Magri, A., Germano, G., Lorenzato, A., Lamba, S., Chilà, R., Montone, M., Amodio, V., Ceruti, T., Sassi, F., Arena, S. *et al.* (2020) High-dose vitamin c enhances cancer immunotherapy. *Sci. Transl. Med.*, **12**, eaay8707.
- Wculek, S.K., Cueto, F.J., Mujal, A.M., Melero, I., Krummel, M.F. and Sancho, D. (2020) Dendritic cells in cancer immunology and immunotherapy. *Nat. Rev. Immunol.*, **20**, 7–24.
- Schadendorf, D., Ugurel, S., Schuler-Thurner, B., Nestle, F.O., Enk, A., Bröcker, E.-B., Grabbe, S., Rittgen, W., Edler, L., Sucker, A. *et al.* (2006) Dacarbazine (DTIC) versus vaccination with autologous peptide-pulsed dendritic cells (DC) in first-line treatment of patients with metastatic melanoma: a randomized phase III trial of the DC study group of the DeCOG. *Ann. Oncol.*, **17**, 563–570.
- Liau, L.M., Ashkan, K., Tran, D.D., Campian, J.L., Trusheim, J.E., Cobbs, C.S., Heth, J.A., Salacz, M., Taylor, S., D’Andre, S.D. *et al.* (2018) First results on survival from a large phase 3 clinical trial of an autologous dendritic cell vaccine in newly diagnosed glioblastoma. *J. Transl. Med.*, **16**, 142.
- Godoy-Tena, G. and Ballestar, E. (2022) Epigenetics of dendritic cells in tumor immunology. *Cancers (Basel)*, **14**, 1179.
- Morante-Palacios, O. and Ballestar, E. (2021) shinyÉPICo: a graphical pipeline to analyze illumina DNA methylation arrays. *Bioinformatics*, **37**, 257–259.
- Aryee, M.J., Jaffe, A.E., Corrada-Bravo, H., Ladd-Acosta, C., Feinberg, A.P., Hansen, K.D. and Irizarry, R.A. (2014) Minfi: a flexible and comprehensive bioconductor package for the analysis of infinium DNA methylation microarrays. *Bioinformatics*, **30**, 1363–1369.
- Ritchie, M.E., Phipson, B., Wu, D., Hu, Y., Law, C.W., Shi, W. and Smyth, G.K. (2015) limma powers differential expression analyses for RNA-sequencing and microarray studies. *Nucleic Acids Res.*, **43**, e47.
- Touleimat, N. and Tost, J. (2012) Complete pipeline for infinium(®) human methylation 450K beadchip data processing using subset quantile normalization for accurate DNA methylation estimation. *Epigenomics*, **4**, 325–341.
- Triche, T.J. Jr, Weisenberger, D.J., Van Den Berg, D., Laird, P.W. and Siegmund, K.D. (2013) Low-level processing of illumina infinium DNA methylation beadarrays. *Nucleic Acids Res.*, **41**, e90.
- Hinrichs, A.S., Karolchik, D., Baertsch, R., Barber, G.P., Bejerano, G., Clawson, H., Diekhans, M., Furey, T.S., Hart, R.A., Hsu, F. *et al.* (2006) The UCSC genome browser database: update 2006. *Nucleic Acids Res.*, **34**, D590–D598.
- Kim, D., Paggi, J.M., Park, C., Bennett, C. and Salzberg, S.L. (2019) Graph-based genome alignment and genotyping with HISAT2 and HISAT-genotype. *Nat. Biotechnol.*, **37**, 907–915.
- 1000 Genome Project Data Processing Subgroup, Li, H., Handsaker, B., Wysoker, A., Fennell, T., Ruan, J., Homer, N., Marth, G., Abecasis, G. and Durbin, R. (2009) The sequence alignment/map format and SAMtools. *Bioinformatics*, **25**, 2078–2079.
- Liao, Y., Smyth, G.K. and Shi, W. (2014) featureCounts: an efficient general purpose program for assigning sequence reads to genomic features. *Bioinformatics*, **30**, 923–930.

32. Love, M.I., Huber, W. and Anders, S. (2014) Moderated estimation of fold change and dispersion for RNA-seq data with DESeq2. *Genome Biol.*, **15**, 550.
33. Schindelin, J., Arganda-Carreras, I., Frise, E., Kaynig, V., Longair, M., Pietzsch, T., Preibisch, S., Rueden, C., Saalfeld, S., Schmid, B. *et al.* (2012) Fiji: an open-source platform for biological-image analysis. *Nat. Methods*, **9**, 676–682.
34. McLean, C.Y., Bristor, D., Hiller, M., Clarke, S.L., Schaar, B.T., Lowe, C.B., Wenger, A.M. and Bejerano, G. (2010) GREAT improves functional interpretation of cis-regulatory regions. *Nat. Biotechnol.*, **28**, 495–501.
35. Yu, G., Wang, L.-G., Han, Y. and He, Q.-Y. (2012) clusterProfiler: an R package for comparing biological themes among gene clusters. *OMICS*, **16**, 284–287.
36. Jalili, V., Matteucci, M., Masseroli, M. and Morelli, M.J. (2015) Using combined evidence from replicates to evaluate chip-seq peaks. *Bioinformatics*, **31**, 2761–2769.
37. Zerbino, D.R., Johnson, N., Juettemann, T., Wilder, S.P. and Flicek, P. (2014) WiggleTools: parallel processing of large collections of genome-wide datasets for visualization and statistical analysis. *Bioinformatics*, **30**, 1008–1009.
38. Ramirez, F., Dündar, F., Diehl, S. and Grüning, B.A., (2014) Manke T.deepTools: a flexible platform for exploring deep-sequencing data. *Nucleic Acids Res.*, **42**, W187–91.
39. Fernández, J.M., de la Torre, V., Richardson, D., Royo, R., Puiggròs, M., Moncunill, V., Fragkogianni, S., Clarke, L. and BLUEPRINT Consortium BLUEPRINT Consortium and Flicek, P. *et al.* (2016) The BLUEPRINT data analysis portal. *Cell Syst*, **3**, 491–495.
40. Johnson, J.S., Lucas, S.Y., Amon, L.M., Skelton, S., Nazitto, R., Carbonetti, S., Sather, D.N., Littman, D.R. and Aderem, A. (2018) Reshaping of the dendritic cell chromatin landscape and interferon pathways during HIV infection. *Cell Host Microbe*, **23**, 366–381.
41. Lachmann, A., Xu, H., Krishnan, J., Berger, S.I., Mazloom, A.R. and Ma'ayan, A. (2010) ChEA: transcription factor regulation inferred from integrating genome-wide ChIP-X experiments. *Bioinformatics*, **26**, 2438–2444.
42. Lee, J., Rhee, M.H., Kim, E. and Cho, J.Y. (2012) BAY 11-7082 is a broad-spectrum inhibitor with anti-inflammatory activity against multiple targets. *Mediators Inflamm.*, **2012**, 416036.
43. de la Rica, L., García-Gómez, A., Comet, N.R., Rodríguez-Ubreva, J., Ciudad, L., Vento-Tormo, R., Company, C., Álvarez-Errico, D., García, M., Gómez-Vaquero, C. *et al.* (2015) NF- κ B-direct activation of microRNAs with repressive effects on monocyte-specific genes is critical for osteoclast differentiation. *Genome Biol.*, **16**, 2.
44. Wu, X. and Zhang, Y. (2017) TET-mediated active DNA demethylation: mechanism, function and beyond. *Nat. Rev. Genet.*, **18**, 517–534.
45. Minor, E.A., Court, B.L., Young, J.I. and Wang, G. (2013) Ascorbate induces ten-eleven translocation (Tet) methylcytosine dioxygenase-mediated generation of 5-hydroxymethylcytosine. *J. Biol. Chem.*, **288**, 13669–13674.
46. Pacis, A., Tailleux, L., Morin, A.M., Lambourne, J., MacIsaac, J.L., Yotova, V., Dumaine, A., Danckaert, A., Luca, F., Grenier, J.-C. *et al.* (2015) Bacterial infection remodels the DNA methylation landscape of human dendritic cells. *Genome Res.*, **25**, 1801–1811.
47. Blaschke, K., Ebata, K.T., Karimi, M.M., Zepeda-Martínez, J.A., Goyal, P., Mahapatra, S., Tam, A., Laird, D.J., Hirst, M., Rao, A. *et al.* (2013) Vitamin c induces Tet-dependent DNA demethylation and a blastocyst-like state in ES cells. *Nature*, **500**, 222–226.
48. Ravichandran, M., Jurkowska, R.Z. and Jurkowski, T.P. (2018) Target specificity of mammalian DNA methylation and demethylation machinery. *Org. Biomol. Chem.*, **16**, 1419–1435.
49. Bauer, J., Namineni, S., Reisinger, F., Zöller, J., Yuan, D. and Heikenwälder, M. (2012) Lymphotoxin, NF- κ B, and cancer: the dark side of cytokines. *Dig. Dis.*, **30**, 453–468.
50. Browning, J.L., Miatkowski, K., Sizing, I., Griffiths, D., Zafari, M., Benjamin, C.D., Meier, W. and Mackay, F. (1996) Signaling through the lymphotoxin beta receptor induces the death of some adenocarcinoma tumor lines. *J. Exp. Med.*, **183**, 867–878.
51. Lukashev, M., LePage, D., Wilson, C., Bailly, V., Garber, E., Lukashin, A., Ngam-ek, A., Zeng, W., Allaire, N., Perrin, S. *et al.* (2006) Targeting the lymphotoxin-beta receptor with agonist antibodies as a potential cancer therapy. *Cancer Res.*, **66**, 9617–9624.
52. Cameron, E. and Pauling, L. (1976) Supplemental ascorbate in the supportive treatment of cancer: prolongation of survival times in terminal human cancer. *Proc. Natl. Acad. Sci. U.S.A.*, **73**, 3685–3689.
53. Cabanillas, F. (2010) Vitamin c and cancer: what can we conclude—1,609 patients and 33 years later? *P. R. Health Sci. J.*, **29**, 215–217.
54. Das, A.B., Kakadia, P.M., Wojcik, D., Pemberton, L., Browett, P.J., Bohlander, S.K. and Vissers, M.C.M. (2019) Clinical remission following ascorbate treatment in a case of acute myeloid leukemia with mutations in TET2 and WT1. *Blood Cancer J.*, **9**, 82.
55. Sasidharan Nair, V., Song, M.H. and Oh, K.I. (2016) Vitamin c facilitates demethylation of the foxp3 enhancer in a tet-dependent manner. *J. Immunol.*, **196**, 2119–2131.
56. Kasahara, H., Kondo, T., Nakatsukasa, H., Chikuma, S., Ito, M., Ando, M., Kurebayashi, Y., Sekiya, T., Yamada, T., Okamoto, S. *et al.* (2017) Generation of allo-antigen-specific induced treg stabilized by vitamin c treatment and its application for prevention of acute graft versus host disease model. *Int. Immunol.*, **29**, 457–469.
57. Iamsawat, S., Tian, L., Daenthanasamak, A., Wu, Y., Nguyen, H.D., Bastian, D. and Yu, X.Z. (2019) Vitamin c stabilizes CD8+ iTregs and enhances their therapeutic potential in controlling murine GVHD and leukemia relapse. *Blood Adv.*, **3**, 4187–4201.
58. Galati, D., Zanutta, S., Capitelli, L. and Bocchino, M. (2022) A bird's eye view on the role of dendritic cells in SARS-CoV-2 infection: perspectives for immune-based vaccines. *Allergy*, **77**, 100–110.
59. Garg, A.D., Coulie, P.G., Van den Eynde, B.J. and Agostinis, P. (2017) Integrating next-generation dendritic cell vaccines into the current cancer immunotherapy landscape. *Trends Immunol.*, **38**, 577–593.

Vitamin D receptor, STAT3, and TET2 cooperate to establish tolerogenesis

Graphical abstract



Authors

Francesc Català-Moll,
Anna G. Ferreté-Bonastre,
Gerard Godoy-Tena, ...,
Javier Rodríguez-Ubrea, Tianlu Li,
Esteban Ballestar

Correspondence

eballestar@carrerasresearch.org

In brief

Català-Moll et al. show that vitamin D induces DNA demethylation and transcriptional activation at VDR binding sites, as well as IL-6-JAK-STAT3 pathway activation associated with acquisition of tolerogenesis by dendritic cells. VDR, STAT3, and TET2 interact with each other. Pharmacological inhibition of JAK2 reverts vitamin D-induced tolerogenic properties of DCs.

Highlights

- Vitamin D induces DNA demethylation at VDR binding sites in dendritic cells (DCs)
- Differentiation to tolerogenic DCs associates with IL-6-JAK-STAT3 pathway activation
- VDR, STAT3, and TET2 interact with each other in tolerogenic DCs
- Pharmacological inhibition of JAK2 reverts vitamin D-induced DC tolerogenesis



Article

Vitamin D receptor, STAT3, and TET2 cooperate to establish tolerogenesis

Francesc Català-Moll,^{1,4} Anna G. Ferreté-Bonastre,^{1,4} Gerard Godoy-Tena,^{1,4} Octavio Morante-Palacios,¹ Laura Ciudad,¹ Laura Barberà,¹ Federico Fondelli,^{2,3} Eva M. Martínez-Cáceres,^{2,3} Javier Rodríguez-Ubreva,¹ Tianlu Li,^{1,4} and Esteban Ballestar^{1,5,*}

¹Epigenetics and Immune Disease Group, Josep Carreras Research Institute (IJC), Badalona, 08916 Barcelona, Spain

²Division of Immunology, Germans Trias i Pujol Hospital, LCMN, Germans Trias i Pujol Research Institute (IGTP), Badalona, 08916 Barcelona, Spain

³Department of Cell Biology, Physiology, Immunology, Autonomous University of Barcelona, Bellaterra, 08193 Barcelona, Spain

⁴These authors contributed equally

⁵Lead contact

*Correspondence: eballestar@carrerasresearch.org

<https://doi.org/10.1016/j.celrep.2021.110244>

SUMMARY

The active form of vitamin D, 1,25-dihydroxyvitamin D₃, induces a stable tolerogenic phenotype in dendritic cells (DCs). This process involves the vitamin D receptor (VDR), which translocates to the nucleus, binds its cognate genomic sites, and promotes epigenetic and transcriptional remodeling. In this study, we report the occurrence of vitamin D-specific DNA demethylation and transcriptional activation at VDR binding sites associated with the acquisition of tolerogenesis *in vitro*. Differentiation to tolerogenic DCs associates with activation of the IL-6-JAK-STAT3 pathway. We show that JAK2-mediated STAT3 phosphorylation is specific to vitamin D stimulation. VDR and the phosphorylated form of STAT3 interact with each other to form a complex with methylcytosine dioxygenase TET2. Most importantly, pharmacological inhibition of JAK2 reverts vitamin D-induced tolerogenic properties of DCs. This interplay among VDR, STAT3, and TET2 opens up possibilities for modulating DC immunogenic properties in clinics.

INTRODUCTION

Dendritic cells (DCs) are a heterogeneous group of innate immune cells that have a key role in initiating adaptive responses. Also, DCs are not only central for coordinating immune responses against a threat but also needed to regulate the immune system at steady state and for inducing immune tolerance (Morante-Palacios et al., 2021). Like in other myeloid cell populations, the immunological properties of DCs vary with the environment. In general, terminal myeloid cell differentiation is highly dependent on the activation of specific signaling pathways in response to extracellular signals, such as inflammatory cytokines, hormones, vitamins, and other factors (Álvarez-Errico et al., 2015), which determine the immunogenicity of the resulting myeloid cells. The activation of signaling pathways leads to the activation of specific sets of transcription factors (TFs). Sequence-specific DNA binding of TFs is a pivotal process for establishing gene expression patterns in concert with the epigenetic machinery that determines cell identity and function (Monticelli and Natoli, 2017). Recent evidence has shown that several TFs are associated with DNA demethylation to increase genomic accessibility of their binding genomic regions, thus facilitating the binding of subsequent TFs (Mahé et al., 2017). In this regard, methylcytosine dioxygenase ten-eleven translocation (TET2), the most relevant enzyme involved in active DNA demethylation in the myeloid

compartment, can interact with a variety of TFs, such as PU.1, C/EBP α , KLF4, and others, in order to facilitate their recruitment to different genomic regions (Costa et al., 2013; Guilhamon et al., 2013; de la Rica et al., 2013; Lio et al., 2016; Mendes et al., 2021; Sardina et al., 2018; Wang et al., 2015; Xiong et al., 2016). Recently, it has been demonstrated that TET2 mutations, which are frequent in myeloid leukemias, lead to DNA hypermethylation of enhancer regions and changes in the subsequent binding of TFs, particularly members of the basic helix-loop-helix (bHLH) TF family (Rasmussen et al., 2019). This suggests that TET2 recruitment by TFs leads to epigenetic remodeling that facilitates the binding of subsequent TFs (Rasmussen et al., 2019). Moreover, a reciprocal relationship between DNA methylation and histone modifications has long been established. TET2 has been not only described to modulate trimethylation of K4 of histone H3 (H3K4me3) (Deplus et al., 2013), a mark of active transcription, but also shown to coordinate trimethylation of K27 of histone H3 (H3K27me3), a mark of heterochromatin, in an inverse manner (Ichiyama et al., 2015).

Calcitriol (1,25-dihydroxyvitamin D₃), the active form of vitamin D₃ (henceforth referred to as vitamin D), is a major modulator of the immune system (Barragan et al., 2015; Carlberg, 2019; Mora et al., 2008). DCs are the most susceptible cell type to vitamin D in a mixed immune population (Mora et al., 2008). In these cells, vitamin D can generate a stable maturation-resistant tolerogenic



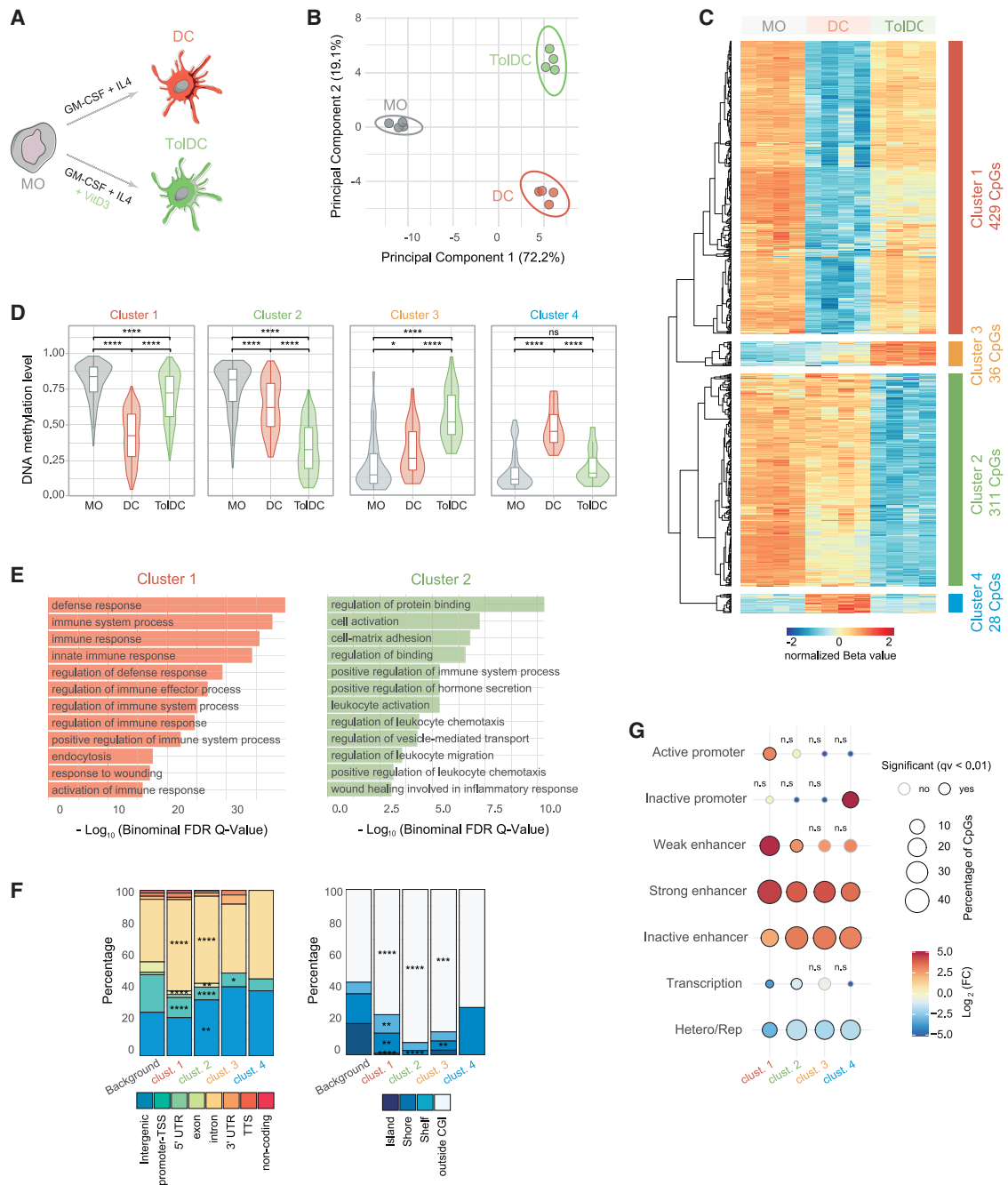


Figure 1. DNA methylation dynamics throughout vitamin D-exposed dendritic-cell differentiation (n = 4, two independent experiments)

(A) Schematic overview of the differentiation model from human peripheral blood MOs to DCs and ToIDCs.

(B) Principal-component analysis of differentially methylated CpGs.

(C) DNA methylation heatmap and cluster analysis of four paired samples of MOs and their derived DCs and ToIDCs at day 5 of differentiation. The heatmap includes all CpG-containing probes displaying significant methylation changes (differential beta value ≥ 0.2 and q value < 0.05) only in the ToIDC-DC comparison. The color annotation of the lateral bar represents the membership to cluster 1 in red (DC-specific DNA demethylation), cluster 2 in green (ToIDC-specific DNA demethylation), cluster 3 in orange (ToIDC-specific DNA hypermethylation), and cluster 4 in blue (DC-specific DNA hypermethylation).

(D) Box and violin plots summarizing the distribution of DNA methylation levels per cell type and cluster.

(E) Gene ontology (GO) terms associated with CpGs from cluster 1 (red) and cluster 2 (green) as analyzed by GREAT software. Bars represent log-transformed binomial q values of the GO term enrichment.

(F) Location proportions of CpGs from each cluster in the context of CpG islands (CGIs) (right) and gene-related regions (left).

(legend continued on next page)

phenotype *in vitro*, with a low level of expression of immunogenic molecules, such as HLA-DR, CD80, and CD86, and increased interleukin (IL)-10/IL-12p70 ratios that are maintained even after removal of the compound (Van Halteren et al., 2002). After ligand recognition, vitamin D receptor (VDR) translocates to the nucleus and acts not only as a TF, controlling the expression of a set of immune and metabolic genes (Carlberg, 2019; Ferreira et al., 2013), but also as a repressor of nuclear factor kappa-light-chain-enhancer of activated B cells (NF- κ B) at different levels (Carlberg, 2019; Fetahu et al., 2014). Several studies have shown the capacity of VDR to interact with a range of TFs, including PU.1 and GABPA, and with chromatin remodeling and histone modification enzymes, such as BRD7 and KDM6B (Pereira et al., 2011; Seuter et al., 2017, 2018; Wei et al., 2018). Previous work has shown that vitamin D may induce DNA methylation changes in myeloid cells (Ong et al., 2021). However, the molecular mechanism that leads to the acquisition of differential methylation patterns remains unexplored.

Vitamin D supplementation is generally used as a preventive agent or a co-adjuvant for diseases with underlying autoimmune or pro-inflammatory states (Bscheider and Butcher, 2016; Dankers et al., 2017). DCs represent an excellent target of vitamin D to dampen autoimmunity and inflammation, not only because these myeloid cells express the whole set of enzymes to generate the active form of vitamin D (Mora et al., 2008) but also because of their unique role as initiators of immune responses. However, the role of DCs in vitamin D-mediated immunomodulation is not fully understood. In addition, DCs with tolerogenic function (ToIDCs) have become a promising immunotherapeutic tool for reinstating immune tolerance in autoimmune diseases and in allogeneic bone marrow and solid organ transplantation (Morante-Palacios et al., 2021). The stability of the tolerogenic phenotype suggests that regulatory mechanisms that allow the maintenance of stable changes of gene expression are involved. In this sense, DNA methylation is a major epigenetic modification closely involved in the acquisition or stabilization of transcriptional states (Luo et al., 2018). Peripheral blood monocyte (MO)-derived DCs represent a useful model for studying the properties of DCs. It has been previously described that DCs differentiated from isolated MOs by the addition of granulocyte-macrophage colony-stimulating factor (GM-CSF) and IL-4 *in vitro* closely resemble CD1c⁺ DCs at the transcriptional level (Goudot et al., 2017). Exposure of MO-derived DCs to vitamin D results in the inhibition of differentiation and maturation into potent antigen-presenting cells and gain in the capacity to inhibit T cell proliferation (Piemonti et al., 2000). Similarly, CD1c⁺ DCs cultured *in vitro* with vitamin D for 2 days acquire a typical semi-mature phenotype after exposure to a DC maturation cocktail, with low CD83 expression, and a tolerogenic phenotype, as they suppressed alloimmunity *in vivo*, in a mouse model (Chu et al., 2012).

In this study, we studied epigenetic determinants critical for the acquisition of tolerogenic properties during *in vitro* human MO-derived DC differentiation in the presence of vitamin D. We demonstrate an interplay between VDR and the Janus kinase (JAK) 2/signal transducer and activator of transcription (STAT) 3 pathway associated with the generation of a specific TET-dependent DNA demethylation signature in ToIDCs. It involves a direct physical interaction between VDR, STAT3, and TET2 that leads to the acquisition and stabilization of the tolerogenic properties of DCs in the presence of vitamin D.

RESULTS

Vitamin D induces the acquisition of a specific DNA methylation profile associated with tolerogenesis during *in vitro* DC differentiation

To investigate the effects of vitamin D in DNA methylation during the acquisition of tolerogenic properties by DCs, we first differentiated *in vitro* peripheral blood MOs from human donors to DCs and ToIDCs for 6 days using GM-CSF and IL-4 in the absence and presence of vitamin D, respectively (Figure 1A). As previously described (Penna and Adorini, 2000; Piemonti et al., 2000), ToIDCs had higher levels of the surface markers CD14 and CD11b and lower levels of HLA-DR, CD1a, and CD86 than did DCs (Figure S1A). To confirm the resemblance between our *in vitro* model with *in vivo* DCs, we integrated the expression profiles of MOs, DCs (12 h and 120 h), and ToIDCs (12 h and 120 h) (Széles et al., 2009) with previously published expression datasets (Goudot et al., 2017; Segura et al., 2013) from MOs, *in vitro*-derived DCs and macrophages (MACs), and *in vivo* DCs and MACs. According to t-distributed stochastic neighbor embedding (t-SNE) analysis, ToIDCs (differentiated in the presence of vitamin D), among different DC subsets, are the ones nearer different MAC types with immunosuppressive phenotypes (Figure S1B).

In concordance with previous studies (Piemonti et al., 2000), we observed that ToIDCs were able to inhibit CD8⁺ T cell proliferation *in vitro*, in contrast to DCs, confirming their immunosuppressive properties (Figure S1C). Furthermore, we also observed increased levels of VDR in the nucleus following vitamin D exposure, in agreement with previous studies, suggesting that VDR preferentially acts in the nucleus (Figure S1D). Altogether, our results confirmed the validity of this *in vitro* model to generate and study ToIDCs by the involvement of VDR through vitamin D exposure.

We then obtained and compared the DNA methylation profiles of MOs, DCs, and ToIDCs using BeadChip arrays (see STAR Methods), which interrogate the methylation status of >850,000 CpG positions across the entire genome, covering 99% of the reference sequence genes. Principal-component analysis (PCA) showed that most of the variability observed at the DNA methylation level may be explained by events common to the two differentiation processes (principal component 1;

(G) Bubble chart depicting the enrichment (red) or depletion (blue) of the CpGs from each cluster in the chromatin states from DCs (Pacis et al., 2015). The circle filling color represents the logarithmic value of the ratio between the percentage of CpGs with the feature in each cluster and the percentage of CpGs with the feature in the background. Circle size indicates the percentage of CpGs from each cluster in the chromatin state, and the circle edge indicates the statistical significance of the enrichment (black: significant; no edge: not significant; q value < 0.01).

Statistical tests: paired two-tailed t test (D), Pearson correlation (E), and two-tailed Fisher's exact test (F and G) (*p < 0.05; **p < 0.01; ***p < 0.001; ****p < 0.0001, ns = not significant). FDR, false discovery rate.

Figure 1B). However, the second principal component is capable of clustering DCs and TolDCs separately (Figure 1B). Differentiation mainly resulted in DNA demethylation in which there were both condition-specific demethylation events and demethylation events common to both differentiation processes (Figure S1E). A small proportion of DNA methylation changes was attributed to gains of DNA methylation during differentiation (Figure S1E). Hierarchical clustering of differentially methylated CpGs between DCs and TolDCs (adjusted $p < 0.05$ and absolute differential $\beta \geq 0.2$) revealed four main groups of CpG sites (Figures 1C and 1D and Table S1): a group of CpGs that underwent specific demethylation in DCs (cluster 1: 429 CpGs); a second group that was specifically demethylated in TolDCs (cluster 2: 311 CpGs); another group that gained methylation in TolDCs (cluster 3: 36 CpGs); and finally a group of CpGs with DC-specific gains in DNA methylation (cluster 4: 28 CpGs).

To confirm these observations in the context of *in vivo* circulating DCs, we obtained the DNA methylation profiles of whole blood-isolated cDCs (CD11c⁺ DCs) cultured in the absence and presence of vitamin D for 3 days and observed that, similar to TolDCs generated *in vitro*, cDCs exposed to vitamin D underwent DNA demethylation in cluster 2 CpGs (Figure S1F). This confirmed that demethylation observed in cluster 2 CpGs were specific to vitamin D exposure.

Functional gene ontology (GO) analysis revealed that CpGs in cluster 1 are associated with immunological categories, such as defense and immune response, whereas those in cluster 2 are more highly enriched in cell activation, positive regulation of immune system process, and wound healing involved in inflammatory response (Figure 1E). For clusters 3 and 4, GO analysis did not show enrichment in any functional categories, probably due to their small size. In all clusters, the majority of changes occurred in introns and intergenic regions with underrepresentation of promoter-transcriptional start sites (TSSs). However, whereas cluster 1 exhibited a marked enrichment of intronic regions with respect to background, the other clusters were enriched in both intronic and intergenic locations (Figure 1F, left). Concordantly, CpGs of all clusters were observed to be located outside of CpG islands, particularly for cluster 2 (Figure 1F, right). Next, we mapped the chromatin states of the CpG sites undergoing changes in methylation in the four clusters using chromatin segmentation data generated in DCs (Pacis et al., 2015) (Figure 1G). We observed an enrichment in enhancer regions for all clusters and an enrichment for inactive promoters for cluster 4. Moreover, cluster 1 (DC-specific demethylation) was enriched in weak (H3K27ac + H3K4me1 + H3K4me3) and strong (H3K27ac + H3K4me1) enhancers, while cluster 2 (TolDC-specific demethylation) was more enriched in inactive enhancers (H3K4me1) in DCs, suggesting that these inactive regions in DCs are activated in TolDCs. In all, our results indicated that vitamin D-driven demethylation events occurred in regions that may play important roles in regulating gene expression and establishing the tolerogenic phenotype of TolDCs.

DNA demethylation in TolDCs is an active process and is associated with changes in gene expression

DNA methylation has long been established to influence gene expression (Jones, 2012), although the dynamics are complex

and highly dependent on genomic location. CpGs that underwent TolDC-specific DNA demethylation during differentiation were largely situated in open seas corresponding to enhancers; hence, it is plausible to envision that they control gene expression, which results in the final tolerogenic phenotype. We therefore integrated our DNA methylation dataset with publicly available expression data generated in the same *in vitro* models (Széles et al., 2009). We observed a significant inverse relationship between levels of DNA methylation and mRNA expression at 12 h ($r = -0.5926$; $p = 4.90e-14$) and 5 days of differentiation ($r = -0.4108$; $p = 4.57e-11$) (Figure 2A). Furthermore, dividing cluster 1 and 2 CpGs based on their genomic location in relation to previously identified enhancer regions (Pacis et al., 2015), we observed that genes associated with cluster 1 CpGs located at active enhancers of DCs displayed higher expression levels in DCs than in TolDCs (Figure 2B).

To explore the dynamics of the relationship between DC- (cluster 1) and TolDC-specific demethylation (cluster 2), we performed bisulfite pyrosequencing and qRT-PCR in a selected group of genes of a set of samples over time. A few genes from each cluster were selected for further analysis based on the conditions that they had the maximum possible difference in DNA methylation during differentiation within their corresponding cluster, that they were differentially expressed, and that there were previous reports relating them with relevant immune properties. For instance, from cluster 1, we chose *IRF4* and *C1QB*, which are important for normal DC differentiation from MOs (Teh et al., 2011; Murphy et al., 2016), and from cluster 2, *CD14* and *DPF3* were selected for being specific markers of TolDCs and being involved in DC chemotaxis, respectively (Liu et al., 2019; Torres-Aguilar et al., 2010). Bisulfite pyrosequencing of these genes showed a high concordance ($r = 0.978$; $p < 2.2 \times 10^{-16}$) with the data obtained from the EPIC arrays (Figure 2C). DC-specific (cluster 1) genes, such as *IRF4* and *C1QB*, were upregulated in DCs in parallel with their specific DNA demethylation (Figure 2D). Similarly, for TolDC-specific (cluster 2) genes, such as *CD14* and *DPF3*, transcript upregulation occurred only in TolDCs in parallel with their corresponding DNA demethylation (Figure 2E). In agreement with previous reports, stimulus-induced DNA demethylation occurred succeeding specific gene expression changes (Pacis et al., 2019). In all, our results suggested that vitamin D-driven DNA demethylation occurred in association with upregulation of TolDC-specific genes.

To further characterize the mechanisms driving DNA demethylation during MO-to-DC and MO-to-TolDC differentiation, we next investigated whether the demethylation was due to active demethylation or replication-mediated passive demethylation. Utilizing BrdU proliferation assay, no proliferation was observed in DCs and TolDCs up to 6 days of differentiation (Figure S2A); hence, all DNA demethylation events observed were driven by active demethylation. In this regard, we and others have previously shown that loss of methylation in terminal differentiation from MOs is accompanied by a transient increase in 5-hydroxymethylcytosine (5hmC) and involves the participation of TET2 methylcytosine dioxygenase (Garcia-Gomez et al., 2017; Klug et al., 2013). We then determined the 5hmC levels of CpGs that became demethylated during DC and TolDC differentiation and observed that there was indeed a gain of 5hmC in these

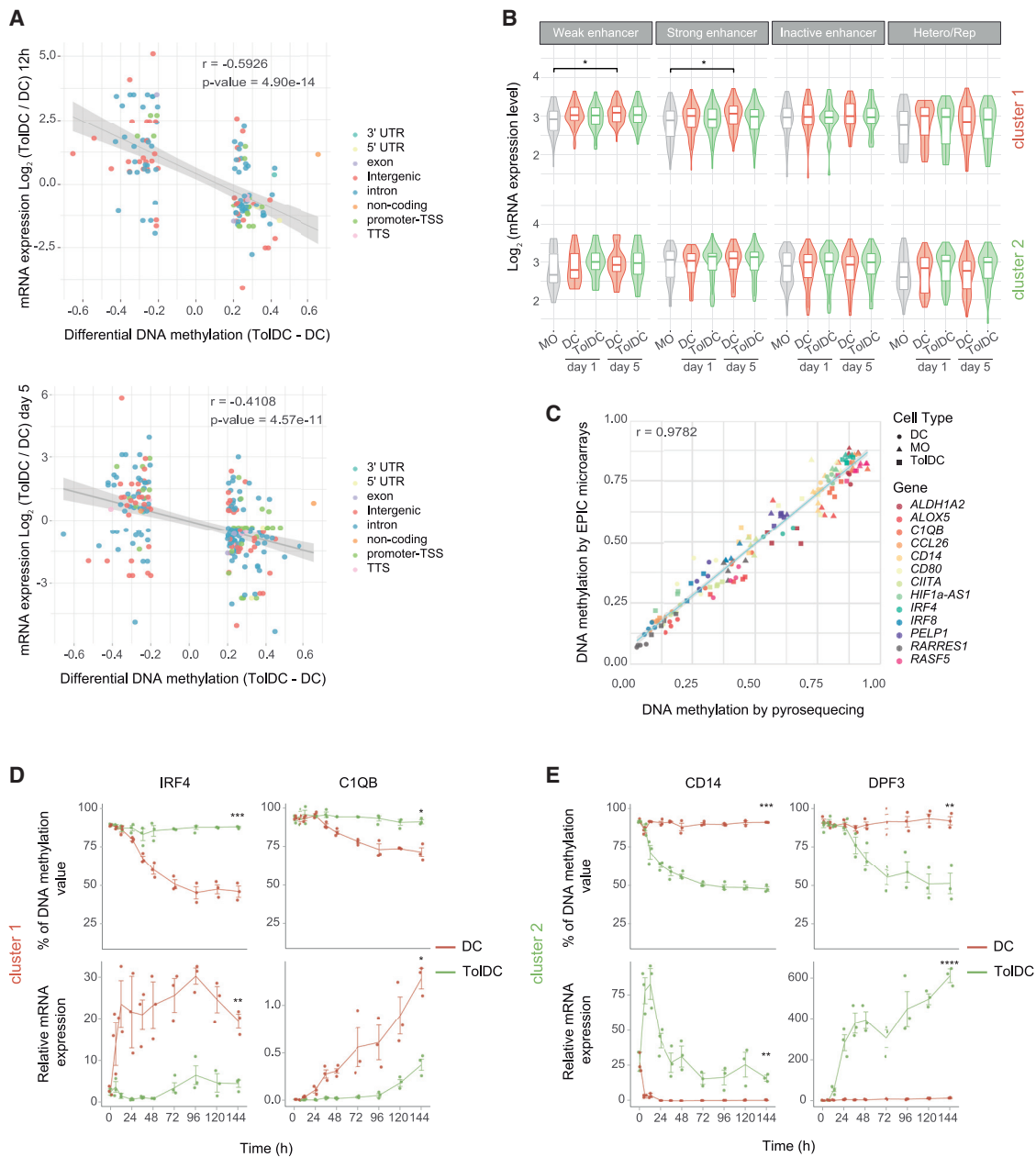


Figure 2. Integration of gene expression with DNA methylation

(A) Scatter plot showing the correlation between DNA methylation differences and gene expression changes between DCs and ToIDCs at 12 h (top) and day 5 (bottom) of differentiation. Only differentially methylated CpGs are represented. Dot color indicates gene-related associations.

(B) Box and violin plots summarizing the mRNA expression levels per cell type of genes annotated to CpGs from cluster 1 (top) and cluster 2 (bottom) divided by chromatin state annotation of the associated CpG. Adjustment for multiple comparisons was performed with false discovery rate.

(C) Scatter plot showing the correlation between methylation array values and bisulfite pyrosequencing DNA methylation values ($n = 4$, two independent experiments).

(D) DNA methylation (top) and mRNA expression (bottom) kinetics of two representative examples of cluster 1 genes. CpGs studied include cg10630015 (IRF4) and cg04097715 (C1QB) ($n = 3$, one single experiment).

(E) DNA methylation (top) and mRNA expression (bottom) kinetics of two representative examples of cluster 2 genes ($n = 3$, two independent experiments). CpGs studied include cg05620710 (CD14) and cg25205844 (DPF3).

Statistical tests: Pearson correlation (A) and unpaired two-tailed t test (B, D, and E) (* $p < 0.05$; ** $p < 0.01$; *** $p < 0.001$; **** $p < 0.0001$).

CpGs (Figure S2B). Finally, utilizing publicly available DNase-sequencing (seq) datasets from MOs (Feingold et al., 2004), we observed that more than 75% of cluster 2 CpGs corresponded to closed chromatin in MOs (Figure S2C), which reinforced the hypothesis that DNA demethylation was mediated by an active event. Altogether, our results suggested that specific active DNA demethylation following vitamin D exposure is mediated through methylcytosine dioxygenase activity, most likely associated with TET2.

VDR binding is associated with DNA demethylation and active chromatin during MO-to-ToIDC differentiation

In concordance with previous work (Jakob et al., 1992), we observed that exposure to vitamin D during DC differentiation increased the nuclear levels of VDR (Figure S1D). Hence, it is plausible that liganded VDR plays a direct role in driving DNA demethylation following vitamin D exposure during ToIDC differentiation. Hence, we performed chromatin immunoprecipitation (ChIP)-seq analysis of VDR in DCs and ToIDCs. First, we observed that exposure to vitamin D during ToIDC differentiation led to a sharp increase in overall VDR genomic binding (Figures 3A and 3B).

Interestingly, motif discovery analysis revealed promiscuity of VDR with respect to its genomic binding preferences, with only 37% of regions having the canonical VDR binding motif (Figure 3C), which suggests the cooperation of VDR with other TFs during ToIDC differentiation. Second, functional annotation of VDR-bound genes revealed enrichment of immune- and signaling-related categories, such as myeloid and granulocyte activations and cytokine receptor activity (Figure 3D). In fact, several genes previously described to be related to the tolerogenic properties of ToIDCs, such as *IL10*, *ANXA1*, and *CD163* (Navarro-Barriuso et al., 2018), are direct targets of VDR (Table S2). Third, global inspection of VDR genomic occupancy showed that VDR preferentially binds to promoters and introns in comparison with background (Figure 3E, left). We also observed enrichment of VDR binding in CpG islands, shores, and shelves, which was compatible with the enrichment noted in promoters (Figure 3E, right). Annotation of VDR peaks in relation to previously published data of DC chromatin states (Pacis et al., 2015) showed the preference of VDR for binding regions that correspond to promoters and enhancers in DCs (Figure 3F).

To further characterize the relationship between VDR and DNA methylation, we overlapped our generated DNA methylation data with VDR ChIP-seq data and observed a specific enrichment of VDR binding in ToIDCs to CpGs that became demethylated in ToIDCs (cluster 2), and this was not observed for the other clusters (Figures 4A, 4B, and S3A). In fact, we observed that over 40% of CpG sites in cluster 2 had significant VDR binding (Figure 4C). For instance, cluster 2 CpGs mapped to genes, such as *GAB2* and *HIF1A*, situated within the binding peaks of VDR in ToIDCs (Figure 4D) and located in closed chromatin regions in MOs (Figure S3B). These genes are of particular interest because *GAB2* has been implicated in phosphatidylinositol 3-kinase (PI3K) pathway activation (Pratt et al., 2000), a pathway implicated in DC tolerogenesis (Ferreira et al., 2015). Furthermore, hypoxia-inducible factor 1- α (HIF1A) is a key factor for the tolerogenic properties of myeloid-derived suppressor cells (MDSCs) in the tumor microenvironment (Corzo et al.,

2010). The dynamics of DNA methylation and gene expression of these two genes confirmed specific DNA demethylation in ToIDC, and differential gene expression changes in relation to DCs (Figures 4E and 4F).

As indicated in the introduction, TET-mediated demethylation is associated with histone modifications, such as H3K4me3 (Deplus et al., 2013) and H3K27me3 (Ichiyama et al., 2015). Hence, we speculated that changes in DNA methylation were accompanied by changes in histone modifications, and their dynamics might be associated with VDR recruitment following vitamin D exposure. Therefore, we performed ChIP-qPCR of VDR together with these activating (H3K4me3) and repressive (H3K27me3) histone modifications. We also added an antibody against H3 acetylation (H3ac), characteristic of active chromatin. To discriminate between the effects of a tolerogenic phenotype acquired through a 6-day differentiation and the effects directly caused by the presence of vitamin D in the medium, we performed ChIPs in MOs, DCs, ToIDCs, and also DCs treated with vitamin D for 30 min (DC + vitD). First, we observed a significant increase in VDR binding (Figure 4G) in DCs treated with vitamin D and in ToIDCs. Second, in the aforementioned cluster 2 genes *GAB2* and *HIF1A*, we only observed a significant increase, associated with VDR binding, for H3ac (Figure 4G). This finding was extendable to other cluster 2 genes, such as *HOPX*, *IL6*, *INHBA*, and *LYRM1* (Figure S3C).

Hence, altogether, our data suggested the coordination between VDR binding, specific DNA demethylation, changes in histone H3 acetylation, and gene expression upregulation in ToIDC differentiation.

Differentiation to DCs in the presence of vitamin D associates with activation of IL-6-JAK-STAT3 signaling pathway, and both VDR and STAT3 interact with TET2

Vitamin D, through its receptor VDR, induces changes in cytokine production and a profound metabolic reprogramming in human DC (Ferreira et al., 2015). For this reason, we hypothesized that autocrine/paracrine activation of secondary signaling pathways during differentiation could lead to the activation of a set of TFs downstream to VDR that could be relevant to ToIDC differentiation. To explore this possibility, we adapted a tool initially designed to explore intercellular communication in bulk and single-cell expression data to test autocrine/paracrine signal activation (Browaeys et al., 2020). Note that our differentiation model does not allow to distinguish between autocrine or paracrine activation. With this approach, and using genes associated with both demethylation clusters with significant expression differences (fold-change <0.5 or >2, and adjusted $p < 0.05$) as input, we inferred potential ligands that may regulate these processes (Figure 5A). One of the most interesting ligands due to its role in immune suppression in the context of tumorigenesis is IL-6 (Park et al., 2017). In fact, the *IL6* gene is significantly overexpressed in ToIDCs compared with DCs (Figure 5B), and its target genes were also observed to be overexpressed in ToIDCs (Figure 5C).

We then performed gene set enrichment analysis (GSEA) of differentially expressed genes between DCs and ToIDCs and visualized that genes differentially overexpressed in ToIDCs were enriched in IL-6-JAK-STAT3 signaling pathway (Figure 5D).

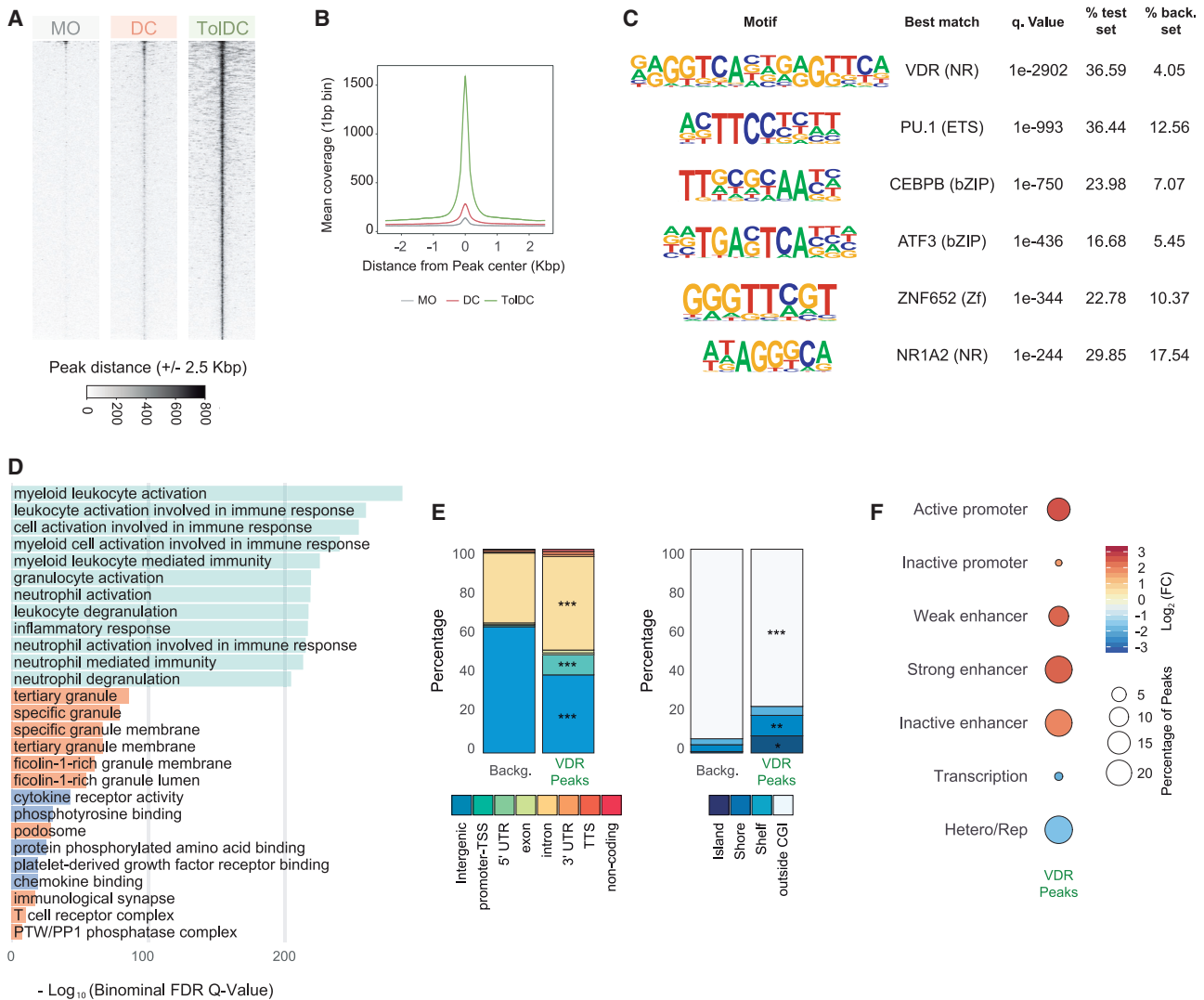


Figure 3. Genomic occupancy of vitamin D receptor (ChIP-seq, n = 2, one experiment)

(A) Heatmaps showing signal intensity of vitamin D receptor (VDR) ChIP-seq at ± 2.5 Kbp window of significant VDR peaks in MO, DCs and ToIDCs (q value < 0.01 and irreproducible discovery rate [IDR] < 0.05).

(B) Composite plots of VDR ChIP-seq distribution ± 2.5 Kbp around CpGs in MO (gray), DCs (red), and ToIDCs (green) for significant VDR peaks. The statistics were computed by comparing the intensity averages of the entire window.

(C) Motif discovery analysis using HOMER software showing q values and the percentage of test and background regions with each motif.

(D) Results of gene set enrichment analysis using GREAT software. The plot depicts the top enriched terms for biological processes (green), molecular function (orange), and cellular component (purple) categories, based on adjusted p values from the binomial distribution.

(E) Location proportions of VDR peaks in the context of CpG islands (CGIs) (right) and gene-related regions (left).

(F) Bubble chart depicting the enrichment (red) or depletion (blue) of VDR peaks in the chromatin states of dendritic cells (Pacis et al., 2015). The circle filling represents the logarithm of the ratio between the percentage of VDR peaks with the feature within the background. Circle size indicates the percentage of VDR peaks in the chromatin state, and the circle edge indicates the statistical significance of the enrichment (black: significant; no edge: not significant; q value < 0.01).

Statistical tests: two-tailed t test (A and B), cumulative binomial distribution (C and D), and two-tailed Fisher's exact test (E and F) (*p < 0.05; **p < 0.01; ***p < 0.001; ****p < 0.0001).

In fact, VDR binds in several regions upstream of the *IL6* gene TSS, suggesting that VDR directly regulates its expression (Figure 5E). Furthermore, we detected an increase in IL-6 production and release into the medium in ToIDCs (Figure S4A), which was concordant with an upregulation of its gene expression

compared with DCs (Figure 5B). Additionally, significant DNA demethylation was observed in 2 CpG sites of the promoter region of *IL6* in ToIDCs, and this was coupled with a gain in 5hmC (Figures S4B and S4C), which suggested the involvement of TET2 in its regulation.

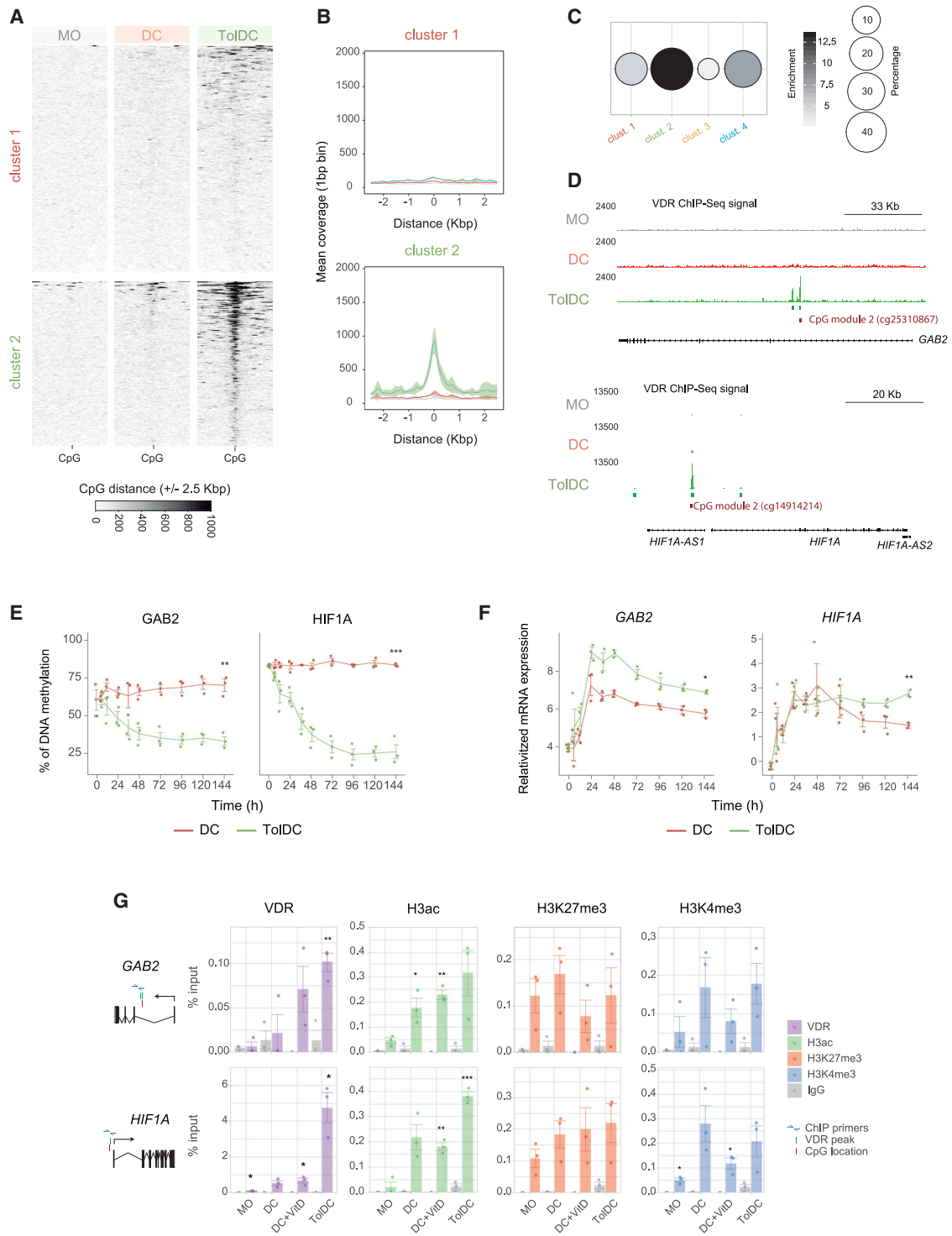


Figure 4. Binding of vitamin D receptor correlates with ToIDC-specific DNA demethylation (ChIP-seq, n = 2, one single experiment; DNA methylation, n = 4, two independent experiments)

(A) Heatmaps showing signal intensity of vitamin D receptor (VDR) ChIP-seq at ± 2.5 Kbp window from CpGs of cluster 1 (top) and cluster 2 (bottom) in MO, DCs, and ToIDCs.

(B) Composite plots of VDR ChIP-seq distribution ± 2.5 Kbp around CpGs from cluster 1 (top) and cluster 2 (bottom) in MO (gray), DC (red), and ToIDC (green). Smooth represents the Cls.

(legend continued on next page)

Remarkably, when we blocked IL-6 with an anti-IL-6 antibody during TolDC differentiation, we observed the production of decreased levels of IL-10 (Figure S4D), which is involved in tolerogenesis (Morante-Palacios et al., 2021). This result is consistent with recent findings in T helper type 1 (Th1) cells (Chauss et al., 2022). However, blocking IL-6 during TolDC differentiation did not result in a reduced ability of TolDCs to suppress CD8⁺ T cell proliferation (Figure S4E). In contrast, in proliferation assays performed with TolDCs in the presence of anti-IL-6 antibody, we found slightly reduced suppression (Figure S4E). These results suggest that IL-6 is a contributor to the ability to suppress CD8⁺ T cell proliferation by TolDCs but not critical to the acquisition of such properties during TolDC differentiation.

In parallel, we utilized DoRothEA (discriminant regulon expression analysis), a manually curated human regulon for estimating single-sample TF activities through the expression of their target genes (Garcia-Alonso et al., 2019) to analyze TF activities of several STATs in genes differentially expressed in TolDCs compared with DCs, and observed a specific increase in STAT3 activity that was not observed for other members of the STAT family, at 5 days of differentiation (Figure 5F). Furthermore, we observed a marked increase in phosphorylation of STAT3 in TolDCs compared with DCs, which was not observed for STAT5 (Figures 5G and S4E). Although a statistically significant increase in phosphorylation was observed for STAT1, this increase was not to the same extent as STAT3 and may be due to indirect activation, as previously described (Haan et al., 2005) (Figures 5G and S4F). Thus, our results suggested that vitamin D played a role in STAT3 activation.

To explore the possibility that the observed interplay between VDR and STAT3 involves a physical interaction, we performed co-immunoprecipitation experiments in TolDCs. Our analysis revealed a specific interaction between VDR and phosphorylated (p)-STAT3 in TolDCs (Figure 5H). We also observed that both VDR and p-STAT3 interacted with TET2 (Figure 5I), which suggests that these two TFs play a role in the targeting of TET2-mediated demethylation to their cognate sites.

Inhibition of JAK2-mediated STAT3 activation affects the acquisition of vitamin D-dependent tolerogenesis

We investigated the consequences of inhibiting the JAK2-STAT3 pathway by using TG101348, a pharmacological inhibitor of JAK2 (Lasho et al., 2008), during DC and vitamin D-dependent TolDC differentiation. Following TG101348 treat-

ment, we confirmed the inhibition of STAT3 phosphorylation by western blot (Figure 6A). Given that TG101348 is an inhibitor of JAK2, and therefore can affect upstream signaling of STAT1, STAT3, and STAT5, we checked their phosphorylation and observed that the partial inhibition of p-STAT5 and p-STAT1 did not reach statistical significance in TolDCs, unlike p-STAT3 (Figures S5A and S5B). TG101348 treatment also resulted in a sharp decrease in the production of IL-10 (Figure 6B), an archetypical anti-inflammatory cytokine that is also a *bona fide* target for STAT3 (Schaefer et al., 2009; Ziegler-Heitbrock et al., 2003). In fact, IL-10 secretion by TolDCs is a contributor to the suppression of CD8⁺ T cell proliferation that is halted when adding anti-IL-10 to proliferation assays (Figure S4E). We also tested the effects of JAK2 inhibition on surface markers and observed that JAK2 inhibition resulted in an increase of CD14 and CD86 protein levels and downregulation of CD1a and CD11b (Figure 6C). In parallel, we investigated the effects of JAK2 inhibition on the DNA methylation and expression levels of TolDC-specific demethylated genes. We did not observe any clear reversion of DNA demethylation (Figure 6D), but we did note alterations at the transcriptional level (Figure 6E). Changes were observed not only in cluster 2 genes (TolDC-specific), such as *CD14* and *DPF3*, but also in those of cluster 1, such as *IRF4* and *RASF5* (Figure 6E). These are likely to be the result of the partial inhibition of phosphorylation of STAT1 and STAT5, which might also be involved in activating these and other DC and TolDC genes.

Most importantly, JAK2 inhibition by TG101348 treatment during differentiation resulted in the loss of the ability to suppress CD8⁺ T cell proliferation of DC differentiated in the presence of vitamin D. This reinforces the idea that the activities of VDR and the JAK2-STAT3 pathway coordinate the acquisition of tolerogenic properties of DCs in the presence of vitamin D (Figure 6F).

DISCUSSION

In this study, we demonstrate that vitamin D is able to induce tolerogenesis in DCs through a mechanism that involves VDR-specific demethylation and activation of key immune genes in a manner that is coordinated with JAK2-mediated STAT3 activation. VDR not only is able to orchestrate a direct response on key immune targets but also associates with activation of the IL-6-JAK-STAT signaling pathway. We also prove the recruitment of TET2 and p-STAT3 by VDR, associated with the

(C) Bubble plot representation of significant VDR binding enrichment in each cluster of CpGs. Dots are colored according to their enrichment value, defined as the logarithm of the ratio between the percentage of CpGs with VDR peak within the cluster and the percentage of CpGs with the VDR peak within the background. Bubble size corresponds to the percentage of CpGs in each cluster overlapping with significant VDR peaks. The presence of a black border indicates significant enrichment (q value < 0.01).

(D) VDR ChIP-seq signal profiles in the vicinity of the representative genes of CpGs from cluster 2. VDR signals are colored by cell type. At the bottom, the significant VDR binding sites are shown in green and CpG position in red.

(E) DNA methylation kinetics of two representative CpGs annotated to *GAB2* (cg25310867) and *HIF1A* (cg14914214) in DCs and TolDCs ($n = 3$, one experiment).

(F) Gene expression kinetics of *GAB2* and *HIF1a* in DCs and TolDCs ($n = 3$, one experiment).

(G) Bar plot representation of ChIP-qPCR results for VDR binding and three histone modifications (H3ac, H3K27me3, and H3K4me4) in the vicinity of VDR peaks close to *GAB2* and *HIF1A* gene sequences ($n = 3$, one experiment). This analysis was performed in MOs, DCs, and TolDCs and DC + vitD. DC + vitD involves adding vitamin D for 30 min at the end of a 6-day differentiation to DCs. Immunoprecipitation with IgG was used as control. The location of the ChIP primers, the CpG site and the VDR peaks are indicated.

Statistical tests: two-tailed Fisher's exact test (C) and unpaired two-tailed t test (E, F, and G) (* $p < 0.05$; ** $p < 0.01$; *** $p < 0.001$).

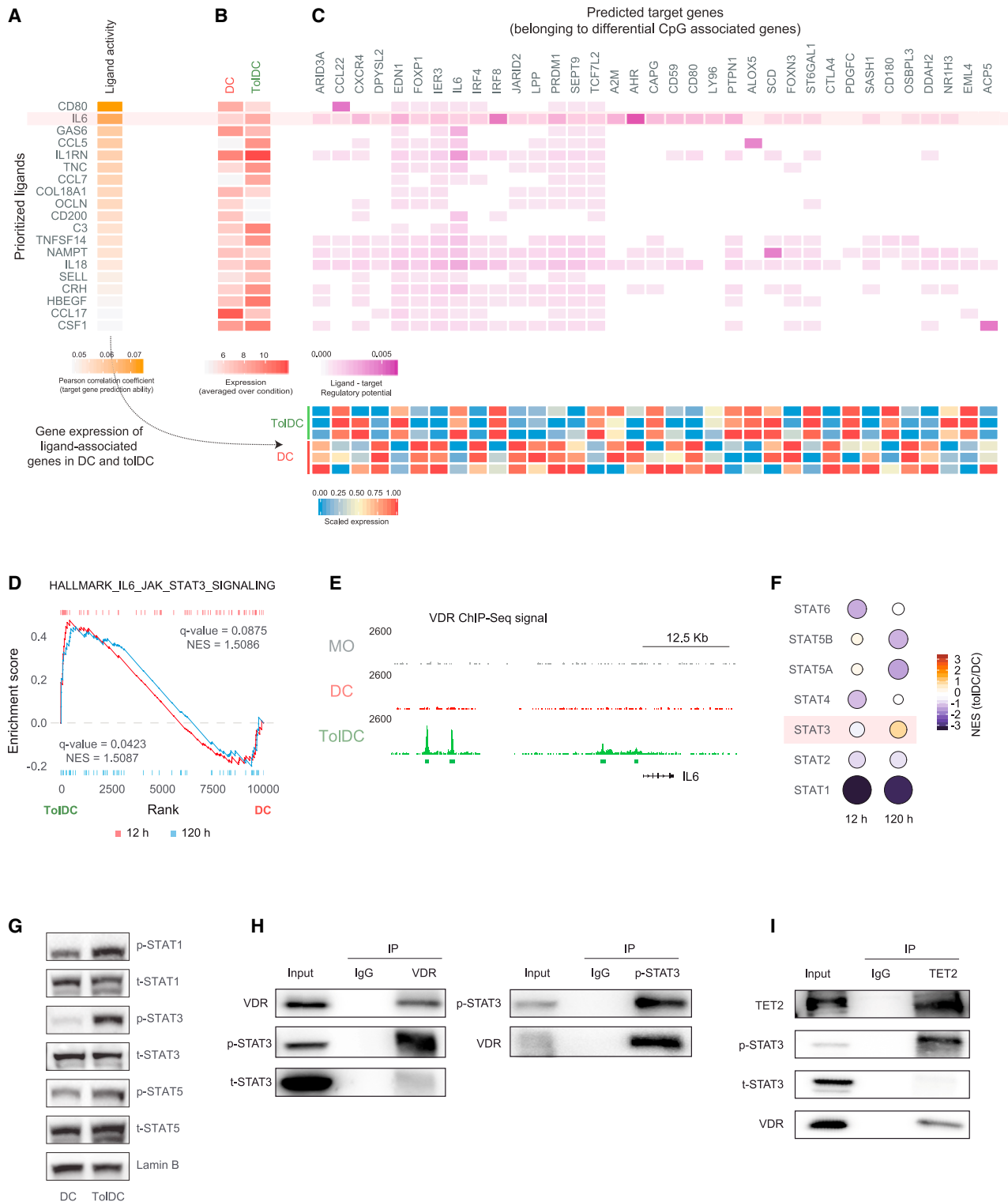


Figure 5. Vitamin D-dependent autocrine/paracrine activation of the IL-6-JAK2-STAT3 pathway

(A) Heatmap showing ligand activity prediction based on the Pearson correlation with its target genes.

(B) Heatmap displaying average gene expression of ligands for DCs and TolDCs on day 5.

(C) Heatmap showing the regulatory potential of each ligand on the target genes based on nichenetr package database (upper panel) and the expression levels of these target genes in each sample (lower panel).

(legend continued on next page)

demethylation and activation of target genes. The essential role of the JAK2-STAT3 pathway in the acquisition of tolerogenesis is demonstrated by the functional impact of the pharmacological inhibition of this pathway.

Our results show the direct role of VDR in guiding TET-mediated DNA demethylation to specific genomic sites during TolDC differentiation. We have shown that, in the presence of vitamin D, VDR levels are increased in the nucleus and that interaction with p-STAT3 and TET2 occurs, thereby promoting TolDC-specific demethylation. A recurrent question in the DNA methylation field is whether DNA methylation is causally involved in shaping gene expression profiles or if it passively reflects transcriptional states (Schübeler, 2015). Our own data support both possibilities, and some DNA methylation changes appear to be more likely to occur after a change in expression than others (Pacis et al., 2019). In our study, we present evidence that TET-mediated demethylation acts as a mechanism facilitating subsequent participation of other TFs, in this case STAT3. In fact, the absence of interference with DNA demethylation, while activation is impeded following pharmacological inhibition of STAT3 phosphorylation, suggests that VDR-dependent demethylation is necessary and precedes STAT3-mediated gene activation. This proposed mechanism was consistent with the alterations in TF activity reported in TET2 knockout mice (Rasmussen et al., 2019). TET2-associated functions may ensure the binding of some TFs, thereby contributing to enhancer-dependent activity and gene expression.

Our study identifies a crucial role for the JAK2-STAT3 pathway in the acquisition of tolerogenesis in innate immunity. The involvement of STAT3 is also relevant in the context of MDSCs, which are also characterized by their tolerogenic properties (Corzo et al., 2009; Kumar et al., 2016). We show that the pharmacological impairment of STAT3 phosphorylation, by inhibiting JAK2, directly results in the loss of the tolerogenic properties of TolDCs, which facilitate T-cell proliferation, demonstrating the essential role of this pathway for the tolerogenic phenotype. Our results raise the possibility that tolerogenic properties can be reverted, not only in the context of vitamin D but also in others. These findings could be clinically relevant both in the context of pathological situations where tolerogenic properties are not desired, like in the tumor microenvironment or in metastatic processes (reviewed in DeVito et al., 2019), as well as in those where they are intentionally pursued (reviewed in Cauwels and Tavernier, 2020), including their therapeutic use in the treatment of inflammatory conditions, such as rheumatoid arthritis and multiple sclerosis (Morante-Palacios et al., 2021).

Limitations of the study

One of the limitations of our current study is that we have not fully explored the impact of the VDR and the IL-6-JAK-STAT3 pathway *in vivo*, in patients treated or supplemented with vitamin D. It would have also been relevant to analyze the direct impact of STAT3 in the epigenetic remodeling in TolDCs, by analyzing their binding sites and associated expression changes. This partly limits our conclusions on the extent and relevance of STAT3 in determining the acquisition of the tolerogenic phenotype.

STAR★METHODS

Detailed methods are provided in the online version of this paper and include the following:

- KEY RESOURCES TABLE
- RESOURCE AVAILABILITY
 - Lead contact
 - Materials availability
 - Data and code availability
- EXPERIMENTAL MODEL AND SUBJECT DETAILS
 - Differentiation of TolDCs and DCs from peripheral blood monocytes
 - Isolation and culture of peripheral blood DCs
- METHOD DETAILS
 - CD8⁺ cell proliferation assay
 - BrdU proliferation assay
 - Flow cytometry
 - Cytokine measurements
 - Genomic DNA and total RNA extraction
 - Bisulfite (BS) and oxidative-bisulfite (oxBS) pyrosequencing
 - Real-time quantitative Polymerase Chain Reaction (RT-qPCR)
 - Western blot
 - Co-immunoprecipitation (Co-IP)
 - DNA methylation profiling
 - ChIP-seq analysis
 - ChIP-qPCR
 - Microarray reanalysis
 - Data analysis
- QUANTIFICATION AND STATISTICAL ANALYSIS

SUPPLEMENTAL INFORMATION

Supplemental information can be found online at <https://doi.org/10.1016/j.celrep.2021.110244>.

(D) Gene set enrichment analysis of differentially expressed genes (fold-change < 0.5 or >2 and q-value < 0.05) at 12 h (red) and 120 h (blue). Results for the IL-6-JAK-STAT signaling pathway are shown.

(E) VDR ChIP-seq signal profiles in the vicinity of the *IL6* gene. VDR signals are colored by cell type. The significant VDR binding sites are shown below in green.

(F) Bubble chart depicting the TF activity predicted from mRNA expression of target genes with DoRoThEA v2.0. The circle filling represents the normalized enrichment score (NES) (blue: more activity in DCs; red: more activity in TolDCs). Bubble size corresponds to the logarithm of adjusted p values.

(G) Representative western blot assays showing the phosphorylated and total protein levels of STAT1, STAT3, and STAT5 on day 3 of differentiation of DCs and TolDCs (n = 4, two independent experiments).

(H) Representative western blots showing the results of co-immunoprecipitation assays performed in MOs differentiated to DC and TolDC for 3 days. Protein extracts were immunoprecipitated using anti-VDR or anti-p-STAT3 antibodies (n = 3, two independent experiments).

(I) Representative western blots showing the results of co-immunoprecipitation assays performed in MOs differentiated to TolDC for 3 days (n = 3, two independent experiments). Protein extracts were immunoprecipitated using anti-TET2 antibodies.

In both (H and I), IgG was used as a negative control and total protein extract was used as input.

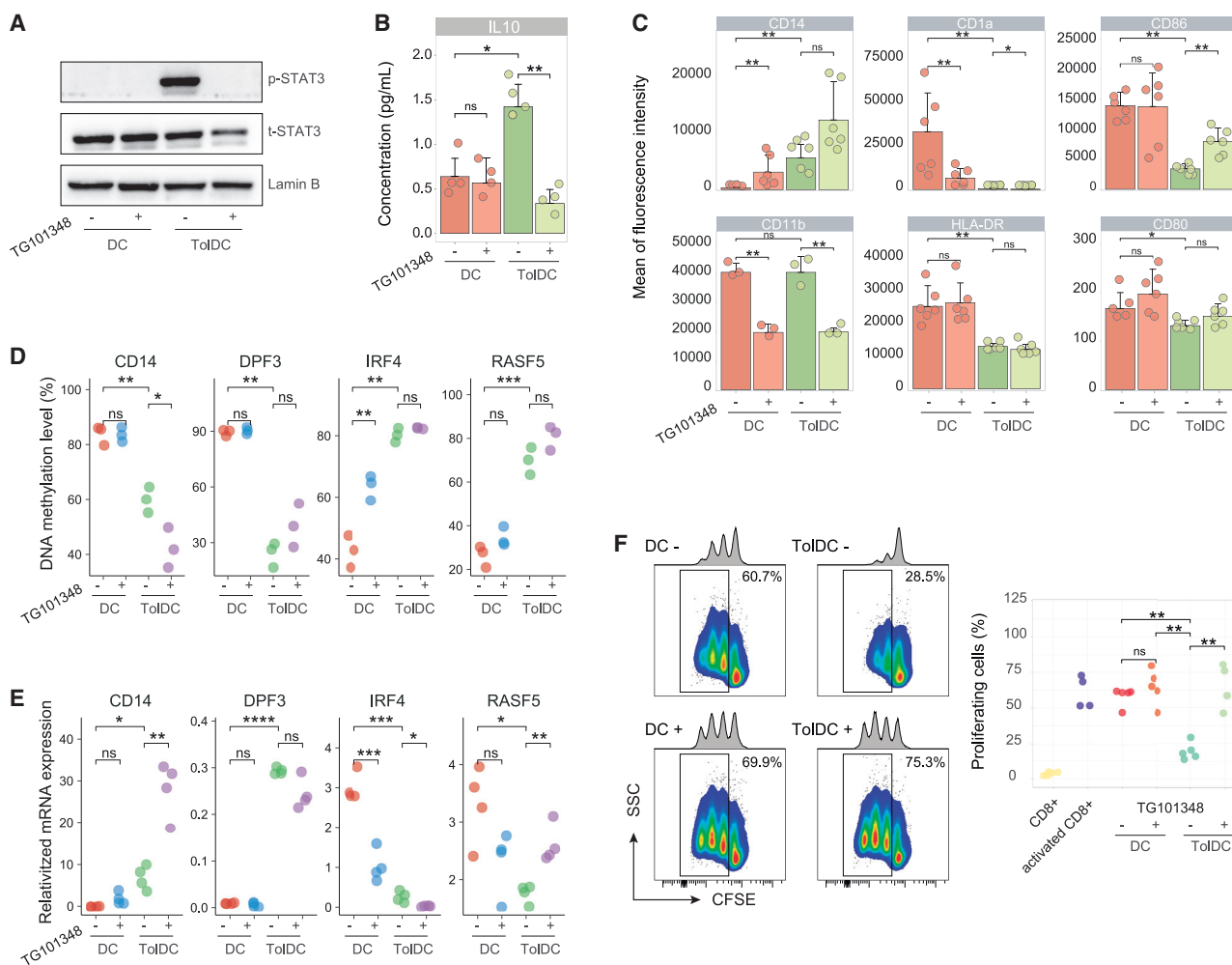


Figure 6. Inhibition of STAT3 phosphorylation reverts immunosuppressive properties of vitamin D exposed dendritic cells

(A) Representative western blot assays showing the effects of STAT3 at the protein phosphorylation level after pharmacological inhibition of JAK2 with TG101348 (n = 3, two experiments).

(B) Bar plot representation of the effect of JAK2 inhibition with TG101348 on IL-10 released by DCs and ToDCs (n = 4, two independent experiments). Protein levels were measured by ELISA.

(C) Bar plots showing the impact of JAK2 inhibition with TG101348 on membrane receptor expression (n = 6, two independent experiments). Protein levels were measured with flow cytometry.

(D) Dot plot representation of bisulfite pyrosequencing results of four example CpGs, two from cluster 1 (CD14 and DPF3) and two from cluster 2 (C1QB and RAS5), displaying the consequence of JAK2 inhibition with TG101348 in DCs and ToDCs (n = 3, two independent experiments).

(E) Dot plot showing mRNA expression of four example genes from cluster 1 and cluster 2 as measured by RT-qPCR, showing the effect of JAK2 inhibition with TG101348 in DCs and ToDCs (n = 4, two independent experiments). Expression was relativized with respect to RPL38 gene expression.

(F) Representative example and dot plot showing the effect on CD8⁺ cell proliferation of DCs and ToDC generated from MO in presence or absence of TG101348 (n = 5, two independent experiments).

Statistical tests: two-tailed Wilcoxon rank-sum test (B–F) (*p < 0.05; **p < 0.01; ***p < 0.001; ****p < 0.0001).

ACKNOWLEDGMENTS

We are very grateful to Dr. José Luis Sardina for useful feedback. We thank CERCA Programme/Generalitat de Catalunya and the Josep Carreras Foundation for institutional support. E.B. was funded by the Spanish Ministry of Science and Innovation (MICINN; grant number PID2020-117212RB-I00/AE/10.13038/501100011033). E.M.-C. is funded with RESTORE project (EU H2020 Research and Innovation Programme, number 779316) and Spanish projects PI17/01521 and PI20/01313, integrated in the Plan Nacional de I+D+I and co-supported by the ISCIII-Subdirección General de Evaluación

and FEDER. O.M.-P. holds an i-PFIS PhD fellowship (grant number IF17/00034) from Acción Estratégica en Salud 2013–2016 ISCIII, co-financed by Fondo Social Europeo. F.F. holds a PhD fellowship from the INSTRUCT Consortium, which receives Innovative Training Network subsidy from the EU H2020 program.

AUTHOR CONTRIBUTIONS

F.C.-M. and E.B. conceived and designed the study; F.C.-M., A.G.F.-B., G.G.-T., O.M.-P., L.C., L.B., F.F., and T.L. performed the differentiation,

chromatin immunoprecipitation, co-immunoprecipitation experiments, and immunological assays; F.C.-M. performed the bioinformatic analyses; F.C.-M., A.G.F.-B., G.G.-T., E.M.-C., and E.B. analyzed results; J.R.-U. and E.B. supervised the study; F.C.-M., T.L., and E.B. wrote the manuscript; all authors participated in discussions and interpreting the results.

DECLARATION OF INTERESTS

The authors declare no competing interests.

Received: June 29, 2021

Revised: September 27, 2021

Accepted: December 20, 2021

Published: January 18, 2022

REFERENCES

Álvarez-Errico, D., Vento-Tormo, R., Sieweke, M., and Ballestar, E. (2015). Epigenetic control of myeloid cell differentiation, identity and function. *Nat. Rev. Immunol.* *15*, 7–17.

Aryee, M.J., Jaffe, A.E., Corrada-Bravo, H., Ladd-Acosta, C., Feinberg, A.P., Hansen, K.D., and Irizarry, R.A. (2014). Minfi: a flexible and comprehensive bioconductor package for the analysis of infinium DNA methylation microarrays. *Bioinformatics* *30*, 1363–1369.

Assenov, Y., Müller, F., Lutsik, P., Walter, J., Lengauer, T., and Bock, C. (2014). Comprehensive analysis of DNA methylation data with RnBeads. *Nat. Methods* *11*, 1138–1140.

Barragan, M., Good, M., and Kolls, J.K. (2015). Regulation of dendritic cell function by vitamin D. *Nutrients* *7*, 8127–8151.

Bibikova, M., Lin, Z., Zhou, L., Chudin, E., Garcia, E.W., Wu, B., Doucet, D., Thomas, N.J., Wang, Y., Vollmer, E., et al. (2006). High-throughput DNA methylation profiling using universal bead arrays. *Genome Res.* *16*, 383–393.

Browaeys, R., Saelens, W., and Saeyns, Y. (2020). NicheNet: modeling intercellular communication by linking ligands to target genes. *Nat. Methods* *17*, 159–162.

Bscheider, M., and Butcher, E.C. (2016). Vitamin D immunoregulation through dendritic cells. *Immunology* *148*, 227–236.

Carlberg, C. (2019). Vitamin D signaling in the context of innate immunity: focus on human monocytes. *Front. Immunol.* *10*, 2211.

Carvalho, B.S., and Irizarry, R.A. (2010). A framework for oligonucleotide microarray preprocessing. *Bioinformatics* *26*, 2363–2367.

Cauwels, A., and Tavernier, J. (2020). Tolerizing strategies for the treatment of autoimmune diseases: from ex vivo to in vivo strategies. *Front. Immunol.* *11*, 674.

Chauss, D., Freiwald, T., McGregor, R., Yan, B., Wang, L., Nova-Lamperti, E., Kumar, D., Zhang, Z., Teague, H., West, E.E., et al. (2022). Autocrine vitamin D signaling switches off pro-inflammatory programs of TH1 cells. *Nat. Immunol.* *23*, 62–74.

Chu, C.C., Ali, N., Karagiannis, P., Di Meglio, P., Skowera, A., Napolitano, L., Barinaga, G., Grys, K., Sharif-Paghaleh, E., Karagiannis, S.N., et al. (2012). Resident CD141 (BDCA3) + dendritic cells in human skin produce IL-10 and induce regulatory T cells that suppress skin inflammation. *J. Exp. Med.* *209*, 935–945.

Corzo, C.A., Cotter, M.J., Cheng, P., Cheng, F., Kusmartsev, S., Sotomayor, E., Padhya, T., McCaffrey, T.V., McCaffrey, J.C., and Gabrilovich, D.I. (2009). Mechanism regulating reactive oxygen species in tumor-induced myeloid-derived suppressor cells. *J. Immunol.* *182*, 5693–5701.

Corzo, C.A., Condamine, T., Lu, L., Cotter, M.J., Youn, J.I., Cheng, P., Cho, H.I., Celis, E., Quiceno, D.G., Padhya, T., et al. (2010). HIF-1 α regulates function and differentiation of myeloid-derived suppressor cells in the tumor microenvironment. *J. Exp. Med.* *207*, 2439–2453.

Costa, Y., Ding, J., Theunissen, T.W., Faiola, F., Hore, T.A., Shliaha, P.V., Fidalgo, M., Saunders, A., Lawrence, M., Dietmann, S., et al. (2013).

NANOG-dependent function of TET1 and TET2 in establishment of pluripotency. *Nature* *495*, 370–374.

Dankers, W., Colin, E.M., van Hamburg, J.P., and Lubberts, E. (2017). Vitamin D in autoimmunity: molecular mechanisms and therapeutic potential. *Front. Immunol.* *7*, 697.

de la Rica, L., Rodríguez-Ubreva, J., García, M., Islam, A.B.M.M.K., Urquiza, J.M., Hernando, H., Christensen, J., Helin, K., Gómez-Vaquero, C., and Ballestar, E. (2013). PU.1 target genes undergo Tet2-coupled demethylation and DNMT3b-mediated methylation in monocyte-to-osteoclast differentiation. *Genome Biol.* *14*, R99.

Deplus, R., Delatte, B., Schwinn, M.K., Defrance, M., Méndez, J., Murphy, N., Dawson, M.A., Volkmar, M., Putmans, P., Calonne, E., et al. (2013). TET2 and TET3 regulate GlcNAcylation and H3K4 methylation through OGT and SET1/COMPASS. *EMBO J.* *32*, 645–655.

DeVito, N.C., Plebanek, M.P., Theivanthiran, B., and Hanks, B.A. (2019). Role of tumor-mediated dendritic cell Tolerization in immune evasion. *Front. Immunol.* *10*, 2876.

Feingold, E.A., Good, P.J., Guyer, M.S., Kamholz, S., Liefer, L., Wetterstrand, K., Collins, F.S., Gingeras, T.R., Kampa, D., Sekinger, E.A., et al. (2004). The ENCODE (ENCyclopedia of DNA elements) project. *Science* *306*, 636–640.

Ferreira, G.B., Overbergh, L., Verstuyf, A., and Mathieu, C. (2013). 1 α ,25-Dihydroxyvitamin D3 and its analogs as modulators of human dendritic cells: a comparison dose-titration study. *J. Steroid Biochem. Mol. Biol.* *136*, 160–165.

Ferreira, G.B., Vanherwegen, A.S., Eelen, G., Gutiérrez, A.C.F., VanLommel, L., Marchal, K., Verlinden, L., Verstuyf, A., Nogueira, T., Georgiadou, M., et al. (2015). Vitamin D3 induces tolerance in human dendritic cells by activation of intracellular metabolic pathways. *Cell Rep.* *10*, 711–725.

Fetahu, I.S., Höbaus, J., and Kállay, E. (2014). Vitamin D and the epigenome. *Front. Physiol.* *5*, 164.

García-Alonso, L., Holland, C.H., Ibrahim, M.M., Turei, D., and Saez-Rodriguez, J. (2019). Benchmark and integration of resources for the estimation of human transcription factor activities. *Genome Res.* *29*, 1363–1375.

García-Gomez, A., Li, T., Kerick, M., Català-Moll, F., Comet, N.R., Rodríguez-Ubreva, J., De La Rica, L., Branco, M.R., Martín, J., and Ballestar, E. (2017). TET2- and TDG-mediated changes are required for the acquisition of distinct histone modifications in divergent terminal differentiation of myeloid cells. *Nucleic Acids Res.* *45*, 10002–10017.

Goudot, C., Coillard, A., Villani, A.C., Gueguen, P., Cros, A., Sarkizova, S., Tang-Huau, T.L., Bohec, M., Baulande, S., Hacothen, N., et al. (2017). Aryl hydrocarbon receptor controls monocyte differentiation into dendritic cells versus macrophages. *Immunity* *47*, 582–596.e6.

Guilhamon, P., Eskandarpour, M., Halai, D., Wilson, G.A., Feber, A., Teschen-dorf, A.E., Gomez, V., Hergovich, A., Tirabosco, R., Fernanda Amary, M., et al. (2013). Meta-analysis of IDH-mutant cancers identifies EBF1 as an interaction partner for TET2. *Nat. Commun.* *4*, 2166.

Haan, S., Keller, J.F., Behrmann, I., Heinrich, P.C., and Haan, C. (2005). Multiple reasons for an inefficient STAT1 response upon IL-6-type cytokine stimulation. *Cell. Signal.* *17*, 1542–1550.

Heinz, S., Benner, C., Spann, N., Bertolino, E., Lin, Y.C., Laslo, P., Cheng, J.X., Murre, C., Singh, H., and Glass, C.K. (2010). Simple combinations of lineage-determining transcription factors prime cis-regulatory elements required for macrophage and B cell identities. *Mol. Cell* *38*, 576–589.

Ichiyama, K., Chen, T., Wang, X., Yan, X., Kim, B.S., Tanaka, S., Ndiaye-Lobry, D., Deng, Y., Zou, Y., Zheng, P., et al. (2015). The methylcytosine dioxygenase Tet2 promotes DNA demethylation and activation of cytokine gene expression in T cells. *Immunity* *42*, 613–626.

Jakob, F., Gieseler, F., Tresch, A., Hammer, S., Seufert, J., and Schneider, D. (1992). Kinetics of nuclear translocation and turnover of the vitamin D receptor in human HL60 leukemia cells and peripheral blood lymphocytes-coincident rise of DNA-relaxing activity in nuclear extracts. *J. Steroid Biochem. Mol. Biol.* *42*, 11–16.

Jones, P.A. (2012). Functions of DNA methylation: islands, start sites, gene bodies and beyond. *Nat. Rev. Genet.* *13*, 484–492.

- Klug, M., Schmidhofer, S., Gebhard, C., Andreesen, R., and Rehli, M. (2013). 5-Hydroxymethylcytosine is an essential intermediate of active DNA demethylation processes in primary human monocytes. *Genome Biol.* *14*, R46.
- Koressaar, T., and Remm, M. (2007). Enhancements and modifications of primer design program primer3. *Bioinformatics* *23*, 1289–1291.
- Korotkevich, G., Sukhov, V., and Sergushichev, A. (2019). Fast gene set enrichment analysis. *BioRxiv*. <https://doi.org/10.1101/060012>.
- Kumar, V., Cheng, P., Condamine, T., Mony, S., Languino, L.R., McCaffrey, J.C., Hockstein, N., Guarino, M., Masters, G., Penman, E., et al. (2016). CD45 phosphatase inhibits STAT3 transcription factor activity in myeloid cells and promotes tumor-associated macrophage differentiation. *Immunity* *44*, 303–315.
- Langmead, B., and Salzberg, S.L. (2012). Fast gapped-read alignment with Bowtie 2. *Nat. Methods* *9*, 357–359.
- Lasho, T.L., Tefferi, A., Hood, J.D., Verstovsek, S., Gilliland, D.G., and Pardanani, A. (2008). TG101348, a JAK2-selective antagonist, inhibits primary hematopoietic cells derived from myeloproliferative disorder patients with JAK2V617F, MPLW515K or JAK2 exon 12 mutations as well as mutation negative patients. *Leukemia* *22*, 1790–1792.
- Leek, J.T., Johnson, W.E., Parker, H.S., Fertig, E.J., Jaffe, A.E., Zhang, Y., Storey, J.D., Torres, L.C., 2021. *Bioconductor*. sva: Surrogate Variable Analysis. R package version 3.42.0.
- Li, H., Handsaker, B., Wysoker, A., Fennell, T., Ruan, J., Homer, N., Marth, G., Abecasis, G., and Durbin, R. (2009). The sequence alignment/map format and SAMtools. *Bioinformatics* *25*, 2078–2079.
- Li, T., Garcia-Gomez, A., Morante-Palacios, O., Ciudad, L., Özkaramehmet, S., Van Dijk, E., Rodríguez-Ubreva, J., Vaquero, A., and Ballestar, E. (2020). SIRT1/2 orchestrate acquisition of DNA methylation and loss of histone H3 activating marks to prevent premature activation of inflammatory genes in macrophages. *Nucleic Acids Res.* *48*, 665–681.
- Lio, C.W., Zhang, J., González-Avalos, E., Hogan, P.G., Chang, X., and Rao, A. (2016). Tet2 and Tet3 cooperate with B-lineage transcription factors to regulate DNA modification and chromatin accessibility. *Elife* *5*, e18290.
- Liu, J., Zhang, X., Chen, K., Cheng, Y., Liu, S., Xia, M., Chen, Y., Zhu, H., Li, Z., and Cao, X. (2019). CCR7 chemokine receptor-inducible Inc-Dp3 restrains dendritic cell migration by inhibiting HIF-1 α -Mediated glycolysis. *Immunity* *50*, 600–615.e15.
- Luo, C., Hajkova, P., and Ecker, J.R. (2018). Dynamic DNA methylation: in the right place at the right time. *Science* *361*, 1336–1340.
- Mahé, E.A., Madigou, T., Sérandour, A.A., Bizot, M., Avner, S., Chalmel, F., Paliere, G., Métivier, R., and Salbert, G. (2017). Cytosine modifications modulate the chromatin architecture of transcriptional enhancers. *Genome Res.* *27*, 947–958.
- McLean, C.Y., Bristor, D., Hiller, M., Clarke, S.L., Schaar, B.T., Lowe, C.B., Wenger, A.M., and Bejerano, G. (2010). GREAT improves functional interpretation of cis-regulatory regions. *Nat. Biotechnol.* *28*, 495–501.
- Mendes, K., Schmidhofer, S., Minderjahn, J., Glatz, D., Kiesewetter, C., Raithel, J., Wimmer, J., Gebhard, C., and Rehli, M. (2021). The epigenetic pioneer EGR2 initiates DNA demethylation in differentiating monocytes at both stable and transient binding sites. *Nat. Commun.* *12*, 1556.
- Monticelli, S., and Natoli, G. (2017). Transcriptional determination and functional specificity of myeloid cells: making sense of diversity. *Nat. Rev. Immunol.* *17*, 595–607.
- Mora, J.R., Iwata, M., and Von Andrian, U.H. (2008). Vitamin effects on the immune system: vitamins A and D take centre stage. *Nat. Rev. Immunol.* *8*, 685–698.
- Morante-Palacios, O., Fondelli, F., Ballestar, E., and Martínez-Cáceres, E.M. (2021). Tolerogenic dendritic cells in autoimmunity and inflammatory diseases. *Trends Immunol.* *42*, 59–75.
- Müller, F., Scherer, M., Assenov, Y., Lutsik, P., Walter, J., Lengauer, T., and Bock, C. (2019). RnBeads 2.0: comprehensive analysis of DNA methylation data. *Genome Biol.* *20*, 55.
- Murphy, T.L., Grajales-Reyes, G.E., Wu, X., Tussiwand, R., Briseño, C.G., Iwata, A., Kretzer, N.M., Durai, V., and Murphy, K.M. (2016). Transcriptional control of dendritic cell development. *Annu. Rev. Immunol.* *34*, 93–119.
- Navarro-Barriuso, J., Mansilla, M.J., and Martínez-Cáceres, E.M. (2018). Searching for the transcriptomic signature of immune tolerance induction-biomarkers of safety and functionality for tolerogenic dendritic cells and regulatory macrophages. *Front. Immunol.* *9*, 2062.
- Ong, L.T.C., Schibeci, S.D., Fewings, N.L., Booth, D.R., and Parnell, G.P. (2021). Age-dependent VDR peak DNA methylation as a mechanism for latitude-dependent multiple sclerosis risk. *Epigenetics Chromatin* *14*, 9.
- Pacis, A., Tailleux, L., Morin, A.M., Lambourne, J., Maclsaac, J.L., Yotova, V., Dumaine, A., Danckær, A., Luca, F., Grenier, J.C., et al. (2015). Bacterial infection remodels the DNA methylation landscape of human dendritic cells. *Genome Res.* *25*, 1801–1811.
- Pacis, A., Mailhot-Léonard, F., Tailleux, L., Randolph, H.E., Yotova, V., Dumaine, A., Grenier, J.-C., and Barreiro, L.B. (2019). Gene activation precedes DNA demethylation in response to infection in human dendritic cells. *Proc. Natl. Acad. Sci. U S A* *116*, 6938–6943.
- Pageaud, Y., Plass, C., and Assenov, Y. (2018). Enrichment analysis with Epi-annotator. *Bioinformatics* *32*, 1781–1783.
- Park, J.H., Van Wyk, H., McMillan, D.C., Quinn, J., Clark, J., Roxburgh, C.S.D., Horgan, P.G., and Edwards, J. (2017). Signal transduction and activator of transcription-3 (STAT3) in patients with colorectal cancer: associations with the phenotypic features of the tumor and host. *Clin. Cancer Res.* *23*, 1698–1709.
- Penna, G., and Adorini, L. (2000). 1 α ,25-Dihydroxyvitamin D 3 inhibits differentiation, maturation, activation, and survival of dendritic cells leading to impaired alloreactive T cell activation. *J. Immunol.* *164*, 2405–2411.
- Pereira, F., Barbáchano, A., Silva, J., Bonilla, F., Campbell, M.J., Muñoz, A., and Larriba, M.J. (2011). KDM6B/JMJD3 histone demethylase is induced by vitamin D and modulates its effects in colon cancer cells. *Hum. Mol. Genet.* *20*, 4655–4665.
- Piemonti, L., Monti, P., Sironi, M., Fraticelli, P., Leone, B.E., Dal Cin, E., Allavena, P., and Di Carlo, V. (2000). Vitamin D3 affects differentiation, maturation, and function of human monocyte-derived dendritic cells. *J. Immunol.* *164*, 4443–4451.
- Pratt, J.C., Igras, V.E., Maeda, H., Baksh, S., Gelfand, E.W., Burakoff, S.J., Neel, B.G., and Gu, H. (2000). Cutting edge: gab2 mediates an inhibitory phosphatidylinositol 3'-kinase pathway in T cell antigen receptor signaling. *J. Immunol.* *165*, 4158–4163.
- Ramírez, F., Dündar, F., Sarah Diehl, S., Björn A Grüning, B.A., and Manke, T. (2014). deepTools: a flexible platform for exploring deep-sequencing data. *Nucleic Acids Res.* *42*, W187–W191.
- Rasmussen, K.D., Berest, I., Keßler, S., Nishimura, K., Simón-Carrasco, L., Vassiliou, G.S., Pedersen, M.T., Christensen, J., Zaugg, J.B., and Helin, K. (2019). TET2 binding to enhancers facilitates transcription factor recruitment in hematopoietic cells. *Genome Res.* *29*, 564–575.
- Ritchie, M.E., Phipson, B., Wu, D., Hu, Y., Law, C.W., Shi, W., and Smyth, G.K. (2015). Limma powers differential expression analyses for RNA-sequencing and microarray studies. *Nucleic Acids Res.* *43*, e47.
- Sardina, J.L., Collombet, S., Tian, T.V., Gómez, A., Di Stefano, B., Berenguer, C., Brumbaugh, J., Stadhouders, R., Segura-Morales, C., Gut, M., et al. (2018). Transcription factors drive Tet2-mediated enhancer demethylation to reprogram cell fate. *Cell Stem Cell* *23*, 727–741.e9.
- Schaefer, A., Unterberger, C., Frankenberger, M., Lohrum, M., Staples, K.J., Werner, T., Stunnenberg, H., and Ziegler-Heitbrock, L. (2009). Mechanism of Interferon-gamma mediated down-regulation of Interleukin-10 gene expression. *Mol. Immunol.* *46*, 1351–1359.
- Schübeler, D. (2015). Function and information content of DNA methylation. *Nature* *517*, 321–326.
- Segura, E., Touzot, M., Bohineust, A., Cappuccio, A., Chiocchia, G., Hosmalin, A., Dalod, M., Soumelis, V., and Amigorena, S. (2013). Human inflammatory dendritic cells induce Th17 cell differentiation. *Immunity* *38*, 336–348.

- Seuter, S., Neme, A., and Carlberg, C. (2017). Epigenomic PU.1-VDR crosstalk modulates vitamin D signaling. *Biochim. Biophys. Acta Gene Regul. Mech.* *1860*, 405–415.
- Seuter, S., Neme, A., and Carlberg, C. (2018). ETS transcription factor family member GABPA contributes to vitamin D receptor target gene regulation. *J. Steroid Biochem. Mol. Biol.* *177*, 46–52.
- Széles, L., Keresztes, G., Töröcsik, D., Balajthy, Z., Krenács, L., Póliska, S., Steinmeyer, A., Zuegel, U., Pruenster, M., Rot, A., et al. (2009). 1,25-Dihydroxyvitamin D3 is an autonomous regulator of the transcriptional changes leading to a tolerogenic dendritic cell phenotype. *J. Immunol.* *182*, 2074–2083.
- Teh, B.K., Yeo, J.G., Chern, L.M., and Lu, J. (2011). C1q regulation of dendritic cell development from monocytes with distinct cytokine production and T cell stimulation. *Mol. Immunol.* *48*, 1128–1138.
- Torres-Aguilar, H., Aguilar-Ruiz, S.R., González-Pérez, G., Munguía, R., Bajaña, S., Meraz-Ríos, M.A., and Sánchez-Torres, C. (2010). Tolerogenic dendritic cells generated with different immunosuppressive cytokines induce antigen-specific anergy and regulatory properties in memory CD4⁺ T cells. *J. Immunol.* *184*, 1765–1775.
- van der Maaten, L. (2014). Accelerating t-SNE using Tree-based algorithms. *J. Machine Learn. Res.* *15*, 3221–3245.
- Van Halteren, A.G.S., Van Etten, E., De Jong, E.C., Bouillon, R., Roep, B.O., and Mathieu, C. (2002). Redirection of human autoreactive T-cells upon interaction with dendritic cells modulated by TX527, an analog of 1,25 dihydroxyvitamin D3. *Diabetes* *51*, 2119–2125.
- Wang, Y., Xiao, M., Chen, X., Chen, L., Xu, Y., Lv, L., Wang, P., Yang, H., Ma, S., Lin, H., et al. (2015). WT1 recruits TET2 to regulate its target gene expression and suppress leukemia cell proliferation. *Mol. Cell* *57*, 662–673.
- Wei, Z., Yoshihara, E., He, N., Hah, N., Fan, W., Pinto, A.F.M., Huddy, T., Wang, Y., Ross, B., Estepa, G., et al. (2018). Vitamin D switches BAF complexes to protect β cells. *Cell* *173*, 1135–1149.e15.
- Xiong, J., Zhang, Z., Chen, J., Huang, H., Xu, Y., Ding, X., Zheng, Y., Nishinakamura, R., Xu, G.-L., Wang, H., et al. (2016). Cooperative action between SALL4A and TET proteins in stepwise oxidation of 5-methylcytosine. *Mol. Cell* *64*, 913–925.
- Ziegler-Heitbrock, L., Lötzerich, M., Schaefer, A., Werner, T., Frankenberger, M., and Benkhart, E. (2003). IFN- α induces the human IL-10 gene by recruiting both IFN regulatory factor 1 and Stat3. *J. Immunol.* *171*, 285–290.

STAR★METHODS

KEY RESOURCES TABLE

REAGENT or RESOURCE	SOURCE	IDENTIFIER
Antibodies		
Fc Block reagent, human antibody	Miltenyi Biotec	Cat# 130-059-901; RRID: AB_2892112
Anti-human CD14, FITC conjugated (clone TÜK4)	Miltenyi Biotec	Cat# 130-080-701; RRID: AB_244303
Anti-human CD80, PE conjugated (clone 2D10)	Miltenyi Biotec	Cat# 130-097-202; RRID: AB_2659259
Anti-human CD86, APC conjugated (clone FM95)	Miltenyi Biotec	Cat# 130-113-569; RRID: AB_2726174
Anti-human CD11b, APC conjugated (clone ICRF44)	BioLegend	Cat# 301310; RRID: AB_314162
Anti-human CD1a, PE conjugated (clone HI149)	BioLegend	Cat# 300106; RRID: AB_314020
Anti-human HLA-DR, Pe-Cyanine7 conjugated (clone LN3)	Thermo Fisher Scientific	Cat# 25-9956-42; RRID: AB_1582284
LIVE/DEAD™ Fixable Violet Dead Cell Stain Kit	Thermo Fisher Scientific	Cat# L34964
Anti-acetyl-Histone H3 Antibody	Millipore	Cat# 06-599; RRID: AB_2115283
Anti-trimethyl-Histone H3 (Lys27) Antibody	Millipore	Cat# 07-449; RRID: AB_310624
Anti-Trimethyl-Histone H3 (Lys4)	Millipore	Cat# 17-614; RRID: AB_11212770
Rat IgG1 kappa Isotype Control (clone eBRG1)	Thermo Fisher Scientific	Cat# 16-4301-85; RRID: AB_470154
IL-10 Monoclonal Antibody (clone JES3-9D7)	Thermo Fisher Scientific	Cat# 16-7108-85; RRID: AB_469229
IL-6 Monoclonal Antibody (clone MQ2-13A5)	Thermo Fisher Scientific	Cat# 16-7069-85; RRID: AB_469219
Vitamin D receptor	Cell Signaling Technology	Cat# 12550; RRID: AB_2637002
Anti-TET2 antibody	Abcam	Cat# ab124297; RRID: AB_2722695
Anti-Pstat3 [Y705], (clone 4/P-STAT3)	Fluidigm	Cat# 3158005A; RRID: AB_2811100
Anti-STAT3, (clone 79D7)	Cell Signaling Technology	Cat# 4904; RRID: AB_331269
Anti-pSTAT1 [Y701], (clone 58D6)	Cell Signaling Technology	Cat# 9167; RRID: AB_561284
Anti-STAT1, (clone 42H3)	Cell Signaling Technology	Cat# 9175; RRID: AB_2197984
Anti-pSTAT5 [Y694], (clone 47)	Fluidigm	Cat# 3150005A; RRID: AB_2744690
Anti-STAT5 beta, (clone ST5b-10G1)	Thermo Fisher Scientific	Cat# 13-5300; RRID: AB_2533021
Anti-Lamin B1	Abcam	Cat# ab16048; RRID: AB_443298
Anti-alpha-Tubulin, (clone DM1A)	Sigma-Aldrich	Cat# T6199; RRID: AB_477583
Normal Rabbit IgG Antibody	Millipore	Cat# 12-370; RRID: AB_145841
Normal Mouse IgG Antibody	Millipore	Cat# 12-371; RRID: AB_145840
Biological samples		
Buffy Coats	Catalan Blood and Tissue Bank (CBTB)	Cat# BB014
Chemicals, peptides, and recombinant proteins		
Recombinant Human IL-4	Peprotech	Cat# 200-04; GenPept: P05112
Recombinant Human GM-CSF	Peprotech	Ca# 300-03; GenPept: P04141
1 α ,25-Dihydroxyvitamin D3	Sigma-Aldrich	Cat# D1530; CAS: 32222-06-3
TG101348, JAK/STAT pathway inhibitor	STEMCELL	Cat# 73472; CAS: 936091-26-8
Potassium perruthenate (VII) (KRuO4)	Thermo Fisher Scientific	Cat# 11877; CAS: 10378-50-4
Triton™ X-100	Sigma-Aldrich	Cat# T8787; CAS: 9036-19-5
Benzonase® Nuclease	Sigma-Aldrich	Cat# E1014; CAS: 9025-65-4
DMP (Dimethyl Pimelimidate)	Thermo Fisher Scientific	Cat# 21666; CAS: 58537-94-3
Critical commercial assays		
MACS CD14 Microbeads	Miltenyi Biotec	Cat# 130-050-201
CD1c (BDCA-1)+ Dendritic Cell Isolation Kit	Miltenyi Biotec	Cat# 130-119-475
Dynabeads™ Untouched™ Human CD8 T Cells Kit	Thermo Fisher Scientific	Cat# 11348D
Cell Trace CFSE	Thermo Fisher Scientific	Cat# C34554

(Continued on next page)

Continued		
REAGENT or RESOURCE	SOURCE	IDENTIFIER
APC BrdU Flow Kit	BD Pharmingen	Cat# 552598
ELISA MAXTM Deluxe Set Human IL-10	BioLegend	Cat# 430604
Access IL-6 reagent kit	Beckman-Coulter	Cat# A16369
Maxwell RSC Cultured Cells DNA Kit	Promega	Cat# AS1620
Maxwell RSC simplyRNA cells Kit	Promega	Cat# AS1390
EZ DNA Methylation-Gold Kit	Zymo Research	Cat# D5005
PyroMark Q48 Advanced CpG Reagents	Qiagen	Cat# 974022
Transcriptor First Strand cDNA Synthesis Kit	Roche	Cat# 04897030001
IMMOLASE DNA polymerase Kit	Bioline	Cat# BIO-21047
LightCycler® 480 SYBR Green I Master	Roche	Cat# 0487352001
Infinium MethylationEPIC BeadChip	Illumina	Cat# 20042130
iDeal ChIP-seq kit for Transcription Factors	Diagenode	Cat# C01010055
Magna ChIP™ Protein A+G Magnetic Beads	Sigma-Aldrich	Cat# 16-663
cOmplete™, EDTA-free Protease Inhibitor Cocktail	Sigma-Aldrich	Cat# 11873580001
PureProteome™ Protein G Magnetic Bead System	Sigma-Aldrich	Cat# LSKMAGG02
Micro Bio-Spin® P-6 SSC columns	Bio-Rad	Cat# 7326200
Deposited data		
DNA methylation profile of <i>in vitro</i> generated DC and TolDC	This paper	GSE145483
VDR ChIP-Seq	This paper	GSE145584
Oligonucleotides		
Primers for bisulphite pyrosequencing, RT-qPCR and ChIP-qPCR, see Table S2	This paper	N/A
Software and algorithms		
PyroMark Assay Design 2.0 software	Qiagen	Cat# 9019079
Pyromark Q48 Autoprep software	Qiagen	Cat# 9024325
Minfi (R package)	Aryee et al., 2014	https://www.bioconductor.org/packages/release/bioc/html/minfi.html
RnBeads (R package)	Assenov et al. (2014)	https://bioconductor.org/packages/release/bioc/html/RnBeads.html
Limma (R package)	Ritchie et al. (2015)	https://bioconductor.org/packages/release/bioc/html/limma.html
Bowtie2 Aligner v2.2.6	Langmead and Salzberg, 2012	http://bowtie-bio.sourceforge.net/bowtie2/index.shtml
MarkDuplicates software v1.126	Broad institute	https://broadinstitute.github.io/picard/
Sequence Alignment/Map (SAMtools) v1.2	Li et al. (2009)	https://doi.org/10.1093/bioinformatics/btp352
bamCoverage function (deepTools (v2.0))	Ramirez et al. (2014)	https://deeptools.readthedocs.io/en/2.1.0/content/tools/bamCoverage.html
HOMER Motif Analysis	Heinz et al. (2010)	http://homer.ucsd.edu/homer/motif/
GREAT (version 3.0.0.)	McLean et al. (2010)	http://great.stanford.edu/public/html
EpiAnnotator (R package)	Pageaud et al. (2018)	http://epigenomics.dkfz.de/EpiAnnotator/
fgsea (R package)	Korotkevich et al. (2019)	http://bioconductor.org/packages/release/bioc/html/fgsea.html
tSNE	van der Maaten, 2014	https://github.com/lvdmaaten/bhtsne/
sva (R package)	(Leek et al., 2021)	https://bioconductor.org/packages/release/bioc/html/sva.html
DoRothEA (R package)	Garcia-Alonso et al. (2019)	https://bioconductor.org/packages/release/data/experiment/html/dorothea.html
Nichenetr (R package)	Browaeys et al. (2020)	https://github.com/saeyslab/nichenetr

RESOURCE AVAILABILITY

Lead contact

Further information and requests for resources should be directed to the lead contact, Esteban Ballestar (eballestar@carrerasresearch.org).

Materials availability

This study did not generate new unique reagents.

Data and code availability

- DNA methylation and ChIP-seq data for this publication have been deposited in the NCBI Gene Expression Omnibus and are accessible through GEO Series accession numbers GSE145483 and GSE145584.
- This paper does not report original code.
- Any additional information required to reanalyze the data reported in this paper is available from the lead contact upon request

EXPERIMENTAL MODEL AND SUBJECT DETAILS

Differentiation of ToIDCs and DCs from peripheral blood monocytes

For *in vitro* differentiation experiments, we obtained buffy coats from anonymous donors through the Catalan Blood and Tissue Bank (CBTB). The CBTB follows the principles of the World Medical Association (WMA) Declaration of Helsinki. The Committee for Human Subjects of Bellvitge Hospital approved the study (PR275/17). Given the anonymous nature of the volunteers, no information about the gender and age was provided by the CBTB. Before providing the first blood sample, all donors received detailed oral and written information, and signed a consent form at the CBTB. Peripheral blood mononuclear cells (PBMCs) were isolated by Ficoll-Paque gradient centrifugation. MOs were isolated from PBMCs using positive selection with MACS CD14 microbeads (Miltenyi Biotec). Cells were resuspended in RPMI Medium 1640 + GlutaMAX™-1 (Gibco, Life Technologies) containing 10% fetal bovine serum, 100 units/mL penicillin, and 100 µg/mL streptomycin. For ToIDC differentiation, the medium was supplemented with 10 ng/mL human IL-4, 10 ng/mL GM-CSF (PeproTech), and 10 nM of vitamin D3 or calcitriol (Sigma Aldrich). For DCs, the medium did not contain vitamin D. Anti-IL-6 1 µg/mL (Invitrogen) and rat IgG isotype 1 µg/mL (eBioscience) was added during differentiation process when required. In some cases, specified in the text, vitamin D3 was added for 30 min following differentiation to DCs (DC + vitD). In other experiments, differentiation was performed in the presence of a JAK2 inhibitor (TG101348, STEMCELL) at 500 nM.

Isolation and culture of peripheral blood DCs

For the validation of our differentiation model, peripheral blood CD1c⁺ DCs were isolated and cultured for three days with or without 100 nM vitamin D (Sigma Aldrich). These samples were also obtained from anonymous donors through the Catalan Blood and Tissue Bank (CBTB). The CBTB follows the principles of the World Medical Association (WMA) Declaration of Helsinki. The Committee for Human Subjects of Bellvitge Hospital approved the study (PR275/17). Given the anonymous nature of the volunteers, no information about the gender and age was provided by the CBTB. Before providing the first blood sample, all donors received detailed oral and written information, and signed a consent form at the CBTB. For this, PBMCs were isolated by Ficoll-Paque gradient centrifugation followed by a CD1c⁺ DCs purification with CD1c (BDCA-1)⁺ Dendritic Cell Isolation Kit (Miltenyi Biotec) according to manufacturer instructions. Obtained cells were cultured at a concentration of 10⁶ cells/mL in RPMI Medium 1640 + GlutaMAX™-1 (Gibco, Life Technologies) containing 10% fetal bovine serum and 100 units/mL penicillin with or without vitamin D.

METHOD DETAILS

CD8⁺ cell proliferation assay

Allogenic CD8⁺ T-cells isolated using negative selection with the human CD8 T Cells Kit (Invitrogen) were labeled with carboxyfluorescein succinimidyl ester (CFSE) and seeded in 96-well plates at 200,000 cells/well, with ToIDCs or DCs at different ratios (ToIDC/DC:CD8⁺ T-cell ratios: 1:2, 1:4, and 1:6). CD8⁺ cells were then stimulated with anti-CD3/CD28 Dynabeads 5 µL/mL (Invitrogen) and cultured for 5 days. Anti-IL-6 1 µg/mL (Invitrogen), anti-IL-10 1 µg/mL (eBioscience) and rat IgG isotype 1 µg/mL (eBioscience) was added during co-culture process when required. CD8⁺ T-cell proliferation was analyzed by FACS and determined by considering the proliferating CD8⁺ T-cells those where CFSE staining had decreased compared to unstimulated CD8⁺ T-cells.

BrdU proliferation assay

MOs were differentiated to DCs and ToIDCs as described above and BrdU (APC BrdU Flow kit, BD Pharmingen) pulses were added to a final concentration of 10 µM at days 2 and 4. On days 3, 4 and 5 cells were harvested and 10⁶ cells were prepared for flow cytometry as described by the manufacturer. In brief, cells were fixed for 30 minutes on ice, permeabilized for 5 minutes on ice and

treated with DNase for 1 h at 37°C to expose incorporated BrdU. Cells were then stained with fluorescent anti-BrdU antibody for 20 minutes at room temperature and analyzed in a BD FACSCanto-II flow cytometer. The HAFTL pre-B cell line was used as control for proliferation.

Flow cytometry

For the study of surface cell markers, cells were harvested after differentiation culture and washed once with PBS. Cell staining was performed in a staining buffer (PBS with 4% fetal bovine serum and 0.4% EDTA) after blocking for non-specific binding with Fc block (BD Pharmingen) for 5 minutes on ice. Cells were stained for 20 minutes on ice. Antibodies used included: CD14-FITC, CD80-PE, CD86-APC (Miltenyi biotec), CD11b-APC, CD1a-PE (Biolegend), HLA-DR-PeCy7 (eBioscience). Cells were also stained with the viability dye LIVE/DEAD™ Fixable Violet (Invitrogen) according to manufacturer's conditions. After staining, cells were fixed with PBS + 4% paraformaldehyde and analyzed in a BD FACSCanto-II flow cytometer in the following 48 h.

Cytokine measurements

For *in vitro* experiments, the concentration of IL-10 cytokine was measured from the cell culture supernatants using an enzyme-linked immunosorbent assay (ELISA), according to the manufacturer's instructions (BioLegend, San Diego, CA, USA). The concentration of IL-6 was measured with Beckman DXI Immunoassay analyzer using the access IL-6 reagent kit (Beckman Coulter) following the manufacturer's instructions.

Genomic DNA and total RNA extraction

DNA was extracted with a Maxwell RSC Cultured Cells DNA kit (Promega) following manufacturer's instructions. Similarly, total RNA was extracted with Maxwell RSC simplyRNA cells kit (Promega) following manufacturer's instructions.

Bisulfite (BS) and oxidative-bisulfite (oxBS) pyrosequencing

500 ng of genomic DNA was BS-converted with an EZ DNA Methylation-Gold kit (Zymo Research), following the manufacturer's instructions. The oxBS samples were purified via buffer exchange with Micro Bio-Spin® P-6 SSC columns (Bio-Rad Laboratories, Inc., USA) and eluted in ~22 μ L MilliQ-water. After DNA denaturation with 1.25 μ L NaOH (1M) for 30 min in a shaking incubator at 37°C, DNA was oxidized with 2 μ L KRuO₄ (15 mM) (Alfa Aesar, Germany) for 60 min in an ice-water bath (vortexing the reaction twice) and centrifuged at 16000 g for 15 min. Finally, oxidized DNA were BS converted using the EZ DNA Methylation™ kit (Zymo Research, CA, USA). BS- and oxBS-treated DNA was PCR-amplified using IMMOLASE DNA polymerase kit (bioline). Primers were designed with PyroMark Assay Design 2.0 software (Qiagen) (see [Table S3](#) for primer sequences). Finally, PCR amplicons were pyrosequenced with the PyroMark Q24 system and analyzed with PyroMark Q48 Autoprep (Qiagen). 5mC levels were derived from the oxBS data, while 5hmC levels were calculated by subtracting the oxBS values from the BS values (5mC+5hmC) using the same biological replicate, as described in ([Garcia-Gomez et al., 2017](#)).

Real-time quantitative Polymerase Chain Reaction (RT-qPCR)

250 ng of total RNA were converted to cDNA with Transcriptor First Strand cDNA Synthesis Kit (Roche) following manufacturer's instructions. RT-qPCR primers were designed with Primer3 software ([Koressaar and Remm, 2007](#)) (see [Table S3](#)). RT-qPCR reactions were prepared with LightCycler® 480 SYBR Green I Master (Roche) according to manufacturer's instructions and analyzed with a LightCycler® 480 instrument (Roche).

Western blot

Protein expression and downregulation was visualized by western blotting, performed using standard Western blot. The following antibodies were used for Western blotting and Co-immunoprecipitation: Anti-Vitamin D3 Receptor (Cell Signaling), anti-TET2 (Abcam), anti-pStat3 (Fluidigm), anti-Stat3 (Cell Signaling Technology), anti-pStat1 (Cell Signaling Technology), anti-Stat1 (Cell Signaling Technology), anti-pStat5 (Fluidigm), anti-Stat5 (Thermo Fisher Scientific), anti-Lamin B1 (Abcam), anti- α Tubulin (Sigma-Aldrich). anti-rabbit IgGs (Merck Millipore) and anti-mouse IgGs (Merck Millipore).

Co-immunoprecipitation (Co-IP)

Co-IP assays were performed using ToIDCs differentiated from CD14 + monocytes for 3 days. Cell extracts were prepared in lysis buffer [50 mM Tris-HCl, pH 7.5, 1 mM EDTA, 150 mM NaCl, 1% Triton-X-100, protease inhibitor cocktail (cOmplete™, Merck)] with corresponding units of Benzonase (Sigma) and incubated at 4°C for 4 h. 100 μ L of supernatant was saved as input and diluted with 2 \times Laemmli sample buffer (5 \times SDS, 20% glycerol, 1M Tris-HCl (pH 8.1)). Supernatant was first incubated with PureProteome™ Protein A/G agarose suspension (Merck Millipore) for 1 h to remove background signal. The lysate was then incubated overnight at 4°C with respective crosslinked primary antibody. The cross-linking was performed in 20 mM dimethyl pimelimidate (DMP) (Pierce, Thermo Fisher Scientific, MA, USA) dissolved in 0.2 M sodium borate (pH 9.0). Subsequently, the beads were quenched with 0.2M of ethanolamine (pH 8.0) and resuspended at 4°C in PBS until use. Beads were then washed three times with lysis buffer at 4°C. Sample elution was done by acidification using a buffer containing 0.2 M glycine (pH 2.3) and diluted with 2 \times Laemmli. Samples and inputs were denatured at 95°C in the presence of 1% β -mercaptoethanol.

DNA methylation profiling

Infinium MethylationEPIC BeadChip (Illumina, Inc., San Diego, CA, USA) arrays were used to analyze DNA methylation. This platform allows >850,000 methylation sites per sample to be interrogated at single-nucleotide resolution, covering 99% of the reference sequence (RefSeq) genes. The samples were bisulfite-converted using EZ DNA Methylation-Gold™ Kit (Zymo Research, Irvine, CA, USA) and were hybridized in the array following the manufacturer's instructions. Image processing and intensity data extraction software and procedures were as previously described (Bibikova et al., 2006). Each methylation data point was obtained from a combination of the Cy3 and Cy5 fluorescent intensities from the methylated and unmethylated alleles. Background intensity computed from a set of negative controls was subtracted from each data point. For representation and further analysis, we used beta and M values. The beta value is the ratio of the methylated probe intensity to the overall intensity (the sum of the methylated and unmethylated probe intensities). It can take a value between 0 and 1, and was used to derive heatmaps and to compare DNA methylation percentages from bisulfite-pyrosequencing experiments. The M value is calculated as the \log_2 ratio of the intensities of the methylated versus unmethylated probes. For the purpose of statistical analysis, M values are more suitable because they are normally distributed.

Raw methylation data were preprocessed with the minfi package (Aryee et al., 2014). Data quality was assessed using the minfi and RnBeads packages (Aryee et al., 2014; Assenov et al., 2014; Müller et al., 2019). After Snoob normalization, data were analyzed using aneBayes moderate t test available in the limma package (Ritchie et al., 2015). Several criteria have been proposed as representing significant differences in methylated CpGs, but in this study we considered a probe to be differentially methylated if it had a methylation differential of 20% and if it was significant ($q < 0.05$).

ChIP-seq analysis

Chromatin immunoprecipitation was performed using the iDeal ChIP-seq kit for Transcription Factors (Diagenode), according to the manufacturer's instructions. Briefly, cells on day 3 of differentiation were cross-linked with 1% formaldehyde for 15 min and glycine was added to quench the reaction (final concentration 125 mM, incubated for 5 min at room temperature). Cells were washed once with cold PBS, scraped off the plates, and pelleted. To obtain a soluble chromatin extract, cells were resuspended in 1 mL LB1 (50 mM HEPES, 140 mM NaCl, 1 mM EDTA, 10% glycerol, 0.5% NP-40, 0.25% Triton X-100 and 1× complete protease inhibitor) and incubated while rotating at 4°C for 10 min. Samples were centrifuged, resuspended in 1 mL LB2 (10 mM Tris-HCl pH 8.0, 200 mM NaCl, 1 mM EDTA, 0.5 mM EGTA and 1× complete protease inhibitor) and incubated while rotating at 4°C for 10 min. Finally, samples were centrifuged, resuspended in 1 mL LB3 (10 mM Tris-HCl pH 8.0, 100 mM NaCl, 1 mM EDTA, 0.5 mM EGTA, 0.1% sodium deoxycholate, 0.5% *N*-lauroylsarcosine, 1% Triton X-100 and 1× complete protease inhibitor). Chromatin extracts were sonicated for 12.5 min using a Covaris M220 focused ultrasonicator at a peak power of 75, and a duty factor of 10 and 200 cycles per burst. The lysates were incubated with anti-VDR antibody (12,550, Cell Signaling) bound to 30 μ L protein A or protein G Dynabeads and incubated overnight at 4°C, keeping 5% as input DNA. Magnetic beads were sequentially washed with low-salt buffer (150 mM NaCl, 0.1% SDS, 1% Triton X-100, 1 mM EDTA and 50 mM Tris-HCl), high-salt buffer (500 mM NaCl, 0.1% SDS, 1% Triton X-100, 1 mM EDTA and 50 mM Tris-HCl), LiCl buffer (150 mM LiCl, 0.5% sodium deoxycholate, 0.1% SDS, 1% Nonidet P-40, 1 mM EDTA and 50 mM Tris-HCl) and TE buffer (1 mM EDTA and 10 mM Tris-HCl). For ChIP-seq, beads were resuspended in elution buffer (1% SDS, 50 mM Tris-HCl pH 8.0, 10 mM EDTA and 200 mM NaCl) and incubated for 30 min at 65°C. After centrifugation, the eluate was reverse-cross-linked overnight at 65°C. The eluate was then treated with RNaseA for 1 h at 37°C and with Proteinase K (Roche) for 1 h at 55°C and the DNA was recovered using a Qiagen PCR purification kit.

Sequencing reads from ChIP-seq experiments were mapped to the hg19 assembly of human reference genome using Bowtie2 Aligner v2.2.6 (Langmead and Salzberg, 2012). After removing reads with MAPQ < 30 with Sequence Alignment/Map (SAMtools) v1.2 (Li et al., 2009), PCR duplicates were eliminated using the Picard function available in MarkDuplicates software v1.126. Peak calling was determined using SPP (with parameters $-npeak=300000 -savr -savp -rf$). The irreproducible discovery rate (IDR) was used to filter peaks (IDR < 0.05). To visualize individual ChIP-seq data on Integrative Genomics Viewer (IGV), we converted bam output files to normalized bigwig format using the bamCoverage function in deepTools (v2.0).

ChIP-qPCR

ChIP assays were performed as previously described (Li et al., 2020). Briefly, MOs, DCs and ToIDCs were crosslinked with 1% methanol-free formaldehyde (Thermo Fisher) for 15 min and subjected to immunoprecipitation after sonication. ChIP experiments were performed using the LowCell# ChIP kit™ protein A (Diagenode, Liège, Belgium). We used antibodies against vitamin D3 Receptor (Cell Signaling), acetylated H3 (H3ac), trimethylated lysine 27 of histone H3 (H3K4me3Millipore) and trimethylated lysine 4 of histone H3. Corresponding rabbit IgG (Diagenode) is used as control. Protein binding was analyzed by real-time quantitative PCR, and data are represented as ratio of the enriched fraction with respect to input. ChIP primers were designed for the areas flanking differentially methylated CpGs and their sequences are shown in Table S3.

Microarray reanalysis

Affymetrix datasets from human monocytes, and from *in vitro*- and *in vivo* DCs and MACs were obtained from GSE40484 (Segura et al., 2013) and GSE102046 (Goudot et al., 2017). Affymetrix raw data from MOs, DCs and ToIDCs were obtained from GSE13762 (Széles et al., 2009). Affymetrix raw data files were normalized by the robust multiarray average (RMA) algorithm and summarized,

after background correction, using the R package oligo (Carvalho and Irizarry, 2010). Normalized expression datasets were then merged and corrected for batch effects using ComBat function of the sva package. Finally, t-Distributed Stochastic Neighbor Embedding (tSNE) of 1000 most variant genes was performed in R using Rtsne package.

Data analysis

Hierarchical clustering was carried out based on Pearson correlation distances and average linkage criteria. For low-dimensional analysis, we used principal component analysis (PCA). Transcription-factor motifs were enriched for each set using HOMER software v4.10.3. Specifically, we used the findMotifsGenome.pl algorithm (with parameters -size 200 -cpg) to search for significant enrichment against a background sequence adjusted to have similar CpG and GC contents. Genomic regions for genetic context location were annotated using the annotatePeaks.pl algorithm in the HOMER v4.10.3 software application (Heinz et al., 2010). To determine the location relative to a CpG island (CGI), we used 'hg19_cpigs' annotation in the annotatr v1.8 R package. GREAT software (McLean et al., 2010) was used to enrich downstream pathways and gene ontologies. We used the single nearest gene option to identify associations between genomic regions and genes. Chromatin state analysis for DCs were assessed using the EpiAnnotator R package (Pageaud et al., 2018). Inference of TF activities from expression values were calculated using DoRothEA (Garcia-Alonso et al., 2019). We used the nichenetr package (Browaeys et al., 2020) to predict ligand activity.

QUANTIFICATION AND STATISTICAL ANALYSIS

All statistical analyses were done in R v3.5.1. Data distributions were tested for normality. Normally distributed data were tested using two-tailed unpaired Student's t-tests; non-normal data were analyzed with the appropriate non-parametric statistical test. Levels of significance are indicated as: *, $P < 0.05$; **, $P < 0.01$; ***, $P < 0.001$; ****, $P < 0.0001$. Non-significance ($P \geq 0.05$) is indicated as 'ns'.

Targeting aberrant DNA methylation in mesenchymal stromal cells as a treatment for myeloma bone disease

Antonio Garcia-Gomez^{1,2,11}, Tianlu Li^{1,2,11}, Carlos de la Calle-Fabregat^{1,2}, Javier Rodríguez-Ubreva^{1,2}, Laura Ciudad^{1,2}, Francesc Català-Moll^{1,2}, Gerard Godoy-Tena¹, Montserrat Martín-Sánchez³, Laura San-Segundo³, Sandra Muntión³, Xabier Morales⁴, Carlos Ortiz-de-Solórzano⁴, Julen Oyarzabal⁵, Edurne San José-Enériz⁶, Manel Esteller^{7,8,9,10}, Xabier Agirre⁶, Felipe Prosper⁶, Mercedes Garayoa³ & Esteban Ballestar^{1,2}

Multiple myeloma (MM) progression and myeloma-associated bone disease (MBD) are highly dependent on bone marrow mesenchymal stromal cells (MSCs). MM-MSCs exhibit abnormal transcriptomes, suggesting the involvement of epigenetic mechanisms governing their tumor-promoting functions and prolonged osteoblast suppression. Here, we identify widespread DNA methylation alterations of bone marrow-isolated MSCs from distinct MM stages, particularly in Homeobox genes involved in osteogenic differentiation that associate with their aberrant expression. Moreover, these DNA methylation changes are recapitulated in vitro by exposing MSCs from healthy individuals to MM cells. Pharmacological targeting of DNMTs and G9a with dual inhibitor CM-272 reverts the expression of hypermethylated osteogenic regulators and promotes osteoblast differentiation of myeloma MSCs. Most importantly, CM-272 treatment prevents tumor-associated bone loss and reduces tumor burden in a murine myeloma model. Our results demonstrate that epigenetic aberrancies mediate the impairment of bone formation in MM, and its targeting by CM-272 is able to reverse MBD.

¹Epigenetics and Immune Disease Group, Josep Carreras Leukaemia Research Institute (IJC), Badalona, 08916 Badalona, Barcelona, Spain. ²Chromatin and Disease Group, Cancer Epigenetics and Biology Programme (PEBC), Bellvitge Biomedical Research Institute (IDIBELL), 08908 L'Hospitalet de Llobregat, Barcelona, Spain. ³Centro de Investigación del Cáncer, IBMCC (Universidad de Salamanca-CSIC) and Hospital Universitario de Salamanca-IBSAL, 37007 Salamanca, Spain. ⁴Imaging Platform, Center for Applied Medical Research (CIMA), University of Navarra, IDISNA, Ciberonc, 31008 Pamplona, Spain. ⁵Small Molecule Discovery Platform, Molecular Therapeutics Program, Center for Applied Medical Research (CIMA), University of Navarra, 31008 Pamplona, Spain. ⁶Division of Hemato-Oncology, Center for Applied Medical Research (CIMA), University of Navarra, IDISNA, Ciberonc 31008 Pamplona, Spain. ⁷Josep Carreras Leukaemia Research Institute (IJC), Badalona, Barcelona, Catalonia, Spain. ⁸Centro de Investigación Biomedica en Red Cancer (CIBERONC), Madrid, Spain. ⁹Institució Catalana de Recerca i Estudis Avançats (ICREA), Barcelona, Catalonia, Spain. ¹⁰Physiological Sciences Department, School of Medicine and Health Sciences, University of Barcelona (UB), Barcelona, Catalonia, Spain. ¹¹These authors contributed equally: Antonio Garcia-Gomez, Tianlu Li. ✉email: nonogarcia85@gmail.com; eballestar@carrerasresearch.org

Multiple myeloma (MM) is an incurable hematological malignancy characterized by clonal expansion of plasma cells in the bone marrow (BM) that accounts for 1% of all cancers^{1,2}. Nearly 90% of myeloma patients suffer from skeletal-related events during the course of the disease, including severe bone pain, hypercalcemia, pathological fractures, and spinal cord compression³, that not only affect the quality of life but also their overall survival⁴. Myeloma-associated bone disease (MBD) is characterized by an increase in bone-resorptive activity and number of osteoclasts (OCs), as well as impairment of bone-forming activity and differentiation of osteoblasts (OBs), which ultimately lead to the development of osteolytic lesions⁵.

In most cases, symptomatic myeloma is preceded by sequential asymptomatic stages of monoclonal gammopathy of undetermined significance (MGUS) and smoldering myeloma (SMM), with increasing BM plasmocytosis and monoclonal component as well as augmented risk of progression to active MM^{6,7}. The biological behavior and clinical outcome of MM are partly dependent on genetic and epigenetic abnormalities of tumor subclones that arise from MGUS and SMM stages⁸. However, the clinical stability of MGUS cases, despite displaying shared genetic lesions with MM cells, suggests that the BM microenvironment may critically modulate disease progression^{6,9,10}. In this regard, it has been widely shown that a complex and bidirectional relationship exists between MM cells and the BM niche, which results in oncogenesis support, anemia, immunosuppression, and uncoupling of the bone remodeling process¹¹.

Mesenchymal stromal cells (MSCs) are an essential cell type in the formation and function of the BM microenvironment, being the progenitors of bone-forming OBs, adipocytes, and chondroblasts, as well as the hematopoietic-supporting stroma components of the BM¹². It is well-documented that BM-derived MSCs from MM patients contribute to MM progression (reviewed in ref. ¹¹) and show an impaired ability to differentiate into OBs^{13,14}. Moreover, MM-MSCs are considered inherently abnormal, as their dysfunctionality remains even following *ex vivo* culture in the absence of MM cells¹⁵. Furthermore, bone lesions persist in many MM patients even after therapeutic remission, suggesting a long-term defect in MSCs that inhibit their ability to properly differentiate into functional OBs¹⁶.

Previous studies described that MSCs from MM patients are cytogenetically normal^{17,18}, but show alterations in their transcriptional^{13,19} and proteomic¹¹ profiles even in the absence of myeloma cell interaction. This suggests that epigenetic mechanisms could be governing the tumor-promoting functions of MSCs and their prolonged OB suppression in MM. In fact, Adamik and colleagues²⁰ reported abnormal recruitment of chromatin remodelers in MSCs from myeloma patients, contributing to the transcriptional repression of *Runx2*, a master regulator of OB differentiation. Yet, there is a lack of information about DNA methylation-related mechanisms that may contribute to MM progression and subsequent bone defects. DNA methylation is an essential epigenetic modification involving the addition of a methyl group to the 5-carbon of the cytosine ring by a family of DNA methyltransferase (DNMT) enzymes²¹, which has been described to play a critical role in MSC lineage determination²², as well as in tumor progression and immunosuppression in other cancer types²³.

In this study, we identify DNA methylation alterations in MSCs of MM patients mediated by MM cells resulting in the dysregulation of osteogenesis, and this is reversed by the treatment with CM-272, a dual inhibitor of DNMTs and the histone methyltransferase G9a.

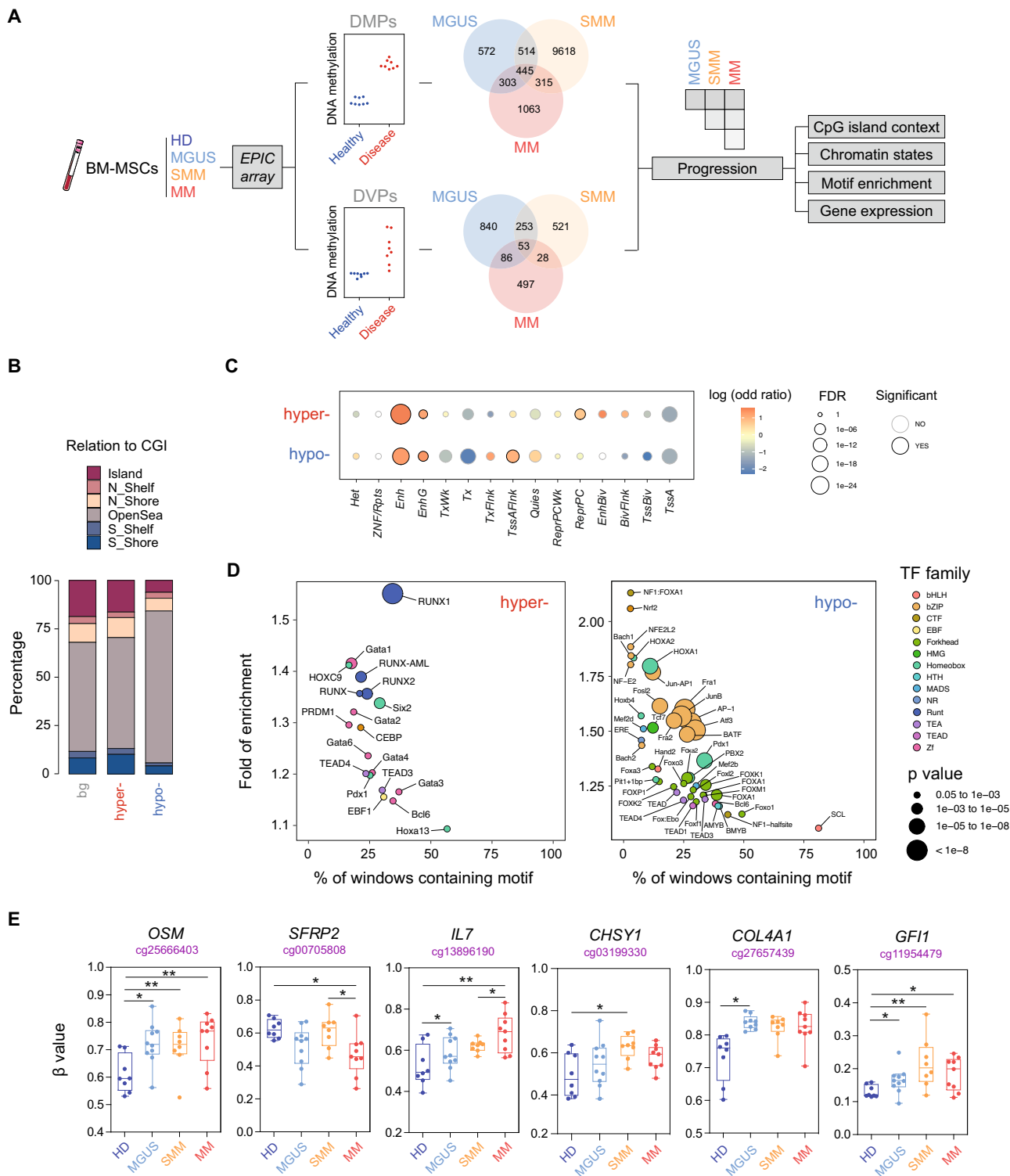
Results

BM-derived MSCs of distinct MM stages exhibit altered DNA methylation profiles. We first obtained genome-wide DNA methylation profiles of BM-derived MSCs isolated at different stages of MM (newly diagnosed MGUS, high-risk SMM, and MM) and healthy controls. DNA methylation changes were identified using two different statistical approaches (Fig. 1A): (i) detection of differentially methylated CpG positions (DMPs) based on differences in DNA methylation means between the patient (MGUS, SMM, and MM) and healthy MSCs ($\Delta\beta \geq 0.1$ and $**p < 0.01$) (Supplementary Data 1); and (ii) detection of differentially variable CpG positions (DVPs) based on differences in variance of DNA methylation levels ($qval < 0.05$ and $*p < 0.05$) between the sample groups (Supplementary Data 2). In regards to DMPs, the largest number of altered CpGs was found in MSCs from patients of the SMM stage compared to healthy donors (Supplementary Fig. 1A, B). On the other hand, we observed the highest number of DVPs in comparison to healthy donors in MSCs isolated from MGUS followed by SMM and MM patients (Supplementary Fig. 1C, D), supporting the notion that these stochastic and heterogeneous DNA methylation patterns are associated with early stages of carcinogenesis, as previously reported^{24,25}. We also observed that the majority of identified DMPs and DVPs are disease stage-specific, although the asymptomatic stages showed a moderate proportion of overlap (Fig. 1A).

Given that myeloma is a multi-stage disease, we then analyzed the accumulative changes of DNA methylation associated with MM progression by selecting DMPs (Supplementary Data 3) and DVPs (Supplementary Data 4) that were found either only in the MM stage, shared by SMM and MM and in all three stages (Fig. 1A). With this analysis, we identified 872 hyper- and 951 hypomethylated DMPs, and 260 hyper- and 318 hypomethylated DVPs.

Analyzing the distribution of MM progression-associated CpGs in relation to CpG islands (CGI), we observed a significant enrichment of CpGs in open sea regions in the hypomethylated DMP data set (Fig. 1B) and in CpG islands in the hypermethylated DVP data set (Supplementary Fig. 1E). Utilizing publicly available chromatin state maps of BM-derived MSCs from healthy individuals²⁶, we found a significant enrichment of both hyper- and hypomethylated DMPs sites that correspond to enhancers (Fig. 1C). In addition, we observed an enrichment in flanking transcription start sites (TSS) in the hypomethylated set, and regions repressed by Polycomb Group (PcG) in hypermethylated CpGs (Fig. 1C). On the other hand, hypermethylated DVPs were enriched in TSSs, bivalent regions, and regions repressed by Polycomb (Supplementary Fig. 1F).

To determine whether these MM progression-associated loci shared any common DNA elements, we performed a search for enriched transcription factor (TF)-binding sites in these regions using the HOMER algorithm²⁷. We observed a significant overrepresentation of binding sites for the Runt and Tead family in differentially hypermethylated DMPs associated with MM progression ($**p < 0.01$; Fig. 1D). These results suggest that key transcription factors involved in the upregulation of osteogenic genes, such as *RUNX2*²⁸ or *TEAD2*²⁹, may participate in aberrant DNA hypermethylation. Since DNA methylation has been originally linked to transcriptional repression, these results suggested that the hypermethylation of these regions could compromise the ability of MSCs to undergo proper OB differentiation. On the other hand, DMP sites that experienced aberrant DNA hypomethylation were highly enriched in binding motifs of the bZip and Homeobox families ($**p < 0.01$; Fig. 1D). In this respect, the loss of DNA methylation could be selectively driving the occupancy of TF



that have been reported as negative regulators of OB differentiation such as *HOXA2*³⁰ and *ATF3*³¹. In addition, we observed transcriptional deregulation of some members of these TF families using expression array data from BM-derived MSCs of healthy controls, MGUS, SMM, and MM patients. Some of these TFs were specifically downregulated in MSCs of active myeloma (*RUNX2* and *TEAD2*), others were already downregulated in precursor myeloma stages (*HOXC9* and *CEBP*), whereas other TFs, including *HOXA2* and *ATF3*, did not change their expression in any myeloma stages

(Supplementary Fig. 1G). In all, these findings suggested that MM progression-associated DNA methylation changes in MSCs might be mediated by the sequential activity of specific TF families, which are also functionally deregulated in MM³². Furthermore, other genes that play important roles in the pathophysiology of MM (such as the cytokines *IL6* and *OSM*) and associated MBD (secreted factors such as *RANKL*, *SFRP2*, *IL7*, *CHSY1*, *COL4A1*, and the transcriptional repressor *GF11*) were also found to alter their DNA methylation levels (Fig. 1E and Supplementary Fig. 1H).

Fig. 1 High-throughput stepwise DNA methylation changes in BM-derived MSCs associated with MM progression. **A** Workflow depicting the methodological approach for selecting DNA methylation changes in bone marrow-derived mesenchymal stromal cells (BM-MSCs) from monoclonal gammopathy of undetermined significance (MGUS; $n = 10$), smoldering myeloma (SMM; $n = 8$), and multiple myeloma (MM; $n = 9$) patients versus healthy controls (HD; $n = 8$). An example of a CpG site experiencing increased mean (differentially methylated position, DMP) or variance (differentially variable position, DVP) in the disease versus the control condition is shown. Venn diagrams show the number of DMPs or DVPs resulting from each comparison. **B** Distribution of DNA methylation changes in relation to CpG islands (CGI), including shores (south, S; north, N), shelves (south, S; north, N), and open sea regions for differentially hyper- or hypomethylated CpG sites. **C** Enrichment analysis of differentially hyper- and hypomethylated CpG sites located in different genomic regions, annotated by 15 chromHMM states. Color scale refers to log odd ratio and circle size refers to p -value significance. **D** Bubble plot representation of HOMER transcription factor (TF) motif enrichment analysis of differentially hyper- and hypomethylated CpGs in MSCs during MM progression (left and right panel, respectively). Color range depicts different transcription factor families and circle size refers to p -value significance. **E** Box plots showing β -values from DMPs obtained from the EPIC array in MSCs from healthy donors and MGUS, SMM, and MM patients of relevant genes involved in the pathogenesis of MM and associated bone disease. HD is represented in dark blue, MGUS in light blue, SMM in orange, and MM in red. eBayes-moderated ANOVA t -test was performed to calculate statistical significance ($*p < 0.05$, $**p < 0.01$, and $***p < 0.005$).

Aberrant DNA methylation is associated with differential Homeobox gene expression in MSCs at different MM stages.

To further investigate the relationship between differential DNA methylation and gene expression, we mapped the DMPs to the most proximal gene. Using expression array data from BM-derived MSCs of healthy controls, MGUS, SMM, and MM patients (Supplementary Data 5), differential expression of DMP-associated genes was identified using a cutoff of $*p < 0.05$ comparing MGUS/SMM/MM to healthy controls for both DNA methylation and gene expression (Fig. 2A and Supplementary Data 6). Gene ontology (GO) analysis revealed that the genes displaying both differential methylation and expression were enriched in functional categories important in cell fate commitment and bone phenotype (Fig. 2B). The most enriched functional category corresponded to genes from the Homeobox family. Within the Homeobox family, we found the subset of *Hox* genes that encodes a large family of highly conserved TFs responsible for driving the correct differentiation of MSCs³³, namely genes belonging to the HOXA-to-D clusters. Furthermore, we observed a significant enrichment in genes reported to be downregulated in MM-MSCs (Fig. 2B)¹³. Integration of methylation and gene expression data corresponding to the Homeobox and bone formation-related genes revealed that both DNA hyper- and hypomethylation events were associated with both downregulation and upregulation of gene expression in different genomic locations (Fig. 2C). Specifically, hypermethylated genes that showed a reduced expression in patient MSCs include positive regulators of OB differentiation such as *RUNX2* or *NRP2*³⁴ (Fig. 2C and Supplementary Table 1). In contrast, negative regulators of osteogenesis such as *SFRP2*³⁵ or *NFATC2*³⁶ were hypomethylated and consequently upregulated in patient MSCs (Fig. 2C). In all, these factors could potentially contribute to impaired osteoblastogenesis associated with bone disease in MM and this is summarized in Supplementary Table 1.

Upon a closer inspection of several Homeobox-associated genomic regions, we observed a negative correlation between DNA methylation of promoters and gene expression. Specifically, the HOXA gene cluster showed aberrant hypomethylation at the *HOXA4* promoter, and its gene expression was upregulated at different disease stages. Conversely, gene promoters of *HOX-A6*, *-A7*, *-A9*, *-A10*, and *-A11* displayed hypermethylation and these genes were downregulated in MGUS/SMM/MM (Fig. 2D and Supplementary Fig. 2A). A similar pattern of an inverse association between methylation and expression was observed in the HOXB and HOXC gene cluster, where *HOXB5*, *-C5*, and *-C8* were aberrantly hypomethylated and upregulated, whereas *HOXC9*, *-C10*, and *-C11* were hypermethylated and downregulated in patients (Fig. 2D and Supplementary Fig. 2A). Other Homeobox genes such as *TBX5*, *PITX1*, or *EMX2* were also reported as regulators of bone formation^{37–39} and showed an

association between DNA methylation at gene promoter and gene expression (Fig. 2D and Supplementary Fig. 2A, B).

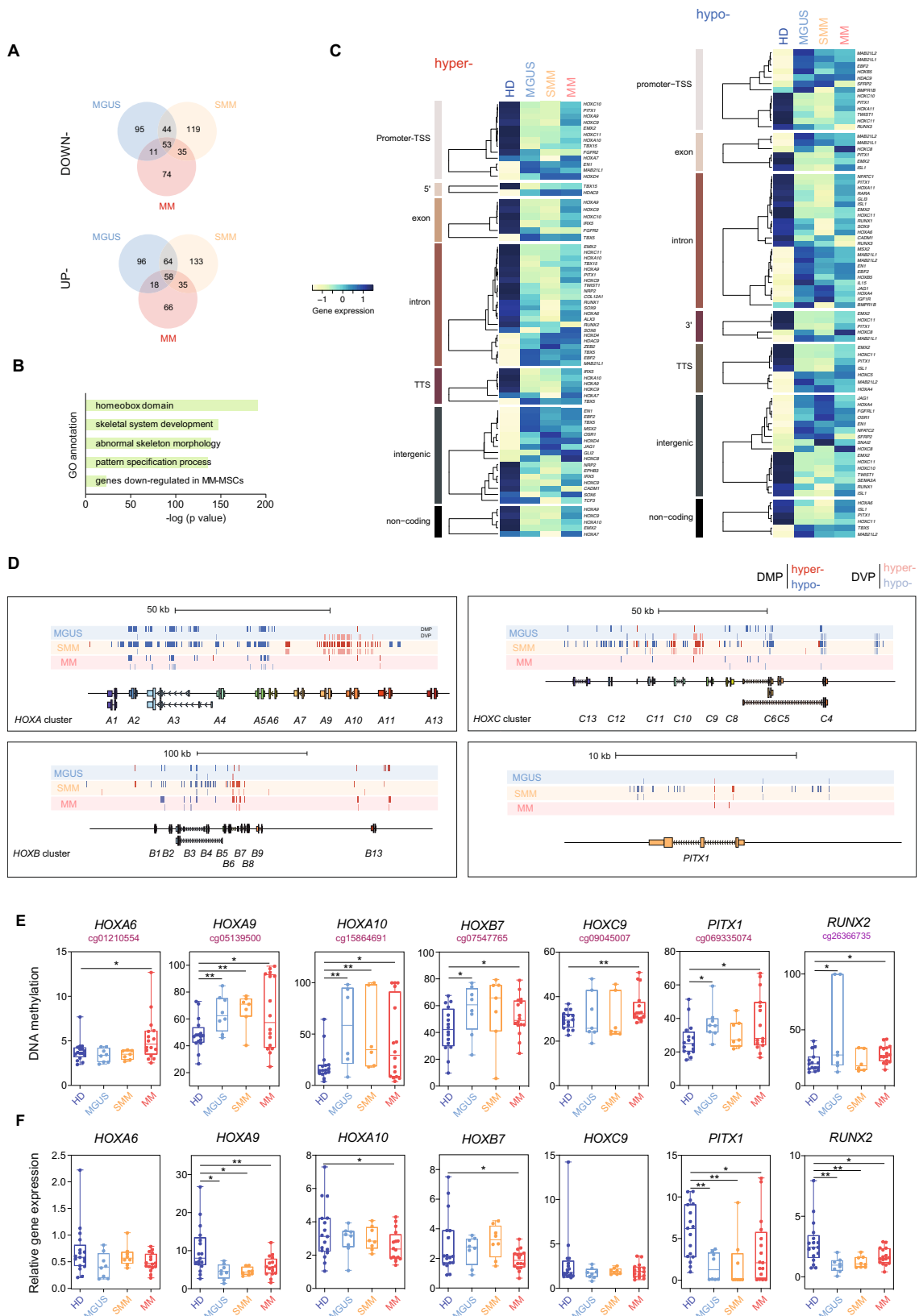
We then validated the aforementioned DNA methylation and gene expression changes in an independent cohort of BM-derived MSCs from different MM disease stages by pyrosequencing and real-time quantitative PCR. Among the differentially methylated genes of the Homeobox family, we selected *HOXA2*, *-A4*, *-A6*, *-A9*, *-A10*, *-B7*, *-C9*, *-C10*, and *PITX1* on the basis of their reported role in MSC pluripotency (Fig. 2E, F and Supplementary Fig. 2C, D)⁴⁰. Furthermore, we validated differentially methylated genes with osteogenic roles in the myeloma context, including *RUNX2* and *IBSP* (Fig. 2E, F and Supplementary Fig. 2C, D). In most cases, we observed that DNA methylation negatively correlated with gene expression.

Healthy MSCs change their DNA methylation profile to one partially resembling that of MSCs from MM patients upon interaction with MM plasma cells.

To address the potential contribution of MM cells in mediating aberrant DNA methylation changes in MSCs, we evaluated whether the epigenetic changes observed in MM-MSCs could be mimicked in vitro by direct contact of healthy MSCs with MM cells. Thus, we co-cultured BM-derived MSCs from healthy donors with the human MM cell line MM.1S for 2 weeks. Subsequently, MSCs were sorted by CD13⁺ expression and subjected to DNA methylation analysis (Fig. 3A).

Under these conditions, MM.1S cells were able to induce the expression of genes known to be upregulated in MM-MSCs (*IL1B*, *IL6*, and *HGF*) in HD-MSCs compared with monocultured HD-MSCs (Fig. 3B). Additionally, we validated the inhibitory effect of MM cells in MSC-to-OB differentiation and observed a decrease in both ALP activity and OB mineralization in OBs differentiated in the presence of conditioned media from the MM.1S cell line as compared to OBs differentiated alone (Fig. 3C).

We then investigated the DNA methylation profiling of MSCs from healthy donors generated upon interaction with MM cells. We observed that 142 CpGs that change their methylation levels upon co-culture with MM.1S cells were shared with aberrant DNA profiles found in MSCs isolated from MGUS/SMM/MM patients (Fig. 3D and Supplementary Data 7). Although this accounted for a small percentage of DMPs identified in MM patient MSCs, GO analyses revealed enrichment in Homeobox genes and categories related to bone formation, similar to that observed in primary patient MSCs (Fig. 3E). Specifically, we found that healthy MSCs exposed to MM cells underwent gains (*HOXA9*, *ACVR2A*, *EBF2*) and losses (*HOXA2*, *HOXA3*, *HOXC5*) of DNA methylation in the direction of those observed for MSCs from myeloma patients (Fig. 3F).



Moreover, we validated the DNA methylation and gene expression changes in healthy MSCs driven by co-culture with MM.1S with another MM cell line, RPMI-8226. Here, we observed a similar effect of co-culture with RPMI-8226, in which there was a clear inhibition of Homeobox and osteogenic

gene expression coupled with hypermethylation of these loci (Fig. 3G, H).

Altogether, these results support the notion that MM cells not only are capable of inducing changes in the global methylome of MSCs but also have a significant impact at specific osteogenic loci.

Fig. 2 DNA methylation changes are associated with differential gene expression of Homeobox genes in MSCs from MGUS, SMM and MM patients. A Venn diagrams showing differentially methylated or downregulated (upper) and upregulated (lower panel) genes when comparing MGUS (blue), SMM (orange), and MM (red) samples with healthy individuals. **B** Gene ontology (GO) enrichment analysis of CpG sites undergoing DNA methylation and gene expression changes in MSCs of patients compared to controls using the GREAT online tool. A binomial test was performed to calculate statistical significance. **C** Heatmaps showing gene expression of Homeobox and other OB-related genes associated with differentially hyper- (left) or hypomethylated (right) CpG sites. Heatmaps are grouped according to the genomic location (promoter, TSS, 5', exon, intron, intergenic, 3' or non-coding region) of analyzed CpG sites. Color scale ranging from light yellow to dark blue represents low to high expression levels. **D** Scheme depicting differentially methylated and variable CpG sites located in the Homeobox genes (*HOXA-A, -B, and -C clusters*) and *PITX1*. Dark blue lines indicate hypomethylated DMPs, light blue lines indicate hypomethylated DVPs, dark red lines indicate hypermethylated DMPs and light red lines indicate hypermethylated DVPs associated with MGUS, SMM, and MM condition. **E** DNA methylation analysis by pyrosequencing of selected CpGs located at the promoter regions and **F** gene expression of *HOXA6, -A9, -A10, -B7, -C9, PITX1, and RUNX2* in MSCs from healthy controls (dark blue; $n = 17$), MGUS (light blue; $n = 8$), SMM (orange; $n = 8$), and MM ($n = 16$) patients. Gene expression was normalized against *RPL38*. Box plots represent median \pm IQR and whiskers represent maximum and minimum. Statistical significance was calculated using unpaired two-tailed Student *t*-tests (* p -value < 0.05 , ** p -value < 0.01 , and *** p -value < 0.005).

Dual targeting of DNMTs and G9a restores Homeobox gene expression in vitro and promotes osteogenic differentiation of mesenchymal precursors.

Gene expression analysis of DNMTs in MSCs from HD and MM patients co-cultured with MM cells obtained from a previous study⁴¹ showed an aberrant upregulation of the DNA methyltransferase DNMT1 (Fig. 4A). DNMT1 interacts with the methyltransferase G9a to coordinate DNA and H3K9 methylation during cell replication⁴² promoting transcriptional silencing of target genes. Moreover, G9a can suppress transcription by inducing DNA methylation in addition to its activity as a chromatin remodeler⁴³. In this regard, we hypothesized that the dual inhibition of DNMT1 and G9a could reactivate hypermethylated and silenced genes of MSCs from MM patients preserving their osteogenic potential and therefore preventing myeloma-associated bone loss. Thus, we utilized a dual inhibitor of DNMTs and G9a, termed CM-272, which has been previously described to have a potent therapeutic response, both in vitro and in vivo, in other neoplasias^{44–47}.

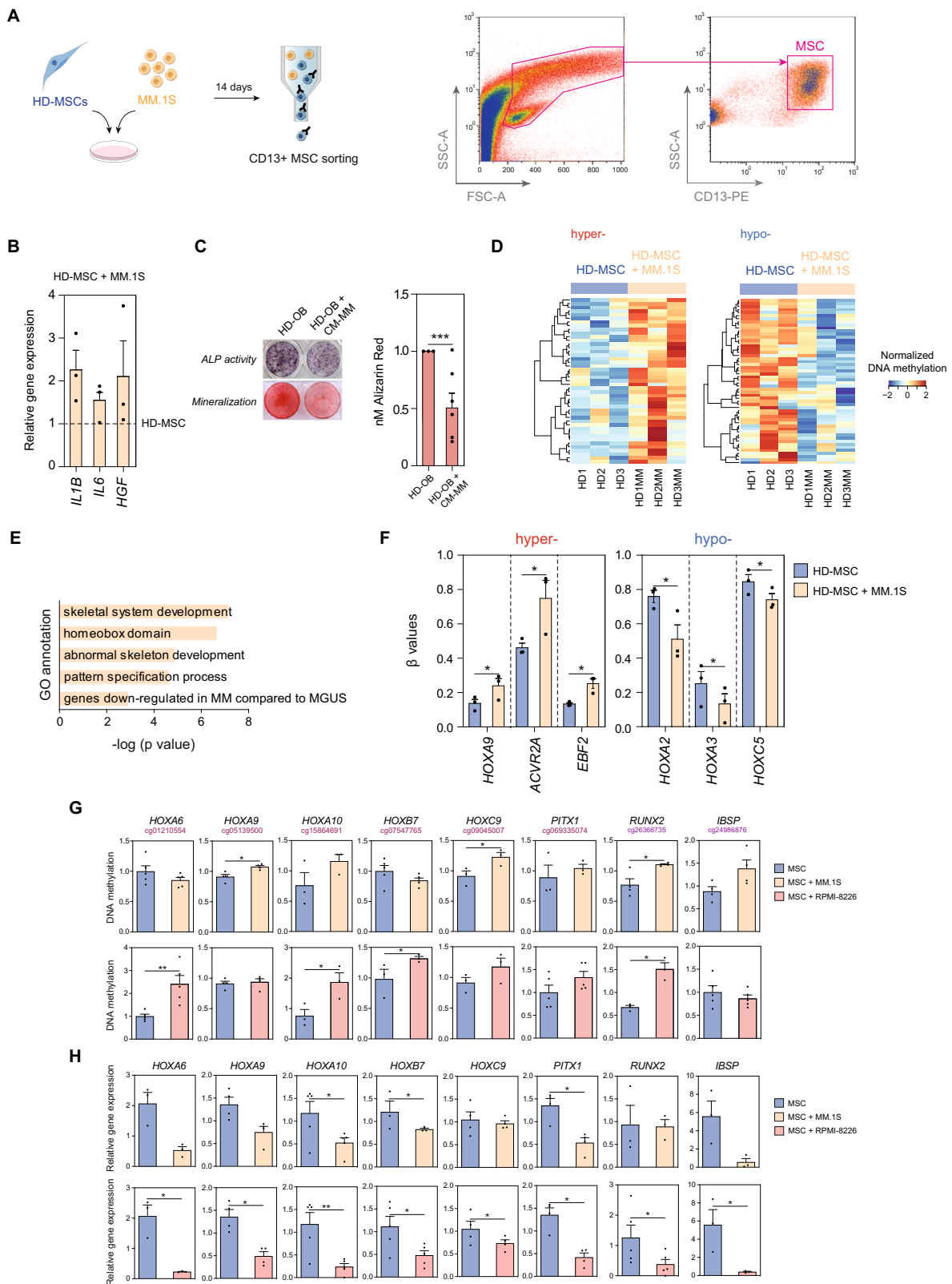
We first checked the effect of CM-272 on the cell viability of mesenchymal progenitors and we selected a dose (50 nM) with no significant toxicity in order to perform further experiments (Fig. 4B). CM-272 treatment was able to restore the expression of Homeobox genes (*HOXA6, -A9, -A10, -C9, PITX1, and RUNX2*) that were epigenetically repressed in MSCs from MM patients (Fig. 4C). Mechanistically, we observed a loss of DNA methylation in the promoter region of the majority of the aforementioned genes after CM-272 treatment in MM-MSCs (Fig. 4D). We then checked the levels of the inactive chromatin mark H3K9me2, a hallmark of methyltransferase G9a activity, at these gene promoters upon CM-272 treatment. The ChIP-qPCR analysis showed a decrease in H3K9me2 levels at the promoter regions of Homeobox genes after CM-272 treatment (Fig. 4E). Taken together, our results suggest that CM-272 acts in vitro by inhibition of both DNMT and G9a methyltransferase activity.

Next, we addressed whether targeting DNMT and G9a may have a role in regulating osteogenic differentiation. For this purpose, we cultured MSCs from myeloma patients in osteogenic media to obtain differentiated OBs in the presence or absence of CM-272. As observed in Fig. 4F, G, CM-272 was able to increase ALP activity in early-stage OBs. Furthermore, CM-272 treatment was able to upregulate the relative expression of several late bone formation markers (namely, bone sialoprotein, osteopontin, and osteocalcin) in MSCs from myeloma patients (Fig. 4H).

Previous research has described that MM cells exert their effect on MSCs through both direct cell–cell contact and soluble factor mechanisms^{11,48}. Our main data show that direct myeloma-MSC co-culture conditions are able to induce changes in the MSC methylome; however, it would be of particular interest to investigate whether MM cells may also mediate the same changes only through soluble factor mechanisms. For this purpose,

utilizing a transwell system avoiding contact between both cell types, we observed that soluble factor secreted by MM.1S and RPMI-8226 cell lines were sufficient to change the expression of several OB-relevant genes in healthy MSCs, including *RUNX2, SPP1, IBSP, and HOXB7* (Fig. 5A), concordantly to direct co-culture. Furthermore, treatment with the dual inhibitor CM-272 was able to partially reverse those changes in gene expression mediated by soluble factors secreted by MM cells (Fig. 5A). Changes in gene expression were accompanied by inverse changes in DNA methylation in some of the genes (*IBSP, HOXB7*) (Fig. 5B), which were also observed to at least be partially reversed by CM-272. However, for some other genes such as *RUNX2* and *SPP1*, transwell co-culture with MM cells induced minimal effect on DNA methylation, suggesting that direct cell–cell contact may be required. Moreover, CM-272 was able to partially reverse the MM cell lines-mediated inhibitory effect on OB mineralization (Fig. 5C). Altogether, these results suggest that MM cells at least partially exert its effects on MSCs through secretory mechanisms, and treatment with CM-272 was able to reserve these effects through the inhibition of DNA methylation.

CM-272 not only controls tumor burden but also prevents the myeloma-associated bone loss. To test the effect of CM-272 in the context of MBD, we used an established murine model of bone marrow-disseminated myeloma. After equivalent engraftment of myeloma cells (RPMI-8226-luc) was verified by bioluminescence measurement, mice were treated for 4 weeks with CM-272 as described in Methods. Compared with the vehicle control group, CM-272 controlled tumor progression as measured by bioluminescence (Fig. 6A) or by serum levels of hlg λ secreted by RPMI-8226 cells (Fig. 6B). Representative microCT images at the metaphyses of distal femurs showed a tumor-associated bone loss in vehicle-treated mice, in contrast with trabecular structures observed in CM-272-treated animals (Fig. 6C). In the vehicle control group, 3D reconstruction images of distal femurs revealed a marked bone loss evidenced by a thin trabecular network (in red) but also by loss of cortical bone (in gray) in vehicle-treated mice (Fig. 6D). By contrast, CM-272-treated mice presented a gain in both trabecular and cortical bone (Fig. 6D). This was also reflected by bone morphometric parameters that resulted in increased trabecular bone volume, occupancy, and connectivity and reduced trabecular separation in CM-272-treated animals, as compared with vehicle control (Fig. 6E). Finally, these findings correlated with a significant increase in serum levels of the bone formation marker P1NP analyzed after CM-272 treatment compared to untreated control (Fig. 6F). In summary, these data demonstrate that CM-272 exerts in vivo anti-myeloma activity along with bone-anabolic effects in human MM-bearing mice.



To further examine the in vivo effect of CM-272 on DNA methylation of myeloma-associated MSCs, we performed reduced representation bisulfite sequencing (RRBS) analysis of MSCs isolated from vehicle- and CM-272-treated myeloma-bearing mice using healthy mice as controls. First, we observed significant alterations in the DNA methylome of MSCs from myeloma-bearing mice compared to healthy mice (Supplementary Data 8).

Myeloma-bearing mice that were treated with CM-272 displayed a partial reversion of aberrant hypermethylation of MSCs caused by the presence of myeloma cells (Fig. 6G). These DNA methylation changes occurred at genomic loci enriched for genes involved in cell commitment and differentiation, such as Homeobox genes (Fig. 6H). Specifically, we were able to identify CpGs that experienced a gain in DNA methylation in vehicle-

Fig. 3 MSCs from healthy donors recapitulate DNA methylation changes observed in MSCs from MM patients upon interacting with MM plasma cells. **A** Scheme depicting workflow (left panel) and sorting strategy (right panel) for selecting CD13 + MSCs after 14 days of co-culture with the MM.1S cell line. **B** Gene expression analysis of *IL1B*, *IL6*, and *HGF*, normalized against *RPL38*, of the hMSC-TERT cell line (HD-MSC) co-cultured with the MM.1S cell line for 14 days. Expression levels were normalized against MSCs in monoculture. Data are represented as the mean \pm SEM from three independent experiments. **C** ALP activity and matrix mineralization were assessed in differentiated osteoblasts from HD-MSCs in the presence (HD-OB + CM-MM) or absence (HD-OB) of conditioned media from the MM.1S cell line (CM-MM). Representative images of each experimental condition are shown. Barplot represents the mean \pm SEM from six independent experiments, and a paired two-tailed *t*-test was performed to evaluate statistical significance (****p* < 0.005). **D** Heatmap showing differentially methylated CpG sites (eBayes-moderated paired *t*-test **p* < 0.05) in sorted HD-MSCs (three independent donors) in monoculture (HD1-3) or co-cultured with the MM.1S cell line (HD1-3MM) for 14 days that overlaps with previously identified DMPs. The color scale from blue to red represents low to high methylation levels. **E** GO enrichment analysis of DMPs in HD-MSCs co-cultured with the MM.1S cell line overlapping with myeloma-associated DMPs analyzed using the GREAT online tool. *p*-values were calculated using a binomial test. **F** Bar plots showing β -values obtained from the DNA methylation array presented in **D**, representing mean and \pm SEM of three independent experiments. **G** DNA methylation and **H** gene expression levels of DMPs validated in HD-MSCs monoculture (blue) or co-cultured with MM.1S (orange) or RPMI-8226 (red) cell lines as indicated. Gene expression data were normalized against *RPL38* and all data were normalized against HD-MSC monoculture. Statistical significance was calculated using paired one-tailed Student *t*-tests and bar plots represent mean \pm SEM of 3–5 independent experiments (**p*-value < 0.05, ***p*-value < 0.01, and ****p*-value < 0.005).

treated MSCs compared to healthy controls at the same genomic loci previously identified in human MM-MSCs, including *HOXA7*, *-B4*, *-B7*, *-B9*, and *-D10* (Fig. 6I and Supplementary Data 9). Importantly, CM-272 treatment was able to restore the DNA methylation levels at these loci to resemble that of healthy mice, which was concomitant with the reduced tumor burden as well as bone loss recovery observed in these mice (Fig. 6I).

Discussion

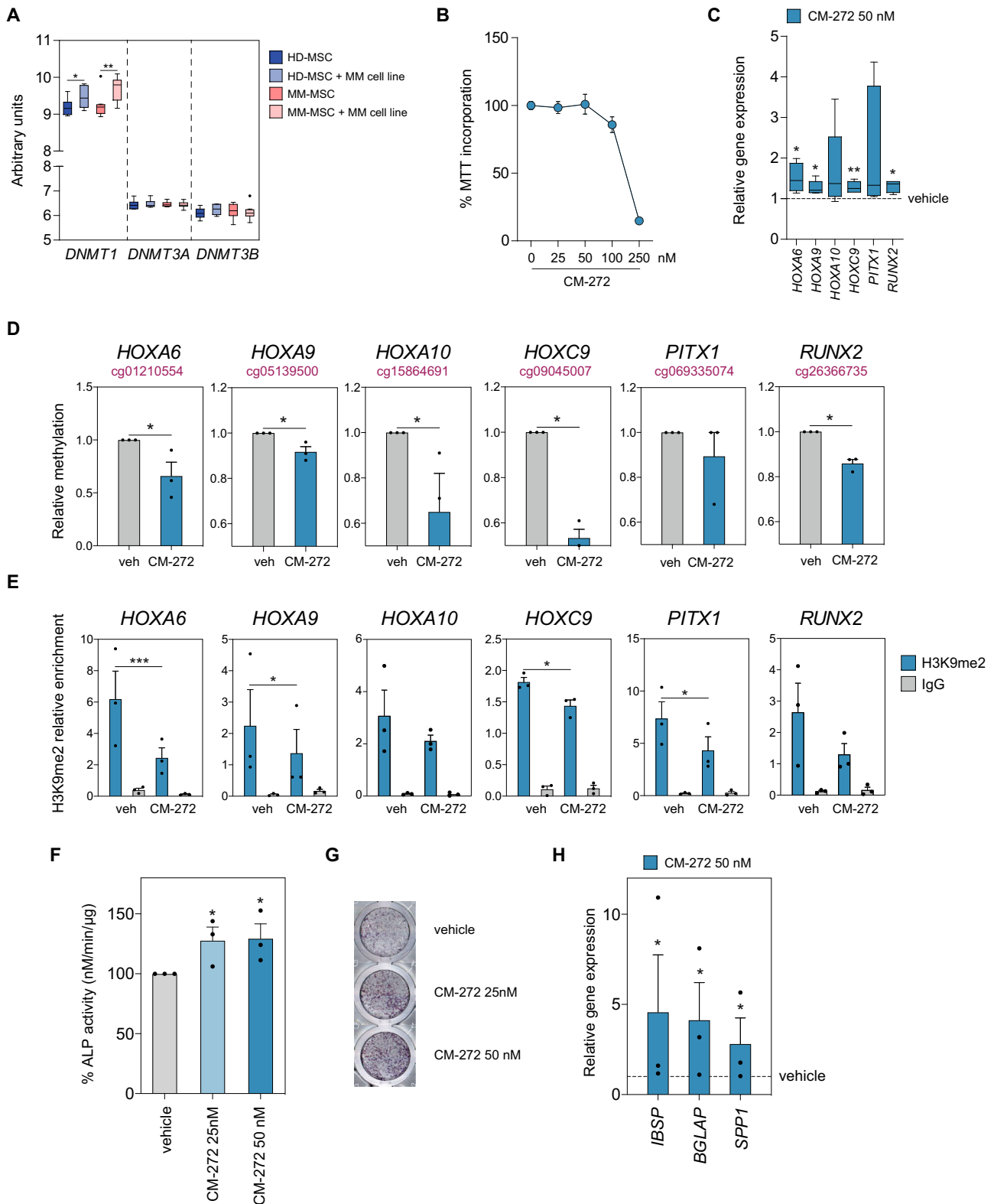
The pathogenic transition from premalignant stages to active MM is complex and not well understood. One example of this complexity is that although all MM cases emerge from the pre-existing asymptomatic MGUS/SMM stage, not all MGUS progress into MM and may exist as a stable and independent disease. Nevertheless, despite being an asymptomatic stage, transformed plasma cells in MGUS present cytogenetic alterations similar to that of myeloma plasma cells, as well as significant abnormalities in bone remodeling^{49,50}. This indicates that both genetic and microenvironmental alterations exist from the early stages of the disease. In our study, we show that epigenetic alterations in MSCs already occur in the early asymptomatic stages of both MGUS and SMM, and although many alterations are shared between all stages, the majority of DNA methylation changes are specific to each stage. These results are in accordance with previous studies that indicate the existence of stage-specific epigenetic alterations during MM progression in malignant plasma cells^{51,52}. This phenomenon could be explained by the expansion of sub-populations of MSCs during MM disease progression, which may favor tumor development and drug resistance, similar to what was observed to occur in MM cells^{53,54}.

Deregulation of methylome in MM-MSCs mediates transcriptional and phenotypical alterations. Interestingly, many genes of the Homeobox family displayed both epigenetic and transcriptional dysregulation in patient MSCs, and these changes were observed in earlier stages of the disease. In this regard, members of the HOX family have been recently described to be key drivers of OB differentiation, in which their expression is fine-tuned by demethylation of their promoters during the osteogenic process⁵⁵. Furthermore, we observed that healthy MSCs exposed to MM cells, similarly to that observed in patient MSCs, not only displayed an altered methylome but also showed impaired MSC-to-OB differentiation, as previously described²⁰. We also observed that some of these methylome changes in MSCs occur in the absence of direct cell–cell contact with MM cells, suggesting the contribution of secretory mechanisms. Hence, our results suggest that the impairment of osteogenesis in all stages of

MM arises from early transcriptional deregulation of Homeobox genes, and altered DNA methylation may be the primary mediator in this process. Nevertheless, we cannot overlook the limitations of our *in vitro* studies, as other cell types of the BM microenvironment may also play important roles in perpetuating the methylome alterations observed in MSCs.

Although the biology of MBD is relatively well described, there is still a lack of pharmacological treatments to improve bone loss. Clinically approved bone-modifying agents for the treatment of MBD include bisphosphonates⁵⁶, which inhibit bone resorption by suppressing OC activity, and denosumab⁵⁷, a monoclonal antibody against the osteoclastogenic cytokine RANKL. However, these drugs only target the OC compartment, and bone disease persists due to the absence of bone formation. Thus, therapeutic agents targeting OBs are needed. In this study, we demonstrated a strategy for treating MBD by targeting aberrant DNA methylation in MSCs. Firstly, we showed that co-culture of healthy MSCs with MM cell lines yielded epigenetic and transcriptional changes similar to that observed for MSCs from myeloma patients, and treatment with CM-272 was able to at least partially reverse these changes. Additionally, this agent promoted the ability of MSCs to differentiate into OBs. These *in vitro* effects on bone were mirrored in a mouse model of disseminated MM. Of note, CM-272 treatment not only prevented bone loss by bone-anabolic effects but also showed anti-myeloma activity. This is in line with previous reports showing that DNMTs are targets for the treatment of MM^{58–60} and also for improving the osteogenic differentiation ability of MSCs⁶¹. Additionally, we cannot discard the possibility that the observed effects on tumor growth inhibition may be a consequence of the impairment of the cross-talk between MSCs and MM cells. Moreover, the dual targeting effects of CM-272 also inhibit the dimethylation of H3K9, which has been described to be crucial in the establishment of DNA methylation^{42,43}. It is therefore rational to envision that the bone-anabolic effects mediated by CM-272, both *in vitro* and *in vivo*, involves the reversion of aberrant hypermethylation at Homeobox loci and other OB-related genes in the MSC population. Nevertheless, it is possible that reduced tumor burden could be partially responsible for restoring the bone-forming capacities of MM-MSCs.

In summary, our findings highlight the existence of aberrant DNA methylation patterns in the BM-derived MSC population which may impact myeloma progression and the development of MBD. Moreover, our preclinical results support the idea that therapeutic targeting of aberrant DNA methylation would result in an anti-myeloma effect and preservation of the appropriate osteogenic differentiation of MSCs to combat myeloma bone disease.



Methods

Participants. BM samples were obtained from the iliac crest of patients with newly diagnosed MGUS ($n = 10$), SMM ($n = 8$), and MM ($n = 9$), according to the International Myeloma Working Group criteria. BM samples from healthy controls ($n = 8$) were obtained from participants undergoing orthopedic surgery not related to oncology disease. Each sample was obtained after receiving the informed written consent of all participating subjects and following approval from the committees listed below for obtaining them and for the study protocol using them. The study was approved by the Cancer Research Center-IBMCC Review Board (CICIC 2015/

02156), the Clinical Ethics Committee for drug research in the Salamanca Health Area (CEIC 73/07/2015), the Clinical Research Committee of the Bellvitge University Hospital (ref. PR076/15) and the Research Ethics Committee of the University of Navarra (ref. 2017.218). Clinical characteristics of MGUS, SMM, and MM patients are listed in Supplementary Table 2.

Inhibitor. CM-272 (dual DNMTs and G9a inhibitor) was synthesized at the Center for Applied Medical Research (University of Navarra)^{44,47,62}.

Fig. 4 CM-272 treatment reactivates Homeobox gene expression and promotes the osteogenic differentiation of MSCs from MM patients. A

Expression of DNA methyltransferases 1, 3A, and B (*DNMT1*, -3A, and -3B) in HD and MM-MSCs co-cultured for 24 h with the MM.1S cell line comparing with monoculture as assessed by the GeneChip Human Gene 1.0 ST Array. Box plots present mean \pm SEM for 8 healthy donors and 9 MM patients. *p*-values were calculated by paired two-tailed Student's *t*-test ($*p < 0.05$, $**p < 0.01$). **B** MSCs from MM patients were treated with the indicated doses of CM-272 for 72 h and subjected to MTT assay for viability. Mean and SEM are indicated on the line chart from 3 independent experiments. **C** Real-time RT-PCR was performed to determine the expression of hypermethylated Homeobox genes (*HOX-A6*, -A9, -A10, -C9, *PITX1*, *RUNX2*) in MM-MSCs treated with vehicle or 50 nM of CM-272 for 7 days. Box plots represent median \pm IQR, with whiskers representing minimum and maximum, of 9 independent experiments. A paired two-tailed Student's *t*-test was performed to calculate statistical significance ($*p < 0.05$, $**p < 0.01$). **D** DNA methylation analysis by pyrosequencing of selected CpGs located at the promoter regions of Homeobox genes in MM-MSCs treated with vehicle (gray) or CM-272 (blue) for 7 days. Bar plots present mean \pm SEM for 3 independent experiments and paired two-tailed Student's *t*-tests were performed ($*p < 0.05$). **E** ChIP assays showing the H3K9me2 (blue) enrichment at the promoter regions of Homeobox genes in MM-MSCs treated with vehicle or CM-272 for 7 days. IgG (gray) was used as a negative control. Data are shown as a relative enrichment of the bound fraction with respect to the input DNA. Bar plots present mean \pm SEM for 3 independent experiments and paired two-tailed Student's *t*-tests were performed ($*p < 0.05$, $**p < 0.01$, and $***p < 0.005$). ALP activity was assessed in MM-MSCs ($n = 3$) cultured in osteogenic media in the presence of 25 nM (light blue) and 50 nM (dark blue) of CM-272, compared to vehicle (gray), by **F** p-NPP hydrolysis and **G** NBT-BCIP. **H** Expression of osteoblastogenesis markers *IBSP* (bone sialoprotein), *BGLAP* (osteocalcin) and *SPPI* (osteopontin) was checked by qRT-PCR in MM-MSCs cultured in osteogenic media in the absence (vehicle) or presence of CM-272. For **F** and **H** data are shown as mean values \pm SEM from three different experiments. Statistically significant tests (paired two-tailed Student's *t*-tests) are represented as $*p < 0.05$, $**p < 0.01$, and $***p < 0.005$ between vehicle and CM-272 condition.

Cell lines. The human multiple myeloma cell line MM.1S was provided by Dr. Steven Rosen (Northwestern University, Chicago, IL), whereas RPMI-8226 cells were purchased from the American Type Culture Collection. The human mesenchymal stem cell (MSC) line immortalized by expression of the telomerase reverse transcriptase gene (*hMSC-TERT*) was a generous gift from Dr. D Campana (Department of Pediatrics, Yong Loo Lin School of Medicine, National University of Singapore, Singapore). Both cell lines were cultured in RPMI 1640 medium supplemented with 10% heat-inactivated fetal bovine serum (FBS), 100 U/ml penicillin and 100 mg/ml streptomycin, and 1% L-glutamine. All the cell culture media and reagents were purchased from Invitrogen (Paisley, UK). All cell types were cultured at 37 °C in a humidified atmosphere in the presence of 5% CO₂-95% air.

Bone marrow-derived MSC isolation and culture. MSCs were isolated and characterized as described by Garayoa et al.¹⁷. Briefly, bone marrow aspirates were obtained from the iliac crest and subjected to centrifugation on Ficoll-Paque (GE Healthcare, Uppsala, Sweden) to obtain mononuclear cells (BMMCs). BMMCs were plated and plastic-adherent cells were expanded until passage 3 (P3) in low-glucose DMEM supplemented with 10% heat-inactivated fetal bovine serum, 100 U/ml penicillin, 100 mg/ml streptomycin, and 1% L-glutamine. Selected MSCs from both MM patients ($n = 4$) and healthy donors ($n = 4$) at P3 were tested to meet minimal criteria as defined by the International Society for Cellular Therapy for multipotent mesenchymal stromal cells⁶⁵. Specifically, MSCs were evaluated by FACS for positive expression of CD73, CD90, CD105, CD44, and CD166 and negative staining for HLA-DR and hematopoietic markers (CD19, CD34, and CD45) (Supplementary Fig. 3A). In addition, the capability to differentiate into osteoblast, adipocyte, and chondrocyte was assessed (Supplementary Fig. 3B–D). Analyses and experiments were performed with MSCs at P3, with a maximum of 3 weeks at each passage.

DNA and RNA isolation and quantification. Genomic DNA was isolated by the proteinase K method or using the Maxwell[®] RSC Cell DNA Purification Kit (Promega) for samples containing low cell number. RNA was isolated using Maxwell[®] RSC simplyRNA Cells Kit (Promega) according to the manufacturer's instructions. DNA and RNA were quantified using Qubit[®] DNA Assay Kit (Invitrogen) or NanoDrop ND-1000, respectively.

DNA methylation and gene expression profiling using arrays. DNA samples were bisulfite-converted using an EZ DNA methylation kit (Zymo Research, Orange, CA) and hybridized onto an Infinium[®] MethylationEPIC BeadChip array (Illumina, Inc.). The array platform allows the assessment of DNA methylation status at >850,000 CpG sites at single-nucleotide resolution and covers 99% of RefSeq genes and 95% of CpG islands with an average number of six probes per island.

RNA samples were obtained from healthy donors ($n = 8$), MGUS ($n = 10$), SMM ($n = 10$), and MM patients ($n = 24$) at diagnosis and 100 ng of excellent quality RNA (RIN > 9) was hybridized onto a GeneChip Human Gene 1.0 ST (Affymetrix).

Quality control, data normalization, and detection of differentially methylated and variable CpGs. Methylation array data were processed in the statistical language R v4.0 in RStudio 1.3 (<https://rstudio.com>) using methods from the Bioconductor libraries *minfi* (v1.36.0), *lumi* (v2.42.0), and *limma* (v3.46.0)^{64–66}.

Probes were annotated using *IlluminaHumanMethylationEPICmanifest* v0.3.0⁶⁷. Data quality was assessed using the standard pipeline from the *minfi* package. The data were quantile-normalized and chromosomes X and Y were removed to avoid technical and biological bias. Furthermore, we discarded the DNA methylation changes associated with the long-term culture of BM-MSCs based on the previous studies⁶⁸. *M* values (log₂-transformed β -values) were utilized to obtain a *p*-value between sample groups by an eBayes-moderated paired *t*-test using the *limma* package, in which age and sex were added in the interaction matrix. For the analysis of MSCs isolated from MM patients and healthy controls, we considered a probe to be differentially methylated when the difference between the mean of β at disease versus control was over 10% ($\Delta\beta \geq 0.1$) and the statistical test was significant ($**p < 0.01$). In addition, we used the iEVORA algorithm⁶⁹, provided by *matrixTests* v0.1.9 (<https://CRAN.R-project.org/package=matrixTests>), to designate a probe as differentially variable. This algorithm detects the homogeneity of variances using the Bartlett's test (FDR < 0.05) and then selects those probes whose *t*-test is significant ($*p < 0.05$) in order to regularize the variability test which is overly sensitive to single outliers.

To evaluate the contribution of various covariates, including age and sex, we performed either a Pearson correlation or Wilcoxon signed-rank test depending on whether the covariate of interest was continuous or categorical. This is represented in Supplementary Fig. 4, in which a covariate with a *p*-value < 0.05 was considered to significantly contribute to DNA methylation.

For the direct co-culture of healthy MSCs with MM cell line, samples were normalized utilizing Noob and Quantile normalizations provided by *minfi*. The paired analysis was performed and a probe was considered differentially methylated if $\Delta\beta$ was more than 10% and *p*-value was < 0.01.

Gene ontology, motif, and chromatin state analysis. Functional annotation enrichment analysis was performed using GREAT tool v4.0.4 (<http://great.stanford.edu/public/html>)⁷⁰ by mapping differentially methylated CpG site to the single nearest gene. CpGs annotated in the EPIC 850K array were used as background. GO categories with *p*-value of < 0.01 were considered significantly enriched.

For TF binding motif analysis, HOMER motif discovery software v4.5 was used²⁷, where a 500 bp-window upstream and downstream of the differentially methylated CpG sites was applied. CpGs annotated in the EPIC array were used as background.

To analyze chromatin states associated with DMPs, ChromHMM²⁶ data sets from healthy donor MSCs were downloaded from the UCSC Genome Browser (<https://genome.ucsc.edu/>). Overlap was performed in R using the *GenomicRanges* package v1.42.0⁷¹, where CpGs annotated in the EPIC array were used as background.

Gene expression array normalization and analysis. Data processing and normalization were carried out using the R statistical language. Background correction was performed using Robust Microarray Analysis (RMA) normalization provided by *oligo* package v1.54.1⁷² and probes were annotated utilizing the *hugene10st-transcriptcluster.db* R package v8.7.0⁷³. Average expression was calculated for probes mapping to the same gene. For comparisons between groups, eBayes-moderated *t*-test provided by the *limma* R package⁶⁵ was applied, where a *p*-value < 0.05 was considered statistically significant. DMPs were mapped to the nearest gene utilizing the GREAT online tool, and overlap with differentially expressed genes were performed by overlapping gene names.

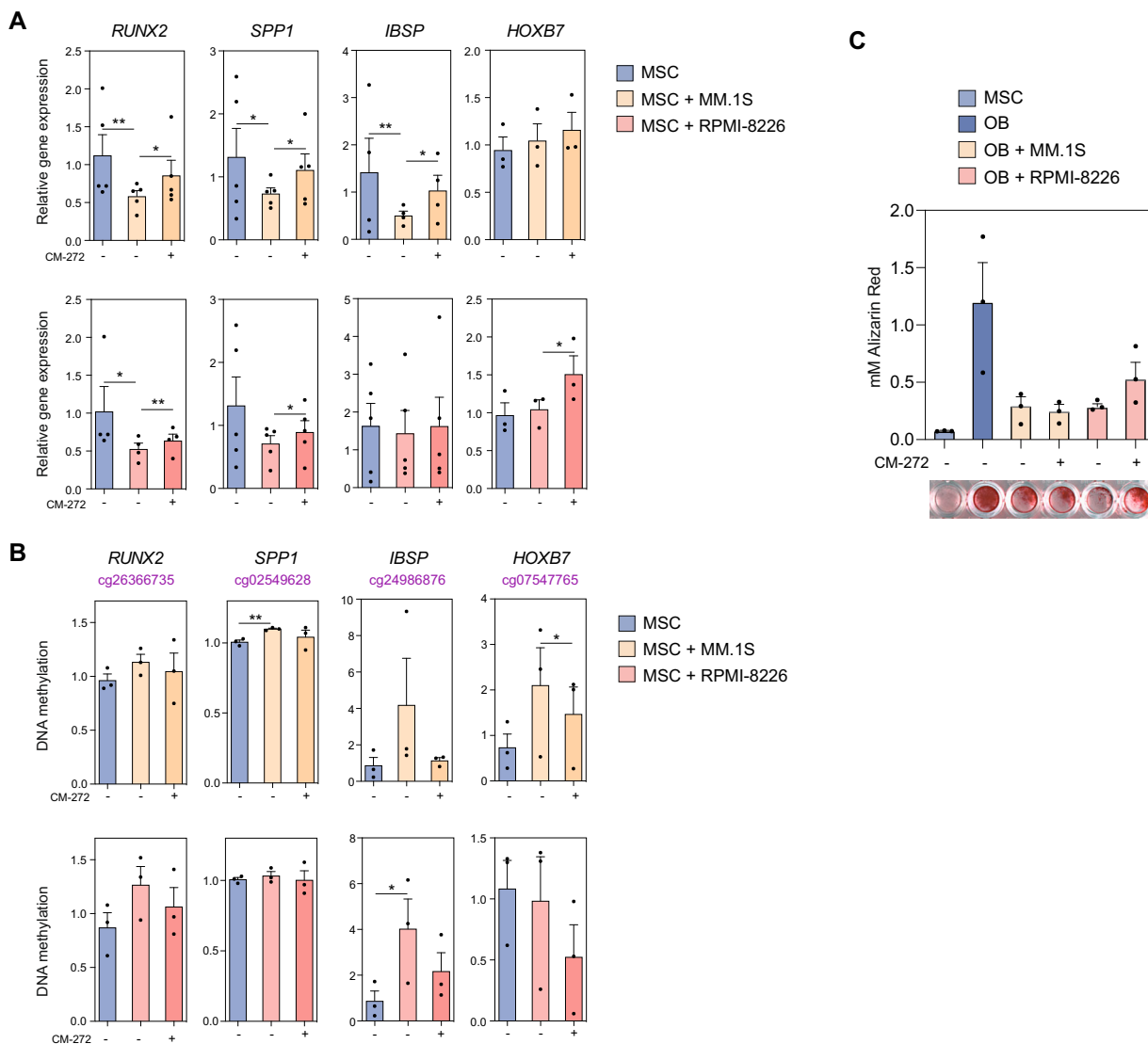


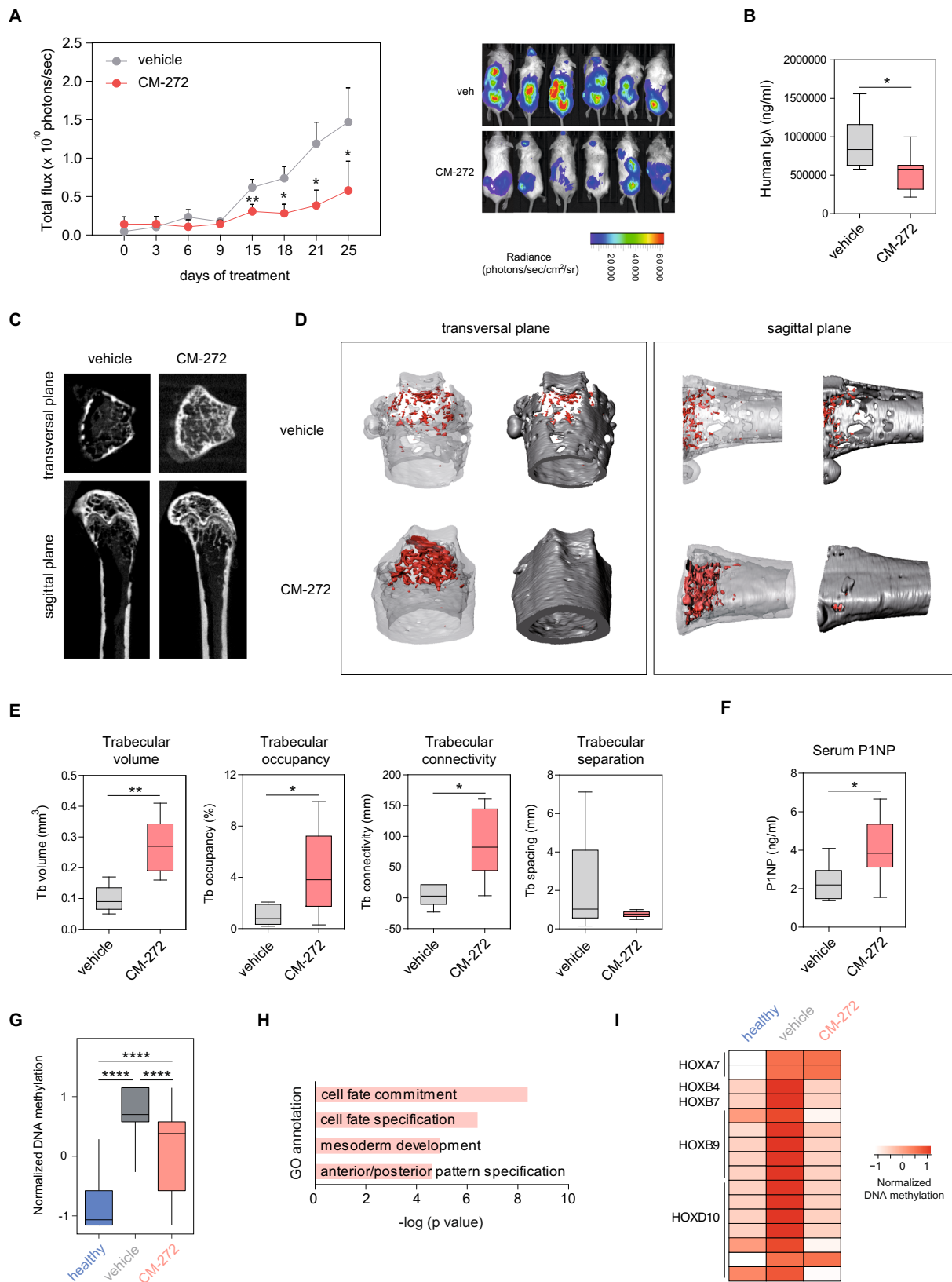
Fig. 5 CM-272 restores the gene expression levels and suppression of mineralization in MSCs from healthy donors exposed to MM cells. HD-MSCs (MSC; blue) were co-cultured with MM.1S (orange) or RPMI-8226 (red) cell lines separated by a transwell system in the presence (darker shade) or absence (lighter shade) of CM-272. **A** Relative expression and **B** DNA methylation of genes *RUNX2*, *SPP1*, *IBSP*, and *HOXB7* was assessed. Gene expression was by normalization against *RPL38*. Bar plots represent mean \pm SEM of 3–5 independent experiments and statistical significance was calculated by paired one-tailed Student’s *t*-test (* $p < 0.05$, ** $p < 0.01$). **C** Mineralization was assessed by alizarin red staining in differentiated OBs from HD-MSCs co-cultured with MM.1S or RPMI-8226 cell lines in the presence or absence of CM-272. Representative micrographs show matrix mineralization by alizarin red staining of corresponding differentiated OBs. Data are represented as the mean \pm SEM from three independent experiments and paired two-tailed Student’s *t*-tests were performed (* $p < 0.05$, ** $p < 0.01$).

Bisulfite pyrosequencing. For total DNA extraction, cells were lysed using lysis buffer (50 mM Tris pH 8.8, 10 mM EDTA pH 8.3, 100 mM NaCl, 1% SDS) in the presence of Proteinase K (Roche). Repeated centrifugation was performed to separate nucleic acids from lipids, in which DNA was subsequently precipitated using isopropanol and washed with 75 % ethanol. 100–300 ng of isolated DNA were bisulfite (BS)-converted using EZ DNA Methylation-Gold™ Kit (Zymo Research, CA, USA) according to manufacturers’ instructions. BS-converted DNA (~10 ng) was used as a template for amplification by conventional PCR using IMMOLA-SE™ DNA Polymerase kit (Bioline, London, UK). PCR primers were designed with the PyroMark Assay Design v2.0.2 software (Qiagen). PCR products were pyrosequenced with the Pyromark™ Q24 system (Qiagen), according to the manufacturer’s protocol.

Quantitative real-time PCR (qRT-PCR). Reverse transcription was performed using the Transcriptor First Strand cDNA Synthesis Kit (Roche) according to the manufacturer’s instructions. qRT-PCR was performed using LightCycler® 480 II System with LightCycler® 480 SYBR Green Mix and data were analyzed with LightCycler® 480 II Software, version 1.5, all provided by Roche. Reactions were performed in triplicate for both the target and the housekeeping gene ribosomal

protein L38 (*RPL38*) used for normalization. Relative quantification of the target gene expression was calculated by the comparative threshold cycle (Ct) method.

Co-culture system and MSC sorting. MSCs from healthy donors at passage 3 (8×10^3 cells/cm²) or the hMSC-TERT cell line (10×10^3 cells/cm²) were first cultured in 100 mm culture dishes until they reached ~85% confluency, and then MM.1S cells (1:3 MSC:MM.1S ratio) were added in RPMI 1640 medium supplemented with 10% FBS and antibiotics. MM cells were changed twice a week until day 14 when MSCs were recovered by trypsinization and flow cytometry-based sorting of CD13⁺ cells (BD Biosciences). For transwell experiments, MSCs from healthy donors were seeded on bottom chambers and MM.1S and RPMI-8226 cells were seeded on PET membrane inserts containing 1 μ m size pores to allow an exchange of soluble molecules. Transwell experiments were performed as in direct co-cultures. For OB differentiation studies, MSCs from healthy donors were cultured in an osteogenic medium supplemented with 20% of conditioned media from the MM.1S cell line. This medium was changed twice a week until day 10 (ALP activity) or day 20 (OB mineralization). For the isolation of mouse MSCs, cells were stained with a combination of CD45-PE, Ter-119-PE, Sca-1-FITC, and PDFGFR-APC (BD Biosciences) as previously reported⁷⁴ (Supplementary Fig. 5). Cell sorting



experiments were performed by the Flow Cytometry Core Facility at Germans Trias i Pujol Research Institute utilizing FACSaria II cell sorter and analyzed using BD FACSDiva version 6.1.1 (BD Biosciences, San Jose CA).

OB differentiation assays. OBs were generated from mesenchymal precursors by culture in osteogenic medium (containing 5 mM β -glycerophosphate and 50 mg/ml

ascorbic acid) and assayed as in Garcia-Gomez et al.⁷⁵. Briefly, primary MSCs (P2–3) were cultured in osteogenic medium for the analysis of alkaline phosphatase (ALP) activity, expression of osteogenic markers (day 10), and formation of mineralized-nodules formation (day 20). ALP activity was determined by hydrolysis of *p*-nitrophenylphosphate (Sigma-Aldrich) into *p*-nitrophenol and NBT/BCIP substrates (Roche), whereas mineralization was assessed by quantitative measurement of Alizarin Red (Sigma-Aldrich) staining and absorbance was

Fig. 6 CM-272 prevents tumor-associated bone loss besides reducing multiple myeloma tumor burden. RPMI-8226-luc cells (8×10^6) were intravenously injected into NSG mice. After 4 weeks, mice were randomized into 2 groups [receiving vehicle (gray) and CM-272 (red); $n = 6/\text{group}$] and treated for additional 4 weeks with dosing and regimen schedules as specified in Supplementary Methods. Tumor dissemination was checked by **A** bioluminescence measurement and **B** serum levels of human Ig λ secreted by RPMI-8226-luc cells at specified time points. Line plots represent mean and SEM. Box plots represent median \pm IQR, with whiskers representing the minimum and maximum. Statistical significance was determined utilizing paired two-tailed Student's *t*-test ($*p < 0.05$, $**p < 0.01$). **C** Representative microCT cross-sections at the metaphyses of distal femurs in a vehicle and CM-272-treated mice in transversal (upper) and sagittal (down) planes. **D** Transversal (left) and sagittal (right) planes of corresponding 3D renderings from microCT images at distal femurs (trabecular bone in red, cortical bone in gray). **E** Trabecular bone morphometric parameters from microCT images were quantitated for trabecular bone volume, occupancy, connectivity, and separation. **F** Serum levels of the bone formation marker PINP were quantified by ELISA. Graphs represent mean values \pm SEM with whiskers representing minimum and maximum values. CM-272-treated (red) mice were compared to the vehicle group (gray), where $*p < 0.05$; $**p < 0.01$ versus the vehicle control group. **G** Box plots showing DNA methylation levels of pooled MSCs obtained from healthy, vehicle- and CM-272-treated animals corresponding to hypermethylated CpGs between healthy and tumor-bearing animals. **H** GO enrichment analysis of CpG sites undergoing DNA hypermethylation changes in vehicle-treated MSCs versus MSCs from healthy mice. **I** Heatmap showing normalized DNA methylation levels of individual CpGs at selected Homeobox loci among animal groups. Data pooled from mice ($n = 6$) for each group with sufficient RRBS coverage (≥ 5 valid sequencing reads per CpG). < 0.01 by paired two-tailed Student's *t*-test. **G** Box plots showing mean \pm SEM, with whiskers representing minimum and maximum values, of DNA methylation levels of pooled MSCs obtained from healthy (blue), vehicle- (gray), and CM-272-treated (red) animals corresponding to hypermethylated CpGs between healthy and tumor-bearing animals. A paired two-tailed Student's *t*-test was performed to calculate statistical significance ($****p < 0.001$). **H** GO enrichment analysis of CpG sites undergoing DNA hypermethylation changes in vehicle-treated MSCs versus MSCs from healthy mice. *p*-values were calculated utilizing a binomial test. **I** Heatmap showing normalized DNA methylation levels of individual CpGs at selected Homeobox loci among animal groups. The color scale ranges from white to red, representing low to high levels of DNA methylation. Data pooled from mice ($n = 6$) for each group with sufficient RRBS coverage (≥ 5 valid sequencing reads per CpG).

measured by Multiskan Sky Microplate Spectrophotometer via SkanIt PC software (ThermoFisher).

MTT assay. MSCs were seeded in 96 well plates and treated with increasing concentrations of CM-272. MTT was added at a final concentration of 0.5 mg/ml and incubated at 37 °C for 1 h. Cells were then washed with PBS and incubated in the dark for 10 min in the presence of dimethyl sulphoxide. Absorbance at 570 nm was measured utilizing the Multiskan Sky Microplate Spectrophotometer.

Flow cytometry antibodies. Prior to analysis and sorting by flow cytometry, distinct amounts of MSCs were stained with fluorochrome-conjugated antibodies. Antibody specifications and concentrations used were the following: CD13-PE (BD Biosciences, 347406), CD45-PE (eBioscience, 12-0451-81), Ter-119-PE (eBioscience, 12-5921-81), Sca-1-FITC (eBioscience 11-5981-81), PDFGR α -APC (BD Biosciences, 562777), CD44-FITC (BD Biosciences, 347943), CD19-PerCP (BD Biosciences, 332780), CD90-FITC (BD Biosciences, 555595), HLA-DR-PerCP (BD Biosciences, 347402), CD14-FITC (BD Biosciences, 345784), CD166-PE (BD Biosciences, 559263), Cd45-PerCPcy5.5 (BD Biosciences, 332784), CD34-FITC (Invitrogen, 11-0349-42), CD73-PE (BD Biosciences, 550257), CD105-APC (R&D System, FAB10971A).

Chromatin immunoprecipitation (ChIP)-quantitative PCR. MSCs (15×10^3 cells per IP) were cross-linked with 1% formaldehyde for 15 min and subjected to chromatin immunoprecipitation after sonication. ChIP-qPCR assays were performed using LowCell ChIP kit[™] protein A (Diagenode) and the antibody (5 μ g) against H3K9me2 (H3K9me2 Abcam ChIP-grade, clone:mAbcam 1220, Ref: ab1220, Lot:GR45436-1). Data are represented as the ratio of the bound fraction over the input for each histone modification or factor. IgG was used as a negative control. Primer sequences were designed as close as possible from the CpG undergoing methylation changes. Primer sequences are shown in Supplementary Table 3. These experiments were performed with three biological replicates of each origin.

In vivo model. Animal experiments were conducted according to relevant ethical regulations for the use of laboratory animals and after acquired permission from the University of Salamanca Committee for animal experimentation (ref # 0000061). BALB/c-Rag2^{null} IL2r γ ^{null} (BRG) mice // or NOD-scid IL2r γ ^{null} (NSG) mice were bred and maintained in the SPF area of the University of Salamanca Animal Facility with controlled environment conditions (20–23 °C, 12:12 light/dark cycles, 30–70% relative humidity) and fed ad libitum. CM-272 was solubilized in 0.9% saline solution. RPMI-8226-luc cells (8×10^6) were injected intravenously into 8-week-old NOD-SCID-IL-2R γ ^{-/-} (NSG) mice (Charles River Laboratories) and tumor development was monitored by noninvasive bioluminescence imaging (BLI) with a Xenogen IVIS 50 system (Caliper Life Sciences). After 4 weeks, animals were randomized into two groups ($n = 6/\text{group}$) receiving vehicle (0.9% saline solution) or CM-272 (5 mg/kg, 5 times/week by intraperitoneal injection).

Microcomputed tomography analysis. One femur of each animal was fixed in 10% formalin in order to preserve bone microarchitecture. 3D X-ray tomographic

images were acquired using a Quantum-GX microCT (Perkin Elmer) with the following parameters: 80 kVp X-ray source voltage, 120 μ A current, and the high-resolution scan protocol for a total acquisition time of 14 min and a gantry rotation of 360 degrees. The tomographic three-dimensional images containing the entire bone yielded a total of 512 slices, with isotropic 50 microns voxel size and a resolution of 512 \times 512 pixels per slice. To perform the bone histomorphometry analysis a (10 \times 10 \times 10 mm) ROI containing the bone metaphysis was defined and subsequently reconstructed from the original scan at a resolution of 20 microns per voxel using the Quantum 3.0 software.

Analysis of trabecular microarchitecture in the distal femur was carried out using ImageJ v1.8.0⁷⁶. First of all, cortical and trabecular bones were segmented from the CT volume. To this end, the following steps were followed: (i) segmentation of the entire bone volume by thresholding the original volume to obtain a 3D binary mask; (ii) segmentation of empty volumes inside the cortical volume (trabecular-free zones) using logical operators over filled vs. unfilled versions of the result of step i; (iii) segmentation of the interior volume of the cortical bone by applying 10 morphological dilations followed by 10 morphological erosions to the 3D mask obtained in step ii; (iv) segmentation of the cortical bone by performing an XOR logical operation between the masks obtained in steps i and iii; and finally, (v) segmentation of the trabecular bone by performing an AND logical operation between the masks obtained in steps i and iii. The final cortical and trabecular bone segmentations were further refined by applying a median filter to remove noise in the respective 3D masks. Cortical and trabecular bone volumes were then calculated by applying the segmentation masks on the original volume.

From the obtained trabecular masks, histomorphometry parameters were calculated using the BoneJ plugin (version 1.4.2)⁷⁷. Finally, bone 3D reconstruction and visualization were performed using Amira 5.2 software (ThermoFisher Scientific).

ELISA. Serum levels of human Ig λ (indicating tumor burden) and N-terminal propeptide of type I procollagen (PINP) (indicating bone formation) were measured in mice sera using the Human Lambda ELISA kit (Bethyl Laboratories, Texas, USA) and Rat/Mouse PINP EIA kit (Immunodiagnostic Systems, East Boldon, UK), respectively, following manufacturers' instructions. Absorbance was measured using the Multiskan Sky Microplate Spectrophotometer.

Reduced representation bisulfite sequencing (RRBS). Sorted MSCs from three groups (healthy, vehicle-treated, and CM-272-treated mice) were pooled in order to obtain a significant number of cells for performing the RRBS-seq. Isolated DNA from each pool was subjected to the RRBS pipeline as previously described⁷⁸. In brief, purified DNA was digested with MspI and subjected to bisulfite conversion. Following PCR amplification, RRBS libraries were generated from sequenced DNA following previously published procedures (<http://code.google.com/p/bsmap/downloads/>). Downstream normalization and analyses were performed following a previously published pipeline (<http://rrbs-techdev.computational-epigenetics.org/>). CpG annotation and GO enrichment analysis was performed utilizing the GREAT online tool.

Primers. All primers used are listed in Supplementary Table 3.

Statistical analysis. Data are expressed as mean \pm SEM and the n value for each in vitro assay is specified in the corresponding figure legend. Statistical analyses were carried out with Prism version 6.0 (GraphPad) and were performed using a two-tailed Mann–Whitney U test or Student's t -test.

Reporting summary. Further information on research design is available in the Nature Research Reporting Summary linked to this article.

Data availability

The DNA methylation and expression data supporting the findings of this study have been deposited in the NCBI's Gene Expression Omnibus database under the accession code [GSE137419](https://www.ncbi.nlm.nih.gov/geo/query/acc.cgi?acc=GSE137419). This SuperSeries (GSE137419) is composed of the following SubSeries: [GSE137360](https://www.ncbi.nlm.nih.gov/geo/query/acc.cgi?acc=GSE137360) (methylation), [GSE137369](https://www.ncbi.nlm.nih.gov/geo/query/acc.cgi?acc=GSE137369) (expression), and [GSE137416](https://www.ncbi.nlm.nih.gov/geo/query/acc.cgi?acc=GSE137416) (methylation II). All the other data supporting the findings of this study are available within the article and its supplementary information files and from the corresponding author upon reasonable request. Source data are provided with this paper.

Received: 9 October 2019; Accepted: 14 December 2020;

Published online: 18 January 2021

References

- San-Miguel, J. F. & Kantarjian, H. M. Multiple myeloma and chronic leukaemias in 2014: Improved understanding of disease biology and treatment. *Nat. Rev. Clin. Oncol.* **12**, 71–72 (2014).
- Kumar, S. K. et al. Multiple myeloma. *Nat. Rev. Dis. Primers* **3**, 17046 (2017).
- Raje, N. & Roodman, G. D. Advances in the biology and treatment of bone disease in multiple myeloma. *Clin. Cancer Res.* **17**, 1278–1286 (2011).
- Saad, F. et al. Pathologic fractures correlate with reduced survival in patients with malignant bone disease. *Cancer* **110**, 1860–1867 (2007).
- Panaroni, C., Yee, A. J. & Raje, N. S. Myeloma and bone disease. *Curr. Osteoporos. Rep.* **15**, 483–498 (2017).
- Dhodapkar, M. V. MGUS to myeloma: a mysterious gammopathy of underexplored significance. *Blood* **128**, 2599–2606 (2016).
- Sundararajan, S., Kumar, A., Korde, N. & Agarwal, A. Smoldering multiple myeloma: emerging concepts and therapeutics. *Curr. Hematol. Malign. Rep.* **11**, 102–110 (2016).
- Amodio, N., D'Aquila, P., Passarino, G., Tassone, P. & Bellizzi, D. Epigenetic modifications in Multiple Myeloma: recent advances on the role of DNA and histone methylation. *Expert Opin. Ther. Targets* **21**, 91–101 (2016).
- Das, R. et al. Microenvironment-dependent growth of preneoplastic and malignant plasma cells in humanized mice. *Nat. Med.* **22**, 1351–1357 (2016).
- Ghobrial, I. M., Detappe, A., Anderson, K. C. & Steensma, D. P. The bone-marrow niche in MDS and MGUS: implications for AML and MM. *Nat. Rev. Clin. Oncol.* <https://doi.org/10.1038/nrclinonc.2017.197> (2018).
- García-Gómez, A., Sánchez-Guijo, F., Del Cañizo, M. C., San Miguel, J. F. & Garayoa, M. Multiple myeloma mesenchymal stromal cells: contribution to myeloma bone disease and therapeutics. *World J. Stem Cells* **6**, 322–343 (2014).
- Friedenstein, A. J., Petrakova, K. V., Kurolesova, A. I. & Frolova, G. P. Heterotopic of bone marrow. Analysis of precursor cells for osteogenic and hematopoietic tissues. *Transplantation* **6**, 230–247 (1968).
- Corre, J. et al. Bone marrow mesenchymal stem cells are abnormal in multiple myeloma. *Leukemia* **21**, 1079–1088 (2007).
- Xu, S. et al. Impaired osteogenic differentiation of mesenchymal stem cells derived from multiple myeloma patients is associated with a blockade in the deactivation of the Notch signaling pathway. *Leukemia* **26**, 2546–2549 (2012).
- Reagan, M. R. & Ghobrial, I. M. Multiple myeloma mesenchymal stem cells: characterization, origin, and tumor-promoting effects. *Clin. Cancer Res.* **18**, 342–349 (2012).
- Rajkumar, S. V. Multiple myeloma: 2016 update on diagnosis, risk-stratification, and management. *Am. J. Hematol.* **91**, 719–734 (2016).
- Garayoa, M. et al. Mesenchymal stem cells from multiple myeloma patients display distinct genomic profile as compared with those from normal donors. *Leukemia* **23**, 1515–1527 (2009).
- Giuliani, N. et al. Bone osteoblastic and mesenchymal stromal cells lack primarily tumoral features in multiple myeloma patients. *Leukemia* **24**, 1368–1370 (2010).
- Todoerti, K. et al. Distinct transcriptional profiles characterize bone microenvironment mesenchymal cells rather than osteoblasts in relationship with multiple myeloma bone disease. *Exp. Hematol.* **38**, 141–153 (2010).
- Adamik, J. et al. EZH2 or HDAC1 inhibition reverses multiple myeloma-induced epigenetic suppression of osteoblast differentiation. *Mol. Cancer Res.* **15**, 405–417 (2017).
- Goll, M. G. & Bestor, T. H. Eukaryotic cytosine methyltransferases. *Annu. Rev. Biochem.* **74**, 481–514 (2005).
- Cakouros, D. et al. Specific functions of TET1 and TET2 in regulating mesenchymal cell lineage determination. *Epigenet. Chromatin* **12**, 3 (2019).
- García-Gómez, A., Rodríguez-Ubrea, J. & Ballestar, E. Epigenetic interplay between immune, stromal and cancer cells in the tumor microenvironment. *Clin. Immunol.* **196**, 64–71 (2018).
- Teschendorff, A. E. et al. Epigenetic variability in cells of normal cytology is associated with the risk of future morphological transformation. *Genome Med.* **4**, 24 (2012).
- Teschendorff, A. E. et al. The dynamics of DNA methylation covariation patterns in carcinogenesis. *PLoS Comput. Biol.* **10**, e1003709 (2014).
- Ernst, J. & Kellis, M. ChromHMM: automating chromatin-state discovery and characterization. *Nat. Methods* **9**, 215–216 (2012).
- Heinz, S. et al. Simple combinations of lineage-determining transcription factors prime cis-regulatory elements required for macrophage and B cell identities. *Mol. Cell* **38**, 576–589 (2010).
- Ducy, P., Zhang, R., Geoffroy, V., Ridall, A. L. & Karsenty, G. Osf2/Cbfa1: a transcriptional activator of osteoblast differentiation. *Cell* **89**, 747–754 (1997).
- Häkeli, A.-M. et al. The regulatory landscape of osteogenic differentiation. *Stem Cells* **32**, 2780–2793 (2014).
- Kanzler, B., Kuschert, S. J., Liu, Y. H. & Mallo, M. Hoxa-2 restricts the chondrogenic domain and inhibits bone formation during development of the branchial area. *Development* **125**, 2587–2597 (1998).
- Jeong, B.-C. ATF3 mediates the inhibitory action of TNF- α on osteoblast differentiation through the JNK signaling pathway. *Biochem. Biophys. Res. Commun.* **499**, 696–701 (2018).
- Giuliani, N. et al. Myeloma cells block RUNX2/CBFA1 activity in human bone marrow osteoblast progenitors and inhibit osteoblast formation and differentiation. *Blood* **106**, 2472–2483 (2005).
- Seifert, A., Werheid, D. F., Knapp, S. M. & Tobiasch, E. Role of *Hox* genes in stem cell differentiation. *World J. Stem Cells* **7**, 583 (2015).
- Verlinden, L. et al. Nrp2 deficiency leads to trabecular bone loss and is accompanied by enhanced osteoclast and reduced osteoblast numbers. *Bone* **55**, 465–475 (2013).
- Oshima, T. et al. Myeloma cells suppress bone formation by secreting a soluble Wnt inhibitor, sFRP-2. *Blood* **106**, 3160–3165 (2005).
- Kaneshiro, S. et al. Bruton tyrosine kinase (Btk) suppresses osteoblastic differentiation. *J. Bone Miner. Metab.* **33**, 486–495 (2015).
- Pizard, A. et al. Connexin 40, a target of transcription factor Tbx5, patterns wrist, digits, and sternum. *Mol. Cell. Biol.* **25**, 5073–5083 (2005).
- Lancôt, C., Moreau, A., Chamberland, M., Tremblay, M. L. & Drouin, J. Hindlimb patterning and mandible development require the Ptx1 gene. *Development* **126**, 1805–1810 (1999).
- Wei, X.-F., Chen, Q.-L., Fu, Y. & Zhang, Q.-K. Wnt and BMP signaling pathways co-operatively induce the differentiation of multiple myeloma mesenchymal stem cells into osteoblasts by upregulating EMX2. *J. Cell. Biochem.* **120**, 6515–6527 (2018).
- Iyyanar, P. P. R. & Nazarali, A. J. Hoxa2 inhibits bone morphogenetic protein signaling during osteogenic differentiation of the palatal mesenchyme. *Front. Physiol.* **8**, 929 (2017).
- García-gomez, A. et al. Transcriptomic profile induced in bone marrow mesenchymal stromal cells after interaction with multiple myeloma cells: implications in myeloma progression and myeloma bone disease. *Oncotarget* **5**, 8284–8305 (2014).
- Estève, P.-O. et al. Direct interaction between DNMT1 and G9a coordinates DNA and histone methylation during replication. *Genes Dev.* **20**, 3089–3103 (2006).
- Tachibana, M., Matsumura, Y., Fukuda, M., Kimura, H. & Shinkai, Y. G9a/GLP complexes independently mediate H3K9 and DNA methylation to silence transcription. *EMBO J.* **27**, 2681–2690 (2008).
- San José-Enériz, E. et al. Discovery of first-in-class reversible dual small molecule inhibitors against G9a and DNMTs in hematological malignancies. *Nat. Commun.* **8**, 15424 (2017).
- Bárcena-Varela, M. et al. Dual targeting of histone methyltransferase G9a and DNA-methyltransferase 1 for the treatment of experimental hepatocellular carcinoma. *Hepatology* **69**, 587–603 (2019).
- Segovia, C. et al. Inhibition of a G9a/DNMT network triggers immune-mediated bladder cancer regression. *Nat. Med.* **25**, 1073–1081 (2019).
- Rabal, O. et al. Discovery of reversible DNA methyltransferase and lysine methyltransferase G9a inhibitors with antitumoral in vivo efficacy. *J. Med. Chem.* **61**, 6518–6545 (2018).
- Xu, S., De Veirman, K., De Becker, A., Vanderkerken, K. & Van Riet, I. Mesenchymal stem cells in multiple myeloma: a therapeutic tool or target? *Leukemia* **32**, 1500–1514 (2018).
- Kristinsson, S. Y. et al. Monoclonal gammopathy of undetermined significance and risk of skeletal fractures: a population-based study. *Blood* **116**, 2651–2655 (2010).

50. Capp, J.-P. & Bataille, R. Multiple myeloma exemplifies a model of cancer based on tissue disruption as the initiator event. *Front. Oncol.* **8**, 355 (2018).
51. Agirre, X. et al. Whole-genome analysis in multiple myeloma reveals DNA hypermethylation of B cell-specific enhancers. *Genome Res.* **25**, 478–487 (2015).
52. Heuck, C. J. et al. Myeloma is characterized by stage-specific alterations in DNA methylation that occur early during myelomagenesis. *J. Immunol.* **190**, 2966–2975 (2013).
53. Ledergor, G. et al. Single cell dissection of plasma cell heterogeneity in symptomatic and asymptomatic myeloma. *Nat. Med.* **24**, 1867–1876 (2018).
54. van Nieuwenhuijzen, N., Spaan, I., Raymakers, R. & Peperzak, V. From MGUS to multiple myeloma, a paradigm for clonal evolution of premalignant cells. *Cancer Res.* **78**, 2449–2456 (2018).
55. da Silva, R. A. et al. HOXA cluster gene expression during osteoblast differentiation involves epigenetic control. *Bone* **125**, 74–86 (2019).
56. Terpos, E., Ntanasis-Stathopoulos, I. & Dimopoulos, M. A. Myeloma bone disease: from biology findings to treatment approaches. *Blood* **133**, 1534–1539 (2019).
57. Raju, N. et al. Denosumab versus zoledronic acid in bone disease treatment of newly diagnosed multiple myeloma: an international, double-blind, double-dummy, randomised, controlled, phase 3 study. *Lancet Oncol.* **19**, 370–381 (2018).
58. Zhou, W., Chen, H., Hong, X., Niu, X. & Lu, Q. Knockdown of DNA methyltransferase-1 inhibits proliferation and derepresses tumor suppressor genes in myeloma cells. *Oncol. Lett.* **8**, 2130–2134 (2014).
59. Das, D. S. et al. A novel hypoxia-selective epigenetic agent RRx-001 triggers apoptosis and overcomes drug resistance in multiple myeloma cells. *Leukemia* **30**, 2187–2197 (2016).
60. Harada, T. et al. HDAC3 regulates DNMT1 expression in multiple myeloma: therapeutic implications. *Leukemia* **31**, 2670–2677 (2017).
61. Yan, X. et al. 5-Azacytidine improves the osteogenic differentiation potential of aged human adipose-derived mesenchymal stem cells by DNA demethylation. *PLoS ONE* **9**, e90846 (2014).
62. Rabal, O. et al. Detailed exploration around 4-aminoquinolines chemical space to navigate the lysine methyltransferase G9a and DNA methyltransferase biological spaces. *J. Med. Chem.* **61**, 6546–6573 (2018).
63. Dominici, M. et al. Minimal criteria for defining multipotent mesenchymal stromal cells. The International Society for Cellular Therapy position statement. *Cytotherapy* **8**, 315–317 (2006).
64. Aryee, M. J. et al. Minfi: A flexible and comprehensive Bioconductor package for the analysis of Infinium DNA methylation microarrays. *Bioinformatics* **30**, 1363–1369 (2014).
65. Ritchie, M. E. et al. Limma powers differential expression analyses for RNA-sequencing and microarray studies. *Nucleic Acids Res.* **43**, e47 (2015).
66. Du, P., Kibbe, W. A. & Lin, S. M. lumi: A pipeline for processing Illumina microarray. *Bioinformatics* **24**, 1547–1548 (2008).
67. Hansen, K. D. IlluminaHumanMethylationEPICmanifest: manifest for Illumina's EPIC methylation arrays (2016).
68. Koch, C. M. et al. Pluripotent stem cells escape from senescence-associated DNA methylation changes. *Genome Res.* **23**, 248–259 (2013).
69. Teschendorff, A. E. et al. DNA methylation outliers in normal breast tissue identify field defects that are enriched in cancer. *Nat. Commun.* **7**, 10478 (2016).
70. McLean, C. Y. et al. GREAT improves functional interpretation of cis-regulatory regions. *Nat. Biotechnol.* **28**, 495–501 (2010).
71. Lawrence, M. et al. Software for computing and annotating genomic ranges. *PLoS Comput. Biol.* **9**, e1003118 (2013).
72. Carvalho, B. S. & Irizarry, R. A. A framework for oligonucleotide microarray preprocessing. *Bioinformatics* **26**, 2363–2367 (2010).
73. MacDonald, J. hugene10stranscriptcluster.db: Affymetrix hugene10 annotation data (chip hugene10stranscriptcluster) (2017).
74. Houlihan, D. D. et al. Isolation of mouse mesenchymal stem cells on the basis of expression of Sca-1 and PDGFR- α . *Nat. Protoc.* **7**, 2103–2111 (2012).
75. Garcia-Gomez, A. et al. Dasatinib as a bone-modifying agent: anabolic and anti-resorptive effects. *PLoS ONE* **7**, e34914 (2012).
76. Schneider, C. A., Rasband, W. S. & Eliceiri, K. W. NIH Image to ImageJ: 25 years of image analysis. *Nat. Methods* **9**, 671–675 (2012).
77. Doube, M. et al. BoneJ: free and extensible bone image analysis in ImageJ. *Bone* **47**, 1076–1079 (2010).
78. Gu, H. et al. Preparation of reduced representation bisulfite sequencing libraries for genome-scale DNA methylation profiling. *Nat. Protoc.* **6**, 468–481 (2011).

Acknowledgements

We thank CERCA Program/Generalitat de Catalunya and the Josep Carreras Foundation for institutional support. E.B. was funded by the Spanish Ministry of Science and Innovation (grant numbers SAF2014-55942-R and SAF2017-88086-R), co-funded by FEDER funds/European Regional Development Fund (ERDF)—a way to build Europe, and a Senior Research Award from the Multiple Myeloma Research Foundation (MMRF). C.O.-d.-S. was funded by the Spanish Ministry of Science, Innovation and Universities, under grant RTI2018-094494-B-C22 (MCIU/AEI/FEDER, UE). M.G. received financial support from the Spanish FIS-ISCI (PI15/02156 and PI19/01384) and FEDER. A.G.G. is funded by a postdoctoral contract of the Asociación Española Contra el Cáncer (AECC). F.P. was funded by grants from Instituto de Salud Carlos III (ISCIII), PI17/00701 and PI19/01352, TRASCAN (EPICA and Immunocell), Fundació La Marató de TV3, the Accelerator award CRUK/AIRC/AECC joint funder-partnership, CIBER-ONC (CB16/12/00489) and co-financed with FEDER funds and Fundación Ramón Areces (PREMAMM).

Ethical declaration

We have complied with all relevant ethical regulations for work with human participants in which informed written consent was obtained and the collection of samples and the study protocol for the use of those samples was approved by the Cancer Research Center-IBMCC Review Board (CICIC 2015/02156), the Clinical Ethics Committee for drug research in the Salamanca Health Area (CEIC 73/07/2015), the Clinical Research Committee of the Bellvitge University Hospital (ref. PR076/15) and the Research Ethics Committee at Universidad de Navarra (code 2017.218). Bone marrow samples were obtained conforming to ethical standards and good clinical practice for research work with principles expressed in the Declaration of Helsinki. All animal work was conducted according to relevant national and international guidelines for animal research and approved by the Bioethics Committee of the University of Salamanca (ref # 0000061).

Author contributions

A.G.-G., T.L., J.R.-U., and E.B. conceived and designed experiments; A.G.-G., T.L., C.C.-F., J. R.-U., L.C., G.G.-T., and L.S.-S. performed experiments; A.G.-G., T.L., and F.C.-M. performed biocomputing analysis; M.M., L.S.-S., S.M., X.M., J.O., C.O.-d.-S., E.S.J.-E., M.E., X.A., F.P., and M.G. participated in the data acquisition (performed patient selection, provided drugs, samples, animals, and facilities); A.G.-G., T.L., J.R.-U., and E.B. analyzed and interpreted the data; A.G.-G., T.L., and E.B. wrote the paper. All authors read and approved the final manuscript.

Competing interests

The authors declare no competing interests.

Additional information

Supplementary information is available for this paper at <https://doi.org/10.1038/s41467-020-20715-x>.

Correspondence and requests for materials should be addressed to A.G.-G. or E.B.

Peer review information *Nature Communications* thanks Stuart Rushworth and the other, anonymous, reviewer(s) for their contribution to the peer review of this work.

Reprints and permission information is available at <http://www.nature.com/reprints>

Publisher's note Springer Nature remains neutral with regard to jurisdictional claims in published maps and institutional affiliations.



Open Access This article is licensed under a Creative Commons

Attribution 4.0 International License, which permits use, sharing, adaptation, distribution and reproduction in any medium or format, as long as you give appropriate credit to the original author(s) and the source, provide a link to the Creative Commons license, and indicate if changes were made. The images or other third party material in this article are included in the article's Creative Commons license, unless indicated otherwise in a credit line to the material. If material is not included in the article's Creative Commons license and your intended use is not permitted by statutory regulation or exceeds the permitted use, you will need to obtain permission directly from the copyright holder. To view a copy of this license, visit <http://creativecommons.org/licenses/by/4.0/>.

© The Author(s) 2021